Style and Setting of Volcanic-hosted Massive Sulphide Mineralisation in the Early Permian Berserker beds, Mount Chalmers, Queensland.

A thesis submitted in fulfilment of the requirements for the degree of

Doctor of Philosophy

in the

School of Earth Sciences,
University of Tasmania

Steven Robert Hunns B.Sc (Hons)

November, 2001

To my past
Robert Arthur Hunns
2nd Dec 1921 to 12th Jan 1998

and to my future
wherever they may be, I will always be by their side

Marc Robert Hunns
21st Sept 1998

Anna Mary Hunns
1st November 2000

DECLARATION AND AUTHORITY OF ACCESS

This thesis contains the results of four years research conducted at the School of Earth Sciences, University of Tasmania, between April 1992 and June 1998. A number of papers and conference abstracts have either been published or have been submitted to international journals. These are listed below and are attached in full in Appendix A (Field guide and conference abstracts not appended).

Hunns, S. R., and McPhie, J. 1999. **Pumiceous peperite in a submarine volcanic succession at Mount Chalmers, Queensland, Australia.** Journal of Volcanology and Geothermal Research. Vol. 88. p. 239 - 254.

Khin Zaw., Gemmell, J. B., **Hunns, S.R.**, Mernagh, T. P., Ryan, C. G., Large, R.R., and Both, R. A. 1995. **Composition of fluid inclusions from the Hellyer and Mt. Chalmers VHMS deposits, Australia: Implications for ore-forming fluids.** *In* Maulk, J. L., and St. George, J. D. (Eds) *Proceedings of the 1995 Pacrim Congress.* Australasian Institute of Mining and Metallurgy Pub. Series N° 9/95. Melbourne. p. 663 – 668

McPhie, J., and **Hunns, S. R.** 1995. **Secondary welding of submarine, pumice-lithic breccia at Mount Chalmers, Queensland, Australia.** Bulletin of Volcanology. Vol. 57. p. 170 –178

Field Guide

Hunns, S. R. 1994. **Geology of the Mount Chalmers volcanic-hosted massive sulfide, and implications for its formation.** *In* Holcombe, R. J., Stephens, C. J., and Fielding, C. R. (Eds). 1*994 Field Conference Guide Book Capricorn Region Central Coastal Queensland.* Geol. Soc. Aust. Qld. Div. p. 80 - 92.

Conference Abstracts.

Hunns, S. R., and Khin Zaw 1996. **Mount Chalmers deposit - a shallow water VHMS deposit:** Mineral Exploration '96, Gold Coast, Queensland, Australia, 24-26 July, 1996.

Hunns, S. R., and Khin Zaw 1997. **Mount Chalmers deposit - a shallow water exhalative VMS deposit:** GAC/MAC Annual Meeting. Abstracts Vol. No. 22. p. 70.

Hunns, S. R., Khin Zaw., Large, R. R., Dean, J. A., Ryan, C. G., and McPhie, J. 1994. **Preliminary geochemical results constraining the formation of the Mount Chalmers volcanic-hosted massive sulfide deposit** *In* Henderson, R. A., and Davis, B. K. (Eds). *New Developments in geology and metallogeny: Northern Tasman Orogenic Zone.* Extended Abstracts. Economic Geology Research Unit Contrib. N° 50. James Cook University of North Queensland. p. 117 - 124.

Hunns, S. R., Kuronen, U., and Taube, A. 1993. **Volcano-sedimentary stratigraphy of the Mount Chalmers massive sulphide ore body.** 1993 IAVCEI General Assembly Abstract Volume, Canberra, 1993. p. 51.

McPhie, J., and **Hunns, S. R.** 1998. **Pumiceous sills, peperite and vesicular sediment at Mount Chalmers, Australia** 1998 IAVCEI General Assembly Abstract Volume, Cape Town, 1998.

The author acknowledges that:

i) the material contained in thesis has not been submitted for a degree or diploma at any other institution;

ii) to the best of the author's knowledge and belief, this thesis contains no material previously published or written by another person except where due reference has been made;

iii) publications arising from this study, as of the date below, are appended;

Authority of Access

This thesis may be made available for loan and limited copying in accordance with the Copyright Act 1968.

Steven R Hunns

16th November 2001

Goslar - Germany

ACKNOWLEDGMENTS

An Australian Postgraduate Award (Industry) in part funded this PhD project, an understanding bank manager the rest. Firstly I would like to thank Urpo Kuronen and Ian Neuss of Outokumpu Exploration Australia and Mining Project Investors for providing the initial support and funding for the PhD project, and then to Bob Cotton of Great Fitzroy Mines for continuing that support to the completion of the thesis. I would also like to thank John Fraser of Federation Resources for allowing me access to drill holes at Mount Chalmers drilled by Federation Resources. Without the support of these companies then this thesis would not have been possible.

I especially would like to acknowledge Alex Taube for the logistical assistance and stimulating discussions on the history and geology of Mount Chalmers, especially during the early stages of the thesis. Rod Sainty is also to be thanked for showing me the light in the sense that you do not need one thousand plus metres of seawater to form an exhalative VHMS deposit. ***"a phase diagram has never found an ore deposit" P. Ruxton (1987) - enough of the numbers - Long Live Palaeontology!.***

I would like the acknowledge the help that I have received from the following people: Byron McKavanagh of University of Central Queensland for providing access to computing facilities. Drs. Ross Both of Adelaide University and Dave Huston of AGSO for providing unpublished isotopic data. Khin Zaw for showing me the wonderful joys of watching tiny weeny bubbles and the information that can be extracted from them, and also to his wife Nilar for her friendship. Garry Davidson for showing me the light on oxygen isotopes and just what you can do with numbers. Ross Large for providing stimulating discussions on the origins of Mount Chalmers and VHMS deposits in general and for allowing a dream to come true. Prof. Bernd Lehman of the Technical University of Clausthal. for providing a place to study and access to library facilities at the university. To Jocelyn McPhie, my supervisor, for all of the patience you have shown me over the life of this thesis, I hope that you may still have a little faith in me.

I am greatly indebted to my fellow post-graduate students especially; Anthea Hill, Bruce Anderson, Mark Duffett, Karin Orth, Ali Raos, Catherine Reid, "Rowdy" (*nee* David Rawlings), Peter Winefield, Rohan Wolfe, and Bill Wyman who through the life of this project have at times kept me either sane or drove me very close to becoming insane. Ali and Catherine are to be especially acknowledged for providing stimulating but somewhat biased opinions on the ongoing "battle of the sexes" Bill Wyman and his wife Tina are especially thanked for being there when I needed them most.

I cannot thank Christine Higgins enough for the friendship that she has shown me over the years, and June Prongratz for the patience and friendship over what are now so many years

Robert Freitag of Capricorn Reef Diving, for the friendship, and for some memorable dives and times in Rock Vegas (Rockhampton). If you want to meet a beautiful German lady, fall in love with her, and marry her, visit Rob in his dive shop. It worked for me and incidentally it has worked for Rob as well.

Dave Polya of the University of Manchester deserves a huge vote of thanks for reading a large number of chapters that make up this thesis and for an entertaining night out in Manchester.

Clive Burrett thanks for everything, especially the patience and obviously a little bit of faith, and many wonderful memories of nights shared together solving the worlds' problems, I miss them.

However, there are three people who have made all of this possible:

Firstly, I owe my parents a debt that I will never be able to repay. I only hope that the final production of this thesis will go some way to expressing my undying gratitude and love for them.

Finally, I would like to thank my wife Eva for not only enduring my moods while this thesis was being written up and the especially the months of separation during the early stages of writing. Without her help, this thesis would not have come into existence. But, most importantly, I would like to thank her for providing the love, the friendship, the warmth, and the understanding when it mattered the most. I cannot thank her enough.

ABSTRACT

Mount Chalmers is a Kuroko-style volcanic-hosted massive sulphide (VHMS) deposit that is hosted within the Early Permian Berserker beds of central, eastern Queensland. The Berserker beds occur within tectonic units that comprise the New England Orogen. During the Early Permian horst-graben style extension occurred throughout the New England Orogen and across the back arc region. These fault basins accumulated marine sediments, commonly diamictites and volcanics. It is in one of these extensional basins that the sediments, volcaniclastics and volcanics that form the Berserker beds were probably deposited.

The Berserker beds are a complex unit of graded, mass flow emplaced, pumiceous breccias, volcano-lithic sandstone units, graded polymict, feldspar phyric pumiceous breccias, rhyolite intrusives, coherent to auto-brecciated rhyolite flows and their autoclastic products, andesitic intrusives, lavas and their autoclastic products. In the vicinity of the Mount Chalmers, mine the Berserker beds are represented by a dynamic and constantly evolving stratigraphic succession of proximal and distal volcanics interbedded with distally derived turbidites. A significant feature of this evolving and variable stratigraphy is the cyclic nature of the volcanism that is represented by the change in volcanism from rhyolite dominant to andesitic dominant and back to rhyolite again. The differing volcanic facies indicate that both subaerial and submarine volcanism were occurring within the general vicinity of each other.

The Berserker beds contain a diverse invertebrate fauna and trace fossil assemblage. The invertebrate fauna contains bryozoans, echinoderms, brachiopods and molluscs. The fossil assemblage and its mode of preservation are typical of a shallow shelf (near wave base) sand and silt environment. The faunal assemblage indicates a water depth in the range of 50 - 300 m. The trace fossils are mainly temporary fodinichnia (feeding traces) structures and comprise mainly *Teichichnus* and *Planolites,* with scattered *Rhizocorallium* and *Zoophycus* type burrows. The trace fossils have a restricted faunal diversity, and may be assigned to the *Cruziana* ichnofacies. This ichnofacies is normally understood as characterising the region between daily wave base and storm wave base, in low to moderate energy regimes.

The mineralisation at Mount Chalmers occurs in two main ore lenses, the Main Lode and the West Lode, and one minor lens, the South Lode. The massive sulphide mineralisation occurs on the flank of a rhyolite dome. The massive sulphide mineralisation consists of massive, layered and fragmental sulphides. Underlying the massive sulphide mineralisation is an extensive well developed network stringer veins. Footwall alteration at Mount Chalmers is dominated by silica along with extensive zones of chlorite alteration. Dolomite, sericite and kaolinite alterations are spatially restricted to high angle normal faults.

Textural, petrographic and microthermometric investigations of primary fluid inclusions yielded homogenisation temperatures of 160-268°C and salinities of 5-8 NaCl equiv. wt %. Semi-quantitative SEM/WDS microprobe analyses of fluid inclusion decrepitates indicate that the Mt. Chalmers ore fluids were enriched in potassium and calcium but depleted in magnesium relative to seawater. PIXE microanalysis of fluid inclusions in quartz also indicates a significant base metal concentration in these fluids. Cation composition and higher salinities relative to seawater suggests that a magmatic input of ore metals during seawater leaching of the footwall volcanic pile was a distinct possibility.

The $\delta^{34}S$ values for pyrite from Mount Chalmers range from -17.6 to -1.6 ‰, with a median value of -5.7 ‰ Chalcopyrite has a narrower range of $\delta^{34}S$ values compared to that for pyrite Both sphalerite and galena have restricted ranges in their $\delta^{34}S$ values compared to pyrite and chalcopyrite. Barite has a broad range in $\delta^{34}S$ values and has a skewed distribution. In combination with the fluid inclusion evidence, the favoured model to explain the $\delta^{34}S$ values in sulphides and barite was hydrothermal fluid that was probably dominated by evolved seawater, but one that had a minor, but significant input of sulphur from a magmatic source. The departures from the "normal" range of $\delta^{34}S$ values to values as low as -17.1 ‰ can be explained by the hydrothermal fluid interacting with biogenic sulphur within microniches within the sediments as the fluids passed through the volcano-sedimentary pile.

Mount Chalmers has a very narrow range of $\delta^{18}O$ values (+9.1 to +9.8 ‰). Modelled w/r ratios for both open and closed systems indicate that the Mount Chalmers hydrothermal fluid was dominated by seawater, with the possibility of the minor input of magmatic fluid. Calculated high water fluxes over a short time period (5,000 years) indicates that high water/rock ratios ($\geq$1) prevailed throughout most of the life the Mount Chalmers hydrothermal system.

Palaeontological evidence shows that the Berserker beds were deposited in a shallow-submarine environment ($\leq$300 m). Contact relationships between the volcanics and sedimentary facies reveals that peperitic facies are widespread. Silicic and mafic magmas have intruded at shallow levels into volcano-sedimentary pile. The Mount Chalmers VHMS mineralisation is spatially and temporally associated with the intrusion of a rhyolitic lava dome(s) into the volcano-sedimentary pile. Studies to date on modern and ancient VMS deposits have indicated that a minimum water depth between 1,000 to 1,500 m is required to prevent boiling of hydrothermal fluids and therefore concentrate metal deposition on the seafloor. However, these minimum water depths are in strong disagreement with the minimum water depth as suggested by the palaeontological and fluid inclusion evidence for the Mt. Chalmers VHMS deposit, indicating that is possible for a hydrothermal system to form an exhalative VHMS in a shallow-marine environment. Fluid inclusion and isotopic evidence suggests that there was a minor but significant input of metals, vapour and S from a magmatic source.

ABBREVIATIONS, SAMPLE NUMBER AND DRILL HOLE INFORMATION

Abbreviations

Listed below are the abbreviations that have been used in this thesis

MC = Mt. Chalmers Mine diamond drill hole *e.g.* MC25
MCP = Mt. Chalmers Mine percussion drill hole e.g MCP3A
MCP3A/MC25 = percussion drill hole (MCP3A) with a diamond drill hole tail (MC25)
MCD = Tungamull prospect diamond drill hole
WS = Woods Shaft prospect
PDH = percussion drill hole
DDH = diamond drill hole

All elevations are related to the Mt. Chalmers mine grid = sea level + 2,000 metres. *e.g.* RL 2200 means that the reference point is 200 metres above sea level

Drill name and samples

e.g. MC25-26.4 indicates that the sample came from drill hole MC25 at a depth of 26.4 metres below the collar (*i.e.* 0 metres).

Drill Hole Orientation

Unless otherwise stated all drill holes were drilled vertically. The drill holes that have been continually survey have only deviated from the vertical by a maximum of 5.5° (see Table below).

Sample downhole drill hole surveys.
Azimuth's are relative to the Mount Chalmers mine grid

Hole ID	Survey Depth	Azimuth	Dip
FDR19	0.00	360.00	-90
FDR19	92.00	313.00	-84.5
FDR19	122.00	94.00	-85.5
FDR19	152.00	179.00	-85
FDR25	120.45	72.00	-89
FDR25	150.00	173.00	-89
FDR25	180.50	360.00	-90
FDR26	0.00	360.00	-90
FDR26	120.00	135.00	-86.6
FDR26	150.20	126.00	-87
FDR26	177.00	340.00	-87

LCA = long core axis: any structural measurement *e.g.* 10° to the LCA means that the structure is at an angle 10° from the vertical.
SCA = short core axis.

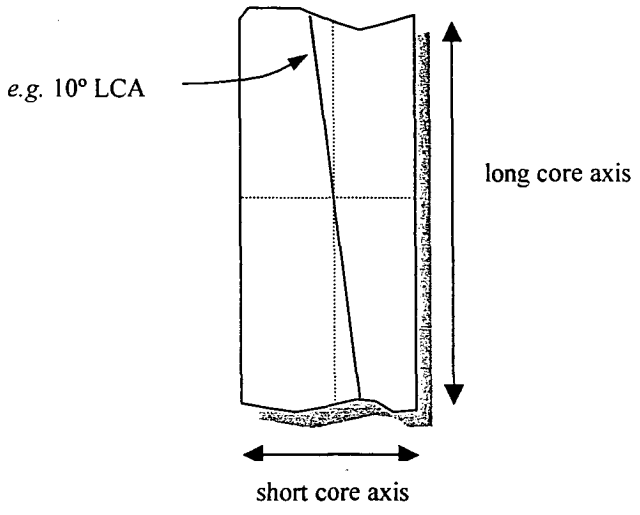

TABLE OF CONTENTS

LIST OF FIGURES

LIST OF TABLES

CHAPTER 1
INTRODUCTION

"Think well to the end, consider the end first"
Leonardo da Vinci

1.1 INTRODUCTION

Ancient volcanic sequences are the immediate host rocks for many of Australia's ore deposits, and in most cases, mineralisation and volcanism are genetically related. Controls on ore deposition are therefore closely linked with volcanic processes. Research into ore genesis and identification of favourable sites for ore deposition both depend on understanding the character and facies architecture of the volcanic host rocks.

The Berserker beds are well-preserved example of submarine volcano-sedimentary succession and based upon palaeontological evidence have been dated as Early Permian. The Berserker beds host the Mount Chalmers mine, a rich gold and copper volcanic-hosted massive sulphide (VHMS) ore deposit, and a number of small, nearby base metal and gold deposits and prospects. The mine operated intermittently between 1896 and 1982. During this period 1.2 million tonnes of ore was extracted yielding, 3,620 kg of Au, 21,751 kg of Ag, 22,624 tonnes of Cu, 19,021 tonnes of Pb and 7,099 tonnes of Zn (Willmott *et al.*, 1986).

1.2 AIMS AND SIGNIFICANCE

The vast majority of ancient VHMS deposits have undergone at least one if not more than one episode of structural deformation, and generally have a minimum greenschist metamorphic grade. These structural and metamorphic complications may produce ambiguities and uncertainties in the interpretation of the genesis of these deposits *e.g.* water depth of formation, and volcano-sedimentary environment. The study of an ancient VHMS deposit that has not undergone high degrees of metamorphism or structural deformation enables a more accurate interpretation of the genesis of these types of deposits to be made. Mount Chalmers is one such deposit. Careful reconstruction of an ancient volcanic terrain provides a powerful predictive tool with which to discern those parts of the volcanic sequence that are most highly prospective for yet undiscovered mineral deposits. The volcanic setting is also of fundamental importance as the framework within which ore genesis models can be developed.

The main aims of this PhD are:

- document the internal stratigraphy and structure of the Berserker beds in the Mount Chalmers region;
- provide an interpretation of the style and setting of the Permian volcanic activity, including identification of proximal facies associations;
- characterise the style of mineralisation and related host rock alteration at Mount Chalmers in terms of mineralogy, textures and alteration facies association.
- evaluate the genetic links between volcanic and mineralising processes.
- use isotopic characteristics and fluid chemistry to possibly fingerprint the source of the hydrothermal fluids and metals *i.e* magmatic versus seawater leaching

1.3 CHARACTERISTICS OF THE BERSERKER BEDS

The Berserker beds are a complex unit of graded, mass flow emplaced, pumiceous breccias, volcanolithic sandstone units, graded polymict, rhyolite intrusions, coherent to auto-brecciated rhyolite flows andesitic intrusions and lavas (Hunns *et al.*, 1993 and Hunns, 1994). The Berserker beds have undergone lower greenschist grade metamorphism, with little if any structural deformation. Regionally, northwest-southeast trending folds have gently folded the Berserker beds. Locally, and normally adjacent to andesitic intrusions the Berserker beds may have steep to near vertical dips.

1.4 METHODOLOGY AND THESIS ORGANISATION

Road sections along the Emu Park and Rockhampton Yeppoon Roads, were mapped at 1:100 000. Pilbeam Drive (access to Mt. Archer) was mapped in detail onto maps provided by the Rockhampton City Council. The area south of Mount Chalmers extending to the Emu Parl Road was mapped at 1:25,000, as this was the prime exploration area for Outokumpu Exploration Australia and Mining Project Investors Pty Ltd, who were sponsoring the project at the time of field mapping. All available diamond drillholes (total - 119) were logged in detail (1: 200) and sections of individual drillholes were logged at 1:10 (MCD4) and 1:40 (MCD11) scale respectively. The drill holes were logged using graphic logs, with emphasis placed on recognition of emplacement and flow units, contact relationships between units and textural variation within units and hydrothermal alteration mineral assemblages. Figure 1.1 shows the location of all holes that were logged, not including the Mount Chalmers mine holes.

Grid coordinates given throughout this thesis are either prefaced with AMG (Australian Map Grid - Australian Geodetic Datum Zone 1966) or by MG (Mount Chalmers Mine Grid coordinates). The Mount Chalmers Mine Grid is aligned parallel too magnetic north and the grid origin 5 000m E : 5 000 mN is centred over the Main Lode shaft. The relationship between AMG and the Mount Chalmers Mine Grid is shown on Figure. 1.2. The interpretations and discussions within this thesis are primarily based on the field data collected.

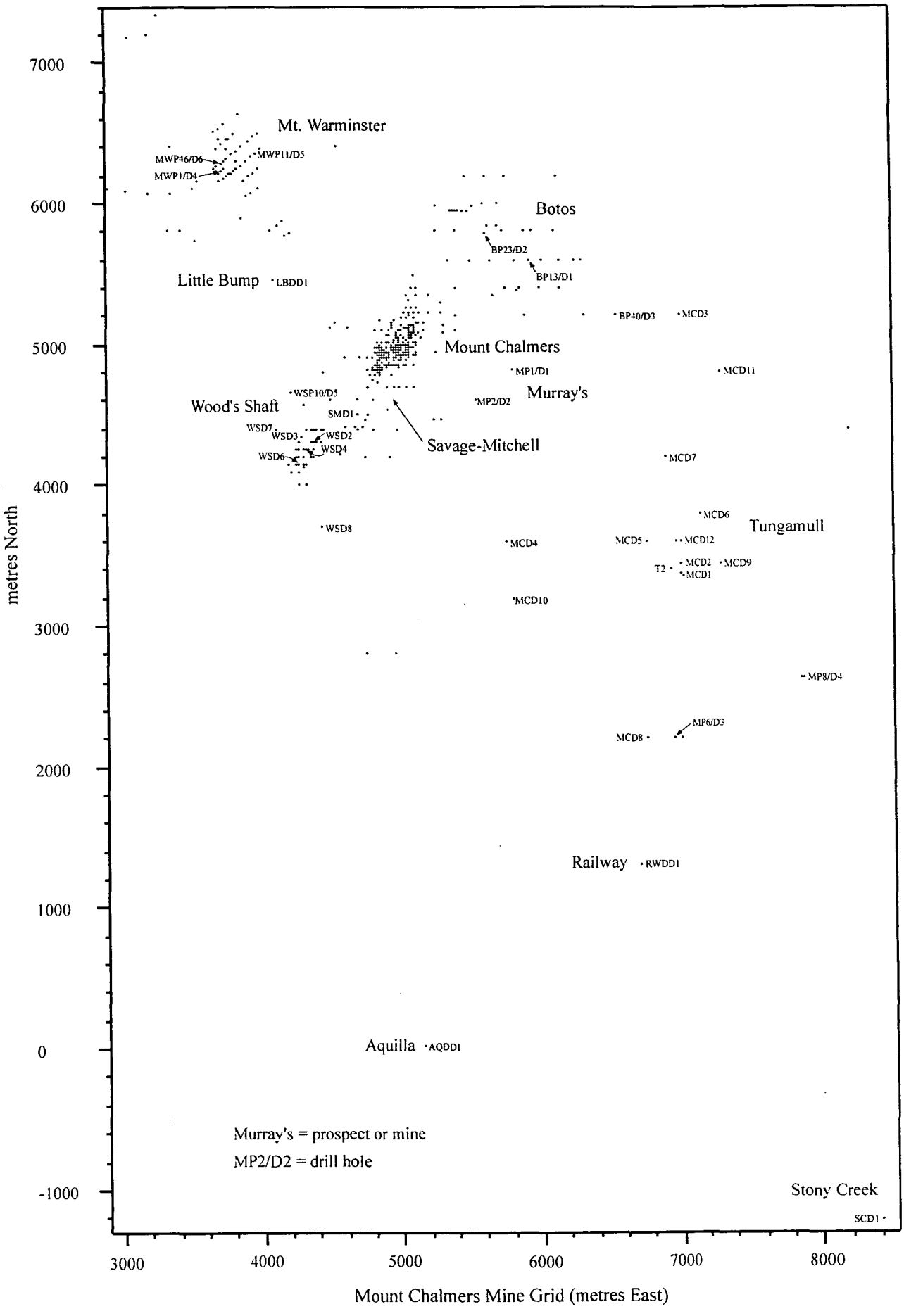

Figure 1.1. Location of prospects and of all diamond and percussion holes drilled at and within the vicinity of the Mount Chalmers mine. Labelled holes have been logged by the author, not labelled are the holes logged at Mount Chalmers

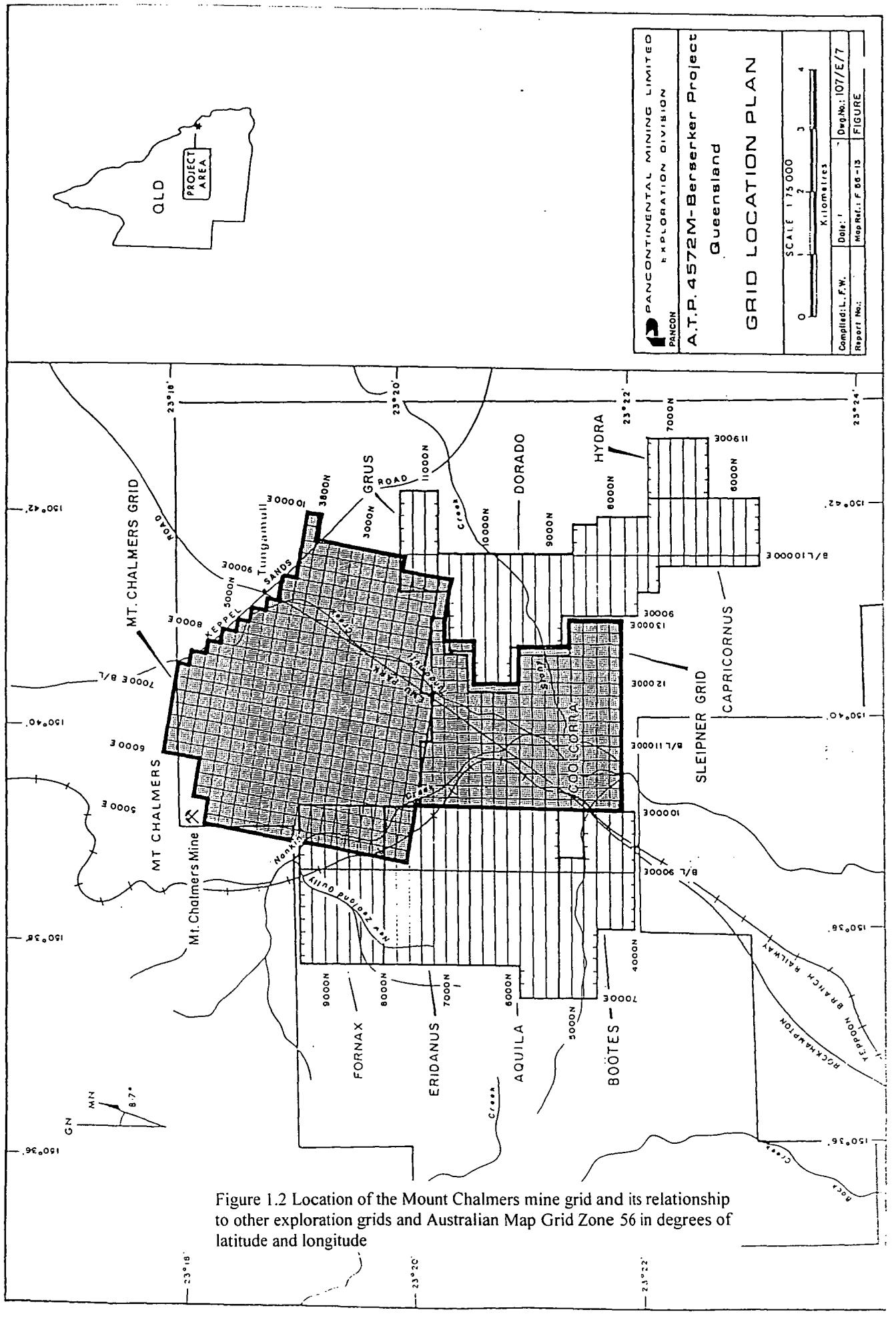

Figure 1.2 Location of the Mount Chalmers mine grid and its relationship to other exploration grids and Australian Map Grid Zone 56 in degrees of latitude and longitude

Rock and drill core samples collected during the field mapping were chosen for geochemical, petrographic and mineragraphic analyses. Selected mineralised and alteration assemblages were selected for sulfur, oxygen and carbon and oxygen isotope analyses.

The thesis is organised into 13 chapters

1 Introduction. -
2 Discusses the regional geology and tectonic setting of the Berserker beds
3 Describes the volcano-sedimentary facies and volcanic facies architecture and palaeoenvironmental setting of the Berserker beds in the vicinity of the Mount Chalmers mine.
4 Describes and discusses the origin of secondary welding textures in pumice breccias adjacent to andesitic and rhyolitic intrusions.
5 Describes and discusses the origin of pumiceous sills and their associated peperitic margins.
6 This chapter describes the style of mineralisation present at the Mount Chalmers mine and its environs, establishes the link between the mineralisation and volcanism as well as the palaeoenvironmental setting for the formation of the Mount Chalmers mineralisation.
7 Underlying the Mount Chalmers deposit is a well-developed extensive and variable alteration zone. This chapter describes the various alteration facies and their spatial distribution.
8 The compositional variation of fluid inclusions from the stringer zone mineralisation was used as constraints for the source of the ore-forming fluids at Mount Chalmers.
9 This chapter describes the massive dolomite lenses associated with the Mount Chalmers VHMS deposit, and proposes a model for their origin using covariance modelling of carbon and oxygen isotopes.
10 Sulphur isotopes from sulphides and barite are used to determine the source of the sulphur and to evaluate any possible spatial variation in the isotopic composition of the sulphur.
11 This chapter examines the oxygen isotope signature of the hydrothermal alteration within the stringer zone of the Mount Chalmers VHMS deposit as an aid for determining some the hydrological characteristics such as water/rock ratio and water flux estimates of the hydrothermal system.
12 Metal zonation and metal association studies were undertaken to delineate zones of hydrothermal activity within the Mount Chalmers and to evaluate the classification of VHMS deposits based upon their metal content.
13 Conclusion - summarises the major findings of this thesis.

1.5 LOCATION AND ACCESS

The Berserker beds extend from the Gladstone area in the south, to north of the central Queensland city of Rockhampton. Access to the low-lying areas of the Berserker beds is by sealed and unsealed roads. The Berserker beds are generally poorly exposed, due to extensive cultivation, and forests. These factors, coupled with the steep and rugged topography have made regional correlations difficult. The best exposures of the Berserker beds are along the Emu-Park Road, Rockhampton-Yeppoon Road and the Mount Archer Road, as well as the open cut exposures at Mount Chalmers. However, the best subsurface information was provided by the logging of approximately 17, 500 metres of drill core, drilled mainly at

Mount Chalmers and at other nearby prospects. The Mount Chalmers mine is located 17 km NE of the central Queensland city of Rockhampton (Fig. 1.3) on the Rockhampton (SF 56-13) 1:250,000 and Rockhampton (9051) 1:100,000 scale map sheets.

1.6 PHYSIOGRAPHY

Willmott *et al.* (1986) divided the Rockhampton region into a number of distinct physiographic regions. The mountainous terrain of the Flat Top Range and the Berserker Range (Mount Archer 608 m), and their continuations to the North dominate the Rockhampton/Yeppoon district. North of the Rockhampton-Yeppoon Road, the terrain changes from mountainous to hilly/mountainous. The Berserker and Flat Top Ranges are flanked on either side by undulating to hilly topography and alluvial plains. Between Mount Hedlow and Mount Wheeler, a series of isolated, resistant trachyte plugs rise out of the alluvial plains.

1.7 SUMMARY OF PREVIOUS WORK ON THE BERSERKER BEDS

Reid and Morton (1928), Whitehouse (1928) and Reid (1930) made the first attempts at a regional geological interpretation of the Rockhampton district. Hawkins and Whitcher (1962) conducted the first systematic regional mapping of the volcanics and sedimentary rocks that now comprise the Berserker beds. The name "Berserker beds" was formally defined by Kikegaard *et al.* (1970) with the type section for the Berserker beds being the Berserker Range.

The Berserker beds contain diverse invertebrate fauna and trace fossil assemblages. The invertebrate fauna contains bryozoans, echinoderms, brachiopods and molluscs. These have been described by Crockford (1945), Armstrong *et al.* (1967), McKellar (1969), and McKellar *et al.* (1970). Hawkins and Whitcher (1962) and Sainty (1992) reported a number of new fossil localities. Sainty (1992) also described a trace fossil assemblage from within and near the Mount Chalmers mine.

Reid (1935; 1936; 1938a) described several small gold prospects in the vicinity of the Mount Chalmers mine. The first published report on mineralisation within the Berserker beds was by Dunstan (1908), who described the geology and style of mineralisation of the Great Fitzroy mine (now the Mount Chalmers mine). Dunstan (1908) suggested that the concentration of sulphides beneath the hangingwall was the result of the replacement of a limestone lens along the crest of a plunging anticlinal fold. Reid (1938b) published the first ore reserve figures for the Mount Chalmers mine. The first comprehensive study of the Mount Chalmers mine was conducted by Fisher and Owen (1952), who described the style of mineralisation and its possible origins, and gave a brief introduction to the stratigraphy and its relationship to the mineralisation. Fisher and Owen (1952) concluded that the mineralising fluids differentially replaced a breccia horizon and that regional and local shearing due to andesitic and quartz porphyry intrusion localised the favourable ore horizons. A systematic stratigraphy for Mount Chalmers mine was initially established by Okill (1974) who recognised nine stratigraphic units based upon the

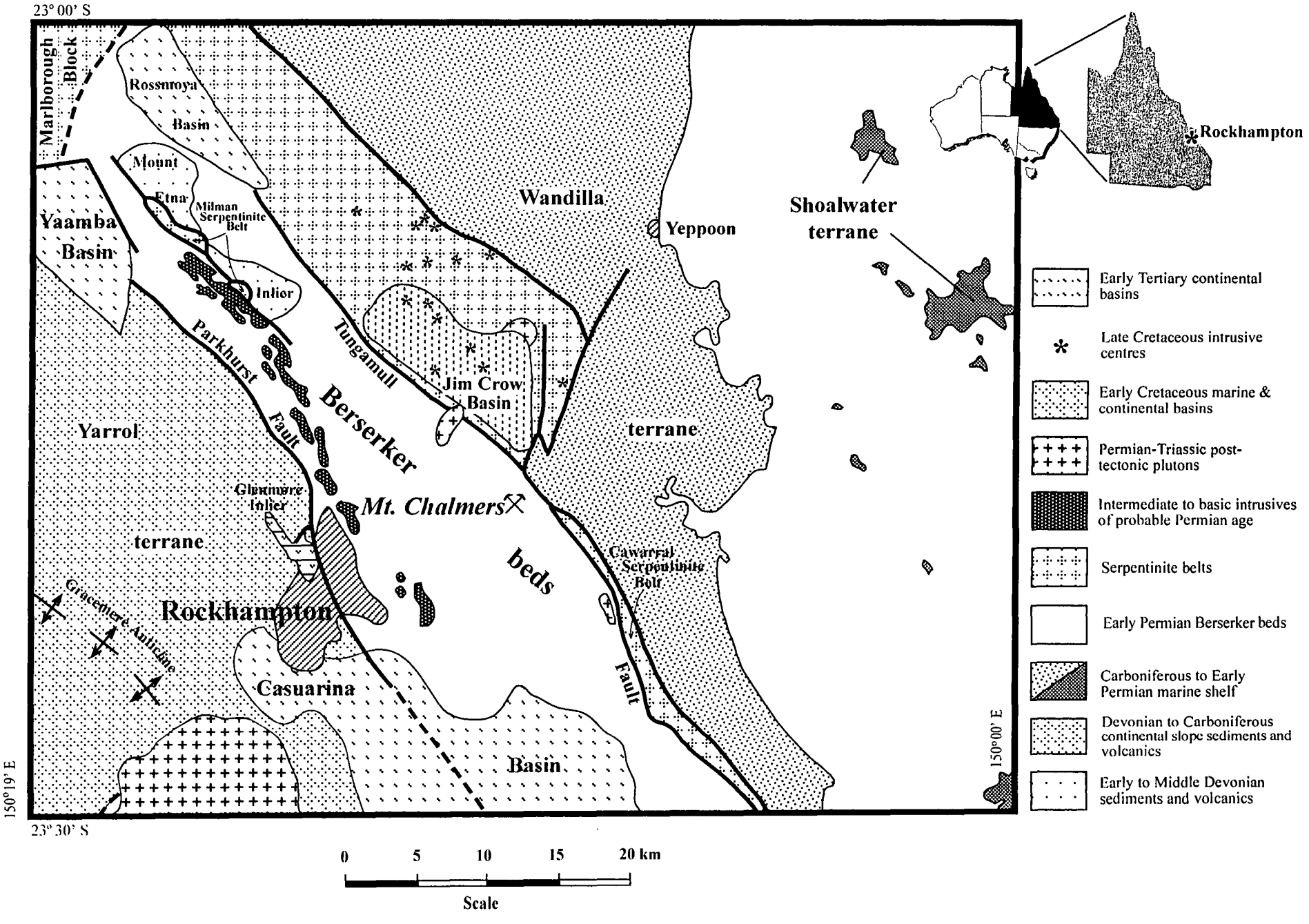

Figure 1.3. Regional geology of central coastal Queensland, showing the location of the Berserker beds, Mount Chalmers and Rockhampton

then available diamond drill holes. Large and Both (1982) recognised 11 stratigraphic units within the immediate vicinity of the Mount Chalmers mine, based upon pit exposures and diamond drill core. Sainty (1992) grouped the units recognised by Large and Both (1982) into six stratigraphic units, based upon regional and mine scale mapping.

Okill (1974) compared the Mount Chalmers style of mineralisation and alteration to the Japanese Kuroko deposits and interpreted a volcano-exhalative origin for the massive sulphide. Fletcher (1975) suggested that metasomatic replacement and alteration of the brecciated country rock formed the Mount Chalmers mineralisation. Large and Both (1980), Taube and van der Helder (1983) and Taube (1990) concluded that the mineralisation was formed by the venting of hydrothermal fluids onto the palaeo sea-floor and that the form, mineralogy, and volcanic setting of the Mount Chalmers massive sulfide are consistent with a submarine volcanogenic origin, similar to the Japanese Kuroko deposits. Hunns (1994) suggested that the hydrothermal fluids never vented onto the seafloor. Instead, they replaced a favourable horizon at some depth below the palaeo-seafloor. Sainty (1992) inferred a shallow water origin (≤300 m bsl) for the formation of the Mount Chalmers mineralisation, based upon the presence of shallow water invertebrate fauna and trace fossil ichnofacies in the host succession. Hunns and Zaw (1997) also favoured a shallow marine (≤ 280-m bsl) setting for the formation of the Mount Chalmers massive sulfide, based upon palaeontological and fluid inclusion evidence.

CHAPTER 2
REGIONAL GEOLOGY

2.1 INTRODUCTION

This chapter describes the regional geology and the relationship between the Berserker beds and other formations, as well as the broad tectonic setting of the Berserker beds.

The Berserker beds occur within an elongate fault-bounded graben-like structure, the Berserker Block (Willmott *et al.*, 1986). To the east, the Berserker beds are in faulted contact with serpentinites of the Cawarral Serpentinite Belt and rocks of the Siluro-Devonian Doonside Formation. To the west, the Berserker beds are in faulted contact with rocks of the Lower Carboniferous Rockhampton Group (Fig. 1.3).

The name Berserker was first used by Whitehouse (1930) as the Berserker Series for the volcanics and sedimentary rocks that form the Berserker Range. The Berserker beds include beds referred to as the Thozet's Creek Beds (Jack and Etheridge, 1892) and Lake's Creek Beds (Smith 1889). Both these names were not formally defined and Berserker was considered more applicable (Kirkegaard *et al.*, 1970). The type area for the Berserker beds is the Berserker Range (Kirkegaard *et al.*, 1970).

2.2. BERSERKER BEDS

The Berserker beds occupy a northwest-trending elongate fault bounded graben-like structure, which measures approximately 110 x 5-15 km wide, and have been dated on palaeontological evidence as Upper Sakmarian to Lower Artinskian (Early Permian ~280 - 265 Ma) (Kirkegaard *et al.*, 1970).

The Berserker beds comprise a mixture of sedimentary and volcanic facies associations. Thin to thickly bedded volcanolithic graded and massive sandstone and laminated to thinly bedded mudstone dominate the sedimentary facies association. *In situ* fossils thought to be typical of shelf environments occur at several localities, and many intervals of both sandstone and mudstone contain trace fossils characteristic of the ichnofacies *Cruziana* (Sainty 1992). The volcanic facies association comprises rhyolitic, dacitic and andesitic lavas and related autoclastic breccia, peperite, pumice-lithic breccia and synvolcanic intrusions (Hunns *et al.*, 1993).

There are regional variations in the proportions of sedimentary versus volcanic facies associations in the Berserker beds. In the Mount Chalmers district the volcanic facies association is dominant and represented by: rhyolitic and andesitic lavas, and autoclastic breccia; dacite mudstone peperite; rhyolitic and andesitic intrusions (sills and dykes), and very thick, graded, rhyolitic pumice and lithic breccia. Rhyolitic intrusions are principally dykes and are strongly discordant to bedding. Andesitic intrusions are mainly sills or else are

slightly discordant to bedding, and up to 200 m in thickness. Near Mount Chalmers mine, andesitic sills have been intersected in drill holes over an area of 6 km x 4 km (McPhie & Hunns 1995).

The Berserker beds unconformably overlie the early Devonian Etna Beds to the North of Rockhampton (Willmott *et al.*, 1986; Fig. 1.3).

The Tungamull Fault and the Parkhurst Fault bound the Berserker beds to the East and west respectively (Fig. 1.3), which have been interpreted as thrust faults by Willmott *et al.* (1986). Reinterpretation of the aeromagnetic data has shown that the Tungamull Fault dips at approximately 80° to the East (U. Kuronen, *verb. comm.* 1993).

The Berserker beds occur within tectonic units that make up the New England Fold Belt (New England Orogen). The New England Fold Belt is the easternmost and youngest part of the Tasman Fold Belt. The Tasman Fold Belt is a composite tectogenic or structural feature which has developed from several pre-cratonic tectonic provinces during the Palaeozoic in eastern Australia (Scheibner, 1978).

2.3. REGIONAL TECTONICS AND GEOLOGY

The New England Fold Belt can be divided into three provinces, the Yarrol Province to the north, the Gympie Province to the east, and the New England Province to the south.

During the Middle to Late Carboniferous the tectonic setting of the Australian continental margin changed from a convergent plate margin with a west dipping subduction zone with attendant arc volcanism to a combination of subduction and transform faulting (Murray *et al.*, 1987). Murray *et al.* (1987) interpreted the change from a purely convergent margin to a transform plate margin was initiated in the northern part of the Yarrol Province and migrated gradually southwards.

In the Rockhampton - Gladstone region of Queensland the New England Fold Belt from west to east is composed of a number of different structural units: the Gogango Overfolded Zone, the Yarrol terrane (Calliope Island Arc, Rockhampton Group and the Berserker beds), the Marlborough terrane, the Wandilla and Shoalwater terranes (Table 2.1. and Fig. 2.1).

2.3.1. Yarrol Terrane

The Yarrol terrane (Table 2.1) is composed of sedimentary rocks deposited on the Yarrol Shelf east of the Connors-Auburn Volcanic Arc during the Late Devonian to Early Carboniferous, and overlies Late Carboniferous - early Permian shallow marine sedimentary rocks.

Table 2.1. Characteristics of structural terranes in central Queensland, New England Fold Belt. (After Day *et al.*, 1978).

Structural Terrane	Rock Types & Age Range	Depositional Environment	Folding	Metamorphism	Intrusives
Connors-Auburn Arches	Late Devonian to Early Carboniferous calc-alkaline volcanics	Continental margin volcanic arc	Slight; gently dipping in most area; no penetrative deformation	Local contact metamorphism around granitic plutons	Post-orogenic granitic batholiths of Late Carboniferous and Early Permian and Early Cretaceous
Gogango Over-folded Zone	Permian pillow basalts & clastic sediments, calc-alkaline volcanics in south & north	Moderately deep water marine	Tight to isoclinal folds overturned to the west; slaty cleavage in argillaceous rocks; later generation of open mesoscopic folding	Unknown; probably locally metamorphosed to greenschist facies	
Yarrol Terrane	Late Devonian to Early Permian volcaniclastic sediments, limestone & calc-alkaline volcanics	Unstable marine continental shelf (fore-arc basin); some terrestrial deposition in the Early Permian	Dominantly open folds along north-northwest axes	Unknown; probably low grade burial metamorphism	Post-orogenic granitic batholith, widespread granitic plutons, and small layered gabbros of Late Permian and Triassic age in Yarrol Block
Calliope Terrane	Late Silurian to Middle Devonian calc-alkaline volcanics, volcaniclastic sediments, & limestone	Shallow to moderately deep marine and terrestrial deposits; probably island arc	Open to tight folding along north to north-north-west axes; slaty cleavage in argillaceous rocks	Widespread metamorphism to lower greenschist facies	Small post-orogenic Late Devonian granodiorite and diorite plutons in Calliope Block
Marlborough Terrane	Mainly serpentinite, with greenschist & amphibolite facies metamorphics	Thrust sheet of fragment of oceanic crust and mantle	Tight, steeply plunging overfolded folds in metamorphic rocks with axial plane slaty cleavage; local second generation kinks	Greenschist and amphibolite facies metamorphics at contacts of serpentinite	Small post-orogenic Late Permian to Early Triassic granitic and gabbroic plutons
Wandilla & Shoalwater terranes	Interbedded arenite & argillite, chert, jasper, minor pillow basalts, conglomerates and limestone of probable Devonian to Carboniferous age	Cherts, jaspers and possibly basalts are abyssal plain deposits; clastics are turbidites of continental slope and possibly trench	Mesoscopic isoclinal folds with steeply dipping axial plane cleavage in argillaceous rocks; up to 3 later generations of open mesoscopic folds including kink folds; axial planes trend north-north-west	Widespread metamorphism to prehinite-pumpellyite and lower facies with local amphibolite and transitional blue schist facies	Widespread post-orogenic granitic plutons and rare small layered gabbros of Late Permian and Triassic Age

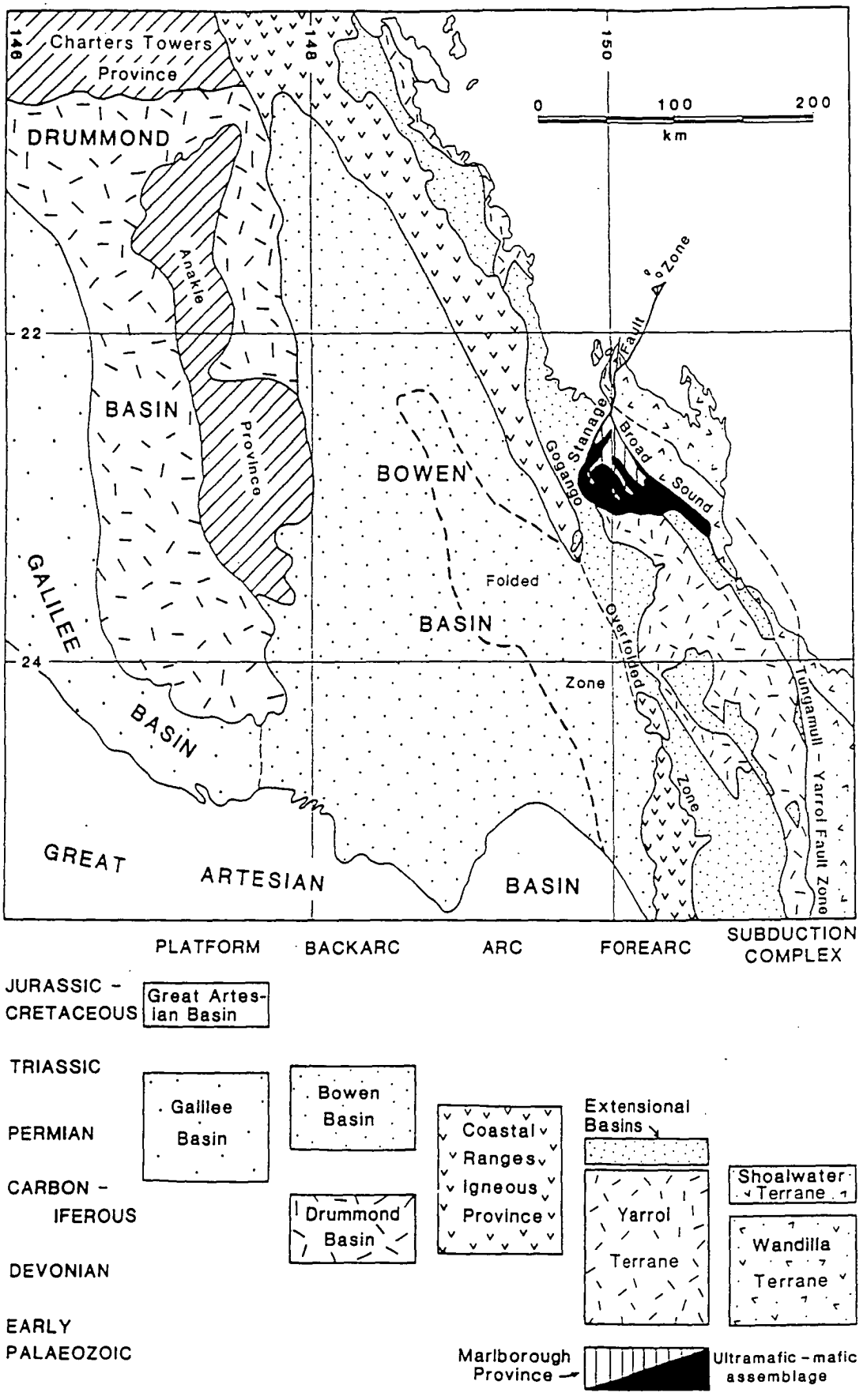

Figure 2.1 Major elements of the northern New England Orogen and the tectonic context attributed to them (From Henderson *et al.*, 1993).

The Yarrol terrane contains a rare record of continuous marine shelf deposition almost throughout the Carboniferous and extending past a brief lacuna (286-280 Ma) into the Early Permian, in the form of the Burnett Formation and the equivalent volcanic fluvial to marginal marine Youlambe Conglomerate. The succeeding Yarrol Formation comprises 500 m of limestone, siltstone and lithic sandstone with interbedded andesitic lava (Veevers *et al.*,1994). Veevers *et al.*, (1994) consider the Berserker beds to be the eastern equivalent of the Yarrol Formation.

The base of the Yarrol terrane is composed of ?Silurian to Middle Devonian aged thick succession of interbedded silicic to andesitic volcanics, volcaniclastics and limestones, which have been intruded by Middle Devonian intermediate plutons. Younger strata are composed of Late Devonian andesitic volcanics and volcaniclastics which overlie the Calliope Island Arc succession with a low angle unconformity; a thick Carboniferous succession of shallow marine strata, consisting of oolitic limestone in the west and coeval deeper marine clastics further west; areally restricted Late Carboniferous marine clastics with a disconformity at their base and scattered Permian clastic units which unconformably overlie older successions. The eastern boundary of the Yarrol terrane is occupied by Permian volcanics, volcaniclastics and sedimentary rocks, which are largely faulted bounded, and locally unconformably overlie Middle Devonian volcanics (Fergusson *et al.*, 1988).

In the Rockhampton-Gladstone district the contact between the Yarrol terrane and the Wandilla terrane is marked by a major fault (Tungamull-Boyne River Fault) and by a series of discontinuous serpentinite bodies. North of Rockhampton areally extensive serpentinised ultramafics grouped as the Marlborough terrane separate the Yarrol and Wandilla terranes (Fergusson *et al.*,1988).

2.3.2. Wandilla and Shoalwater Terranes

Highly deformed rocks that occur to the east of the Tungamull Fault in the Rockhampton - Gladstone district of central Queensland were termed the Curtis Island Group by Kirkegaard *et al.*, (1970). Kirkegaard *et al.*, (1970) subdivided the group into the Shoalwater Formation, Wandilla Formation and the Doonside Formation. Fergusson *et al.*, (1988) referred the Wandilla Formation and the Doonside Formation to the Wandilla terrane and the Shoalwater Formation to the Shoalwater terrane.

Both the Wandilla and Shoalwater terranes have undergone four stages of deformation. D_1 formed a widespread lenticular melange during subduction accretion in a Devonian to Carboniferous fore-arc (Fergusson *et al.*, 1990; Fergusson *et al.*, 1993). D_2 is widespread and formed a moderately to shallowly dipping cleavage and tight to open F_2 folds, and was produced during the Late Permian to Triassic Hunter-Bowen Orogeny (Fergusson *et al.*,1990; Fergusson *et al.*, 1993). D_3 and D_4 developed as a progressive sequence during the same general deformation as D_2, but occurred in the Middle to Late Permian (Fergusson *et al.*, 1990).

2.3.2.1. Wandilla Terrane

The Wandilla terrane (Fig. 1.3 and Table 2.1) is a tectonic melange composed of mudstone, greywacke, chert and greenstone. An Early Carboniferous age is inferred from the abundant detrital ooids and crinoid ossicles contained in the greywacke (Fergusson *et al.*, 1990). Bedded cherts within the Wandilla terrane contain radiolarians, and are inferred to have formed from pelagic deposition on an oceanic plate (Fergusson *et al.*, 1993).

The lithological characteristics and structural styles indicate a subduction complex setting for much of the Wandilla terrane. Radiolarians (Carboniferous age) from cherts within the subduction complex are consistent with a major accretionary episode in the late Early and Late Carboniferous (Fergusson *et al.*, 1993).

2.3.2.2. Shoalwater Terrane

The Shoalwater terrane (Fig. 1.3 and Table 2.1) is a variably metamorphosed succession of quartzose turbiditic sandstone and mudstone containing trace fossils. A Late Carboniferous age is inferred for the Shoalwater terrane, because it is ocean ward of the Wandilla terrane, and therefore, presumably a younger part of the subduction complex (Fergusson *et al.*, 1990). The first phase of deformation seen within the Shoalwater terrane is characteristic of subduction accretion of coherent strata and is thought to indicate continued accretion of the subduction complex (Fergusson *et al.*, 1990).

2.3.3. Marlborough Terrane

The ultramafic rocks of the Marlborough terrane (Fig. 1.3 and Table 2.1) are considered to be fragments of oceanic crust and mantle material, which were emplaced by thrusting during deformation and upthrusting of the continental slope deposits of the Wandilla terrane in the middle to late Permian. A belt of small intrusions of gabbro, dolerite and diorite occur along the western margin of the Berserker Block may be related to these thrusting movements and the emplacement of the serpentinite belts (Willmott *et al.*, 1986).

2.4 EARLY PERMIAN TECTONICS

Between 300 - 295 Ma a major volcanic arc developed — the Camboon Volcanic arc, along the site of the former Connors-Auburn Arc (Murray *et al.*, 1987). Jones (1994) considers that the Camboon Volcanic Arc was activated by either subduction (associated with a trench seaward of the present continental margin. Murray *et al.*, 1987), or related to widespread extension during the Early Permian.

In the late Carboniferous intensive extension was occurring within the old accretionary complex. By the Early Permian horst-graben style extension occurred throughout the New England Fold Belt and across the back arc region. These fault basins commonly accumulated marine sedimentary rocks, commonly diamictites and volcanics (Holcombe *et al.*, 1994). It is in one of these extensional basins that the sedimentary rocks, volcaniclastics and volcanics that form the Berserker beds were probably deposited.

The Berserker beds have been moderately deformed and metamorphosed to zeolite - prehnite-pumpellyite grade. The Berserker beds were deformed during the middle to late Permian orogeny that resulted in the development of north-northwest trending open upright folds (Day *et. al.*, 1983, Donchak and Holmes, 1991) and the development of a weak although not pervasive northerly striking vertical cleavage. The late Devonian to early Carboniferous Curtis Island Group was thrusted against the eastern side of the Tungamull Fault. The Berserker beds were probably thrust westwards against the early Carboniferous Rockhampton Group along the Parkhurst Fault. Thrusting also occurred within the Berserker beds along the Caves Fault (Willmott *et al.*, 1986). A large east-northeast-striking fault at the mouth of the Fitzroy River appears to have displaced the Berserker beds. It has probably undergone movement in the Quaternary, as it is defined by the present coastline (Murray, 1975).

CHAPTER 3
VOLCANIC AND SEDIMENTARY FACIES AND VOLCANIC FACIES ARCHITECTURE OF THE BERSERKER BEDS IN THE VICINITY OF THE MOUNT CHALMERS MINE

"On the morning of his departure he put his planet in perfect order. He carefully cleaned out his active volcanoes. He possessed two active volcanoes; and they were convenient for heating his breakfast in the morning. He also had one volcano that was extinct. But, as he said 'One never knows!' *So he cleaned out the extinct volcano, too. If they are well cleaned out, volcanoes burn slowly and steadily, without any eruptions. Volcanic eruptions are like fires in a chimney.*
On our earth we are obviously much too small to clean out our volcanoes. That is why they bring no end of trouble upon us."

Antoine de Saint-Exupéry - *The Little Prince* 1945

3.1. INTRODUCTION

The Berserker beds are a complex assemblage of graded mass-flow emplaced pumiceous breccias, volcanolithic sandstone units, graded polymict, feldspar phyric pumiceous breccias, rhyolite intrusives, coherent to auto-brecciated rhyolite flows and their autoclastic products, basaltic intrusions, andesitic intrusions, lavas and their autoclastic products.

Okill (1974) initially established a systematic stratigraphy for the Mount Chalmers mine and divided the succession into 11 units (Table 3.1). Large & Both (1982) modified the stratigraphy as defined by Okill (1974), and defined a regional stratigraphy that could be correlated to the mine stratigraphy (Table 3.1). Taube and van der Helder (1983) from mapping of the open cut detailed the structure of the mine, and Sainty (1992) reevaluated both the mine scale and the regional stratigraphy. Figure 3.1 shows the generalised surface geology of the mine prior to mining, the surface projection of the "10 m% Cu" contour, and the outer limit of the final open pit.

A number of local terms have been used by previous workers, that for sake of clarity and ease of separation of some similar rock types will be used throughout this thesis. The two main terms are the Ellrott Rhyolite and the Sleipner Andesitic Breccia. The term Ellrott Rhyolite was first used by Taube (1979) to describe the flow banded, feldspar-phyric rhyolite that forms the low hills on the northern side of the Emu Park Road. Taube (1979) first coined the phrase Sleipner Andesitic Tuff, which Sainty (1992) renamed the Sleipner Andesitic Breccia. The term Sleipner Andesitic Breccia is preferred, as it is a non-generic term. Sainty (*ibid*) introduced the following terms; Lower Chalmers Sediment and Upper Chalmers Sediment to separate two sedimentary horizons that he mapped, one of which hosts the Mount Chalmers massive sulphide mineralisation (Lower Chalmers Sediment) and the second that occurs higher up in the stratigraphy (Upper Chalmers Sediment). The separation and naming of volcanolithic sandstone units within the Berserker beds is not considered to be valid for the following two main reasons:

- more than two unique sedimentary units have been mapped in the field and logged in drill core
- due to the lack of continual exposure, regional correlations are difficult to make.

Table 3.1. Comparison between lithological associations and stratigraphic nomenclature used by various workers for the Berserker beds at and in the vicinity of the Mount Chalmers mine

This Thesis	Okill (1974)	Large & Both (1980)	Taube & van der Helder (1983)	Sainty (1992)
		Footwall Lithologies		
Chlorite-silica-sericite altered dacitic breccias	Unit 10 - Silicified breccia	Unit 1 - Coarse-grained siliceous fragmental	Silicified pyritic tuffs	Footwall dacite
Footwall rhyolite, ±sulphide stringers	Unit 10 - Silicified breccia	Unit 2 - Siliceous pyroclastics		
Silica-sericite-kaolin-chlorite-dolomite alteration, ±sulphide stringers	Unit 12 - Grey clayey fragmental tuff			
Massive dolomite alteration	Unit 11 - Calcareous tuff limestone	Unit 4 - Dolomite-pyrite horizon	Dolomite	Not described
		Mineralised Horizon		
Massive to semi-massive sulphide	Massive sulphide	Unit 5 - Massive sulphide-barite lens	Massive bedded sulphide	Not described
Altered & mineralised volcanolithic sandstone	Unit 10 - Silicified tuff & tuffaceous sandstone	Unit 6 - Chloritic-talcose-pyritic siltstone	Mineralised sequence - ash tuff or fg sediments	Lowers Chalmers Sediment
		Hangingwall Lithologies		
Peperites	Unit 13 & 14 - Silicified crystal tuff breccia	Unit 7 - Contorted tuff	Contorted feldspathic rhyolitic tuffs & siltstones	Not described
Feldspar-phyric, pumiceous lithic mass-flow emplaced breccia	Unit 18 - Crystal tuff breccia	Unit 10 - Rhyolitic breccia	Mill rock	Facies variant within the North Star Pumice Breccia
Feldspar-phyric, pumiceous mass-flow emplaced breccia	Unit 18 - Crystal tuff breccia	Unit 9 & 11 - Rhyolitic volcaniclastics	Rhyolite tuffs	North Star Pumice Breccia
Graded, volcanolithic conglomerate	Not described	Unit 8 - Greywacke siltstone	Greywackes	Not described
Well bedded, graded volcano- lithic sandstone	Unit 17 - Andesite tuff or siltstone	Unit 8 - Greywacke siltstone	Greywackes	Upper Chalmers Sediment
Andesitic lava & hyaloclastite	Not described		Not described	Not described
Sleipner Andesitic Breccia	Not described	Andesitic lithic tuffs & lavas	Not described	Sleipner Andesitic Breccia
Ellrott Rhyolite	Not described		Not described	Ellrott Rhyolite
		Intrusives		
Andesite	Amygdaloidal andesites	Andesites	Andesites	Andesites
Quartz-feldspar porphyries	Quartz porphyries	Quartz-feldspar porphyries	Quartz-feldspar porphyries	Quartz-feldspar porphyries
Feldspar-quartz porphyries	Not described	Not described	Not described	Not described
Diorite	Not described	Not described	Not described	Not described

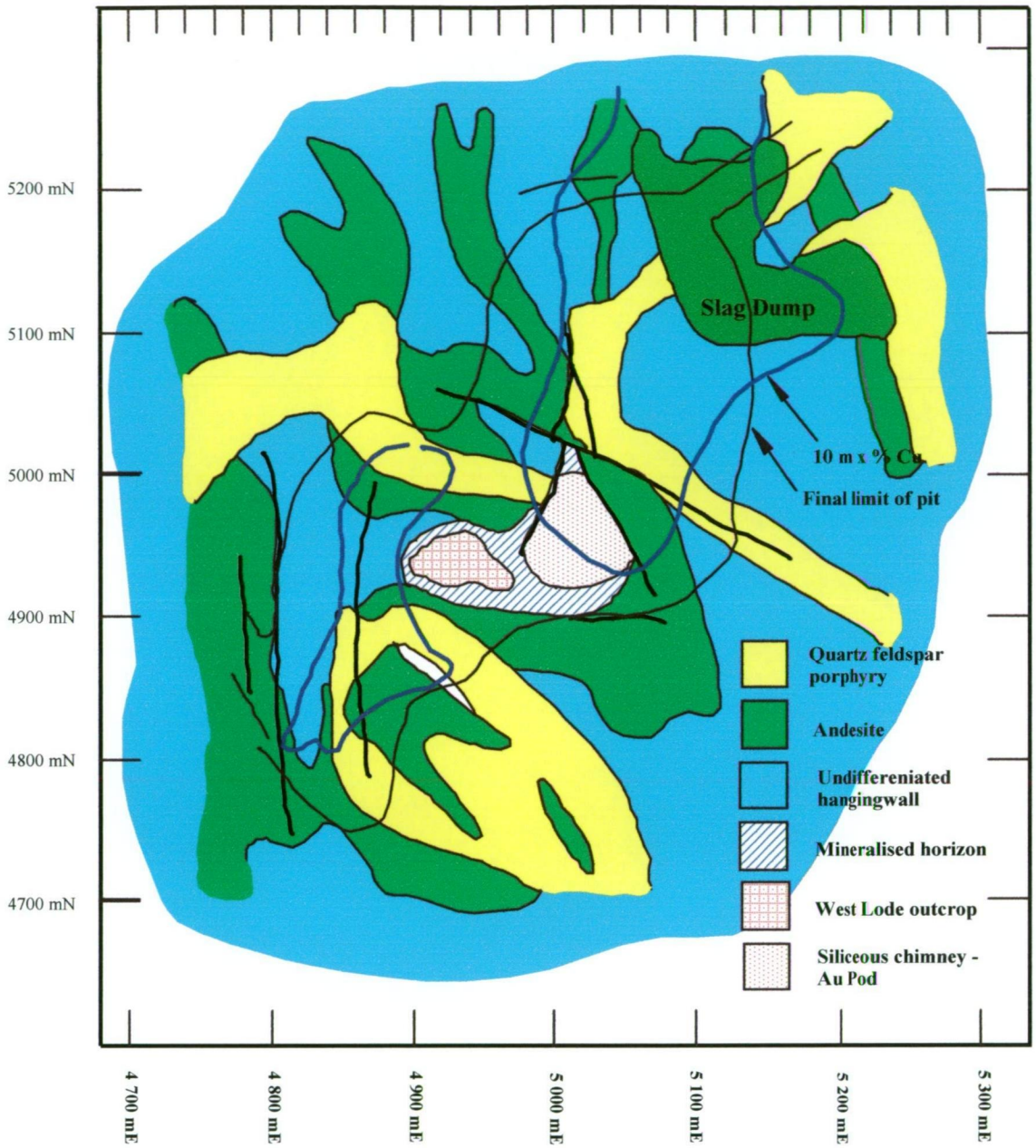

Figure 3.1 Generalised surface geology of Mount Chalmers (After Large and Both, 1981 and Taube and van der Helder, 1982).

The area immediately south and southeast of the Mount Chalmers mine was the focal point of the mapping program, as this was the area of prime interest to the mining exploration companies that partly sponsored the research for this thesis.

Due to the relatively flat lying stratigraphy, steep topography and extensive farming practices, regional correlations are difficult. Therefore, most of the descriptions and subsequent interpretations rely heavily upon the logging of both percussion and diamond drill holes. A total of 17,300 m of percussion and diamond drill holes were logged at 1:200 and sections of individual drillholes (MCD4 and MCD11) were logged at 1:10 scale. The drill holes were logged using graphic logs, with emphasis placed on recognition of emplacement and flow units, contact relationships between units and textural variation within units and hydrothermal alteration mineral assemblages.

The aim of this chapter is to document the volcano-sedimentary facies at the Mount Chalmers mine and within the immediate area of the mine. To distinguish between proximal and distal volcanic facies and to provide a basis upon which the volcanic facies architecture of can be established.

The geology south of Mount Chalmers towards the Emu Park Road is shown on Plate 1

3.2. FOOTWALL FACIES

In this chapter and thesis the term "footwall" is used to describe any lithology that is interpreted as being below the ore equivalent horizon, which itself may be defined as a characteristic sediment or exhalite that occurs at the same stratigraphic level as the massive sulphide mineralisation and may form a marker horizon for mapping and exploration (Large, 1992). The footwall units within the Mount Chalmers mine are no longer exposed due to flooding of the mine (Fig. 3.2). Okill (1974) and Large and Both (1980) described the footwall units within the Mount Chalmers mine as a coarse-grained siliceous volcanic fragmental, composed of andesitic to rhyolitic fragments in a siliceous and weakly pyritic matrix.

Within the Mount Chalmers mine a number of distinct footwall units were observed in drill core. The footwall units are composed of variable lithologies, which are not that dissimilar to the hangingwall volcaniclastics. The most areally extensive lithology at Mount Chalmers is the volcanolithic sandstones.

3.2.1. Altered and Mineralised Volcanolithic Sandstone and Siltstone.

In large numbers of drill holes massive to well bedded and graded quartz-sericite-pyrite altered volcanolithic sandstone and siltstone were intersected *e.g.*MC23, MC24, MC27A, MC28, MC30, MC31, MC32, MC33, MC34 and MC62. When siltstone occurs without a sandstone component it is massive and generally featureless. The volcanolithic sandstone forms a series of graded beds that have cobble to granule -size bases that grade up into siltstone. The beds vary in thickness from ~0.5 - ~11.0 m. Within the cobble-size base the clasts are generally angular to subangular in form and are matrix supported.

Figure 3.2. Various views overlooking the Main Lode and West Lode open cuts at the Mount Chalmers mine

Figure 3.2a.View looking towards southwest overlooking the Main Lode (foreground) and the West Lode open cuts. The line of hills in the background is the Berserker Range. The prominent peak on the left-hand side of the range is Mount Sleipner.

Figure 3.2b View looking east over the Main Lode open cut towards the eastern benches. The lower most two benches are 11 m high.

Figure 3.2c View looking north over the Main Lode open cut towards the northern benches. The lower most two benches are 11 m high.

The clasts have a varied provenance that include:

- chlorite altered spherulitic lava clasts
- pale-grey silica altered feldspar-phyric rhyolite clasts
- feldspathic sandstone clasts
- epidote altered fine-grained andesitic clasts
- pale grey siliceous clasts

The cobble- to granule-sized bases grade uphole into sericite-chlorite altered fine-grained sandstone and siltstone. In MC70 the sandstone displays an overall upward fining sequence from a cobble-size basal unit to a granule-size sandstone units uphole. The contacts between individual beds are generally planar and sharp. The sandstone and siltstone host the massive sulphide mineralisation at Mount Chalmers and the disseminated and vein style mineralisation at Wood's Shaft (~ 1 km SW of Mount Chalmers) . The volcanolithic sandstone has been weakly to very strongly altered by chlorite, quartz-sericite-pyrite and dolomite-kaolin-pyrite. Locally the alteration has been so intense (especially quartz), that the original lithological textures have been destroyed.

The massive featureless nature of the siltstone could be due to bioturbation and fluidisation during compaction (Walker, 1984). Away from the main focus of hydrothermal activity trace fossils were observed in four drill holes (MC23: 46.0 m; MC24: 154.7 m; MC47: 56.3 m and MC70: 174.6 m).The graded nature of the pebble to granule-sized sandstone and clasts indicates that they are volcaniclastic mass-flow deposits. The graded tops to the coarser-grained basal units may have been formed from the deposition of fine dilute suspended material that enclosed the mass flow deposit, so that when quiet conditions were restored the fine-grained particles settled out of suspension.

3.2.2. Graded, Sericite-Silica-Chlorite Altered Polymictic Lithic Breccia

Graded, sericite-silica-chlorite altered polymictic lithic breccia was intersected in MC32, MC35, MC40 (Fig. 3.5b), SMDD1 and WS4. The breccia is composed of clast supported, polymict, variable sized (1-3 mm up to 60-80 mm) altered lithics. The smaller lithics are generally rounded to well rounded and siliceous. The larger clasts vary in angularity from very angular to surrounded. The clasts are set within a pale-grey silica altered groundmass that contains dark-green coloured specks. In SMDD1 euhedral feldspar grains were observed within the groundmass. In SMDD1 and MC32 the breccia grades uphole into medium- to coarse grained lithic-rich sandstone. The clasts have a varied provenance:

- chlorite, epidote-altered andesitic clasts.
- feldspar-phyric rhyolitic clasts.
- chlorite altered flow banded rhyolitic clasts.
- spherulitic flow banded rhyolite
- chloritic, feldspar-phyric rhyolitic-dacitic clasts.
- strongly sericite-silica altered clasts.
- very fine-grained siliceous sandstone clasts.

The dominant clast-type is feldspar-phyric or amygdaloidal andesitic clasts. In MC35 the andesitic clasts are brecciated and display jigsaw-fit texture, and smaller andesitic fragments can be seen to be spalling off from the larger clasts.

Contact relationships were difficult to establish due to a number of factors, the most important of which that the Mount Chalmers drill holes were pre-collared as percussion drill holes and then a diamond tail

was added later. Consequently, no drill core was available to establish the relationship between the breccia and other lithologies. In SMDD1, the breccia is overlain by a thick (~85 m) andesite intrusion.

The graded nature and varied clast provenance argues that these breccias are volcaniclastic mass flow deposits. The dominance of andesitic clasts over the other clasts indicates that the parental source for the breccia was possibly either an andesitic lava or small dome that collapsed and produced a high energy turbulent flow. Quench fragmented andesitic clasts with jigsaw-fit texture argues that some of the andesitic clasts were still hot at the time of emplacement. The different styles of alteration within the clasts suggest that the alteration could be related to syn-volcanic alteration processes, completely unrelated to any mineralising hydrothermal system.

3.2.3. Feldspar-phyric, Lithic Pumice Breccia

Feldspar-phyric, lithic pumice breccia was intersected in a number of diamond drill holes (MC20, LBDD1, WS4, and WS6). The breccia is massive, silica, chlorite altered feldspar-phyric, lithic, pumice breccia. The breccia is characterised by the presence of irregularly to angular shaped chlorite alteration patches, of which some may be true lithics (andesite?). Others have gradational boundaries and are the result of silica alteration overprinting an earlier chlorite alteration phase. The tube pumice fragments are uncollapsed and have a random orientation, and they may be altered either by chlorite or silica. The feldspar crystals are euhedral and 1 - 2 mm long and have been altered to silica. The lithics are predominantly feldspar-phyric rhyolitic lava(?) fragments and possible chlorite altered andesitic clasts. Locally, the alteration may be so intense the original lithological textures have been obscured. In LBDD1 the pumiceous breccias are strongly altered by silica. Possible relict bedding structures were also recognised in LBDD1.

The presence of randomly oriented tube pumice fragments indicates that the pumice breccias are not welded. Graded tops to the pumice breccia were logged in WS4 and WS6 implying that they have undergone some degree of transport and resedimentation. The non-welded nature and graded tops to the breccia argues that they are resedimented mass-flow deposits. They were formed as a result of the submarine transformation of subaerially to shallow-marine erupted pyroclastic deposits into mega-turbidity currents.

3.2.4. Coherent to Autobreccia Feldspar-phyric Rhyolite

Coherent to brecciated feldspar-phyric rhyolite was intersected in a large number of diamond drill holes (23 in total) from both the Main Lode and the West Lode (*e.g.* West Lode: MC20, MC28, MC30, MC34, MC35 and West Lode: MC50, MC53, MC55, MC58, MC66 and MC74) and in diamond drill hole from the Tungamull prospect (MCD10; 333.7 - 386.5 m). The rhyolite is composed of two sub-facies; coherent rhyolite or brecciated rhyolite.

Structure contours were constructed for the top of the footwall rhyolite at Mount Chalmers in order to determine the spatial distribution and the palaeo topography of the rhyolite (Fig. 3.3). The rhyolite forms a topographic high and that has a prominent ridge that trends NNE. It also forms the central core around

which the massive sulphide lenses of the Main Lode and West Lode are positioned. Figure 3.4 shows the distribution of the coherent versus brecciated rhyolite from the available diamond drill hole information. For this purpose the rhyolite intersected in the drill hole was classified either as coherent or brecciated when the drill hole intersection contained greater than 50 % of one sub facies compared to the other. This approach is based upon the assumption that a carapace of autoclastic breccia surrounds a rhyolite flow or dome. This is a simplistic approach to determine the distribution of the two sub facies. However, the distribution of the coherent sub-facies is in good agreement with the NNE trending ridge of rhyolite determined from the structure contours (Fig 3.4) and is therefore considered to give a good approximation of the distribution of the two sub-facies. Using this approach the rhyolite forms, a number of separate bodies that may be domes with the possibility of the northern most rhyolite body being formed from coalesced domes.

The rhyolite is composed of silicified euhedral feldspar crystals (1 - 3 mm and 10 - 15 %) set in white silicified groundmass (Fig. 3.5a). The rhyolite may be composed of alternating intervals of coherent and brecciated rhyolite. Alternating intervals of coherent and brecciate rhyolite were observed in a number of drill holes (Fig 3.6). The contacts between the coherent and brecciated rhyolite are gradational. Spherulites are locally developed within the coherent rhyolite (*e.g.* MC24; MC52; MC58; MC74). The spherulites are $\leq$2 mm, circular and composed of translucent quartz. Faintly developed flow banding may also be evident. Brecciated rhyolite commonly overlies the coherent rhyolite.

The brecciated rhyolite is composed of clast supported (with little or no interstitial granular material), poorly sorted generally angular to subrounded with occasional well-rounded rhyolite clasts. The clast size varies between 10 to 80 mm. Clasts within the rhyolite breccia sub-facies display either good jigsaw-fit texture indicating that very little movement of the clasts has occurred post brecciation, or alternatively, they have no spatial relationship to each other indicating that they have been rotated or transported post brecciation (Fig 3.6). The clasts generally display few internal structures, however sparse flow banded and spherulitic clasts were observed (*e.g.* MC24: 157 - 167 m).

The rhyolite has been extensively altered by silica and locally by sericite and chlorite. The intensity of the alteration generally increases uphole. As the intensity of the alteration increases, the internal structures and feldspar crystals disappear. Locally the overprinting of the chlorite by the quartz-sericite has produced a pseudo-fragmental texture (e.g. MC30 57.77 - 60.81 m, MC58, 136.2 - 144.5 m). Translucent and milky white quartz veins commonly brecciate the rhyolite. These have hydraulically brecciated the rhyolite to produce a pseudo breccia. Pyrite and chalcopyrite locally form an extensive network of sulphide stringer veins.

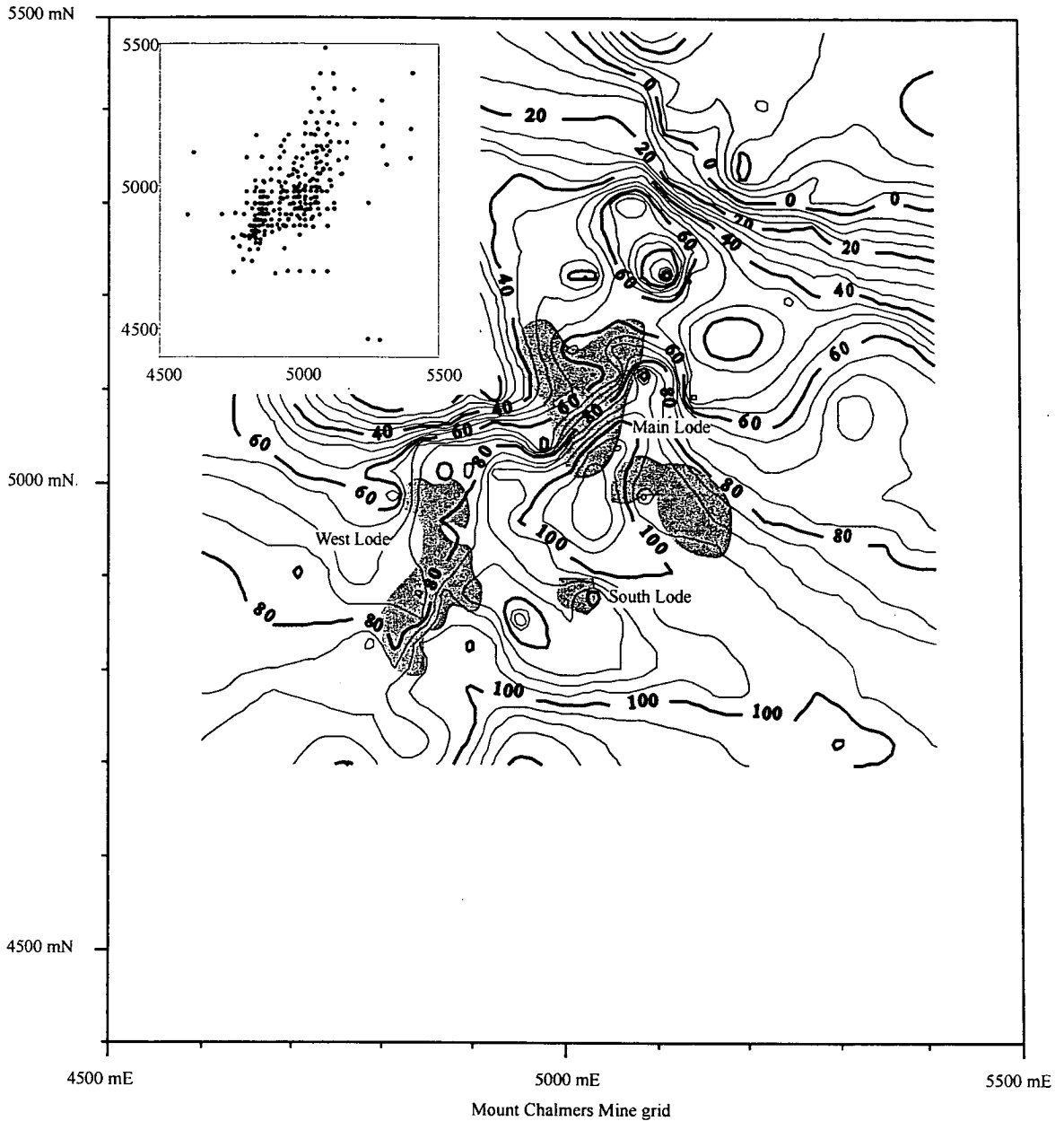

Figure 3.3. Structure contours to the top of the footwall rhyolite at the Mount Chalmers mine, the massive sulphide ore lenses have been superimposed for comparative purposes. Contour interval = 5 m. The inset shows the distribution of drillholes on which the contouring is based. The corner coordinates of the inset are identical to those of the main diagram. Grid coordinates are in metres.

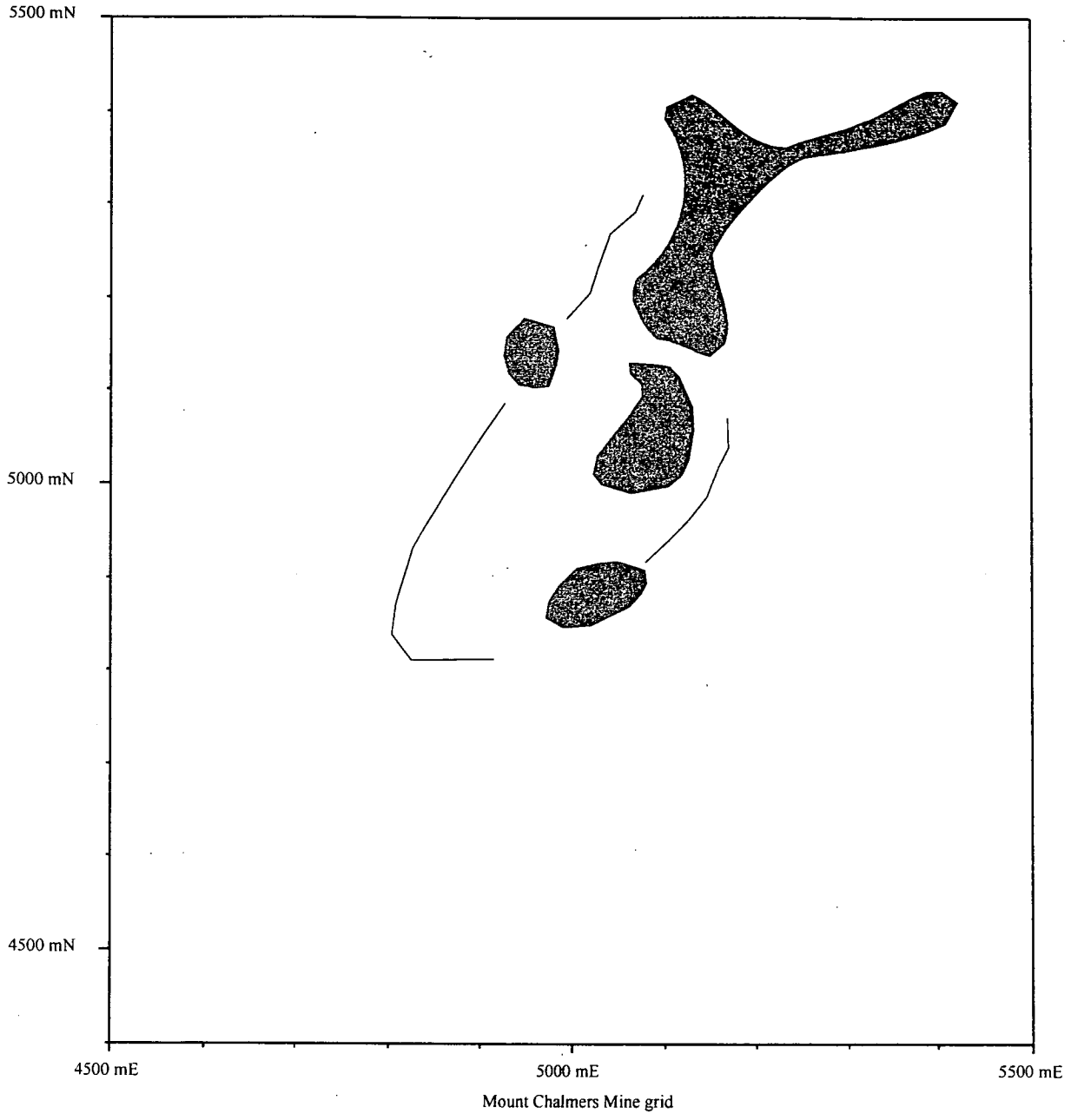

Figure 3.4. Distribution of coherent rhyolite versus brecciated rhyolite. Gray areas represent areas dominated by coherent rhyolite. Solid line indicates the extent of brecciated rhyolite

Examples of footwall lithologies from the Mount Chalmers mine

Figure 3.5a Drill core sample of the rhyolite 1. Jigsaw-fit texture is evident on the right-hand side of the drill core. This has been over printed and hydraulically brecciated by translucent quartz veins. Quartz altered euhedral feldspar crystals are visible in the feintly flow banded rhyolite in the left-hand side of the sample. (MC58 138.4 m).

Figure 3.5b Graded, sericite-silica-chlorite altered polymictic lithic breccia. Clast types include: chlorite, epidote-altered andesitic clasts; . chloritic, feldspar-phyric rhyolitic-dacitic clasts; feldspar-phyric rhyolitic clasts; strongly sericite-silica altered clasts; chlorite altered flow banded rhyolitic clasts; very fine-grained siliceous sandstone clasts and spherulitic flow banded rhyolite clasts.


a


b

Figure 3.6. Graphic lithological logs for parts of MCP/52 and MCP47/MC53 depicting the relationship between the coherent and brecciated facies of the footwall rhyolite.

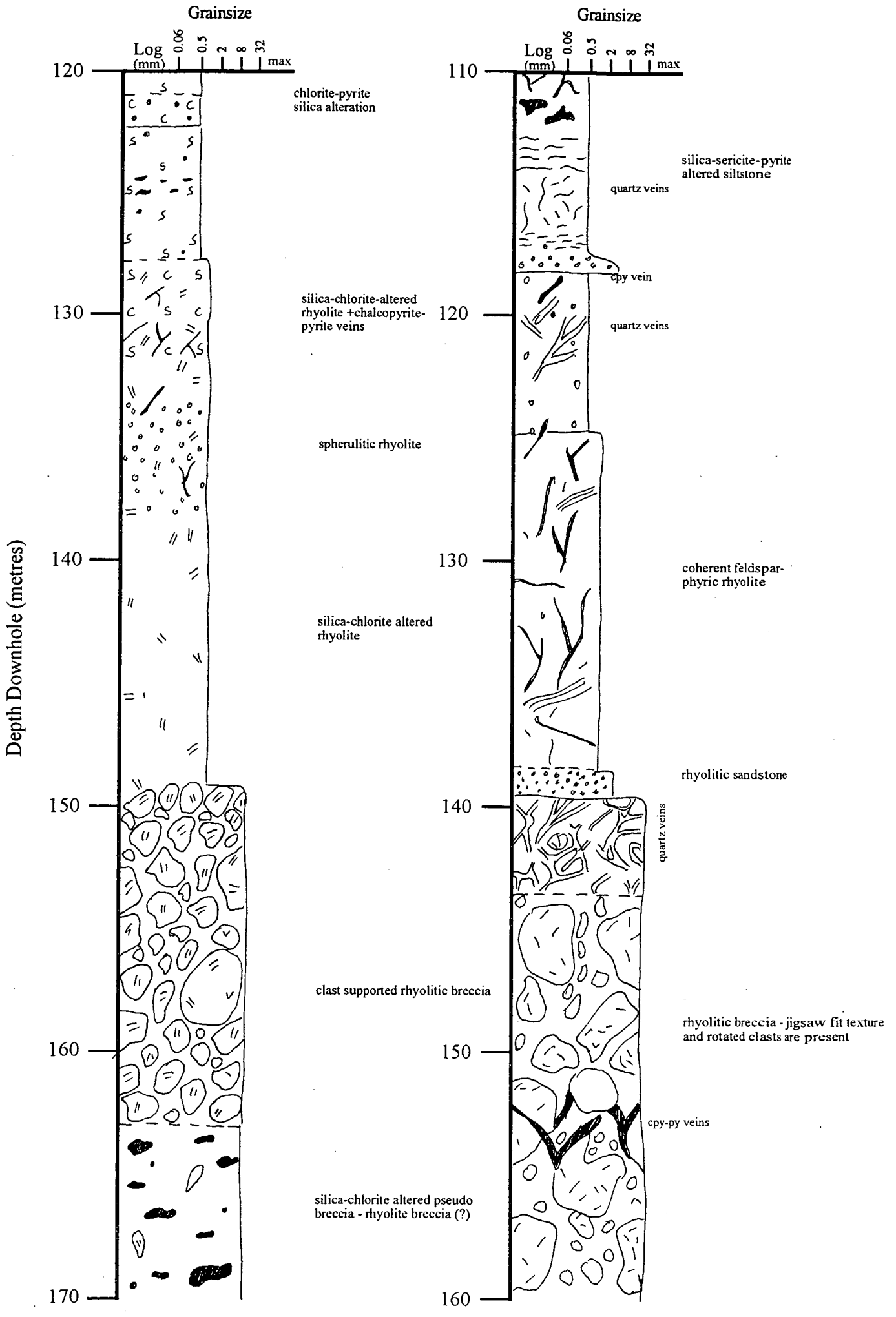
MCP52/MC52
MCP47/MC53
Grainsize
Log (mm)
0.06
0.5
2
8
32
max
Depth Downhole (metres)
120
130
140
150
160
170
110
120
130
140
150
160
chlorite-pyrite silica alteration
silica-chlorite-altered rhyolite +chalcopyrite-pyrite veins
spherulitic rhyolite
silica-chlorite altered rhyolite
clast supported rhyolitic breccia
silica-chlorite altered pseudo breccia - rhyolite breccia (?)
silica-sericite-pyrite altered siltstone
quartz veins
cpy vein
quartz veins
coherent feldspar-phyric rhyolite
rhyolitic sandstone
quartz veins
rhyolitic breccia - jigsaw fit texture and rotated clasts are present
cpy-py veins

Alteration or broken drill core generally obscures the majority of contact relationships between rhyolite and other lithologies. Where the contacts are visible, they are sharp. In MC30 a mixed contact zone between the overlying siltstone and rhyolite occurs between 40.5 - 50.0 m. In MC30 the contact between the overlying siltstone and the rhyolite composed of a chaotic mixture of angular rhyolite fragments and siliceous siltstone. Smaller angular rhyolite clasts with jigsaw-fit texture can be seen to be spalling off the larger clasts. This suggests that the rhyolite has been quench fragmented and the contact zone is a blocky peperite.

The structure contours show that the rhyolite is elongated in a NNE direction and forms a topographic high (Fig 3.3). The spatial distribution between the coherent rhyolite and the rhyolite breccia indicates that the rhyolite forms a series of isolated small domes surrounded by autoclastic lava (Fig 3.4). The elongate nature of the rhyolite suggests that its extrusion was largely structurally controlled. The presence of gradational contacts and angular clasts identical to the underlying coherent rhyolite indicates that the brecciated rhyolite was derived from the fragmentation of the coherent rhyolite. The angular nature, lack of interstitial granular material, poor sorting and spatial relationship to the coherent rhyolite argues that the breccia was derived from autoclastic processes. Autobrecciation involves the non-explosive fragmentation of flowing lava (McPhie *et al.*, 1993). If a viscous congealed lava continues to flow or alternatively if the congealed viscous crust is moved by continual flow of the lava inside then the congealed lava becomes stressed, is deformed and breaks into slabs or blocks (Cas and Wright, 1987). The blocks of lava can be fused together or else remain loose and are easily dislodged during continual flow of the lava. This results in a lava that has a coherent interior encased in a carapace and floor of autobreccia (McPhie *et al.* 1993). The alternating intervals of coherent rhyolite and autobreccia suggests either:

- narrow lava flows separated by intervals of autobreccia, or
- autobrecciated rhyolite has foundered into the flow interior.

Autobrecciation is commonly associated subaerial lava flows (McPhie *et al.*, 1993), however bioturbated siltstones were logged immediately overlying autobreccia in MC24 (~154.0 m). The trace fossils assemblage is identical to those seen elsewhere within the Berserker beds, which are indicative of a shallow marine environment (see Section 3.3 for a fuller discussion on the palaeoenvironmental setting of the Berserker beds).

In this thesis this rhyolite is informally referred to as the "footwall rhyolite".

3.2.5 Silica-Chlorite Altered Dacitic Lithic Breccia

The silica-chlorite dacitic lithic breccia was intersected in MC32, MC35 and WS7 and is characterised by the large (50 mm) chlorite altered feldspar-phyric (?) matrix supported dacitic clasts set within an amorphous siliceous groundmass. Smaller (≤10 mm) rounded siliceous clasts are also present. The clasts are generally angular and matrix supported. Smaller (10 mm), rounded, siliceous cherty clasts are also found. Amorphous silica alteration and smaller angular chlorite altered and "cherty" clasts dominate the groundmass.

Some of the clasts have diffuse margins, indicating that they have been replaced by the silica alteration, or that breccia may be partly due to the silica alteration overprinting an earlier chlorite alteration phase.

3.3. HANGINGWALL FACIES

The hangingwall facies are dominated by primary and secondary volcanic facies. The primary volcanic facies include rhyolite lavas and their autoclastic products, andesitic intrusions and lavas and their autoclastic products. Voluminous and areally extensive feldspar-phyric, pumice-lithic breccia and feldspar-phyric breccia dominate the secondary volcanic facies. In this chapter and thesis the term "hangingwall" is used to describe any lithology that is interpreted as being stratigraphically above the ore equivalent horizon. The hangingwall units within the Mount Chalmers mine are exposed on the upper most two or three benches of the now flooded Mount Chalmers mine (Figs. 3.2a,b and c).

3.3.1. Volcanolithic Sandstone and Siltstone

The volcanolithic sandstone and siltstone facies occur throughout the mine and regional stratigraphy. This facies has not been previously described in detail. Sainty (1992) recognised two main units, the Lower Chalmers Sediment and the Upper Chalmers Sediment separated by units of feldspar-phyric, pumice-lithic breccia and feldspar-phyric pumice breccia. The separation and naming of these two volcanolithic sandstone units is not considered to be valid, as volcanolithic sandstone units occur at more than two unique stratigraphic positions within the Berserker beds.

Both within the mine and in diamond drill core the volcanolithic sandstone and siltstone grade upwards from a base composed of lithic fragments, crystal fragments, (predominantly feldspar, with rare quartz) or a combination of both, to finer grained sedimentary rocks. Contacts between individual beds are generally planar, although highly irregular contacts with well-developed load cast and flame structures are also evident. The upper finer grained tops to the sandstone and siltstone beds are commonly weakly to extensively bioturbated, such that any primary sedimentary structures such as bedding, ripples, convolute laminations have been destroyed. Where internal structures have been preserved, the coarser-grained bases are commonly overlain by laminated siltstone that may have convolute laminations.

Sections of two drill holes were logged in detail; MCD4 (at 1:10 scale (165.0 - 177.55 m)) and MCD11 (at 1:40 scale (110.0 - 159.7 m)) to better define the internal structures of individual beds and the relationships between beds.

The structure of the volcanolithic sandstone and siltstone argues that they are turbidites. A turbidite may be defined as a grade bed consisting of a sandstone/siltstone couplet which has been deposited by a turbidity current and is commonly overlain by hemipelagic mudstone. The Bouma sequence typifies this ideal kind of deposit (Fig. 3.7), but is considered to be an oversimplification of the many possible expressions of turbidite sandstone beds (Mutti *et al.*, 1999). Pickering *et al.* (1989) amongst many others have adopted a facies approach to the description and interpretation of turbidites.

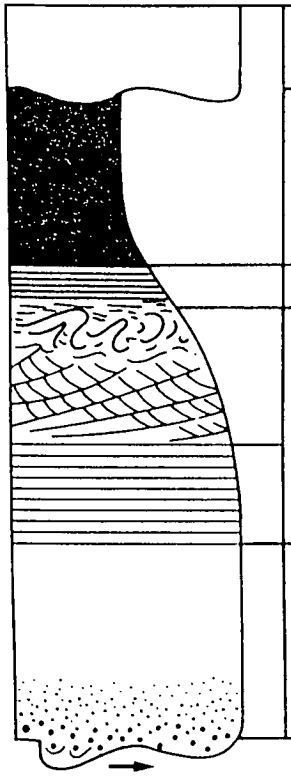

GRAIN SIZE	BOUMA (1962) DIVISIONS	INTERPRETATION
Mud	E Laminated to homogeneous mud	Deposition from low-density tail of turbidity current ± settling of pelagic or hemipelagic particles
Silt	D Upper mud/silt laminae	Shear sorting of grains & flocs
Sand	C Ripples, climbing ripples, wavy or convolute laminae	Lower part of lower flow regime of Simons *et al* (1965)
	B Plane laminae	Upper flow regime plane bed
Coarse Sand	A Structureless or graded sand to granule	Rapid deposition with no traction transport, possible quick (liquefied) bed

Figure 3.7 Ideal sequence of sedimentary structures in turbidite beds (From Pickering *et al.*, 1989)

In the ongoing discussion the description of the different turbidite facies exposed within the Berserker beds follows that of Pickering *et al.* (1989 - Fig. 3.8).

The two most common facies present within the Berserker beds are Facies Class C2.1 (Bouma ABD). Facies Group C2 consists of moderately well sorted to poorly sorted sand-mud couplets showing partial to complete Bouma sequences (Pickering *et al.*, 1989). Individual beds vary in thickness from a minimum of 20 mm up to 2.5 m. Compaction structures are common; flames of the underlying siltstone can be seen to be "intruding" in between lithic fragments of the overlying division A.

Facies C2.1 (Bouma Division ABD): Characterised in drill core and outcrop by thin sandstone bases comprised of broken and intact feldspar grains and small angular to subrounded lithic fragments. These sandstones have sharp abrupt bases and grade upwards very rapidly, over millimetres into apparently massive to infrequently delicately laminated siltstones (Figs. 3.9a, b, c and d). The basal sandstone beds commonly contain feldspar grains, lithic fragments and tube pumice fragments. The size of the lithics varies between individual sandstone beds from 1 - 2 millimetres up to 10 mm The larger lithics have a varied provenance, but are generally a siliceous siltstone, a felsic volcanic or a fine to medium grained sandstone. Some of the lithics are rip-up clasts that have been derived from the underlying siltstones. The lithics are generally clast supported, with any original primary pore space now infilled by silica.

The massive siltstone tops are commonly bioturbated, which probably destroyed any original fine laminations. The presence of division A suggests that the grains settled very rapidly out of suspension, causing water to be rapidly expelled upward, and momentarily the grain/water mixture became fluidised (Walker, 1984).

Contacts between individual beds are generally planar but load structures are also very common. The tops of the beds are generally planar to smooth and may be bioturbated throughout. Laminations within the siltstone may be disrupted or convoluted due to soft sediment deformation. The non-recognition of Bouma division C may be due to bioturbation and fluidisation during compaction destroying parallel laminations normally associated with division C (Walker, 1984).

Facies C2.1 (Bouma Division ACD): On the northern face of the Mount Chalmers open pit and within diamond drill holes the sedimentary rocks are characterised by a series of individual volcanolithic sandstone deposits. The bases to the beds are very sharp and generally planar, and are composed of angular to rounded lithic fragments (maximum size 8 mm) and feldspar grains. Divisions C and D are composed of fine to silt to sand size fractions. Also included with division C and D are large (10 mm) scattered rounded lithics. Divisions C and D are generally weakly to strongly bioturbated. Where strong bioturbation is present, the fine convolute bedding commonly present within division C has been destroyed.

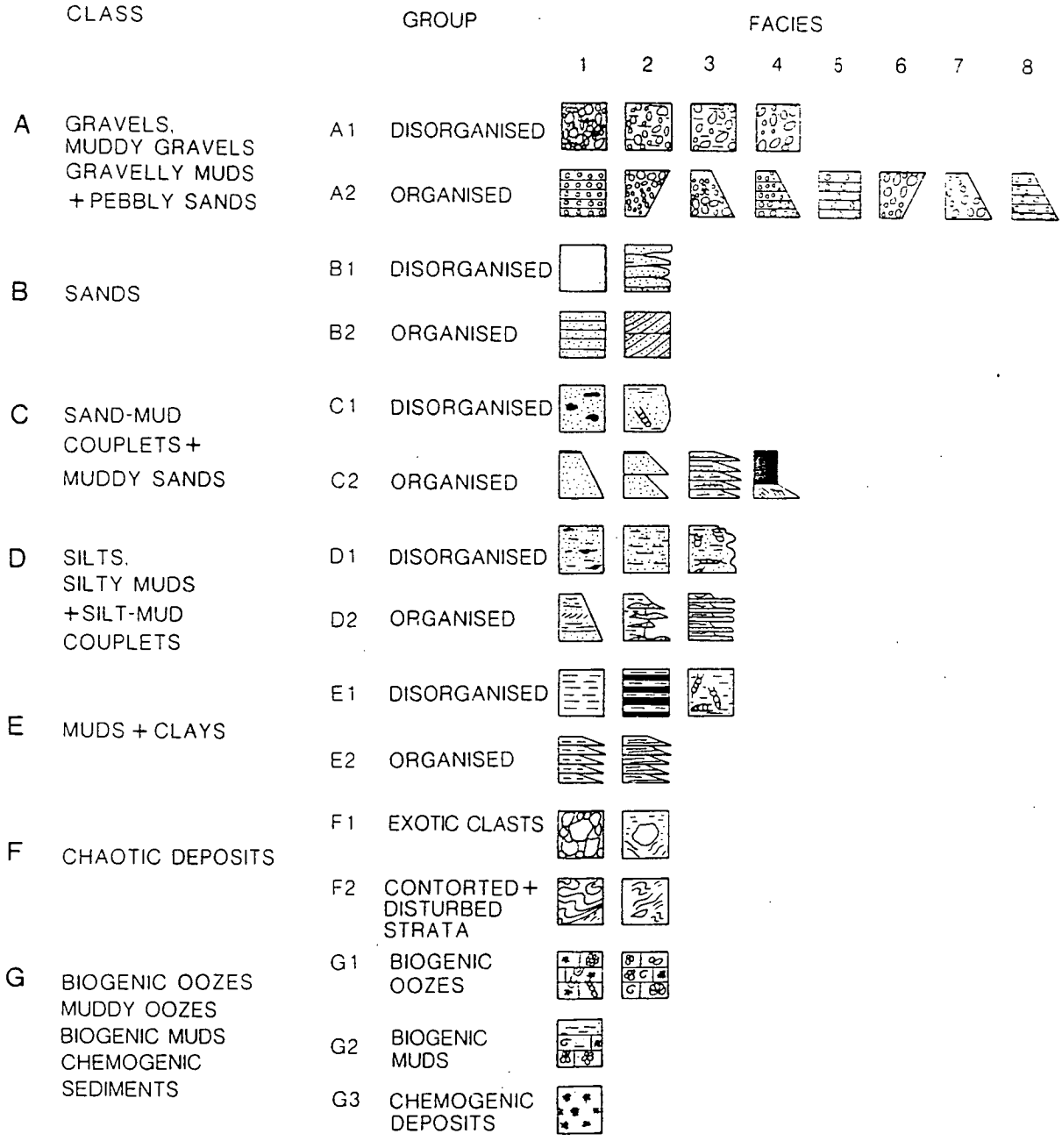

Figure 3.8 Classification scheme for deep-water sediments (From Pickering *et al.*, 1989).

Figure 3.9.
Figure 3.9a and b Outcrop photographs of Facies C2.1 (Bouma Divisions ABD) illustrating thin sandstone bases that grade rapidly up into thinly laminated to massive siltstone mudstone.

Figure 3.9c and d Outcrop and slabbed examples of Facies C2.1 (Bouma Divisions ACD) illustrating volcanolithic sandstone to pebble size beds with sharp planar contacts with underlying siltstone.

Figure 3.9a Mount Chalmers mine - Main Lode open cut, northern benches.
Figure 3.9b Emu Park Road - roadside cutting (AMG 255150 mE : 7410200 mN).
Figure 3.9c Mount Chalmers mine - track side exposure immediately north of the Main Lode open cut.
Figure 3.9c Sample (AQ108d) from a track leading from Mount Chalmers mine to the summit of Mount Chalmers (AMG 260900 mE :7420230 mN).


a

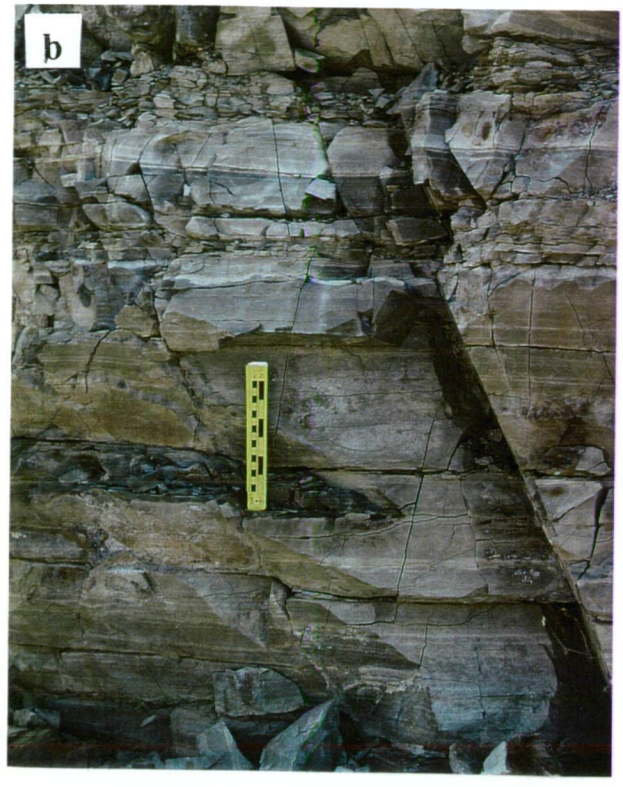
b


c
50mm

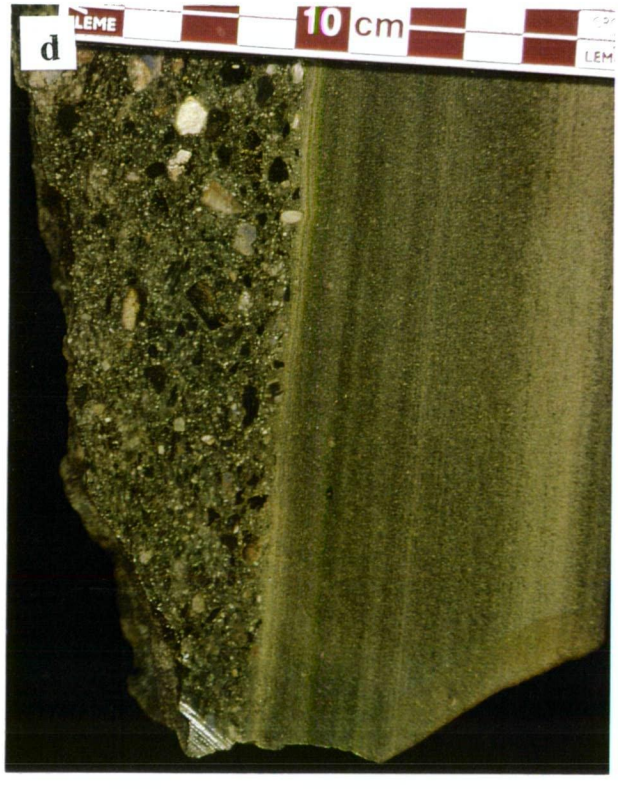
d
10 cm

Figure 3.10. Graphic lithological logs for parts of MCD11 and MC21 depicting the structure of Facies C2.1 (Bouma Divisions ABD - MCD11) illustrating thin sandstone bases that grade rapidly up into thinly laminated to massive siltstone mudstone. and Facies C2.1 (Bouma Divisions ACD - MC21) illustrating volcanolithic sandstone to pebble size beds with sharp planar contacts with underlying siltstone.

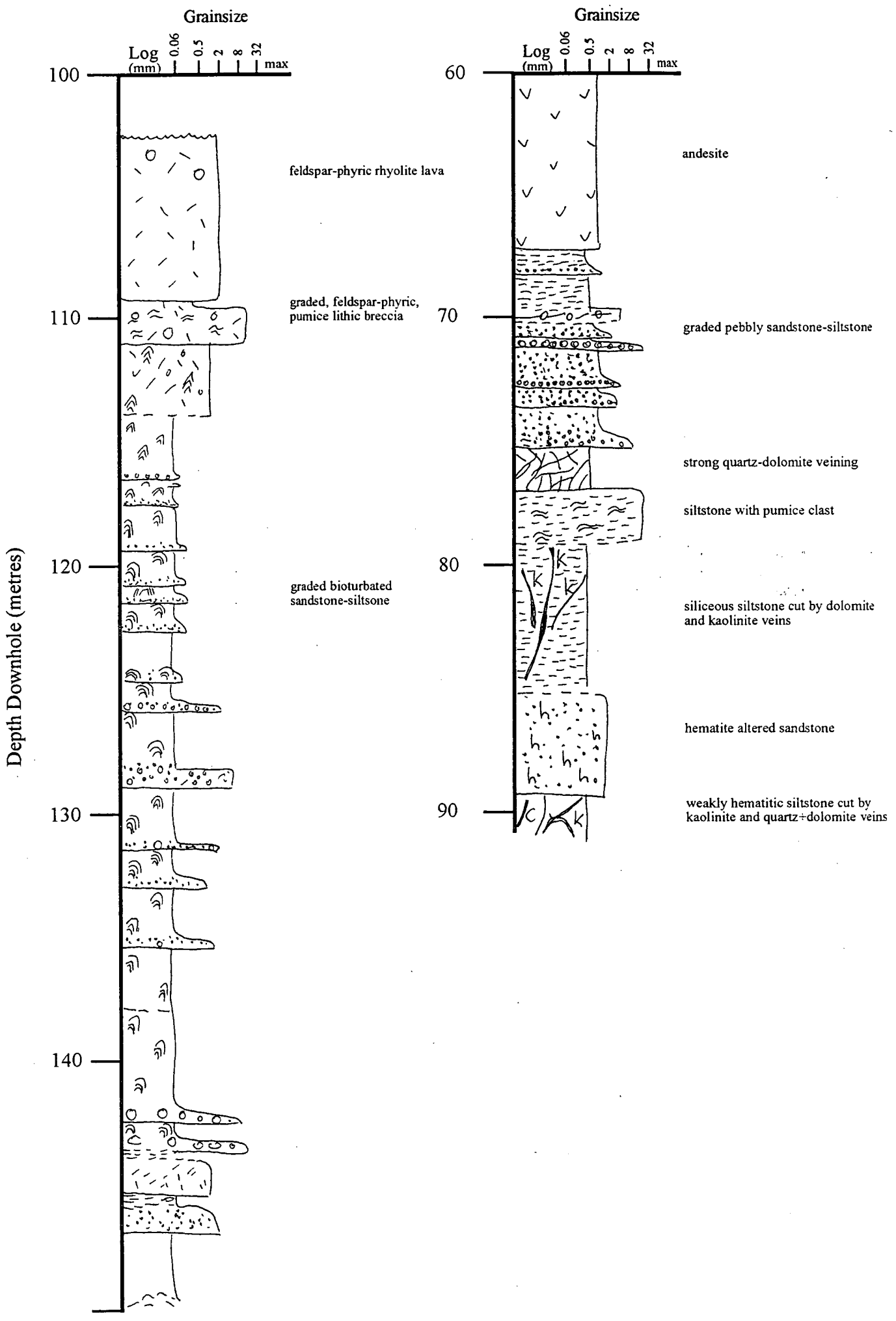
MCD11
MC21
Grainsize
Log (mm)
0.06
0.5
2
8
32
max
Depth Downhole (metres)
100
110
120
130
140
60
70
80
90
feldspar-phyric rhyolite lava
graded, feldspar-phyric, pumice lithic breccia
graded bioturbated sandstone-siltsone
andesite
graded pebbly sandstone-siltstone
strong quartz-dolomite veining
siltstone with pumice clast
siliceous siltstone cut by dolomite and kaolinite veins
hematite altered sandstone
weakly hematitic siltstone cut by kaolinite and quartz+dolomite veins

Facies C2.4: This facies dominates the intervals logged in detail in MCD4 and MCD11. These detailed logs show that the sedimentary rocks are dominated by fine-grained feldspathic bases or infrequent lithic-rich bases that grade uphole very rapidly into massive, extensively bioturbated siltstone/mudstone. Some of the coarser-grained bases maybe as thin as 1 - 2 mm and have a thicker graded mud dominated top that is up to 8 m thick. Turbidites of Facies C2.4 normally show internal evidence of flow reversal during deposition. However, no internal structures are evident within the silt to mud size upper fraction of the facies. This lack of internal structure may be attributable to the extensive bioturbation of the sedimentary rocks that has occurred.

All beds of facies C2.1 may be considered to be the deposited from turbidity currents and are deposited from high concentration flows. The predominant depositional process is grain-by-grain deposition from suspension, followed either by burial (Bouma Division A) or by tractional transport as bed load (Bouma Divisions B and C). The muddy upper divisions were possibly deposited by grain-by-grain deposition from suspension, with subsequent pervasive bioturbation destroying most of the original physical sedimentary features (Pickering *et al*, 1989).

3.3.2. Graded Volcanolithic Conglomerate Facies

The graded volcanolithic conglomerates are composed of a variety of clast types. The clasts range in size from 10 - 600 mm and are poorly sorted; the beds are generally clast supported. The clasts vary from well rounded to very angular. The clasts have a varied provenance and are predominantly comprised of fine-grained and bedded sediment, feldspar-phyric dacitic lava (?), flow banded rhyolitic lava clasts, sericite altered tube pumice clasts, andesite, amorphous silica clasts, and chlorite altered feldspar-phyric clasts. One sulfide clast was observed in a bed to the northwest of the mine. The clasts are set within a matrix composed of significantly smaller clasts (≤25 mm), and feldspar grains. The smaller matrix clasts like the larger clasts are also angular to subrounded in form. On an east-west trending ridge 200 m to the north of the mine, a conglomerate unit grades rapidly vertically and laterally into coarse grained sandstone and then into siltstone. This outcrop has the only exposure of cross bedding that was mapped in the field. This suggests that the conglomerate may be a channel-fill. The clast-dominated basal portions of the conglomerates grade rapidly upward into finely laminated sandstone and siltstone beds (≤0.30 m). The graded tops are commonly bioturbated.

3.3.3. Sedimentary Structures

The Berserker beds contain a wide spectrum of soft sedimentary deformation structures, most of which are restricted to a handful of outcrops or are only known from single exposures or drill core. These include; convolute laminations, current ripples, slump structures, load casts and dewatering structures. The most widespread soft sedimentary structure is load casts. Convolute laminations are only known from a small number of outcrops, while the remaining structures are known only from single outcrops.

The structures described in the ongoing discussion are not indicative of any one particular marine environment. Rather they are indicative of particular processes that were operating at the time of shortly after the deposition of a bed.

3.3.3.1 Convolute Laminations

Convolute laminations although rare within the Berserker bed were observed in a siltstone unit that occurs in the hangingwall to the Main Lode mineralisation (Fig 3.11 a and b) in fine-grained sandstones and siltstones exposed on Pilbeam Drive and near Nerimbera Quarry (Fig 3.11 c and d). Convolute laminations or bedding consists of intraformational folds that occupy a distinct interval in a sandstone/siltstone bed or the bed as a whole. The folds increase in amplitude upward from flat or almost flat laminations at the base to steep-limbed structures which are either truncated or pass upward into lower amplitude folds and flat laminations (Conybeare and Crook, 1982; Lucchi, 1995). Convolute laminations occur within a variety of environments and therefore can not be considered to be a diagnostic feature of turbidites (Allen, 1977; Reineck and Singh, 1980; Collinson and Thompson, 1989) *e.g.*

- present-day tidal zone deposits (Einsele, 1963; Wunderlich, 1967; De Boer, 1979);
- river flood plains (McKee 1966; Coleman, 1969)
- natural levees of distributary channels of the Mississippi delta (Coleman and Gagliano, 1965);
- non-marine sandstones (Davies, 1965)

Convolution involves the plastic deformation of partially liquefied sediment soon after deposition. Convolute laminations are used as evidence for rapid deposition (Collinson and Thompson, 1989),

The convolute laminations at Mount Chalmers comprise flat topped, symmetrical and steep cuspate folds that are separated by broad anticlines. On Pilbeam Drive the amplitude of the folds increase from almost flat laminations at the base to steep-limbed folds near the top, some of which have been truncated. The axial planes of the folds are inclined to the right of the image (Fig. 3.11 c and d). Where convolute laminations have inclined axial planes, this normally coincides with the palaeocurrent, suggesting that convolution formed during deposition. This indicates that the current flowed from north to south *i.e.* from left to right of the picture. Along the entrance road into the Nerimbera Quarry a low-lying outcrop of fine-grained turbidites are exposed. Near the top of the beds, the convolute laminations have inclined axial planes. These indicate that the current has flowed from west to east. These are the few indicators of palaeocurrent direction that have been found in the Berserker beds.

3.3.3.2 Current Ripples

At the top of the truncated convolute laminations asymmetrical ripples are visible (Fig. 3.11 d). These have formed on top of the eroded bed containing the convolute laminations. The lower boundary of the set is irregular and undulating and the adjacent ripple sets are dissimilar. The presence of an eroded top to the underlying bed containing the convolute laminations and the asymmetrical ripples indicates the presence of current activity with the palaeobasin.

Figure 3.11. Outcrop examples illustrating different styles of convolute laminations within the siltstone to mudstone upper fraction of turbidite Facies C2.1.

Figure 3.11 a and b Mount Chalmers mine - Main Lode open cut - northern benches.
Figure 3.11c and d Pilbeam Drive (AMG ~253000 mE : 7415500 mN).


a
0
20 mm


b
0
20 mm


c


d

Ripple marks are a common feature of in both nonmarine and marine sandstones and siltstones deposited in shallow water, but they form at all depths in which ocean bottom-currents are flowing, such ripples are asymmetrical (Kolpack, 1965). As opposed to symmetrical ripples that are commonly formed by oscillatory movements produced by waves, and therefore are restricted to comparatively shallow depths (Conybeare and Crook, 1982). A bottom current if it is sufficiently strong can drag coarse particles; in a weak current only mud can be carried in suspension (Lucchi, 1995). When the velocity of a current flowing over a sand bed exceeds a certain critical value, grains begin to move. With widespread movement of grains finer than approximately 0.6 mm in diameter, asymmetrical ripples begin to form almost immediately (Collinson and Thompson, 1989). Therefore a low velocity current that flowed from north to south most likely formed the asymmetrical ripples at MAR15. This current direction agrees with the current direction obtained from the underlying inclined convolute laminations.

3.3.3.3 Slump Structures

Slump structures are not indicative of any particular depositional environment, but can form on the slopes of ocean floor, on lake bottoms, and in the upper parts of point deposits along riverbanks. Slumping is a common feature in sediments deposited on slopes with gradients as low as 1°. Compaction of the sediment, caused by gravity may result in the gradual steepening of the gradient and slumping of the upper layers. A critical point is reached where shock such as that induced by an earthquake or the load imposed by an unusually large influx of sediment initiates the development of rapid slumping (Conybeare and Crook, 1982). Only one example of a slump structure has been recognised within the Berserker beds. This example comes from Pilbeam Drive where a feldspar-phyric dacite overlies silicified finely bedded sandstones. The slump structure or fold occurs within graded, finely bedded feldspathic sandstone, interbedded with siltstone. The fold axis is subhorizontal to overturned (Fig 3.12). No cleavage was observed within the sedimentary rocks or the overlying dacite to suggest that the fold structure is a tectonic fold. Therefore, the slump structure - fold is interpreted as having been formed by the loading of the sediment by the overlying dacite. Evidence for the sedimentary rocks still being wet and unconsolidated at the time of slump formation is the presence of a peperitic contact between the sedimentary rocks and the dacite.

One possibility that the fold shown in Figure 3.12 may be a Type1a - internal convolute lamination of Allen (1977). In Type 1 convolute laminations, deformation affects laminae within a single sedimentation unit, but not the upper and lower boundaries. Type 1a structures are interpreted to have formed from deformed cross-bedding (Allen, 1977).

3.3.3.4. Load Casts

Although not ubiquitous, load casts were observed at a number of localities. They range from centimetre scale to structures that are only clearly visible on cut and polished slabs. Load structures most commonly occur on the lower surfaces of sandstone beds interbedded with mudstones, *i.e.* they are a type of sole mark (Collinson and Thompson, 1989). Load casts are formed from the density difference between higher

Figure 3.12. Slump structures within finely bedded feldspathic sandstone (Pilbeam Drive – AMG 252500 mE : 7416400 mN

density sand overlying less dense mud. The intervening surface is potentially unstable, because of the inverted density stratification. The sand tends to sink and the mud to inject upwards. A convective-like motion is initiated, but the attempts of the two "fluids" to overturn the bedding and replace one another completely is stopped at some stage due to frictional resistance. More commonly, the mud was more viscous than sand and the resulting profile is a lateral alternation of rounded down bulging lobes of sand and narrower, pointed crests of mud (Lucchi, 1995). This is clearly seen in Figure 3.13a and b, where the overlying narrow massive sand bed has sunk into the mudstone to produce rounded lobes. Small scale load casts on the millimetre scale are visible in a finely laminated siltstone-mudstone sequence. Where the mud was less viscous than the sand, the "typical" profile of a load cast would be inverted. This is seen in Figure 3.9 where lobes of intensely bioturbated siltstone have sunk into the sandstone. Adjacent to the lobe of siltstone where bioturbation has been negligible and bedding has been preserved then the contact between the overlying siltstone and the sandstone remains planar. This indicates that one of the consequences of intense bioturbation is to change the viscosity of sediment. Although many load casts are simple protrusions on the sandstone base, some are more globular being attached to the overlying sandstone by a thin neck or they may even be completely detached (Collinson and Thompson, 1989). The resulting pockets and pillow-like shapes are termed pseudonodules or ball-and-pillow structure. The detached pseudonodules appear to float in the darker green mudstone. Figures 3.14b and c illustrate a series of load clasts along one bedding plane. The sandstone base of the overlying bed is composed of densely packed, grain supported feldspar grains, that have sunk into the underlying siltstone top to a graded bed. The load casts vary between lobes composed of multiple feldspar grains to load casts caused by individual grains. Also visible within Figure 3.14c are semidetached to completely detached pseudonodules composed of feldspar grains. Further possible evidence for the upward expulsion of water from the underlying siltstone is provided by the detached rafts of siltstone that occur within and near the base of the feldspathic sandstone.

3.3.3.5 Dewatering Structures?

Within the middle of Figure 3.14c is a "fissure" of feldspar grains that occurs within the underlying siltstone. The top of the siltstone bed on either side of the feldspar-rich "fissure" is marked by the presence of two upwardly projecting "ramps". One of three possibilities may be able to explain this feature.

- an injection of feldspar grains from below *i.e.* a sandstone dyke
- infilling of a crack developed in the mudstone on the palaeoseafloor
- dewatering structure

Each of these three possibilities will be examined in turn.

The upward displacement of the siltstone suggests that perhaps the feldspar grains have penetrated the siltstone from below. However, there is no feldspar-rich bed lying immediately below the siltstone from which the feldspar grains may have been derived. This would therefore exclude the injection of feldspar grains from an underlying bed to form a sandstone dyke as a possible mechanism for the formation of the "fissure".

Figure 3.13. Load casts within thinly bedded (3.13a) and thickly bedded (3.13b) turbidite Facies C1.2. In both examples, stratigraphic up is to the left of the figure.

Figure 3.13a DDH T2 - 235.2 m.
Figure 3.13b Emu Park Road.(AMG 255150 mE : 7410200 mN).


a

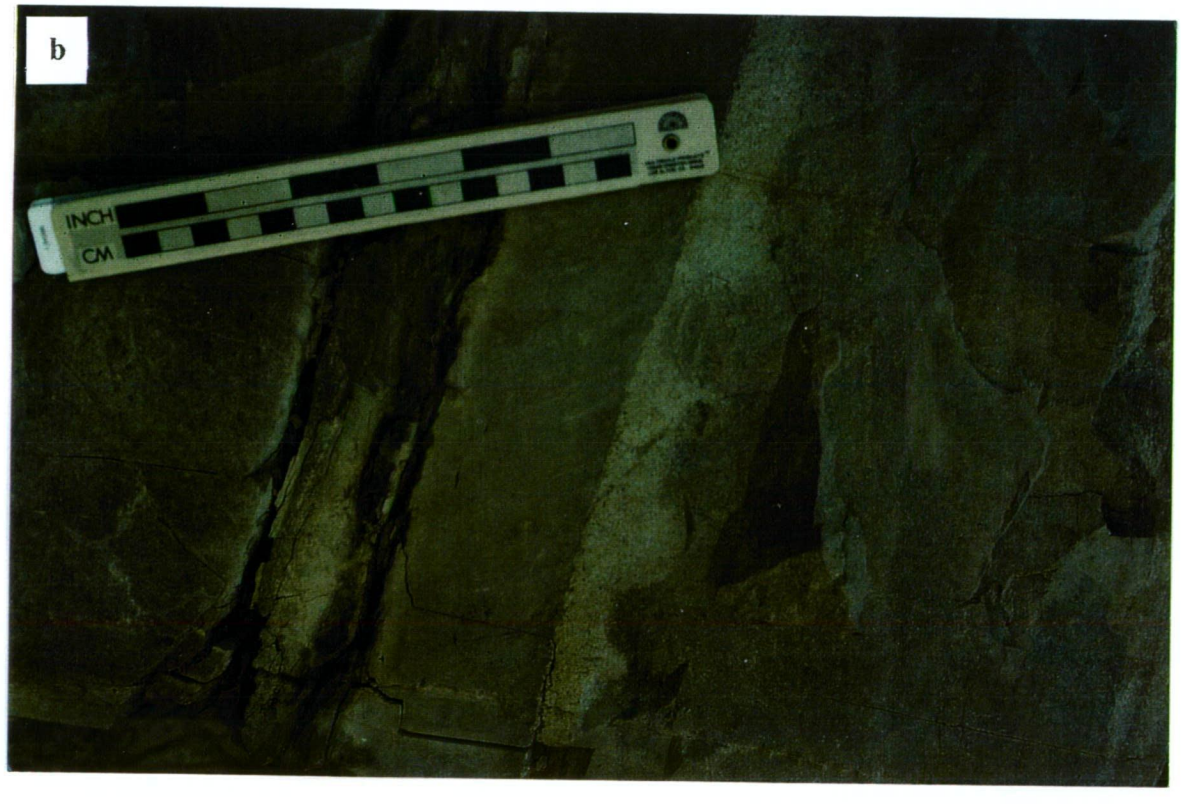
b
INCH
CM

Figure 3.14. Load structures within turbidite Facies C1.2.

Figure 3.14a Mount Chalmers mine - Main Lode open cut, northern benches.
Figure 3.14b Emu Park Road.(AMG 255150 mE : 7410200 mN).
Figure 3.14c Nerimbera Quarry


a


b
0
20
mm


c

The other possibility is that the feldspar grains have infilled a synaeresis crack that developed on the seafloor. Synaeresis cracks are thought to develop due to the loss of pore water from the sediment because of the reorganisation of originally highly porous clays, either due to:

- flocculation (Collinson and Thompson, 1989), or
- salinity-induced changes of volume of certain clay minerals (Collinson and Thompson, 1989; Lucchi, 1995), or
- mechanical disturbances (Lucchi, 1995).

The development of a singular synaeresis crack would tend to exclude flocculation or by salinity induced volume changes of clay minerals as possible mechanism for the formation of the "fissure". However, a single synaeresis crack produced by mechanical disturbances such as loading cannot be ruled out.

The base of the feldspathic sandstone is interpreted as being equivalent to Bouma division A and as such was probably deposited from rapid suspension with little or no bed transport. Then the rapid deposition of the sandstone and subsequent loading of the mudstone could have induced the rapid expulsion of pore water from the mudstone and in doing so causing the upward ramping of the upper 5 mm of the mudstone bed. The "fissure" would have then been subsequently infilled by the feldspar grains. Loading of the mudstone by the overlying feldspathic sandstone is provided by the presence of numerous load casts and pseudonodules of feldspathic sandstone.

3.3.4. Pumiceous Breccias

Within the Berserker beds three types of pumiceous breccias have been recognised:

- graded feldspar-phyric, pumice-lithic breccia - characterised by the presence of polymict lithics,
- feldspar-phyric pumice breccia - characterised by the presence of monomict rhyolitic lithics.
- feldspar-phyric, pumice-lithic breccia - characterised by the presence of rhyolitic and andesitic lithics.

Pumice–lithic breccia units in the drill core intersections, pit exposures and outcrops to the southwest are texturally very similar. The units are generally very thick, some in excess of 100 m, and have sharp basal contacts above which there is a massive to weakly graded interval overlain gradationally by diffusely bedded tuffaceous sandstone and mudstone. The units comprise very poorly sorted feldspar-phyric tube pumice and less abundant polymict volcanic lithic clasts. Delicate tube vesicles are preserved within the pumice clasts, and overall, there is a very weak alignment due to diagenetic compaction. However, many clasts are uncompacted and randomly oriented. *In situ* trace fossils in interbedded sedimentary facies indicate that the depositional environment was submarine. Although composed of pumice, presumably of pyroclastic origin, the units show no signs of hot emplacement and the internal organisation is consistent with deposition from water supported, submarine, high particle concentration, volcaniclastic mass flows. The abundance of pumice clasts and the large volumes represented by the units strongly suggests that the parent mass flows were syn-eruptive. Resedimentation of temporarily stored, non-welded, pumice-rich, primary pyroclastic deposits is also plausible.

3.3.4.1. Graded, Feldspar-phyric, Pumice-Lithic Breccia

The graded feldspar-phyric, pumice-lithic breccia were mapped in east wall of the Main Lode open cut, crop out to the south of the Mount Chalmers mine and were intersected in a number of drill holes. The breccia is characterised by the presence of polymictic lithics, tube pumice clasts and euhedral to broken feldspar crystals. The feldspars range in size between, 1 - 3 mm in size and comprise between 20 - 30% of the deposits. Locally the feldspars may occur in concentrations up to 50%. The clasts within the breccia have a varied size range and degrees of angularity and sphericity. The pumice clasts are uncollapsed and randomly oriented and are up to 150 mm long. Some the pumice clasts have a red/orange colour to them indicating that they have been thermally oxidised.

The units are generally thick (≤100 m) but deposits down to ~1 m thick were mapped to south of Mount Chalmers and were also logged in a number of drill holes. The variety in clast types generally increases downhole in any given deposit, so that near the top a deposit the lithics are dominated by feldspar-phyric rhyolitic clasts. The clasts range in size from a 1 - 2 mm up to 120 mm (Figs. 3.15a, b, and c). The clasts vary in their angularity from very angular with low degrees of sphericity to well rounded with a high degree of sphericity. The variation in lithic types is listed below.

- feldspar-phyric rhyolitic lava fragments
- lithic-rich sandstone
- granite (?)
- feldspar-phyric andesite
- bleached, siliceous amygdaloidal andesite clasts.
- orange/red coloured siliceous lava (?) clasts
- fine-grained andesite
- granodiorite
- siltstone
- milky white quartz clasts
- feldspathic sandstone

The graded nature of the breccia is best observed in drill core. Diffusely bedded tuffaceous sandstone and mudstone (Fig. 3.16 - MCD1) commonly overlie the breccia. Where the breccia is not overlain by tuffaceous sandstone and mudstone, then the grading within the breccias is in respect of the lithics, which generally decrease in size and proportion uphole in any given deposit (Fig. 3.16 - MC 24). Possible reverse grading in the pumice clasts was observed in LBDD1 between 142.0 - 145.0 m.

Contact relationships between the breccia and other lithologies *e.g.* the volcanolithic sandstone and siltstone and other pumice breccias in drill core are generally planar and sharp. South of the Mount Chalmers mine and on the track leading to Mount Chalmers, proper, the contact between the volcanolithic sandstone and breccia is exposed. The breccia has eroded down into the top of the sandstone (Fig. 3.15d). Rip up clasts of the underlying sandstone occur in the base of the breccia.

Figure 3.15. Drill core and outcrop examples of feldspar-phyric, pumice-lithic breccia.

Figure 3.15a Boulder of feldspar-phyric, pumice-lithic breccia exposed on the entrance ramp to the Main Lode
Figure 3.15b Drill core intersection of feldspar-phyric, pumice-lithic breccia. MC24 87.95 - 93.87 m. Mount Chalmers mine, Main Lode
Figure 3.15c Cut and polished slab of feldspar-phyric, pumice-lithic breccia. Randomly oriented uncollapsed tube pumice are visible as well as a variety of lithic types, including amygdaloidal andesitic clasts, siliceous clasts, and dark green andesitic (?) clasts. Sample AQ109 - Sleipner Railway Siding. Sample AQ109 (AMG 206876 mE : 7416082 mN)
Figure 3.15d Erosional contact between feldspar-phyric, pumice-lithic breccia (upper half of figure) and the underlying tuffaceous siltstone. Plan view. (AQ108 AMG 260900 mE :7420230 mN)


a


b

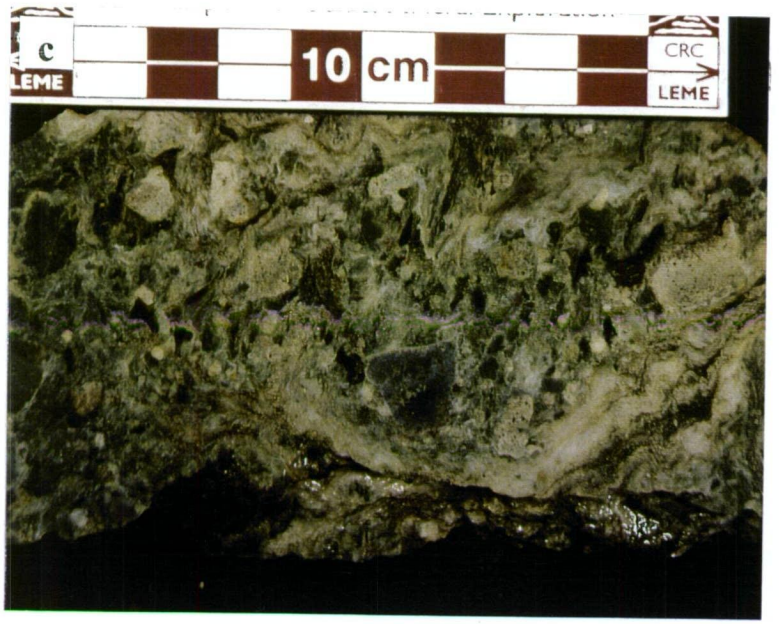
c
10 cm
CRC
LEME


d

Figure 3.16. Graphic lithological logs for parts of MC24 and MCD6 illustrating the structure of feldspar-phyric, pumice-lithic breccia. MC24 grading is only evident within the variation in the clast size. The graphic log from MCD6 shows the graded top to the breccia and the downhole contact with where secondary welding texture has developed adjacent to the contact with the andesite.

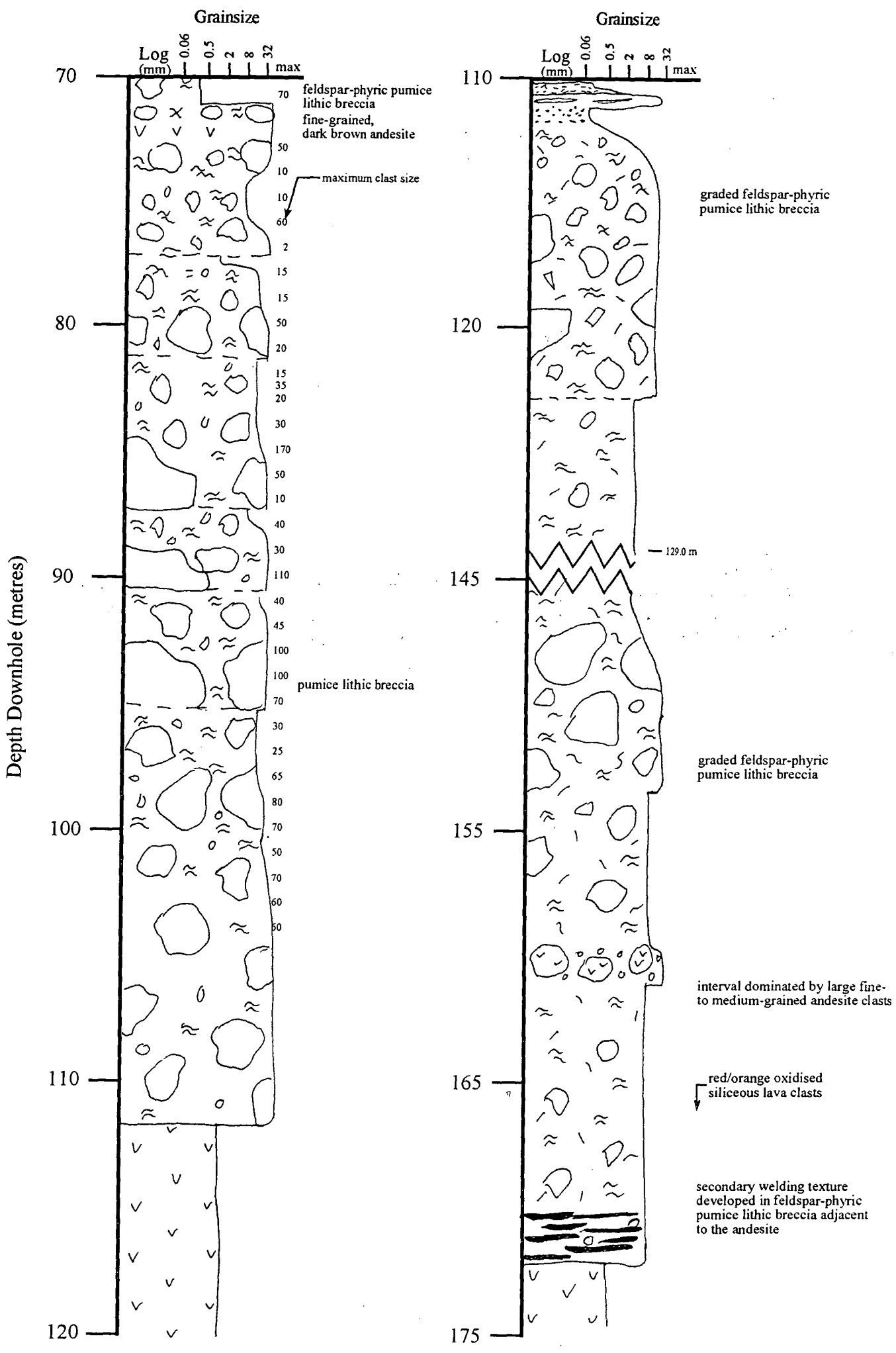
MC24
MCD6
Grainsize
Log (mm)
0.06
0.5
2
8
32
max
Depth Downhole (metres)
70
80
90
100
110
120
feldspar-phyric pumice lithic breccia
fine-grained, dark brown andesite
maximum clast size
pumice lithic breccia
110
120
145
155
165
175
129.0 m
graded feldspar-phyric pumice lithic breccia
graded feldspar-phyric pumice lithic breccia
interval dominated by large fine- to medium-grained andesite clasts
red/orange oxidised siliceous lava clasts
secondary welding texture developed in feldspar-phyric pumice lithic breccia adjacent to the andesite

3.3.4.2. Feldspar-phyric Pumice Breccia

Feldspar-phyric pumice breccia occurs throughout the field area. The feldspar-phyric pumice breccia dominates the geology to the south and west of the mine. The best exposures of the breccia is along Nankin Creek, the northern benches of the Main Lode open cut and in the creeks leading up to the North Star prospect. The breccia is composed of evenly distributed feldspar-phyric crystals (1-3 mm, 15 -20 %; Fig. 3.17b). The groundmass of the pumice breccia is composed of randomly oriented tube pumice that has now been altered to sericite and or silica. Feldspar-phyric and flow banded rhyolitic and feldspar-phyric andesitic clasts are scattered throughout the breccia (Fig. 3.17c). The clasts are generally angular, but clasts with scalloped margins were also observed. In MCD11 between 383.75 to 401.2 m the flow banded and feldspar-phyric rhyolitic clasts are partially to wholly oxidised. Deformation of tube pumice around some clasts was also observed. The only evidence for grading is seen in the size reduction and abundance of lithics within the breccia. In Nankin Creek a possible contact between two feldspar-phyric pumice breccias were observed. A thin faint line that can be traced for some metres marks the possible contact. A feature of this possible contact is the presence of a tongue of the overlying breccia that has sunk into the underlying breccia (Fig. 3.17a). Exposed on the second most top northern bench of the Main Lode open cut is the contact between the feldspar-phyric pumice breccia and the underlying siltstone (Fig. 3.17d). Here the contact is clearly erosional as rip up clasts of the underlying siltstone ($\leq$300 mm) occur in the base of the breccia. The clasts are aligned parallel to the contact between the two units.

Separate domains of silica and sericite have commonly altered the feldspar-phyric pumice breccia (Fig. 3.17b). This style of alteration has locally produced attenuated sericite altered domains that resemble fiamme, that parallel S_0. This style of alteration has produced pseudo clastic textures. These pseudoclasts are distinguished from real clasts by their diffuse margins and the presence of euhedral unbroken feldspar crystals that transect both alteration domains.

3.3.4.3. Feldspar-phyric pumice-lithic breccia (andesitic and rhyolitic clasts)

Narrow intervals of this pumice breccia facies were intersected in three drill holes, (MCD7 (171.3 - 184.7 m); MCD10 (129.85 - 139.0 m) and MCD11 (191.25 - 211.3 m). The groundmass is composed of randomly oriented tube pumice clasts and euhedral feldspar crystals (1 - 3 mm; 15 - 20 %). The breccia has only three clast types visible: fine-grained andesitic and feldspar-phyric (1 - 3 mm; 15 - 20 %) and flow banded rhyolitic clasts. The clasts have varying degrees of angularity, but are generally angular. The flow banded rhyolitic clasts are invariably red/orange colour indicating that they have been oxidised.

3.3.5. Flow Banded, Spherulitic Rhyolitic Breccia

The flow-banded aphyric spherulitic rhyolite crops out in two places, at the Mount Chalmers open cut, in the southern corner of the upper benches of the Main Lode open cut and on a small hill approximately 1.3 km south-southwest of Woods Shaft prospect. The breccia is composed of clast supported, angular, aphyric; flow-banded rhyolitic clasts set within a chlorite altered feldspar-phyric (1 - 3 mm, 20 - 25%)

Figure 3.17. Drill core and outcrop examples of feldspar-phyric, pumice-lithic breccia.

Figure 3.17a Contact between two feldspar-phyric pumice breccias. Nankin Creek (AMG 259000 mE : 7419500 mN).
Figure 3.17b Cut and polished slab of feldspar-phyric pumice breccia. Evenly porphyritic nature of the breccia is visible. Silica and sericite (dark green) alteration domains are visible.
Sample AQ1 - Nankin Creek. (AMG 259000 mE : 7419500 mN).
Figure 3.17c Representative drill core samples of feldspar-phyric breccia, with bleached amygdaloidal volcanic clast and chlorite alteration domains WSDD8: 265 - 302 m
Figure 3.17d Contact between the feldspar-phyric pumice breccia (to the left of the picture) and silicified siltstone (to the right of picture. The contact between the two units is immediately below the joint running diagonally across the photo.

a

b
10 cm
CRC
LEME

c

d

matrix (Figs. 3.18a and b). The clast size varies between 5 - 200 mm. Flow banding within the clasts is generally planar, but distorted flows bands are also present. A feature of this rhyolite is the presence of nodular to cauliflower-shaped aggregates of anhedral quartz. The nodules may be up to 30 mm across and are surrounded by smaller spherulites. The spherulites have developed along the flow bands and within the matrix (Figs. 3.18a and b). Within some of the spherulites flow bands can be traced through them, indicating that crystallisation occurred after the lava had stopped flowing, while with other spherulites the flow bands wrap around them.

The disparity in feldspar crystal content between the clasts and the matrix suggests that they are not cogenetic with each other. No contact relationships with the other lithologies at Mount Chalmers were mapped, except one where the breccia is cut by quartz-feldspar porphyry. Therefore, no definite conclusions on the origin or likely source of the clasts can be made. However, the hill south-southwest of Woods Shaft prospect is composed almost solely of the rhyolite. Given the relatively undeformed nature of the Berserker beds, then possibly the rhyolitic breccia represents a chilled brecciated carapace to a rhyolite dome.

3.3.6. Andesite and Andesitic Breccia, Intrusions, Lavas and Hyaloclastite

Andesitic intrusion, lava, hyaloclastite and resedimented hyaloclastite were intersected in drill holes MCD4 (190.86 - 210.1 m)(Fig 3.19a), MCD10 (164.05 - 216.5 m), MCD11 (219.9-243.1)(Fig 3.19b), RWDD1 (60.1-290.2), T2 (209.0 - 212.0 m) and WS7 (88.0 - 119.6 m). All these intervals are true thickness as the holes were all drilled vertically. The hyaloclastites are composed of variably shaped and sized andesitic clasts set within a pale yellow-brown coloured matrix, which may contain smaller andesitic fragments. Some groups of clasts show jigsaw-fit arrangement, indicating that the clasts are still largely *in situ*. Some of the clasts were still "plastic" when brecciation occurred as some individual clasts show evidence of plastic deformation and some adjacent clasts have been "welded" together or are deformed or draped by adjacent clasts. A number of the clasts have narrow (≤20 mm) reaction/alteration rims, that may have been glassy chilled margins.

The andesitic clasts may be weakly to strongly amygdaloidal and are infilled by epidote, chlorite and rarely quartz. The amygdales are generally spherical in shape, but irregularly shaped amygdales are also present.

In WS7, MCD4 and MCD10 MCD11 (Fig. 3.20a) graded beds of andesitic breccia overlie the *in situ* andesitic breccia. The contacts between beds are gradational. In MCD4 the resedimented hyaloclastite intervals are composed of a series of graded units (max. 10 m thick) in which the clasts have a bimodal size distribution (10 mm and max. 40 mm). The aggregates have an open framework, but are clast supported. The contacts between beds are gradational, possibly indicating that there was very little time between the generation of each individual bed. The resedimented hyaloclastite is strongly bioturbated and contains a trace fossil fauna identical to that seen elsewhere within the Berserker beds. Shallow-water trace fossil assemblages are present within volcanolithic sandstone that occurs above and below the andesitic hyaloclastite. The presence of identical trace fossils above and below the andesitic hyaloclastite implies a near constant shallow marine environment. The upper most resedimented unit grades up into a

Figure 3.18. Examples of flow-banded spherulitic rhyolitic breccia from Mount Chalmers mine - Main Lode southern end of eastern benches.

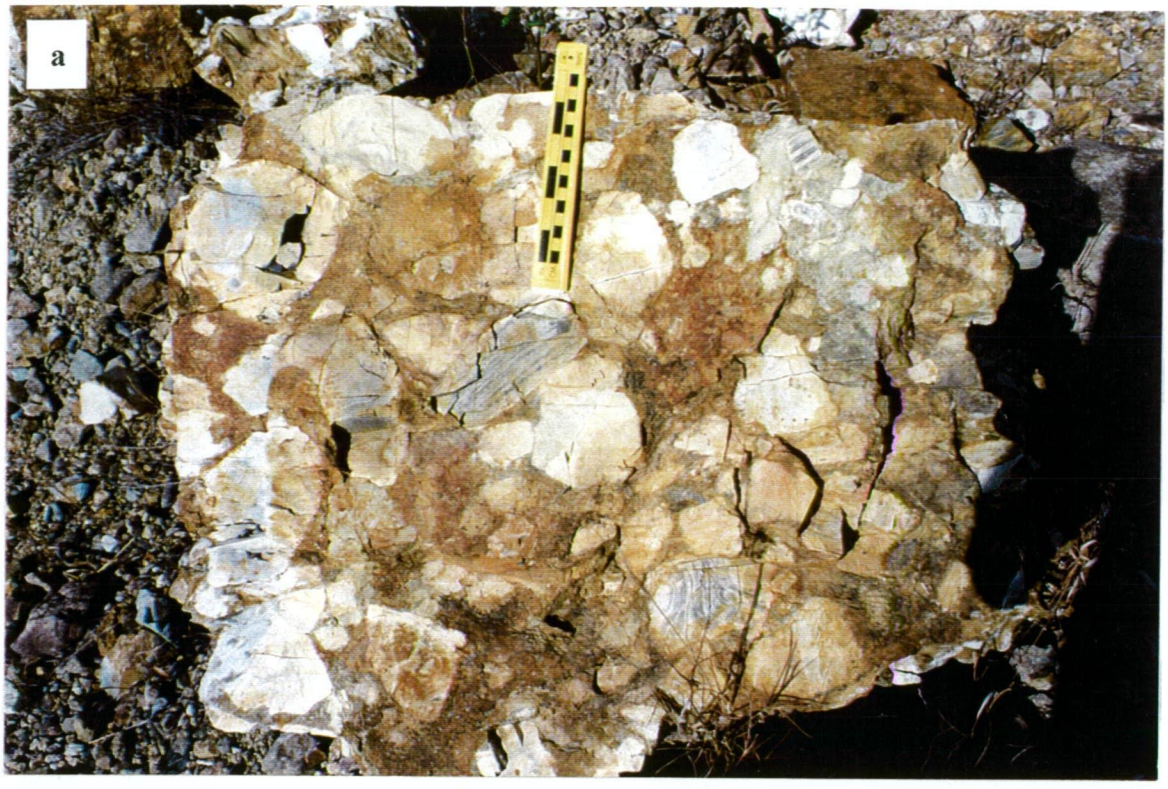
a


b
INCH
CM

Figure 3.19. Graphic lithological logs for parts of MCD4 and MC11 depicting the structure and variation within andesitic breccia intersected in drillholes at the Tungamull prospect. The andesitic breccia in MCD4 grades up into a number of andesitic pebble beds and sandstone. The fine-grained sandy to the uppermost graded bed is bioturbated. The andesitic breccia in MCD11 has a coherent amygdaloidal margin with the overlying siltstone. Within the breccia, smaller clasts can be seen to be spalling off the larger clasts with a jigsaw-fit texture.

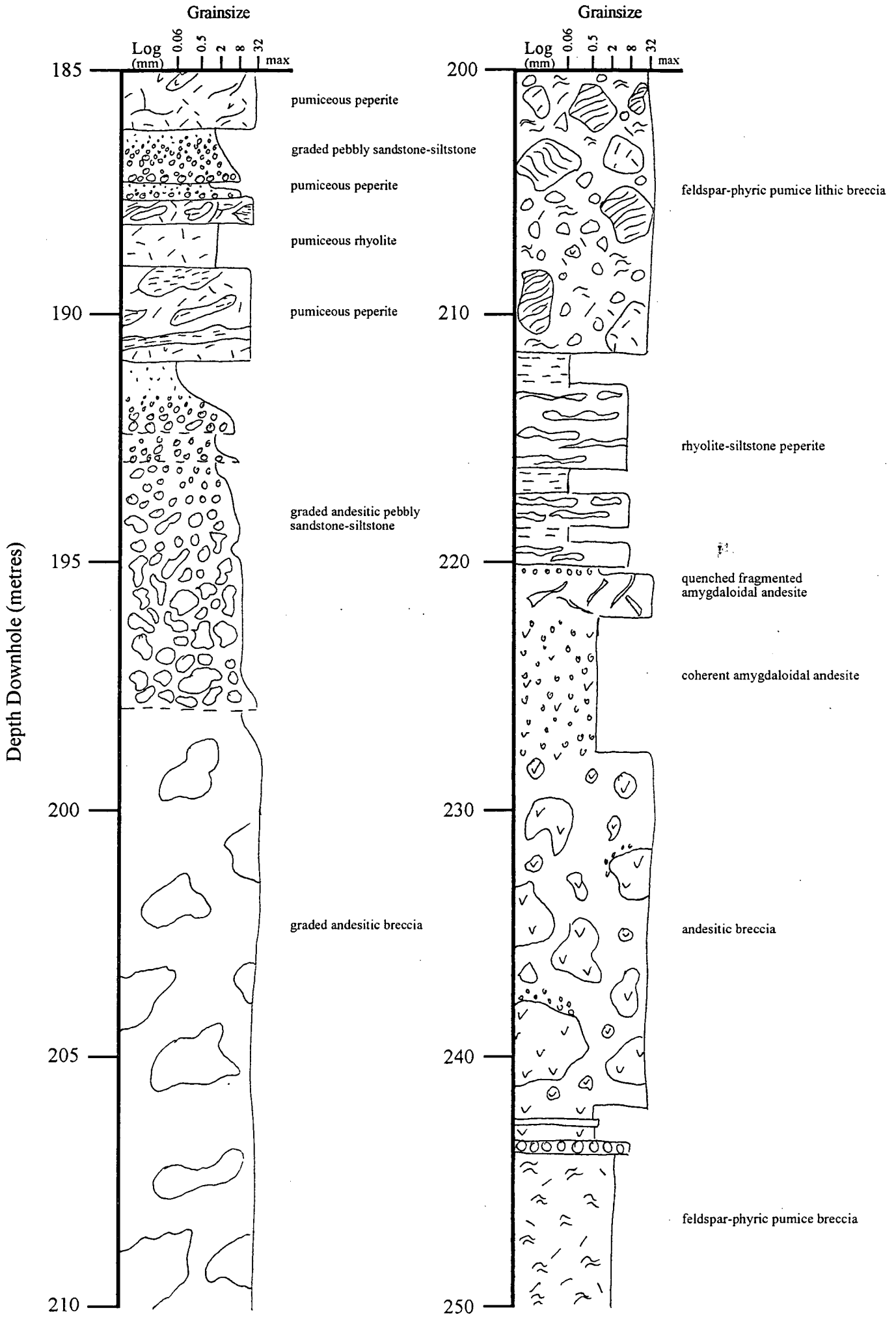
MCD4
MCD11
Grainsize
Log (mm)
0.06
0.5
2
8
32
max
Depth Downhole (metres)
185
190
195
200
205
210
pumiceous peperite
graded pebbly sandstone-siltstone
pumiceous peperite
pumiceous rhyolite
pumiceous peperite
graded andesitic pebbly sandstone-siltstone
graded andesitic breccia
200
210
220
230
240
250
feldspar-phyric pumice lithic breccia
rhyolite-siltstone peperite
quenched fragmented amygdaloidal andesite
coherent amygdaloidal andesite
andesitic breccia
feldspar-phyric pumice breccia

Figure 3.20. Graphic lithological logs for parts of MCD4 and MC11 depicting the structure and variation within andesitic breccia intersected in drillholes at the Tungamull prospect. The andesitic breccia in MCD4 grades up into a number of andesitic pebble beds and sandstone. The fine-grained sandy to the uppermost graded bed is bioturbated. The andesitic breccia in MCD11 has a coherent amygdaloidal margin with the overlying siltstone. Within the breccia, smaller clasts can be seen to spalling off the larger clasts with a jigsaw-fit texture.


a


b

siltstone. The upper most beds have also been intruded by feldspar phyric (pumiceous?) rhyolitic sills that have produced peperites.

In MCD10, (177.3 - 216.5 m) (Fig 3.20b) the andesitic breccia also contains very well rounded, feldspar-phyric (dacitic?) lava clasts, a flow banded rhyolitic lava clasts and subangular to subrounded siliceous siltstone clasts. The base of the breccia is composed of andesitic clasts. Flames of siltstone derived from underlying beds have been injected between the andesite clasts. This interval is interpreted as andesitic lava that flowed onto and incorporated a pre-existing polymictic conglomerate as it was brecciating.

In MCD7 an autobrecciated/hyaloclastite intrusive andesite is present between 94.4 - 148.3 m. The andesite is identical in composition to those described above. Locally the clasts have jigsaw-fit texture, where smaller clasts have spalled off from the larger clasts. Downhole the andesite becomes more massive, with incipient brecciation being evident. Between the start of coring (74.3 m) to 94.4 m, the andesite has produced a peperite in which stringers and lobes of the andesite occur within a siltstone.

RWDD1 intersected a thick sequence of andesitic breccia intruded by a number of andesitic dykes. The clasts are all very angular and are generally clast supported. The clasts range in size from ≤10 mm up to 150 mm. The clasts are very fine-grained and amygdaloidal. The amygdales are generally spherical, although stretched or elongated amygdales are also present. The clasts generally do not display jigsaw-fit texture, although locally this texture was observed. Towards the bottom of the drill hole (266.8 - 290.2 m) the clasts have been plastically deformed and moulded back together. Below approximately 287.0 m, red coloured oxidised flow banded rhyolite clasts are present. The andesitic breccia has been intruded by a number of andesitic dykes or sills. The dykes may either be texturally identical to the andesitic breccia or they are texturally similar to the Type 1 andesitic sills and dykes described in Section 3.3.10.

The andesitic breccia is composed of variably shaped and sized andesitic clasts set within a pale yellow-brown coloured matrix, which may contain smaller andesitic fragments. Some groups of clasts show jigsaw-fit arrangement, indicating that the clasts are still largely *in situ*. A number of the clasts have narrow (≤20 mm) reaction/alteration rims, that may have been glassy chilled margins. This indicates that the clasts may have formed by quench fragmentation and can therefore be interpreted as being a hyaloclastite or a resedimented hyaloclastite. Some of the clasts were still hot when brecciation occurred as some individual clasts show evidence of plastic deformation and some adjacent clasts have been "welded" together or are deformed or draped by adjacent clasts.

In RWDD1, jigsaw-fit texture is generally lacking and none of the clasts appear to have quenched glassy margins, suggesting that may be resedimented autobreccia. However, they have been intruded by a number of sills or dykes that are texturally similar to the andesitic breccia. This suggests that the sills or dykes may be andesitic feeder lava lobe dykes that have intruded into unconsolidated autobreccia.

3.3.7. Peperites

Two main types of peperitic associations have been recognised within the Berserker beds. Peperites associated with the andesitic intrusions at the Tungamull prospect and peperites associated with syn-volcanic rhyolitic pumiceous sills.

An andesite-siltstone peperite was intersected in MCD7 (74.3 - 96.4 m) The peperite occurs at the top of a brecciated andesitic intrusive. The peperite is composed of fluidal stringers of andesite within a pale grey coloured siltstone matrix. No structures such as laminations were observed within the siltstone. This suggests that the sediment has possibly been homogenised by the and is mainly composed of siltstone and stringers of andesitic magma. In MCD7, the top of the peperite is not seen as it was not cored.

The host sediment involved in the peperite is homogeneous in texture and unstratified whereas elsewhere, it is bedded and beds are graded. Local destruction of bedding and grading requires considerable re-arrangement of the original grain packing which can only take place in sediment that is unconsolidated or weakly consolidated.

Syn-volcanic rhyolitic pumiceous sills and associated peperite were mapped in the field and logged in a number of drill holes. This peperite variety is fully described and discussed in Chapter 5. However, the key features of pumiceous peperite are listed here for reference:

- highly irregular contacts between pumiceous rhyolite and host sediment,
- gradational to sharp contacts between coherent pumiceous rhyolite and pumiceous peperite
- presence of vesicles and thermal metamorphic effects in the host sediment adjacent to the rhyolite
- local destruction of bedding in the sediment involved in the peperite.

3.3.8. Sleipner Andesitic Breccia

The Sleipner Andesitic Breccia (SAB) occurs in the southern half of the mapped area (Plate 1) and is comprised of three main facies:

- coherent to brecciated highly vesicular andesite (SAB_M)
- andesitic agglutinate deposit
- poorly sorted polymictic andesitic breccia (SAB_P)

3.3.8.1. Coherent to Brecciated Vesicular Andesite (SAB_M)

A coherent to brecciated highly vesicular andesitic breccia was mapped in the southern part of the area, and also just south of the North Star Mine (Plate 1). The SAB and its contact relationship between the coherent and brecciated andesite and feldspar-phyric, pumice-lithic breccia are well exposed along the railway cutting near the Sleipner Railway Siding. The railway cutting was mapped in detail and is shown

graphically in Figure 3.21. The andesitic breccia is composed of alternating intervals of highly vesicular, coherent andesite surrounded by zones containing highly vesicular andesitic clasts, set within an andesitic matrix. The clasts may have a very good jigsaw-fit texture, indicating that they have not moved far, or they may be sub-rounded to rounded (low degree of sphericity), indicating some movement of the clasts has occurred. Elsewhere the clasts are set within a sericite, epidote, carbonate-altered groundmass that has locally enhanced the breccia texture. Minor angular very fine-grained siliceous clasts are also present. The contacts between the coherent andesite and the andesitic breccia are either gradational or sharp. A gradational narrow contact zone (≤1 m) between the SAB_M and feldspar-phyric, pumice-lithic breccia occurs approximately 284 m along the mapped section. The SAB_M contains chlorite altered uncollapsed tube pumice clasts, plus minor amounts of siliceous clasts, identical to those found in the adjacent feldspar-phyric, pumice-lithic breccia. Clasts of highly vesicular andesite are found within the feldspar-phyric, pumice-lithic breccia to approximately 284 m along the mapped section.

A number of highly vesicular andesitic dykes have intruded into the feldspar-phyric pumice breccias at the mapped railway cutting (Fig. 3.21). The contacts between the andesite and the feldspar-phyric pumice breccia, are vertical, and may be faulted. In terms of their vesicularity, the dykes are commonly zoned with a chilled outer margin (≤10 cm), that contains little or no visible vesicles, a middle zone (adjacent to the chilled margin) where upwardly and inwardly inclined stretched vesicles are present, and a central zone composed of roughly circular vesicles (Fig. 3.22). The upwardly and inwardly inclined vesicles show that the magma was still flowing after formation of the vesicles and that it behaving as a laminar flow on its margins, while in the middle it was flowing as a rigid plug.

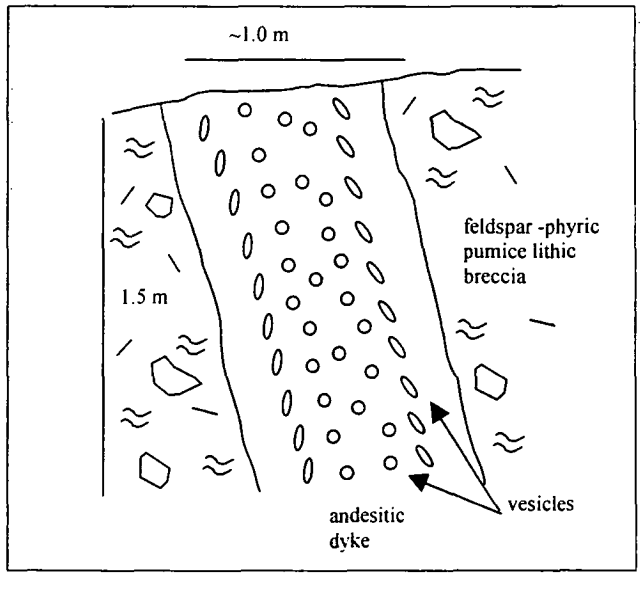

Figure 3.22 Field sketch of highly vesicular andesitic dyke intruding into feldspar-phyric, pumice-lithic breccia at Sleipner Railway Siding. Size of vesicles has been enlarged to show their orientation and shape within the dyke.

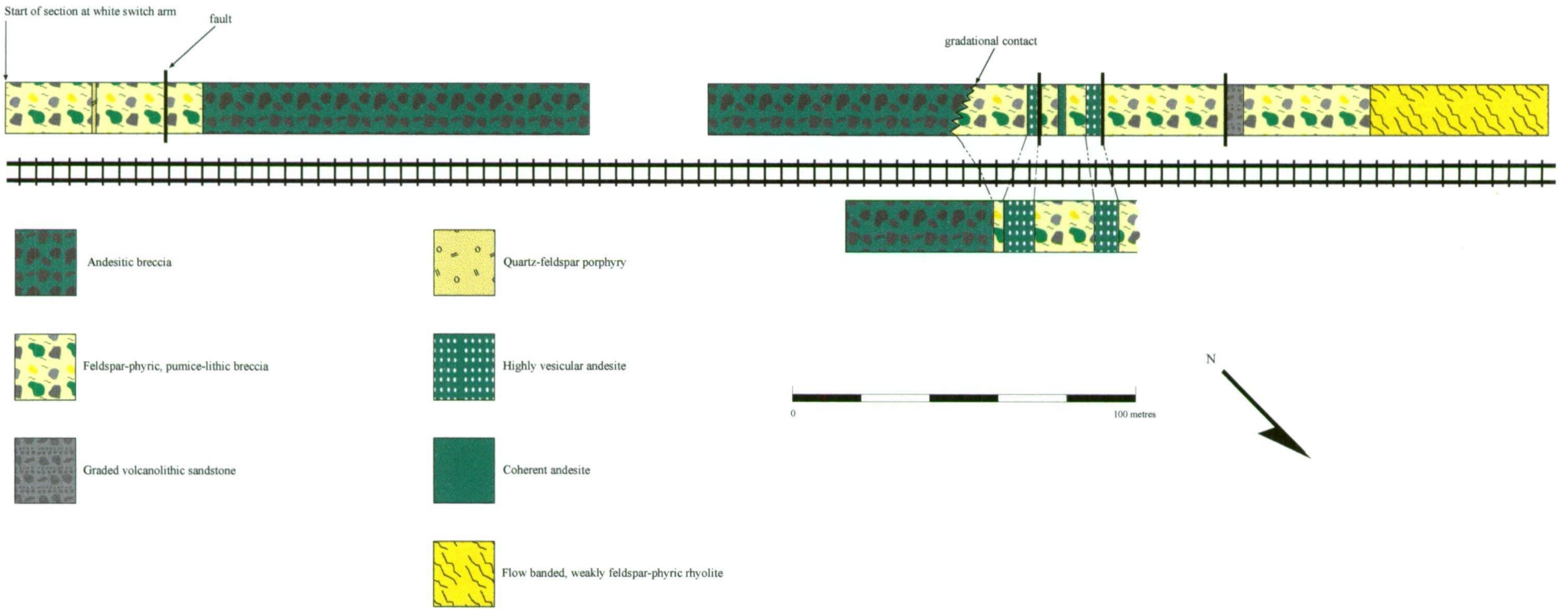

Figure 3.21. Geological sketch map of the railway cutting near the Sleipner Railway Siding.

The gradational contacts between the coherent andesite and the presence of jigsaw-fit texture between groups of clasts within the andesitic breccia indicate that the breccia is an hyaloclastite. Further away from the contact, the *in situ* hyaloclastite has been disturbed so that jigsaw fix texture is no longer visible, and the clasts become more matrix supported. Disturbance of the hyaloclastite can be caused by a number of factors including continued movement of the more ductile interior lava, flowage over steep slopes or by intrusions of magma into the hyaloclastite pile or by seismic activity (McPhie *et al.*, 1993). Contact relationships between the coherent highly vesicular andesite and the enveloping highly vesicular andesitic breccia argues that the coherent andesite is a feeder lava lobe-dyke intruding into contemporaneous unconsolidated hyaloclastite of the same composition (Fig 3.23). The presence of mixed zone or gradational contact between the andesitic hyaloclastite and the feldspar-phyric pumice breccia suggests that two separate facies have mixed at their margins. Alternatively, that andesitic magma intruded into unconsolidated feldspar-phyric, pumice-lithic breccia. As the magma brecciated along it margins to form hyaloclastite it continued to flow upwards and outwards, causing the outward expansion of the hyaloclastite into the unconsolidated feldspar-phyric pumice-lithic breccia.

The SAB_M is interpreted as being produced from the sequential build up of and intrusion of andesitic magma into a pile of contemporaneous unconsolidated hyaloclastite of the same composition. As the initial lava was extruded onto the seafloor, its margin was rapidly chilled by the seawater and quenched fragmented to form hyaloclastite. As more lava was injected, and was exposed to seawater, both within the hyaloclastite and also by direct exposure to seawater, more hyaloclastite was formed. This process built up a cone composed of *in situ* and resedimented hyaloclastite, with interior feeder lava lobe-dykes and sills. The presence of highly vesicular lava and hyaloclastite indicates that the magma was volatile-rich and had vesiculated substantially prior to interaction with the seawater. The highly vesicular andesitic dykes that have intruded into the feldspar-phyric pumice-lithic breccia provide evidence for this.

3.3.8.2. Andesitic Agglutinate Deposit

A small outcrop of andesitic breccia was mapped on the northwest trending ridge leading to the North Star prospect, and represents the highest exposure of SAB on the ridge. Three basic clast shapes have been recognised in the outcrop:

- lapilli to bomb size tabular shaped clasts
- lapilli size spindle-shaped clasts, and
- lapilli size spheroidal-shaped clasts

All clasts are dark green in colour (fresh surface) and are aphyric and non-vesicular.

The tabular-shaped clasts define a layering within the outcrop that is parallel to S_0 *i.e.* horizontal (Fig.3.24a). The clasts have also been deformed such that they have moulded into each other. Visible within Figure 3.24b are a number of lapilli-size spheroidal clasts that have also been moulded into the underlying tabular shaped clasts. In Figure 3.24b a spheroidal clast has deformed the underlying thin tabular clast while overlying the spheroidal clast a thin tabular-shaped clast is draped and deformed around the spheroidal clast. The moulding of one clast onto another indicates that the clasts were still hot

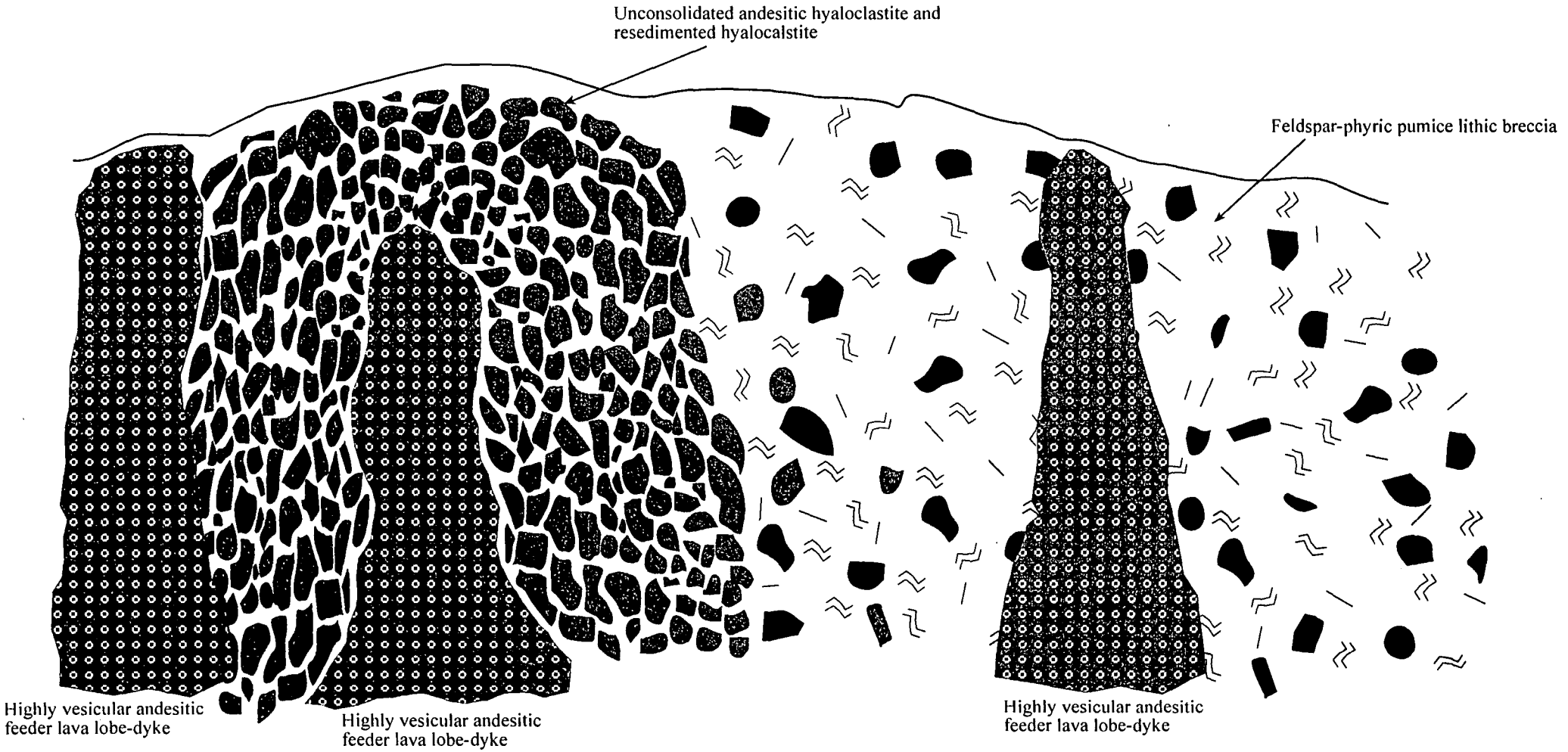

Figure 3.23. Schematic representation of the relationship between the highly vesicular andesitic dykes, unconsolidated andesitic hyaloclastite, resedimented hyaloclastite and feldspar-phyric pumice breccia, at the Sleipner Railway Siding

Figure 3.24. Outcrop photos of surface textures andesitic agglutinate deposit, below the North Star prospect. For explanation of textures, see text.


a


b

and plastic at the time of formation. These clasts are interpreted as cowdung bombs formed by the explosive ejection of andesitic magma.

The spheroidal and spindle shaped clasts are also interpreted as being formed by the explosive ejection of andesitic magma. The difference in clast shapes is possibly reflecting subtle changes in the fluidity of the magma. The breccia is interpreted as having been formed by the explosive eruption of andesitic magma. The eruption of fluidal bombs produces agglutinate. Agglutinate is a fall deposit comprising spatter (poorly vesicular, fluidal, juvenile pyroclasts) and bombs that accumulate near vents in explosive eruptions of low viscosity magma (McPhie *et al.* 1993). The eruptions may form small agglutinate-cones over cylindrical vents or agglutinate-ramparts bordering fissures (Williams and McBirney, 1979).

3.3.8.3. Polymictic Sleipner Andesitic Breccia (SAB_P)

The SAB_P is a poorly sorted polymictic andesitic breccia that is up to 150 m thick. The SAB_P clast assemblage is dominated by large ($\leq$ 0.5 m) dark brown, vesicular and non-vesicular andesitic clasts (Figs. 3.25a, b, c and d), with subordinate dacitic and feldspar-phyric rhyolitic lava clasts, sedimentary clasts, andesitic pillow fragments and rare gabbroic clasts set within a fine-grained andesitic and feldspar-bearing matrix. As well as the andesitic clasts a number of other clast types have also been recognised:

- feldspar-phyric (10%; 0.5 - 1.0 mm) dark grey andesite
- strongly vesicular, feldspar-phyric (10%; 0.5 - 1.0 mm) andesite
- very dark grey siliceous clast
- flow banded rhyolite clasts
- feldspar-phyric (20 - 25%; 1 - 1.5mm) dacite
- andesitic pillow fragments
- rare gabbroic clasts

The andesitic, dacitic and siliceous siltstone clast types dominate the breccia. The andesitic clasts are generally angular to subrounded and have a maximum size range between 100 - 120 mm (Fig 3.25d). The other clast types vary between having an angular to subrounded form. The siliceous siltstone clasts are generally angular and have a maximum size of 300 mm.

The clasts are set within a fine-grained andesitic and feldspar-bearing matrix. The matrix and andesitic clasts have been extensively altered to an assemblage of calcite, sericite and epidote. Individual units grade up into fine- to coarse-grained andesitic sandstones, and are between 5-10 m thick. The base of the SAB_P is interbedded with the uppermost volcanolithic sandstone and siltstone mapped within the field area. The SAB also crops out on the southwestern flanks of Mount MacDonald as a series of isolated outcrops of graded pebble-boulder breccia that grade up into feldspathic sandstone with scattered lithics. The clast size varies from pebble to boulder size (Fig. 3.25a).

Figure 3.25. Outcrop and hand specimen examples of the different sub-facies within the Sleipner Andesitic Breccia.

Figure 3.25a Reverse-graded polymictic andesitic breccia, western foothills of Mount MacDonald.
Figure 3.25b Hand specimen example of polymictic andesitic breccia - Nankin Creek.
Figure 3.25c and Hand specimen example of vesicular andesitic breccia. Jigsaw-fit texture is evident in Figure 3.25c.


a

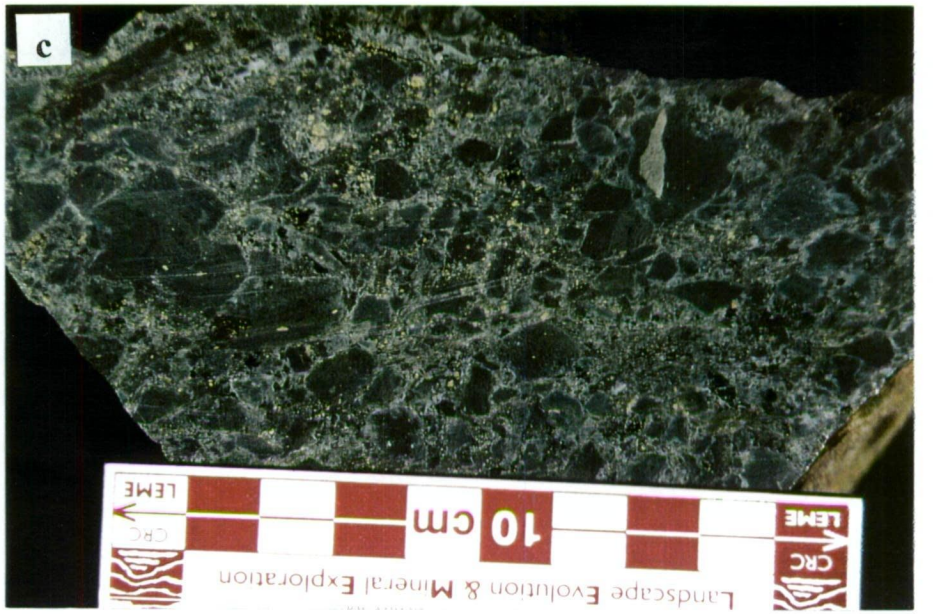
c
10 cm
CRC
LEME

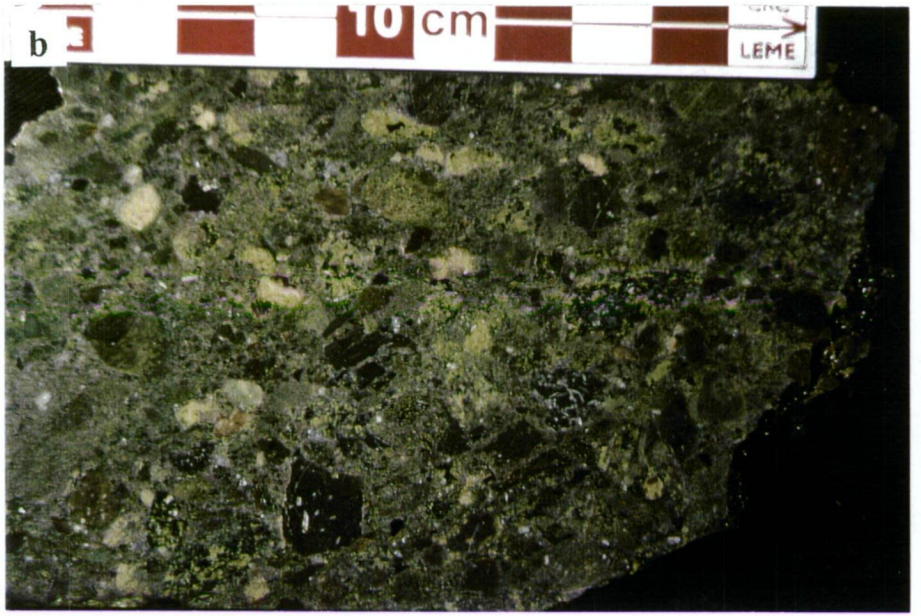
b
10 cm
LEME


d
Landscape Evolution & Mineral Exploration
CRC
LEME
10 cm
CRC
LEME

The smaller clasts tend to be more rounded than the larger clasts. The pebble-boulder breccia grades up into feldspathic sandstone with scattered small lithics (≤10 mm). The larger more angular clasts tend to occur near the top of the breccia layer. The contact between the pebble-boulder bed and the underlying sandstone is relatively sharp. Reverse to normal grading within the pebble-boulder breccia clasts is evident (Fig. 3.25a). Reverse grading is likely to occur where concentration values and therefore viscosity, density and strength of the fluid are high (Fisher and Schmincke, 1984).

The coherent and brecciated SAB are interpreted as having been a small andesitic dome that grew by the accumulation of *in situ* and resedimented hyaloclastite that was fed by highly vesicular andesitic magma. The small outcrop of andesitic agglutinate is interpreted as being produced by small-scale pyroclastic eruptions of the andesitic magma within a shallow-marine setting. As there is no evidence for oxidation of the clasts this would suggest that the deposit was not formed in a subaerial environment, it is interpreted that the eruption occurred either wholly within a submarine environment or within a subaerial environment and that the lava settled through the water column to form the agglutinate deposit. As the dome grew and expanded, sectors of the dome would become unstable due to steepening gradients. This combined with possible seismic activity and injection of more magma could have caused the slumping of the andesitic breccia and the subsequent generation of high-energy submarine turbidity currents. Extraneous lithics, either from erosion of the seafloor or from earlier deposited pebble or boulder beds would have become entrapped within the current as it flowed across the seafloor. The presence of normally graded beds within the SAB_P suggests that the deposits were formed from deposition of low concentration turbidity currents. Whereas the reverse to normal grading seen in the pebble-boulder breccia beds of the SAB_P at Mount MacDonald suggests that they were deposited from high concentration turbidity currents.

3.3.9. Rhyolites

To the south and east of Mount Chalmers two distinct rhyolitic lavas and intrusives were mapped and intersected in drill core the flow banded, auto brecciated to massive Ellrott Rhyolite; and a weakly feldspar phyric siliceous rhyolite.

3.3.9.1. Ellrott Rhyolite

Massive to finely to coarsely flow banded rhyolites crop out on either side of the Emu Park road. On the southern side of the Emu Park Road, rhyolite occurs as low isolated hills. The rhyolite has also been intersected in a number of drills at the Tungamull Prospect and in Stony Creek drill hole. Rhyolite also crops out along the Rockhampton-Yeppoon Road, where it also forms low ridges and hills. Two facies have been recognised within the Ellrott Rhyolite:

- brecciated rhyolite and massive to flow banded coherent feldspar-phyric rhyolite
- graded sandstone and lithic breccias

Outcrop exposures and drill core intersections of have shown that the Ellrott Rhyolite is composed of alternating intervals of flow banded rhyolite (Fig. 3.26a) and flow banded and feldspar-phyric breccia (Fig. 3.26b). In outcrop, the clasts may display excellent jigsaw-fit texture to non-jigsaw-fit texture where the clasts have been rotated (Fig. 3.26c and d). Some the clasts also have smaller clasts spalling off them that form a narrow carapace to the parental clast. Within some of the flow-banded intervals, rhyolite clasts have been rotated and flow bands have been distorted around clasts. In some outcrops, the flow banding is so fine that taken out of context, it could be easily mis-identified as a finely bedded siltstone. Locally the rhyolites are strongly altered and pyritic. The alteration varies between strong sericite and silica to very strong kaolinisation. Locally alteration may be so strong that positive identification of textures and structures within the rhyolite at times can be difficult.

3.3.9.1.1. Brecciated Rhyolite and Massive to Flow Banded Coherent Feldspar-Phyric Rhyolite

Within drill core and outcrops the Ellrott Rhyolite is composed of alternating intervals (various thicknesses) of feldspar-phyric finely to coarsely flow banded to massive rhyolite, and brecciated rhyolite composed of predominantly of two clasts types: flow banded ± feldspars and feldspar-phyric clasts (Figs. 3.27). The Ellrott Rhyolite tends to have a uniform feldspar size range of 1 - 3 mm and comprises between 15 - 20 % of the rhyolite. The clasts may be up to 100 mm in size, although the normal clast population size is between 20 - 70 mm. Interstitial to these larger clasts are smaller clasts (≤20 mm) of feldspar-phyric rhyolite. The clasts generally do not display jigsaw-fit texture (Fig 3.27b). However, jigsaw-fit texture was intersected in three drill holes (T2, 181.55 - 182.70 m; P8/D4, 154.3 - 169.2 m; MCD12, 130.4 - 131.8 and a narrow interval at 160.5 m) display jigsaw-fit texture with little or no rotation of the clasts evident. The flow banding within clasts may either be planar or contorted.

The clasts are set within a siliceous feldspar-phyric groundmass. In MCD5 the top 15 - 20 m (188.0 - ~208.0 m) of the rhyolite breccia and in P8/D4 (154.3 - 169.2 m) and MCD11 (171.11 - 178.6 m) the clasts have a red/orange colouration due to thermal oxidation of the breccia. In MCD5, the red/orange colouration decreases in intensity downhole.

Intervals of massive to flow banded feldspar-phyric rhyolite where intersected in three drill holes (MCD8, 99.4 - 132.5 m; MCD9, 129.9 - 200.4 m; MCD12, 122.1 - 162.6 m). Within these intersections the rhyolite is composed of evenly distributed euhedral feldspar crystals that range in size from 1 - 3 mm and comprise 15 - 20 % of the rhyolite. Commonly within these apparent massive units are narrow rhyolitic breccia intervals. One thick interval of flow banded rhyolite was intersected in MCD9 (129.9 - 200.4 m) where the flow banded rhyolite has a narrow (≤2 m) breccia zone composed of flow banded rhyolite clasts. In MCD8 between the start of coring (99.4 m) and 132.5 m the Ellrott Rhyolite is dominated by massive feldspar-phyric rhyolite, within which are four narrow intervals (≤4 m) composed of angular feldspar-phyric rhyolite clasts.

The contact relationships between the rhyolite breccia and the coherent to flow banded rhyolite are gradational (Figs. 3.27a and b). However, where the rhyolite breccia or coherent rhyolite is in contact with sedimentary rocks the contact relationships are more complex. Invariably the contact between the rhyolite and volcanolithic sediment is mixed zone.

Figure 3.26. Outcrop examples of the Ellrott Rhyolite.

Figure 3.26a Illustrates finely planar flow banded Ellrott Rhyolite.
Figure 3.26b Contorted flow bands.
Figure 3.26c and d *In situ* to locally transported rhyolite breccia.
(All examples: AMG 261500 mE : 7416700 mN).


a


b


c
INCH
CM


d

Figure 3.27. Graphic lithological logs (P8/D4 and MCD1) illustrating the relationship between the coherent, brecciated and rhyolitic sandstone facies of the Ellrott Rhyolite.

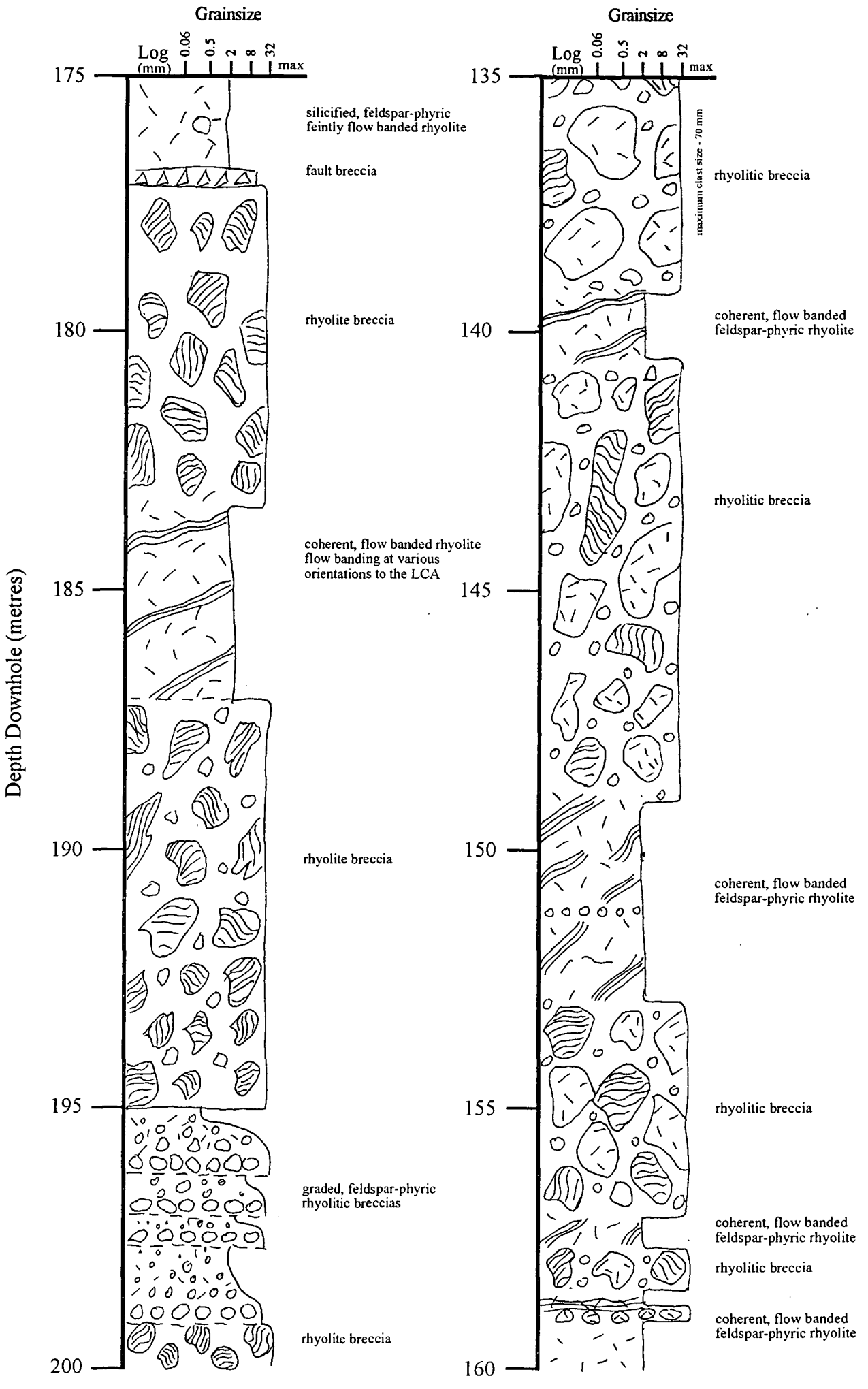
P8/D4 (Murray's 4)
MCD1
Grainsize
Log (mm)
0.06
0.5
2
8
32
max
Depth Downhole (metres)
175
180
185
190
195
200
silicified, feldspar-phyric feintly flow banded rhyolite
fault breccia
rhyolite breccia
coherent, flow banded rhyolite flow banding at various orientations to the LCA
rhyolite breccia
graded, feldspar-phyric rhyolitic breccias
rhyolite breccia
135
140
145
150
155
160
maximum clast size - 70 mm
rhyolitic breccia
coherent, flow banded feldspar-phyric rhyolite
rhyolitic breccia
coherent, flow banded feldspar-phyric rhyolite
rhyolitic breccia
coherent, flow banded feldspar-phyric rhyolite
rhyolitic breccia
coherent, flow banded feldspar-phyric rhyolite

These mixed contact zones are composed of rhyolite clasts separated by apophyses of siltstone. In P8/D4 between 223 - ~227.0 m a mixed contact zone between the overlying siltstone and the underlying massive coherent feldspar-phyric rhyolite occurs. In this interval, angular feldspar-phyric rhyolite fragments occur within a siltstone matrix. The clast size of the rhyolite clasts increases and the amount of interstitial sediment decreases downhole. The coherent rhyolite has either intruded into the siltstone from below or produced a peperitic margin or it has burrowed down into the sediments and likewise produced a peperitic contact. The thickness of the coherent rhyolite would suggest that the rhyolite has intruded up into the sediment, rather than burrowed down into it. In MCD9, the coherent rhyolite is bounded on both its upper and lower contact by feldspar-phyric pumice breccia. The contacts are very sharp with no evidence for mixing between the two lithologies.

The remaining mixed contact zones between the underlying sedimentary rocks and the breccias may be the result of one of two possible processes:

- rhyolite blocks tumbled off an advancing lava front and became embedded within the sediment and the lava continued to flow over the blocks.
- an advancing lava with a flow foot breccia flowed over the sediments, consequently the weight of the lava flow pushed the lava blocks down into the sediment and squeezed the sediment up and in between the lava blocks.

3.3.9.1.2. Graded Rhyolitic Lithic Breccia

In two drillholes (MCD12, 111.0 - 119.0; P8/D4, 194.9 - 199.1 m) a series of graded rhyolitic lithic breccia conformably overly the rhyolitic breccia (Fig 3.27a). Individual beds vary between 0.7 - 3.0 m thick. Each breccia has a basal component composed of angular to subrounded feldspar-phyric and/or feldspar-phyric flow banded rhyolite clasts set within a now silica altered sandy matrix. The basal breccias rapidly grade uphole into sandstone and siltstone. Clasts within the basal breccias are clast supported and attain a maximum size of 70 mm. The contact between individual beds is gradational. In MCD12 the uphole contact (110.0 m) between the uppermost graded lithic breccia and sandstone/siltstone and the overlying rhyolitic breccia is marked by the presence of pale grey stringers ($\leq$10 mm wide) of the underlying siltstone occurring between the rhyolitic clasts. The rhyolitic lithic breccia and graded sandstone/siltstone are interpreted as being the product of debris flow processes. The angularity of the clasts and the similarity in clast composition to the rhyolite breccia indicates that they are locally derived and have not been transported any significant distance where rounding of the clasts would have occurred.

In MCD5 and P8/D4 thermally oxidised rhyolite breccia is present. The presence of thermally oxidised rhyolite indicates that at least locally the rhyolite was exposed above the water and that cooling occurred in a subaerial environment (McPhie *et al.*, 1993).

The alternating intervals of coherent and brecciated rhyolite are interpreted as having been formed by successive lava flows flowing over the autobrecciated tops to earlier lava flows (Fig. 3.28), or alternatively the brecciated intervals may be product of blocks of autobrecciated rhyolite that have foundered into the still flowing lava

The Ellrott Rhyolite is areally restricted and its distribution south of Mount Chalmers parallels the Rockhampton to Emu Park Road. The surface expression of the Ellrott Rhyolite is elongated in approximately an east-west direction. This suggests that the emplacement of the Ellrott Rhyolite was structurally controlled and that the effusive phase of the rhyolite did not flow far.

3.3.9.2. Weakly Feldspar-phyric Siliceous Rhyolite

Mapping in the New Zealand Gully, Sleipner Railway Siding areas, identified a second rhyolite phase intruding into massive feldspar-phyric, pumiceous ± lithic breccias. The rhyolite is composed of euhedral lathe-shaped feldspar crystals (1 - 2 mm, 2 - 5 %) set in an aphyric siliceous groundmass. Small (≤1 mm) spherulites were also observed. Locally the rhyolite is weakly to moderately flow banded, and has no preferred orientation. The contacts between the rhyolite and the feldspar-phyric, pumiceous ± lithic breccia are generally near vertical, but occasional faulted contacts were mapped.

3.3.10. Andesitic Sills and Dykes

Within the Mount Chalmers mine and elsewhere within the Berserker beds, a large number of sub-horizontal andesitic sills and near vertical dykes have intruded the hangingwall stratigraphy. Logging of drill core and face mapping of the Mount Chalmers mine has shown that there are at least three generations of andesite intrusions, based upon their differences in crystal size, colour and the presence or absence of magnetite.

- Type 1: grey to brown coloured, fine to medium grained plagioclase, pyroxene-phyric non-magnetic andesite.
- Type 2: dark brown coloured, fine grained, amygdaloidal magnetic andesite.
- Type 3: almost black, fine grained interlocking acicular plagioclase crystals, magnetic amygdaloidal andesite.

Type 1 andesite is the most common andesite mapped and logged within the field area. It forms sills up to 270.0 m thick (*e.g.* DDHMW6). Isopachs of Type 1 andesite were generated to determine the areal extent of the andesite at Mount Chalmers and whether the massive sulphide mineralisation and andesite are spatially related (Fig. 3.29). The isopachs show that the Type 1 andesite has a "U" shaped distribution. The distribution of the thickest zones of Type 1 andesite is similar to the distribution of the footwall rhyolite (Fig. 3.3). This suggests that both the emplacement of the footwall rhyolite and the Type 1 andesite was controlled by the same structures.

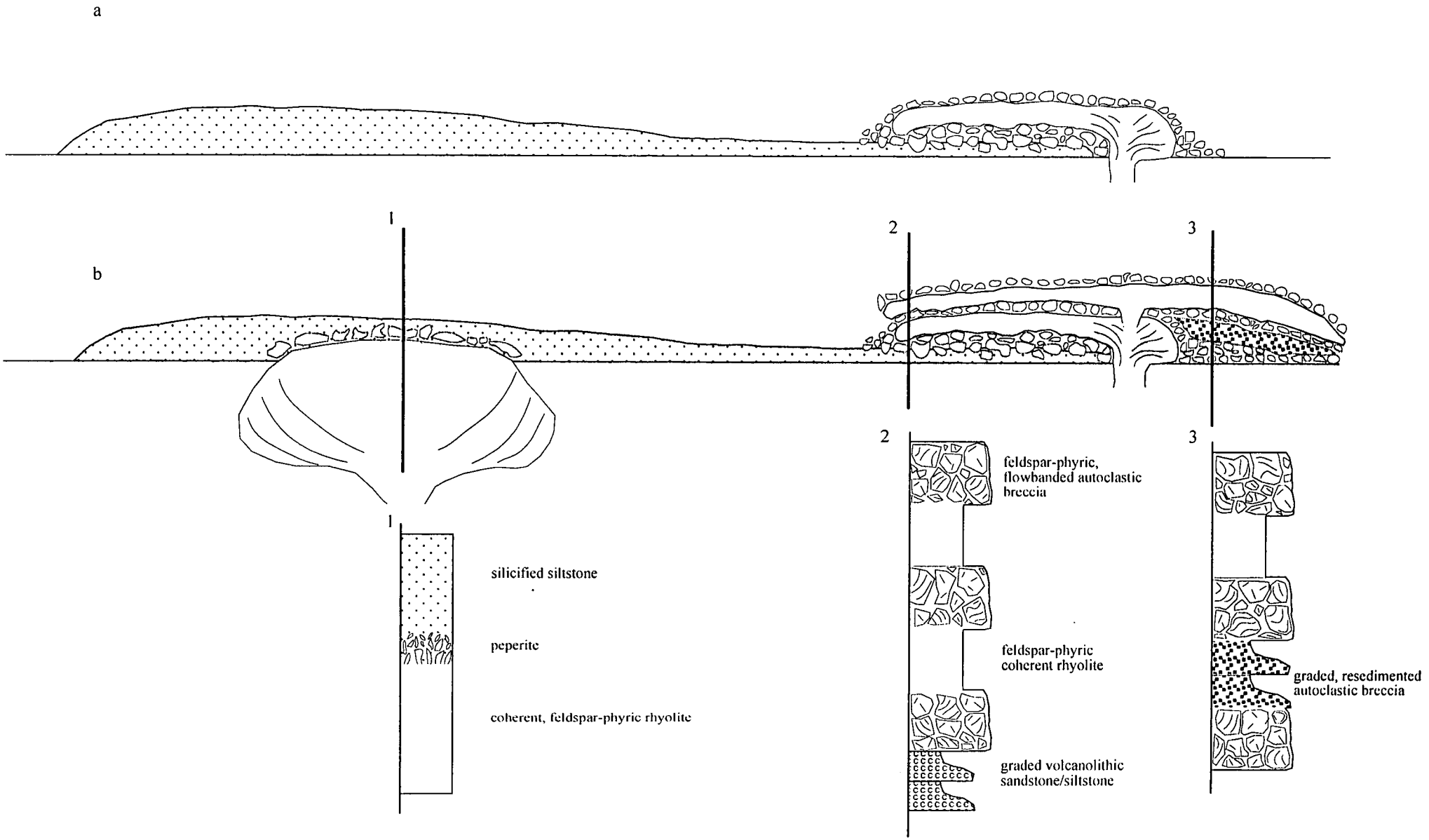

Figure 3.28. Schematic representation of the formation of the volcanic facies that comprise the Ellrott Rhyolite and their relationship with volcanolithic sandstone and siltstone. On each volcanic facies diagram, (1), (2), (3) mark the sites of sections depicted by graphic logs

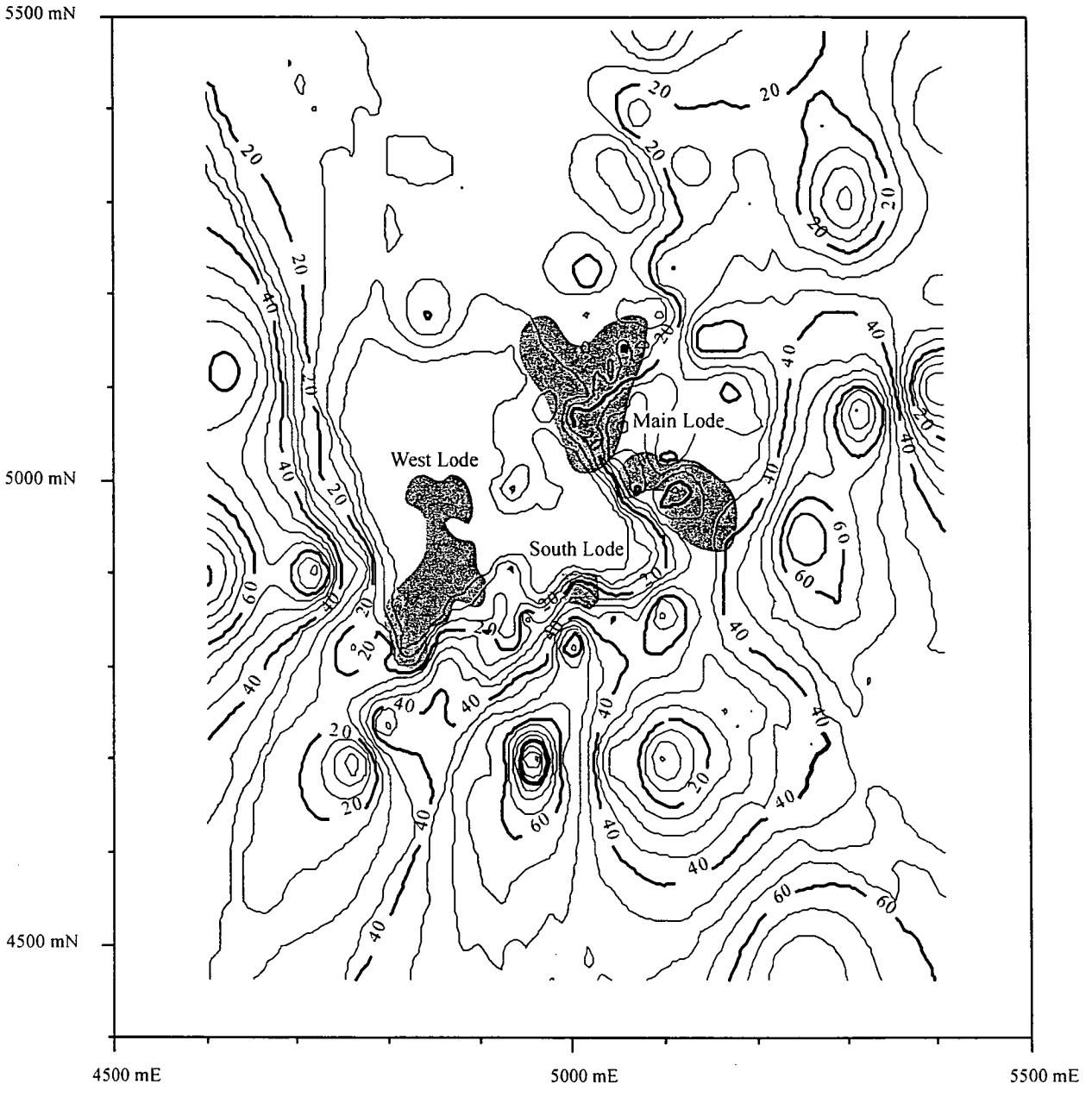

Figure 3.29. Isopachs of Type 1 andesite at the Mount Chalmers mine, with the massive sulphide lenses superimposed. Contour interval = 5 m.

Furthermore, the massive sulphide ore lenses (Fig. 3.29) appear to have been controlled by the same structures that controlled the emplacement of the Type 1 andesite.

In drill hole P1/D1 (Murray's 1) at 162.5 m a contact between two separate Type 1 andesites can be seen. The contact is marked by an inverted "flame" of one andesite intruding into the underlying andesite (Fig. 3.30a). The "flame" of andesite has a chilled margin to it. On the upmost bench on the eastern face of the Mount Chalmers mine a "flame" of feldspar-phyric pumice breccia intrudes into the andesitic dyke, suggesting that the andesite intruded the feldspar-phyric pumice breccia before consolidation of this unit occurred (Fig. 3.30b). Commonly along the contact between the andesite and the pumice breccias an eutaxitic texture is developed and is interpreted to be the result of secondary welding of the pumice breccias adjacent to the andesites Figs. 3.30c). Zones of secondary welding extend up to a few metres away contact with the andesite intrusions. Beyond this narrow zone the pumice breccias are non-welded and show no evidence of hot emplacement. For a more detailed description and discussion on the origin of secondary welding textures in the pumice breccias in the Berserker beds the reader is referred to Chapter 4. Exposed on the two uppermost northern benches of the mine are two andesitic lopoliths. The lowermost one has intruded into the base of the volcanolithic sandstone (Fig. 3.30d), and has caused upward doming of the sandstone and the overlying feldspar-phyric, pumice, lithic breccias. On the upmost bench of the north face of the Mount Chalmers Main Lode open cut the andesite lopolith contains very large (up to 2 x 3m) xenoliths of feldspar-phyric pumice breccia.

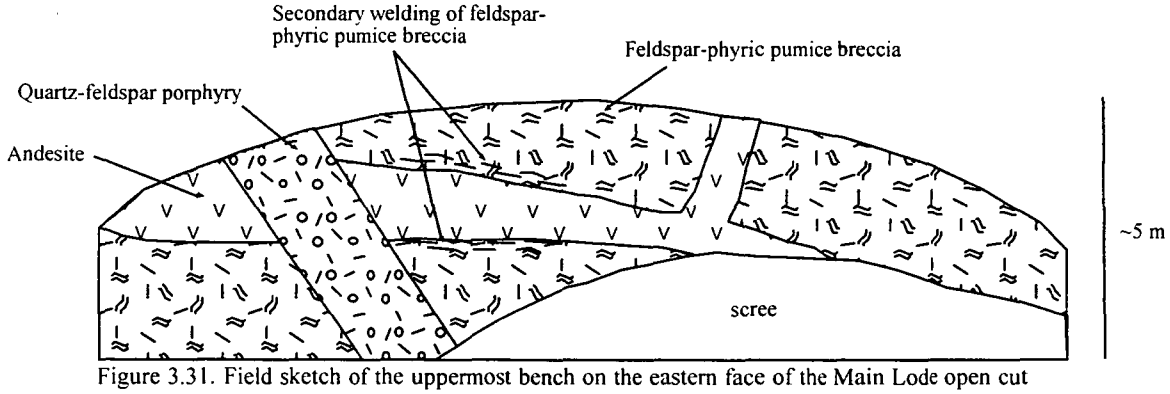

Figure 3.31. Field sketch of the uppermost bench on the eastern face of the Main Lode open cut illustrating the relationship between the feldspar-phyric pumice breccia, andesite and quartz-feldspar porphyry. Adjacent to the contact with the andesite the feldspar-phyric pumice breccia has developed secondary welding texture (see Chapter 4 for a detailed description and discussion on the origin of secondary welding in pumice breccia).

The vertical dykes appear to be a later generation than the Type 1 andesites as they crosscut the sub-horizontal andesites. They are associated with late vertical faults, and consequently are sheared and badly weathered. The vertical dykes are best seen in the pit wall of the Mount Chalmers mine and in the Nerimbera Quarry (AMG 254300 mE : 7410830 mN). Type 3 andesite intrudes both Type 1 and Type 2 andesites. In the Nerimbera Quarry, Type 3 andesite intrudes the quartz-feldspar porphyry, where it has developed a chilled margin adjacent to the contact with the porphyry.

Figure 3.30. Drill core and outcrop examples of contact relationships for Type 1 andesite.

Figure 3 30.a Contact between tow sills of Type 1 andesite. A tongue of the later Type 1 andesite protrudes down into an earlier Type 1 andesite (P1/D3 -162.5 m). Stratigraphic up is to the right of picture.
Figur e3 30.b Flame of feldspar-phyric, pumice "intruding" into the base of Type 1 andesite sill. Mount Chalmers-Main Lode open cut, upper most bench, eastern face.
Figur e3 30.c Development of secondary welding texture within feldspar-phyric pumice breccia. Mount Chalmers-Main Lode open cut, upper most bench, eastern face.
Figure 3 30.d Contact between andesite and overlying volcanolithic sandstone. The contact is marked by the pen (photo is turned on its side). Mount Chalmers- Main Lode open cut, northern benches.


a


b


c
INCH
CM


d

3.3.11. Porphyritic Intrusions

Throughout the Berserker beds, intrusions of quartz-feldspar, feldspar-phyric and feldspar-quartz-biotite porphyry occur. Contact relationships indicate that these intrusions post-date the andesites mapped within the Berserker beds. At a number of localities *e. g.* Mount Chalmers Nerimbera Quarry, and Nerimbera Quarry, the porphyries can be seen to be transecting the Type 1 and Type 2 andesites. Based upon the phenocryst composition, three different porphyries have mapped in the field and logged in drill core:

- a quartz-feldspar porphyry,
- a feldspar -phyric porphyry, and
- a feldspar-quartz-biotite porphyry.

3.3.11.1. Quartz-feldspar Porphyry

Dykes of quartz-feldspar porphyry (QFP) occur throughout the mapped field area and were intersected in a number of mine and regional diamond drill holes. Within the Mount Chalmers mine, a QFP can be seen to be crosscutting the mine stratigraphy at a low angle to the strata. The porphyry is composed of embayed quartz (up to 5 mm) and euhedral feldspar crystals (up to 3 mm), set within a siliceous and/or sericitic groundmass. In the Nerimbera Quarry, a near vertical QFP, up to 12 m wide, is present. The QFP in the quarry is coarse grained, with evenly distributed feldspars (25-30%) having a bimodal grain size (5 - 10 mm and 2 mm). The feldspars have been altered to sericite and/or clay minerals. The quartz grains are glassy, generally rounded and are strongly embayed. Like the feldspars, the quartz grains have a bimodal size distribution (5 - 10 mm and <2 mm).

In Nankin Creek the QFP has intruded into a feldspar-phyric, lithic pumice breccia. The contact relationship between the pumiceous breccias and the QFP is chaotic, reminiscent of peperite texture. This implies that the pumiceous breccia was still locally unconsolidated at the time of the QFP intrusion.

3.3.11.2. Feldspar-phyric Porphyry and Feldspar-quartz-biotite Porphyry

These two porphyry types are only known from drill core and limited outcrop exposures in road cuttings. The feldspar porphyry occurs as narrow intrusions, and is composed of large (<6 mm) euhedral feldspar crystals set in an aphyric sericitic groundmass.

The feldspar-quartz,-biotite porphyry is composed of lathe shaped feldspar crystals (5 x 2 mm, 10-15%), glassy rounded quartz grains (≤5 mm, 5-10%) and scattered biotite booklets (2%). The groundmass is very fine grained and siliceous.

3.3.12. Serpentinites

In the Rockhampton area two serpentinite bodies occurs, the Milman and Cawarral Serpentinite Belts (comprise part of the Marlborough terrane). Murray (1968,1969 and 1974) identified the original rock type as an harzburgite. Most of the serpentinites are massive and retain an harzburgitic texture, but sheared and foliated serpentinites are also present (Willmott *et al.* 1986). The serpentinites occur as a series of discontinuous bodies that parallel the Tungamull Fault. A serpentinite body has recently been mapped at the Red Hill Quarry near Kawana, occurs adjacent to the Parkhurst Fault. The ultramafic rocks are considered to be fragments of oceanic crust and mantle material, which were emplaced by thrusting during deformation and upthrusting of the continental slope deposits of the Wandilla terrane in the middle to late Permian (Willmott *et al.* 1986).

3.4 STRUCTURE

North-northwest trending open upright folds were formed during the middle to late Permian orogeny (Day *et. al.*, 1983, Donchak and Holmes, 1991). Associated with the folding was the development of a weak although not pervasive northerly striking vertical cleavage. In the Tungamull area, south of the Mount Chalmers mine, two major northwest striking faults (Boto's Fault and Wood's Shaft Fault – Plates 2, 4, 3 and 5) were interpreted from aeromagnetic and gravity data (Hunns, 1993). These two faults parallel the Tungamull Fault to the east. Based upon regional isopachs of the andesites, the Boto's and Wood's Shaft faults are interpreted as having structurally controlled the intrusion of the andesites (Hunns, 1993). A large east-northeast-striking fault at the mouth of the Fitzroy River appears to have displaced the Berserker beds. It has probably undergone movement in the Quaternary, as it is defined by the present coastline (Murray, 1975).

At Mount Chalmers the predominant structure is a north-northwest-trending broad syncline that has produced gentle dips. Steep dips occur adjacent to faults, often associated with the mineralisation and at the contacts with near vertical andesitic dykes. Taube and van der Helder (1983) argued that the succession around the massive sulphide ore lenses forms a structural dome associated with a horstblock . A slaty cleavage is locally developed within the sedimentary rocks, particularly the black mudstones, and along fold hinges.

3.5. PALAEONTOLOGY AND PALAEOENVIRONMENTAL DEPOSITIONAL SETTING FOR THE VOLCANOLITHIC SANDSTONES AND SILTSTONES

Numerous localities where marine body fossils occur are known within the Berserker beds (*e.g.* several of these localities occur within a 4 km radius of the Mt. Chalmers mine (Plate 1). Trace fossil assemblages are also widespread within the Berserker beds (*e.g.* Sainty, 1992). Significantly, trace fossils occur at the same stratigraphic level as the Mount Chalmers massive sulphide ore lenses, both in outcrop (Sainty, 1992) and in diamond drill core (MC23: 46.0 m; MC24: 154.7 m; MC47: 56.3 m and MC70: 174.6 m). The trace fossils in MC23 occur within 20 m of the Main Lode massive sulphide ore lens. The presence

of both trace fossils and body fossils at, and in, the vicinity of the Mount Chalmers massive sulphide deposit provides an opportunity to constrain the depth of seawater that an ancient VHMS deposit has formed in.

Body fossils and microfossils (principally foraminifer) have been reported from sedimentary rocks immediately overlying or hosting the Japanese Kuroko VHMS deposits (*e.g.* Hatai and Kotaka, 1969 *in* Motegi, 1974; Kajiwara, 1970; Hayakawa *et al.*, 1974; Matsukama, 1974; Motegi, 1974; Oshima *et al.*, 1974; Sato and Kusaka 1974; and Tanaka *et al.*, 1974). The presence of fossils within the immediate vicinity of ancient VHMS deposits is not widely known. However, a number of occurrences of fossilised tubeworms and other fauna have been reported from sites where the fossils have an intimate association with semi-massive to massive sulphide mineralisation from a variety of mineralisation styles (Table 3.2). The inferred palaeoenvironmental setting for the sulphide deposits associated with VHMS style of mineralisation are deep-water, high temperature vents, comparable to modern day deep water, high temperature vents communities (*e.g.* see van Dover, 1995 for Mid-Atlantic Ridge descriptions; Hessler and Kaharl, 1995 for an overview of deep-sea hydrothermal vent communities).

The presence of both trace fossils and body fossils within the Berserker beds provides an important basis for defining the palaeoenvironmental setting for the deposition of the Berserker beds and for reconstructing their depositional processes.

3.5.1. Body Fossils Within the Volcanolithic Siltstone Facies

Body fossils have been found at numerous localities throughout the Berserker beds. The fossils mainly comprise brachiopods, gastropods, bivalves and bryozoans (Table 3.3). The degree of reworking of the fossils appears to be minimal as in the case of the bivalves both valves are still co-joined. The presence of co-joined valves indicates that the bivalves are predominantly in their life position and have undergone little if any reworking (Fig 3.32 c,d). This is especially important for the brachiopods, as during life the two valves are held together by two pairs of muscles, that upon death relax and therefore are no longer able to hold the two valves together. Consequently, any reworking of the dead brachiopod will result in the two valves becoming separated. Further evidence for limited or minimal reworking of the fossils is provided by the retention of fine spines on many of the brachipods, the lack of abrasion (*e.g.* broken shells) and the preservation of entire blastoid cups. The age of the assemblage is late Early Permian (Baigendzinian stage of Waterhouse 1976; *i.e* Sakmarian to Artinskian ~280 - ~265 My). Table 3.3 lists the currently known fossil localities and the various phyla and associated species found at each of the localities.

Table 3.2. Fossil faunal assemblages associated with ancient hydrothermal ore deposits and the inferred palaeoenvironment for formation of the deposit.

Location [1]Reference(s)	**Fauna**	**Mineralisation** *Style*	**Proximity to Mineralisation**	**Inferred Palaeoenivronment**
[1]Silvermines, Ireland	tubeworms	hydrothermal pyrite mounds	occur within the pyrite mounds	brine pool dominated by hypersaline Carboniferous seawater
[2]Cyprus deposits	tubeworms	massive sulfide within ophiolite *Cyprus-type?**	within and near the top of the massive sulfide	compared to similar modern hot springs on the East Pacific rise and the Juan de Fuca Ridge
[3]Samail Ophiolite, Oman	tube worms			
[4]Tynagh, Ireland	tubeworms	pyrite mounds & chimneys on top of laminated sulfides *sedimentary exhalative*	associated with hydrothermal sulfide chimneys on top of laminated sulfides	relatively shallow intracontinetal basin
[5]Red Dog, Alaska	tubeworms	*sedimentary exhalative*	silica masses beneath the massive sulfide	
[6]Urals	monoplacophoran molluscs, inarticulate brachiopods, vestimentiferan wormtubes &possible polychaete worms	VHMS deposit	fossils are *in situ* and occur at the top of the massive sulphide	deep-water, high temperature vent, comparable to modern day high temperature vent communities
[7]Port au Port Peninsula, Newfoundland	fossil tube fragments and brachiopods	gossans & sulfide veins within a carbonate mound, *Mississippi Valley style*	fossil tubes occur within carbonate mounds	shallow -marine (≤100 m) low temperature (<200° C) hydrothermal vent community
[8]Figueroa massive sulfide, San Rafael Mts., California	vestimentiferan wormtubes; brachiopods, gastropod filamentous Fe-silica bacteria	massive sulfide associated with basalts of probable OIB or MORB derivation *Cyprus-type?**	occur within the silicified core of the massive sulfide deposit	deep-water, high temperature vent, comparable to modern day high temperature vent communities

* my interpretation of the mineralisation style

References: [1]Boyce *et al.* (1983); [2]Oudin and Constaninou (1984); [3]Haymon *et al.* (1984), [4]Banks (1986), [5]Moore *et al.* (1986); [6]Kuznetsov *et al.* (1991); Zaikov *et al.* (1995); Little *et al.* (1997), Kuznetsov *et al.* (1998); [7]von Bitter *et al.* (1990); [8]Little *et al.* (1999).

Table 3.3. Body fossil sites within the Beserker beds and associated species. Data from: Armstrong *et al.* (1967), Crockford (1945), Hawkins and Whitcher (1962), McKellar (1969), McKellar *et al.* (1970) and Sainty (1992).

Location AMG Coordinates	Phylum(Class/Subclass)	Species
Nerimbera Quarry 252350mE : 7410850mN	Bryozoa	*Cladochonus* sp. *Fenestella cf. canthariformis* *Polypora woodsi*
	Brachiopoda	*Lissochonetes yarrolensis* *Strophalosia preovalis* *Linoproductus* sp. *Neospirifer* sp. *Taeniothaerus subquadratus* *Anidanthus springsurensis* *Ingellarella profunda*
	Mollusca	*Streblopteria* sp.
	Echinodermata	*Austroblastus whitehousei* gen.et sp. nov
Lake's Creek Quarry 252228mE : 7410686mN	Brachiopoda	*Strophalosia preovalis* *Taeniothaerus subquadratus* *Anidanthus springsurensis* *Ingellarella profunda* *Terrakea sp. cf. T. pollex*
	Bryozoa	*Fenestrellina canthariformis* *Fenestrellina granulifera* *Fenestrellina aspratilis* *Polypora woodsi* *Polypora virga* *Minilya duplaris*
Mt. Nicholison Siding 259044mE : 7418777mN	Brachiopoda	*Anidanthus springsurensis* *Echinolosia preovalis* *Ingellarella? Plana* *Trigonatreta*
	Bryozoa	*Stenopora sp.*
	Mollusca (Gastropoda)	*cf. Pseuobaylea* sp. *Warthia* sp. *Unidentified internal moulds*
	Mollusca (Bivalvia)	*Deltopecten (Squameuliferipecten)* sp. *?Etheripecten sp.* *Glyptoleda glomerata* *?Platyschisma* sp.
Frenchman's Creek	Mollusca	*Neocrimites* sp. cf. *N. meridionalis*
Mt. Chalmers	Brachiopoda	*Strophalosia preovalis* *Taeniothaerus subquadratus* *Anidanthus springsurensis* *Ingellarella sp.* *Spirifrellina sp.* *Spirifer cf. tasmaniensis*
	Bryozoa	*Thamnapora* *Fenestella* *Protoretepora* *Polypora*

Figure 3.32. Representative examples of trace and body fossils from within the Berserker beds.

Figure 3.32a Facies C2.1 turbidite dominated by *Lophoctenium* (upwardly branching trace fossil) with scattered *Teichichnus* and *Planolites*. Mount Chalmers - Main Lode open cut, northern benches
Figure 3.32b Finely laminated siltstone from Facies C2.1 with scattered *Planolites* and *Rhizocorallium* transecting the sediment. Emu Park Road (AMG 255150 mE : 7410200 mN)
Figure 3.32c *Echinalosia preovalis waricki* Mount. Nicholson Siding
Figure 3.32d *Taeniothaerus* n. sp (external dorsal valve). Mount. Nicholson Siding


a


c

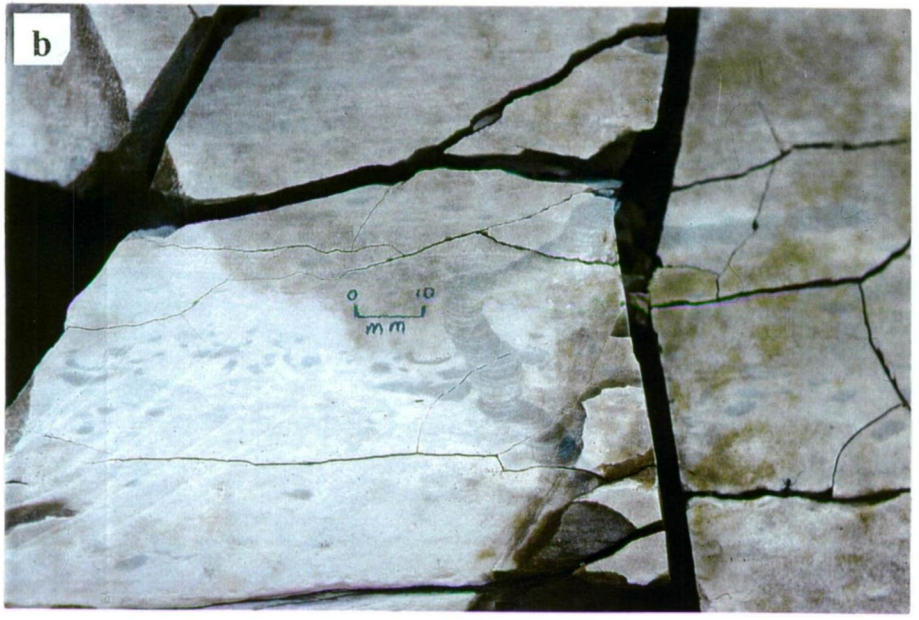
b
0
10
mm


d

3.5.2. Trace Fossils Within the Volcanolithic Sandstone Facies

Traces are structures produced in rocks, sediments and grains by the life processes of organisms. Trace fossils are the fossilised equivalents of those structures (Bromley, 1990). Trace fossils generally include:

- footprints, tracks and burrows in uncemented sediments
- raspings, borings and etchings in rigid substrates
- faecal pellets

Evidence for bioturbation (endobenthic activity re-orders or "unmixs" the sediments by introducing new structures, which may be preservable as discrete trace fossils - Bromley, 1995) within the volcanolithic sandstone of the Berserker beds is relatively common and widespread. Trace fossils were found within volcanolithic sandstone that hosts the massive sulphide at Mt. Chalmers (MC23, MC24, MC47, MC70) and as far away as the junction of the Bruce Highway and the Rockhampton-Yeppoon Road (AMG 247100 mE : 7420100 mN). In contrast to body fossils, trace fossils provide an unequivocal *in situ* record of animal activities within or upon the substrate (Johnson and Baldwin, 1986 and references therein). The trace fossils are mainly temporary fodinichnia (feeding traces) structures and comprise mainly *Teichichnus*, *Planolites (Fig 3.32b)*, *Palaeophycus (Fig 3.32b)*, *Phycosiphon* and *Lophoctenium (Fig 3.32d)* with scattered *Rhizocorallium* and *Zoophycus (Fig 3.32b)* burrows. The trace fossils have a restricted faunal diversity, and may be assigned to the *Cruziana* ichnofacies (Sainty, 1992 and references therein).

The degree of bioturbation varies from very little to almost complete homogenisation of the sediments. The degree of bioturbation can be expressed quantitatively by the Bioturbation Index (Taylor & Goldring, 1993). For the volcanolithic sandstone and siltstone, this varies between 0 to 5 or 6 (Table 3.4).

Table 3.4. Bioturbation Index where each grade is described in terms of the sharpness of the primary sedimentary fabric, burrow abundance and amount of burrow overlap (After Taylor, in Taylor & Goldring 1993).

Grade	Bioturbated %	Classification
0	0	No bioturbation.
1	1-4	Sparse bioturbation, bedding intact, few discrete traces and/or escape structures often common
2	5-30	Low bioturbation, bedding distinct, low trace density, escape structures often common
3	31-60	Moderate bioturbation, bedding boundaries sharp, traces discrete, overlap rare
4	61-90	High bioturbation, bedding boundaries indistinct, high trace density with overlap common
5	91-99	Intense bioturbation, bedding completely disturbed (just visible), limited reworking, later burrows discrete
6	100	Complete bioturbation, sediment reworking due to repeated overprinting

The percentage bioturbation values should be used as a guide and not as an absolute class division.

3.5.3. Palaeoenvironment for the Deposition of the VHMS Deposits - Mount Chalmers

The presence of widespread body and trace fossil assemblages within the Berserker beds can provide an accurate indication of the palaeoenvironment in which the volcanolithic sandstone facies was deposited. Trace fossils have great palaeoecologic utility because they are temporally and spatially, found in *situ*, and are largely the record of animal behaviour and response, making them ideal indicators of environmental conditions (Rhoads, 1975). Table 3.3 lists the body faunas that have been reported from the Berserker beds. It can be seen that Brachiopoda is by far the most dominant phylum. The fossil assemblage and its mode of preservation are typical of a shallow shelf (near wave base) sand and silt environment as defined by Runnegar and Campbell (1975) for the Early Permian of eastern Australia. In this environment, numerous epifaunal and infaunal bivalves, articulate brachiopods, gastropods, bryozoans, sponges, solitary rugosan and branching tabulate corals and echinoderms were represented. More commonly, many brachiopods and a few molluscs dominated this environment (Runnegar and Campbell, 1976). The invertebrate marine fauna of eastern Australia is composed of littoral and shallow-water forms, and is essentially a cold-water assemblage, as suggested by the absence of reef-forming corals and by the abundance of bryozoans (fenestrellinids, stenoporids) and rugose corals (zaphrentids) (David, 1950).

Waterhouse (*writ. comm.* in Sainty, 1992) suggested that the body fossil fauna indicated water depths of 50 to 300 m's, with a 100 to 200 m depth most likely. Crouch and Parfrey (1998) concluded that the fauna of brachipods and molluscs indicate water depths between 30 to 50 m, with a maximum depth of 200 m. The presence of *Eurydesma* specimens within the Berserker beds also provides an accurate estimate of water depth. *Eurydesma* was an opportunistic species that colonised sublitooral substrates that ranged in depth from near low water to below storm wave base (Runnegar 1979b).

The trace fossil assemblage belongs to the *Cruziana* ichnofacies (Fig 3.33), characteristic of water depths between daily wave base and storm wave base, in low to moderate energy regimes (Fig. 3.33 and 3.34); Frey and Pemberton, 1984; 1985). *Cruziana* is the characteristic ichnofacies for shelf environments, particularly where it experiences moderate to high-energy conditions (Johnston and Baldwin, 1986). Marine ichnofacies are not intended to be palaeobathometers, rather, they are archetypical facies models based upon recurring ichnocoenoses (Frey and Pemberton 1984, 1985; 1987). Some authors have noted occurrences of the *Cruziana* ichnofacies in settings outside the zone outlined in the above model. *Cruziana* may appear on the proximal parts of deep-sea fans (Acenolaza and Durand, 1973; Crimes, 1977), and may reach all the way to the intertidal zone or even the shoreline (Frey *et al.*, 1987). However, the trace fossil and body fossil faunas of the Berserker beds have been found in intimate association with each other at a number of localities. It can therefore be concluded that the faunal assemblages inhabited a shallow marine (at or near wave base, 30 - 50 m., and maximum depth of 200 m) palaeoenviroment during the deposition of the volcanolithic sandstones and siltstones of the Berserker beds.

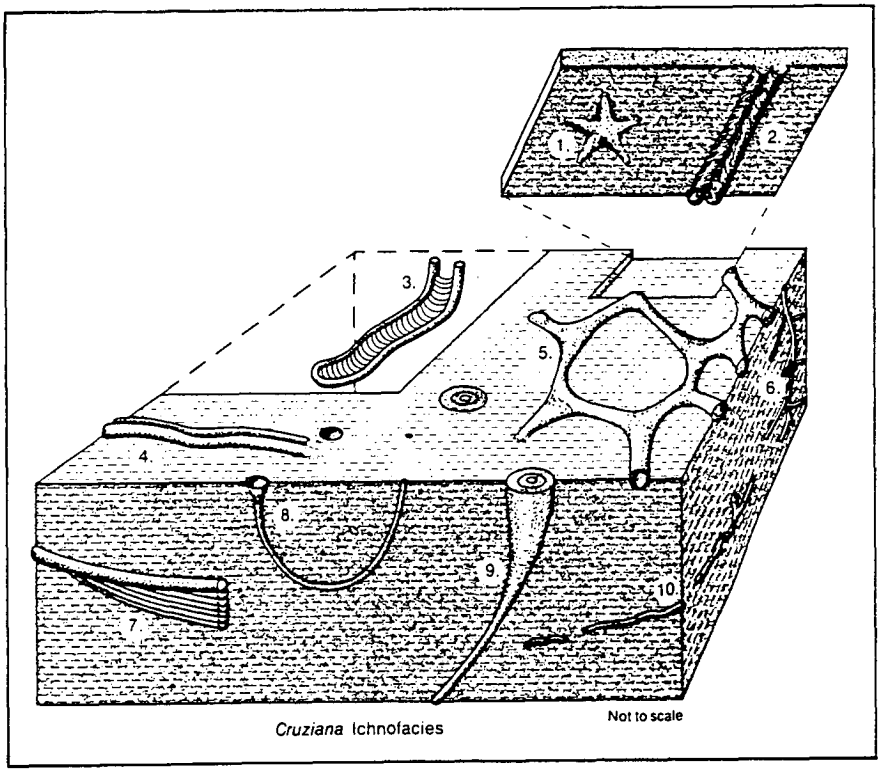

Figure 3.33 Diverse trace fossil association characteristics of the *Cruziana* ichnofacies 1) *Asteriacitses* 2) *Cruziana*; 3) *Rhizocorallium*; 4) *Aulchnites*; 5) *Thalassinoides*; 6) *Chondrites*; 7) *Teichichnus*; 8) *Arenicolites*; 9) *Rosselia*; 10) *Planolites* (From Frey and Pemberton, 1984).

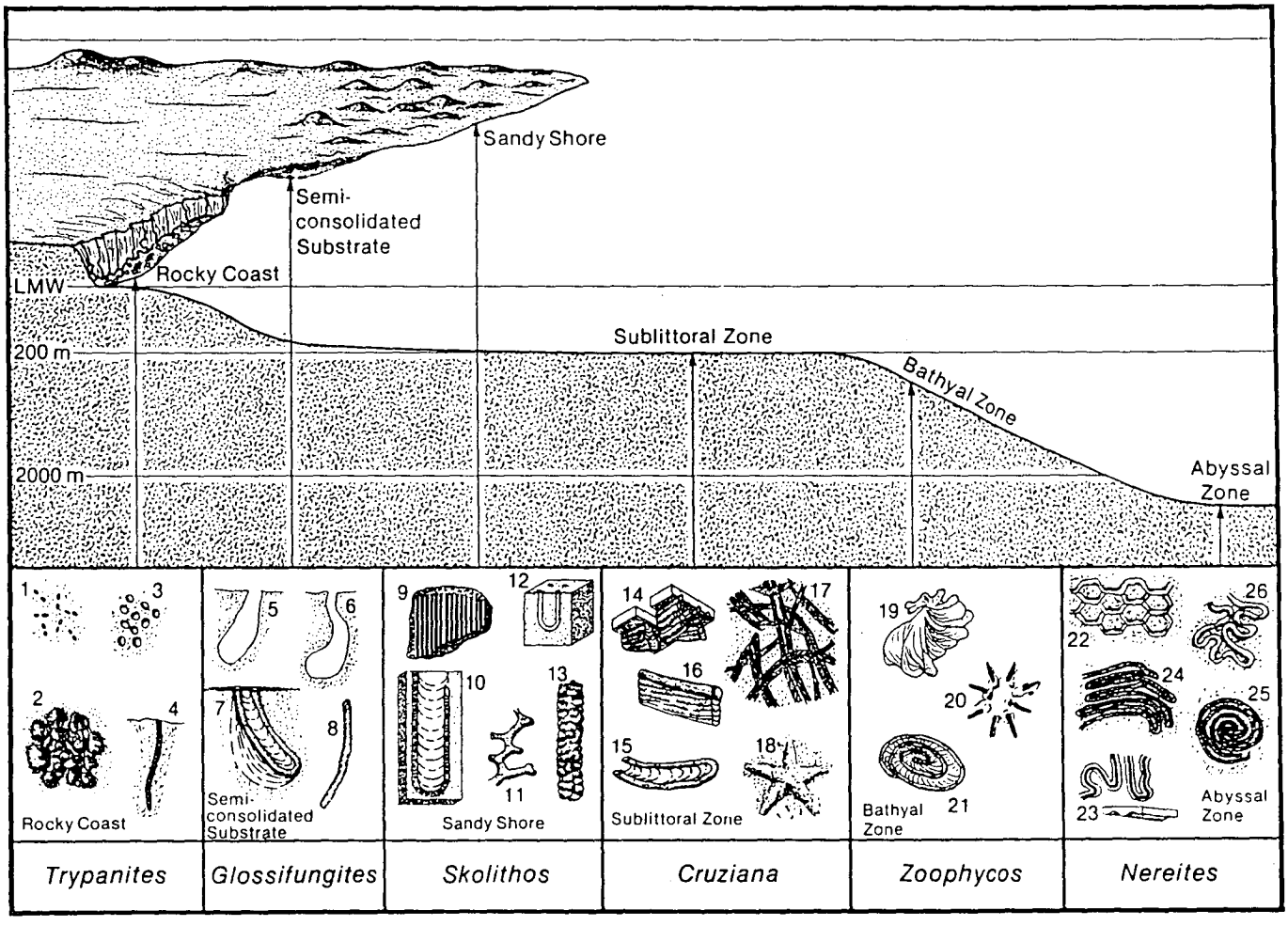

Figure 3.34 Recurring marine ichnofacies set in a representative, but not exclusive suite of environmental gradients. Local physical, chemical, and biological factors ultimately determine which traces occur at which suites. Typical trace fossils for the *Cruziana* ichnofacies include: 14) *Phycodes*; 15) *Rhizocorallium*; 16) *Teichichnus*; 17) *Crossopodia* and 18) *Asteriacites* (From Frey and Pemberton, 1984).

3.5.4. What Does Shallow-marine Actually Mean?

Recently, the concept of shallow-marine VHMS deposits has appeared in the economic geological literature (*e.g.* Sainty, 1992; Allen *et al.*, 1997; Hannington *et al.*, 1997). Also within the economic geological literature, there has been the frequent mentioning of shallow-marine hydrothermal vents and shallow-marine VHMS deposits. Nevertheless, there has been no real definition of what shallow actually means. So, where does "shallow" end and "deep" start in the marine environment? Oceanographers have divided the earths' oceans into four zones, based upon the water depth (Bates and Jackson, 1995):

- littoral zone, zone between high and low tide;
- neritic zone, between low tide and 100 fathoms (600 feet/183 metres);
- bathyal zone, 200 to 950 metres;
- abyssal zone, > 950 metres.

Johnson and Baldwin (1996) defined a shallow sea as having water depths of less than 200 metres. Walker and Plint (1992) defined shallow marine in general terms, as including environments affected by waves, including modern shelves, epeiric seas and the shallow part of foreland basins. In their book on deep marine environments Pickering *et al.* (1989) defined deep marine as occurring where sedimentation occurs below storm wave base (*i.e* ~200 m). This maximum water depth (~200 metres) for defining a shallow-marine environment also corresponds to the approximate maximum water depth of the disphotic zone. That is the zone where penetration of light is so low as to severely limits the rate of photosynthesis (Bates and Jackson, 1995). Therefore, in this thesis the term "shallow-marine" is used as being at a depth not exceeding the neritic zone *i.e* ~200 metres.

3.6. VOLCANIC FACIES ARCHITECTURE

The reconstruction of the facies architecture of the Berserker beds in the vicinity of the Mount Chalmers mine is based upon textural interpretation and volcanic facies analysis of seven drill cross sections from the Mount Chalmers mine (Figs. 3.35a, b, c, d, e, f, g) and six regional cross sections (Plates 2 - 7). The massive sulphide ore lenses at Mount Chalmers are located on the flanks of small rhyolite domes and are overlain by a rhyolitic to andesitic volcano-sedimentary succession. The total stratigraphic thickness of the Berserker beds in the vicinity of the Mount Chalmers mine is not known due to the generally flat lying stratigraphy.

Outside of the Mount Chalmers mine, the footwall lithologies are not exposed due to the generally flat lying stratigraphy. In fact, the footwall stratigraphy is only known from a limited number of diamond drill holes. At the Tungamull prospect, only MCD10 managed to penetrate into the equivalent of the footwall rhyolite at Mount Chalmers.

Taube and van der Helder (1983) indicated that the mapped faults at Mount Chalmers all have steep dips and are normal faults. Normal faults exposed in the Mount Chalmers open cut are either steeply dipping or have near vertical dips. This also true of faults mapped elsewhere in the vicinity of Mount Chalmers *i.e.* they are either have a near vertical dip or are steeply dipping and all are normal faults. Consequently all of the interpreted faults shown on the geological and alteration cross sections are assumed to be vertical faults.

The relationship between the footwall lithologies is largely obscured by alteration or broken or missing core (due to sampling for assay purposes). The footwall lithologies include a number of lithologies, namely:

- altered and mineralised volcanolithic sandstone and siltstone
- graded, sericite-silica-chlorite-altered polymictic breccia,
- feldspar-phyric, lithic-pumice breccia,
- coherent to autobrecciated feldspar-phyric rhyolite (footwall rhyolite)
- silica-chlorite altered dacitic lithic breccia

At Mount Chalmers, the footwall is dominated by the footwall rhyolite. The total thickness and distribution of the rhyolite is not known as a large number of drill holes failed to penetrate deep enough into the footwall volcano-sedimentary stratigraphy. However, structure contours to the top of the footwall rhyolite (generated from the available drill holes) show that the rhyolite forms a number of small domes that are surrounded by resedimented autoclastic rhyolitic breccia and is therefore considered to be proximal facies. The footwall rhyolite overlies the silica-chlorite altered dacitic breccia. The dacitic breccia appears to be areally extensive as it was intersected in WS7 at the Woods Shaft prospect, but is only known from a limited number of drill holes.

Regionally the reconstruction of the facies architecture has not been complicated by either the open folds or interpreted normal faults within the Berserker beds. However, facies reconstruction is limited by the generally flat-lying stratigraphy and lack of continuous lateral and vertical exposures of the footwall and hangingwall. Reconstruction of the regional facies architecture has therefore relied on scattered outcrops and widely spaced exploration drill holes. At Mount Chalmers, original relationships among the various hangingwall lithologies have been complicated by extensive normal faults and by the presence of andesite and quartz-feldspar porphyry intrusions, both of which have displaced large sections of the hangingwall.

The hangingwall stratigraphy at Mount Chalmers is dominated by feldspar-phyric, pumice breccia and feldspar-phyric, pumice-lithic breccia. South of Mount Chalmers and based upon the drill hole intersections these deposits are areally extensive and laterally continuous for distances up to approximately 1 km. The clasts in the feldspar-phyric, pumice-lithic breccia. have a varied provenance. These breccias are interpreted to have been derived from pyroclastic eruptions, however they show no signs of hot emplacement and their internal organisation is consistent with their emplacement from syn-eruptive deposits.

Geological Legend for Figures 3.35a - 3.35g


Gossan


Massive sulphide


Semi-massive sulphide


Disseminated sulphides

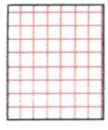
Hematite

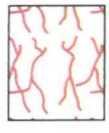
Stringer vein mineralisation

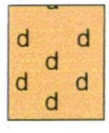

Massive dolomite alteration


Undifferentiated alteration facies

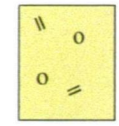
Quartz-feldspar porphyry


Type 1 Andesite

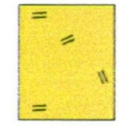
Feldspar-phyric rhyolite


Autobrecciated feldspar-phyric rhyolite

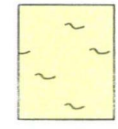
Feldspar-phyric pumice breccia


Feldspar-phyric, lithic pumice breccia


Quartz-feldspar porphyry


Volcanolithic siltstone

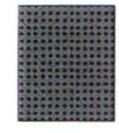
Volcanolithic sandstone


Graded volcanolithic conglomerate facies

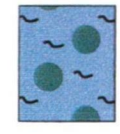
Chlorite-silica altered feldspar-phyric pumice breccia

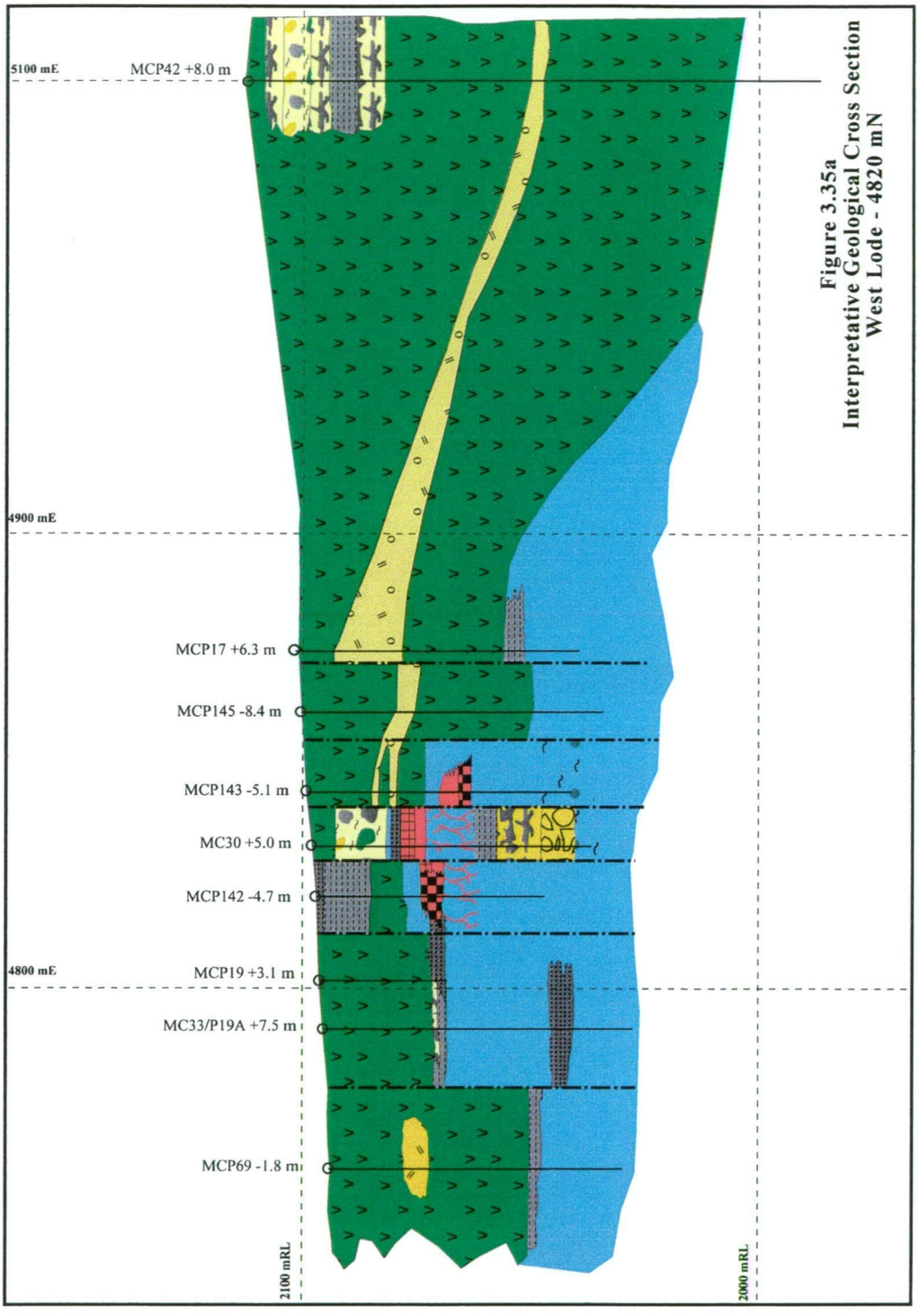

Figure 3.35a
Interpretative Geological Cross Section
West Lode - 4820 mN

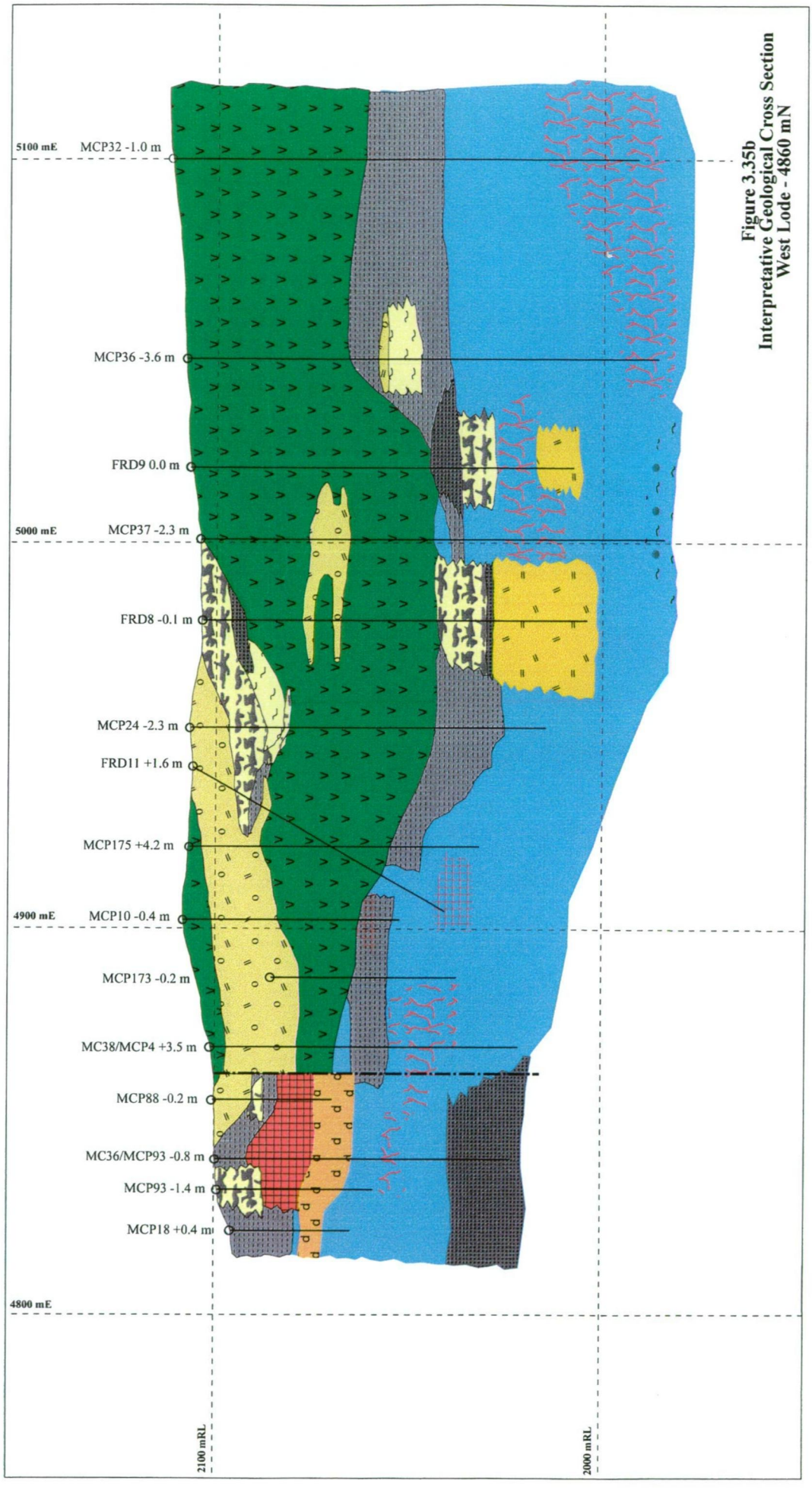

Figure 3.35b
Interpretative Geological Cross Section
West Lode - 4860 mN

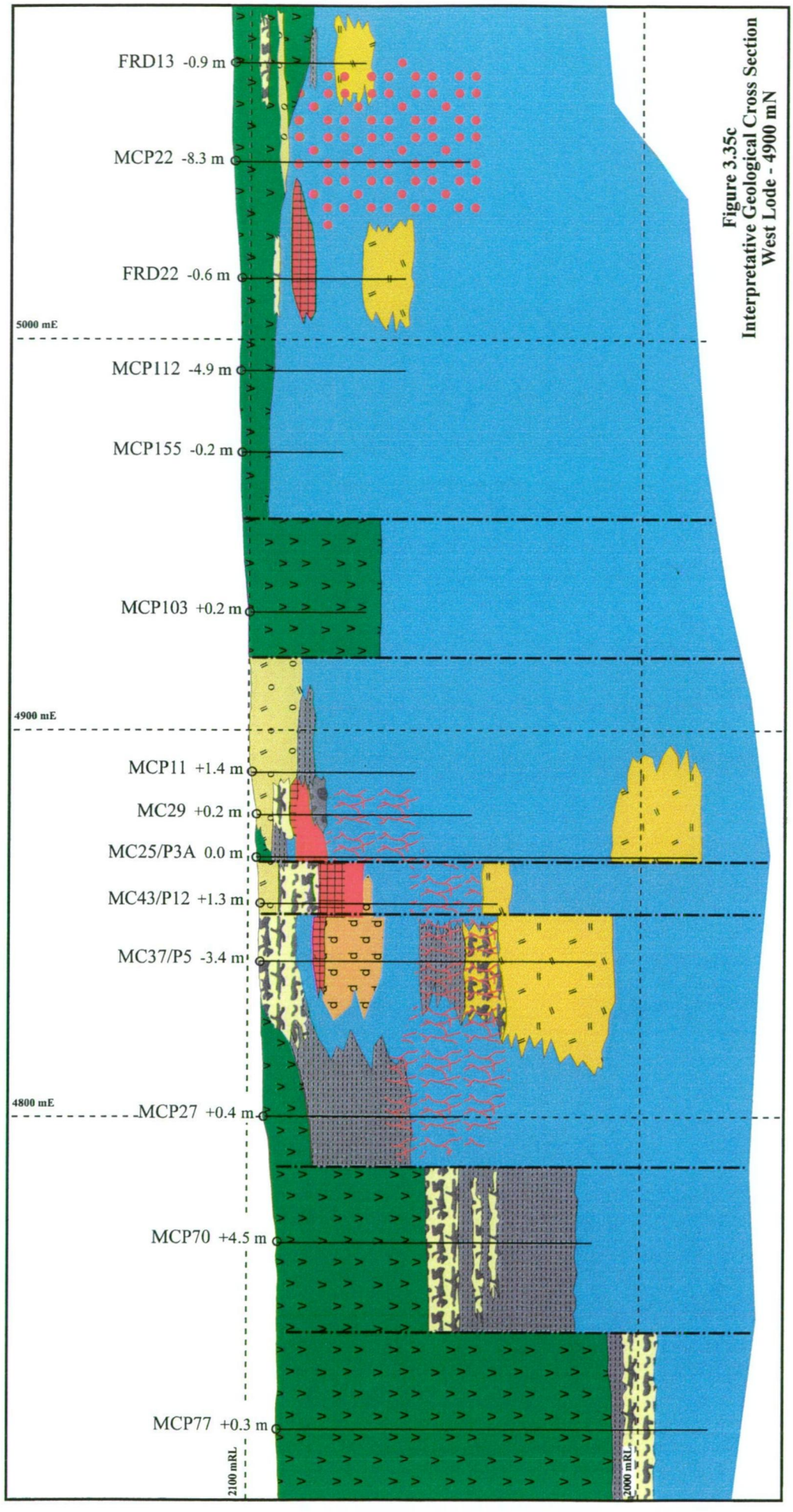

Figure 3.35c
Interpretative Geological Cross Section
West Lode - 4900 mN

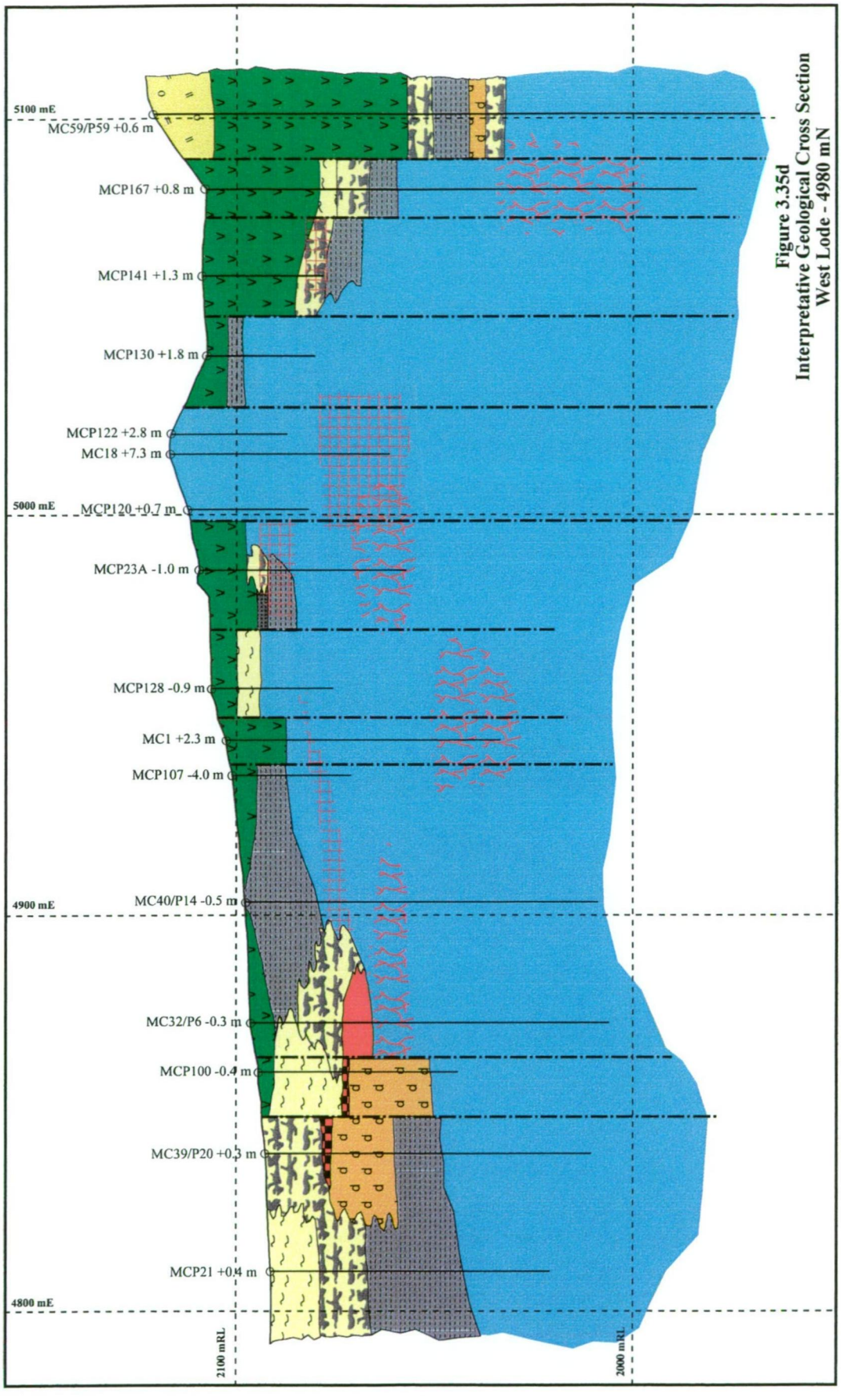

Figure 3.35d
Interpretative Geological Cross Section
West Lode - 4980 mN

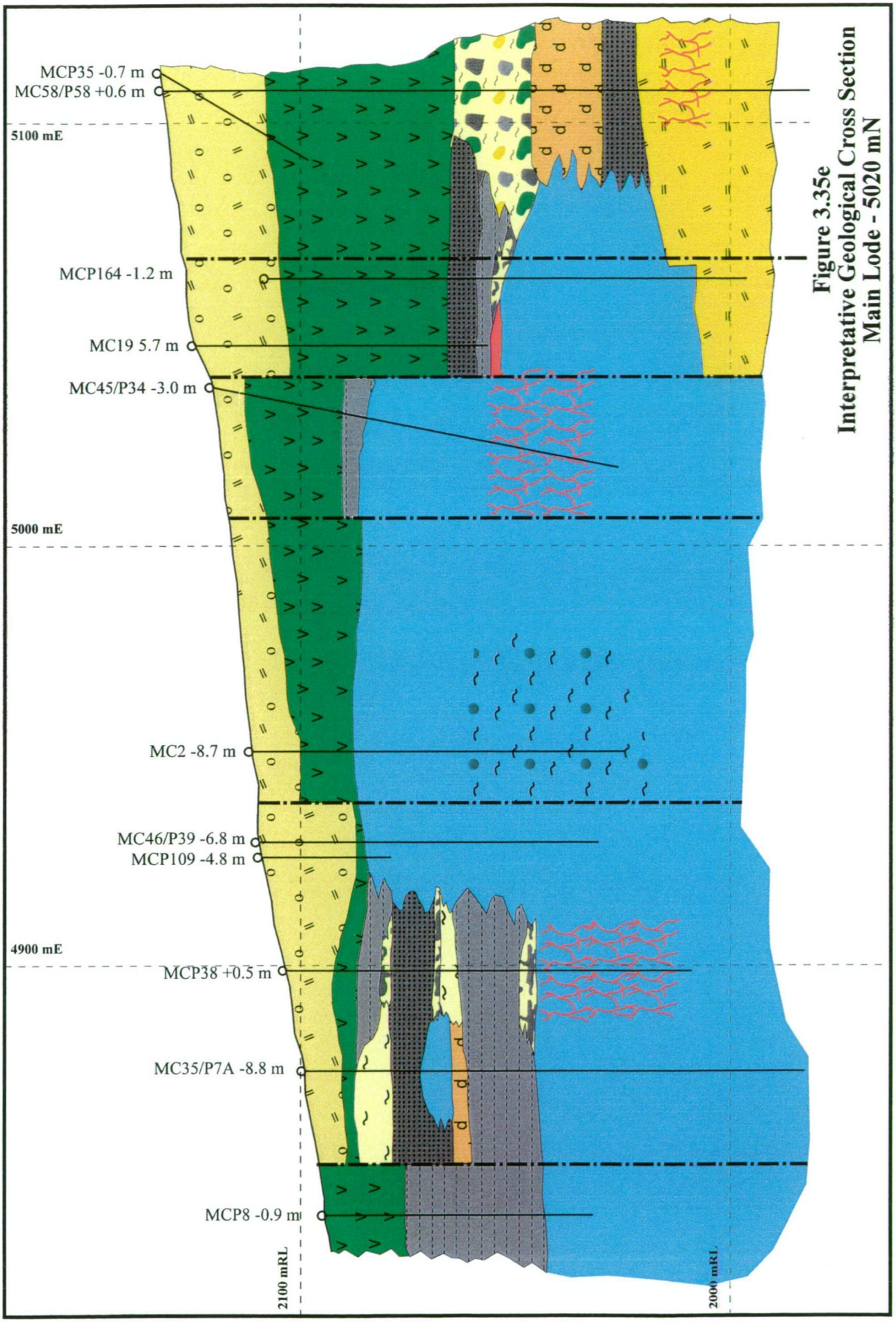

Figure 3.35e
Interpretative Geological Cross Section
Main Lode - 5020 mN

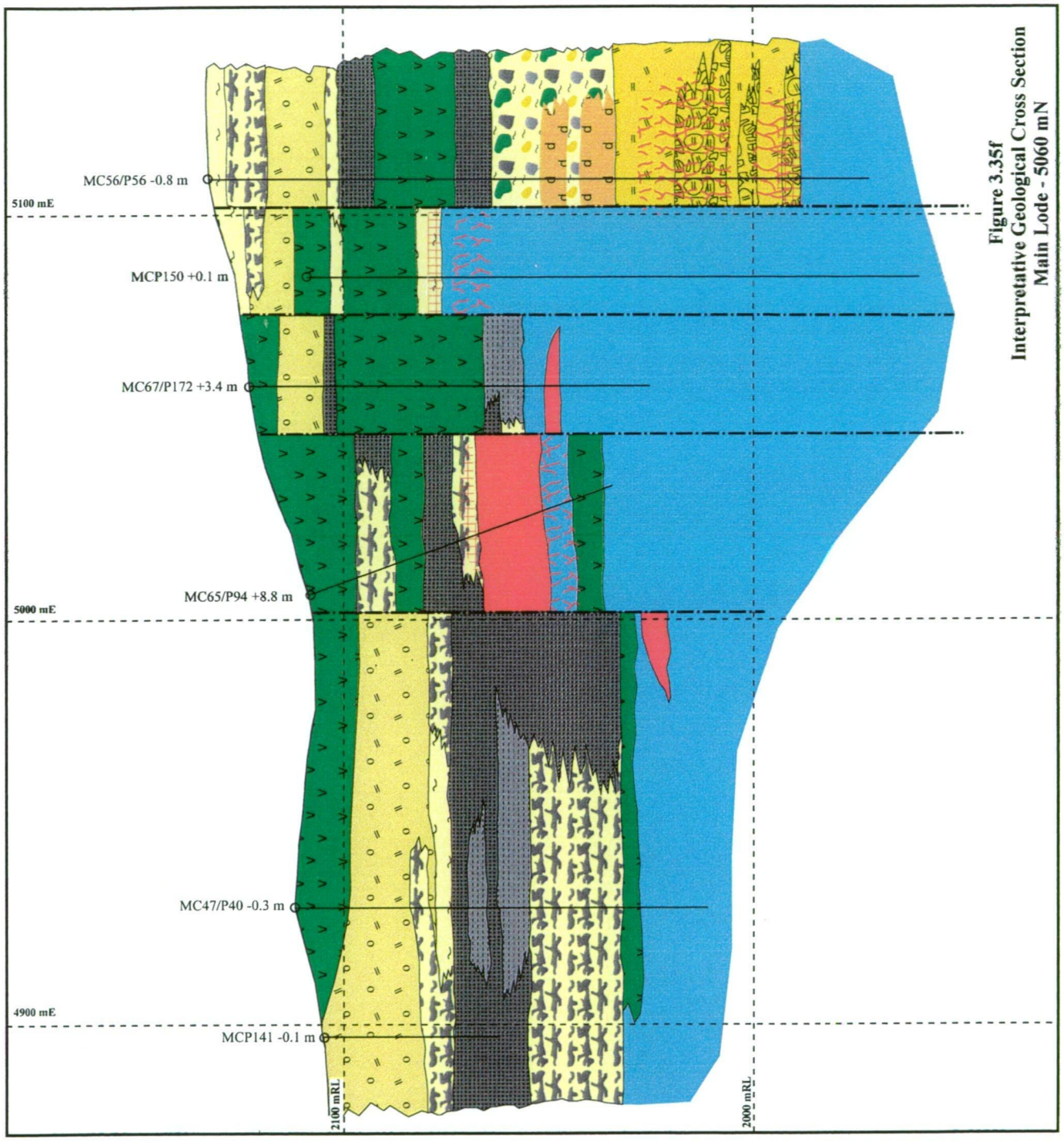

Figure 3.35f
Interpretative Geological Cross Section
Main Lode - 5060 mN

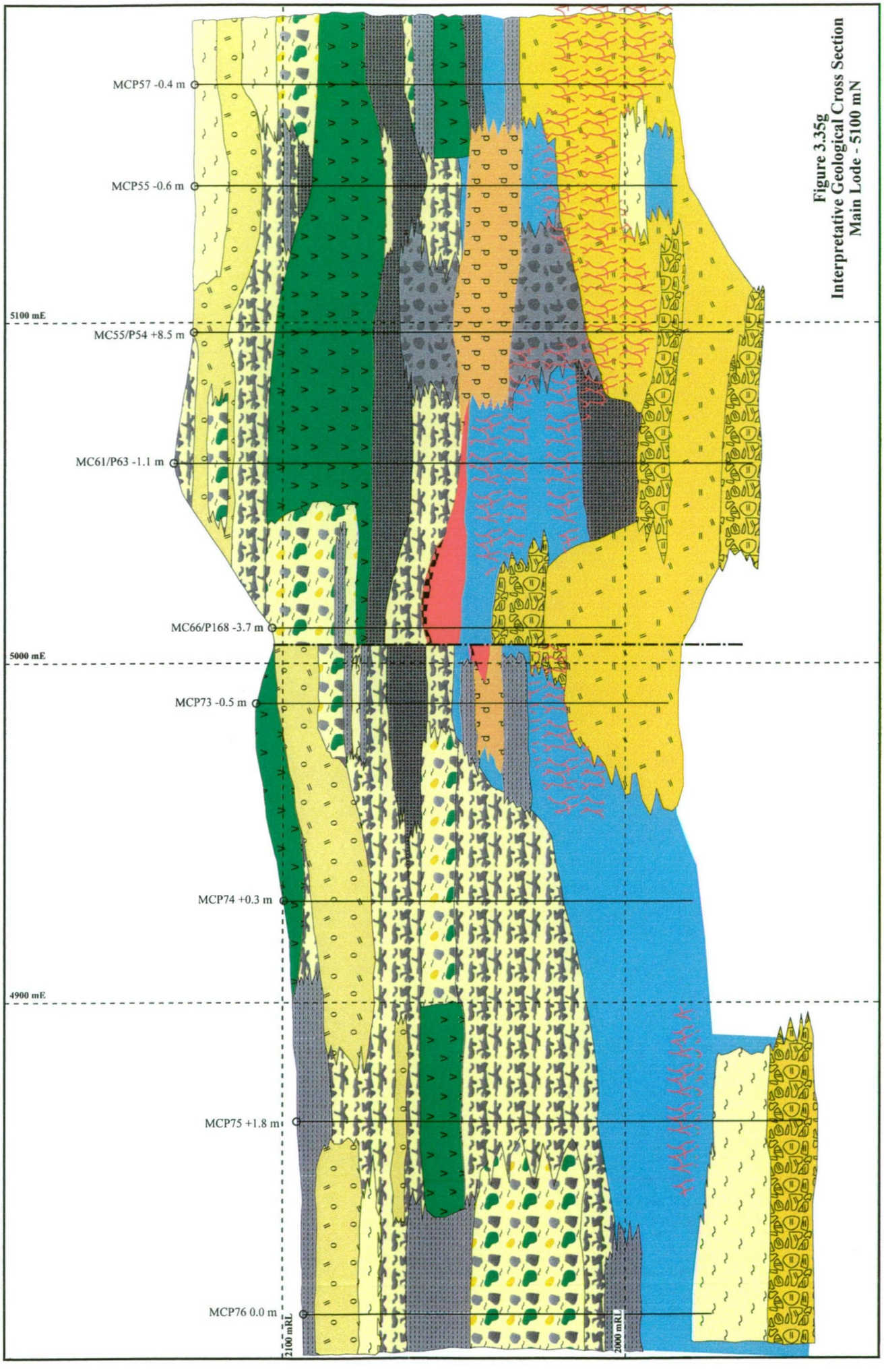

Figure 3.35g
Interpretative Geological Cross Section
Main Lode - 5100 mN

Regionally the reconstruction of the facies architecture has not been complicated by either the open folds or interpreted normal faults within the Berserker beds. However, facies reconstruction is limited by the generally flat-lying stratigraphy and lack of continuous lateral and vertical exposures of the footwall and hangingwall. Reconstruction of the regional facies architecture has therefore relied on scattered outcrops and widely spaced exploration drill holes. At Mount Chalmers, original relationships among the various hangingwall lithologies have been complicated by extensive normal faults and by the presence of andesite and quartz-feldspar porphyry intrusions, both of which have displaced large sections of the hangingwall.

The presence of oxidised rhyolitic lava clasts within the pumice breccia suggests that they were initially erupted in a subaerial, environment before being emplaced from water supported submarine, high particle concentration, volcaniclastic mass flows.

Andesitic lavas and intrusions were intersected in a number of drill holes in the Tungamull prospect area. The internal structure of the andesites are exposed within the drill cores indicate that there is a coherent and a brecciated phase. Contact relationships visible only in drill core indicate that the andesite has both an intrusive as well as an extrusive phase. The intrusive phase is marked by the presence of peperitic margins between the overlying siltstone and andesite. A constructional phase of the andesite was intersected in RWDD1. This drill hole intersected a thick sequence (~ 200 m) of autoclastic andesitic lava that has been intruded by andesitic feeder lava lobe-dykes. This would have been a substantial topographic feature on the Early Permian seafloor.

A second interval of andesite centred on the Sleipner Railway Siding also occurs within the hangingwall, but at a higher stratigraphic position compared to the first one. The andesite is dominated by autoclastic breccia and andesitic feeder dykes and lava lobe, implying that this initial phase of andesitic volcanism was non-explosive. Further upslope, below the North Star prospect, there is an agglutinate deposit that suggests a change in the style of volcanism to weakly explosive.

The last phase of effusive volcanism within the study is represented by the Ellrott Rhyolite and has both intrusive and extrusive facies, which are composed of both coherent and autobrecciated facies. The Ellrott Rhyolite has intruded into the Sleipner Andesitic Breccia and into the feldspar-phyric pumice breccia at the Tungamull prospect. The extrusive facies is represented by a series of small domes the emplacement of which was largely structurally controlled. The coherent Ellrott Rhyolite is commonly overlain by the brecciated facies. The presence of oxidised clasts within some zones of the brecciated rhyolite indicates that some segments of the Ellrott Rhyolite were exposed to subaerial conditions.

Andesitic sill and dykes intruded into the hangingwall lithologies sometime before lithification of the pumice breccias had occurred. Commonly within the pumice breccias and adjacent to the contact with the andesitic sills secondary welding texture is developed.

3.7. DISCUSSION - EVOLUTION OF THE BERSERKER BEDS IN THE VICINITY OF THE MOUNT CHALMERS MINE

The Mount Chalmers mine and the Tungamull prospect area were a was a submarine volcanic centre dominated by the products of effusive eruptions comprising lavas and domes, together with their resedimented autoclastic and hyaloclastic products. Prior to the onset of hydrothermal activity at Mount Chalmers the volcanism was dominated by the footwall rhyolite and dacitic lavas and pumiceous mass-flow emplaced units. Coeval sedimentation was dominated by graded, polymictic lithic breccia, massive to well-bedded and graded volcanolithic sandstone and siltstone. The footwall rhyolite was emplacement formed constructional topography on the seafloor as a series of small domes.

Monomictic resedimented autoclastic breccia collected in the topographic lows between and on the outside flanks of the domes. The emplacement of the footwall rhyolite and the hydrothermal activity that formed the sulphide mineralisation were controlled by the same structures. Consequently, it is thought that the onset of hydrothermal activity was initiated shortly after emplacement of the footwall rhyolite. During this period of hydrothermal activity sedimentation continued until the massive sulphide was effectively buried by the sediments.

The Mount Chalmers mine area as well as the Tungamull prospect area remained a centre of volcanic activity, however, the volcanism was dominated by the intrusion of pumiceous sills into the unconsolidated sediments. Subaerial to very shallow-marine pyroclastic volcanism was re-initiated, as evident from the emplacement of the feldspar-phyric, pumice-lithic mass-flow emplaced breccias. Shortly after the emplacement of the feldspar-phyric, pumice-lithic breccias, in the Tungamull prospect area there was a shift in the style of volcanism from rhyolite dominant to andesitic dominant. Eruption and emplacement of andesitic lavas and magmas occurred. At the Railway prospect, constructional andesitic volcanism is evident from the thick pile of autobrecciated lava and feeder lava lobe-dykes that were intersected in RWDD1.

After the emplacement of the andesitic volcanics, there was again a shift in the style of volcanism, this time back to rhyolite dominant. Areally extensive and voluminous feldspar-phyric pumice mass-flow emplaced deposits dominated this period of rhyolite volcanism. Following the emplacement of the feldspar-phyric pumice mass-flow deposits, there was switch back to effusive, constructional andesitic volcanism. In the Sleipner Railway Siding area a possible andesitic cone was built up by the accumulation of autobrecciated andesite. At some stage this cone breached the surface and was followed by a brief period of explosive andesitic volcanism as evident by the agglutinate deposit. At some stage, part of the cone is thought to have collapsed either due to gravity through oversteeping of the flanks of the cone or seismic activity. This generated high-energy submarine avalanches that travelled over the seafloor before depositing the polymictic variety of the Sleipner Andesitic Breccia. In the Tungamull area, the intrusion and eruption of the Ellrott Rhyolite mark a switch back to rhyolitic volcanism. The Ellrott Rhyolite marks the final phase of volcanic activity in the study area.

During these alternating periods of rhyolitic and andesitic volcanism, sedimentation continued and is marked by the deposition of extensive and thick deposits of coarse to fine-grained turbidites.

CHAPTER 4
SECONDARY WELDING OF SUBMARINE, PUMICE–LITHIC BRECCIA

This chapter has previously been published by - McPhie, J., and Hunns, S. R. 1995. "Secondary welding of submarine, pumice-lithic breccia at Mount Chalmers, Queensland, Australia". *Bulletin of Volcanology*. Vol. 57. p. 170 –178

4.1. INTRODUCTION

Compaction of pumice and bubble-wall shards may occur during high temperature primary welding of hot, primary pyroclastic flow and fall deposits (Smith, 1960; Ross and Smith, 1961; Sparks and Wright, 1979). Thoroughly welded pyroclastic deposits have much lower porosity than their non-welded counterparts, and display eutaxitic texture (Ross and Smith, 1961) comprising plastically deformed, aligned (commonly bedding parallel) pumice lenses in a matrix of flattened shards. In this chapter eutaxitic texture, mass-flow emplaced pumice and lithic clast-rich breccia deposited in a below-wave base submarine setting at Mount Chalmers are described. In this instance, the mass-flow deposit was cold and the eutaxitic texture was generated by re-heating and high-temperature compaction of initially glassy pumice adjacent to synvolcanic intrusions, a process that is referred to as secondary welding. This example adds to the growing number of circumstances where eutaxitic textures can occur and emphasises the need for care in the interpretation of rocks displaying such textures.

One type of secondary welding is already well documented. Glassy pyroclastic deposits and tuffaceous sediments underlying and adjacent to younger subaerial lavas may undergo secondary welding compaction that results in zones of "fused tuff" (Smith, 1960; Ross and Smith, 1961; Christiansen and Lipman, 1966; Schmincke, 1967). Christiansen and Lipman (1966), following Smith (1960:800) used the term "fused" for the induration and deformation of glassy clasts resulting from heating by adjacent lava, but emphasised that the term should not be taken to imply that melting (fusion) had occurred. Similarly, there is no evidence that melting occurred in the Mount Chalmers case, but the term "fused tuff" is nevertheless inappropriate because the pumice-lithic breccia is not a primary pyroclastic deposit (that is, not "tuff"). It is clear that any glassy pumiceous deposits, whether primary non-welded pyroclastic deposits or resedimented and reworked deposits, can be affected by secondary welding adjacent to lava flows, intrusions and other sufficiently hot pyroclastic deposits

Eutaxitic texture is characteristic of, but not restricted to, welded pyroclastic deposits and can also be generated by processes other than either primary or secondary welding compaction. These processes include: (1) diagenetic compaction of pumiceous deposits (Branney and Sparks, 1990; McPhie *et al.*, 1993); (2) devitrification and hydrothermal alteration of coherent lavas and intrusions (Allen 1988, 1992); or (3) re-heating and plastic deformation of autoclastic breccia associated with lava flows (Boyd, 1961; Sparks *et al.*, 1993; Dadd, 1992). Eutaxitic texture resulting from primary welding is limited to volcaniclastic aggregates that are deposited hot, and is most commonly found in subaerial or very shallow subaqueous pyroclastic

deposits. Eutaxitic texture resulting from secondary welding has no specific connotations for emplacement processes, nor for depositional setting, but does imply proximity to a lava flow or intrusion and is restricted to pumiceous (or scoriaceous), initially porous, glassy deposits. Eutaxitic textures generated by other processes can occur in a wide range of volcaniclastic deposits, lavas and shallow intrusions in diverse environments.

4.2. EUTAXITIC TEXTURE IN PUMICE–LITHIC BRECCIA AT MOUNT CHALMERS

4.2.1. Pumice–lithic Breccia

Pumice–lithic breccia units in the drillcore intersections, pit exposures and outcrops are texturally very similar. The units are generally very thick, some in excess of 100 m, and have sharp basal contacts above which there is a massive to weakly graded interval overlain gradationally by diffusely bedded tuffaceous sandstone and mudstone. The units are very poorly sorted and comprised feldspar-phyric tube pumice and less abundant volcanic lithic clasts. Delicate tube vesicles are preserved within the pumice clasts, and overall, there is a very weak alignment due to diagenetic compaction. However, many pumice clasts are uncompacted and randomly oriented. *In situ* trace fossils in interbedded sedimentary facies indicate that the depositional environment was submarine. Although composed of pumice, presumably of pyroclastic origin, the units show no signs of hot emplacement and have an internal organisation (sharp base; massive-graded cause lower part; diffusely stratified; fine upper part) that is consistent with deposition from water supported, submarine, high particle concentration, volcaniclastic mass flows. The abundance of pumice clasts and the large volumes represented by single sedimentation units strongly suggests that the submarine mass flows were fed directly from major pyroclastic eruptions - that is, they were syn-eruptive. Resedimentation of non-welded, pumice-rich, primary pyroclastic deposits temporarily stored in coastal environments is also plausible.

4.2.2. Pumice–lithic Breccia Adjacent to Sills

Pumice–lithic breccia in drillholes MCD 6, MCD 7 and MCD 10 is intruded by andesitic sills (Fig 4.1). In two instances (MCD 6 and MCD 10) a single interval of andesite occurs within very thick, massive pumice–lithic breccia. In the third instance (MCD 7), there are five intervals of andesite, the uppermost 2 of which have faulted contacts. Where contacts between the andesite and the pumice–lithic breccia are preserved and are not fault contacts, a well-developed eutaxitic texture occurs in the pumice–lithic breccia adjacent to the contact. There is a gradual transition towards these contacts from randomly oriented, slightly compacted pumice clasts to strongly aligned and compacted pumice clasts adjacent to the andesite (Fig. 4.2). The compacted pumice clasts are plastically deformed around lithic clasts close to the contacts (*e.g.* MCD 7, Fig 4.2). In addition, pumice–lithic breccia close to the andesite is indurated and silicified. The eutaxitic texture, induration and silicification extend as far as 3 m from the contact with the andesite. Contacts of the sills, the eutaxitic foliation, the weak compaction foliation, and regional bedding are all more or less parallel and sub-horizontal. In these drillhole sections, the eutaxitic texture, induration and silicification occur in the pumice–lithic breccia *only* where it is in contact with intrusive andesite.

Figure 4.1. Graphic logs of drill core from part of MCD6 and MCD7 and MCD10. MCD6 and MCD7 are both located within about 3 km SE of Mount Chalmers pit (Fig. 1.1). The pumice–lithic breccia units in each section are correlated. Eutaxitic texture occurs at both contacts of a single, 50 m thick andesite sill in MCD 6. Of the 5 intervals of andesite in MCD7, only 3 have unfaulted contacts; in each case the adjacent pumice–lithic breccia shows eutaxitic foliation. Drill core samples from one zone of secondary welding and the andesite are illustrated in Figure 4.2. MCD10, located about 2 km south of Mount Chalmers pit (Fig. 1.1). Eutaxitic foliation occurs in pumice–lithic breccia adjacent to both the lower and upper contacts of a 15 m thick andesite sill. F, faulted contact.

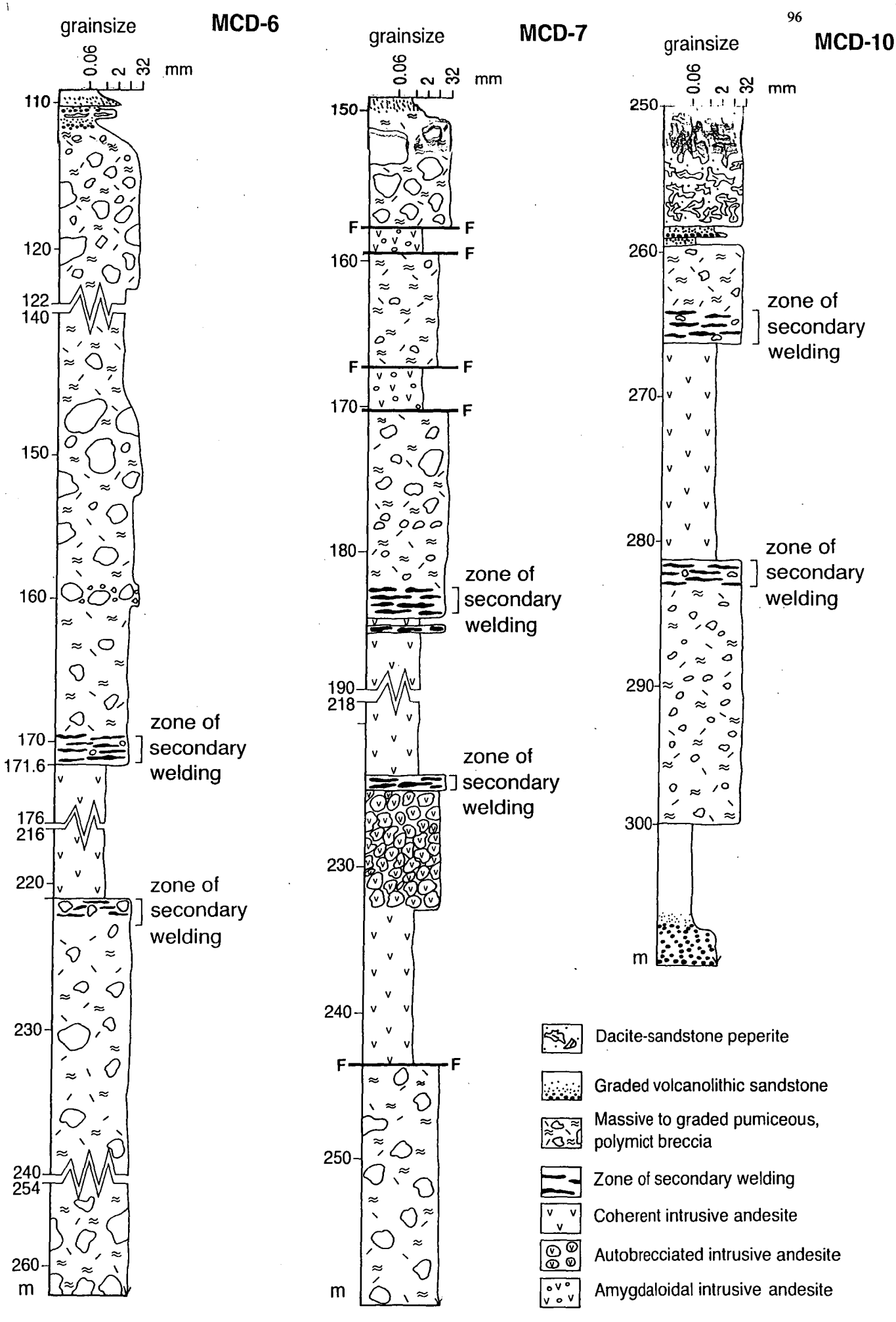
MCD-6
grainsize
0.06
2
32
mm
110
120
122
140
150
160
170
171.6
176
216
220
230
240
254
260
m
zone of secondary welding
zone of secondary welding
MCD-7
grainsize
0.06
2
32
mm
150
F
160
F
170
F
180
190
218
230
240
250
m
zone of secondary welding
zone of secondary welding
MCD-10
grainsize
0.06
2
32
mm
250
260
270
280
290
300
m
zone of secondary welding
zone of secondary welding
Dacite-sandstone peperite
Graded volcanolithic sandstone
Massive to graded pumiceous, polymict breccia
Zone of secondary welding
Coherent intrusive andesite
Autobrecciated intrusive andesite
Amygdaloidal intrusive andesite

Figure 4.2. Drill core samples from MCD7 (Fig. 4.1), showing well-developed eutaxitic texture in pumice–lithic breccia adjacent to andesite sills. The eutaxitic foliation is sub-parallel to the sill contacts and to regional bedding. The samples come from the uppermost zone of secondary welding: upper piece of core (181.6 m), middle piece of core (184.3 m), lower most piece of core (184.7 m; the contact with the andesite occurs at 184.6 m. Sample depths have been measured from the centre of the drill core. Up-hole direction is to the left of the figure.

a

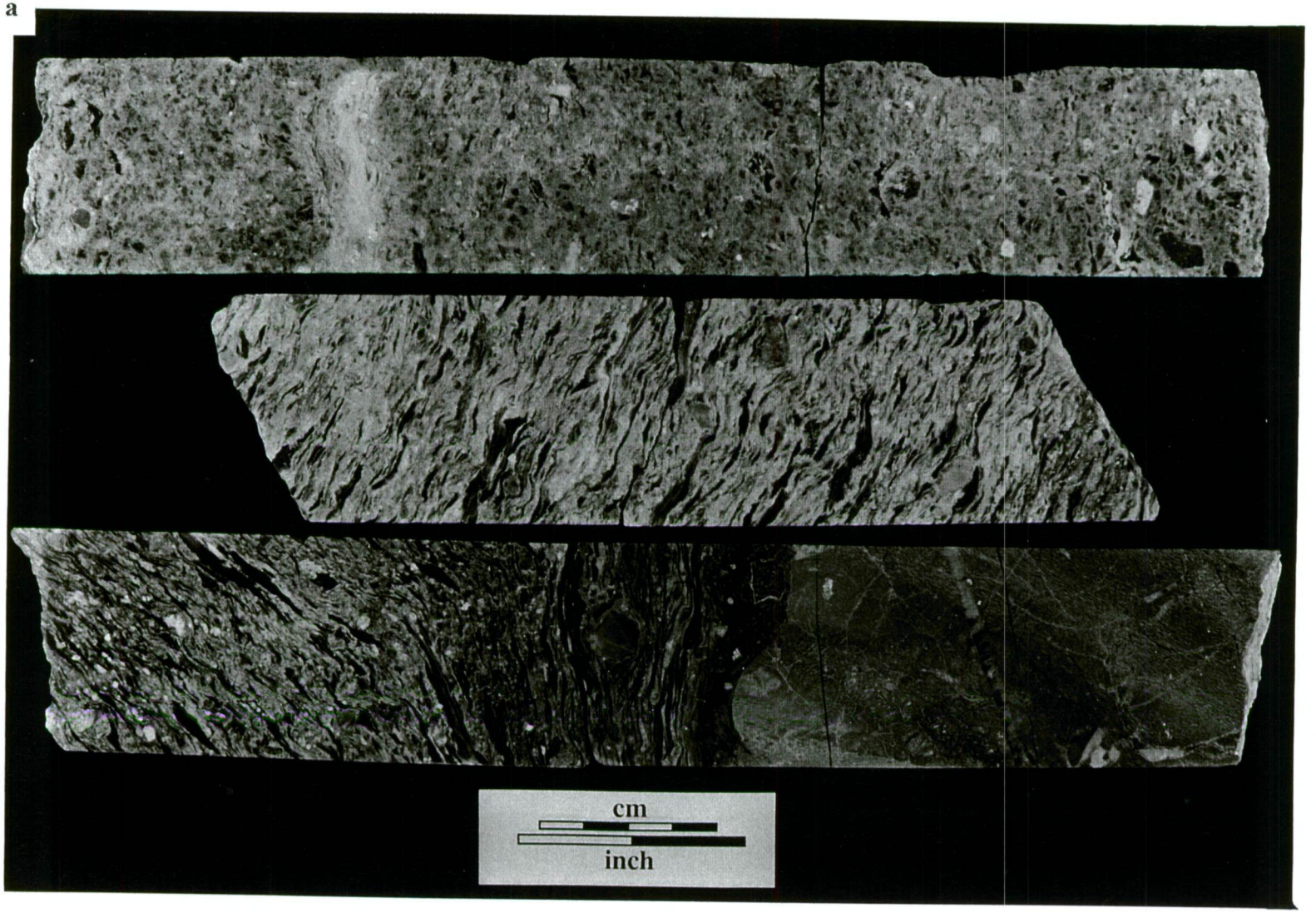

Similar relationships between a gently south-dipping, 3 m thick, andesite sill and pumice–lithic breccia are exposed on the east face of the Mount Chalmers pit. Away from the andesite, the pumice–lithic breccia is massive. Within about 1 m of both the upper and lower contacts of the sill, the pumice–lithic breccia shows a distinct foliation, which is parallel to the contacts and defined by sharply flattened relict pumice clasts. Although everywhere sharp, the lower contact of the sill is locally highly irregular. Flame-like protrusions of pumice–lithic breccia extend upwards into the andesite, suggesting that the pumice–lithic breccia was unconsolidated at the time of intrusion.

4.2.3. Pumice–lithic Breccia Adjacent to Dykes

Pumice–lithic breccia in New Zealand Gully, about 4-km south of Mount Chalmers pit (Plate 1), is intruded by rhyolitic and andesitic dykes. The orientation of bedding is not evident along the gully because all outcrops are within a very thick (at least 200 m) unit of massive pumice–lithic breccia. However, regional bedding dips very gently (<20°) to the west. Contacts between dykes and the pumice–lithic breccia are exposed at localities NZ 22 (258245mE 7417432mN; Rockhampton 1:100000), and NZ 24 (258400mE 7417340mN; Rockhampton 1:100000). The dyke at NZ 22 is rhyolite and about 50 m wide; the single exposed contact with pumice–lithic breccia is oriented 70°/105°. The dyke at NZ 24 is andesite and about 1.2 m wide; its contacts with the pumice–lithic breccia are oriented 80°/016°. Away from the dykes, the pumice–lithic breccia is massive, apart from a very weak, near vertical, N–S trending regional cleavage. In both instances, a well-developed eutaxitic foliation is present in the pumice–lithic breccia adjacent to the dykes (Fig.4.3), and is oriented parallel to the dyke contacts. The texture dies out beyond about 3 m from the contact with the rhyolite (NZ 22), and beyond about 1 m from the andesite (NZ 24). The eutaxitic texture is defined by compacted, aligned pumice clasts; the pumice clasts adjacent to lithic fragments are the most strongly deformed (Fig. 4.3).

A poorly exposed contact between andesite and pumice–lithic breccia occurs on a track leading to the hilltop above the northern face of the Mount Chalmers pit. Relationships are similar to those observed at New Zealand Gully. The contact is near vertical and trends northeasterly. Eutaxitic foliation developed in adjacent pumice–lithic breccia is more or less parallel to the contact and dies out within 1-2 m.

4.2.4. Eutaxitic Texture in Thin-Section

The pumice–lithic breccia consists of close-packed, granule-size and coarser, feldspar-phyric, tube pumice clasts together with lithic fragments. Feldspar crystals are mainly phenocrysts within pumice clasts. Although euhedral, many show jigsaw-fit fracture patterns indicating they have broken *in situ*, perhaps reflecting brittle fracturing during compaction of the enclosing pumice. In massive pumice–lithic breccia, the tube pumice clasts are randomly oriented and vary from equant to lenticular.

Figure 4.3. Samples of pumice–lithic breccia from New Zealand Gully, about 4 km SW of Mount Chalmers (Fig. 1.1). (a). NZ 22, adjacent to a rhyolite dyke, weathered surface. (b). NZ 24, adjacent to an andesite dyke, sawn and polished surface. Both samples show well-developed eutaxitic texture defined by dark grey, wispy, compacted relict tube pumice clasts. The eutaxitic foliation in each case is oriented parallel to the steeply-dipping contacts of the dykes.

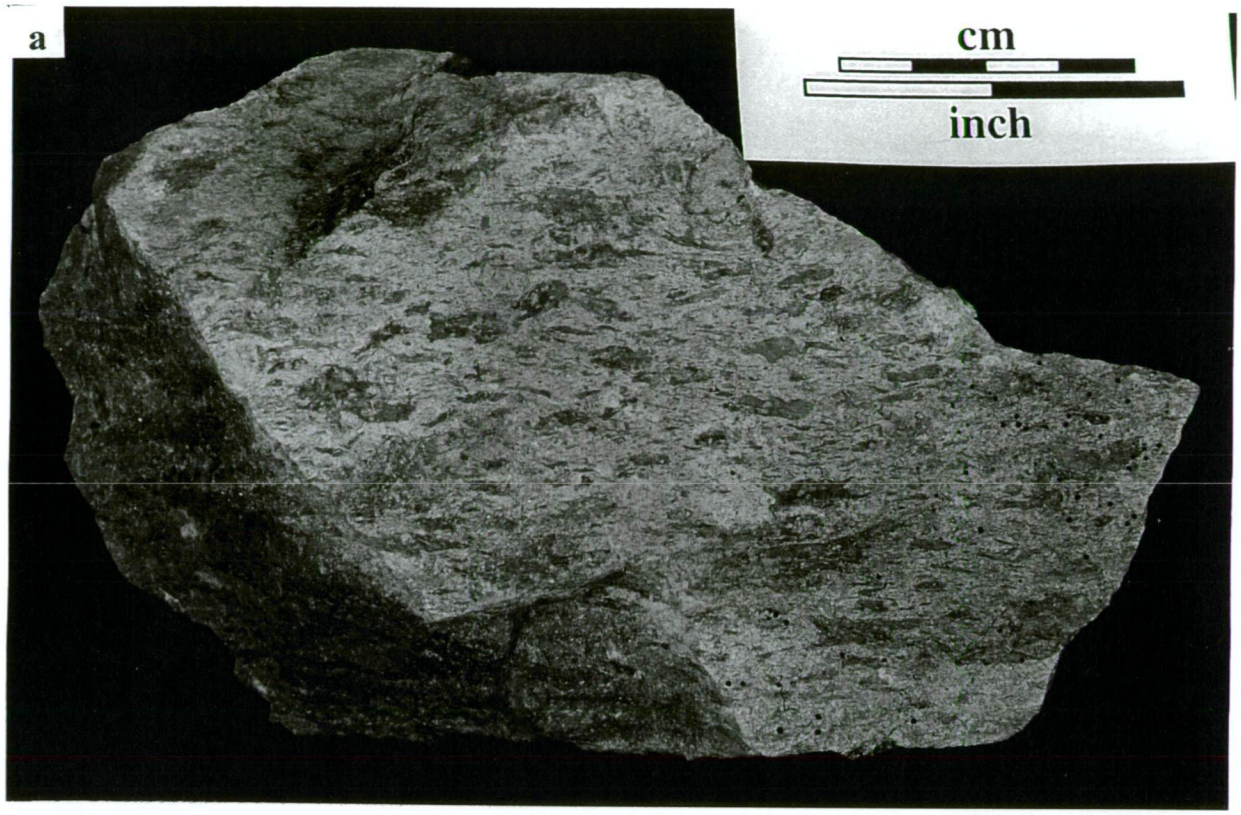
a
cm
inch

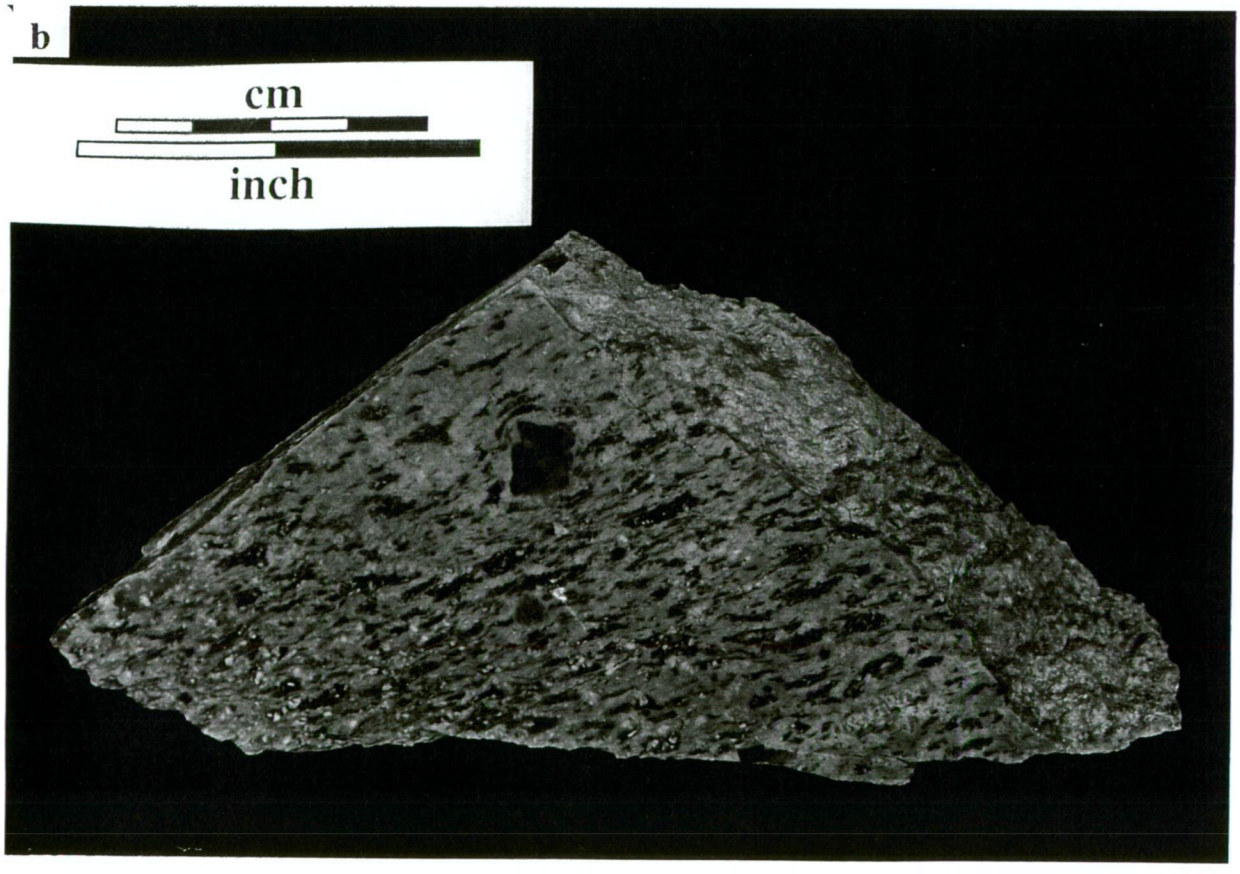
b
cm
inch

Closer to the contacts with the intrusions, most pumice clasts are aligned and the tube vesicles are compacted but some retain a tube vesicle texture oriented at high angles to the eutaxitic foliation. Adjacent to the intrusions, relict pumice clasts have been deformed into long thin "strands" that wrap around rigid phenocrysts and lithic fragments.

In thin-section, the tube pumice structure is clearly preserved where the glass has been replaced by a very fine-grained quartzo-feldspathic mosaic (Fig.4.4A). In instances where phyllosilicates (principally sericite or chlorite) have replaced the glass, the relict pumice clasts are represented by wispy phyllosilicate lenses and patches in which original vesicular microtextures are less distinct (Fig.4.4B). Strongly flattened pumice in samples from close to the intrusions contain abundant, round and ovoid, quartz-filled amygdales (Fig.4.4C). These were small vesicles, generated by secondary vesiculation during re-heating by the adjacent intrusions (cf. Schmincke 1967; Yamamoto *et al.* 1991). Furthest from the intrusions, the vesicles are very small (0.1-mm diameter) and they increase in size up to about 2 mm across at the contacts of the intrusions.

Spherical structures are especially conspicuous in pumice lenses replaced by phyllosilicates (Fig.4.5A). Some are composed of radially arranged, fine, quartz or feldspar crystals and are interpreted to be spherical spherulites (cf. Lofgren 1971a). Others that are identical in mineralogy, size, shape and distribution but lacking distinct radial structure may be recrystallised spherical spherulites. There is a range in size from less than 0.04 mm in the least compacted samples to about 0.1 mm close to the intrusions. Also close to the intrusions, some samples show interlocking quartz patches that overprint the relict pumice and strongly resembles micropoikilitic (or "snowflake") texture (Fig.4.5B, C; cf. Lofgren 1971a; Bigger and Hanson 1992). Samples that contained amygdales (Fig.4.5C) are also spherulitic and characterised by sheath spherulites, many of which nucleated on the amygdale margins.

4.3. ORIGIN: SECONDARY WELDING COMPACTION ADJACENT TO INTRUSIONS

In most outcrops and drill core sections, the pumice–lithic breccia at Mount Chalmers is non-welded and entirely massive or else displays a weak, bedding-parallel, diagenetic compaction foliation. The parent pumice-rich mass flows were submarine although they may have originated from a shallow water or subaerial source. Juvenile pumiceous clasts can remain very hot during transport and after deposition of syn-eruptive, water-supported mass flows (*e.g.* Tamura *et al.*, 1991; Cashman and Fiske, 1991). Nevertheless, primary welding compaction is uncommon, in submarine pumiceous mass flow deposits, either because the clasts are cooler than minimum welding temperatures, or because the lithostatic load is insufficient. A primary welding origin for the eutaxitic foliation observed in pumice–lithic breccia at Mount Chalmers is untenable because the texture is strictly confined to the vicinity of intrusions, including dykes, and dies out a few metres away from the intrusive contacts. Instead, the texture is interpreted to be secondary, and resulted from re-heating and compaction of tube pumice close to the intrusions.

Figure 4.4. Photomicrographs of pumice–lithic breccia in the Berserker beds.
(a). Tube vesicle texture preserved in relict pumice (P) in massive pumice–lithic breccia from the New Zealand Gully area (sample NZ 1b). The tube vesicles within the pumice clasts are uncompacted and have different orientations. Plane polarised light, scale bar 0.5 mm.
(b). Sericite-altered tube pumice (P) clasts in pumice–lithic breccia that shows good eutaxitic foliation (NZ 22, Fig. 4.3a). Pumice clasts have wispy terminations (arrow). Tube vesicles are compacted and deformed adjacent to feldspar (F) phenocrysts. Plane polarised light, scale bar 1 mm.
(c). Abundant amygdales (*e.g.* arrows) within a compacted pumice clast from pumice–lithic breccia with good eutaxitic foliation (MCD 6, 170.4 m, Fig. 4.1). The pumice clast fills the field of view and is crowded with round or ovoid, quartz-filled amygdales up to about 0.3 mm diameter. Between the amygdales are abundant impinging sheath sperulites (cf. Lofgren, 1971a), evident only with crossed nicols. The amygdales record secondary vesiculation of compacted pumice as a result of re-heating by an adjacent andesite sill. Plane polarised light, scale bar 1 mm.Samples of pumice–lithic breccia from New Zealand Gully, about 4 km SW of Mount Chalmers (Fig. 1.1). (a). NZ 22, adjacent to a rhyolite dyke, weathered surface. (b). NZ 24, adjacent to an andesite dyke, sawn and polished surface. Both samples show well-developed eutaxitic texture defined by dark grey, wispy, compacted relict tube pumice clasts. The eutaxitic foliation in each case is oriented parallel to the steeply-dipping contacts of the dykes.

Figure 4.5. Photomicrographs showing devitrification textures in pumice–lithic breccia affected by secondary welding.
(a). Spherulites (*e.g.* arrows; about 0.8 mm dimeter) in a compacted pumice (P) clast from pumice–lithic breccia that shows well-developed eutaxitic foliation (NZ 24, Fig. 4.3b). On the left side, spherulites are isolated within chlorite that replaces compacted former glass; on the right side, the spherulites have coalesced. Plane polarised light, scale bar 0.5 mm. (b) and (c) Micropoikilitic texture in pumice–lithic breccia affected by secondary welding adjacent to an andesite sill (MCD 10, 265.5 m, 4.1). The poikilitic quartz patches are about 0.05 to 0.1 mm diameter. They include abundant very fine feldspar microlites replaced by sericite, and are outlined by narrow seams of very fine phyllosilicates and opaque grains. In both thin-section and hand specimen, pumice clasts are less distinct where micropoikilitic texture occurs. The micropoikilitc texture overprints the eutaxitic foliation and is the result of devitrification during slow cooling after secondary welding of the pumice–lithic breccia. (b), plane polarised light; (c), crossed nicols; scale bar 0.5 mm.

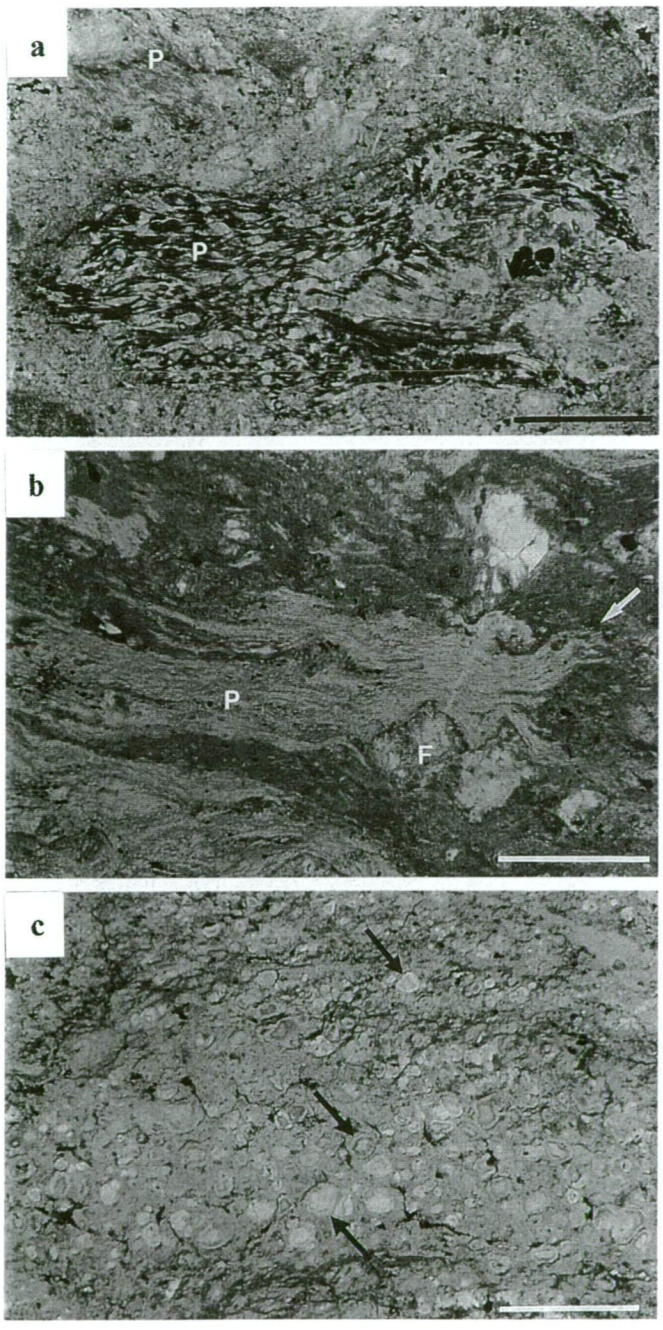

Figure 4.4

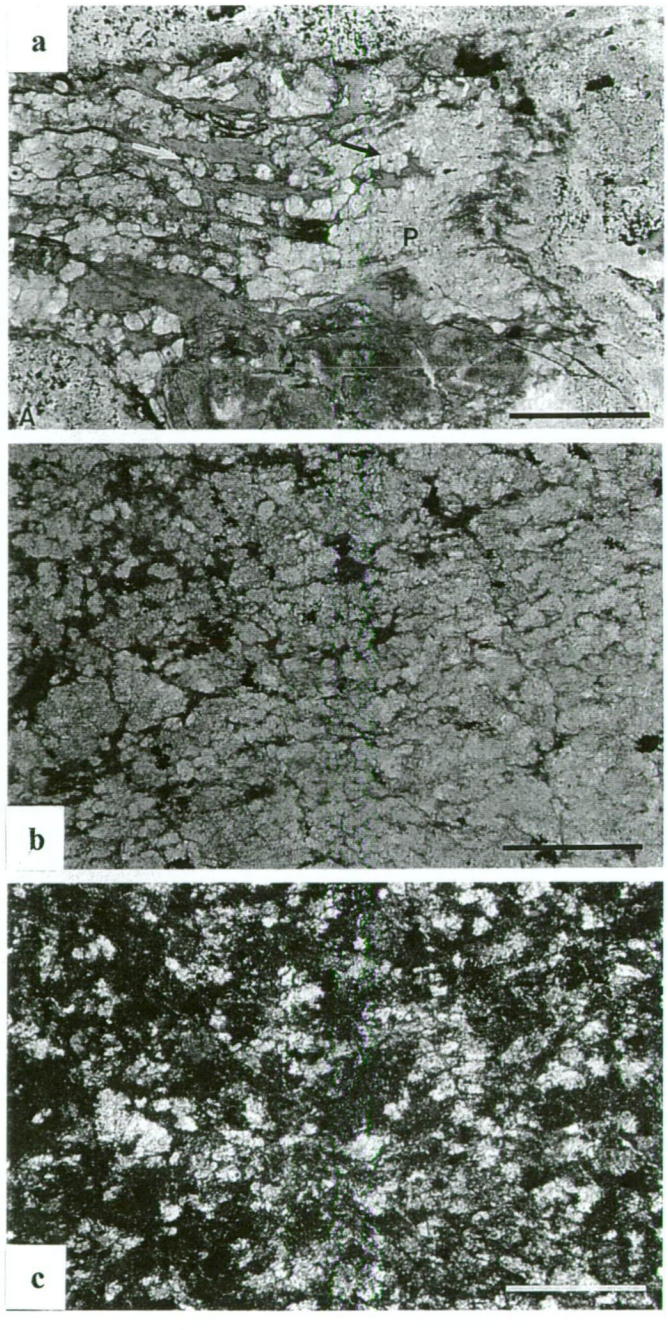

Figure 4.5

The presence of spherulites and round amygdales in flattened relict pumice provides critical evidence that compaction involved high temperature welding, rather than low temperature compaction of pumice that was more altered and, hence, mechanically weak, adjacent to intrusions.

Secondary welding compaction of cold pumice can occur providing: (1) the pumice is still glassy and porous at the time of intrusion; (2) there is sufficient directed stress, either lithostatic load or stress related to intrusion of dykes or sills; and (3) enough heat is transferred to the pumice–lithic breccia so that the glass can deform plastically and compact. Previous workers have highlighted the importance of water vapour pressure, in addition to temperature and load, in promoting primary welding (Smith, 1960; Boyd, 1961; Sparks *et al.*, 1980), and steam generated in porous deposits under lava flows may play a part in the heat transfer involved in forming "fused tuffs" (Christiansen and Lipman, 1966; Schmincke, 1967). The water-saturated condition of the submarine pumice–lithic breccia at Mount Chalmers may thus have been a factor favouring the development of secondary welding compaction when the intrusions were emplaced.

The eutaxitic foliation in the Mount Chalmers pumice–lithic breccia is parallel to the intrusive contacts. In the instances involving sills, this orientation is sub-parallel to bedding and perpendicular to the direction of the greatest principal stress (s_1) generated by lithostatic load. In instances involving dykes, the foliation defined by flattened pumice clasts reflects the local stress field related to the emplacement of the dykes, rather than the lithostatic load. That is, the sub-horizontally directed stress associated with the intrusion of the dykes was evidently more important than lithostatic load during secondary welding of the adjacent pumice–lithic breccia, and produced steeply dipping, contact-parallel eutaxitic foliations. Indeed, the volume reduction in the pumice–lithic breccia reflected by the secondary welding compaction may have facilitated intrusion of the dykes.

Re-heating of the glassy pumice–lithic breccia adjacent to intrusions resulted not only secondary welding compaction but also in high temperature devitrification of the glass. Spherulites and micropoikilitic texture develop during cooling of felsic glass and result from crystallisation at high temperature (Lofgren, 1971a, 1971b), probably above the glass transition temperature (Manly, 1992). Furthermore, such textures develop only in continuous glass and therefore are common in the interiors of lavas, shallow intrusions and thick, densely welded ignimbrites (Anderson, 1969; Lofgren, 1971a, 1971b; Bigger and Hanson, 1992). Lofgren (1971a, 1971b) concluded that spherulitic textures generated during first cooling and during reheating would be similar and that such textures do not alone indicate a particular origin for the glass. Their presence in pumice–lithic breccia at Mount Chalmers can only be explained as a result of re-heating and secondary welding compaction of the tube pumice to continuous non vesicular glass, followed by spherulitic and micropoikilitic devitrification. Very similar textures were recognised immediately north of the Mount Chalmers pit by Sainty (1992) and interpreted by him to indicate primary welding. However, another possibility suggested by this study is that his samples were affected by re-heating adjacent to a concealed intrusion.

4.4. CONCLUSIONS

The eutaxitic texture within pumice–lithic breccia at Mount Chalmers is interpreted to be the result of secondary welding compaction adjacent to intrusions. The critical evidence indicating that reheating was responsible for the compaction is the presence of amygdales due to revesiculation and spherulites, generated by high temperature devitrification, within flattened pumice clasts adjacent to intrusions. As predicted by Lofgren (1971a, 1971b) the high temperature devitrification textures are the same as those formed during initial cooling of hot glass.

Secondary welding is probably common in submarine volcanic sequences because these typically include thick, glassy pumice rich deposits and syn-volcanic intrusions (McPhie and Allan 1992). For example, very similar secondary welding is present in submarine pumice rich volcaniclastic rocks reheated by syn-volcanic andesitic and dacitic intrusions in the southern Izu Peninsula, Japan (Ito *et al.* 1984). Such occurrences of secondary welding compaction differ from "fused tuff" (Christiansen and Lipman 1966; Schmincke 1967) in two main respects: (1) the affected units are submarine-emplaced pumice-rich volcaniclastic mass-flow deposits rather than subaerial, primary pyroclastic deposits, and (2) syn-volcanic intrusions rather than lava flows were involved.

Zones of secondary welding compaction at Mount Chalmers extend to a few metres away from the intrusive contacts of both dykes and sills, and the eutaxitic foliation is parallel to the contacts. Away from the intrusions the pumice–lithic breccia is massive, non-welded and shows no evidence for having been emplaced hot. In instances involving sills, the eutaxitic foliation is approximately parallel to bedding, and large areas (km^2) of pumice–lithic breccia have been affected. Where exposure is poor and the sills or their contacts are concealed, the more or less conformable zones of welded pumice–lithic breccia could easily be misinterpreted as welded, primary, pyroclastic flow deposits (ignimbrite).

CHAPTER 5
INTRUSIVE PUMICEOUS SILLS AND ASSOCIATED PEPERITES AT MOUNT CHALMERS

This chapter has previously been published by - Hunns, S. R., and McPhie, J. 1999. "Intrusive pumiceous sills and associated peperites at Mount Chalmers, Queensland, Australia". *Journal of Volcanolgy and Geothermal Research.* Vol. 88. P. 239 - 254

5.1 INTRODUCTION

Peperite is formed when hot magma or lava comes into contact with wet unconsolidated sediments and the two components are dynamically mixed. The most common circumstances for peperite formation occur at the contacts between an intrusion or lava and sediment. Peperite may involve a wide range of sediment types and the full spectrum of magma compositions and form in diverse settings (*e.g.* Brooks *et al.*, 1982; Hanson and Schweikert, 1982; Kokelaar, 1982; Busby-Spera and White, 1987; Kano, 1989; Sanders and Johnston, 1989; Hanson, 1991; Peltz and Kafri, 1992; Boulter, 1993; Hanson and Wilson, 1993; McPhie, 1993; Rawlings, 1993; Brooks, 1995; Goto and McPhie, 1996).

The igneous component of peperite is commonly non-vesicular to poorly vesicular and may be totally glassy or almost entirely crystalline. Here we report an example of peperite composed almost entirely of formerly glassy, rhyolitic tube pumice. The peperite is associated with sills that are also substantially pumiceous. This example is unusual because the host sediment is vesicular.

The internal textures and facies relationships of the pumiceous peperite and host sediment are described and used to constrain a genetic model. The peperite developed at the margins of rhyolitic intrusions emplaced into a relatively shallow submarine, mixed volcanic and sedimentary succession. Intrusion evidently took place beneath a thin cover of wet sediment that did not impede vesiculation of the rhyolite and that trapped bubbles of steam and/or magmatic volatiles generated during mixing. Such a setting could also have been important in the development of microfractures in vesicle walls (cf. Mungall *et al.*, 1996) that facilitated disintegration of the intrusions and mixing with adjacent wet sediment.

5.2. FIELD RELATIONSHIPS OF THE PUMICEOUS PEPERITE

Pumiceous peperite has been identified throughout the hangingwall stratigraphy to the Mount Chalmers massive sulfide mineralisation and is not confined to one particular stratigraphic position. The peperite occurs within thick sequences of interbedded graded sandstone and siltstone, or within the laminated siltstone to sandstone tops of very thick, graded units of pumice-lithic breccia. In some instances, the peperite is associated with coherent pumiceous rhyolite. Where well constrained by adjacent drill hole intersections, the intervals of pumiceous rhyolite appear to be conformable with the enclosing units.

They are thus interpreted to be sills. However, the facies geometry is complex in detail, comprising a number of relatively thin (<20 m) intervals of pumiceous rhyolite and/or pumiceous peperite of limited lateral extent (< a few tens of m) intercalated with sedimentary facies. Macroscopic textures in the host sedimentary facies, the pumiceous rhyolite (igneous component) and the peperite are described in this section.

5.2.1. Sedimentary Facies

The sedimentary facies that host the Mount Chalmers pumiceous peperite is dominated by normally graded beds of volcaniclastic siltstone, sandstone and pebbly sandstone. Single beds vary from 15 mm to 2.5 m thick. The framework grains are predominantly volcanic lithic fragments, relic pumice clasts and crystals (mainly feldspar, subordinate quartz); minor components are clasts of siliceous siltstone and intraclasts of fine-medium sandstone. The thicker beds of sandstone have sharp bases and commonly grade upward into siltstone, displaying Bouma divisions ABD. The siltstone intervals are massive to delicately laminated; however, in many cases, any original bedding has been destroyed by bioturbation.

The sediment component within and immediately adjacent to the peperite is dominantly siltstone to fine sandstone with a homogeneous texture. Neither bedding nor grading is present. Typically, bedding, grading and bioturbation structures occur and are undisturbed beyond about 0.5 m from the peperite.

The sediment component that occurs mixed with rhyolite in the peperite contains vesicles that are now filled by fine-grained quartz, chlorite or quartz-chlorite assemblages (Figs 5.1A, 5.1B, 5.2A and 5.2B). The vesicles are generally spherical, although elliptical to lenticular forms are also present, and range from <1 mm to 3 mm in diameter. They occur singularly or in groups, and in some cases, they define "trails" that parallel the irregular sediment-rhyolite contacts. Importantly, vesicles have been observed only in the sedimentary facies immediately adjacent to the rhyolite component of the peperite. The sediment component within the peperite is also commonly paler (Fig. 5.1) and more siliceous along contacts with the rhyolite than elsewhere away from the rhyolite.

5.2.2. Rhyolite

The igneous component of the peperite has an evenly porphyritic texture comprising euhedral feldspar phenocrysts (10 - 20%, 1-2 mm in size; plagioclase and K-feldspar) and glomerocrysts set within a formerly glassy, variably vesicular groundmass. The feldspars have been altered to sericite, quartz or quartzo-feldspathic assemblages. Next to contacts with the sedimentary component, some of the feldspars are highly fractured *in situ*. The formerly glassy groundmass has been completely altered to sericite and/or silica. Sericite alteration of the groundmass predominates whereas silica alteration is largely confined to groundmass adjacent to contacts with the host sediment. The phenocryst assemblage suggests that the igneous component is broadly felsic in composition. Texturally similar but less altered feldspar-phyric pumice breccias elsewhere in the succession are predominantly rhyolitic in composition (Ti/Zr ranges from 3 to 22; SR Hunns, unpublished data). Thus, the igneous component was probably originally rhyolitic.

Figure 5.1. Drill core samples of pumiceous peperite composed of highly irregular domains of pumiceous rhyolite (dark grey) and homogeneous host sediment (pale grey). In A and B, the sediment in contact with the pumiceous rhyolite is bleached and contains chlorite- and/or quartz-filled vesicles (arrows). In places, the vesicles define trails parallel to the contacts. In C, the formerly vesicular rhyolite clasts (r) have been compacted and now resemble wispy fiamme. They include intricately crenulated "veins" of sediment (s). a, MCD 10, 217.7 m; b, MCD 10, 175.3 m; c, WS 8, 79.6 m.

a
CM

b
CM

c
CM

Figure 5.2. (a). The highly irregular contact between pumiceous rhyolite (pr) and the host siltstone (s) at 175.3 m in MCD 10. Feldspar crystals (f) from the pumiceous rhyolite and vesicles (v) occur within the host siltstone near the contact. Note the broken feldspar phenocryst (bf) in the rhyolite adjacent to the contact. Plane polarised light. Field of view ~ 7.5 mm across.
(b). Detail of a chlorite-quartz filled vesicle in the host siltstone adjacent to pumiceous rhyolite at 175.3 m in MCD 10. Plane polarised light. Field of view ~ 1.25 mm across.
(c). Tube pumice texture in feldspar-phyric (f) pumiceous rhyolite that intrudes siltstone at 175.3 m in MCD 10. Note the delicate wispy terminations of the rhyolite domain. Plane polarised light. Field of view ~ 3 mm across.

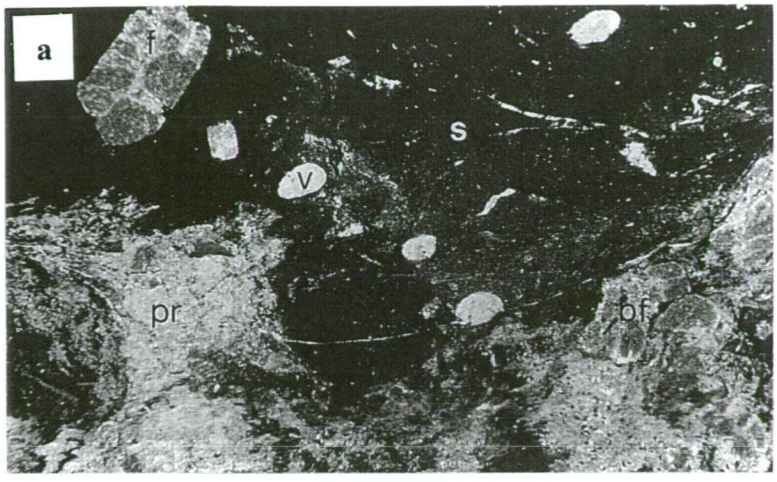
a
f
s
v
pr
bf

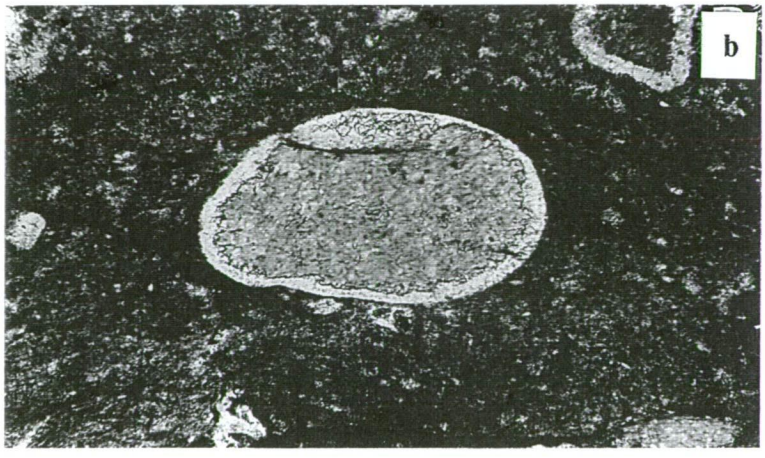
b

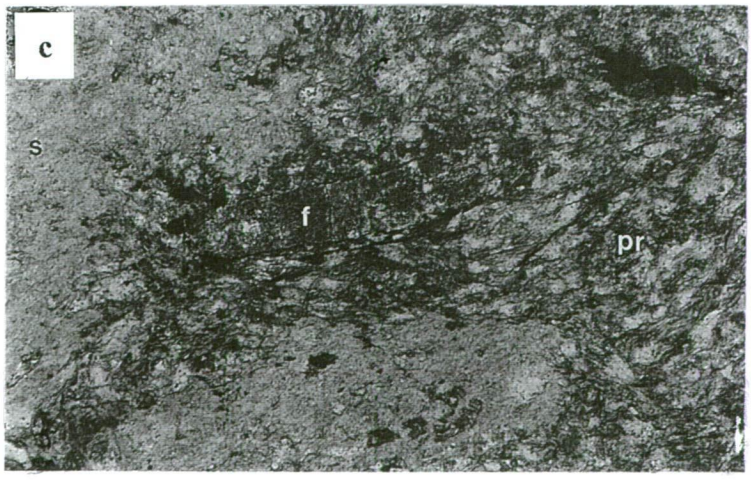
c
s
f
pr

The groundmass of the rhyolite has three textural domains, all of which are transitional to each other: non-vesicular, round vesicle and tube pumice domains. The transition from one domain to the next occurs over short distances (≤2-3mm). In the non-vesicular domains, the groundmass is uniformly and completely altered to sericite ± silica. The round vesicle domains are composed of round quartz-filled vesicles less than 0.1 mm in diameter within sericitic groundmass. The vesicles comprise up to 60% of the round vesicle domains. These round vesicle domains grade into tube pumice domains. In the tube pumice domains, vesicles are infilled by quartz and the vesicle walls have been completely altered to sericite.

The rhyolite is internally massive throughout drill core intersections up to 15 m in thickness. It includes up to 2 modal % feldspar-phyric clasts that have the same size and abundance of feldspar phenocrysts as the surrounding rhyolite but within a non-vesicular, quartz-feldspar-sericite groundmass that was probably originally glassy. These probable rhyolite clasts range up to 25 mm across and are angular to subangular.

5.2.3. Pumiceous Rhyolite - Siltstone Peperite

Peperite composed of pumiceous rhyolite and siltstone at Mount Chalmers occurs in two main settings: (1) peperite associated with intervals of coherent to *in situ* fractured rhyolite (Fig. 5.3); (2) peperite not associated with coherent rhyolite (Fig. 5.4). The latter category includes a spectrum of rhyolite - siltstone mixtures that range from rhyolite-dominated to sediment-dominated peperite. The distinction between the rhyolite- and sediment-dominated types is based on a visual estimate of the relative proportions of the two components.

Examples of peperite associated with coherent rhyolite (1) were intersected in diamond drill holes WSDD 8, MCD 4 and MCD 10 (Fig. 5.3). Intervals of coherent pumiceous rhyolite range from 1 m to 10 m in thickness and have gradational to sharp upper and lower contacts with both rhyolite-dominated and sediment-dominated peperite. The coherent rhyolite is composed of euhedral feldspars set within a sericite -silica altered pumiceous groundmass. Irregularly shaped lobes and worm-like stringers of homogeneous sediment a few mm across also occur within the intervals of coherent pumiceous rhyolite and apophyses of rhyolite locally extend for relatively short distances (≤ 10 cm) into the host sediment.

Peperite that is not associated with coherent rhyolite (2) dominates the peperite occurrences intersected by the Mount Chalmers drill holes (Fig. 5.4). The peperite is composed of predominantly irregular, ragged clasts and stringers of either rhyolite in sediment (*e.g.*, MCD 6) or sediment in rhyolite (*e.g.*, WS 7), although peperite comprising blocky sediment or rhyolite domains was also intersected. In these types, the rhyolite groundmass has been completely altered to sericite, and the sediment lacks bedding and is texturally homogeneous.

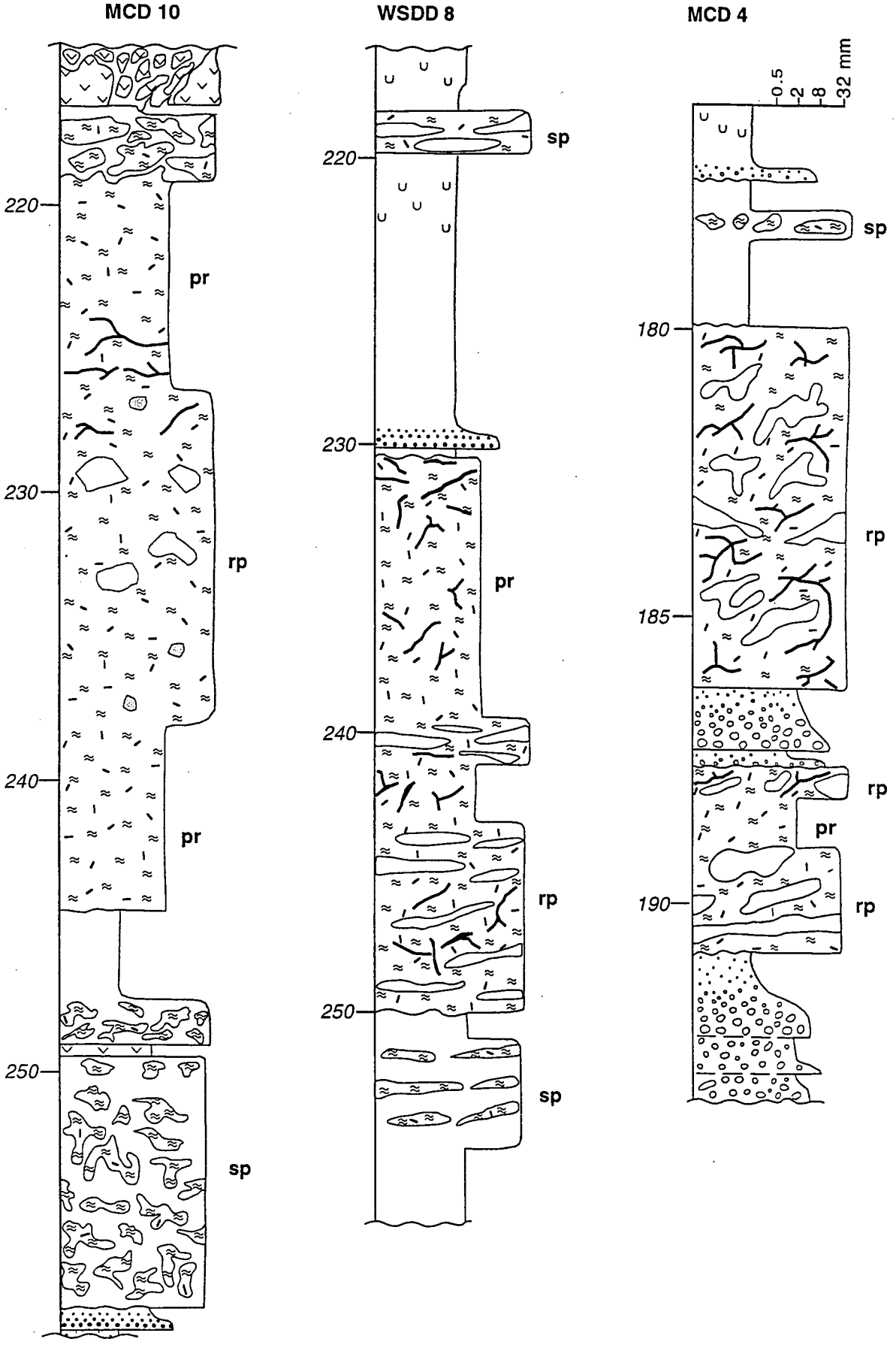

Figure 5.3. Graphic logs of diamond drillholes MCD 10 (215-259 m), WSDD 8 (216-257 m) and MCD 4 (176-193.5 m), each of which intersected pumiceous peperite that is associated with intervals of coherent pumiceous rhyolite (pr). Examples of both rhyolite-dominated (rp) and sediment-dominated (sp) peperite are also present in each intersection. The rhyolite-dominated peperite in MCD 10 (227-238 m) includes a small proportion of non-vesicular, feldspar-phyric rhyolite (?) clasts. Legend for symbols is given on Figure 5.4.

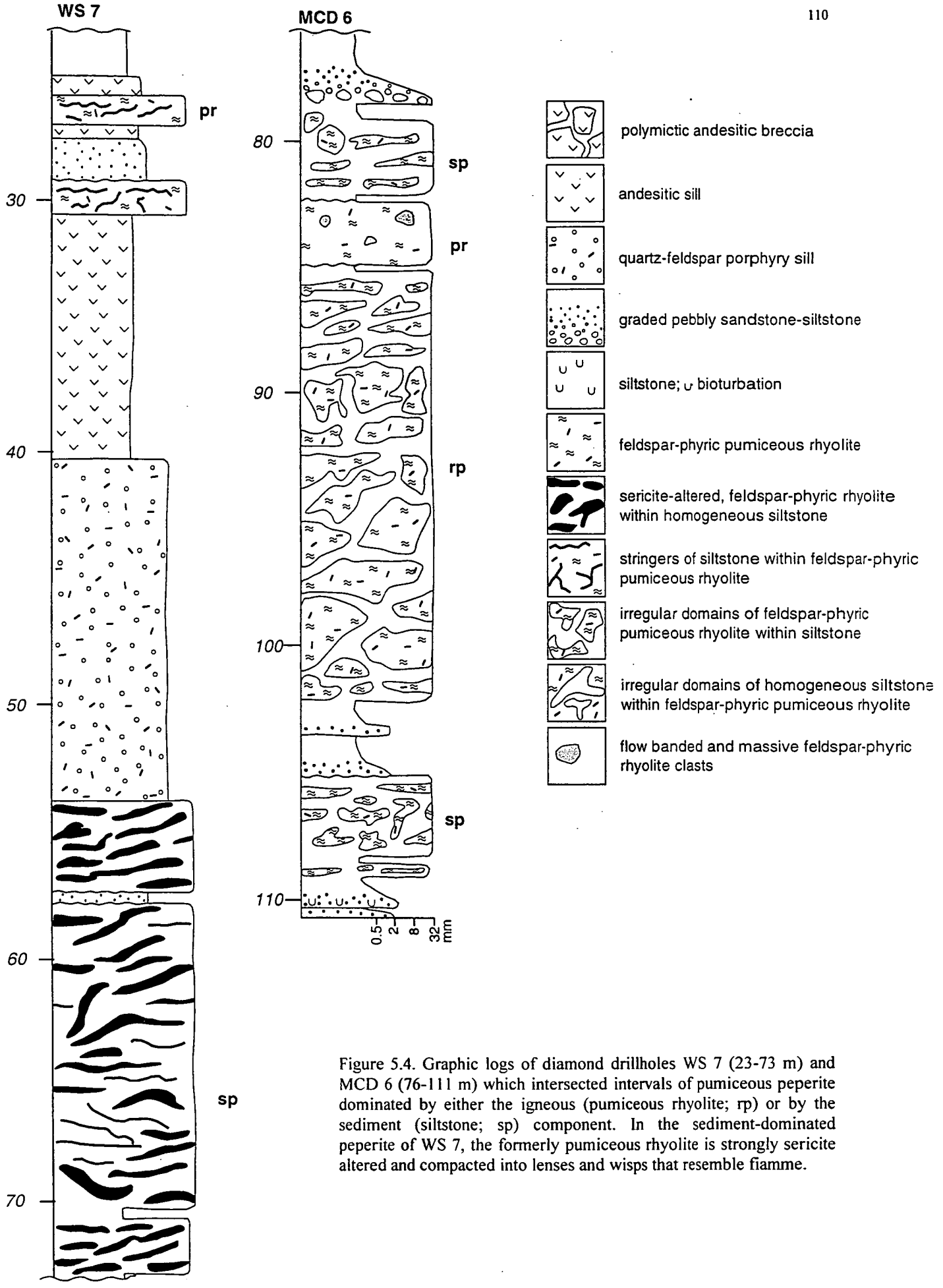

Figure 5.4. Graphic logs of diamond drillholes WS 7 (23-73 m) and MCD 6 (76-111 m) which intersected intervals of pumiceous peperite dominated by either the igneous (pumiceous rhyolite; rp) or by the sediment (siltstone; sp) component. In the sediment-dominated peperite of WS 7, the formerly pumiceous rhyolite is strongly sericite altered and compacted into lenses and wisps that resemble fiamme.

In some cases, the rhyolite clasts in the peperite have very wispy, lenticular shapes and are aligned sub-parallel to bedding (Fig. 5.1C), resembling fiamme. In these clasts, the vesicular texture is not preserved and the groundmass is composed of fine grained structureless sericite. Similar intensely sericitic, wispy domains that lack pumiceous textures occur within some intervals of coherent pumiceous rhyolite. It is likely that initial alteration of the glassy pumiceous rhyolite was patchy. Where the vesicles were infilled and the glassy walls replaced, the tube pumice structure was preserved. However, where alteration of the glassy walls involved mainly sericite (or a clay precursor), and the vesicles remained open, the pumiceous structure did not survive. These more porous domains would have compacted during diagenesis whereas the domains with infilled vesicles were not strongly affected by compaction. Early (pre- or syn-diagenetic compaction), patchy alteration appears to be a relatively common feature of submarine pumiceous facies (*e.g.*, McPhie *et al.*, 1993; Allen and Cas, 1990).

In thin section, intricate mixing of the rhyolite component and the sedimentary component is visible (Figs 5.2A and 5.2C). Delicate, semi-detached to completely detached apophyses of tube pumice extend a few mm into the host sediment; feldspar crystals, some of which have rinds of tube pumice, occur adjacent to the tube pumice apophyses. Shards derived from the pumiceous rhyolite are also a common feature of the peperite. They occur isolated within the sediment adjacent to tube pumice apophyses, or else are connected to the tube pumice. The shards are dominantly cuspate and platy bubble wall shards and pumice shreds. None of the shards show evidence for plastic deformation while still hot, as seen in welded ignimbrites. Some of the vesicles within the tube pumice shreds have been infilled by the host sediment .

5.3. IDENTIFICATION OF PUMICEOUS PEPERITE

Peperite is a variety of volcanic breccia that results from dynamic mixing of unconsolidated, typically wet sediment and molten lava or magma. Positive identification therefore rests on evidence that the sediment was unconsolidated at the time of mixing and that the igneous component was hot. The Mount Chalmers examples are very well constrained as peperite by several arguments:

1. The host sediment involved in the peperite is homogeneous in texture and unstratified whereas elsewhere, it is bedded and beds are graded. Local destruction of bedding and grading requires considerable re-arrangement of the original grain packing which can only take place in sediment that is unconsolidated or weakly consolidated.
2. The sediment immediately adjacent to the rhyolite is vesicular. The vesicles indicate that gas-filled bubbles were trapped within the sediment. Formation of vesicles requires small-scale re-arrangements of the sediment grains and intergranular movement of the entrapped gas phase, both of which can only be accomplished in wet, unconsolidated sediment.

3. The presence of vesicles in the host sediment indicates that the rhyolite was hot when the two components were mixing. Vesicles do not occur elsewhere in the sedimentary facies and show a close spatial relationship with the rhyolite. In this instance, the gas phase could have been steam generated from heating of the pore fluids by the intruding rhyolite and/or magmatic volatiles exsolving from the rhyolite or released from rupturing vesicles within it.
4. Away from the rhyolite, the host sediment is green-grey but it fades to cream or very pale green in a zone about 1-2 cm wide adjacent to the rhyolite. The colour change is gradational and closely mirrors the sediment-rhyolite contacts. The paler sediment at the contacts is more silicified than the host sedimentary facies elsewhere. The subtle, gradational colour change and local silicification of the sediment are interpreted to result from thermal metamorphism of the sediment in contact with hot rhyolite.
5. The shapes of many of the rhyolite clasts in the peperite are highly irregular and suggest that part of the rhyolite was behaving, at least momentarily, in a ductile and plastic fashion during mixing. However, in some cases, the highly irregular and ragged shape of the rhyolite domains is not entirely primary but a consequence of variable compaction of the original pumiceous structure.

In submarine settings, pumice - sediment mixtures can result from mechanisms other than dynamic mixing of a pumiceous intrusion with wet sediment. Large clasts of pumice generated by submarine eruptions, both effusive and explosive, are initially buoyant but eventually become water-logged and sink, together with fine sediment from other sources settling from suspension (*e.g.*, Reynolds *et al.*, 1980; Clough *et al.*, 1981; Kano *et al.*, 1996; Fiske *et al.*, 1998). This process yields a deposit composed of outsize (up to several metres across) pumice clasts in mudstone or siltstone, which after compaction, can strongly resemble the complicated and intricate mixtures of sedimentary and igneous components typical of pumiceous peperite. However, water-settled pumice blocks may be distinguished by the presence of stratification in the enclosing sediment, especially stratification that drapes contacts with the pumice blocks. Water-settled pumice blocks are typically concentrated in laterally continuous beds, and evidence for thermal metamorphism of the sediment component is lacking. Neither do they show gradational relationships with intervals of coherent pumiceous component. On all counts, features of the pumiceous rhyolite - siltstone mixtures at Mount Chalmers are not consistent with an origin involving water-logged pumice but instead, are best interpreted as the result of dynamic mixing of a pumiceous intrusion with wet sediment. The two main categories of pumiceous peperite described above (associated with or separate from coherent rhyolite) are most likely related, representing sections that have intersected either the parent intrusion (1) or its peperitic margins (2) (Fig. 5.5).

5.4. Formation of Pumiceous Sills and Pumiceous Peperite

The setting, facies relationships and textures in the pumiceous sills and peperite at Mount Chalmers provide some constraints on the sequence of events, especially the means by which the pumiceous rhyolite was dismembered and mixed with the enclosing sediment.

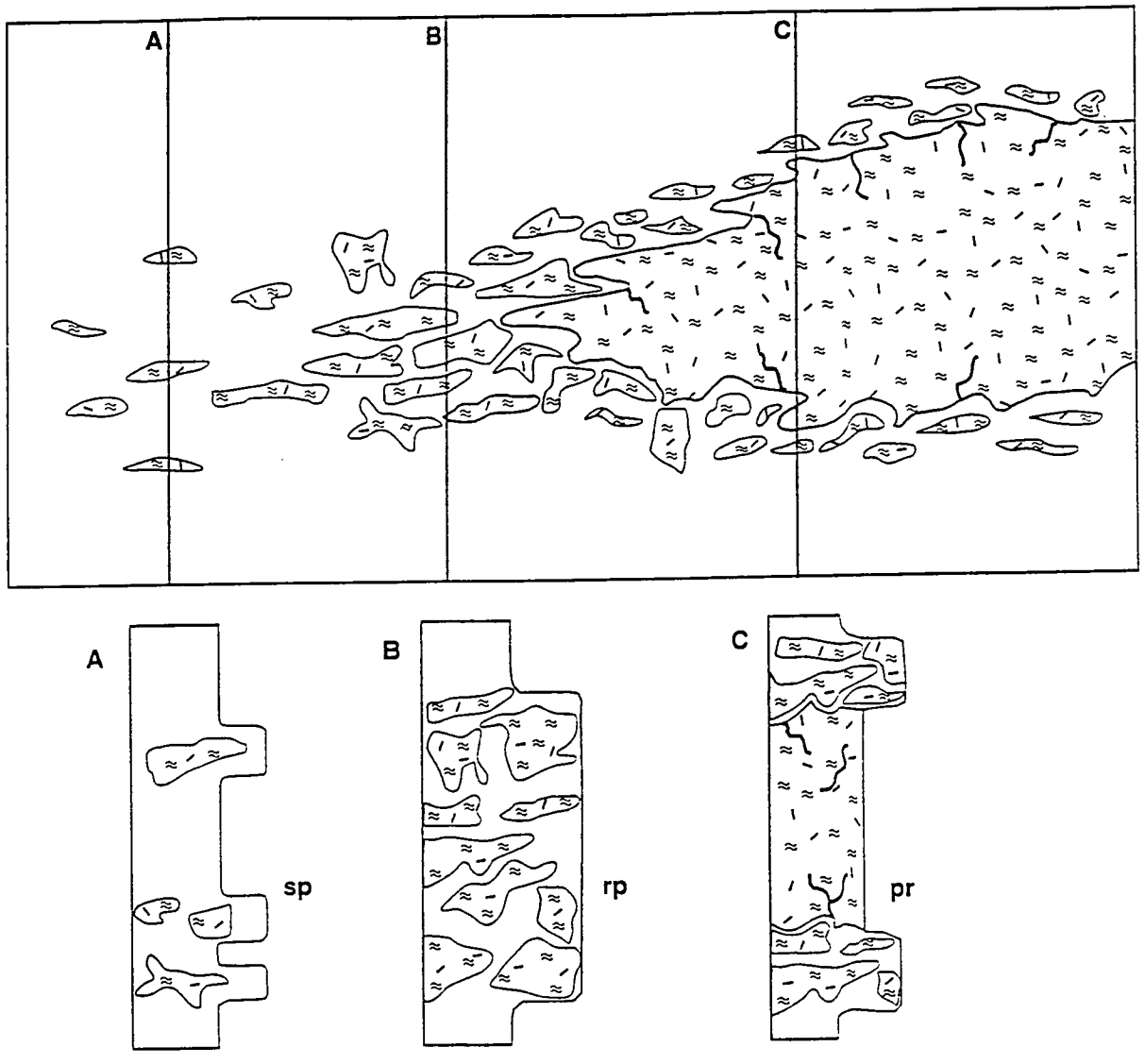

Figure 5.5. Cartoon showing inferred relationships between drill core intersections of pumiceous peperite associated with coherent pumiceous rhyolite (pr) and peperite that apparently occurs separately. It is likely that the latter intersections (A, B) represent settings beyond the margins of the sills where the peperite facies was dominant. In these settings, the peperite ranges from rhyolite-dominated (rp) near the sills (B), to sediment-dominated peperite (sp) farther from the sills (A).

5.4.1 Setting and Confining Pressure

Significant vesiculation of rhyolitic magmas with average water contents (~3 wt%) is probably limited to confining pressures less than 10 MPa (McBirney, 1963). Both the presence of vesicles in the host sediment and the pumiceous nature of the rhyolite at Mount Chalmers imply that the confining pressure was substantially below that limit. The sedimentary succession that hosts the pumiceous rhyolite has facies characteristics and trace fossil and body fossil assemblages consistent with a shallow submarine shelf setting (Sainty, 1992). The abundance of turbidites suggests that the setting was below storm wave base. These constraints provide an indication that the water depth most likely ranged from a minimum of a few tens of metres to a maximum of about 200 m.

Constraints on the thickness of sediment cover above the rhyolite sills at Mount Chalmers are less precise. The position of the palaeoseafloor at the time of intrusion can not be recognised in the stratigraphy above the sills. However, the sediment cover may have been as little as a few tens of metres up to more than 100 m thick. At the likely maximum water depth of 200 m, the confining pressure limit of 10 MPa would not have been exceeded until the wet sediment cover was more than about 400 m thick (Fig. 5.6). Thus, the confining pressure did not prevent vesiculation.

5.4.2. Geometry and Size of the Pumiceous Intrusions

The lack of correlation among intervals of pumiceous rhyolite and associated peperite suggests that the initial rhyolitic intrusion comprised separate lobes or digits with dimensions in the order of 10 m across and up to a few tens of metres thick (Fig. 5.7A). Such a facies geometry has been described in felsic, submarine and subglacial rhyolites (*e.g.*, Yamagishi, 1987; De Rosen-spence *et al.*, 1980; Furnes *et al.*, 1980), and in subaerial felsic lavas (*e.g.*, Nakada, 1992) and in felsic intrusions (*e.g.*, McPhie and Goto, 1996).

5.4.3. Model for intrusion, fragmentation and mixing

The rhyolite lobes intruded wet sediment and rapidly developed chilled, glassy margins that thermally insulated the interior (Figs 5.7A and 5.7B). Intrusion was accommodated by expansion of the enclosing water-saturated sediment in response to heating of the pore fluid, progressive disruption of grain contacts and displacement of the sediment cover. The confining pressure exerted by the sediment cover and the overlying shallow seawater was sufficiently low to allow vesiculation of the hot interior of the rhyolite lobes. Concurrently, new magma was being fed into the lobe interiors. Thus the lobes inflated (Fig. 5.7C) in response to vesiculation and to continued magma supply. Early formed vesicles became increasingly elongate in the direction of shear within the growing lobes.

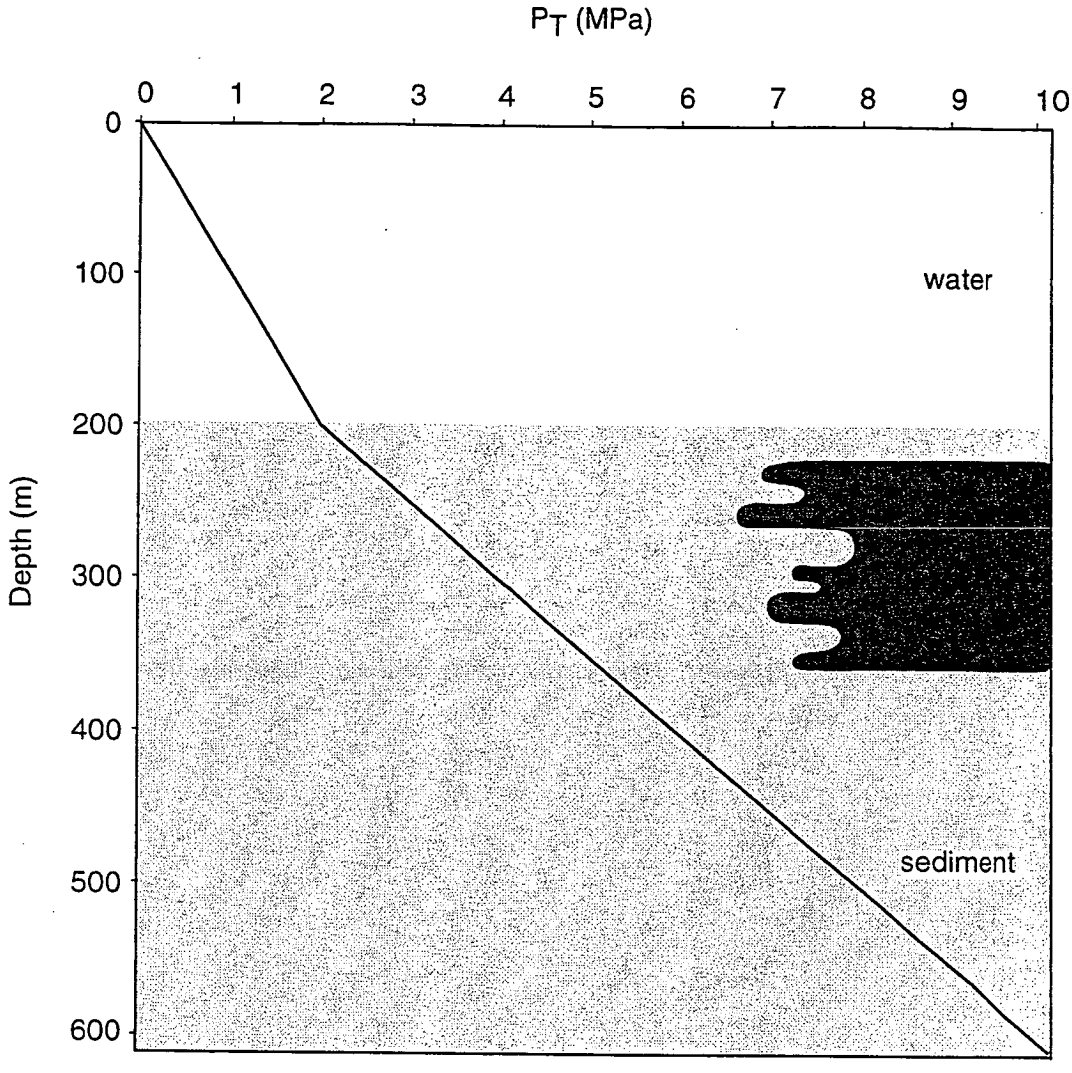

Figure 5.6. Graph showing the likely range of confining pressure (P_T) experienced by the Mount Chalmers pumiceous rhyolite sills. P_T includes the pressure exerted by the seawater and the pressure exerted by the wet sediment covering the sills. The depth of the seawater was probably less than 200m. The thickness of the wet sediment cover is poorly constrained, but may have been in the range of 30-150m. Pt exerted by a 150-m thick layer of wet sediment with density 2000 kg/m^3 (*e.g.* Moore, 1962) and 200 m of seawater is ~5 MPa. Vesiculation of rhyolite can occur for confining pressures up to about 10 MPa (McBirney, 1963), which corresponds to a sediment cover of ~400m.

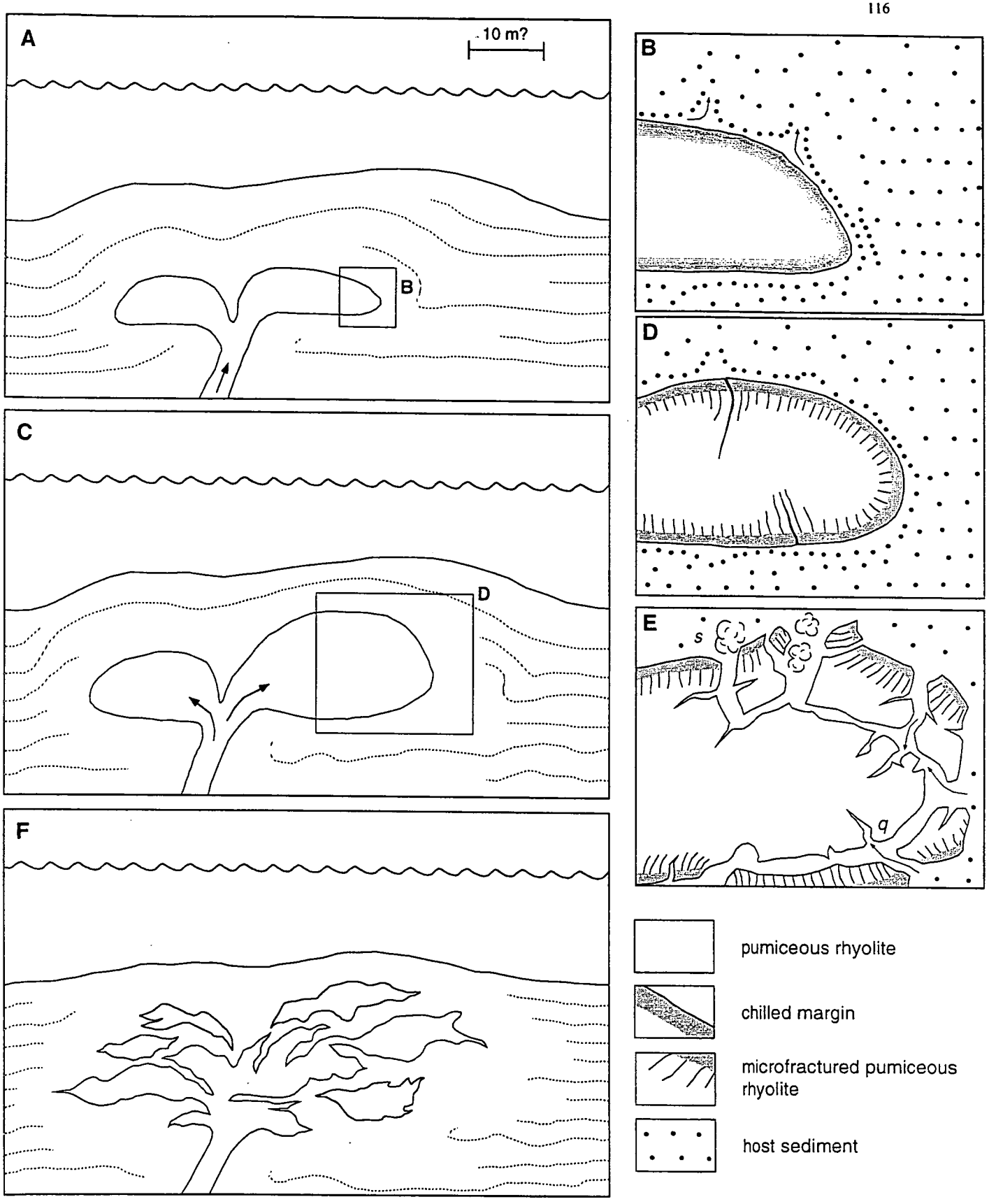

Figure 5.7. Schematic reconstruction of the sequence of events involved in the formation of pumiceous sills and associated peperite at Mount Chalmers. (A). Intrusion of rhyolite lobes into wet silt and fine sand. (B) Space was created by expansion and fluidisation of the sediment at the contact The lobes developed a glassy, nonvesicular chilled margin. (C). Inflation of the lobes occurred in response to vesiculation and to continued magma supply. (D) Parts of the lobes that cooled through the glass transition temperature developed microfractures in the walls of the vesicles. (E) Failure of the microfractured vesicular domains dismembered the lobes and allowed ingress of wet sediment. Direct interaction of wet sediment with the hot rhyolite resulted in further disintergration and mixing caused steam explosions (s) and / or quench fragmentation (q). (F) Fragmentation of the intrusive lobes and mixing with the wet host sediment produced a complex arrangement pumiceous rhyolite, rhyolite-dominated peperite and sediment-dominated peperite. Bedding in the host sediment was destroyed where mixing with the pumiceous rhyolite occurred, but was undisturbed elsewhere.

The intricate mixtures of pumiceous rhyolite and sediment in the Mount Chalmers peperite indicate that at some point, the rhyolite lobes were dismembered and invaded by wet sediment. The non-vesicular, formerly glassy rhyolite clasts in the pumiceous sills could represent fragments of the ruptured chilled margin. A number of processes probably contributed to fragmentation of the lobes. Depressurisation of the inflated lobes may have triggered fragmentation. Mungall *et al.* (1996) have shown that cooling of vesicular shallow intrusions is accompanied by development of microfractures in vesicle walls due to dehydration and shrinkage. This greatly reduces the strength of the vesicular glass so that a small reduction in confining pressure can cause disintegration. This process would have affected portions of the vesicular rhyolite that had cooled below the glass transition temperature and were subject to small, probably local reductions in confining pressure. Cooling and microfracturing of the rhyolite were heterogeneous, proceeding faster in proximity to the chilled margins and quench fractures (Fig. 5.7D). Mechanisms for reducing confining pressure in these circumstances include (1) local unloading by slumping of the overlying, up-domed sediment pile, and/or (2) propagation of fractures through the chilled margins of the lobes and into the more slowly cooled vesicular domains. Microfracture-driven disintegration could yield fragments ranging from mm size, being bubble-wall shards from disruption of vesicles, to several metres, governed by the distribution of domains that had cooled through the glass transition. Wet and/or steam-rich sediment would have immediately invaded fractures propagating through the rhyolite and engulfed detached apophyses of rhyolite.

Failure of the cooler parts of the lobes allowed wet sediment to interact directly with hot rhyolite that remained in the interior of the lobes (Fig. 5.7E). Because the confining pressure was relatively low, direct contact between the hot rhyolite and wet sediment may have generated steam-driven explosions capable of fragmenting the rhyolite. In addition, rapid cooling and contraction of the hot rhyolite in contact with wet sediment would have promoted dismembering of the lobes. Quench fractures that opened in the hot vesicular rhyolite were rapidly invaded by the host sediment.

Gas released by rupture of vesicles in the rhyolite and/or steam from vaporised pore fluid formed bubbles in the sediment immediately adjacent to the rhyolite. Intrusion of the rhyolite into the sediment together with heating, expansion and possible fluidisation by the pore fluid led to destruction of bedding and other original structures in the host sediment adjacent to the rhyolite. Heat and magmatic fluids released from the rhyolite resulted in induration, bleaching and silicification of the sediment in direct contact with it.

5.4.4. Other Examples of Pumiceous Peperite

Although by no means common, pumiceous peperite is not unique to the Mount Chalmers locality. Other examples of felsic pumiceous intrusions and associated peperite have been reported from the Miocene submarine successions of the Green Tuff Belt on Honshu, Japan and the Mount Read Volcanics of western Tasmania (*e.g.*, Gifkins *et al.*, 1996). These are also known from drill core intersections and involve complex arrangements of coherent pumiceous to non-vesicular rhyolite enclosed by *in situ* intrusive hyaloclastite and pumiceous peperite.

The apparent paucity of examples most likely reflects a combination of the rarity of the special circumstances required for vesiculation of intrusions, and the difficulty of identifying the critical diagnostic features of such facies. In particular, extensive vesiculation requires low confining pressure and delayed quenching which are conditions not easily met by intrusions into water-saturated sediments. The first condition places limits on the thickness of the sediment cover and on the water depth. The second condition depends on the development of an insulating chilled margin that impedes cooling and promotes the build-up of internal volatile pressure.

5.5. CONCLUSIONS

The Early Permian submarine volcanic and sedimentary succession at Mount Chalmers includes syn-volcanic sills and associated peperite in which the igneous component is pumiceous rhyolite. Key features of the pumiceous peperite are: (1) the highly irregular contacts between pumiceous rhyolite and host sediment, (2) the gradational to sharp contacts between coherent pumiceous rhyolite and pumiceous peperite, (3) the presence of vesicles and thermal metamorphic effects in the host sediment adjacent to the rhyolite, and (4) local destruction of bedding in the sediment involved in the peperite.

Formation of the pumiceous sills and associated pumiceous peperite involved intrusion of rhyolite lobes that developed chilled margins. The lobes inflated in response to magma supply and vesiculation. A number of processes may have operated to fragment and dismember the lobes. In this setting, microfracturing of vesicle walls probably occurred during cooling, weakening the vesicular rhyolite so that even a small reduction in confining pressure would have been sufficient to cause disintegration (*e.g.*, Mungall *et al.*, 1996). Where hot rhyolite came in direct contact with wet sediment, both quench fragmentation and steam explosions may have operated. Heating of the sediment pore fluid led to expansion and possible vaporisation that disrupted grain packing and completely destroyed bedding in the vicinity of the lobes. Gas released from the pumiceous rhyolite and/or steam from vaporised pore fluid was entrapped as bubbles in the host sediment.

The formation of pumiceous sills and peperite in a water-saturated host sedimentary succession requires a special combination of low confining pressure, vesiculation and delayed quenching. The facies characteristics of the Mount Chalmers pumiceous sills and peperite suggest that the depositional setting was a submarine shelf below wave base but no more than a couple of hundred metres deep and possibly substantially shallower. Delayed quenching was achieved by development of a chilled margin that effectively insulated the interior from the surrounding wet sediment.

CHAPTER 6
VOLCANIC-HOSTED MASSIVE SULPHIDE MINERALISATION

6.1. INTRODUCTION

The only known mineralised occurrence of any economic significance within the Berserker beds occurs at the Mount Chalmers mine. Within a 2 - 3 km radius of the mine are a number of old workings and prospects (Fig. 6.1). The styles of mineralisation within the Berserker beds fall into one of two broad types, volcanic-hosted disseminated to massive sulphide mineralisation as at Mount Chalmers, Wood's Shaft, Mount Warminster, Boto's and Tungamull and Au lode-style mineralisation as in the New Zealand Gully area.

The Mount Chalmers volcanic-hosted massive sulphide (VHMS) deposit has been compared to the VHMS Kuroko-style deposits of Japan (Okill, 1974; Large and Both, 1980; Taube and van der Helder, 1983). The style of mineralisation at the prospects that surround Mount Chalmers, namely, Wood's Shaft, Mount Warminster, Boto's and Tungamull may also be analogous with the VHMS style of mineralisation.

This chapter describes the style of mineralisation present at the Mount Chalmers mine and its environs, establishes the link between the mineralisation and volcanism and also establish the palaeoenvironmental setting for the formation of the Mount Chalmers mineralisation.

6.2. VOLCANIC-HOSTED MASSIVE SULPHIDE MINERALISATION

Here a volcanic-hosted massive sulphide deposit is defined as a stratabound accumulation of sulphide minerals that were precipitated from a hydrothermal fluid at or below the seafloor and are hosted within a sequence dominated by submarine volcanics. The deposits generally have a crosscutting stringer zone or massive replacement pipe (Franklin *et al.*, 1981; Lydon, 1988; Large, 1992; Barrie and Hannington, 1997). Based upon this classification Mount Chalmers can be classified as a VHMS deposit. VHMS deposits are found within a wide range of tectonic settings, they occur within volcano-sedimentary successions, and are commonly coeval or coincident with volcanic rocks. The ores characteristically consist of more than 60 percent sulphide, most of which are pyrite and/or pyrrhotite and variable amounts of sphalerite, chalcopyrite and galena. The deposits are further characterised by an internal metal zoning, commonly characterised by an upward and outward decrease in the Cu/(Cu+Zn+Pb) ratio (Franklin *et al.*, 1981; Lydon, 1988; Barrie and Hannington, 1997).

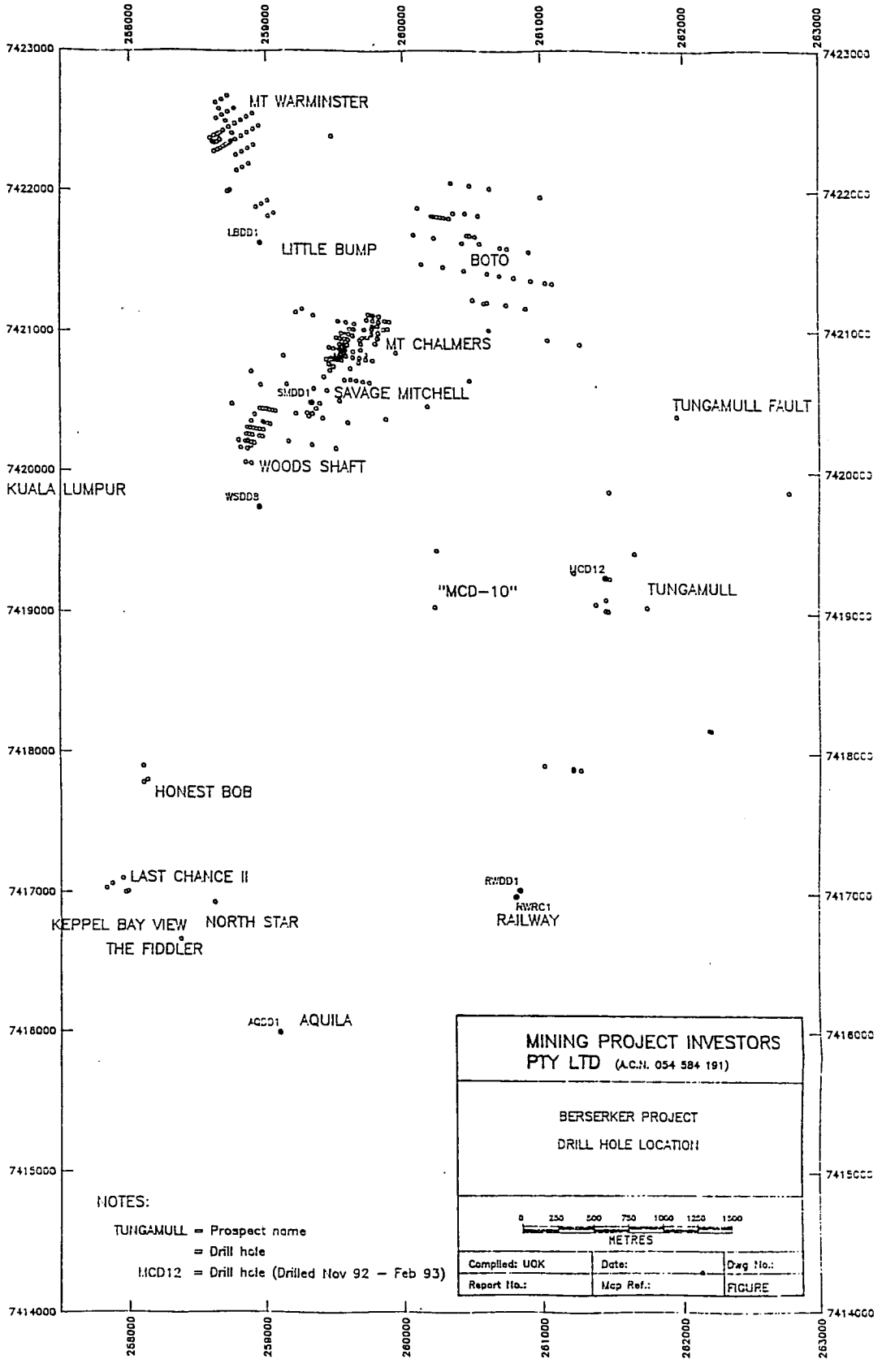

Figure 6.1. Location of Mount Chalmers mine and surrounding prospects

6.2.1. Mount Chalmers - Style of Mineralisation

The mineralisation at Mount Chalmers occurs in two main ore bodies, the Main Lode and the West Lode, and one minor lens, the South Lode. In 1860 the highly siliceous "chimney" of the Main Lode was found to contain gold, and copper was discovered in 1898. The significance and extent of the mineralisation at the West Lode remained unknown until it was drilled and defined by Geopeko in 1977 (Large and Both, 1980). Large and Both (1980) reported a proven reserve of 3,860,000 tonnes at 1.65 % Cu and 1.87 g/t Au. Between 1898 and 1943, 434,899 tonnes at 2.70% Cu and 4.68 g/t Au were mined from Mount Chalmers (Table 6.1). This gives a total resource for Mount Chalmers of 4,294,899 tonnes at 1.76 % Cu and 2.15 g/t Au (Hunns, 1994). Geopeko commenced mining operations in 1979 and ceased in 1982.

Table 6.1. Resource and mine production data estimate for Mount Chalmers. From Taube and van der Helder (1983) and Hunns (1994). NA = not available

Lode	Ore Mined (tonnes)	Au g/t	Cu %	Zn %	Pb %	Ag g/t
Main Lode Underground (1898 -1943)	434,899	4.68	2.70	NA	NA	19.9
Main Lode Open Cut (1979 - 1982)	561,930	2.57	1.60	0.52	0.21	17.4
West Lode Open Cut (1979 – 1980)	217,567	3.41	1.57	1.92	0.82	31.2
Total Production	1,214,396	3.48	1.99			20.8
Total Resource	4,294,899	2.15	1.76			

6.2.1.1. Massive Sulphide Mineralisation

6.2.1.1.1. Massive Sulphide Distribution

Isopachs of the massive sulphide were generated using all available drillhole data in order to determine the spatial distribution of the massive sulphide ore lenses (Fig.6.2). The massive sulphide lenses have a limited spatial distribution compared to the stringer zone mineralisation. The isopachs show that the massive sulphide mineralisation for both the Main Lode and the west Lode is oriented predominantly in a northerly direction, with a northwest and a north northeast component to the spatial distribution of the massive sulphide also evident (Fig. 6.2). The isopachs also show that the Main Lode massive sulphide is thicker and spatially more extensive than the West Lode.

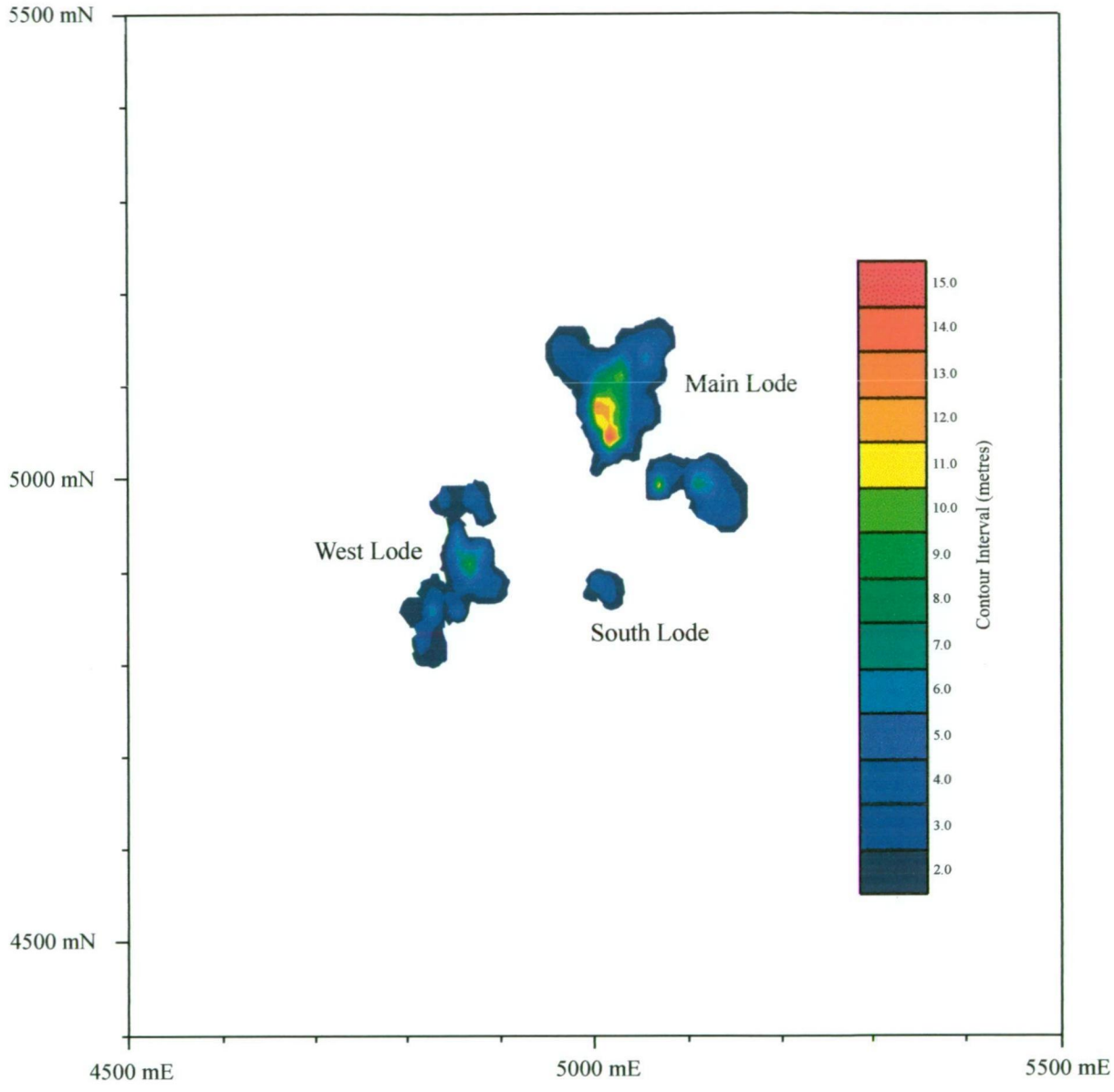

Figure 6.2. Isopachs of massive sulphide thickness

6.2.1.1.2. Main Lode

The Main Lode mineralisation is approximately 500 m long and 100 m wide and up to 60 m thick (including the stringer zone). The massive sulphide mineralisation attains a maximum thickness of approximately 17 m, with a number of drill holes having intersections of massive sulphide over 10 m. The massive sulphide mineralisation is continuous, *i.e* no identifiable breaks in the mineralisation were observed (Fig. 6.3), however, the massive sulphide mineralisation consists of three zones:

1. upper laminated zone - composed of fine-grained pyrite with chalcopyrite (Figs. 6.4a and 6.4b).
2. middle zone - dominated by fine-grained to coarse-grained (2 - 10 mm) fragmental pyrite with chalcopyrite set within a fine-grained pyritic matrix (Figs. 6.4c and 6.4d).
3. lower zone - composed predominantly of massive fine-grained pyrite ± chalcopyrite.

Within the upper laminated zone, individual layers are generally monomict and are predominantly composed of fine-grained pyrite and later chalcopyrite. The laminae may either be continuous or discontinuous. Individual laminations are between 5 - 40 mm thick (Figs 6.4a and 6.4b). In MC66 the sulphide laminae are disrupted and contorted. Individual laminations may be separated by intervals of fragmental sulphide. Rare sphalerite and galena groundmass may also be present. Matrix supported pyrite grains and fragments of pyrite aggregations dominate the fragmental sulphides (Figs. 6.4c and 6.4d). The groundmass to the massive sulphide may be composed of silica-chlorite alteration and may also contain barite crystals. The lower zone massive sulphide is composed of densely packed individual pyrite grains, fragments of pyrite agglomerations, and is structureless.

The Main Lode massive sulphide is overlain predominantly by peperite or sediments (Fig. 6.3), except where an andesite has intruded along the contact. The base of the hangingwall lithologies is invariably altered by one or more of the following alteration phases: hematite, chlorite, silica, sericite and dolomite. Minor sulphide mineralisation may also extend up into the base of the hangingwall lithologies. A well-developed and intense footwall alteration underlies the massive sulphide mineralisation and is dominated by silica, chlorite, dolomite, kaolin and sericite mineral assemblages (Fig. 6.3). The contact between the massive sulphide and the underlying stringer zone mineralisation and footwall alteration is gradational.

6.2.1.1.3. West Lode

The West Lode mineralisation is centred approximately 150 m southwest of the of the Main Lode outcrop. The orebody is elongated in a north-northeast direction, with maximum dimensions of 200 x 90 x 25 m (including stringer zone mineralisation). The massive sulphide mineralisation attains a maximum thickness of approximately 15 m, but the majority of drill holes have intersections of massive sulphide less than 5 m.

Figure 6.3. Graphic lithological logs illustrating the relationship between the Main Lode massive sulphide ore lens, footwall and hangingwall lithologies

Legend for Figures 6.3 and 6.5


Gossan

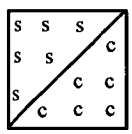

Silica/chlorite

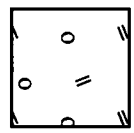
Quartz-feldspar porphyry


Massive sulphide

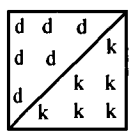

Dolomite/kaolinite

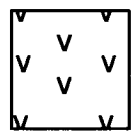

Andesite

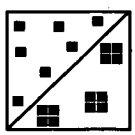
Dessiminated/ agglomerations of pyrite

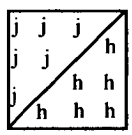

Jasper/hematite

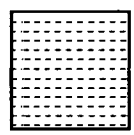
Siltstone


Pyrite-chalcopyrite veins

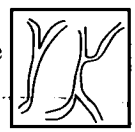
Dolomite & quartz veins

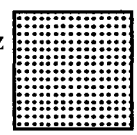
Sandstone

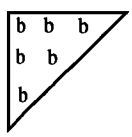

barite


Peperite


Feldspar-phyric pumice breccia


Feldspar-phyric rhyolire/ +/- flowbands


Feldspar-phyric rhyolitic breccia

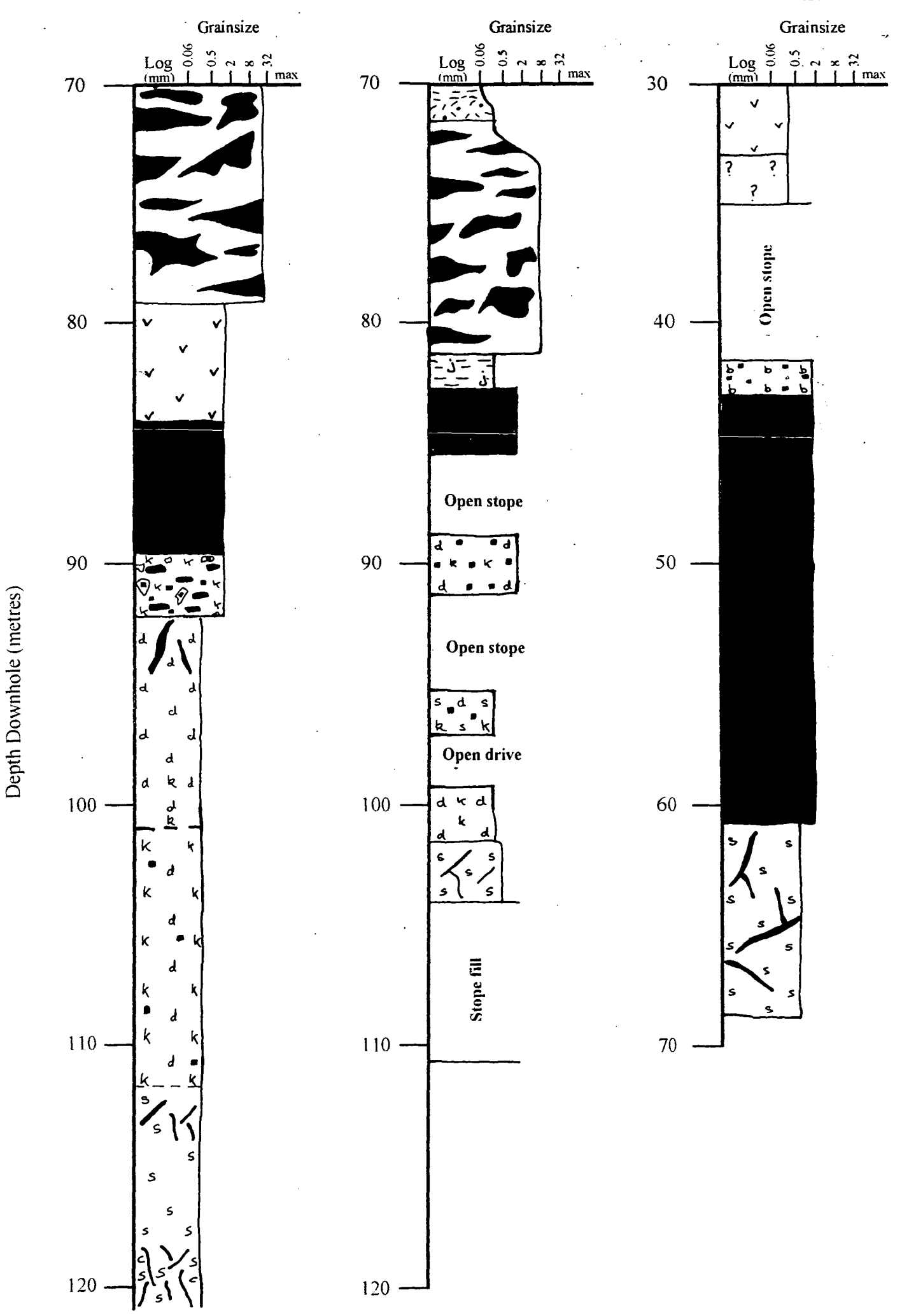
MCP49/MC49
MCP53/MC54
MCP81/MC64
Grainsize
Log (mm)
0.06
0.5
2
8
32
max
Depth Downhole (metres)
70
80
90
100
110
120
30
40
50
60
Open stope
Open stope
Open stope
Open drive
Stope fill

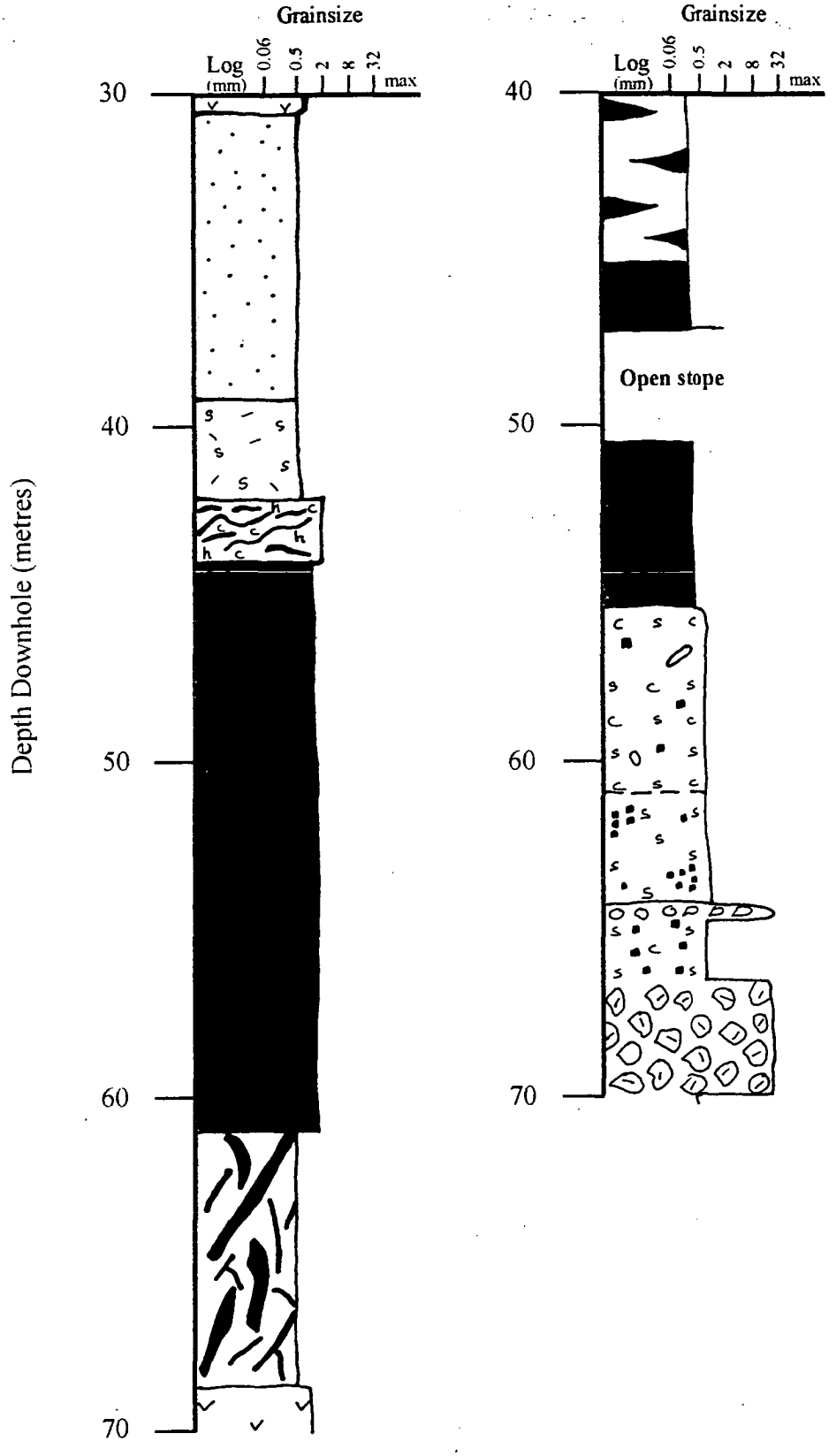

Figure 6.3. con't

Figure 6.4. Representative examples of the Main Lode massive sulphide mineralisation.

Figure 6.4a MC64 - 46.30 m; Figure 6.4b. MC64 - 44.30 m; Figure 6.4c MC64 - 45.15 m; Figure 6.4d MC64 - 43.17 m

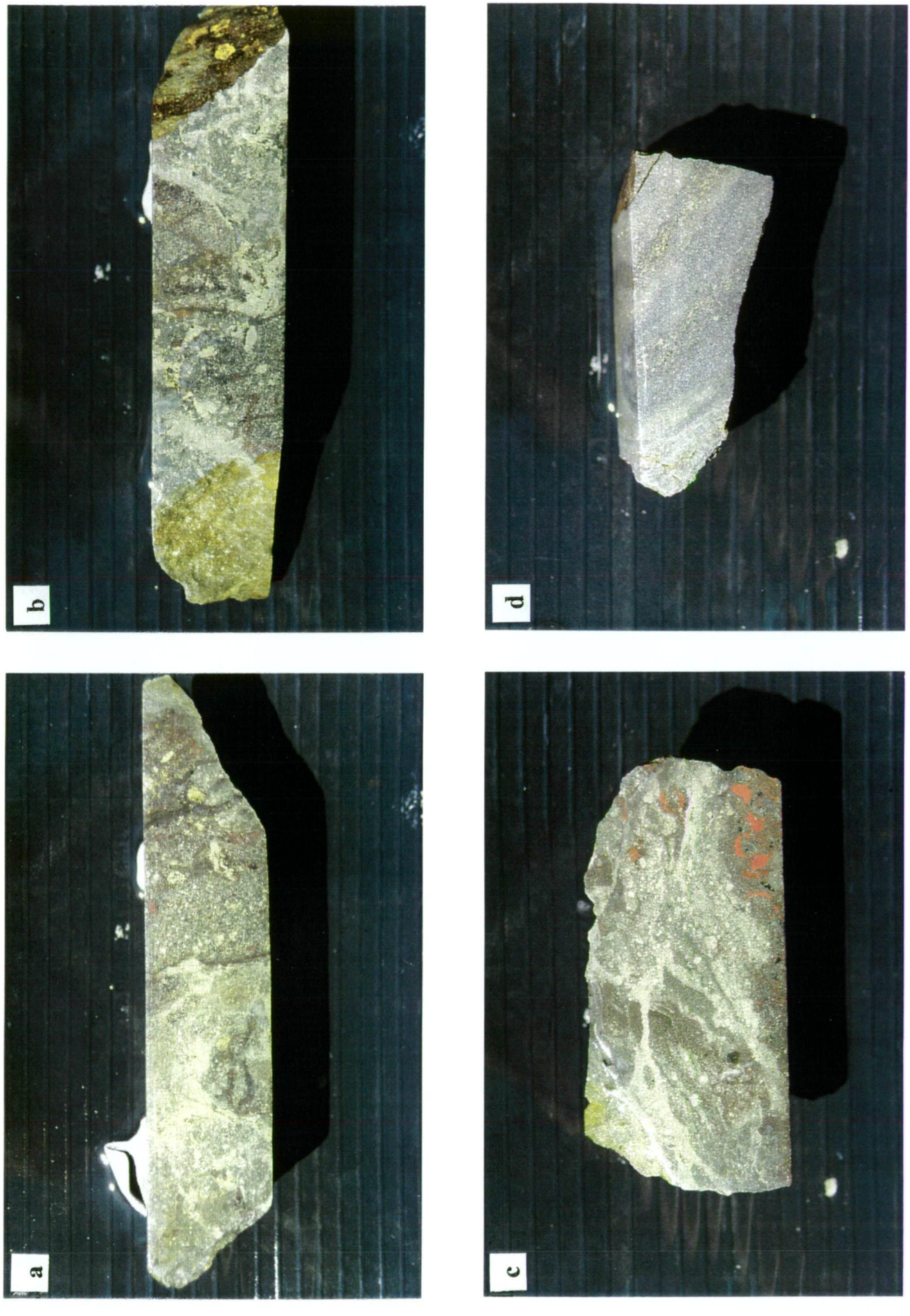
b
d
a
c

Locally the West Lode massive sulphide mineralisation is not continuous with some intersections of massive sulphide being separated by zones of sulphide veins that transect silica and or chlorite alteration *e.g.* MC25, MC44 and MC48 (Fig. 6.5). The West Lode mineralisation consists of an upper zone of massive Cu-Au-Zn-Ag ore, 6 - 10-m thick, with a lower stringer zone of Cu-Au mineralisation, 6 - 25 m thick.

The West Lode massive sulphide like the Main Lode massive sulphide has three readily identifiable zones:

- upper laminated zone is composed of fine-grained pyrite, sphalerite ± galena ± chalcopyrite. The laminae may either be continuous or discontinuous, and may be inter mixed with the fragmental sulphides (Figs. 6.6a and 6.6b).
- middle zone is dominated by fine-grained to coarse-grained fragmental pyrite, sphalerite ± chalcopyrite ± galena (Figs. 6.6c and 6.6d). Round chalcopyrite fragments may be up to 20 mm in diameter (Fig. 6.6c). The fragmental sulphides occur within a groundmass of fine-grained pyrite. Barite crystals may occur within the groundmass were they are rimmed and being replaced by pyrite.
- lower zone - composed predominantly of massive fine-grained pyrite ± chalcopyrite ± sphalerite.

Both the Main Lode and the West Lode have a locally developed an uppermost fourth zone that is composed of semi-massive sulphide. In this zone the sulphides are dominated by disseminated individual pyrite grains ± chalcopyrite ± sphalerite ± galena and disseminated agglomerations of pyrite all set within a matrix composed of sericite *e.g.* MC66, sericite + chlorite *e.g.* MC28 or within a kaolin rich matrix *e.g.* MC39. Locally cross cutting the massive sulphide are near vertical fine-grained pyrite ± chalcopyrite veins. These veins cut across the all the three main sulphide zones, and locally may dominate the massive sulphide. The relationships between the various zones that comprise the massive sulphide ore lenses are shown schematically in Figure 6.7.

The West Lode massive sulphide is overlain by a well-developed gossan. The contact between the massive sulphide and the gossan is gradational (Fig. 6.8a,b,c and d). The transition zone between massive sulphide and gossan is marked by the presence of oxidised pyrite, malachite, covellite, azurite and chalcocite. Where the gossan is not well-developed or has not developed at all a feldspar-phyric rhyolite generally immediately overlies the massive sulphide (Fig. 6.8a). In MC34, the massive sulphide is overlain by brecciated rhyolite, where tongues of the massive sulphide have intruded up in between the rhyolite clasts. The West Lode massive sulphide mineralisation is underlain by an intense footwall alteration zone of composed different mineral assemblages, but generally dominated by silica, chlorite, sericite, dolomite and kaolin. The downhole contacts between the massive sulphide and the underlying stringer zone mineralisation and footwall lithologies are gradational, except in MC30 where the contact is very sharp.

Figure 6.5. Graphic lithological logs illustrating the relationship between the West Lode massive sulphide ore lens, footwall and hangingwall lithologies. Key is facing page 124.

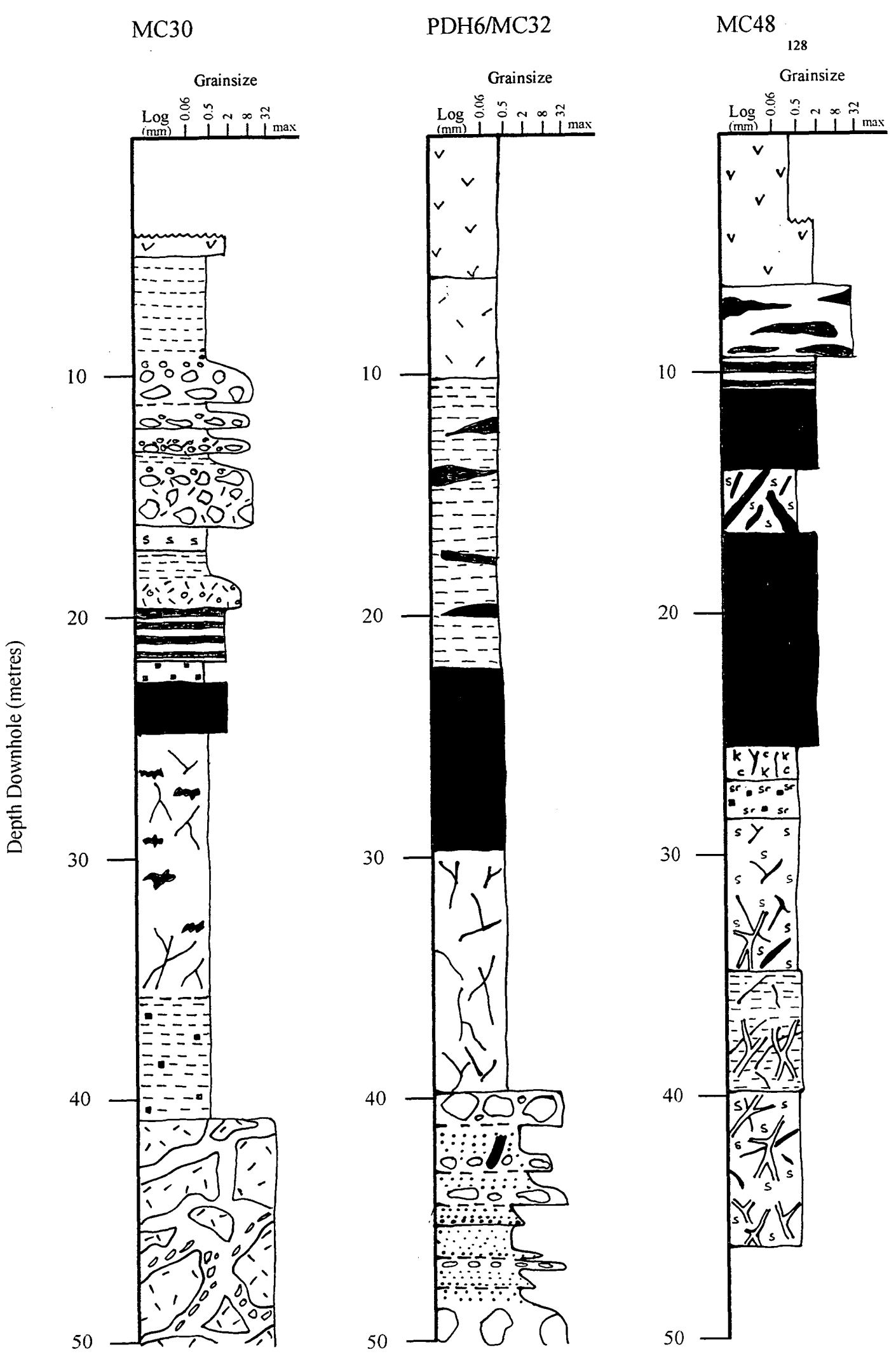
MC30
PDH6/MC32
MC48
Grainsize
Log (mm)
0.06
0.5
2
8
32
max
Depth Downhole (metres)
10
20
30
40
50

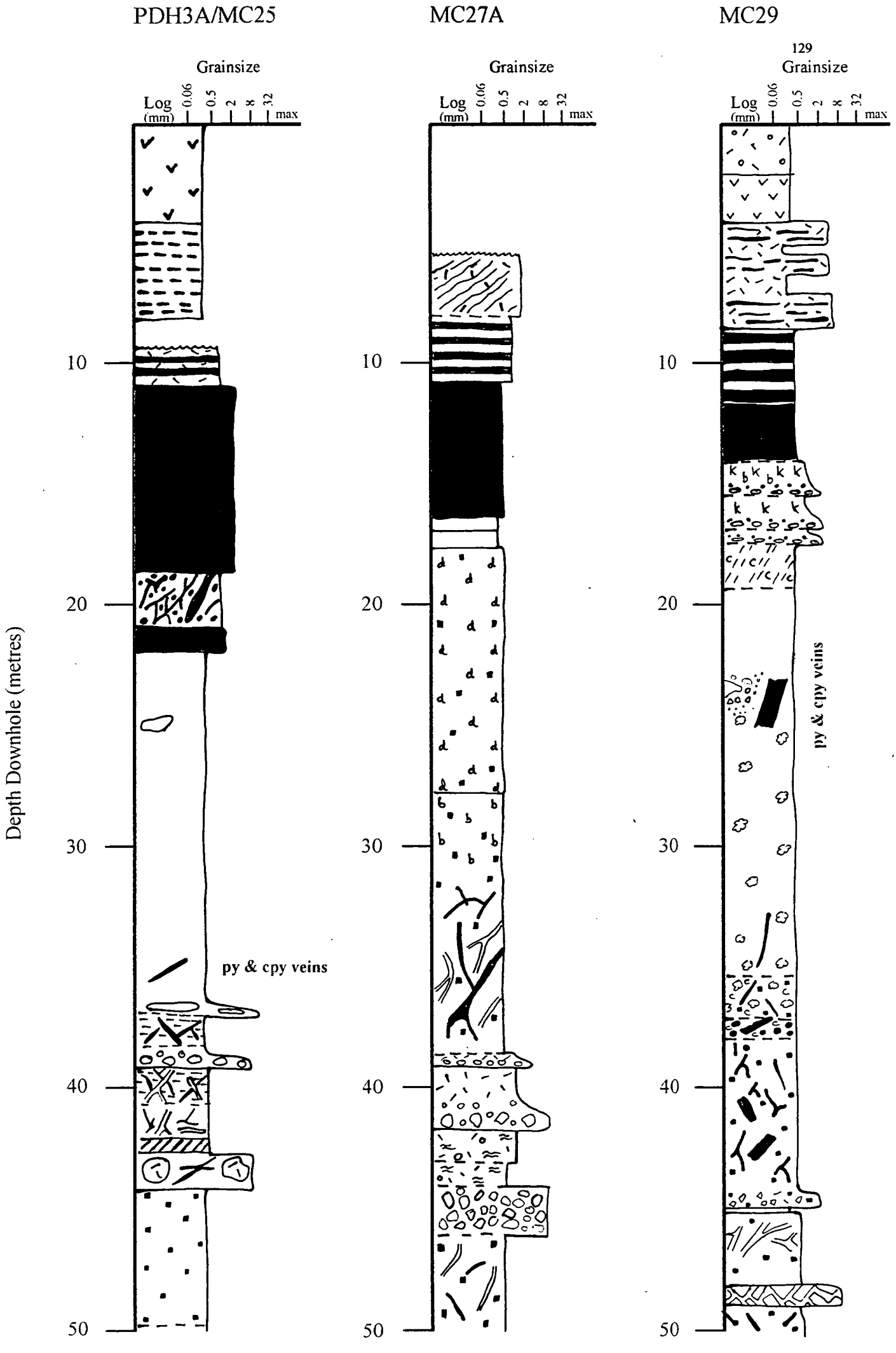
PDH3A/MC25
MC27A
MC29
129
Grainsize
Log
(mm)
0.06
0.5
2
8
32
max
Depth Downhole (metres)
10
20
30
40
50
py & cpy veins
py & cpy veins

Figure 6.6. Representative examples of the West Lode massive sulphide mineralisation.

Figures 6.6a,b and d from MC25. Figure 6.6c, cut and polished grab sample from the West Lode (sample provided by A. Taube).


b


d


a


c

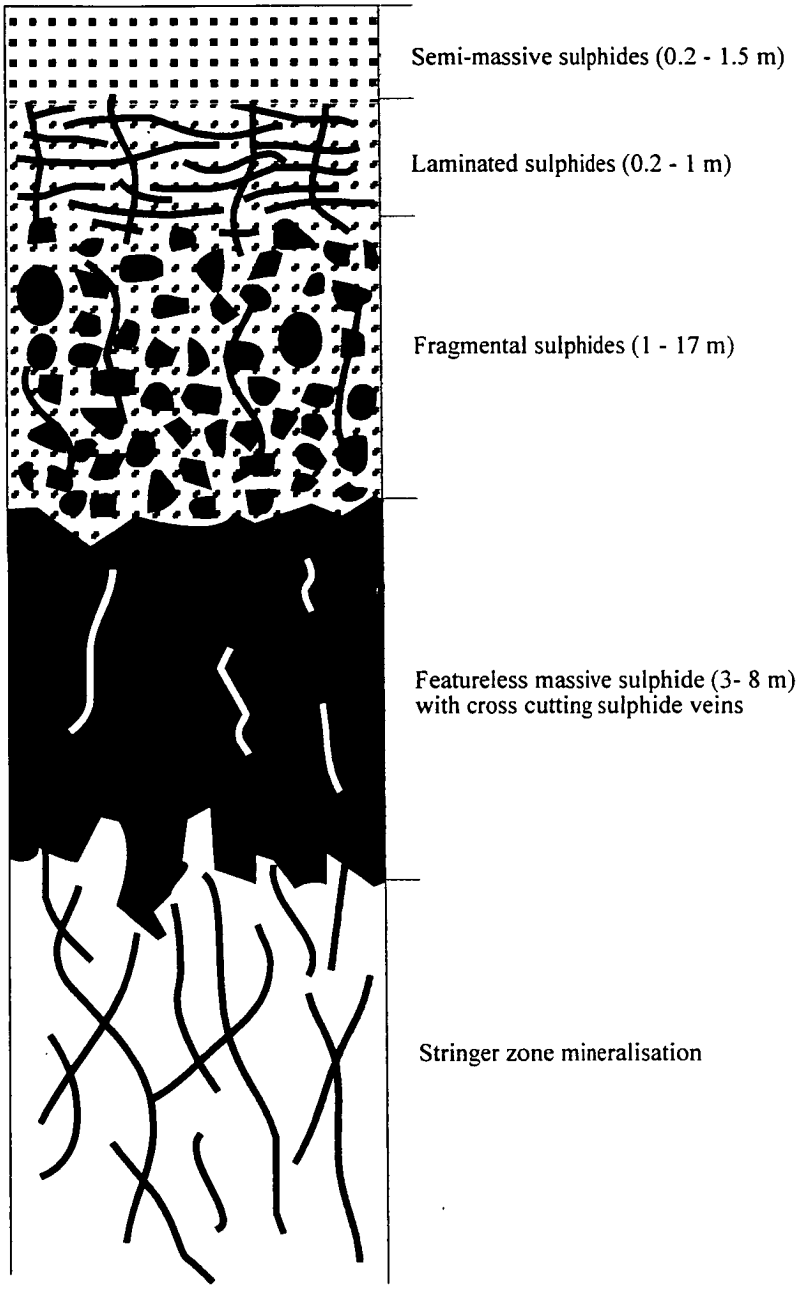

Figure 6.7. Schematic representation of the relationship between massive featureless sulphides, fragmental sulphides and laminated sulphides within the Mount Chalmers massive sulphide lenses

Figure 6.8. Examples of the West Lode gossan, illustrating the transition form the partially oxidised massive sulphide (Fig. 6.8c: MC29- 11.80 m) into the overlying gossan (Fig. 6.: MC29- 11.20 m) and oxidised rhyolite (Fig. 6.8a: MC29- 8.90 m).

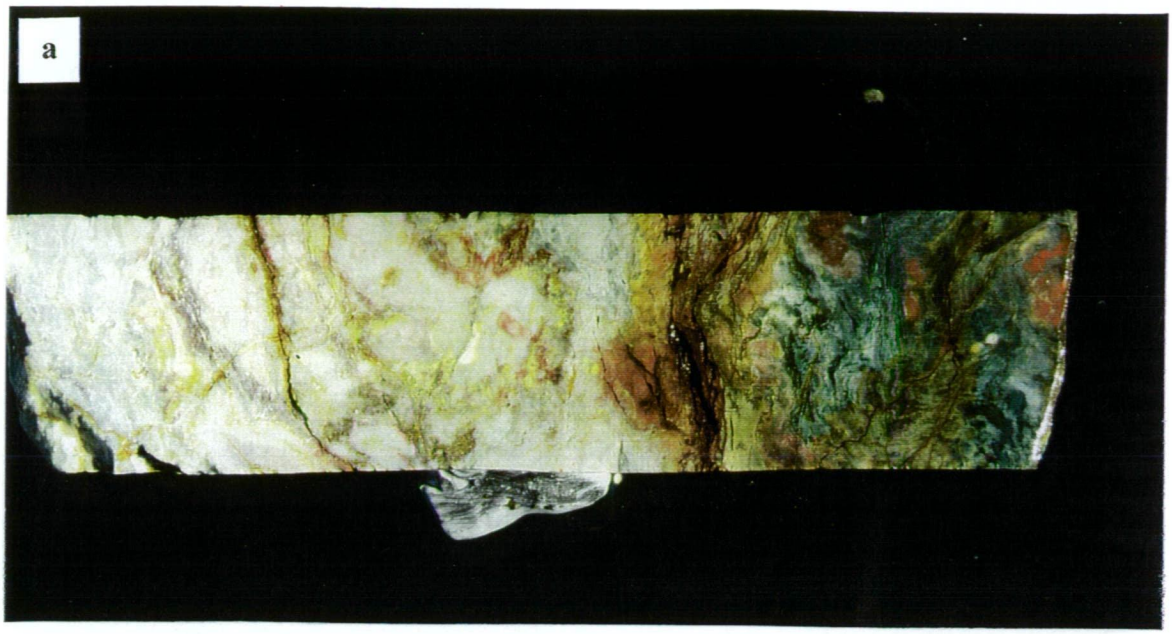
a


b

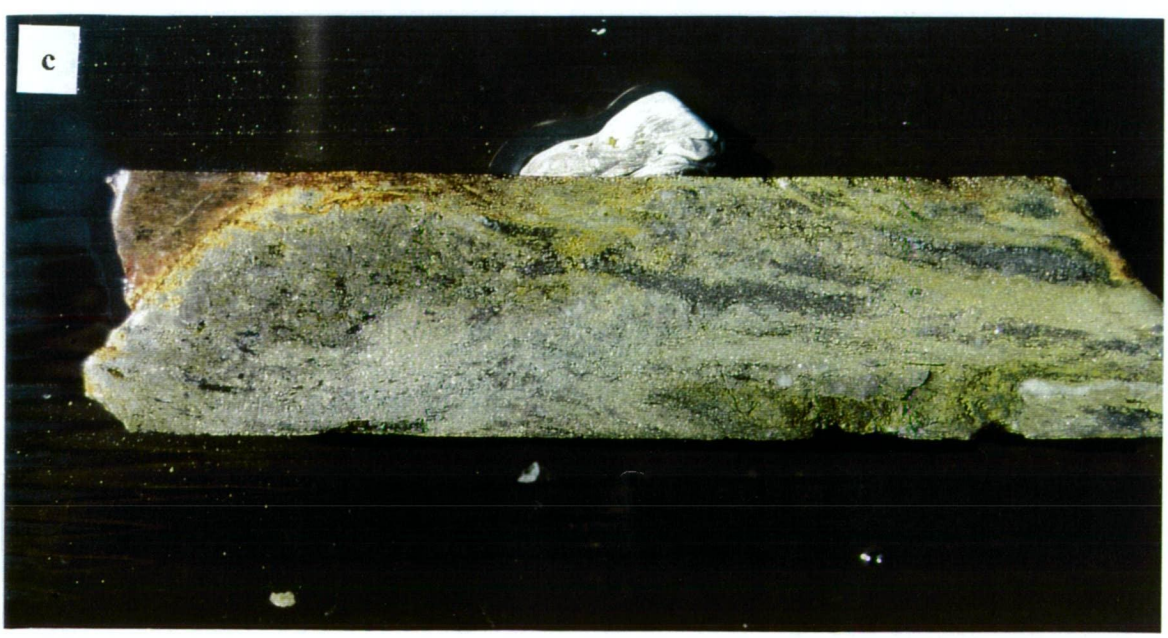
c

6.2.1.1.4. South Lode

The South Lode occurs to the east and south of the Main Lode (Fig. 6.3). It was mined before the main underground operations began. Old plans suggest that the South Lode probably consisted of a thin bed of stratiform massive sulphide ore. One percussion hole returned values of 12.2% Zn and 6.1% Pb over a 2 m intersection - higher grades than intersected from either from the Main or West Lodes (Taube and van der Helder, 1983).

6.2.1.2. Stringer Mineralisation

Commonly underlying a VHMS deposit is a complex network of veins, (commonly termed either the stringer zone or stockwork zone) that are considered to be the conduits for hydrothermal fluids responsible for massive sulphide mineralisation that formed on or below the seafloor. The stringer zone mineralisation is contained within a halo of hydrothermally altered rock (Lydon, 1984). The development and preservation of the Mount Chalmers footwall alteration and stringer vein system allows a study of the plumbing system of a VHMS deposit to be made. The study of a stringer zone can also provide valuable information on the chemistry of the hydrothermal fluid as it evolved over time.

6.2.1.2.1. Stringer Vein Paragenesis

Detailed core logging revealed a complex array of 18 stages of veining in the footwall alteration zone, some of which extend up into the hangingwall lithologies. The differentiation of the veins and vein sets is based upon consistent crosscutting relationships and mineralogy. Although, in some drill holes, some crosscutting relationships were not able to be established, *e.g.* in MC38 dolomite veins immediately overlie sericite veins, without one vein set cutting across another. However, the dolomite veins crosscut earlier generation veins, that have cut the sericite veins, thereby allowing a timing relationship to be established. A schematic representation of the crosscutting relationships for each individual stage is shown in Figures 6.9a, 6.9b and 6.9c.

- Stage 1 - pre-mineralisation veins
- Stage 2 - syn-mineralisation veins
- Stage 3 - post-mineralisation veins

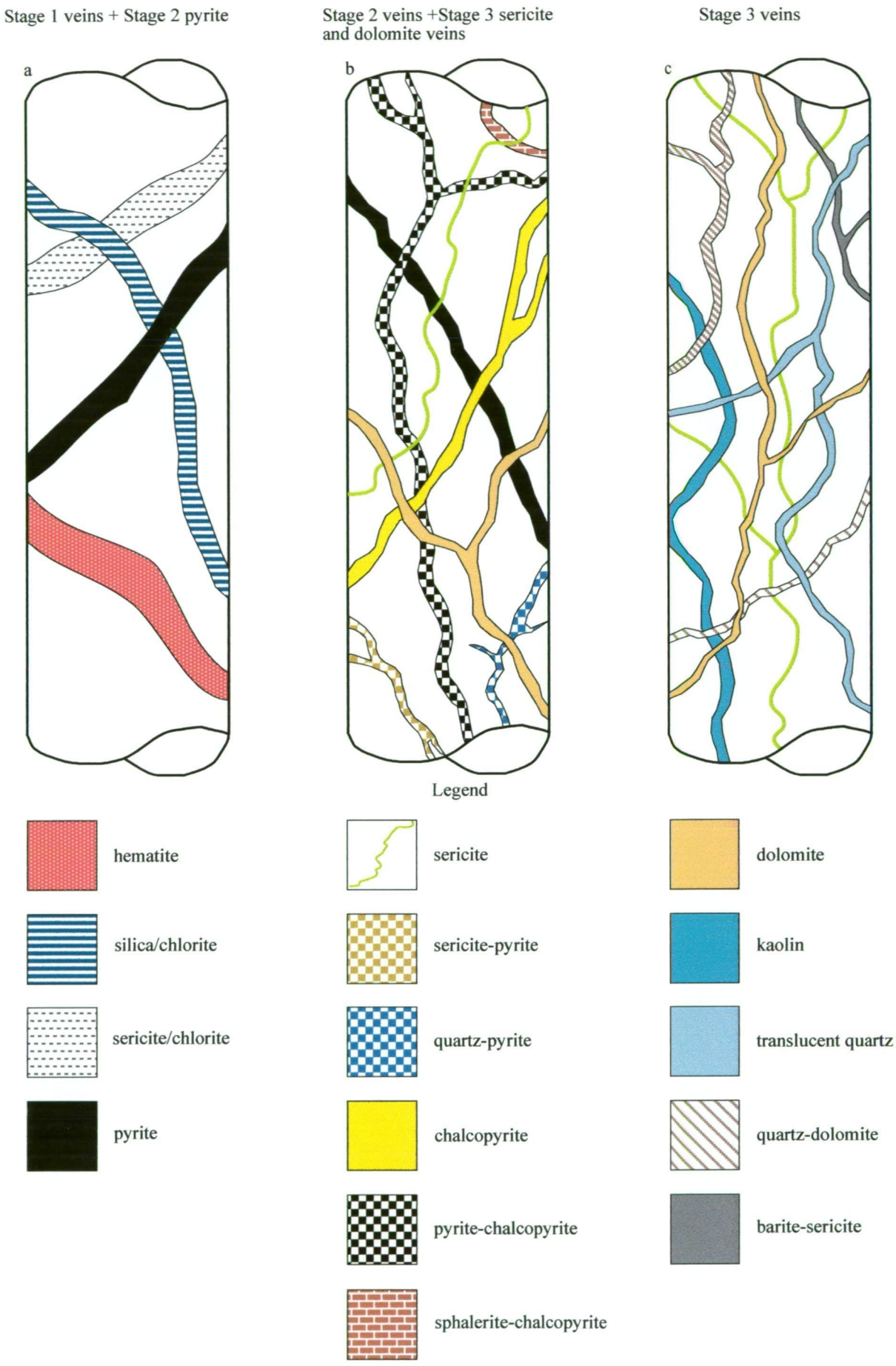

Figure 6.9. Schematic relationship of Stage1 to Stage 3 veins from the Mount Chalmers VHMS deposit

Stage 1: consists of three vein sets (Fig. 6.9):

- hematite veins
- sericite-chlorite veins
- silica-chlorite veins

Stage 1 veins form an irregular network of narrow veins and veinlets. They occur exclusively within the footwall lithologies, and are generally in close proximity to the sulphide bearing stringer veins of Stage 2.

Stage 2 consists of four vein sets (Fig. 6.9b):

- pyrite veins
- sphalerite-chalcopyrite veins
- pyrite-chalcopyrite veins
- chalcopyrite veins

The stage 2 sulphide veins form an irregular network of sub-vertical veins cutting predominantly strongly silicified and/or chloritised footwall rhyolite and volcaniclastic sandstone (Fig. 6.10a,b,c and d), and are considered to be conduits for the hydrothermal fluid that formed the massive sulphide mineralisation. Within the West Lode, the sulphide stringer veins vary in thickness from 0.2 cm to 30.0 cm with a quartz and/or chlorite matrix, while in the Main Lode individual veins may be up to 1 m wide. Pyrite dominated the early stages of mineralisation within the stringer zone veins. Chalcopyrite ± sphalerite, plus rare galena have subsequently overprinted the early pyrite mineralisation. The veins exhibit no evidence of crustiform banding, indicative of multiple episodes of sealing, brecciation and fluid upflow. Instead, they tend to be composed of fine- to medium-grained granular pyrite or agglomerations of pyrite grains. In MC25 between 37.8 to 38.3 m the sulphide veins have no well-defined vein walls *i.e.* they do not have sharp margins, instead the vein margins are diffuse, with the sulphides spreading out into the siltstones. Suggesting that the siltstones at least locally were not yet consolidated or silicified at the time of veining.

Stage 3 consists of nine vein sets, all of which post date the massive sulphide mineralisation (Fig. 6.9c):

- barite
- clear to translucent quartz veins or veinlets
- dolomite
- sericite veins
- milky white quartz veins
- kaolinite
- dolomite-pyrite veins
- quartz-dolomite
- quartz-chalcopyrite veins

Except for the barite and quartz-chalcopyrite veins, the remaining Stage 3 veins are found both within the footwall stringer and footwall alteration zones as well as extending up into the overlying hangingwall lithologies. Barite veins are rare within the stringer zone and are generally found in drill holes near to the massive sulphide mineralisation. Barite veins also cut both pyrite and chalcopyrite veins. Kaolinite veins occur predominantly within the footwall alteration zone, and are most noticeable where they crosscut the massive dolomite alteration. Rarely kaolinite veins may carry some minor chalcopyrite. Whether these veins are of the same generation or not or related to the massive sulphide mineralisation of Stage 2 veins is not possible to tell.

Figure 6.10. Representative examples of stringer zone mineralisation from Mount Chalmers. Figures 6.10a and b - floor of the Main Lode open cut, showing the pyrite, chalcopyrite veins cutting across strongly chlorite altered footwall lithic breccias. Figure 6.10c; Chalcopyrite replacing an earlier formed pyrite veins cutting across Stage 1 pale blue/grey silica alteration (MC33 -48.8 m). Figure 6.10d. Fine-grained, massive to semi-massive pyrite and "clastic" pyrite cutting across milky white stage 2 silica alteration (MC57 - 153.21 - 153.57 m).


b


d


a


c

Dolomite and quartz dolomite veins crosscut most alteration types, including the massive dolomite alteration (see Chapter 7 for description of alteration lithologies) and other vein sets and are found from deep within the footwall alteration zone to crosscutting the massive sulphide as well as an andesitic sill in the hangingwall.

6.2.1.3 Gossan Development at Mount Chalmers

The West Lode massive sulphide lens has a thick and well-developed gossan that sits on and laterally to the massive sulphide (Fig 6.11). A small thin gossan has also developed over the massive sulphide at the South Lode. No gossan development occurred on the Main Lode massive sulphide. The gossan attains a maximum thickness of ~12 metres over the West Lode massive sulphide (Fig. 6.11). The gossan was intersected in a number of drill holes. Unfortunately, the majority of these were percussion drill holes. No formal investigation of the gossan was undertaken as part of this research. However, logging of the gossan where it was intersected in diamond drill holes allows a few observations to be made.

The thickest interval (~17 m) of gossan was intersected in MCP13/MC36. The gossan is composed predominantly of Fe and Mn-oxides. Disseminated fine-grained to coarse-grained barite, especially at the base of the gossan may be present. Locally delicate boxwork textures may also be developed. Azurite and malachite are the most visible supergene Cu-bearing mineral phases present. Spheroidal silica with fine-grained pyrite is also developed locally.

A fuller approximation of the development and mineralogy of the Mount Chalmers gossan may be obtained by comparison with the gossan developed over the Mount Warminster massive sulphide prospect. The sulphide mineralogy is identical to that seen at Mount Chalmers, and the genesis of the mineralisation is considered to be analogous to that for Mount Chalmers (Leggo, 1980). A well-developed gossan and underlying supergene oxidation zone cap the Mount Warminster massive sulphide. The mineralogy (Table 6.2) of the gossan was determined by X-ray diffraction, microscopic and by visual identification (Leggo, 1980).

Table 6.2. Minerals identified within the Mount Warminster gossan (After Leggo, 1980).

Mineral	Formula	Mineral	Formula
Limonite/Goethite	$Fe_2O_3.nH_2O$	Covellite	CuS
Quartz	SiO_2	Hematite	Fe_2O_3
Limonitic Jasper	$xSiO_2.Fe_2O_3.nH_2O$	Azurite	$Cu_3(CO_3)_2(OH)_2$
Malachite	$Cu_2CO_3(OH)_2$	Jarosite	$KFe_3(SO_4)_2(OH)_6$
Cerussite	$PbCO_3$	Cuprite	Cu_2O
Manganese Oxide	MnO_2	Chlorite	$(Mg,Al,Fe)_{12}[(Si,Al)_8O_{20}](OH)_{16}$
Chalcocite	Cu_2S	Smithsonite	$ZnCO_3$

In addition, relict sulphides: Chalcopyrite, pyrite, galena and bornite

Silica and 'limonite' dominate the mineralogy of the Mount Warminster gossan. Leggo (1980) grouped the different mineral assemblages from the gossan into five distinct assemblages (Table 6.3).

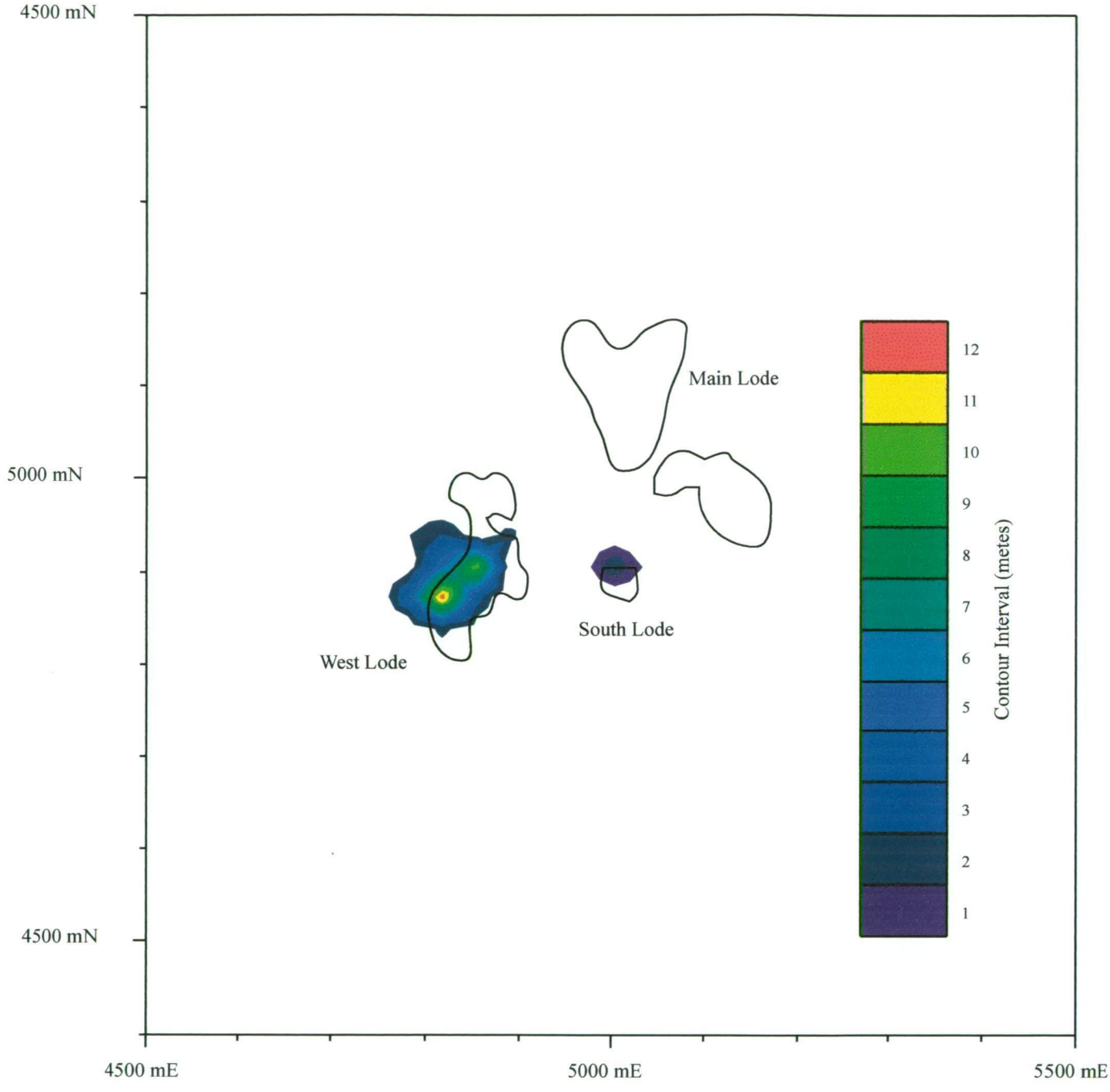

Figure6.11. Isopachs of gossan thickness, with the outline of the massive sulphide lenses superimposed

Table 6.3. Assemblage mineralogy of the Mount Warminster gossan (After Leggo, 1980)

Assemblage	Major Mineralogy	Minor Mineralogy
Siliceous	quartz, limonite/limonitic jasper	malachite, clay, jarosite, anglesite
Limonite - Quartz - Manganese Oxide	limonitic jasper, quartz, limonite, manganese oxide	pyrite, hematite, kaolinite
Limonite - Malachite	limonite, malachite, goethite	pyrite, chalcopyrite, hematite
Carbonate	cerussite, malachite, limonite, quartz, ± clay, ± limonitic jasper	chalcocite, covellite, jarosite, manganese oxide, azurite, goethite, cuprite
Pyritic Tuffaceous	chlorite, limonite, goethite, hematite	

6.2.2. Hydrothermal Vent Bacteria?

In drill hole MC25 (West Lode) within the amorphorous silica groundmass surrounding some pyrite grains is a distinct green colouration. Within this green colouration are singular but predominantly clusters of spheroidal to ellipsoidal structures. These spheroids are up to 10 to 12 μm across and have an internal wall that is generally less than 0.5 μm thick. No internal structures were observed within the spheroids (Fig. 6.12). The spheroids are associated with and may also be found on the pyrite grains and within the spaces between individual pyrite grains. By focusing up and down through the thin section and observing paragenetic relations to the pyrite grains and one another it is easily possible to determine that the spheroids are not surface contaminants.

The spheroids may be one of two possibilities:

- the structures are silica spheroids formed during precipitation of the silica groundmass to the pyrite, or
- the spheroids are fossilised bacteria.

Both of the above alternatives will be considered in the ongoing discussion.

Modern day VHMS vent environments are characterised by the lack of ambient light, high temperatures, acidic sulphide and metal-rich fluids. Despite these hostile conditions, hydrothermal vents are also home to complex high-biomass animal communities, which live entirely on geochemical energy sources. Bacteria have been reported and described from modern hydrothermal vent communities ranging from the shallow marine (<60 m) to the deep oceans (*e.g.* Concetta and Maugeri, 1993; Haymon *et al.*, 1993; Wirsen *et al.*, 1993; Dando *et al.*, 1995; Jannasch, 1995; Sudarikov and Galkin, 1995). The form of the bacteria varies from unicell organisms to large mats. Bacteria have been found within the plumes above the hydrothermal vent complex, colonising the external and internal surfaces of high temperature sulphide chimneys (*e.g.* Winn *et al.*, 1986). The presence of bacteria within modern shallow-marine to deep-marine hydrothermal vents suggests that bacteria may have also colonised ancient hydrothermal vents.

Figure 6.12. Photomicrographs depicting the fossilised vent bacteria from the West Lode massive sulphide ore lens. The fossilised bacteria are represented by agglomerations of green coloured spherical structures that display cell walls (Figure12c and d). The black mineral phase in all photomicrographs is pyrite. The clear interstitial material is quartz and in Figure 6.12, the fibrous mineral in top centre of the photomicrograph is muscovite. All examples from MC25 - 16.0 m. Field of view for Figure 6.12a ≈ 6 mm across, 6.12b and c ≈ 3 mm and for 6.12d ≈ 1.25 mm. All photomicrographs were taken in plane polarised light.

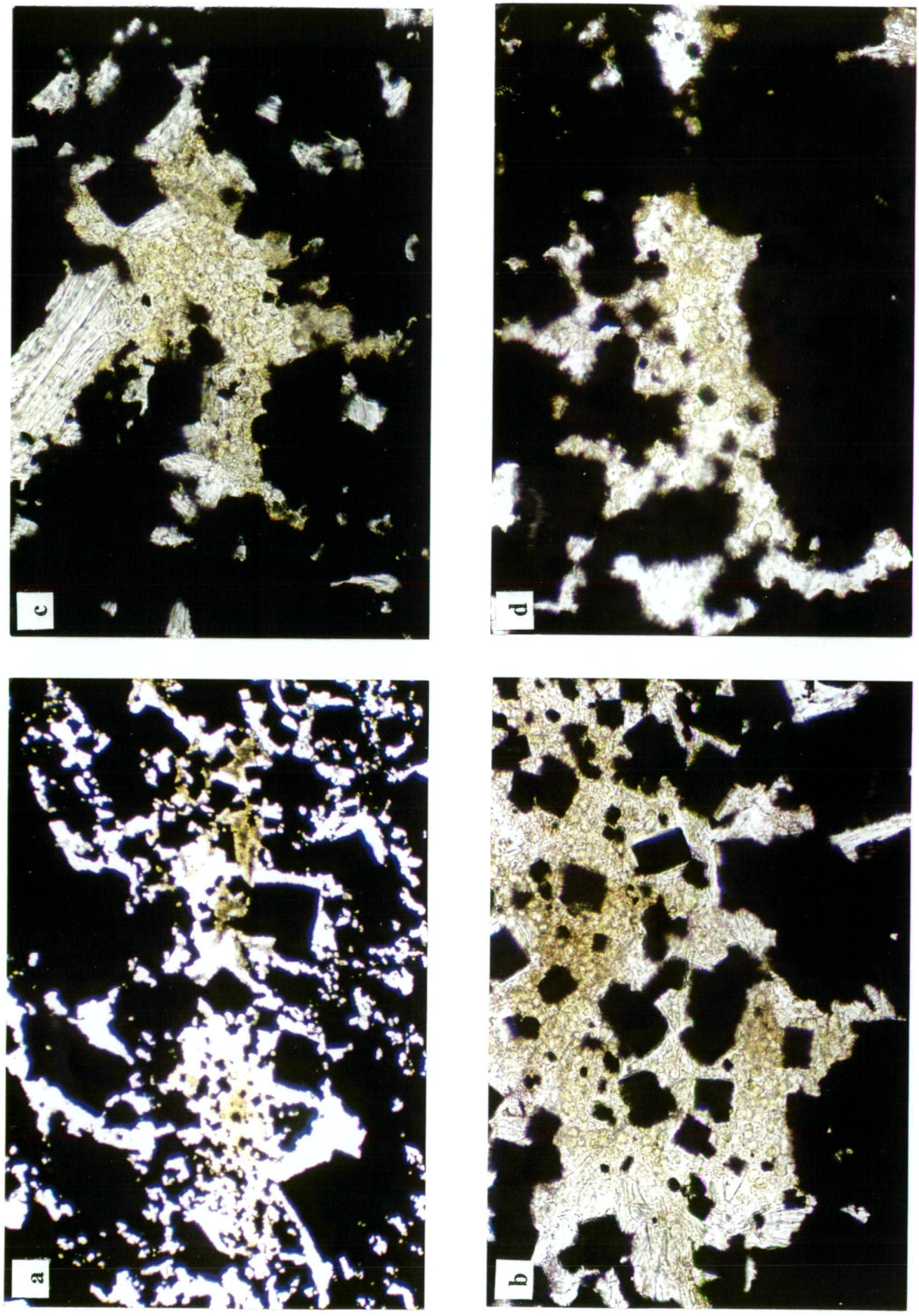
a
b
c
d

Although not common, fossilised bacteria have been reported from a number of ancient low-temperature hydrothermal sites. Juniper and Fouquet (1988) suggested that some of the iron-silica filamentous structures they studied from both ancient and modern hydrothermal vents were formed in association with filamentous microorganisms. Duhig *et al.* (1992) described hematitic filaments within ironstones associated with low-temperature hydrothermal fluids within the Mount Windsor Volcanics of northern Queensland, which they interpreted as being fossilised bacteria. Little *et al.* (1999) interpreted iron-silica filaments within a low-temperature iron-silica exhalite bed associated with the Jurassic Figueroa massive sulphide deposit as being fossilised bacteria.

Walter *et al.* (1972) indicated that algal and bacterial stromatolites lining the outflow channels of hot-spring geyser effluents of Yellowstone National Park are primarily composed of amorphorous silica. Kornhauser and Ferris (1996) reported that microbial mats from hot springs in Iceland were being encrusted and partially to totally replaced by silica and or iron. They also showed that silica-rich spheroids formed epicellularly on cell walls and surrounding sheaths and capsules of microorganisms and in some cases intracellularly when the cells had lysed. Commonly, these precipitates were observed coalescing to form a matrix of amorphorous silica that completely encapsulated the cells and/or replaced their cytoplasmic material. Kornhauser and Ferris (*ibid*) argued that the complete encrustation of bacterial cells by silica might greatly enhance their preservation potential. The presence and of silicified bacteria within modern day hydrothermal systems and their potential for preservation also suggests that fossilised bacteria may have flourished within ancient hydrothermal vents and their deposits.

Lebedev (1967 *in* Juniper and Fouquet, 1988) described the formation of tubular and spheroidal structures of amorphorous silica during crystallisation of siliceous gels. However, Juniper and Fouquet (1988) in their study of filamentous iron-silica structures form modern and ancient hydrothermal sites argued that the solutions that Lebedev (1967) used in his experiments were dense and viscous with a silica concentration much higher than modern hydrothermal fluids and contained only silica. Juniper and Fouquet (*ibid*) concluded that although the structures they studied have some resemblance to the structures produced by Lebedev their origin do not seem attributable to the same processes. Duhig *et al.* (1992) described chalcedonic and chalcedony spherulites within ironstones. The spherulites have a diameter between 0.5 to 5 mm, have irregular forms and are composed of transparent megaquartz (*sic*) and chalcedony. The outer margins are often chalcedonic, whereas the megaquartz becomes coarser towards the centre. The spherules almost without exception have cores, concentric zones and rims of chert and iron oxide granules. Duhig (*ibid*) interpreted the spherulites as being formed by inorganic maturation of amorphorous silica gel.

Following the arguments of Juniper and Fouquet (1988), the spheroidal structures in MC25 are not interpreted as having been precipitated out of a silica gel. Furthermore the structure form and size of the spheroids described by Duhig *et al.*, precludes the MC25 spheroids having been precipitated out of a silica gel. In addition, although the MC25 spheroids occur within amorphorous silica, they do not occur within iron-silica exhalites that would have been close to if not saturated with respect to silica.

The preservation potential of bacteria is greatly enhanced when they have been silicified. Kornhauser and Ferris (1996) showed that complete encrustation of bacterial cells by silica might greatly enhance their preservation potential as fossils. Therefore, the spheroids within the West Lode are interpreted as silicified and fossilised bacteria. Their intimate association with pyrite suggests that they may have been chemolithautotrophic sulphur reducing bacteria.

6.3. PROSPECTS

Within the immediate vicinity of Mount Chalmers, are a number of old mine workings and prospects occur (Fig. 6.1). These vary between old prospecting pits to small mines with underground development. The style of mineralisation that was exploited or potentially was going to be exploited was one of three categories:

- base metal sulphides with Au - Woods Shaft, Mount Warminster, Boto's, Savage Mitchell, Tungamull and Murray's
- lode Au - North Star/New Zealand Gully area, Kay's prospect and Emu Park Road
- alluvial Au - no data available

6.3.1. Base Metal Prospects

The Woods Shaft prospect is located 1km southwest of the Mount Chalmers mine (Fig. 6.1). A gossanous outcrop was discovered to be auriferous and in 1900 a shaft was sunk to a depth of 30 m. The geology of the Wood's Shaft is very similar to that of the Mount Chalmers mine. The Woods Shaft prospect has a well defined surface geochemical anomaly, with peak values of 4400 ppm Cu, 1200 ppm Pb, 3100 ppm Zn, 4 ppm Ag, and 0.6 ppm Au, with a Au resource of 379,000 *t* at 1.33 g/t Au (Cran, 1985). The mineralisation at Wood's Shaft occurs in one of two modes; either within crosscutting quartz veins, or as disseminated grains or agglomerations of sulphides within graded siltstones and sandstones. Although no analyses of the sphalerite at Woods Shaft have been made, the honey colour indicates that the sphalerite is Fe poor compared to the darker and brown coloured sphalerite at Mount Chalmers.

The Mount Warminster mine is a small Pb-Zn-Cu prospect, approximately 1.6 km NNW of the Mount Chalmers mine (Fig. 6.1). The mine was discovered in 1871 and was worked intermittently until 1915, yielding approximately 200 *t* of high-grade lead and copper ore. The discovery mineralisation comprised a small outcrop of secondary Pb-Zn-Ag-Au gossan. The subsequent underground development revealed several small erratic lenticular bodies with sericitised and kaolinised aureoles, hosted by volcanically derived sediments.

Total production was less than 200 *t* of high-grade ore (Okill, 1974; Taube and van der Helder, 1983). The prospect consists of a broad alteration zone which is strongest adjacent to an andesite sill. The sequence is dipping towards the east. Along strike to the north the alteration intensity decreases (Taube and van der Helder, 1983). The mineralisation is hosted within a pyrite-altered siltstone (Leggo, 1980).

The Boto's Prospect is located 1.2 km northeast of the Mount Chalmers mine (Fig. 6.1). A shaft and several pits had been put down on the gossanous alteration zones, but no record exists of any production. Soil geochemical values from the area have peak values of 2000 ppm Cu, 1.1% Pb, 4600 ppm Zn and 11 ppm Ag. Taube and van der Helder (1983) concluded that the Boto's Prospect represented the re-emergence of the Mount Chalmers mine stratigraphy in a local domal feature. Logging of the available drill holes has shown that the alteration extends up into the overlying andesites. The alteration visible in PDH13/DDH1 is split roughly into two domains. An upper domain that is dominated by intense silicification which is cross cut by sericite veinlets that define a foliation at a low angle to the LCA *i.e* near vertical. A lower domain that is dominated by sericite/chlorite alteration. Visible mineralisation is largely restricted to disseminated fine-grained pyrite, with an overall content of $\leq$3 %. Locally over narrow intervals (2 -3 m), the pyrite content may be as high as 40 %. However, no significant base metal or precious metal values occur within these zones. Perusal of the drill hole assay database shows that the mineralisation although low-grade can extend over tens of metres (Table 6.4).

Table 6.4. Selected assay intervals from the Boto's prospect

Hole	Sample Interval (metres)	Cu %	Zn %	Pb %	Ag g/t	Au g/t
PDH23/DDH2	140		0.5	0.2		
PDH17	1.5	2.9				
PDH13/DDH1	66	0.1	1.2	0.6		
	includes 21 m	0.2	2.8	1.4	63	1.2

The Savage-Mitchell prospect occurs immediately to the south of the Mount Chalmers mine (Fig. 6.1). The mineralisation occurs in strongly silica-altered sedimentary rocks, pumice breccia and quartz-carbonate ± pyrite veins within the andesites. The base of SMDD1 (367.0 - 395.4 m) is composed of graded, sericite-silica-chlorite-altered polymictic lithic breccia. Plate 5 is a geological cross section that extends from the West Lode in a southwesterly direction through the Savage-Mitchell prospect and to the east of the Woods Shaft prospect, and illustrates the relationship between the lithologies intersected in SMDD1 and the West Lode. Within the andesites (SMDD1), the mineralisation and alteration are associated with quartz-carbonate ± pyrite veins (Stage 3 post-massive sulphide mineralisation). Peak assay values for Cu, Zn and Pb all occur within the andesites, although the sedimentary rocks and pumice breccia are also weakly mineralised (Table 6.5). The style of alteration and alteration mineral assemblages within the sedimentary rocks and pumice breccias are identical to those described from the Mount Chalmers mine, where they are have not been intruded by andesites, and are therefore considered not to be the result of syn-volcanic alteration processes. The assay values for the andesites, sedimentary rocks and pumice breccias are far greater than the average values for Cu, Zn and Pb from unaltered andesites, sedimentary rocks and pumice breccias from the Berserker beds (Table

6.5). This indicates that the metals have been added to the rocks either by contact with a metalliferous-bearing hydrothermal fluid or by assimilation of previously mineralised sediment by the intruding andesite. This latter process is similar to the process suggested by Boulter (1997) to account for the presence of altered and mineralised intrusions near the Rio Tinto deposit in the Iberian Pyrite Belt. The post-mineralisation intrusions were altered and mineralised through interaction with unconsolidated stratiform sulphides or sulphidic sediments. This process may explain why the peak assay values within the andesites at the Savage-Mitchell prospect occur at or near the contacts between the andesites and the sedimentary rocks. However, the mineralisation is associated with quartz-carbonate veins, that at the Mount Chalmers mine, post-date the massive sulphide mineralisation (see Section 6.2.1.2.1 Stringer Vein Paragenesis), suggesting that the mineralisation may have been generated by local post-Mount Chalmers mineralisation and post-intrusion hydrothermal processes.

Table 6.5. Selected assay intervals from SMDD1 – Savage Mitchell prospect

Lithology	From - To (m)	Cu %	Zn %	Pb %
Sedimentary rocks	149.0 - 152.6	0.003	0.13	0.015
Andesite	155.6 - 160.6	0.006	0.35	0.14
Sedimentary rocks	240.3 - 252.3	0.009	0.03	0.016
Andesite	252.3 - 253.3	0.13	0.04	0.015
Pumice breccia	261.0 - 277.0	0.014	0.04	0.013
Andesite	297.2 - 302.2	0.25	0.28	0.12
Andesite	308.6 - 313.6	0.08	0.26	0.013
Graded lithic breccias	367.9 - 390.6	0.01	0.04	0.006
Average unaltered				
Andesite	(N=58)	0.005	0.009	0.0004
Sedimentary rocks	(N=48)	0.002	0.01	0.002
Pumice breccia	(N=9)	7*	66*	9*

* = ppm

The mineralisation and the alteration at the Tungamull prospect (Fig. 6.1) occurs as two distinct styles. The most dominant style of mineralisation and alteration is the massive dolomite/kaolin alteration that was intersected in drill holes T2, P6/D3, MCD2 and MCD12. Dolomite and later kaolin alteration of the dolomite dominate the alteration. The massive dolomite/kaolin alteration is a late stage event, as the alteration phases are clearly overprinting a feldspar-phyric pumice lithic breccia. In MCD2 significant Zn and Ba values were intersected over a 63.4 m interval (138.6 - 202.0 m). Au values are anomalous where the Ba values are close to or above percent values.

Murray's is a prospect that extends approximately 3.5 km southeast from Mount Chalmers that was delineated by surface geochemistry and geophysical methods (Fig. 1.1). The style of alteration and mineralisation is known only from two diamond drill hole tails to percussion holes. The first style is represented by intense kaolinisation of a sericite altered feldspar phyric-brecciated rhyolite and was intersected in P6/D3 (Murray's 3, Fig. 1.1). The kaolinite alteration is cut by kaolinite and carbonate veins. At the base of the drill hole the rhyolite is strongly hematised and contains ovoid carbonate alteration spots. Intense silicification of a siltstone is the second style of alteration and was intersected in P8/D4 (Murray's 4,Fig. 1.1).

6.3.2. Lode Au

A number of other prospects and small mines within the Berserker beds have been worked for gold. This includes a number of old mines and prospects within the near vicinity of Mount Chalmers.

The North Star/New Zealand Gully (Fig. 6.1) area was prospected and mined for both alluvial and hard rock gold from the 1890's to the 1930's. Available production figures for gold from a limited number of prospects were in the range of 1 to 12.5 kg of Au (Hunns and Kuronen, 1993). The geology of this area is dominated by a thick sequence of pumice breccias, volcanogenic sediments, intrusive rhyolite domes and dykes and andesitic dykes. The mineralisation at in the North Star/New Zealand Gully area occurs predominantly within quartz veins within a thick pile of pumiceous breccias or is associated with weak to moderate pyrite alteration developed along the contacts between the intrusive rhyolites and the pumice breccias. Overall, the base metal component of these styles of mineralisation is negligible (Taube, 1987; Hunns and Kuronen, 1993). The only recognised sulphide mineral phases within the quartz veins were pyrite and galena. Sampled quartz veins have gold values in the range of 0.13 to 9.7 g/t (Hunns and Kuronen, 1993). Silver levels are at or just above analytical detection limits (0.5 ppm). The Au-mineralisation in the New Zealand Gully area is spatially related to the intrusion of rhyolitic cryptodomes into a substantially thick pile of pumice breccias.

Kay's Prospect is located 6 km northeast of Rockhampton and occurs some distance to the north of the main mineralised corridor for the Berserker beds, that hosts the Mount Chalmers VHMS and the North Star/New Zealand Gully Au mineralisation. The mineralisation occurs as disseminated pyrite (20 - 30 %) within a bleached autobrecciated and flow banded rhyolitic cryptodome that has intruded into pumice breccias. No recorded production figures are available. Although given the limited extent of the workings it can be assumed that very little if any payable gold was mined.

The style of alteration and mineralisation is very similar to that seen within the Ellrott Rhyolite near the junction of the Emu Park Road and Artillery Road (Fig. 6.1). Here the Ellrott Rhyolite is extensively altered and bleached and contains disseminated and veinlet pyrite. The hydrothermal alteration does not extend to the top of the rhyolite outcrop, but is overlain by a zone of relatively unaltered rhyolite. The altered rhyolite has also been hydrothermally brecciated, with the fractures infilled by chlorite and sericite.

6.4. FORMATION OF THE MOUNT CHALMERS MASSIVE SULPHIDE MOUND

The Mount Chalmers massive sulphide mineralisation is composed of massive, fragmental and laminated sulphides (Figs. 6.4 and 6.5). The fragmental sulphides are predominantly composed of pyrite and to lesser extent chalcopyrite and sphalerite clasts within a pyritic matrix. In one sample, well-rounded chalcopyrite nodules are present within the granular pyrite matrix (*e.g.* Fig. 6.5c). A number of ancient and modern day VHMS deposits have fragmental sulphides associated with them (Table 6.6). The Buchans (Newfoundland, Canada) massive sulphide deposits are distinguished by the extensive development and preservation of transported ore (Thurlow, 1988). The ore breccias are considered proximal resedimented breccia-conglomerates emplaced by a series of gravity-driven subaqueous debris flows (Thurlow and Swanson, 1981). Numerous Japanese workers have reported on the sedimentary origin of some of the Kuroko ore deposits in Japan, these include: Matsukama and Horikoshi (1970); Ishikawa and Yanagisawa (1974); Ito *et al.* (1974); Lee *et al.* (1974); Mukaiyama *et al.* (1974); Takahashi and Suga (1974); Tanaka *et al.* (1974); Tanimura *et al.* (1974); Watanabe (1974). Textural evidence for the sedimentary origin include: lateral transition from massive to bedded ores, vertical size grading of ore fragments and pyrite grains, soft sedimentary deformation structures, such as flames and scours and breccia composed of both sulphide fragments and volcaniclastic fragments. Dereky *et al.* (1989) reported fragmental sulphides from the Iron Dyke deposit in northeastern Oregon, (USA), in which a significant portion of bedded Kuroko-type massive sulphide ore is composed of multiple sourced clastic sulphides, quartz and clay minerals. The sulphide fragments range in size from sand-silt size fraction up to boulders.

For the examples cited above, *i.e.* Buchans, Kuroko and the Iron Dyke massive sulphide deposits, the evidence for the resedimentation of the massive sulphides is unequivocal. Especially where transitions between massive, fragmental to bedded ores is well documented, and also where the breccia ore is composed of both sulphide clasts and clasts derived from the surrounding country lithologies. Unfortunately, evidence for the lateral transition from massive to fragmental to bedded sulphides is lacking at Mount Chalmers, although a vertical transition from massive to fragmental sulphides to laminated/bedded sulphides is present.

Brecciated sulphide textures may also be produced by hydrothermal explosions or by phreatomagmatic explosions as suggested by Clark (1971, 1983) for some of the Kuroko fragmental ores. If the fragmental and layered sulphides at Mount Chalmers were produced by one of these two methods, then as well as the sulphides being fragmented, there should be evidence of the surrounding volcaniclastic lithologies being fragmented and incorporated into the fragmental and bedded sulphides.

Table 6.6. Selected VHMS deposits with fragmental sulphides and their interpreted mode of origin.

Location	Deposit	Age	Description	Origin	Reference
Japan - Akita Prefecture	Hanaoka Mine	Tertiary	laminated beds, grading,	reworking and redeposition of sulphides	
			breccia ores	reworking and redeposition of fragments of preexisting ore crushed by explosion during mineralisation and sedimentation	Matsukuma and Horikoshi (1970)
	Shakanai Mine		fragmental ore with vertical and lateral grading, with development of imbricate structures, cross-laminae and erosion channels	slumping or sliding of accumulated massive sulphide after and during ore deposition	Kajiwara (1970)
	Ainai Mine		bedded ores with vertical grading	slumping, transportation and deposition by dense turbulent flows	Ishikawa and Yanagisawa (1974)
	Furutobe Mine		bedded and fragmental ore	submarine sliding or slumping of accumulated massive sulphide after and/or during ore deposition	Tanaka *et al.* (1974)
	Kosaka Mine		bedded, transported and blocky ore	fragmentation and transportation caused by intrusion of rhyolite domes and dacite sills	Hashiguchi (1983)
Japan - Aomori Prefecture	Kamikita Mine		fragmental ore composed of sulphide, sedimentary and volcanic clasts	slumping of massive sulphides	Lee *et al.* (1974)
Japan - Fukushima Prefecture	Kurosawa Mine		conglomeratic ore with lateral grading	transported and resedimented kuroko ore	Motegi (1974)
Japan	Kuroko deposits		stratiform layers of clastic sulphides	fragmentation and sedimentation of sulphides produced by phreatomagmatic explosions induced by clogging of the hydrothermal plumbing system	Clark (1971, 1983)
U.S.A - Alaska Prince William Sound	Midas Mine		clastic pyrite		Newberry *et al.* (1997)

Table 6.6 con't. Selected VHMS deposits with fragmental sulphides and their interpreted mode of origin.

Location	Deposit	Age	Description	Origin	Reference
SW China - Sanjiang region	Gacun, Gayiqong, Shengmelong and Ronggong deposits	Triassic	conglomeratic, fragmental ore and massive ore with graded beds and laminations	slumping, brecciation and local transportation of the sulphides	Hou and Mo (1993)
China - Sanjiang area - SW Yunnan Province	Laochang Mine	Early Carboniferous	graded bedding, ripples, cross-laminated graded beds, brecciated and deformed ore clasts, and chaotically emplaced blocks	slumping and displacement and resedimentation	Yang and Mo (1993)
Cyprus - Troodos ophiolite		late Cretaceous	sulphide balls within a sandy pyritic matrix	colloform pyrite initially precipitated from a gel-like mass and then underwent soft-rock deformation	Clark (1971)
			conglomeratic ore	secondary leaching of compact ore	Costantinou and Govett (1973)
			massive pyrite breccias, pyrite-silica breccias and "conglomeratic" ore	dissolution of anhydrite supported portion of the mound has caused extensive *in situ* brecciation of the mound, analogous to the TAG sulphide mound	Hannington *et al.* (1998)
Canada - Newfoundland	Buchans orebodies	Middle Ordovician	angular(competent) and wispy (plastic) sulphide fragments mixed with a large variety of angular to rounded lithic fragments	fragmentation of *in situ* orebodies occurred intermittently throughout sulphide deposition and were transported sedimentologically downslope as series of gravity-driven debris flows	Thurlow (1977, 1988); Kirkham and Thurlow (1987)
California - West Shasta District	Balaklala deposit	Devonian	chalcopyrite-rich massive sulphide boulders cemented within a pyritic matrix	chalcopyrite boulders derived from an earlier formed topographically higher deposit that was disturbed by seismic activity	Lindberg (1985)
Gulf of California	Guayamas Basin	Modern Day	large angular blocks of sulphide talus scattered around base of sulphide mounds	construction of mounds from talus may be an important process	Peter and Scott (1988)
Galapagos Ridge 0°45'N, 85°50.5'W	Galapagos Ridge		talus slopes and sulphide mounds	mass wasting of mounds and within primary sulphide talus slopes	Embley *et al.* (1988)
Mid-Atlantic Ridge 26°N	TAG		sulphide breccias	dissolution of anhydrite supported portion of the mound has caused extensive in situ brecciation of the mound	Hannington *et al.* (1998)

At Mount Chalmers, there is no evidence of fragmental volcaniclastic lithologies either within the fragmental or layered ore to support these mechanisms. This lack of extraneous lithics within the fragmental sulphides would therefore preclude a hydrothermal breccia origin for the Mount Chalmers fragmental ores.

A possible mechanism for the generation of apparently graded and fragmental massive sulphides was proposed by Yui (1983), who interpreted apparent graded pyritic "beds" from the Motoyaso mine, Japan, as reflecting the rhythmic changes in the degree of supersaturation of the fluids due to intermittent discharge of the hydrothermal fluids. When the degree of supersaturation and the rates of hydrothermal discharge were high, this resulted in the rapid deposition of abundant clots or masses of FeS_2, which were subsequently recrystallised to form the present fine-grained aggregates. When the rates of pyrite nucleation and growth were low, this resulted in the formation of fewer and larger single pyrite crystals. A second line of evidence for the presence of supersaturated fluids and high nucleation rates is provided by the presence of colloform pyrite. Roedder (1968) concluded that the dominant factor controlling the formation of colloform textures is a relatively high degree of supersaturation, resulting in the relatively high rates of nucleation and crystallisation. This would require the hydrothermal fluids to be discharged, and then ponded in a topographic depression on the seafloor to form a brine pool, where the degree of supersaturation of the fluid changes as precipitation of sulphides proceeds, and as new fluid is discharged and then ponded. The palaeoreconstruction of the Mount Chalmers ore body indicates that the massive sulphide mineralisation occurs on the flanks of a rhyolite lava dome and does not sit within a palaeo depression. In addition, the formation of apparent graded beds maybe explained by the process discussed by Yui (1983), however "clastic" textures evident within the Mount Chalmers massive sulphide would also preclude this mechanism.

If there is no clear evidence of how the layered and fragmental sulphides formed from ancient analogies, then how were these textures developed? Recent studies on the active Trans Atlantic Geotraverse (TAG) black smoker complex may supply the answer(s). The TAG massive sulphide mound is composed of an upper zone of massive pyrite and pyrite breccias with locally significant chalcopyrite and sphalerite. Underlying the massive pyrite are pyrite-anhydrite breccias, which in turn overly pyrite-silica breccia that grades into the underlying silicified wallrock breccia (Gemmell and Sharpe, 1998). Knott *et al.* (1998) suggested that the formation of granular pyrite clasts that are abundant in the pyrite and pyrite-anhydrite breccia at the TAG complex were formed by hydrothermal recrystallisation during burial of porous sulphides which formed at the mound surface and became fragmented by collapse and mass wasting. Knott *et al.* (*ibid*) suggested that nodular pyrite and chalcopyrite in the TAG massive sulphide mound formed by *in situ* nucleation of the sulphide, followed by sequential overgrowth in the anhydrite matrix. This process makes it unnecessary to cite processes such as corrosion or rounding during transportation to explain the rounded morphology of the clasts. As the anhydrite dissolves due to its reverse solubility, the pyrite and chalcopyrite nodules and grains are "weathered" out to form a sulphide apron surrounding the complex (Hannington *et al.*, 1998). Such a mechanism can readily explain the fragmental and nodular nature of the Mount Chalmers massive sulphide mound.

In nearly all of the diamond drillholes that have intersected the massive sulphide mineralisation, the mineralisation appears to be continuous (Figs. 6.3 and 6.5). However in MC25, and MC48 (West Lode) two

intervals of massive sulphide mineralisation are separated by an interval of semi-massive sulphide mineralisation or chalcopyrite and pyrite bearing sulphide veins, that cut across silica and or chlorite alteration. This suggests that at some stage in the evolution of the massive sulphide mound the fluid chemistry at least locally changed from precipitating sulphides to silica and or chlorite precipitation, and then back to precipitating sulphides.

Both the Main Lode and West Lode massive sulphide mineralisation are cut by near vertical fine- to medium-grained pyrite and or chalcopyrite veins. These veins cut across the underlying structureless massive sulphide as well as the fragmental and laminated massive sulphides and generally have well-defined margins. This indicates that the massive sulphide mound at the time of fluid flow was locally consolidated and cemented. Otherwise, had the massive sulphide still been unconsolidated and not cemented, then the flow of the hydrothermal fluids would have not been confined to the veins and would have been dispersed through the sulphide mound as a diffuse flow. Therefore, these late stage sulphide veins indicate that hydrothermal system was reactivated after a period of quiescence during which the sulphide mound was consolidated and cemented.

The formation of the Mount Chalmers massive sulphide mound can be summarised as follows

- initial mound formed from the deposition of sulphates from low temperature hydrothermal fluids, these acted as a seal for the hydrothermal fluids.
- temperature increased, dissolution of sulphate species and precipitation of sulphides occurred
- growth of sulphide mound and black smoker chimneys
- collapse of chimneys, mound grows by the build-up of rubble from sulphide chimneys,
- fluids circulating within base of mound cause dissolution, precipitation, and recrystallisation of the various sulphide species as the hydrothermal fluid flows upwards and outwards through the mound. This produces the featureless massive sulphide at the base of the mound.

6.5. DEPOSITIONAL SETTING OF THE MOUNT CHALMERS VHMS DEPOSIT

Typically, polymetallic producing hydrothermal vents are found in water depths exceeding 1,500 m (Rona, 1988). However, recently a number of active hydrothermal vents have been found in water depths considerably shallower than what has previously been thought, some are within safe SCUBA diving range (Table 6.7).

However, in ancient volcanic successions the interpretation of the palaeoenvironmental setting and ultimately the water depth of ancient VHMS deposits have relied largely on detailed facies analysis of the enclosing host lithologies to the mineralisation. Therefore, based upon facies analysis of volcano-sedimentary terranes that host VHMS deposits, a number of authors have proposed a shallow-marine setting for the formation of a number of VHMS deposits, *e.g.*

Table 6.7. Location and description of modern day shallow-marine hydrothermal systems

Location	Water Depth (m)	Geology	Type of Deposit	Mineralogy
Aeolian arc (Tyrrhenian Sea) Basiluzzo Islet (Gamberi *et al.*,1997)	80	Mineralisation occurs on the submerged southern flank of the Basiluzzo extrusive dome.	Strong, diffuse hydrothermal activity, sediment-hosted, barite-rich Pb-Zn sulfides. Sediments (altered pyroclastics) contain abundant disseminated grains of silt-sand size and sparse blocks up to decimetre composed of sph, gn and ba crystals. Authors have drawn analogies with the Kuroko-type deposits of Japan.	sph, gn ba
Ambitle Island, Paua New Guinea (Picler and Dix, 1996)	5 - 10	Venting occurs in a near shore coral reef environment	Two types of venting: (1) focused discharge of clear, two-phase fluid, with phase separation (boiling) occurring at the sea floor. T = 94 – 98°C; (2) dispersed or diffuse discharge	arg, Fe-oxyhydroxide, ferroan cal None observed
Grotta Azzurra, Capo Palinuro, Italy (Stüben *et al.*, 1996)	≤32	Discharge of warm, mildly acidic fluids in and around a submarine limestone cavern	No hydrothermal deposits reported	
Reykjanes Ridge: the Steinahóll vent-field at 63°06'N (German *et al.*, 1994)	250-350	Bubble-rich plumes above the ridge		
Palinuro Seamount, Tyrrhenian Sea (Minniti and Bonavia, 1984; Turfar, 1991)	630	Mineralisation occurs within a volcanic crater on the summit of the Palinuro Seamount. No active venting reported	Complex massive sulphide with sulphosalts and barite gangue paragenesis	py, mel-py, sph, gn, ba, en, ccp
Vulcano - Aeolian Archipelago, Italy (Sedwick and Stüben, 1996)	≤0.30	Venting through beach sands in a shallow embayment of Porto di Levante	Two chemically-distinct submarine hydrothermal fluids recognised: (1) hot gas-rich fluids derived high temperature (>100° C) hydrothermal alteration of a mixture of seawater and ground water overprinted by reactions of CO_2, SO_2 and H_2S in the fluids (2) warm fluids, possibly reflect low-temperature hyrothermal alteration of seawater, also overprinted by reaction of acid volatiles	

Anhy = anhydrite; arg = aragonite; ba = barite; bn = bornite; cal = calcite; ccp = chalcopyrite; cov = covellite; en = enargite; gn = galena; go = goethite; marc = marcasite; mel-py = melnikovite-pyrite; py = pyrite; sph = sphalerite; tn = tennantite; wurz = wurtzite;

Colley and Rice (1975) and Colley (1993) inferred a water depth of <700 m for a Kuroko-type mineralisation (Vanua Levu, Fiji) occurring in proximal position to intrusive rhyolite domes, autoclastic flows and pumiceous deposits produced by explosive eruptions.

- Morton *et al.* (1991), interpreted the Mattabi, F-Group and Sturgeon Lake deposits were formed in water depths of 1,000 m or less due their association with subaqueous pyroclastic flow deposits, that they interpreted as having been emplaced in water depths between 1,000 to <500 m.
- Kerr and Gibson (1993), suggested that the water depth during extrusion of most of the 3,000 m thick Mine sequence of the Noranda cauldron was between 1,000 to 300 m, with a minimum water depth of 300 m most likely.
- Galley *et al.* (1993) argued that the Chisel Lake VHMS deposit was formed in water depths of 1,000 m or less based a number of assumptions, but importantly that the footwall dacite (Powderhouse dacite) had a pyroclastic origin and that it is essentially *in situ.*
- Allen *et al.*, (1996) argued that the massive sulphide ore bodies within the Skellefte district of Sweden span a range in ore deposit styles from deep-water sea-floor ores, to subseafloor replacements, to shallow-water and possibly subaerial synvolcanic replacements.

However, facies interpretations can always be open to re-interpretation especially when new ideas and research come to the fore, *e.g.* the host-rock succession to the Kuroko VHMS of Japan are a submarine succession of volcanics and sedimentary rock, of which a large and significant volume are pyroclastics (Sato *et al.*, 1974; Cas 1992). The pyroclastics have previously been interpreted to have been erupted and deposited in a highly explosive setting in deep-water (3.5 - 4.0 km deep) in an extensional rift basin environment (*e.g.* Kouda and Koide, 1978; Ohmoto, 1978; Burnham, 1983; Cathles *et al.*, 1983; Guber and Green, 1983; Ohmoto, 1983; Ohmoto and Takahashi, 1983; Urabe, 1987). The presence of pyroclastics indicates the explosive fragmentation of magma *i.e.* caused by rapid expansion of gases contained within the magma (Fisher and Schmincke, 1984). McBirney (1963) estimated that for most magmas with known volatile content the practical depth range for explosive subaqueous eruptions is between 500 to 1,000 m. Pecover *et al.*, (1973) calculated the maximum water depth at which hydrovolcanic eruptions can occur as being 700 m. Cas (1992) concluded that explosive submarine eruptions are only likely to occur in water depths of less than 1 km, and generally less than 500 m, thus refuting models of highly explosive, very deep water calderas that have been previously proposed as the host volcanic centres for the Kuroko VHMS deposits.

For ancient deposits other than facies analysis there are few other tools available that will enable an accurate estimate of the water depth that a VHMS may have formed in. One possible and powerful tool is palaeontology. However, few VHMS deposits have a fossil faunal assemblage that is intimately associated with them. Table 3.2 lists the inferred palaeoenvironmental setting for selected fossilised vent faunas associated with known hydrothermal mineralisation. Other sites where fossiliferous VHMS deposits have high temperature vent communities associated with them include the Barlo deposit (Philippines); Azema deposit (New Caledonia).

Altogether, there are 19 known ancient VHMS deposits known with a fossilised vent faunal assemblage. These vent faunal assemblages range in age from the Silurian to the Eocene, and by analogy to modern day deep-sea vent faunas are interpreted to have lived in a deep marine environment (Little *et al.*, 1998; Herrington and Little, 2000). For a discussion on modern day deep-marine vent faunas, the reader is referred to van Dover (1995) for Mid-Atlantic Ridge descriptions and Hessler and Kaharl (1995) for an overview of deep-sea hydrothermal vent communities.

A large number of body and microfossils have been reported from the Kuroko deposits of Japan. Asano *et al.*, (1969) suggested that the Middle Miocene seas of the Oga and Backbone Range regions (N.E. Japan) were in excess of 1,500 m of depth based upon the presence and deep-water nature of two species of foraminfera, *Martinottiella communis* and *Melonis pompilioides*. Hatai and Kotaka (1969 *in* Motegi 1974) reported a molluscan fauna from mudstones within the Takizawaga Formation within 1,500 m of the Kurosawa Mine, Fukushima Prefecture, indicative of a warm to moderate temperature open sea. Whereas Hayakawa *et al.*, (1974) argued that the sea covering the Aizu District during ore formation was not very deep and many islands appeared when the sea level was lowered. Foraminiferal assemblages have been reported from a number of Kuroko-style massive sulphide deposits from Japan (Kajiwara, 1970; Hayakawa *et al.*, 1974; Matsukama, 1974; Motegi, 1974; Oshima *et al.*, 1974; Sato and Kusaka 1974; and Tanaka *et al.*, 1974). Based upon a statistical foraminiferal palaeobathymetric model Guber and Merrill (1983) argued that the Kuroko deposits were formed with a minimum water depth of ~2,000 m and most probably ~3,500 m. However, as discussed above, the presence of primary pyroclastics within the host sequence of the Kuroko deposits argues strongly against a deep marine setting. Therefore, the use of palaeontological evidence for determining the palaeo-water depth that the Kuroko deposits formed in, is at best ambiguous.

For Mount Chalmers the presence of both body and trace fossils enables an accurate estimate of the maximum water depth that the ore deposit formed in to be made. Body and trace fossils occur throughout the Berserker beds and are not restricted to any one horizon. The fauna of brachipods and molluscs indicate water depths between 30 to 50 m, with a maximum depth of 200 m. The trace fossil assemblage belongs to the *Cruziana* ichnofacies which is the characteristic ichnofacies for shelf environments and indicates a maximum water depth of 300 m. Although body fossils have not been found associated with the massive sulphide mineralisation, trace fossils occur within the sediments that host the massive sulphide mineralisation. The body fossils and trace fossils rarely occur together, but where they do, the faunal assemblages remain constant. Therefore, based upon the body and trace fossil assemblages it can be concluded that the Mount Chalmers massive sulphide was formed in a shallow-marine setting of $\leq$ 300 m. Indirect evidence for constraining the depth of formation for the Mount Chalmers VHMS deposit is provided by the presence of peperitic sills that immediately overly the massive sulphide. Hunns and McPhie (1999) concluded that the formation of pumiceous sills and associated peperites required a special combination of low confining pressure, vesiculation and delayed quenching. The facies characteristics of the Mount Chalmers pumiceous sills and peperite suggest that the depositional setting was a submarine shelf below wave base but no more than a couple of hundred metres deep and possibly substantially shallower.

6.6. CONTROLS ON VHMS MINERALISATION

Structure contours to the top of the footwall rhyolite were constructed to determine the palaeotopography at the time of massive sulphide formation. The structure contours were derived from 177 drill hole intersections and were plotted relative to sea level and are shown on Figure 6.13 (sea level = 0 metre contour, a negative value is below sea level and conversely a positive value is above sea level). Even allowing for the vertical displacement of the stratigraphy due to faulting (~20 metres) the footwall rhyolite still forms a prominent topographic high. The Main Lode ore lens on the flanks of and between two small domes of the rhyolite complex, while the West Lode massive sulphide lens located on the southwestern flank of the rhyolite complex (Fig. 6.14). The distribution of the stringer zone mineralisation is spatially related to the narrow ridge of footwall rhyolite that extends northwards (Figs. 6.13 and 6.14). The rhyolite dome is the host rock to the Au Pod mineralisation, around which the massive sulphide mineralisation is also centred. The alteration is most intense within the centre of the rhyolite dome and the intensity of the alteration decreases towards the margin of the dome and also downward. The distribution of the massive sulphide mineralisation around a central siliceous core at Mount Chalmers has a strong similarity to the relationship between massive sulphide mineralisation and "white rhyolite" of the Japanese Kuroko deposits *e.g.* the Uchinotai-nishi deposit (Oshima *et al.*, 1974) VHMS deposits of the Hanaoka Kuroko belt (Takahashi and Suga, 1974) and the Furutobe Mine (Tanaka *et al.*, 1974).

Faults mapped by Taube and van der Helder (1983) were superimposed onto the isopachs of the massive sulphide lenses (Fig. 6.15). Figure 6.15 shows that there is an almost perfect match between the orientation and distribution of the massive sulphide ore lenses as well as the thickest zones of the massive sulphide lenses and the faults. This indicates that the faults had a controlling influence on the orientation and distribution of the massive sulphide ore lenses, and were therefore the main conduits for the hydrothermal fluids. The isopachs of the massive sulphide ore lenses are interpreted as representing the palaeo-vent sites for Mount Chalmers hydrothermal fluid. The northerly elongate nature of the Main Lode massive sulphide is explicable either to the down slope movement of the hydrothermal fluids or more probably the down slope movement and accumulation of sulphide detritus due to gravity, probably derived from collapsed chimney structures.

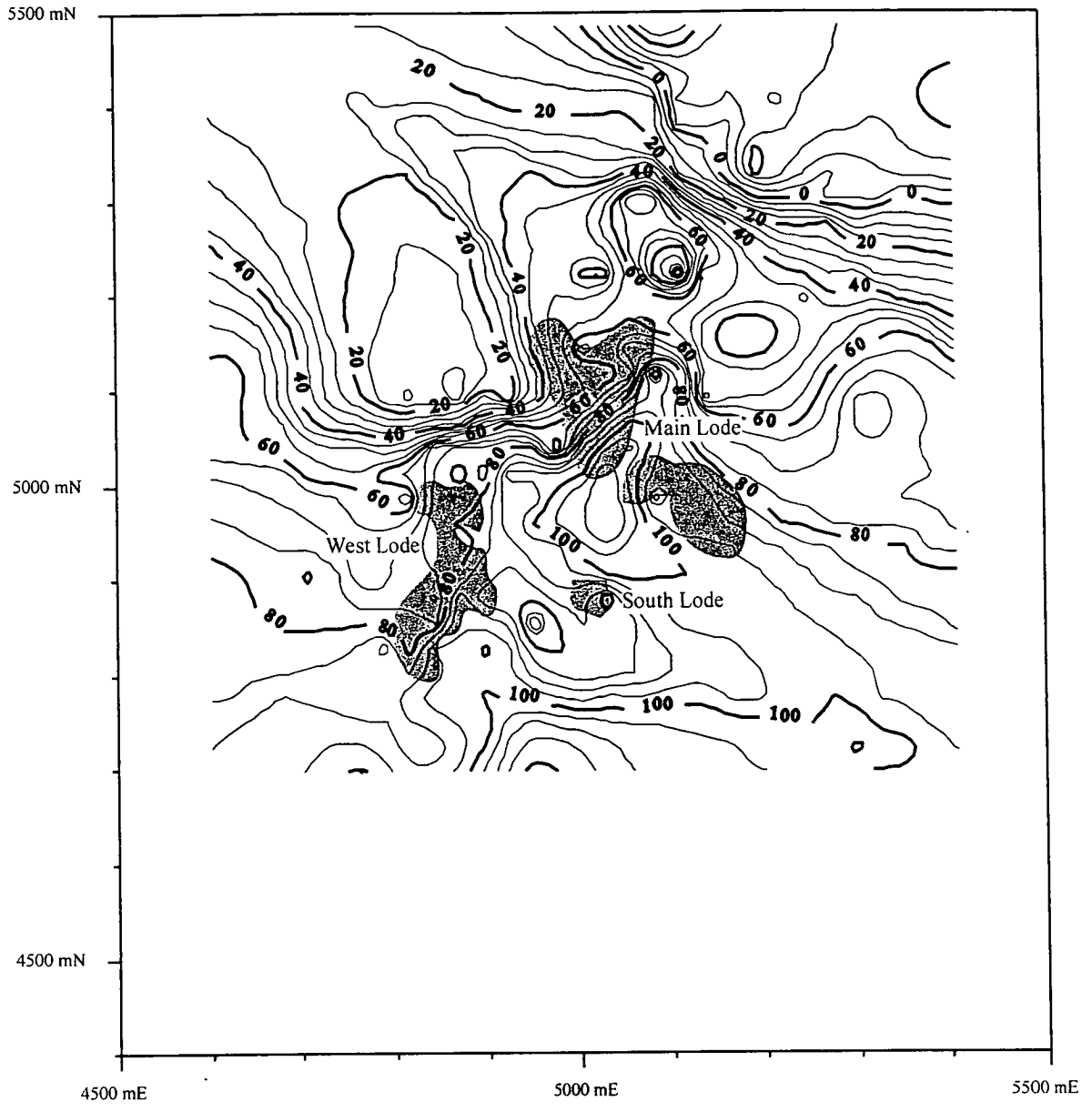

Figure 6.13. Distribution of massive sulphide mineralisation (grey areas) superimposed on the structure contours to the top of the footwall rhyolite

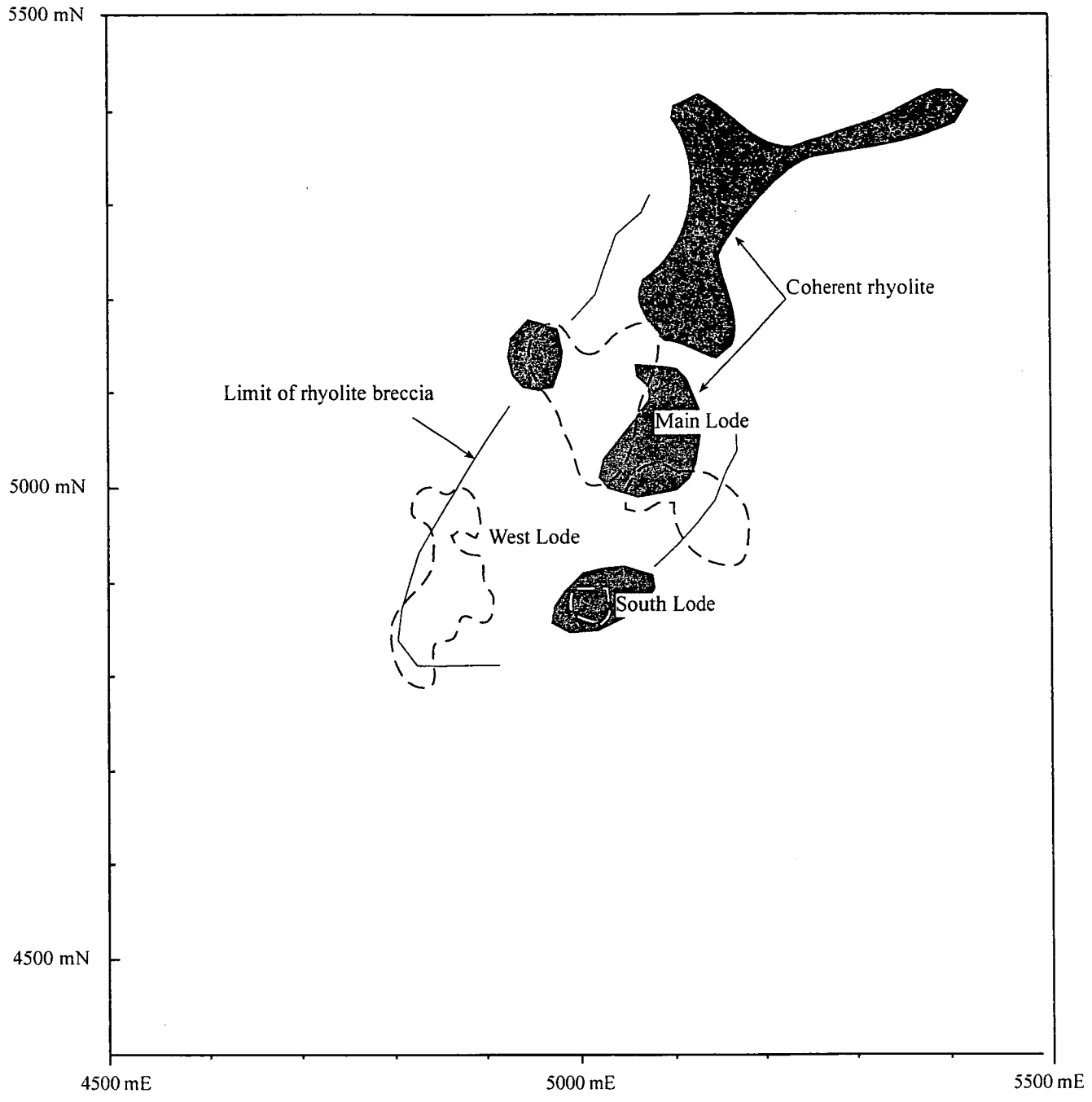

Figure 6.14. Relationship between the massive sulphide mineralisation at Mount Chalmers and the distribution of coherent and brecciated footwall rhyolite

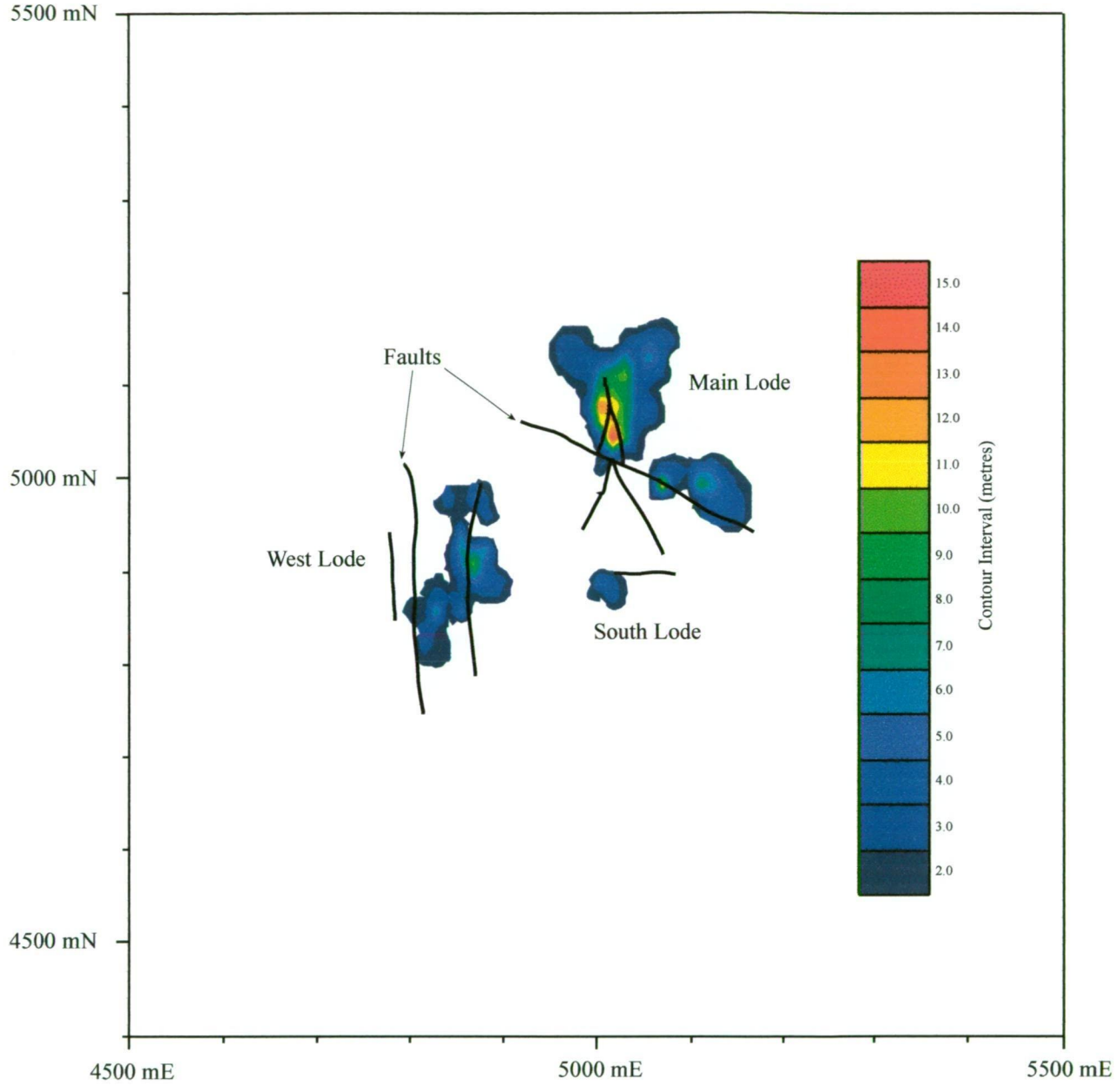

Figure 6.15. Isopachs of massive sulphide thickness with superimposed faults mapped by Taube and van der Helder (1983).

6.7. Comparison With Kuroko Deposits and Modern Analogues

Okill (1974) compared Mount Chalmers to the Kuroko deposits of Japan, and concluded that they are very similar. This analogy with the Kuroko deposits was also proposed by Large and Both (1980) and Taube and van der Helder (1983). Sato (1974) recognised five different deposit styles:

"classical" Kuroko deposit
- Kuroko-type network deposit
- Kuroko-type gypsum deposit
- Kuroko-type barite deposit
- Kuroko-type pyrite-gold deposit

The "classical" Kuroko-type deposit will be discussed as it is considered to be relevant to Mount Chalmers. A Kuroko deposit is generally defined as a strata-bound polymetallic sulfide-sulphate deposit containing economic to subeconomic Cu-Pb-Zn-Ag-Au and an abundance of Ba and Ca sulphates. The deposits occur in Miocene rocks and are typically zoned from laminated black Zn-Pb-Ag-Au ores to layered Cu-rich ore to a siliceous stockwork zone at the base. The "classic" Kuroko orebody has six mineralogical zones that are common between deposits (Shimazaki, 1974) and are described below in ascending stratigraphic order:

- siliceous ore (***keiko***) - stockwork mineralisation characterised by disseminated and veined pyrite and chalcopyrite distributed within an irregular funnel shape in felsic lavas and pyroclastics
- gypsum and/or anhydrite (***sekkoko***) occur as lenticular or irregular mass between the stockwork and stratiform ore bodies or adjacent to the stratiform ore body
- in the stratiform ore body the top half is rich in sphalerite, galena and barite - black ore (***kuroko***), while in the lower half chalcopyrite and pyrite dominate - yellow ore (***oko***)
- stratified ***barite*** mineralisation overlies the kuroko zone.
- small lenses or thin beds of ferruginous chert often occur directly overlying the stratiform ore lens (***tetsusekiei*** bed).

Table 6.7 shows that Mount Chalmers and the Japanese Kuroko deposits have a number of features in common, with one significant difference being the absence of gypsum beds and the presence of dolomite at Mount Chalmers. There are similarities in the alteration mineralogy between the Kuroko deposit and Mount Chalmers. However, the Kuroko deposits tend to have zoned pipe-like alteration halo. Whereas at Mount Chalmers the alteration is related to and controlled by high angle faults, with little if any zonal pattern evident (see Chapter 7 for a fuller discussion on the alteration assemblages and their distribution).

Table 6.7. Comparison between the "classical" Kuroko-type deposits of Japan and Mount Chalmers

Feature	Typical Kuroko-deposit	Mount Chalmers
Intrusive rocks	Spatially and temporally related to intrusive rhyolite dome. Volcano-sedimentary host lithologies intruded by mafic dykes and sills	
Detailed stratigraphy	Occur within a mixed volcano-sedimentary sequence. Mineralisation occurs on the flanks of rhyolite domes	
Mineralisation	barite	local development of small barite lenses in the hangingwall and footwall
	tetsusekiei	locally present
	sekkoko	not present
	Kuroko	locally present in West Lode, but only a minor component and possibly in the South Lode, absent in the Main Lode
	oko	present in both lodes
	keiko	well-developed pyrite-chalcopyrite stockwork stringer zone
Alteration	Regular vertical and lateral alteration (outer to inner zone) I: Montmorillonite, zeolite and cristobalite zone II: Sericite-Fe,Mg-chlorite-albite-K-feldspar and quartz zone III: Sericite, sericite-montmorillonite, Fe-chlorite zone IV: Quartz-sericite zone	Alteration is controlled by high angle normal faults, with silica, pyrite and kaolinite tend to be proximal to mineralisation and sericite and chlorite tending to dominate away from to the mineralisation.

6.8. How Did Mount Chalmers Survive?

The modern oceans are well aerated and therefore the preservation potential of modern day massive sulphide deposits is low, as sulphides within an oxygenated environment are rapidly oxidised. For subaerially exposed, or buried near surface sulphide deposits on land the main oxidising agent is oxygenated groundwater. The sulphide minerals are dissolved ionically under the attack of surface waters, and the constituents then react with dissolved atmospheric oxygen (Guilbert and Park, 1985). For the modern oceans, the oxidising agent is seawater. On the modern ocean seafloor where massive sulphide deposits are currently being formed, once hydrothermal activity has ceased or the focus of hydrothermal discharge in the mound has moved, the sulphide mounds rapidly develop an oxidised crust to them *e.g.* Snake Pit and TAG (Thompson *et al.*, 1988) and the Indian Ocean floor, north of the Rodrigues Triple Junction. (Halbach, 1998). One can easily imagine that unless these deposits are rapidly buried by *e.g.* lava flows or mass-flow deposits then they will not be preserved in the geological record.

The Mount Chalmers VHMS deposit has a well-developed gossan, especially over the West Lode, as does the Mount Warminster VHMS deposit to the northeast of Mount Chalmers. One of the important processes involved in the formation of gossans is the oxidation of S and usually, other elements such as Se, As, Cu, Fe and Au (Thornber and Taylor, 1992). As marine sediments occur within the hangingwall stratigraphy to the Mount Chalmers mineralisation, it is considered to be extremely unlikely that the mineralisation was exposed to subaerial conditions. Therefore, for a gossan to have formed or for the sulphide mound to have been oxidised it must have been exposed to an oxygenated water column. However, a number of authors, notably Goodfellow (1987; 1998), and Eastoe and Gustin (1996) have argued that the formation of sulphide deposits on the Phanerozoic sea floor occurred within widespread anoxic bottom water conditions.

Goodfellow (1987) and Goodfellow *et al.*(1993) argued that sediment-hosted stratiform Zn-Pb deposits (SEDEX) in the Selwyn Basin were formed by the mixing of a Zn- and Pb-rich brine with reduced S enriched in ambient stagnated bottom waters. Goodfellow (*ibid*) also concluded, that other SEDEX deposits occurring worldwide coincide with periods of documented anoxia in the palaeo-oceans. Although controversy exists over whether these events are coeval and truly global or due to a combination of local environmental factors (Stow *et al.*, 1996). Eastoe and Gustin (1996) reviewed the association between Phanerozoic VHMS deposits, the $\delta^{34}S$ values for sulphides and sulphates and argued that the presence of anoxic bottom water (regardless of the scale) is a critical factor in the preservation of Phanerozoic VHMS deposits. They further argued that the link with anoxia is reinforced in the form of numerous associations between VHMS deposits and black shale and the preservation of pyrrhotite. Therefore, it can be argued that the preservation of ancient VHMS and SEDEX deposits is largely dependent upon them being formed in an anoxic environment.

Table 6.8 lists the environmental conditions required for the preservation of SEDEX and VHMS deposits and compares this to the palaeoenvironmental conditions interpreted to have existed at the time of the formation of Mount Chalmers. This shows that where data is available Mount Chalmers fails to meet any of the environmental conditions required to preserve a massive sulphide ore body. Therefore, Mount Chalmers should not have survived in the geological record. So, how did Mount Chalmers survive?

Table 6.9. Comparison between environmental conditions required to preserve a SEDEX or a VHMS deposit and the palaeoenvironmental conditions at Mount Chalmers.

Anoxic Bottom Water Conditions	Mount Chalmers
Black laminated shales (no bioturbation)	Black shales are present at the nearby Woods Shaft Prospect and also are exposed on Pilbeam Drive. At Woods Shaft, the shales are strongly cleaved so no evidence of bioturbation is preserved. At Pilbeam Drive, the shales are extensively bioturbated. Sediments hosting the mineralisation are bioturbated
Lack of benthic fauna	Extensive and wide ranging benthic fauna is present throughout the Berserker beds
Unoxidised clastic sulphides	Development of gossans over the West Lode and South Lode + occasional oxidised sulphides
Sulphur/carbon ratios >>0.36	No data
Positive $\delta^{34}S$ values in laminated pyrite Upward increasing secular trends	$\delta^{34}S$ values for pyrite are all negative. Mount Chalmers as far as is presently known is a "one off "deposit within the Berserker beds, therefore a secular trend cannot be established

As the Main Lode has no gossan developed on it, some mechanism must have protected this area from the oxygenated seawater environment. The lowest sections of the hangingwall lithologies that immediately overlie the massive sulphide are invariably altered to some degree, and locally they may also be mineralised. Therefore, it is envisaged that the Main Lode massive sulphide was rapidly buried prior to cessation of hydrothermal activity or very shortly afterwards, thus excluding it from the oxygenated seawater column.

One possible reason for Mount Chalmers for being relatively small ($\approx$ 4 Mt) is that perhaps like modern day "black smokers" an estimated 90 % of the metals were lost to an oxygenated water column during venting (Goodfellow, 1998). For example, without metal loss the Bent Hill deposit would be approximately 150 Mt instead of the current 15 Mt and TAG would be approximately 27 Mt, instead of the estimated 2.7 Mt (Goodfellow, 1998; Hannington *et al.* 1998). If the hydrothermal fluids that formed Mount Chalmers vented into an anoxic water column then the sulphides would have been deposited onto the seafloor forming laminated apron and therefore would have been preserved.

6.9. DISCUSSION

Based upon the presence of shallow-marine body and trace fossils within the Berserker beds the Mount Chalmers VHMS was formed in an oxygenated shallow-marine ($\leq$300 m) environment. The Mount Chalmers massive sulphide ore lenses were formed and grew from the growth and collapse of black smoker chimneys as well as from hydrothermal fluids circulating within the mound. The fluids dissolved sulphides in the base of the mound and precipitated sulphides near the top of the mound through mixing with seawater. Detailed core logging has revealed a complex and dynamic array of veins within the footwall and hangingwall lithologies. These show that the Mount Chalmers hydrothermal fluid was constantly evolving and changing its fluid chemistry throughout its life.

Within and near the top of the West Lode massive sulphide possible fossilised bacteria occur. No bacteria were found within the Main Lode massive sulphide. The bacteria have very close spatial relationship to the pyrite and are therefore thought to be fossilised chemolithautotrophic sulphur reducing bacteria. Preservation of bacteria within a sulphide mound requires a very unique set of circumstances. Foremost amongst these would be early silicification *via* the processes described by Kornhauser and Ferris (1996). Other considerations would include whether the microniches the bacteria occupy are overprinted by later higher temperature hydrothermal fluids *e.g.* by the process of zone refining.

The Main Lode massive sulphide lens is thicker and more extensive than the West Lode massive sulphide. This may be partially due to the development of a thick gossan over the West, but it may also have been due to the duration of hydrothermal activity. The development a thick gossan over the West Lode massive sulphide further reinforces the argument that the Mount Chalmers VHMS deposit was formed in an oxygenated seawater column. Furthermore, the presence of a gossan over the West Lode and not the Main Lode suggests one of two possibilities:

- that the hydrothermal systems responsible for the formation of the two lenses were not operating at the same time and that the West Lode hydrothermal system was short lived and therefore became subject to oxidation processes prior to burial by the hangingwall lithologies., or
- that the hydrothermal system that formed the West Lode ceased activity sometime before cessation of the Main Lode hydrothermal activity and again was subject to oxidation. The Main Lode massive sulphide mineralisation was buried either before the cessation of hydrothermal activity or shortly afterwards before oxidation of the sulphides could occur.

Either scenario would effectively account for the disparity in thickness between the two lodes and the development of the gossan over the West Lode and not the Main Lode. The preservation potential of VHMS and SEDEX deposits is directly linked to their formation environment. Sulphide deposits, will be more readily preserved in an anoxic water column.

In an oxygenated water column the preservation potential of VHMS deposits is very limited. Mount Chalmers was preserved from total oxidation and therefore destruction by being rapidly buried by mass flow deposits and lava flows. These deposits effectively sealed Mount Chalmers off from the oxygenated water column and thus preserving it. The low preservation potential of massive sulphide deposits formed within an oxygenated environment could explain why they are not largely represented in the geological record compared to the deep-marine VHMS deposits.

The presence of limited hangingwall alteration immediately overlying massive sulphide and the extension of stage three veins up into the hangingwall lithologies indicates that the hydrothermal system continued after burial of massive sulphide by sediments and volcanics, or that the system was reactivated sometime after burial.

The close relationship between the massive sulphide ore lenses to the footwall rhyolite argues that they are a spatially and temporally related. Furthermore, the distribution of the massive sulphide mineralisation and the positioning of the massive sulphide ore lenses over mapped faults shows that there is also a strong structural control on the distribution of the massive sulphide mineralisation. These faults bound the footwall rhyolite dome and were possibly activated at the time of emplacement of the rhyolite dome and also acted as conduits along which the hydrothermal fluids migrated and were eventually discharged out onto the palaeo seafloor. The sequence of events that lead to the formation and preservation of the Mount Chalmers VHMS deposit are summarised in Figure 6.16. This sequence of events outlined below have the West Lode hydrothermal system operating at an earlier stage than the Main Lode hydrothermal system.

a) intrusion of rhyolite and dome and the initiation of the West Lode hydrothermal activity. Formation of white smokers and a sulphate mound by low-temperature hydrothermal fluids (not shown). As fluid temperatures increased sulphide chimneys were formed.

b) growth of the sulphide mound by an ongoing process of chimney collapse and growth and internally by circulating hydrothermal fluids.

c) cessation of hydrothermal activity at the West Lode and possibly the initiation of low-temperature hydrothermal activity on the Main Lode (assuming that there was no prior hydrothermal activity).

d) formation of black smoker chimneys from higher temperature fluids at the Main Lode while oxidation of the West Lode has begun.

e) growth of the Main Lode massive sulphide continues through processes outlined in (b), along with further oxidation of the West Lode and gossan formation.

f) burial of the massive sulphide ore lenses along with the possible cessation of all hydrothermal activity, or continuation of hydrothermal activity at a lower level.

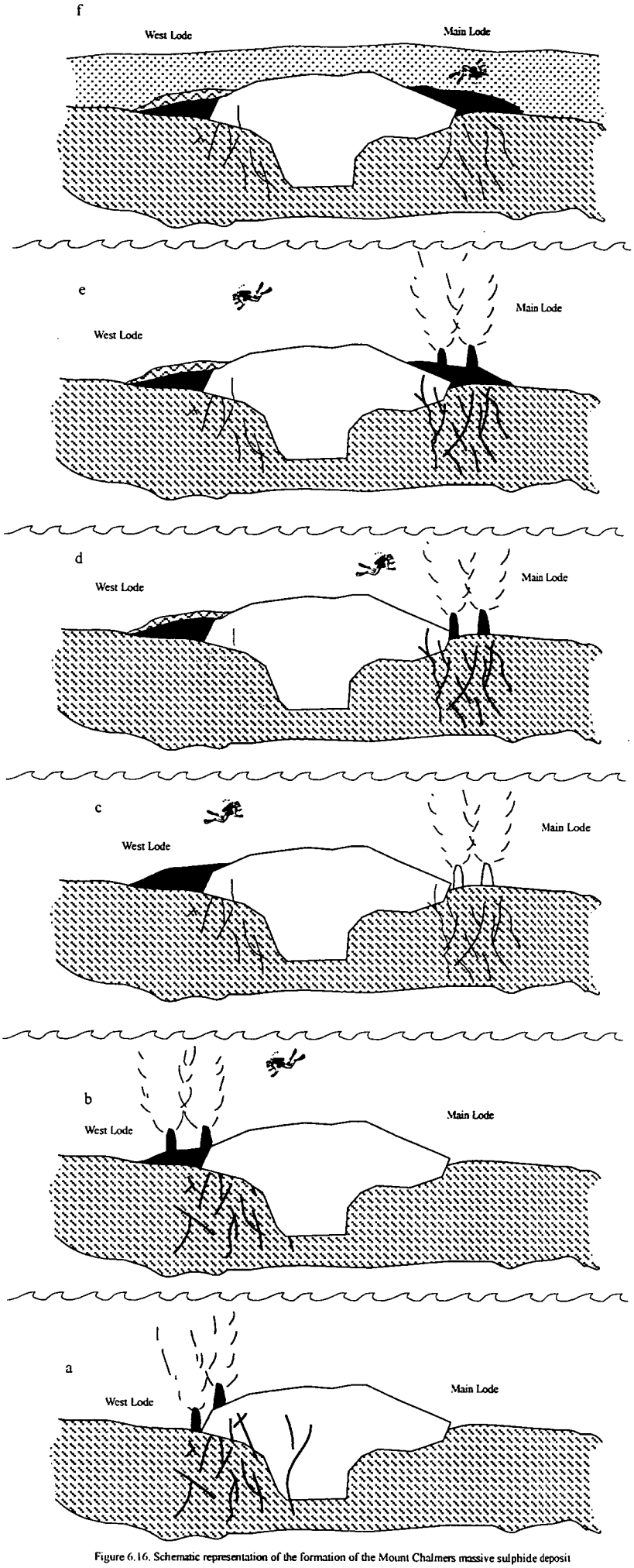

Figure 6.16. Schematic representation of the formation of the Mount Chalmers massive sulphide deposit

CHAPTER 7
HYDROTHERMAL ALTERATION

7.1 INTRODUCTION

"Hydrothermal alteration is a chemical replacement of the original minerals in a rock by new minerals where a hydrothermal fluid delivers the chemical reactants and removes the aqueous reaction products" (Reed, 1997). The hydrothermal alteration zone that underlie, and in some VHMS deposits overly it, are produced by reaction of the hydrothermal fluid with wall rocks that it passes through, and have been the focus of considerable research over the last 30 years (Large, 1992). Alteration zones are important in order to understand the chemical and thermal nature of the mineralising fluids, and as a tool in the exploration for VHMS deposits.

Alteration commonly effects both the chemical and physiological state of the hydrothermal system and extends well beyond the actual deposit. Hydrothermal alteration is generally most intense in the footwall of a deposit resulting in the enrichment of Si, Mg and Fe and depletion in Na and Ca. For example, Na depletion haloes associated with the Kuroko deposits may extend for up to 3 km laterally away from a deposit (Date *et al.*, 1983), and alteration in the hangingwall may extend for up to 200 m above a deposit, as in the case of the Shakanai mine in the Kuroko district of Japan (Matsukama and Horikoshi, 1970). More extensive hangingwall alteration may be traced using oxygen isotopes. Where zonation of the $\delta^{18}O$ values may extend for up to 400 m above a deposit and the lateral extent of the $\delta^{18}O$ anomaly is much larger than the geochemical anomalies (Green *et al.*, 1983).

Due to the metamorphism, structural complexity, and lack of access to alteration pipes away from economic mineralisation (Lydon, 1988), few studies of intact, relatively undeformed and metamorphosed stringer and alteration zones associated with VHMS deposit have been undertaken, the Kuroko deposits of Japan aside (*e.g.* Gemmell and Large, 1992). Although the Mount Chalmers stringer zone and footwall alteration zones are no longer exposed (due to flooding of the open cut), enough diamond drill holes and percussion holes with diamond tails were drilled to enable a study of the alteration zone to be made.

7.2 FOOTWALL ALTERATION

Underlying the Mount Chalmers deposit is a well developed extensive and variable (in terms of mineral associations) alteration zone. The footwall alteration occurs along the entire length and breadth of the deposit and extends for hundreds of metres beyond the limits of the known mineralisation. Extensive zones of alteration of similar style to that found in the footwall of Mount Chalmers have been intersected in a number of drill holes at different prospects up to 6 km away *e.g.* Tungamull (Fig. 7.1).

The mineralogy of the footwall alteration at Mount Chalmers presents only six main mineral phases. To date there have been recognised: Two varieties of chlorite (sudoite - a lithium poor, aluminous di, trioctahedral chlorite; trioctahedral chlorite), two generations of silica (phase 1 and phase 2), sericite/muscovite, dolomite, kaolinite and hematite.

7.2.1 Chlorite Alteration

Chlorite alteration at Mount Chalmers is largely restricted to the footwall volcaniclastics. Within the footwall volcaniclastic pile, the chlorite alteration has extensively altered the Footwall Rhyolite, polylithic breccias and pumiceous breccias. Chlorite alteration is also present within the dolomite alteration, where it occurs as thin planar or kinked veinlets that have imparted a planar appearance to the dolomite. The chlorite alteration has been overprinted by silica-sericite alteration that locally has imparted a pseudo-breccia appearance to the rocks.

Rarely does massive chlorite alteration occur alone, *i.e.* where chlorite is the sole alteration mineral present. However, two intervals of massive chlorite were intersected beneath the West Lode massive sulphide:

- MC25: the chlorite is associated with disseminated to semi-massive and veined chalcopyrite and pyrite in a narrow interval between 20.75 to 21.85 m. In this interval the sulphides are replacing the chlorite. Also in MC 25 at 18.4 m there is a narrow interval of massive pyrite + chalcopyrite that has been "intruded" and split by a chlorite wedge.

- MC29: the massive chlorite is been cut by very fine grained sericite veinlets.

Using XRD and electron microprobe analyses, McLeod (1987) recognised two varieties of chlorite at Mount Chalmers, sudoite - a lithium poor, aluminous di, trioctahedral chlorite and trioctahedral chlorite.

7.2.1.1 Sudoite

Sudoite was observed within the marginal zone of the dolomite horizon within the Main Lode and within the sericite-altered volcaniclastics along strike from the massive sulphide lenses of both the Main Lode and the West Lode. Sudoite was first reported from the Japanese Kuroko deposits where it occurs in the marginal zones Alteration Zone III of many of the Kuroko deposits (Sudo *et al.*, 1954; Sudo and Kodama, 1957; Sudo, 1959; Sudo and Sato, 1967; Hayashi and Oinuma, 1964; Tsukahara 1964; Shiozu, 1969, 1974, 1978; Iijima, 1974; Kimbara and Nagata, 1974 Shirozu, 1974). Sudoite is rarely found in the hangingwall and footwall clays of the Kuroko deposits.

Sudoite was not observed within the massive sulphide or within the underlying stringer zone. In the Main Lode sudoite occurs as laminae and veinlets within the dolomite and within the sericite altered volcaniclastics as patches or randomly oriented flakes within a groundmass of sericite-trioctahedral chlorite and as coarse crystals in halos around pyrite euhedra (McLeod, 1987).

The compositional range of the sudoite is large and the variation from the ideal composition $(Mg_2Al_3)(AlSi_3)O_{10}(OH)_8$ is extensive. Nonetheless, for each analysis the octahedral population approaches the ideal number, five (Al(VI) + Mg) and Ald (the difference between the numbers of octahedral and tetrahedral aluminium) approaches the ideal, two (McLeod, 1987).

7.2.1.2 Trioctahedral Chlorite

Chlorites of the trioctahedral subgroup occur throughout the stratigraphic sequence, but the total content and grain size of the chlorite increases with proximity to the massive sulphide lenses. Within the footwall the chlorite occurs as coarse flakes and rosettes, intimately associated with chalcopyrite within the stringer veins. The chlorites can also be seen to be replacing feldspar crystals, and is commonly intergrown with sericite. Within the dolomite lenses the chlorite occur in laminae and anastomosing veinlets associated with sericite, barite, quartz and pyrite. Along with sudoite, the chlorite also occur at the margin of the Main Lode dolomite horizon (McLeod, 1987).

Chemically the chlorites have a wide range of divalent cation substitutions and Mg numbers {100Mg/(Mg+Fe)} 38.3 - 77.3, with a mean of 59.1. The chlorites exhibit a systematic trend of decreasing Mg numbers as the base of the massive sulphide lenses is approached or to the contact with the along strike mineralised and altered volcaniclastics. This negative trend in Mg as the massive sulphide is approached is also seen in the dolomite (Chapter 10). At the footwall contacts a trend reversal occurs in that the chlorites become increasingly Mg-rich towards the top of the sulphide horizon. Within the mineralised horizon the chlorites are volumetrically insignificant, and have higher Mg numbers (average 85.6) than those of the underlying footwall volcaniclastics. Chlorites along strike from the mineralisation have an average Mg number of 77.1.

7.2.2. Silica Alteration

Silica alteration associated with VHMS deposits commonly occurs adjacent to the stockwork stringer veins , but may also affect the uppermost 50 to 100 metres of the footwall (Barrett and Sherlock, 1996). Logging of the Geopeko drill holes from the Mount Chalmers mine has shown that there are at least two phases of silica alteration within the stringer zone or immediately beneath the massive sulphide mineralisation. The first phase of silica alteration has produced a pale grey/blue "cherty" appearance (Fig 6.10c). Scattered inliers of relatively unaltered feldspar-phyric rhyolite and siltstone occur within the zone of intense silica alteration, indicating that the silica alteration has partially to completely overprinted either a siltstone and or a rhyolite. The second phase of silica alteration is later than Phase 1 silica alteration and is characterised by irregularly shaped milky white coloured blotches within the Phase 1 silica. The Phase 1 silica alteration also forms the "silica chimney", which is an intense zone of silica alteration that forms the core of the footwall alteration system, and divides the Main Lode and West Lode massive sulphide lenses.

7.2.2.1. Timing of Silica Alteration

Phase 1 silica alteration is the dominant form of silica alteration within the footwall alteration zone. It occurs replacing earlier chlorite alteration, producing pseudoclastic textures within the footwall lithologies especially the Footwall Rhyolite. In close proximity to the mineralisation, the silica alteration has completely overprinted the original lithological textures and earlier alteration phases. The phase 1 silica is considered to be late pre-mineralisation to early syn-mineralisation as it contains disseminated pyrite grains and is cross cut by the sulphide stringer veins. The Phase 2 silica alteration is clearly post phase 1 silica alteration as it is overprinting and cross cutting the Phase 1 silica. It is also considered to be post mineralisation as it cross cuts some of the sulphide veins and is also locally replacing the massive sulphide mineralisation.

7.2.3. Sericite/Muscovite Alteration

Convential dioctahedral potassium micas in the mineralised envelope surrounding the Mount Chalmers massive sulphide deposit are fine grained and carry up to 6.5 wt% of the phengite molecule (FeO + MgO). Systematic stratigraphic variations in the composition of the sericites occur at Mount Chalmers. In the hangingwall, deep in the footwall (beneath the stringer zone) and along strike from the mineralised horizon, the sericites are conventional potassium micas with little of the phengite or paragonite molecule. As the massive sulphide mineralisation is approached the sericites become enriched in Ba, and their Mg numbers vary systematically with changes in the Mg numbers of the coexisting chlorites. At the top of the massive sulphide mineralisation in the Main Lode, the barian sericites are replaced by barium-free sodian sericites and are accompanied by barite as the barium bearing phase. (McLeod, 1987).

7.2.3.1. *Timing of Sericite Alteration*

There are at least two generations of sericite alteration. The first stage of sericite alteration occurs post Phase 1 silica alteration, as the sericite is overprinting the silica alteration. The later stage of sericite alteration occurs post dolomite alteration, and maybe slightly earlier or synchronous with the second stage of kaolinite alteration.

7.2.4. Dolomite Alteration

The dolomite alteration at Mount Chalmers is the dealt with in detail in Chapter 10. Therefore, only a brief summary of the salient features of the dolomite alteration are given here. At Mount Chalmers lenses of semi-massive to massive dolomite associated with massive sulphide have replaced hangingwall and footwall rocks. There are five generations of dolomite: texture 1 - anhedral to subhedral very fine-grained cloudy dolomite; texture 2 – radiating blades of cloudy dolomite; texture 3 - clear rhombohedral dolomite overgrowths on the cloudy dolomite; texture 4 - mosaics of interlocking subhedral clear dolomite within

the cloudy dolomite and texture 5 - late stage dolomite infilling veins, vughs and fractures. The cloudy dolomite replaced earlier silica and barite blades.

The five phases of dolomite indicate evolving, episodic hydrothermal replacement. Carbon and oxygen isotopes indicates that the dolomite may have been formed by either: (1) fluid mixing, where an ascending hydrothermal fluid charged with juvenile CO_2 mixed with cold circulating seawater, or (2) fluid/rock interaction where an ascending, hot, but cooling hydrothermal fluid reacted with the wallrocks. Reaction between and ascending CO_2-rich fluid and mafic minerals provided cations for dolomite formation. In both models, it is envisaged that contribution of the seawater to the formation of dolomite was minor and occurred at or near the site of dolomite precipitation. Geological observations favour derivation of the dolomite by fluid/rock interaction.

7.2.5. Kaolinite Alteration

The presence of kaolinite at Mount Chalmers has previously been reported by Finlow-Bates (*in* Wilkin-Smith, 1973) and McLeod (1985, 1987). X-ray diffraction analyses conducted by Mineral Resources Tasmania identified both kaolinite and dickite. There are two generations of kaolinite at Mount Chalmers. The early stage is associated with the massive sulphide mineralisation, where kaolinite occurs as intercalations with the massive sulphide. There is a close association with chalcopyrite in the stringer zone. In the post-mineralisation stage kaolinite is found within the footwall volcaniclastics. Kaolinite is found cross cutting veins and replacing the dolomite alteration. It also occurs along strike from the massive sulphide mineralisation and is a major component of the dolomite alteration.

Under the scanning electron microscope the kaolinite occurs in one of three modes:

- interlocking radially oriented pseudohexagonal plates (Fig. 7.1a),
- stacked pseudohexagonal plate (Fig. 7.1b),
- twisted, wormlike masses elongated on the *c* axis (Fig. 7.1c).

High proportions of the kaolinite plates have well defined straight edges with prominent 60° angles.

7.2.5.1. *Timing of Kaolinite Alteration*

Within the footwall volcaniclastics, both kaolinite and chalcopyrite are intimately associated, suggesting a premetamorphic origin for the kaolinite (McLeod, 1985). An alteration origin for the kaolinite is further suggested by the presence of crosscutting kaolinite veinlets within the dolomite horizons and within the silica-altered footwall. Away from the faults, chlorite and sericite become the dominant phyllosilicates at the expense of the kaolinite.

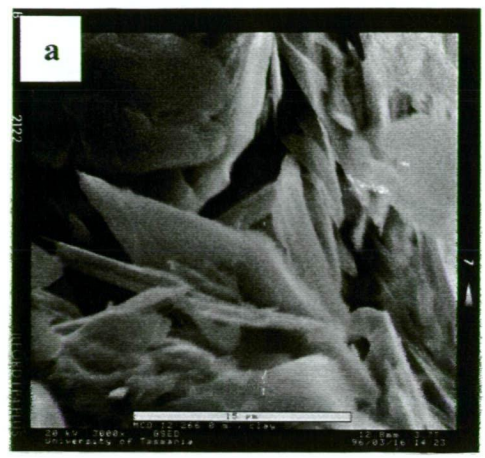

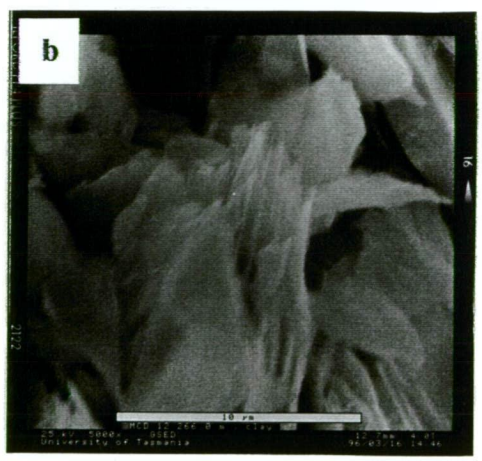

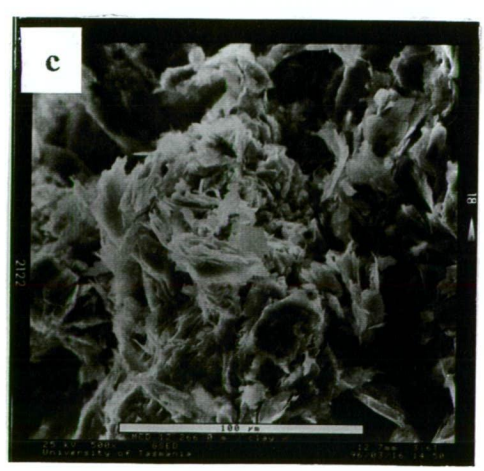

Figure 7.1. SEM photographs of kaolinite (a) interlocking radially oriented pseudohexagonal plates; (b) stacked pseudohexagonal plates; (c) twisted, wormlike masses elongated on the *c* axis.
All samples are from MCD12 @ 266.0 m

7.2.5.2. *Discussion of Kaolinite Alteration*

Kaolinite is usually formed either from weathering of granites and similar Ca-poor igneous and metamorphic rocks and is a major constituent of shales and residual transported soils. It is also a product of hydrothermal alteration and is common in wall rock alteration of sulphide ore veins (Phillips and Griffen, 1981). Kaolinite may also form from the oxidation of pyrite by surficial weathering resulting in supergene acid attack and consequent development of kaolinite. At Mount Chalmers, the kaolinite is associated with sulphide assemblages that exhibit no evidence of oxidation, and this would appear to eliminate the possibility of a supergene origin for the kaolinite.

The presence of kaolinite within ancient or modern day VHMS has not been widely reported. The most widely reported hydrothermal clay mineral from modern day VHMS and sediment-hosted massive sulphide deposits is smectite (Peter and Scott, 1988; Kurnosov *et al.*, 1994; Zierenberg and Shanks) where it occurs as hydrothermal alteration product of the surrounding sediments. In fact, the presence of kaolinite has only been reported from one modern active submarine hydrothermal system - Hine Hina in the Lau Basin (Fouquet *et al*, 1993; Herzig *et al*, 1993). and from the inner alteration zone from an extinct hydrothermal system on the eastern Galapagos (Cocos-Nazca) Spreading Center some 20 to 30 km west of the active Galapagos vents (Malahoff, *et al.*,1993). At the Galapagos (Cocos-Nazca) Spreading Center kaolinite occurs in layered veins composed of kaolinite-smectite-chlorite-cristobalite-sulphide, indicating the presence of multi-phase alteration processes (Embley *et al.*, 1988).

Kaolinite forms an intense zone of argillisation surrounding small pods of massive sulphides from the Undu VHMS deposit on Vanua Levu - Fiji (Colley and Rice, 1975). Kaolinite also occurs within Alteration Zone III of the Kuroko deposits of Japan and beneath and lateral to the Minamishiraoi massive stratiform barite orebody (southwest Hokkaido) and is interpreted to have formed from the hydrothermal fluids responsible for the massive sulphide mineralisation (Shirozu, 1974; Marumo, 1989). Marumo (1989) from an oxygen and deuterium isotope of kaolinite at the Minamishiraoi orebody interpreted the kaolinite to have formed from low temperature hydrothermal fluids (maximum 175°) below the stability fields for sericite and chlorite. However, at Mount Chalmers the kaolinite is associated with chalcopyrite, which suggests that it may have formed at higher temperatures as indicated from the fluid inclusion study.

Part of the reason for the lack of kaolinite within ancient VHMS deposits is that the vast majority of ancient VHMS deposits have undergone moderate to high-grade metamorphism. Experimental work by Hemly *et al.* (1980) in the system Al_2O_3-Al_2O_3-H_2O at 1 kb has shown that the size of the kaolinite stability field increases with decreasing temperature, such that at quartz saturation (*i.e* increasing SiO_2 in solution with increasing temperature), pyrophyllite is in equilibrium with kaolinite at approximately 250° C (Eqn. 7.1, Krauskopf, 1979). The transition from kaolinite to pyrophyllite can also occur at much lower temperatures, but under conditions of high silica saturation *e.g.* Philippine geothermal systems (Reyes, 1990). Alternatively, if kaolinite contains adsorbed K ions muscovite would form instead of pyrophyllite (Eqn. 7.2; Krauskopf, 1979).

The transition of kaolinite to sericite occurs at 200° C and a pH of 4.5. At higher temperatures (400 ° C ± 15° C at 1 kb) pyrophyllite is converted to andalusite or other aluminum-sliciates (Winkler, 1976;

Hedenquist and Reid, 1985; Eqn. 7.3; Winkler, 1976). However, Stanton (1983) observed kaolinite in the metamorphosed Archaean Geco VHMS deposit (Ontario, Canada). The kaolinite occurs in gneisses, and Stanton, suggested that the biotite impurities in the kaolinite prevented the structural readjustment required for the kaolinite + gibbsite → sillimanite transformation.

$$\underset{\text{kaolinite}}{2Al_2Si_2O_5(OH)_4} + 2SiO_2 \Leftrightarrow \underset{\text{pyrophyllite}}{Al_2Si_4O_{10}(OH)_2} + H_2O \qquad \text{Equation 7.1}$$

$$\underset{\text{kaolinite}}{3Al_2Si_2O_5(OH)_4} + 2K^+ \Leftrightarrow \underset{\text{muscovite}}{K_2Al_4(AlSi_3O_{10})_2} + 2H^+ + 3H_2O \qquad \text{Equation 7.2}$$

$$\underset{\text{pyrophyllite}}{Al_2Si_4O_{10}(OH)_2} \Rightarrow \underset{\text{andalusite-kyanite}}{Al_2SiO_5} + \underset{\text{quartz}}{3SiO_2} + H_2O \qquad \text{Equation 7.3}$$

Kaolinite is a widely reported mineral from modern day active geothermal systems, where it is the product of acid alteration and is thermally stable below 200° C (Reyes, 1990), and is one of the key indicator minerals for 'advanced argillic' alteration. Advanced argillic alteration is characterised by extreme hydrolysis and cation leaching, relatively high total sulphur, and oxidising conditions. Therefore, the sulphur is oxidised, and the sulphuric acid carries out the cation leaching, leaving an aluminium-silicate and/or sulphate assemblage (Hedenquist and Reid, 1985). Kaolinite associated with the Kuroko deposits was formed from ascending acidic hydrothermal fluids below the seafloor, where circulation of seawater was prevented. The close spatial association between kaolinite and sulphide mineralisation suggests that the acidic hydrothermal fluids were closely related to the Kuroko mineralisation (Iijima, 1974). This close spatial relationship between sulphides and kaolinite also occurs at Mount Chalmers, also suggesting that the acidic hydrothermal fluids responsible for the formation of the kaolinite may have also been responsible for the formation of the sulphide ores.

7.2.6. Hematite

Hematite alteration was intersected in a number of drill holes in both the hangingwall and footwall position to the massive sulphide mineralisation. The hematite alteration normally occurs within siltstones that either immediately overlie the massive sulfide mineralisation or occur along strike from the massive sulphide mineralisation in the ore equivalent horizon. The hematite has also altered the base of rhyolite (MC27A: 5.4 - 8.0 m) and a peperite (MC22A: 49.2 - 52.0 m). In MC 44 (-16.2 - 17.6m) the sedimentary component of a peperite that overlies a gossan and semi-massive sulphide has been altered by hematite, while the magmatic component has remained relatively unaltered.. In MC51, a narrow interval (89.5 - 89.9 m) of hematite-silica breccia was intersected. The breccia is composed of sub-rounded to rounded hematite fragments within a siliceous matrix.

The breccia overlies an open stope, where presumably either semi to massive sulfide was mined. Hematite alteration was also intersected in the footwall stringer zone, where silica alteration is overprinting the hematite alteration.

7.2.6.1. *Timing of Hematite Alteration*

The timing of the hematite alteration, especially in the footwall is not very clear. In MC45 (34.4 - 36.0 m) the hematite is replacing an earlier chlorite alteration and is being crosscut by pyrite and later kaolinite veins. Between 36.0 - 50.0 m the hematite is being replaced by Phase 1 silica alteration. This has imparted a pseudobreccia appearance to the core, composed of sub-rounded to rounded hematite fragments. Hematite alteration in the hangingwall and in the ore equivalent horizon is considered to be related to the waning stage of the hydrothermal activity and has replaced the sedimentary rocks that immediately overlies the massive sulphide mineralisation or in the ore equivalent position.

7.3. MOUNT CHALMERS

The above alteration phases can occur separately or with one another, presenting a complex history of interacting mineral phases. This interaction between the different mineral phases has produced complex alteration assemblages. This is particularly true near the massive sulphide lenses, where very irregular, and partially to completely different alteration assemblages occur. With this in mind a series of alteration cross sections through the West Lode and the Main Lode have been produced. In an attempt to simplify the number of alteration assemblages present in any given interval, only the two dominant alteration assemblages were used. In addition, for clarity the hangingwall lithologies have been grouped into one entity — undifferentiated hangingwall. In total 11 cross sections were generated, progressing from the southern margins of the West Lode through to the northern margins of the Main Lode (Figs. 7.2a-k).

The most obvious feature of these cross-sections is the ubiquitous nature of the silica alteration. Although this shown as being widespread, no attempt was made to distinguish drill core intervals were the silica alteration has completely destroyed the original lithological textures and those were the silica alteration is present, but the original lithologies and lithological textures are still discernible. In addition, no attempt was also made to distinguish Phase 1 silica from Phase 2 Silica, as Phase 2 is commonly associated with Phase 1. However, the most intense zone of silica alteration occurs beneath the massive sulphide lenses, and in the "silica chimney" between the West Lode and Main Lode sulphide lenses.

The second most dominant alteration assemblage is chlorite. Chlorite alteration is mainly preserved in the deeper parts of the footwall alteration zone and along strike from the massive sulphide mineralisation, and is the only other alteration assemblage other than silica to have any significant lateral or vertical extent. Compared to chlorite, sericite and kaolinite tend to have a limited lateral extent, and do not occur over significant horizontal or vertical distances.

Legend for Figures 7.2a - 7.2k

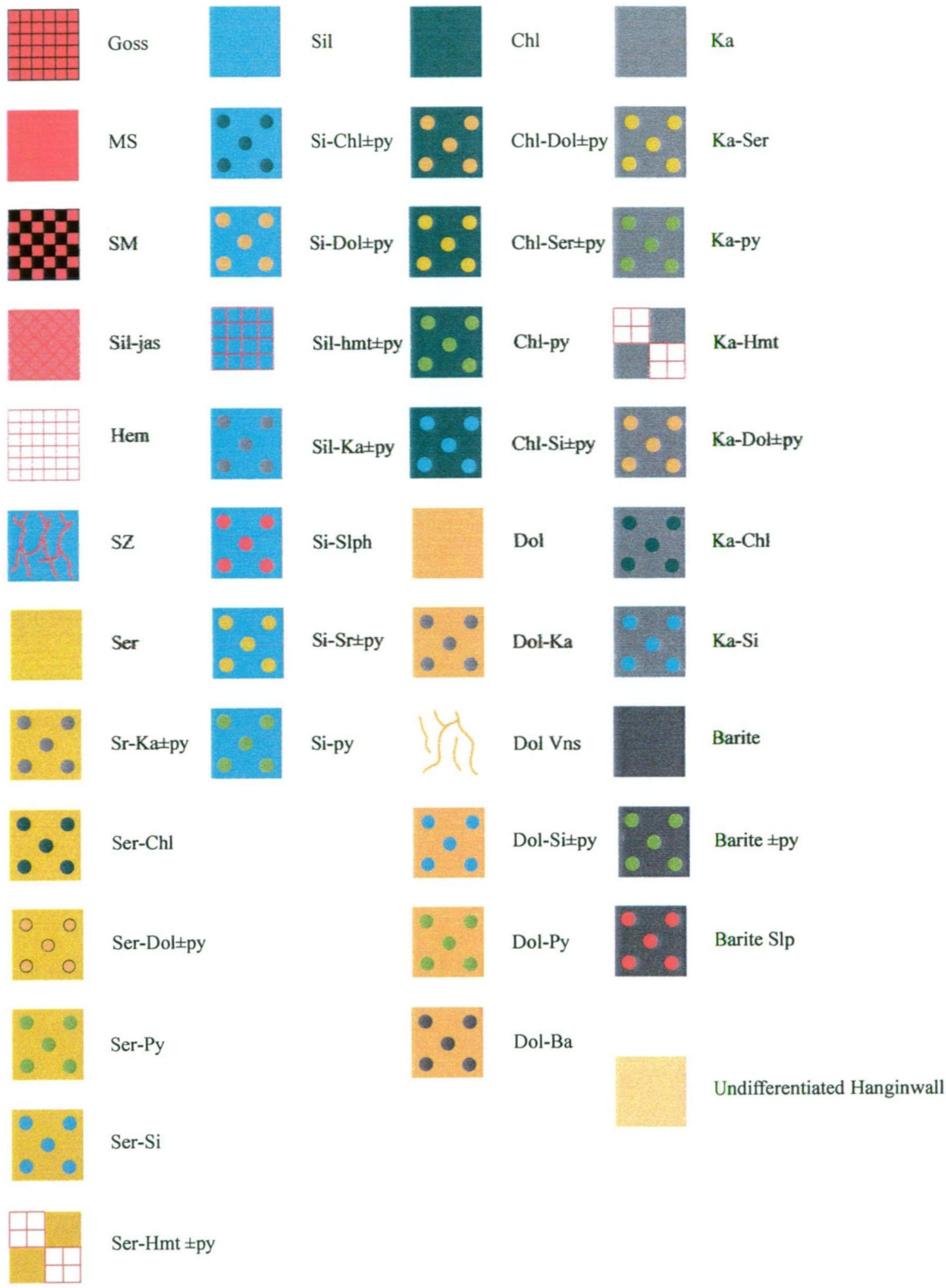

Goss = gossan
SM = semi-massive sulphide
MS = massive sulphide
SZ = stringer zone
Ba = barite

Hmt = hematite
Sil-jas = silica/jasper
Dol = dolomite
Dol Vns = Dolomite veins
py = pyrite
Slp = sulphides

Si = silica
Ser = sericite
Ka = kaolinite
Chl = chlorite

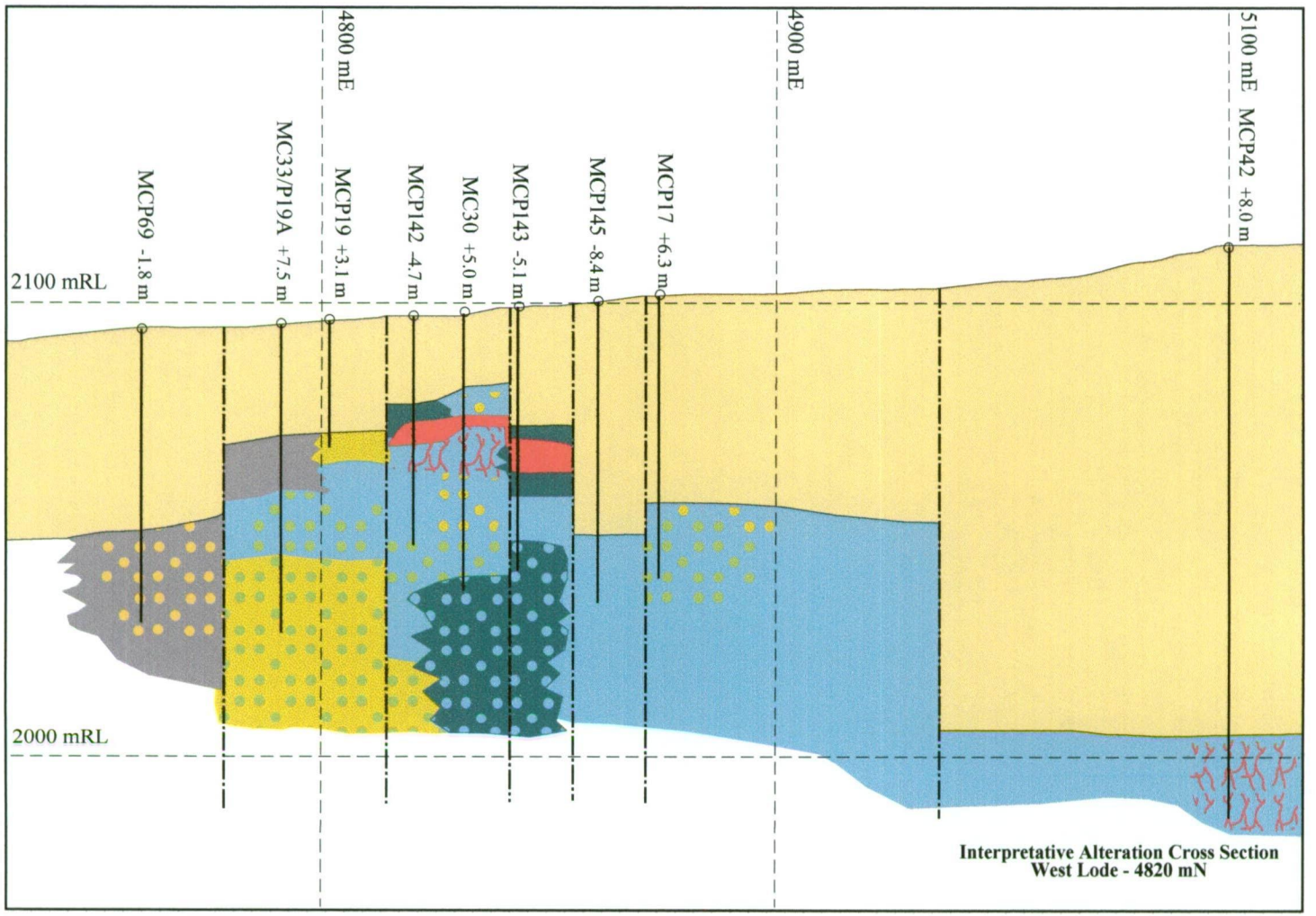

Figure 7.2k. Interpretative alteration cross section: West Lode - 4820 mN

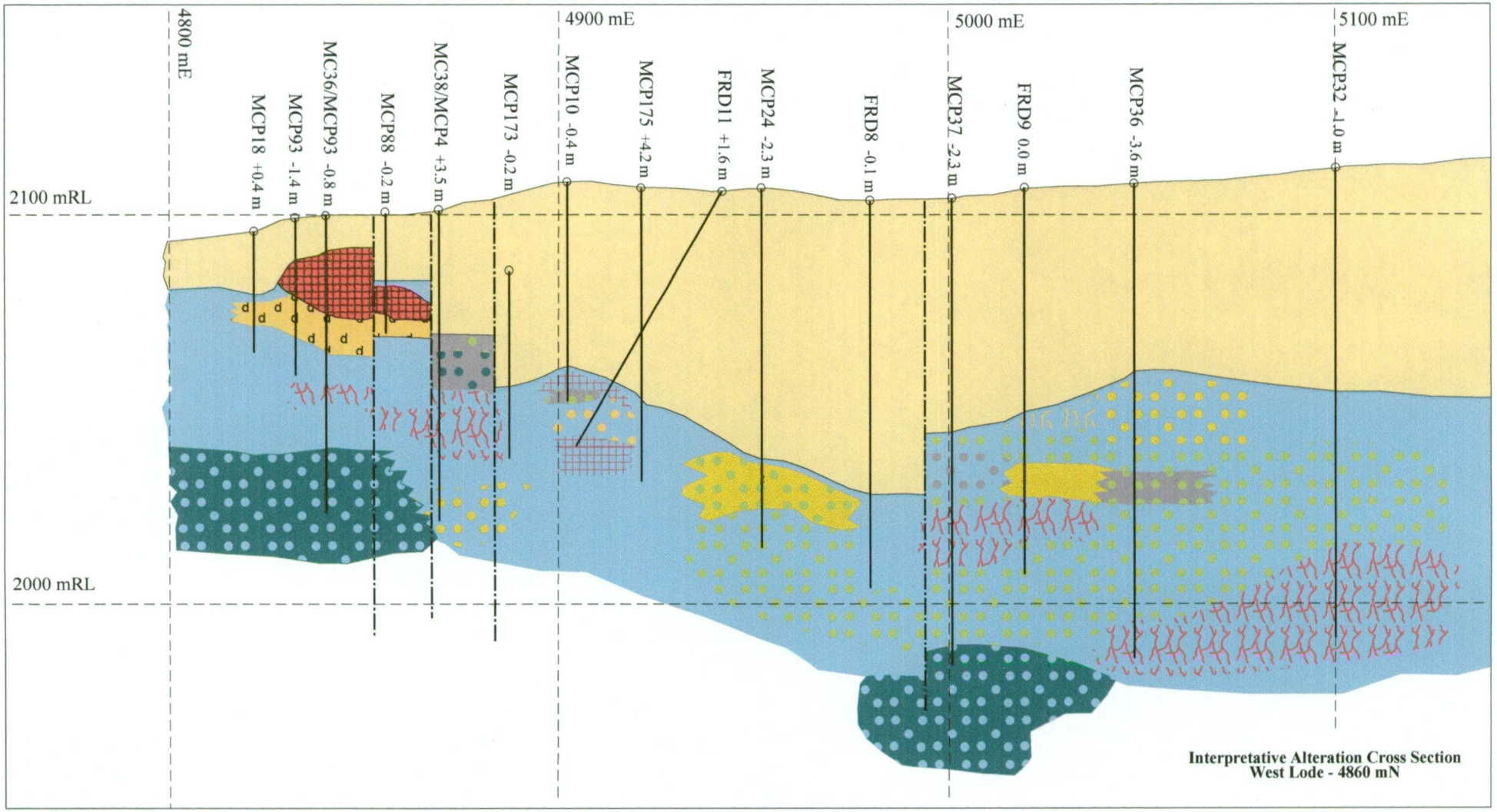

Figure 7.2b. Interpretative alteration cross section: West Lode - 4860 mN

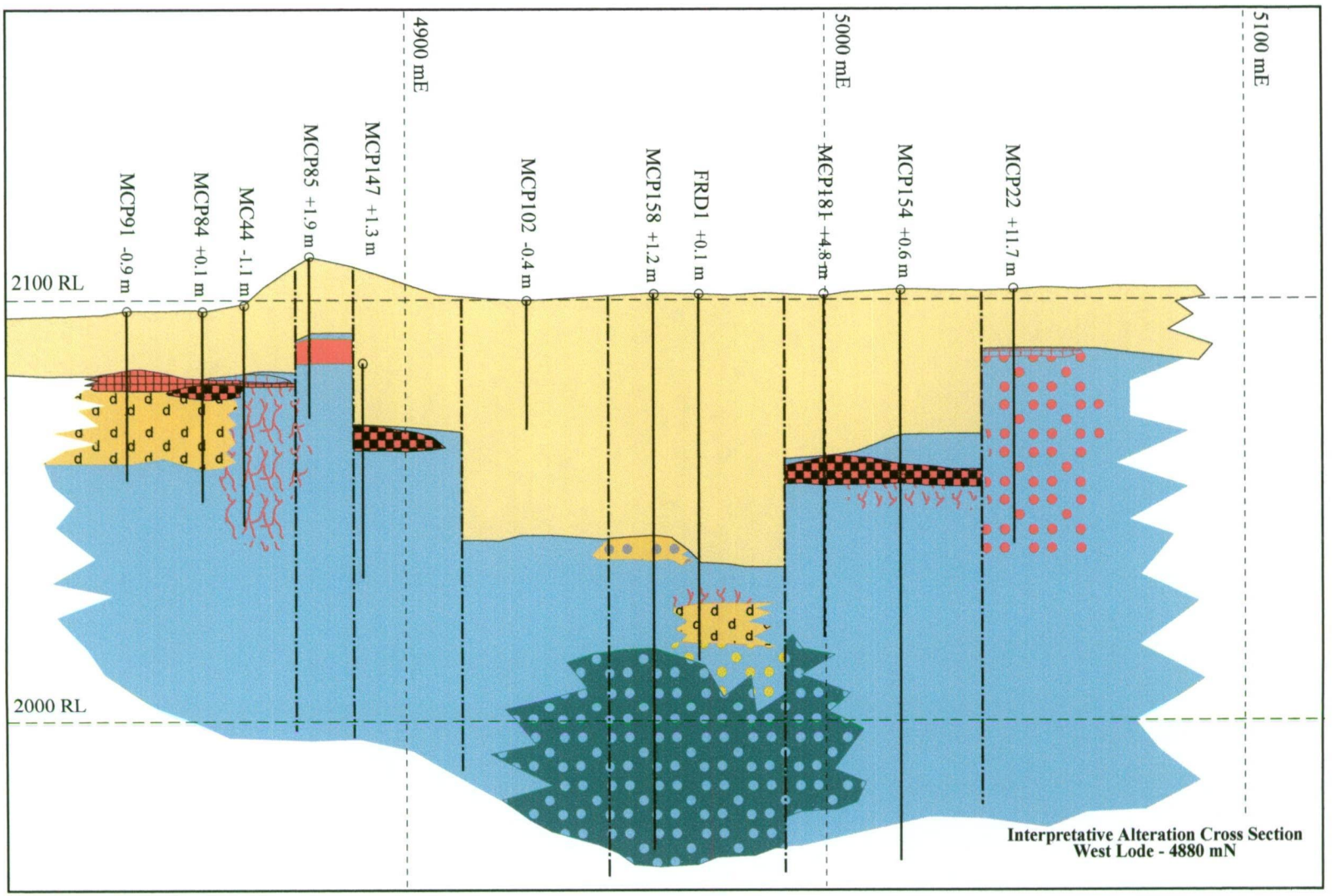

Figure 7.2c. Interpretative alteration cross section: West Lode - 4880 mN

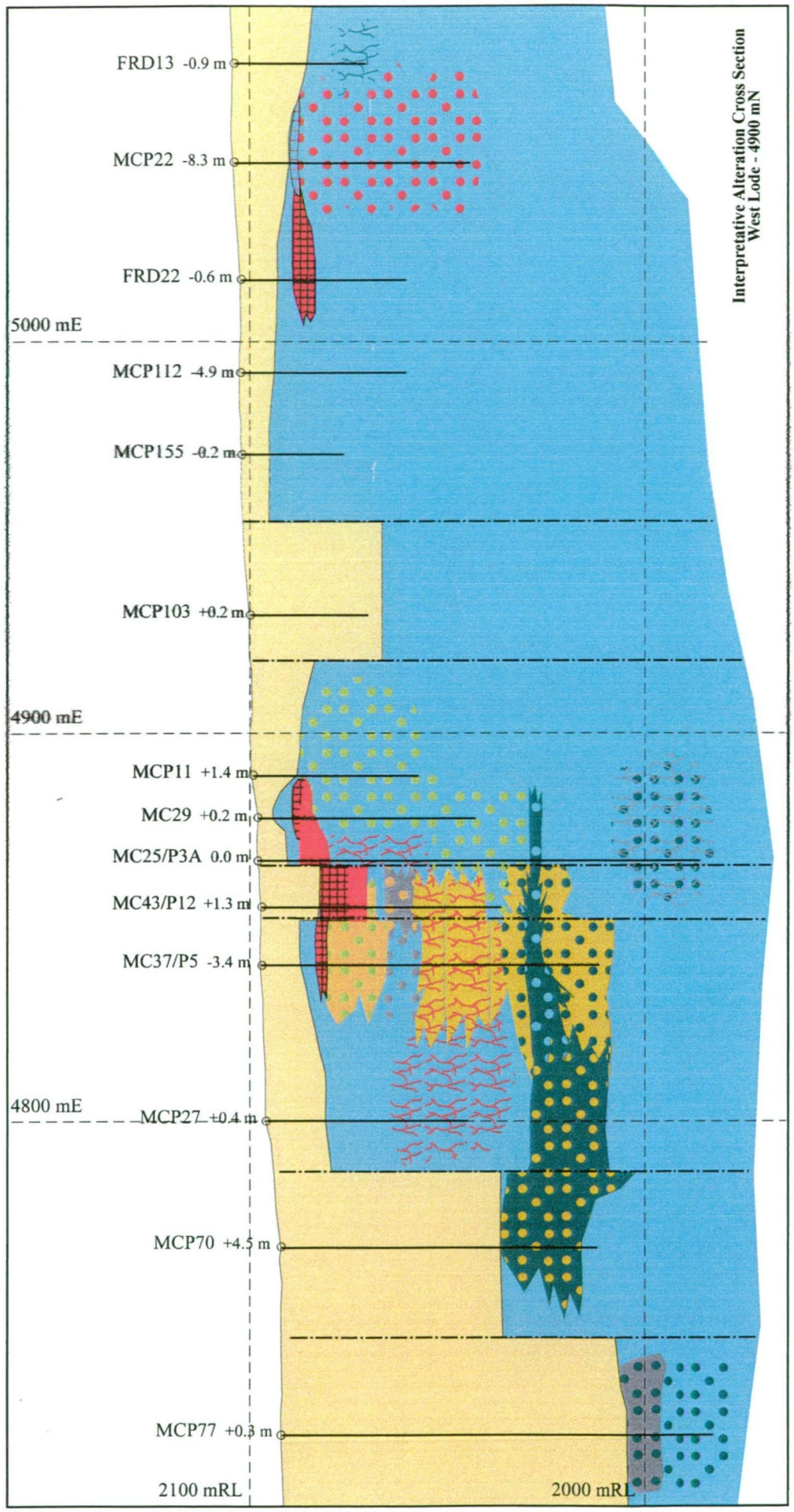

Figure 7.2d. Interpretative alteration cross section: West Lode - 4900 mN

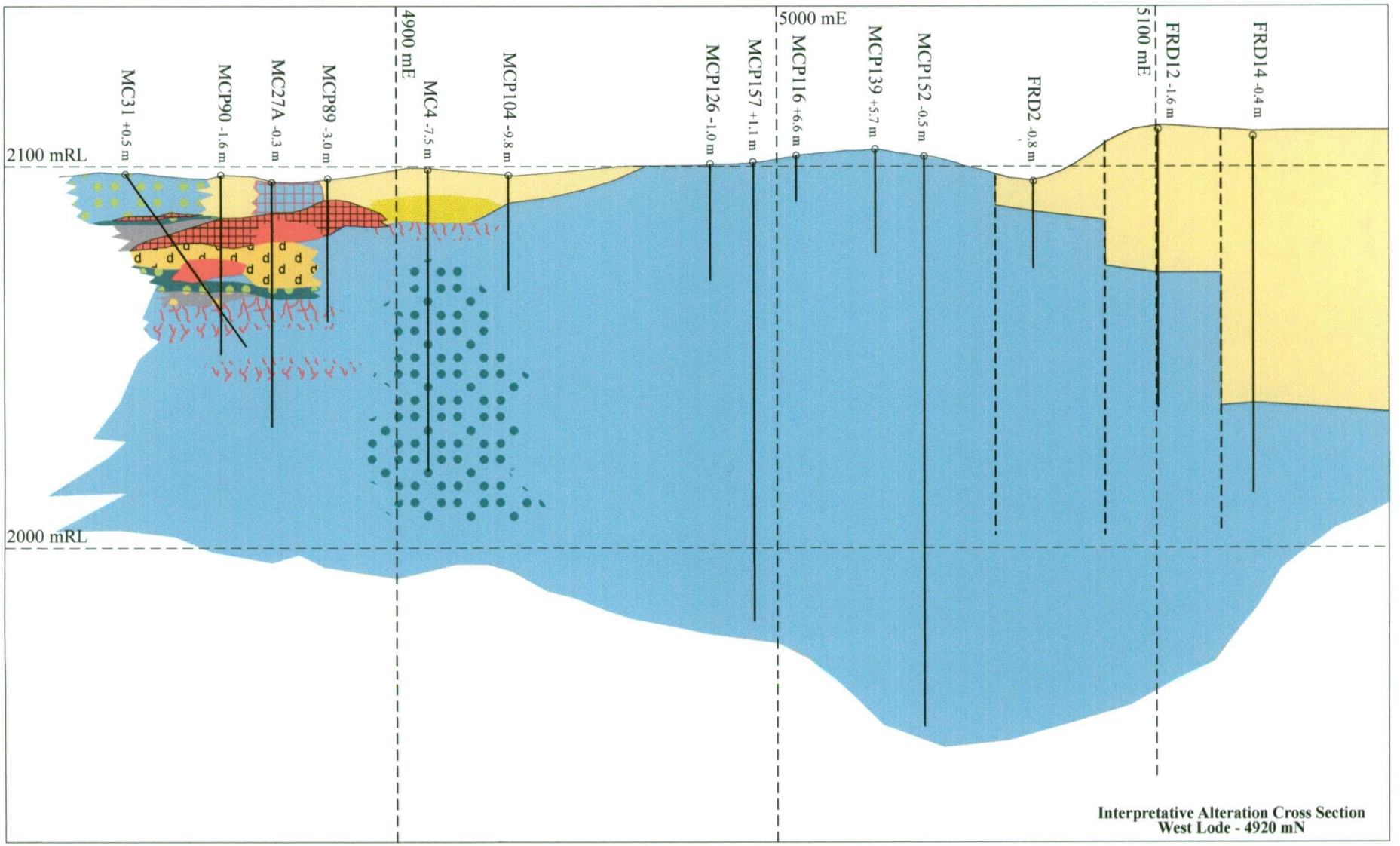

Figure 7.2e. Interpretative alteration cross section: West Lode - 4920 mE

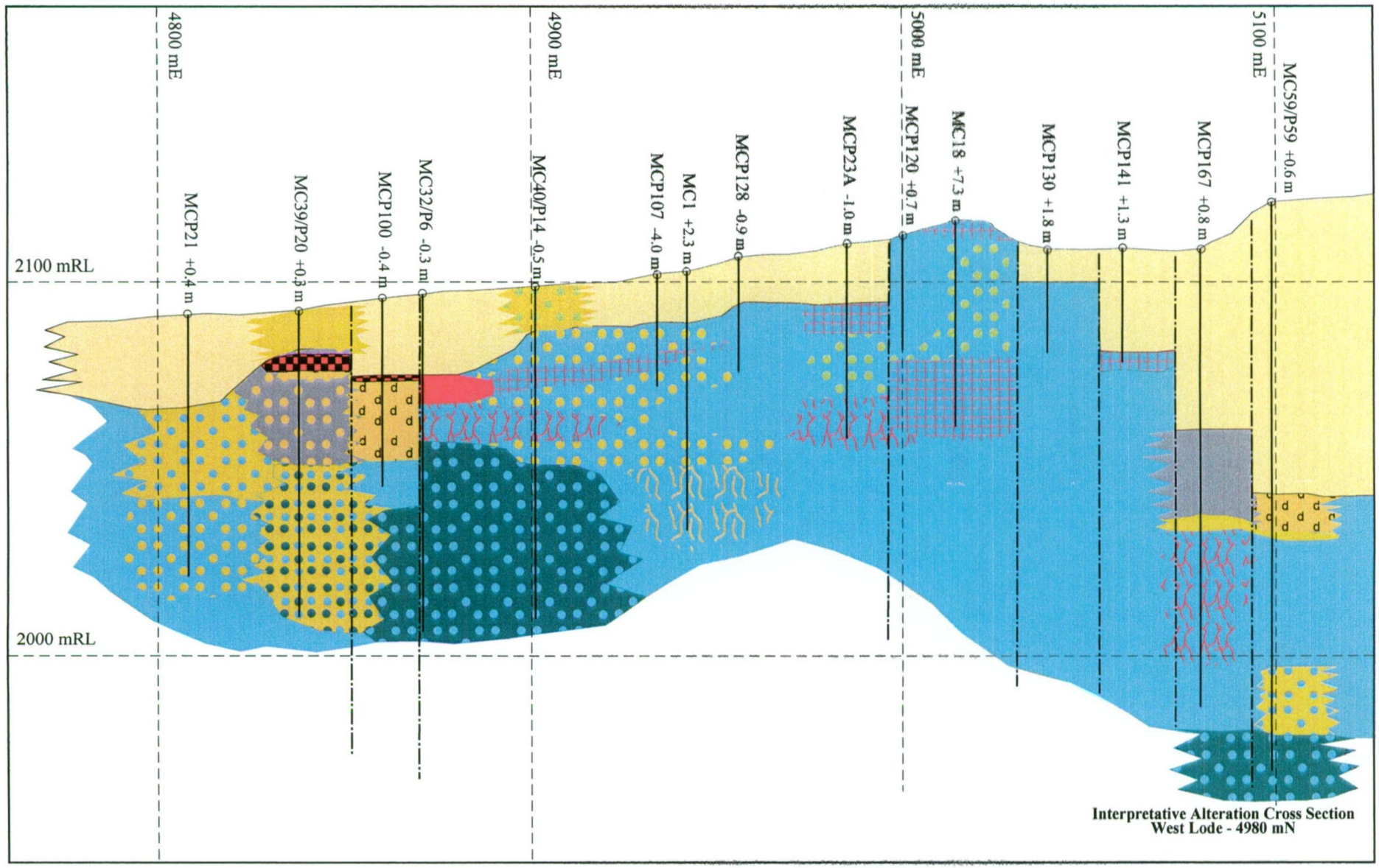

Figure 7.2f. Interpretative alteration cross section: West Lode - 4980 mN

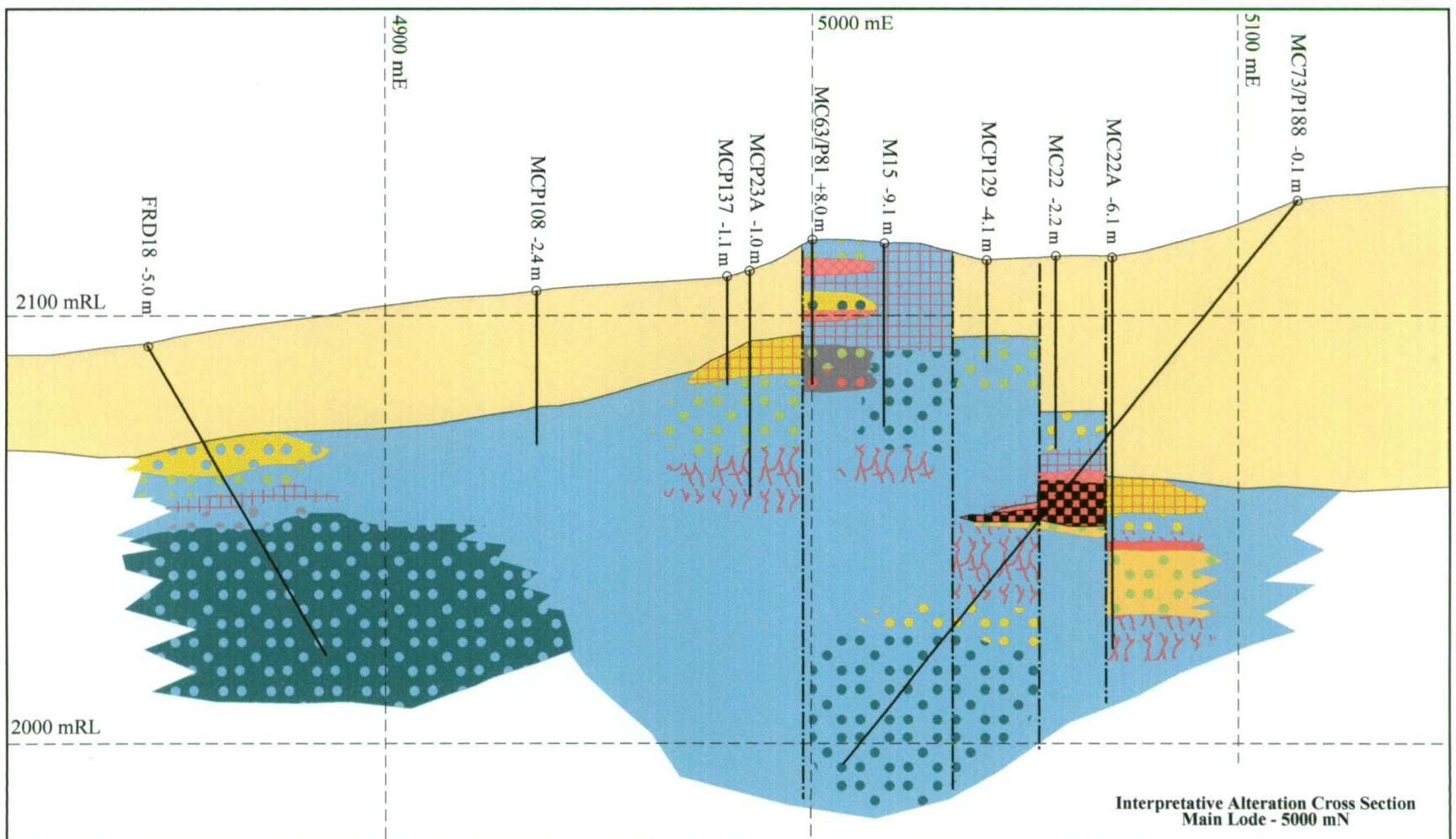

Figure 7.2g. Interpretative alteration cross section: Main Lode - 5000 mE

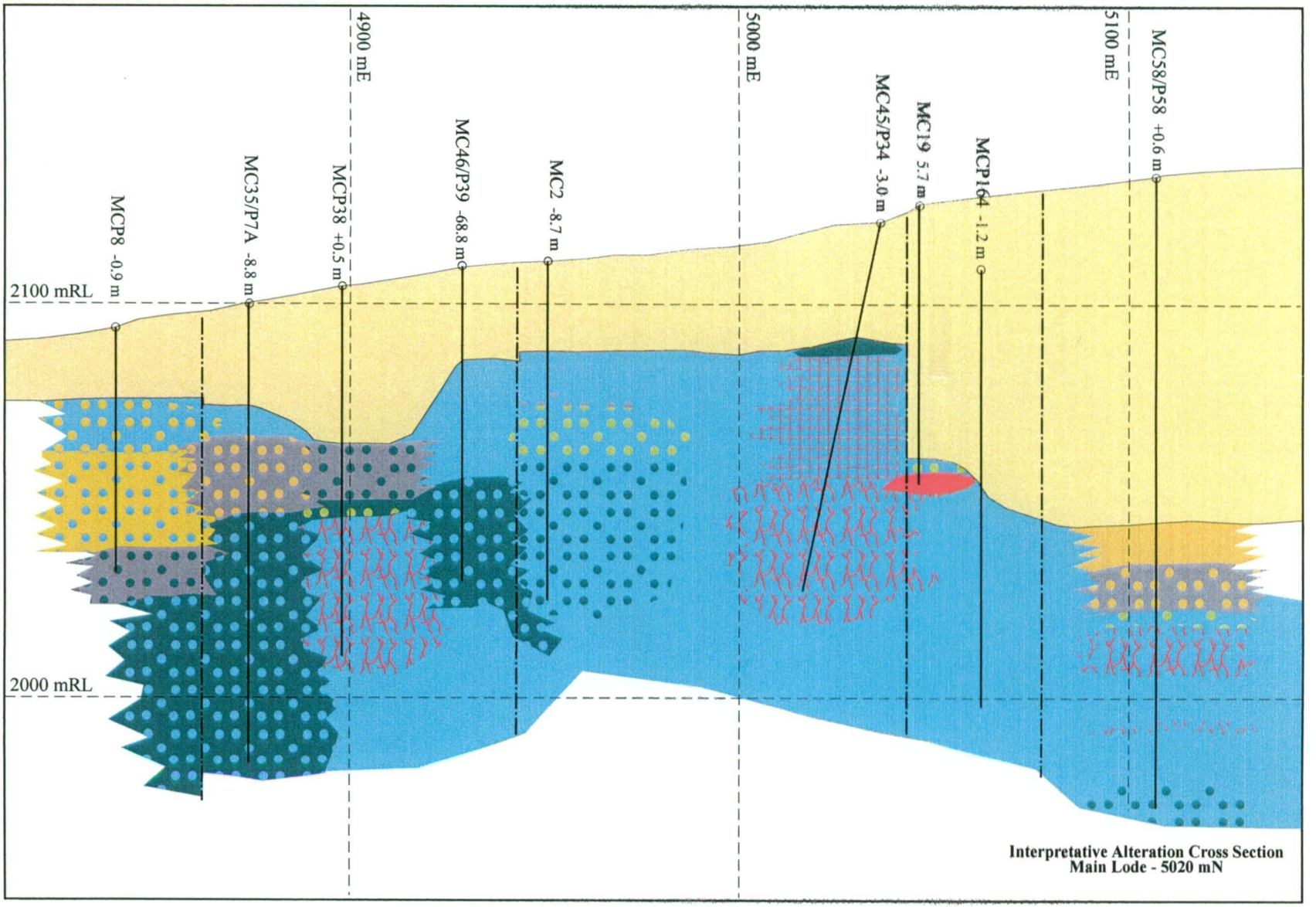

Figure 7.2h. Interpretative alteration cross section: Main Lode - 5020 mN

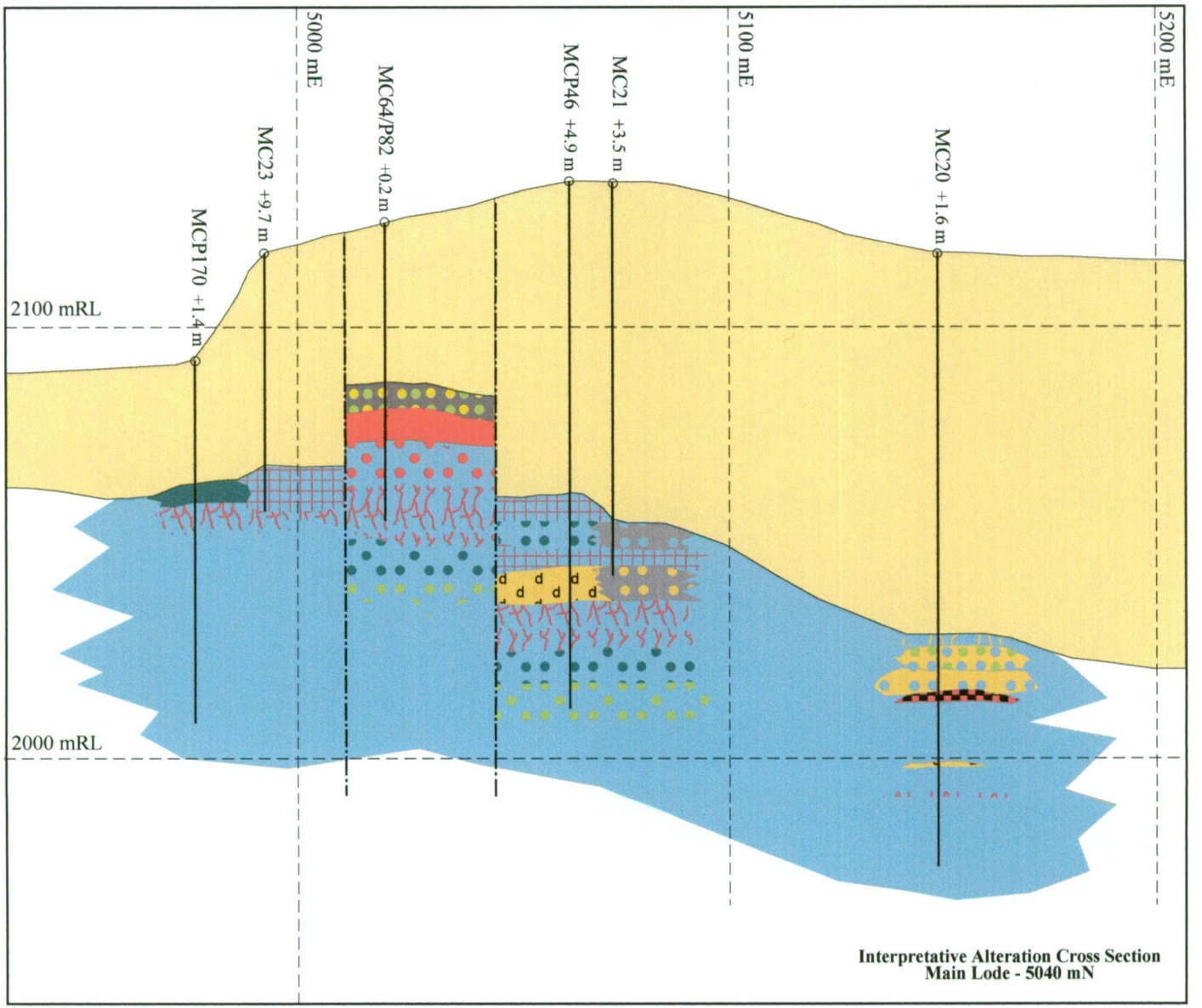

Figure 7.2i. Interpretative alteration cross section: Main Lode - 5040 mN

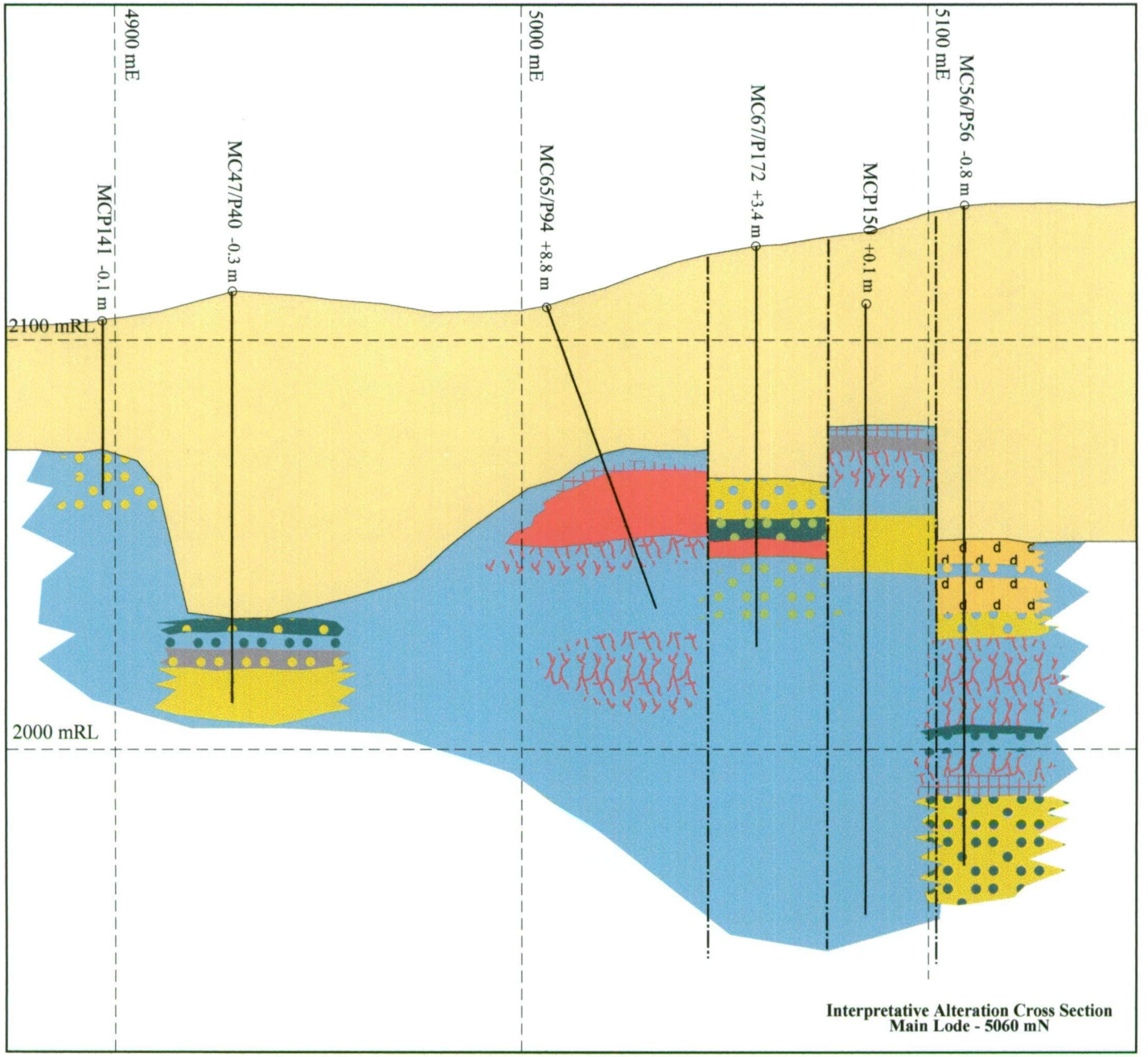

Figure 7.2j. Interpretative alteration cross section: Main Lode - 5060 mN

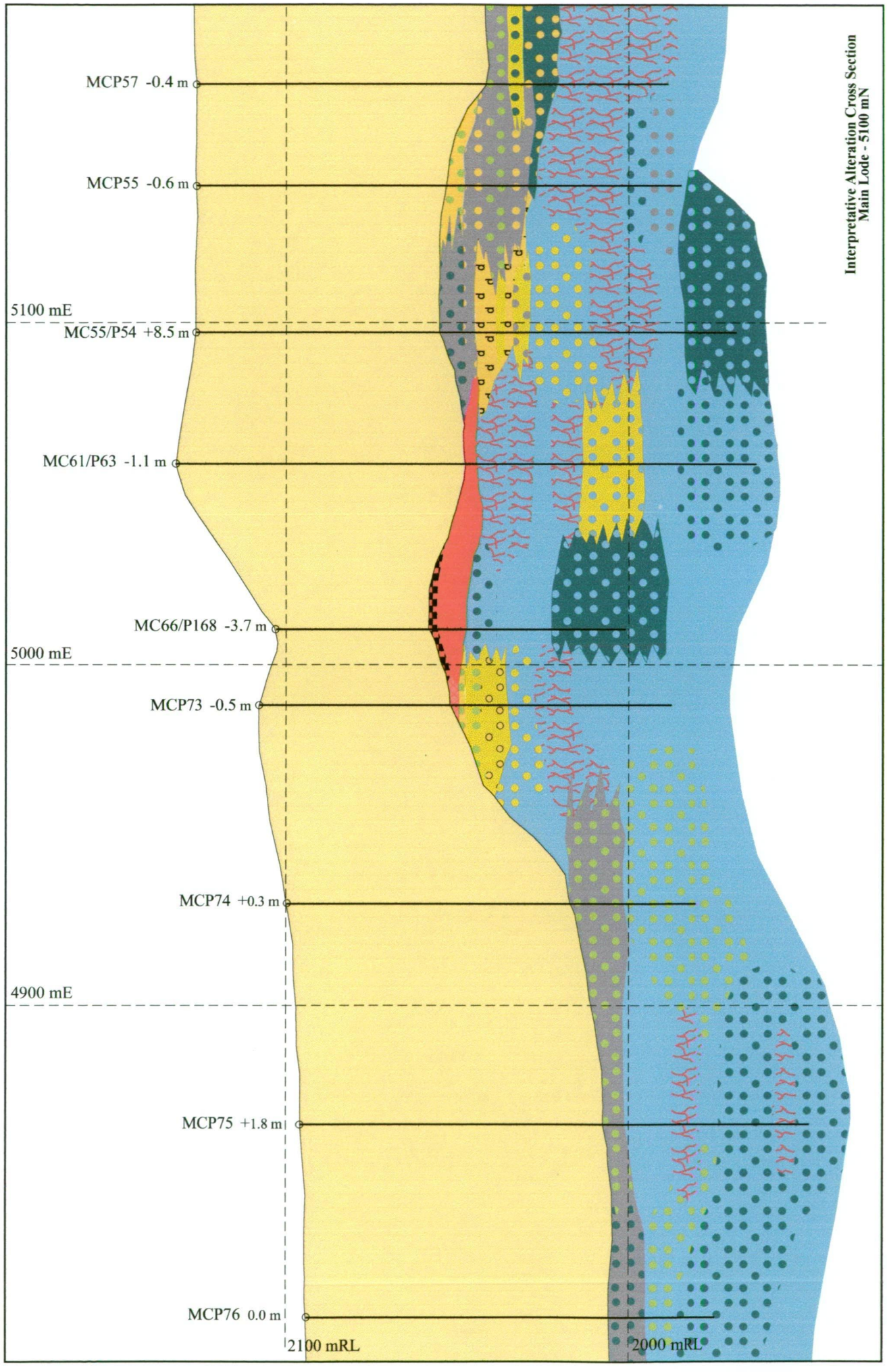

Figure 7.2k. Interpretative alteration cross section: Main Lode - 5100 mN

Sericite alteration tends to occur lateral to or above the chlorite alteration and in addition, tends to be concentrated in proximity to the massive sulphide mineralisation, especially the West Lode. In both the West Lode and the Main Lode, sericite alteration forms a narrow alteration halo around the massive sulphide lenses, as is typical of the Horuroko district deposits.

Kaolinite is generally located in proximity to the massive sulphide mineralisation, but can also be found some distance from the mineralisation, where it is generally associated with faults. Kaolinite can occur in both the hangingwall and footwall position to the massive sulphide mineralisation. The strongest zone of kaolinite alteration occurs on the northern flanks of the West Lode massive sulphide lens. Like sericite, kaolinite forms an alteration halo, especially around the West Lode massive sulphide lens.

Hematite alteration is closely associated with the massive sulphide mineralisation, where it occurs in the immediate hangingwall to it or along strike from it. Although on the Section 4980 mN, the hematite alteration extends from the eastern margins of the West Lode massive sulphide lens to the Main Lode massive sulphide lens.

7.3.1. Discussion of the alteration at Mount Chalmers

The ubiquitous nature of the silica alteration and the extensive zones of chlorite alteration suggest that there has been little structural control on their distribution. The extent of chlorite alteration and its overprinting by other alteration phases, suggests its original areal extent was comparable to that of the silica alteration. This compared to the dolomite, sericite, and kaolinite alteration tend to have a limited areal extent, and are spatially restricted to the high angle normal faults. This limited areal extent of phyllosilicate alteration may have also been controlled by the ubiquitous nature of the silica alteration, in that the silica alteration effectively sealed off any permeable pathways for other hydrothermal fluids away from the faults.

7.4. STYLE OF ALTERATION

Two broad styles of footwall alteration may be present beneath a VHMS deposit, namely:

1. *Alteration pipes,* occur below mound style VHMS deposits and are the product of the upward focussing of hydrothermal fluids towards and to the seafloor. The alteration pipes are associated with stringer-style mineralisation and have a tabular or inverted cone shape, and their depth is many times greater than their width or length (Gemmell, 1996).

Four alteration zones associated with the Japanese Kuroko deposits have been described by Matsukuma and Horikoshi (1970), Shirozu (1974), Iijima (1974) and Date *et al.* (1983) (Fig. 1 *in* Shirozu 1974), and are considered to be analogous to the alteration zones associated with the Canadian VHMS deposits (Franklin, 1995).

- Zone 1 - contains montmorillonite, zeolite and cristobalite (opal)
- Zone 2 - consists of sericite, mixed-layer smectite minerals, sericite, FeMg-chlorite, albite, K-feldspar and quartz
- Zone 3 - composed of sericite, mixed-layer smectite minerals, and Mg-chlorite
- Zone 4 - is the most intense alteration zone and is characterised by intense silicification, sericite and minor amounts of Mg- and FeMg-chlorite.

Four alteration zones have also been recognised for some Australian VHMS deposits (Large, 1992):

- a central core of intense silica-pyrite ± sericite ± chlorite with abundant stringer veins
- chlorite-pyrite ± carbonate zone surrounding the siliceous core
- sericite-chlorite-pyrite
- sericite-quartz-pyrite outer shell

e.g. Hellyer (western Tasmania; Gemmell and Large, 1992); Balcooma (northern Queensland; Huston *et al.*, 1992); Mount Morgan (central, eastern Queensland; Taube, 1986).

2. *Stratabound or semiconformable alteration*, in which the alteration is developed immediately beneath the ore lenses and may extend up to 200 m into the footwall, and for several kilometres around the main ore body (Large, 1992) *e.g.* Rosebery (western Tasmania; Green *et al.*, 1981), Que River (western Tasmania, Large *et al.*, 1988), Phelps Dodge (Matagami, Quebec; Kranidiotis and MacLean, 1987) and on a regional scale the Kuroko deposits of Japan (Matsukuma and Horikoshi; 1970; Iijima, 1974; Utada *et al.*, 1974; Date *et al.*, 1983) VHMS deposits. The style of alteration in Australian VHMS deposits is dominated by silica-sericite ± pyrite alteration with patchy development of chlorite and carbonate (Large, 1992).

The style of alteration at Mount Chalmers has similarity to both the stratabound and semiconformable alteration, and the pipe-like alteration style. The alteration assemblages at Mount Chalmers cross cut and replace the footwall lithologies. The assemblages generally being centred on interpreted high angle normal faults, which are interpreted as being the conduits for the hydrothermal fluids. In this aspect Mount Chalmers differs from the Australian VHMS deposits with a pile-like alteration zone, in that the alteration is related to a large number of relatively closely spaced faults, as opposed to being related to one or two faults of hydrothermal fluid conduits. Given that there are a number of these closely spaced faults within the immediate vicinity of the deposit, then apparent stratabound-styles of footwall alteration may result from the coalescing of a number of pipe-like or fault related alteration styles. A similar style of alteration, *i.e.* alteration associated with closely spaced faults or fractures was mapped at the extinct hydrothermal system on the Galapagos Ridge, 20 to 30 km west of the currently active hydrothermal vents (Embley *et al.* 1988). Alteration is centred on closely spaced fractures or alteration channels and form patches and layers of intensely altered material within well-preserved pillow lavas (Fig. 5 *in* Embley *et al.*, 1988).

7.4.1. High Sulphidation versus Low Sulphidation

Sillitoe *et al.* (1996) proposed that VHMS deposits can be classified on their associated mineralogy, either as a high sulphidation or low sulphidation deposit (Table 7.1) rather than their metal content, geotectonic setting or a combination of these two (see Chapter 10 - Section 10.2.1 for discussion and references). They argue that active "shallow"-marine hydrothermal systems (Hannington and Herzig, 1993) display high sulphidation assemblages, advanced argillic alteration, native sulphur and the epithermal trace element suite (Au, Ag, As, Sb and Hg). In addition samples recovered form the Lau Basin (1,850 - 2,000 m water depth) are alunite bearing indicative of advanced argillisation. Furthermore, Sillitoe *et al.* (1996) argues that VHMS deposits of various ages possess high sulphidation mineralogic characteristics.

Table 7.1. Comparison between high sulphidation and low sulphidation deposits

High Sulphidation			Low Sulphidation		
Alteration	Sulphides	Fluid Chemistry	Alteration	Sulphides	Fluid Chemistry
advance argillic alteration mineral assemblages, including quartz, kaolinite, prophyllite, diaspore, alunite, barite and native sulphur	pyrite, bornite, enargite, luzonite, tennantite and covellite	acidic, relatively oxidised and S-rich fluids, largely of magmatic origin	sericite ± adularia and/or intermediate argillic alteration ± carbonates (dolomite, siderite, ankerite)	sphalerite, galena, chalcopyrite	near-neutral, relatively reduced, and S-poor solutions of meteoric origin

Mount Chalmers has features in common with both the high sulphidation and low sulphidation classification of VHMS deposits. Mount Chalmers has advanced argillic alteration (quartz + kaolinite) overprinting earlier formed intermediate argillic alteration phases (sericite + chlorite). The kaolinite alteration is mainly associated with the massive sulphide mineralisation, while the sericite and chlorite tend to dominate away from the massive sulphide mineralisation, indicating that there is some degree of lateral and vertical zonation to the alteration mineral assemblages. The sulphide mineralogy at Mount Chalmers is dominated by pyrite with lesser amounts of chalcopyrite and minor amounts of sphalerite ± galena. Mount Chalmers has sulphide mineralogy associated with low sulphidation deposits, namely sphalerite, galena and chalcopyrite, but also has covellite (replacing chalcopyrite), which is, associated with high sulphidation deposits. In summary Mount Chalmers has many features in common with both the high and low sulphidation classification for VHMS deposits, but obviously does not readily fit into either category.

7.5. PROSPECTS

As previously discussed in Chapter 6 - Mineralisation, there are number of weakly mineralised to "barren" alteration prospects in the vicinity of Mount Chalmers. These have all been investigated either by diamond drilling and/or percussion drilling. This section of this chapter details the alteration at two of these prospects - the Tungamull and Savage-Mitchell prospects and compares the alteration mineral assemblages and the style of alteration seen here to that at Mount Chalmers.

7.5.1. Tungamull

At the Tungamull Prospect three styles of alteration predominate:

- kaolin-silica- ± pyrite ± dolomite ± chlorite — drill holes - P6/D3, MCD2, MCD12
- dolomite — drill hole - MCD6
- chlorite-sericite — drill hole - MCD9

The alteration in drill hole MCD2 is dominated by kaolinite and dolomite, while in MCD12 and P6/D3 the alteration is dominated by kaolinite. In MCD2 and P6/D3 the alteration occurs within the Ellrott Rhyolite, and in MCD12 the alteration occurs in a pumice, lithic breccia. In P6/D3 and MCD2 the kaolinite has almost completely overprinted the original lithological textures of the rhyolite and has possibly enhanced a pre-existing breccia horizon within the rhyolite. Quartz-dolomite veins (post kaolinite) also occur in the kaolinised interval, further enhancing the brecciated texture. In P6/D3 the kaolinite, alteration is underlain by a zone of intense silicification within the rhyolite. In MCD12, the kaolinite has leached and overprinted a zone of intense silica alteration. The remnants of the silica alteration occur as irregularly shaped nodules and worm-like structures.

The dolomite + pyrite alteration in MCD6 occurs two zones; firstly in a narrow zone, and secondly in a thicker interval as semi-massive to massive dolomite + pyrite. The massive dolomite has a banded appearance that is parallel to the short core axis *i.e.* ~ horizontal. In both zones, the dolomite alteration has nucleated on feldspars and/or spherulites replacing a feldspar-phyric rhyolite.

Two zones of alteration were intersected in MCD9. The first was intersected between 129.9 - ~ 180.0 m occurs within the Ellrott Rhyolite. The rhyolite has been altered to silica + chlorite, and locally altered by hematite. Crosscutting the silica-chlorite alteration are quartz-carbonate veins that have bleached margins associated with them. The second interval occurs between ~350.0 - 418.90 m. In this interval the alteration has overprinted a possible lithic breccia. The groundmass is strongly altered to chlorite-sericite. Associated with the alteration is extensive pyritisation (overall 10 -15 %; locally up to 30 - 40 %) of the host lithology. The pyrite is disseminated and either occurs as individual euhedra or as clots of pyrite grains. Scattered throughout the altered groundmass are angular to well-rounded lithic clasts, of variable provenance, but appear to be dominated by siliceous felsic volcanic clasts. Downhole the clasts become more readily discernible and larger. Some of the clasts contain white alteration spots that may either be alteration that has nucleated on feldspars or has infilled vesicles.

7.5.1.1. *Discussion of the alteration at Tungamull*

The Tungamull prospect has similar alteration mineralogy to that occurs at Mount Chalmers. At Mount Chalmers, the alteration is largely restricted to the footwall lithologies, whereas at Tungamull the most intense alteration occurs within the hangingwall lithologies. For example in MCD12 and P6/D3 the alteration crosscuts the hangingwall stratigraphy and in MCD12 extends for ~70 m (not including the basaltic sill) above the interpreted ore equivalent horizon. However, in MCD9 the position of the alteration *i.e.* hangingwall versus footwall is not so readily discernible as no mineralised horizon was

intersected in the drill hole. In MCD6 dolomite alteration is associated with semi-massive to massive pyrite + minor base metals within chlorite altered siltstones, so it occurs at or near the ore equivalent horizon. Although hangingwall alteration occurs at Mount Chalmers, its extent and intensity are substantially less that what occurs at the Tungamull prospect. As at Mount Chalmers the alteration at Tungamull appears to be related to be related to the inferred faulting that has occurred in the area.

7.5.2. Savage-Mitchell

One diamond drill hole (SMDD1) has intersected the alteration and mineralisation at the Savage-Mitchell prospect. The prospect area is dominated by a thick sequence of andesitic intrusions and lavas. The mineralisation is hosted in strongly silica-altered sedimentary rocks, pumice breccia, graded, sericite-silica-chlorite-altered polymictic lithic breccias and relatively unaltered andesites. Two narrow intervals of altered and pyritised sedimentary rocks were intersected between 149.1 - 152.6 m and 240.1 252.0 m. The sedimentary rocks have been intruded by a thick andesitic sill, splitting the sedimentary rocks into two intervals. The uppermost interval is strongly silica-altered and contains a narrow interval of semi-massive coarse-grained pyrite and minor chalcopyrite veins (149.3 - 149.7 m). The lowermost interval consists of sericite altered, pyritic, graded sandstones and siltstones. Strongly silica-chlorite altered pumice breccia was intersected between 261.0 - 277.0 m. The upper 18 m and lower two metres of the intervening andesitic sill have been altered by pyrite and are crosscut by quartz-carbonate-pyrite veins (Stage 3 post-massive sulphide mineralisation). Graded, sericite-silica-chlorite-altered, polymictic lithic breccias occur between 367.0 - 395.4 m. Two thick andesitic sills have intruded into the sedimentary rocks between 152.6 - 240.1 m and 277.0 – 367.0 m. The andesites are relatively unaltered but are cut by chlorite and silica veinlets and also by quartz-carbonate ± pyrite veins (Stage 3 post-massive sulphide mineralisation). However, within the uppermost andesite, the upper 18 m and lower two metres of andesite, adjacent to the contacts with the sedimentary rocks, are pyritic.

7.5.2.1. *Discussion of the alteration at Savage-Mitchell*

The alteration intersected in the sedimentary rocks in SMDD1 is identical to that seen and described along strike in the sedimentary rocks within the footwall lithologies at Mount Chalmers, and therefore is considered to be related to hydrothermal processes that formed the Mount Chalmers massive sulphide. The andesites are relatively unaltered except for the pyritised contacts of the uppermost andesitic sill, and possibly the result of the assimilation of mineralised sedimentary rocks near its margins. The quartz-carbonate ± pyrite veins within the andesites are similar to the Stage 3 quartz-carbonate veins (*i.e.* post-mineralisation) that occur throughout the stratigraphy at Mount Chalmers.

7.6. CONCLUSIONS

Silica, chlorite, sericite, dolomite and pyrite dominate the alteration at Mount Chalmers and its environs. These mineral assemblages are particularly well developed in the footwall position to the massive sulphide mineralisation at Mount Chalmers and along strike from the deposit.

McLeod (1987) found two varieties of chlorite at Mount Chalmers, sudoite, which occurs in the marginal, zones to the Mount Chalmers massive sulphide, and trioctahedral chlorites, which occur throughout the deposit. Sudoite has also been observed occurring in the marginal zones of many of the Kuroko deposits (Sudo *et al.*, 1954; Sudo and Kodama, 1957; Sudo, 1959; Hayashi and Oinuma, 1964; Tsukahara 1964; Sudo and Sato, 1967; Shiozu, 1969, 1974, 1978; Iijima, 1974; Kimbara and Nagata, 1974). McLeod (1987) suggested that because of where sudoite is located at Mount Chalmers, it has an hydrothermal origin, and that it is stable under conditions of lower temperatures, higher pH and/or higher Eh than those that prevailed during the ore forming processes. The trioctahedral chlorites exhibit a systematic decrease in the Mg number stratigraphically upwards beneath the massive sulphide, which maybe reflecting a decrease in the temperature of the hydrothermal fluids as the site of mineral deposition is approached. Immediately above the footwall alteration the Mg number of the chlorites increase systematically upwards. This upward trend is possibly reflecting an increase in the cation-exchange capacity of neoformed clays as the amount of reduced sulphur in the depositional environment is reduced (McLeod, 1987).

Within the stringer zone and altered host volcano-lithic sandstones convential potassium micas are replaced by barian sericites. Sodian sericites occur at the top of the altered host volcano-lithic sandstones overlying the Main Lode massive sulphide. Divalent cation substitutions results in trends similar to those that occur in the coexisting trioctahedral chlorites, which is indicative of an approach towards equilibrium for these phyllosilicates (McLeod, 1987).

The silica alteration increases in intensity stratigraphically upwards to just beneath the massive sulphide mineralisation. Chlorite is developed within and adjacent to the sulphide veins and within the dolomite lenses. Sericite occurs extensively throughout the footwall lithologies, and is probably the result of hydrothermal destruction of feldspars, volcanic glass and its precipitation within veinlets (McLeod, 1987). Dolomite-kaolin and pyrite alteration is very important on a local scale, and is associated with known mineralised occurrences, such as, Mount Chalmers and the Tungamull prospect. The hangingwall alteration is dominated by weakly developed sericite with minor amounts of chlorite and carbonate alteration. Although, locally within the hangingwall there is extensive alteration by silica, kaolinite, sericite and pyrite.

CHAPTER 8
FLUID INCLUSION MICROTHERMOMETRY AND FLUID COMPOSITION

8.1. INTRODUCTION

Fluid inclusions have long been an important research tool in attempting to understand the genesis of hydrothermal ore deposits. Fluids trapped within primary fluid inclusions are remnants of actual solutions responsible for mineral deposition. They can therefore provide valuable compositional information on salinity, gas compositions and the identification of a variety of dissolved aqueous species that cannot be obtained from any other source. Other equally important information that can be obtained from fluid inclusions by microthermometric and/or petrographic analysis includes temperature, pressure and density estimates. Fluid inclusions can also provide evidence for physical processes that have operated in the ore-forming environment such as phase separation and fluid mixing. The use of fluid inclusions requires some basic but fundamental assumptions to be made. These include that the trapped fluid was a single homogeneous phase, the cavity has not changed in volume, nothing is added or lost after sealing, effects of pressure are insignificant or known, the origin of the inclusion is known and the determinations of homogenisation are both precise and accurate (Khin Zaw and Cooke, 1995).

The major aim of this study is to use the fluid inclusion compositional variation as constraints for the source of the ore-forming fluids at Mount Chalmers. Parts of this chapter have previously been published by Khin Zaw *et al.* (1995) (see Appendix A for full text of the paper).

8.2. METHODOLOGY

A Fluid Inc. modified USGS heating/freezing stage was used in this study. The general method and procedure for heating/freezing experiments are reported elsewhere (*e.g.* Roedder, 1984). The precision of the temperature measurements is better than ±1° C for heating and ±0.3° C for freezing. Accuracy of the measurements was insured by calibration against the triple point of CO_2 (-56.6° C), the freezing point of water (0.0° C), the critical point of water (374.6° C) and synthetic fluid inclusions.

Doubly polished plates were examined in detail under the petrographic microscope prior to the heating and freezing experiments. The fluid inclusions were first located under low magnification to record their distribution, origin, size and types, and to determine their spatial, temporal and textural relationships. Phase relations were studied under high power objectives (x 100). Salinities were calculated from the temperature of melting of ice crystals using the equations of Bodnar (1993) and expressed as NaCl equivalent weight percent (NaCl equiv. wt%).

Laser Raman spectroscopy (LRS) method is an important development in the field of non-destructive fluid inclusion technique for *in situ* pin-point analysis of individual, unopened fluid inclusions (Roedder, 1984). Laser Raman spectroscopy can be used to quantitatively determine the gaseous components (*e.g.* H_2S, CO, CO_2, CH_4, SO_2, H_2, NH_3, N_2) with a detection limit of 0.1 mole % for some species and for identifying daughter minerals. In this study, a DILOR MICRODIL-28® Raman microprobe at the Australian Geological Survey Organisation (AGSO), Canberra was used to quantitatively determine the composition of gaseous components and to identify the daughter minerals in fluid inclusions from the Mt Chalmers samples.

The recent development of non-destructive Particle Induced X-ray Emission (PIXE) microprobe analysis of the chemical composition of fluid inclusions (Ryan *et al.*, 1991, 1993a) has enabled quantitative determination of individual fluid inclusions. From the study of a Cornish tin deposit Ryan *et al.* (1991, 1993a & b, 1994a & b) detected Cl, K, Ca, and other heavy metals such as Cu, Fe and Zn, down to concentration levels of about 50 ppm. The PIXE microprobe technique applied in this study is similar to the method used by Heinrich *et al.* (1992).

8.3. RESULTS

8.3.1. Fluid Inclusion Petrography

The fluid inclusions from Mt. Chalmers can be classified into two major types based on the phases observable in the inclusions at room temperature and their paragenesis. Fluid inclusions were also classified in a temporal sense as primary, secondary and pseudo-secondary relative to the time of trapping as defined by Roedder (1984). The following inclusion types were observed:

Type I: Primary two-phase, liquid and vapour inclusions (Fig. 8.1).
Type II: Secondary two-phase, liquid-rich inclusions with variable liquid and vapour ratios.

Primary fluid inclusions can be distinguished in relation with textural criteria of the host minerals (*e.g.* growth zoning in quartz and colour banding in sphalerite). Negative shape or isolated, solitary nature is not considered as evidence for primary origin in this study.

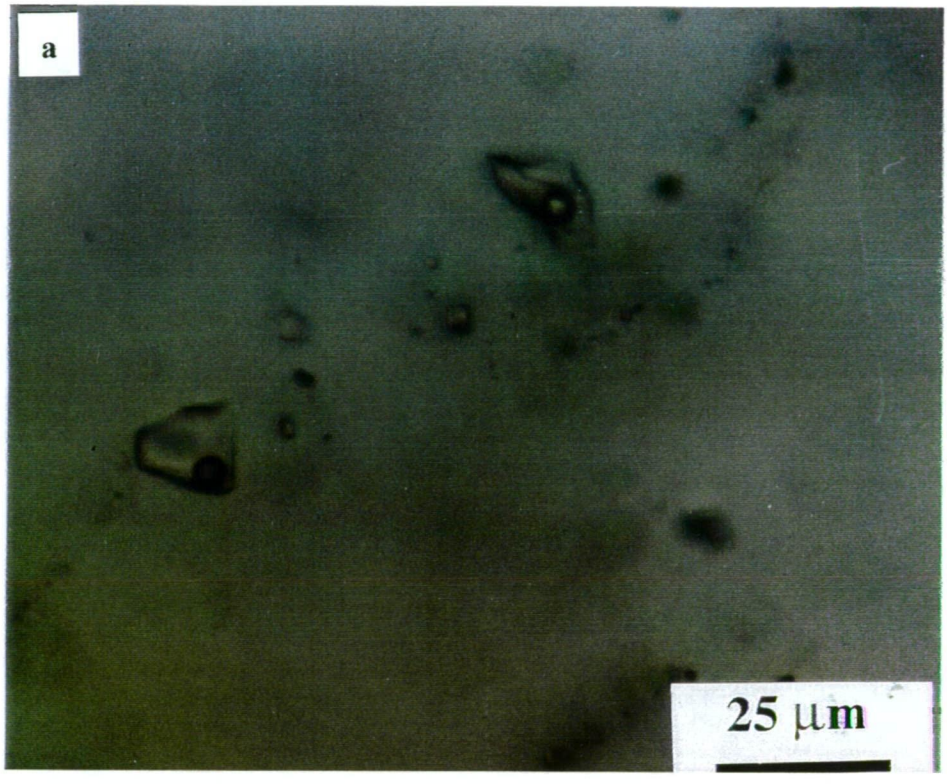

Figure 8.1 Photomicrograph showing the primary Type I fluid inclusion in quartz from the Mount Chalmers stringer zone.

Type I inclusions are found in quartz, sphalerite and barite. In this study, only fluid inclusions in quartz have been investigated (Fig. 8.1). No chalcopyrite daughter mineral is found in the Mt Chalmers deposit, but the presence of chalcopyrite has been reported from the Fukazawa mine, Hokuroko district, Japan (Foley, 1986) and the Hellyer deposit, western Tasmania (Khin Zaw *et al.*, 1996).

Type II inclusions are found in all minerals from Mt. Chalmers. They crosscut all other inclusion types and also grain boundaries of host minerals. The irregular shape, crosscutting nature and randomly distributed array of the inclusions indicate a secondary origin.

8.3.2. Microthermometry

Microthermometry and SEM/WDS semi-quantitative analyses of fluid inclusions have been undertaken for the Mount Chalmers deposit in order to measure the temperature, salinity and composition of the ore fluids (Hunns *et al.*, 1994; Khin Zaw *et al.*, 1995; Hunns and Khin Zaw, 1998). Large and Both (1980) recorded a homogenisation temperature range of 68° - 295° C (average 176°C) and salinities of 2.9 - 13.7 NaCl equiv. wt % (average 10.3) for three barite samples from the West Lode. R. Both (*writ. comm.* to Ross Large) later suggested that most of the fluid inclusions he studied were of a secondary and not a primary nature.

Primary fluid inclusions in quartz from the stringer zone of the Main Lode yielded homogenisation temperatures in the range of 207.5° to 276.6°C and salinities of 4.8 to 7.8 eq. NaCl wt % (Table 8.1). Fluid inclusions from the West Lode yielded homogenisation temperatures in the range of 157.8° to 231.6°C and salinities of 4.9 to 11.2 eq. NaCl wt % (Table 8.1). No evidence for boiling, such as simultaneously formed inclusions of both liquid and vapour phases were recognised either from the Main Lode or from the West Lode. The presence of simultaneously formed inclusions of both liquid and vapour gives the best evidence available that the fluids were actually on the boiling curve.

Table 8.1. Temperature of homogenisation (Th), and salinities (NaCl equiv, wt. %) for the Main Lode and West Lode stringer zone mineralisation.

Sample No./	Th	Tm-ice	NaCl eq wt %	Sample No./	Th	Tm-ice	NaCl eq wt %
MC53@154.4m	207.5	-2.9	4.8	MC26@34.1m	167.4	-4.1	6.6
(Main Lode)	210.6	-3.1	5.1	(West Lode)	177.0	-3.9	6.3
	231.6	-4.1	6.6		179.6	-3.8	6.1
	267.5	-3.9	6.3		160.7	-4.8	7.6
	276.6	-3.9	6.3		170.2	-4.1	6.5
	210.7	-3.3	5.3		231.5	-4.1	6.5
	267.5	-3.8	6.1		207.6	-3.0	4.9
	231.5	-4.1	6.5		231.6	-3.9	6.3
	260.3	-5.0	7.8		170.2	-4.1	6.5
	262.6			median	178.3	-4.0	6.4
median	231.6	-3.9	6.3				

8.3.3 Gas Composition - Laser Raman Analysis

Gaseous components (H_2S, CO, CO_2, CH_4, SO_2, H_2, NH_3, N_2) in fluid inclusions from the Mt. Chalmers were scanned by LRS method. Only CO_2 was detected and other gas species were not detected (Fig. 6 *in* Khin Zaw *et al.*, 1995). The relatively low intensity of the CO_2 bands at 1383-1378 and 1281-1287 cm^{-1} suggests that the CO_2 content is near the detection limits of 0.1 mole %.

8.3.4. Fluid Composition

Three modern day vent fluids were selected for comparison to the Mount Chalmers hydrothermal fluid: Lau Basin North Fiji - White Lady; Okinawa Trough - Minami-Ensei and Izena as well as the Miocene Kuroko deposits of Japan as they occur within a similar tectonic environment to what Mount Chalmers was formed in *i.e* back-arc basin. "White Lady" is an example of a phase-separated (boiling) hydrothermal system, and consists of anhydrite chimneys developed on a 2-m high sulphide mound (Ishibashi and Urabe, 1995).

8.3.4.1. SEM/WDS Analysis

The major element chemistry of fluid inclusion decrepitates from the Mount Chalmers was studied by electron microprobe. The fluid inclusions were thermally decrepitated between 350-400° C to produce salt precipitates and these were analysed semi-quantitatively by SX 50 CAMECA microprobe.

The electron microprobe data of fluid inclusion decrepitates from the synmineralisation veins in the Mount Chalmers stringer zone are listed in Table 8.2. The data are shown in Figures 8.1a and 8.1b, together with the crushed-leached analytical data from the Kuroko deposits and the composition of the end-member vent fluids from the Lau Basin, North Fiji - White Lady and the Okinawa Trough - Minami-Ensei and Izena (Table 8.3).

Table 8.2. CAMECA microprobe data for composition of fluid inclusion decrepitates in quartz from Mount Chalmers

Sample	MC 36@34.1m			MC 36@34.1m			MC 36@34.1m			MC 36@34.1m			MC 36@34.1m			MC 36@34.1m		
Element	wt %	Atomic %	Eq. Cl %	wt %	Atomic %*	Eq. Cl %**	wt %	Atomic %	Eq. Cl %	wt %	Atomic %*	Eq. Cl %**	wt %	Atomic %	Eq. Cl %	wt %	Atomic %	Eq. Cl %
Na	2.25	27.89	5.72	0.72	26.76	1.83	4.08	26.37	10.37	1.41	27.94	3.58	2.40	29.99	6.10	0.73	32.96	1.86
Mg	0.10	1.22	0.39	0.05	1.60	0.20	0.09	0.52	0.35	0.04	0.66	0.16	0.05	0.62	0.20	0.10	4.04	0.39
S	0.38	3.39	-	0.34	9.10	-	0.52	2.42	-	0.29	4.07	-	0.41	3.71	-	0.22	7.06	-
Cl	4.13	33.15	-	1.02	24.72	-	9.14	38.33	-	2.81	36.12	-	4.60	37.37	-	0.64	18.69	-
K	3.62	26.34	6.90	1.31	28.69	2.50	7.79	29.60	14.85	2.48	28.86	4.73	3.39	24.92	6.46	1.10	29.17	2.10
Ca	0.80	5.65	2.22	0.23	4.93	0.64	0.62	2.31	1.72	0.11	1.23	0.30	0.37	2.68	1.02	0.25	6.48	0.69
Mn	0.01	0.04	0.02	0.00	0.00	0.00	0.00	0.00	0.00	0.00	0.01	0.00	0.00	0.00	0.00	0.00	0.00	0.00
Fe	0.45	2.32	1.02	0.27	4.21	0.61	0.17	0.45	0.39	0.14	1.11	0.32	0.14	0.72	0.32	0.09	1.59	0.20
K/Na	1.61	0.94	1.21	1.82	1.07	1.36	1.91	1.12	1.43	1.76	1.03	1.32	1.41	0.83	1.06	1.51	0.89	1.13
Ca/Na	0.36	0.20	0.39	0.32	0.18	0.35	0.15	0.09	0.17	0.08	0.04	0.08	0.15	0.09	0.17	0.34	0.20	0.37
Mg/Na	0.04	0.04	0.07	0.07	0.06	0.11	0.02	0.02	0.03	0.03	0.02	0.04	0.02	0.02	0.03	0.14	0.12	0.21
Mn/Na	0.00	0.00	0.00	0.00	0.00	0.00	0.00	0.00	0.00	0.00	0.00	0.00	0.00	0.00	0.00	0.00	0.00	0.00
Na/Cl	0.54	0.84	-	0.71	1.08	-	0.45	0.69	-	0.50	0.77	-	0.52	0.80	-	1.14	1.76	-
Mg/Fe	0.22	0.53	0.38	0.19	0.38	0.32	-	-	-	0.29	0.59	0.49	0.36	0.86	0.62	1.11	2.54	1.92
Ca/K	0.22	0.21	0.32	0.18	0.17	0.25	0.08	0.08	0.12	0.04	0.04	0.06	0.11	0.11	0.16	0.23	0.22	0.33

*Atomic concentration in percent

Sample	MC107140			MC107140		
Element	wt %	Atomic %	Eq. Cl %	wt %	Atomic %*	Eq. Cl %**
Na	2.66	59.28	6.76	1.16	75.04	2.95
Mg	0.10	2.29	0.39	0.00	0.26	0.00
S	0.67	11.50	-	0.17	7.94	-
Cl	0.21	3.29	-	0.08	3.17	-
K	0.05	0.68	0.10	0.11	4.25	0.21
Ca	1.67	22.96	4.62	0.23	8.53	0.64
Mn	0.00	0.00	0.00	0.00	0.00	0.00
Fe	0.00	0.00	0.00	0.03	0.81	0.07
K/Na	0.02	0.01	0.01	0.09	0.06	0.07
Ca/Na	0.63	0.39	0.68	0.20	0.11	0.22
Mg/Na	0.04	0.04	0.06	0.00	0.00	0.00
Mn/Na	0.00	0.00	0.00	0.00	0.00	0.00
Na/Cl	12.67	18.02	-	14.50	23.67	-
Mg/Fe	0.00	0.00	0.00	0.00	0.32	0.00
Ca/K	33.40	33.76	48.51	2.09	2.01	3.04

*Atomic concentration in percent

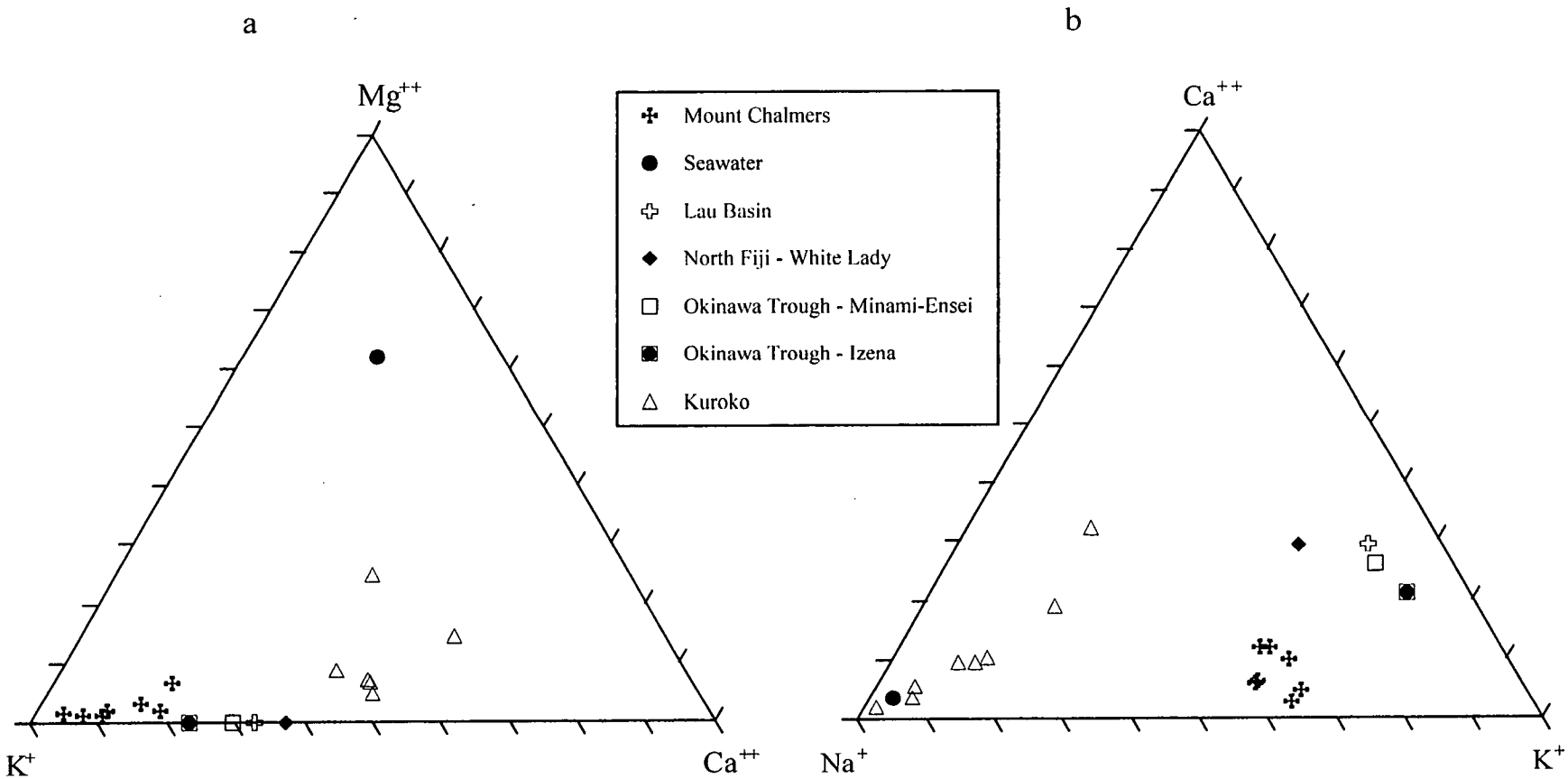

Figure 8.2a. K-Ca-Mg and Figure 8.2b. Na-K-Ca plots of fluid inclusion decrepitates from Mount Chalmers together with end-member vent fluids from Lau Basin (Fouquet *et al.*, 1991), North Fiji - White Lady (Ishibashi and Urabe, 1995 and the references therein) Okinawa Trough (Ishibashi and Urabe, 1995 and the references therein) and fluid inclusion composition of Kuroko deposits (Pisutha-Arnond and Ohmoto, 1983).

Table 8.3. Composition of seawater (von Damm *et al.*, 1985; Butterfield *et al*; 1990; 1994; Fouquet *et al.*, 1991); and selected end-member vent fluids from Lau Basin (Fouquet *et al.*, 1991); North Fiji - White Lady; Okinawa Trough - Minami-Ensei and Okinawa Trough - Izena (Ishibashi and Urabe, 1995 and the references therein).

		Seawater	Lau Basin	North Fiji	Okinawa Trough	
				White Lady	Minami-Ensei	Izena
Cl	mmol/kg	541	725	255.00	527.00	550.00
Br	µmol/kg	838		306.00	0.00	1045.00
Na	mmol/kg	465	567.5	210.00	430.00	446.00
Ca	mmol/kg	10.2	34.5	6.50	22.10	23.20
K	mmol/kg	9.8	67.5	10.50	50.90	73.70
Li	µmol/kg	26	662.5	200.00	1860.00	600.00
Sr	mmol/kg	87	120	30.00	227.00	110.00
Si	mmol/kg	0.18	2	14.00	10.80	12.50
Fe	µmol/kg	0.0034	2050	13.00	0.00	21.00
Mn	µmol/kg	0.005	6450	12.00	94.00	370.00
Cu	µmol/kg	0.007	25			
Zn	µmol/kg	0.01	2150			7.60
Ba	µmol/kg	0.14	40	5.90	55.00	60.00
B	µmol/kg	420	820			
Pb	nmol/kg	0.01	5400			36.00
As	nmol/kg	27	8500			

On a K-Ca-Mg plot, (Fig. 8.2a) Mount Chalmers and the Kuroko deposits form two distinct and separate fields, with the end-member vent fluids falling in between the two. Mount Chalmers and the Kuroko fluids are depleted in Mg relative to seawater. The end-member vent compositions are depleted in Mg as it is removed from hydrothermal fluids during high-temperature reaction with rocks and sediments (Bischoff and Dickson, 1975; Mottl and Holland, 1978) and any Mg present is inferred to be the result of mixing with seawater (von Damm, 1995). All fluids are enriched in K compared to seawater

On a Na-K-Ca plot (Fig. 8.2b), the Kuroko, Mount Chalmers and modern day end-member fluids form three distinct and separate fields. The Kuroko fluids are broadly similar to seawater with a trail of analyses trending towards Ca enrichment. Mount Chalmers is enriched in K and has similar Na concentration to that of seawater. The modern day end-member vent compositions are also enriched in K compared to seawater and are enriched in Ca compared to seawater and Mount Chalmers.

8.3.4.2. PIXE Analysis

In order to further understand the pattern of element abundances within the Mount Chalmers fluid and how they compare to modified seawater end-member vent composition of modern day hydrothermal fluids it is useful to have a reference frame to which the elemental abundances in a particular fluid can be compared. To this effect, the elemental abundances from Mount Chalmers and the end-member vent fluids were normalised to modern day seawater and plotted as a multi-element plot or spidergram (Figure 8.3).

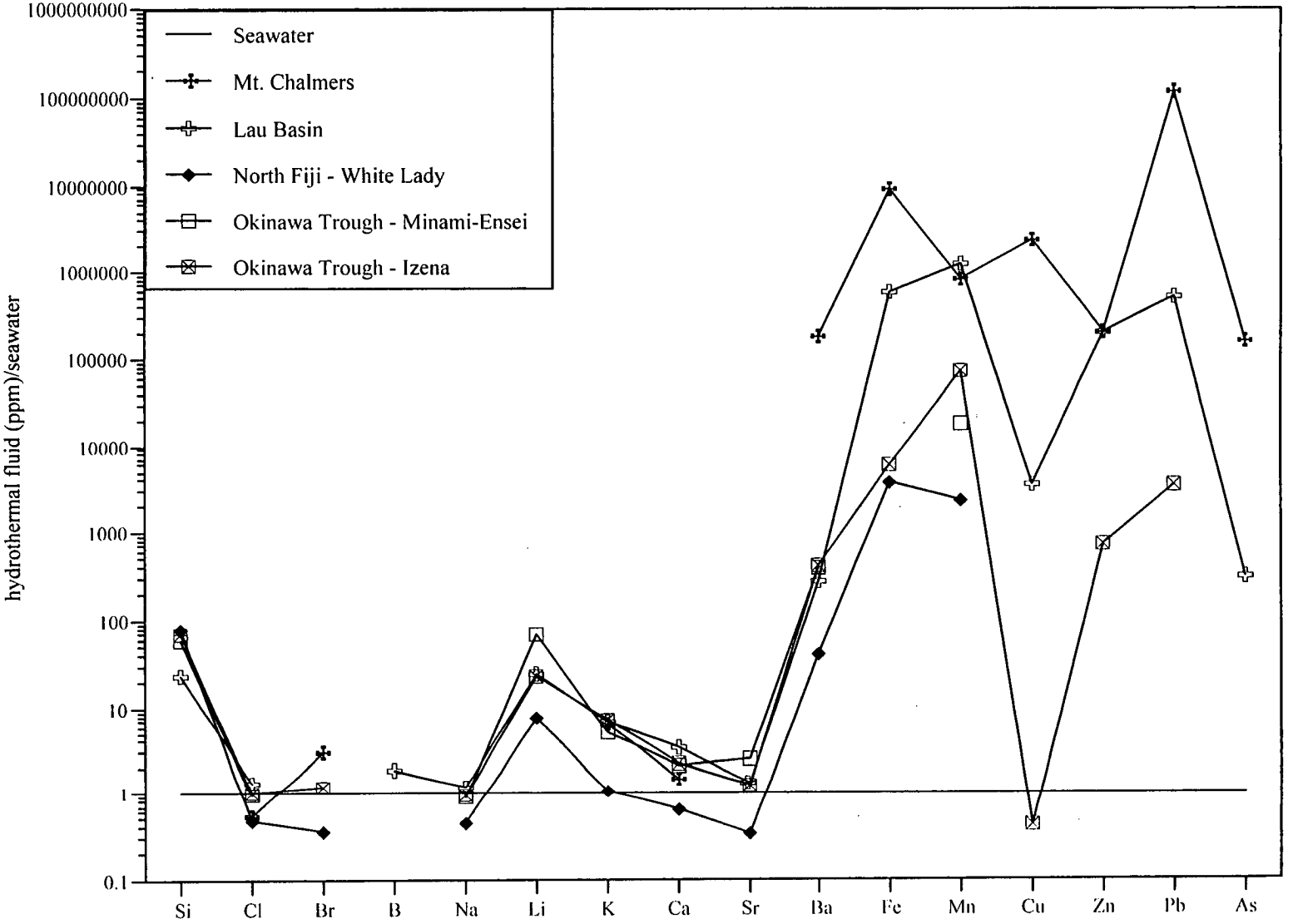

Figure 8.3. Multi-element plot for Mount Chalmers together with end-member vent fluids from Lau Basin (Fouquet *et al.*, 1991); North Fiji - White Lady; Okinawa Trough (Ishibashi and Urabe, 1995 and the references therein).

The average Mount Chalmers PIXE analyses are reported in parts per million (Table 8.4), while the end-member vent fluids are reported as moles/kg (Table 8.3). The end-member vent fluids and seawater values were converted to ppm. This conversion from moles/kg to ppm makes no difference to the relative abundances of the end-member vent fluids and therefore the spidergram pattern that is produced. In the forgoing discussion, the *concentration of element x* means the *relative concentration* of that element in a fluid to that of the element in seawater.

The end-member vent fluids have a Cl similar concentration to that of seawater. However, "White Lady" has concentrations less than that of seawater for both Cl and Br. Mount Chalmers has a lower Cl concentration and a higher Br concentration compared to seawater. Izena from the Okinawa Trough like Mount Chalmers is enriched in Br compared to seawater (Fig. 8.3).

The end-member vent fluids ("White Lady" excepted) have Na concentrations close to that of seawater, while the Na concentration for "White Lady" is less than that of seawater. Na was not analysed at Mount Chalmers. The fluid inclusion decrepitation analyses (Fig. 8.2b) would suggest that the Mount Chalmers fluid was also depleted in Na compared to seawater. The alkali metals (Li and K) are enriched in the end-member vent fluids, except for "White Lady" that has Li concentration similar to that of seawater. Mount Chalmers like the end-member vent fluids is also enriched in K relative to seawater (Fig. 8.3).

Lau Basin, Okinawa Trough end-member fluids and Mount Chalmers are all enriched in Ca and Sr compared to seawater. "White Lady" is depleted in Ca and Sr compared to seawater. Ba is highly enriched in all fluids compared to seawater. Mount Chalmers has approximately 2.5 orders of magnitude more Ba than the end-member vent fluids (Fig. 8.3).

All fluids are highly enriched in the transition metals (Fe, Mn, Zn, Pb) compared to seawater. The Lau Basin and Minami-Ensei fluids have higher concentrations of Mn compared to Fe, whereas Mount Chalmers and "White Lady" have Mn concentrations less than that of Fe. Izena has a Cu concentration less than that of seawater. The end-member vent fluids are enriched in Zn relative to Cu. Mount Chalmers has a higher Cu concentration than either Mn or Zn compared to the end-member fluids (Fig. 8.3).

8.4. DISCUSSION

The Main Lode fluids were ~70°C hotter (232° C - median value), than the West Lode hydrothermal fluids (161° C) and but are generally less saline than the West Lode fluid inclusions. Fluid inclusions in quartz from the West Lode show relatively lower homogenisation temperatures and salinities compared to fluid inclusions in barite. This is probably due to necking and leaking of the fluid inclusions in the barite. These temperatures from the present study indicate that the hydrothermal fluids that formed Mount Chalmers are at the lower end of the temperature range than those thought to have prevailed in the formation of ancient VHMS deposits and modern day VHMS deposits (Table 8.5).

Table 8.4. PIXE microprobe data for the composition of fluid inclusions (in ppm) from the Mount Chalmers deposit,

Sample/Inclusion No.	S	Cl	K	Ca	Mn	Fe	Co	Cu	Zn	As	Br	Mo	Rb	Sr	Ba	Pb
MC61*-139 1**	nd	0.27	486.00	<	<	55.00	50.00	<	<	123	<	<	na	na	723	<
MC61*-139 2**	nd	1.01	623.00	<	<	<	<	<	<	201	<	<	na	na	755	<
MC61*-139 3**	nd	0.21	566.00	<	<	136.00	<	<	<	226	<	<	na	na	0	<
MC61*-139 4**	nd	<	0.17	<	<	509.00	<	<	<	564	<	<	na	na	1	<
MC61*-139 7**	nd	0.39	0.25	<	<	824.00	<	<	<	963	593	<	na	na	1	<
Average	nd	**0.47**	**335.08**	<	<	**381.00**	**50.00**	<	<	**415**	**593**	<	na	na	**296**	<
Stdev	nd	0.37	309.55	<	<	355.40	<	<	<	350	<	<	na	na	405	<
MC66*-70 1**		<	566.00	<	80.00	763.00	<	251.00	<	73	<	na	na	na	0	<
MC66*-70 2**		0.84	0.22	842.00	<	0.24	<	923.00	<	<	<	na	na	na	0	<
MC66*-70 4**		<	0.22	784.00	<	0.45	<	935.00	<	658	<	0	na	na	0	<
MC66*-70 5**		0.49	0.21	836.00	581.00	0.34	365.00	0.10	<	567	<	na	na	na	1	<
MC66*-70 6**		<	0.62	<	<	0.90	<	0.54	<	<	<	<	na	na	1	<
MC66*-70 7**		0.54	0.41	<	<	0.98	<	0.67	<	924	<	<	na	na	1	<
MC66*-70 8**		<	<	0.16	<	0.33	<	867.00	<	330	<	<	na	na	1	<
Average		**0.62**	**94.61**	**615.54**	**330.50**	**109.46**	**365.00**	**425.33**	<	**510**	<	**0**	na	na	**1**	<
Stdev		0.19	230.93	411.08	354.26	288.18	<	460.89	<	324	<	<	na	na	0	<
MC52*-130 1**		<	222.00	<	<	91.00	<	49.00	<	<	<	<	<	<	492	<
MC52*-130 2**		<	0.17	457.00	<	329.00	<	198.00	<	<	168	<	<	<	0	<
MC52*-130 3**		0.24	513.00	197.00	<	17.00	<	<	<	19	21	<	<	<	152	32
MC52*-130 4**		0.47	0.23	410.00	<	288.00	<	168.00	<	<	<	<	<	<	0	<
Average		**0.35**	**183.85**	**354.67**	<	**181.25**	<	**138.33**	<	**19**	**95**	<	<	<	**161**	**32**
Stdev		0.16	243.07	138.55	<	150.94	<	78.81	<	<	104	<	<	<	232	<

Table 8.4. Con't.

Sample/Inclusion No.	S	Cl	K	Ca	Mn	Fe	Co	Cu	Zn	As	Br	Mo	Rb	Sr	Ba	Pb
MC52*-154 4**		0.61	0.19	259.00	<	156.00	<	110.00	<	<	<	179	<	<	<	<
MC52*-154 6**		1.28	0.47	804.00	<	451.00	<	301.00	101.00	114	<	<	<	<	<	<
MC52*-154 7**		4.19	0.71	<	<	414.00	<	227.00	<	<	<	<	<	<	<	<
MC52*-154 8**		0.26	940.00	<	<	272.00	<	256.00	79.00	<	<	<	<	<	<	121
MC52*-154 9**		1.12	0.11	177.00	<	87.00	<	62.00	<	63	29	<	<	<	<	<
MC52*-154 10**		3.21	0.40	417.00	<	210.00	<	116.00	<	495	<	<	<	<	<	<
Average		**1.78**	**156.98**	**414.25**	<	**265.00**	<	**178.67**	**90.00**	**224**	**29**	<	<	<	<	121
Stdev		1.56	383.60	278.27	<	143.83	<	95.43	15.56	236	<	<	<	<	<	<

***Sample number**

****Inclusion number**

< below detection limit or not fitted with proton yields

Table 8.5 Temperature of hydrothermal fluids from recent and ancient seafloor deposits. *Data from Rona (1988 and references therein); Kuroko deposits (Pisutha-Arnond and Ohmoto. 1983); Hellyer (Khin Zaw *et al.*, 1995; 1996); TAG (Lowell *et al.*, 1995).

Site	Fluid Temp. (0° C)	Site	Fluid Temp. (0° C)
EPR vents at 10°57'N*	347	Troodos*	301-351
Endeavour Ridge*	380	Kuroko deposits	200-300
EPR vents at 21°N*	350	Mattagami Lake*	250-300
Explorer Ridge*	291	Hellyer	165-322
Guaymas basin vents*	315	South Hercules	150-250
EPR vents at 12°N50'N*	381		
MAR at 23°35'N:45°W*	<200 - 270		
TAG	366		

Depth of seawater is the primary factor which determines whether or not the rising hydrothermal fluid boils before it reaches the seafloor (Haas, 1971). Based upon palaeontological evidence Mount Chalmers VHMS deposit was formed in a shallow marine environment (maximum water depth of 300 m). This depth range is considered too shallow for the formation of a VHMS without the fluid boiling and therefore not being able to precipitate metals at the seawater-rock interface. Boiling of a hydrothermal fluid has two important effects it directly increases the solution concentration, but more importantly, it is a mechanism whereby volatile constituents can be removed from solution, leaving the residue more alkaline and less capable of metal transport (Skinner *in* Roedder, 1984). In response to boiling a proportion of the dissolved metals will be deposited as disseminated or vein mineralisation below the seafloor. Boiling also selectively removes CO_2, H_2S and other volatiles from the liquid thereby increasing pH and K/H of the hydrothermal fluid (Rose and Burt *in* Roedder, 1984). In this study, no fluid inclusion evidence of boiling (*e.g.*, vapour-rich inclusions and liquid-rich inclusions together in the same healed micro-fracture) was recorded. The median values for the temperature of homogenisation and salinities (eq. wt % NaCl) for the Main Lode (232° C, 6.3 eq. wt % NaCl) and West Lode (161° C, 7.6 eq. wt % NaCl) were plotted on the boiling curves of Haas (1971 - Figure 8.4). Figure 8.4 shows that the hydrothermal fluids may have reached the seafloor without boiling at a water depth of approximately 300 m for the Main Lode and approximately 90 m for the West Lode. The depletion of Cl within a hydrothermal fluid relative to seawater may be considered to be an indicator that the hydrothermal fluids have boiled as Cl is partitioned into the brine phase (Butterfield *et al.*, 1990; Charlou *et al.*, 1996). Such depletion in Cl relative to seawater is seen in the Mount Chalmers fluid. However, in the low Cl vapour-rich fluids there should be a corresponding drop in Fe as it is being precipitated as an Fe-sulphide phase (pyrite or pyrrhotite) (Butterfield *et al.*, 1990; Charlou *et al.*, 1996). This depletion in Fe is also evident in the Fe/Mn ratio, where the ratio drops below unity due to sulphide precipitation (Butterfield *et al.*, 1990). The Fe/Mn ratio for Mount Chalmers is 7.5. This enrichment in Fe relative to Mn also seen in Figure 8.3, the Mount Chalmers fluid has almost an order of magnitude higher Fe concentration relative to seawater than Mn. The depletion in Cl may be possibly explained by the precipitation of a Cl-bearing mineral within the footwall lithologies. Depletion of Zn and Cu within a boiling (boiled) hydrothermal fluid is consistent with the lower Fe-content and is further evidence for subsurface precipitation of sulphides (Butterfield *et al.*, 1990). The depletion in Cl, Cu and Zn is also seen in the boiling "White Lady" hydrothermal vent (Figure 8.3).

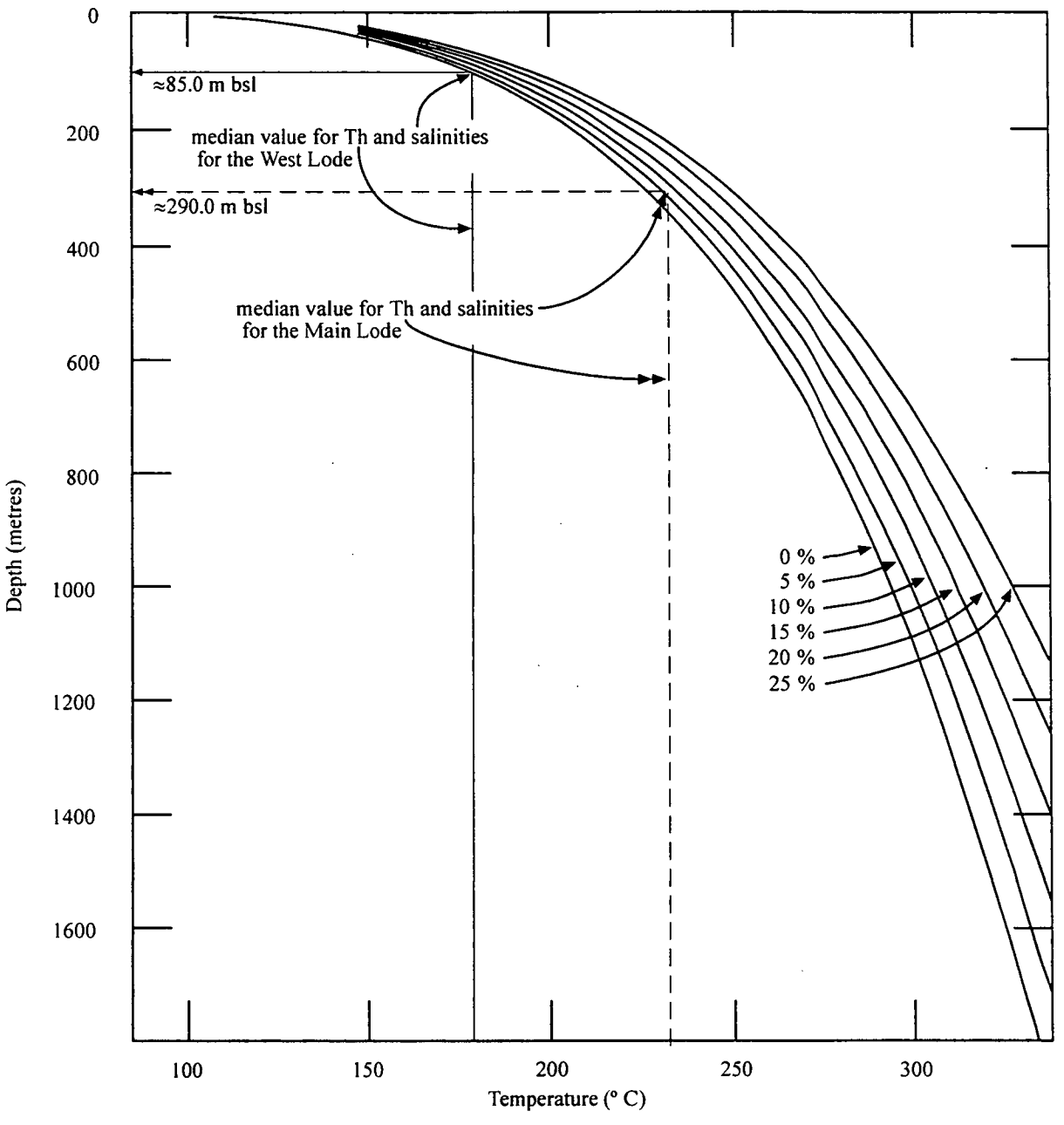

Figure 8.4. Boiling-point curves for H_2O liquid (0 wt percent) and for brine of constant composition given in weight percent NaCl. After Haas (1971). Th = temperature of homogenisation

The end-member vent fluids are enriched in most elements compared to seawater and are considered to be largely derived either from leaching of the footwall lithologies by convecting seawater or are derived from seawater itself (Table 6 *in* von Damm, 1995). Mount Chalmers has a broadly similar pattern and relative elemental abundances to seawater as the end-member vent fluids, which suggests that these elements were incorporated into the hydrothermal fluid by leaching of the footwall stratigraphy.

The enrichment in Ca in the Mount Chalmers, Lau Basin and Okinawa Trough fluids may be explained by the release of Ca when Na is taken up by the albitisation process (von Damm, 1995). At low water/rock ratios, some Na is removed from seawater to make secondary albite or analcime. At water/rock ratios greater than 10, however, Na is leached from the rocks (Franklin, 1986). "White Lady" is depleted in Ca and Sr relative to seawater and can be explained by the precipitation of anhydrite chimneys. For end-member vent fluids, a reliable Ba concentration in the hydrothermal fluid is difficult to determine due to its precipitation as $BaSO_4$ (barite) if small amounts of sulphate are present. However, Ba must be enriched in some hydrothermal fluids as barite-rich chimneys have been recovered from a number of vents sites (von Damm, 1995). The Ba concentration in the Mount Chalmers fluid inclusions is possibly reflecting the original concentration in the fluid as no daughter minerals or sulphate were observed or analysed. However, there are two significant differences between the Mount Chalmers fluid and the end-member vent fluids: the enrichment in Ba and the enrichment of Cu relative to Mn and Zn.

Mount Chalmers is depleted in Mg relative to seawater. This consistent with the theory that all Mg is removed from the fluid during hydrothermal circulation as found in experimental studies (Bischoff and Dickson, 1975; Mottl and Seyfried, 1980).

Na is the most abundant cation in hydrothermal fluids and as such it is closely tied to Cl, and is not conservative in water/rock reactions like Cl is, but has a major sink in the albitisation of basalts. The enrichment in Li and K in the end-member vent fluids is thought to be due to the preferential leaching of Li from basalts by high temperature hydrothermal fluids (von Damm 1995). However, no basalts are known from the footwall stratigraphy at Mount Chalmers, therefore, there must be another source of K for the Mount Chalmers fluid.

Mount Chalmers fluid inclusions are highly enriched in Fe compared to seawater and have an order of magnitude more Fe than Lau basin. The Cu content of the Mount Chalmers hydrothermal fluid is radically different to the end member vent fluids in that the concentration of Cu is greater than either Mn or Zn. The elevated Cu values in the Mount Chalmers fluid suggest that Cu was not derived solely form the leaching of the footwall stratigraphy by circulating modified seawater, but there was another source for the Cu. This is also true for Zn, where the concentration of Zn in the Mount Chalmers and also the Lau Basin fluid are 5 orders of magnitude greater than that of seawater. Pb also has a relative greater enrichment in the Mount Chalmers fluid compared to Lau Basin and Bent Hill. This is based upon two analyses that had Pb values above the detection limit. For Mount Chalmers the low Pb levels are to be expected as the samples come from the Main Lode, which is essentially depleted in Pb. Based upon the Pb isotope signature of the Mount Chalmers massive sulphide, Hunns *et al.* (1994) concluded that the Pb at Mount Chalmers was derived from the mantle. Whether the Pb was subsequently leached out of mantle derived volcanics by the hydrothermal fluid or was precipitated from a magmatic fluid is not possible to say. "White Lady" has no detectable Cu, Zn, or Pb due to subsurface precipitation of ore-forming

elements caused through boiling (Ishibashi and Urabe, 1995). Mount Chalmers and the Lau Basin vent fluids are enriched in As relative to seawater.

The geological and geochemical characteristics of VHMS deposits have been extensively studied for a number of years, yet there still remains disagreement on whether the fluids are magmatic or derived from recycled seawater. Two alternative models have been suggested for the source of metals within VHMS deposits:

- leaching from the footwall volcano-sedimentary lithologies and basement rocks by heated convecting seawater above a magmatic intrusions (*e.g.* Sakai *et al.*, 1970, Sasaki and Kajiwara, 1971; Constantinou and Govett, 1973; Spooner and Fyfe, 1973, Ishihara and Terashima, 1974; Sasaki, 1974; Ohmoto and Rye, 1974, Heaton and Sheppard, 1977; Sheppard, 1977; Solomon, 1981; Stolz and Large 1992)

- direct input of metals from a magmatic volatile phase (*e.g.* Urabe and Sato, 1978; Henley and Thornley, 1979; Kowalik *et al.*, 1981; Sawkins and Kowalik, 1981; Stanton, 1985, 1990, 1994, Urabe, 1987, Urabe and Marumo, 1991).

Ore fluid salinity values (5-8 NaCl equiv. wt %) at Mount Chalmers are higher than seawater. This coupled with the presence of CO_2 suggests that recycled seawater cannot be the sole source of the VHMS ore fluids. The high concentrations of Ba, Cu, Fe, Zn and Pb and the presence of significant concentrations of As and K in the Mount Chalmers ore fluids imply that they were not solely derived from the leaching of the footwall stratigraphy by circulating modified seawater, but that there was some, probably minor, magmatic input of these elements into the hydrothermal system.

CHAPTER 9
ORIGIN OF HYDROTHERMAL DOLOMITE AT MOUNT CHALMERS

This chapter has been submitted to Economic Geology for publication as "Origin of hydrothermal dolomite at Mount Chalmers, Queensland, Australia" by S. R. Hunns and B. R. Anderson.

9.1 INTRODUCTION

Carbonates are commonly associated with both ancient and modern day volcanic-hosted massive sulphide (VHMS) deposits (*e.g.* Braithwaite, 1974; Iijima, 1974; Peter and Scott, 1988; Sagalevich *et al.*, 1992; Larocque and Hodgson, 1993; Baker *et al.*, 1994; Leybourne and Goodfellow, 1994). Calcite and dolomite are the dominant carbonate phases. Although the carbonate-VHMS association is well known, only limited textural studies have been conducted on the carbonates (Dixon, 1980; Hill and Orth, 1994; Orth and Hill, 1994; Hill, 1996).

The hydrothermal fluids considered to be responsible for carbonate formation in VHMS deposits are largely thought to be derived from a mixed fluid source dominated by seawater with a minor magmatic and or meteoric component (Dixon, 1980; Khin Zaw and Large, 1992; Hill, 1996; Huston, 1997). However covariance modelling of the carbon and oxygen isotopes of the carbonates has not been widely applied and has largely been restricted to comparative analyses of the data (Addy and Ympa, 1977; Kowalik *et al.*, 1981; Hill, 1996; Huston, 1997). This chapter describes the massive dolomite lenses associated with the Mount Chalmers VHMS deposit, and proposes a model for their origin using covariance modelling of carbon and oxygen isotopes.

9.2. TIMING OF DOLOMITE FORMATION

Carbonates associated with VHMS deposits are generally considered to have formed either before or contemporaneously with massive sulphide (Dixon, 1980; Peter and Scott, 1988; Khin Zaw, 1991; Galley, 1993 and Orth and Hill, 1994). However at Mount Chalmers the dolomite replaces a number of different rocks, including peperites (*e.g.* MC58 and MC59), sediments (*e.g.* MC22, MC36 and MC56), the base of an andesitic intrusion (MC20) and silica-altered host rocks (*e.g.* MC49, MC55 and MC56) (Figs. 9.1 and 9.2) in both hangingwall and footwall. These features suggest that the fluids responsible for dolomite formation were actively circulating after mineralisation and after deposition and/or intrusion of the hangingwall rocks.

Gossan

Massive sulfide

Semi-massive sulfide mineralization

Siltstone/sandstone (d) dolomite alteration

Massive dolomite

Dolomite veins

Dolomite/kaolin alteration

Silica/sericite alteration

Sulfide veins/b barite

Disseminated pyrite

Pumiceous, feldspar-phyric lithic breccia

Peperite

Altered peperite

Basaltic-andesite intrusives

Graded, feldspar-phyric, pumiceous lithic breccias

Lithic breccias + chlorite altered clasts

Legend for Figures 9.1 and 9.2.

Figure 9.1Graphic logs of drill core from Mount Chalmers mine MC58, MC59 MC36, MC56, MC20 and MC55. The logs illustrate the massive and replacive nature of the dolomite. The dolomite is replacing a number of different lithologies, including peperite, basaltic-andesite, volcanolithic sandstone and lithic breccias. These logs also show that the massive dolomite also occurs peripherally to the massive sulfide mineralisation.

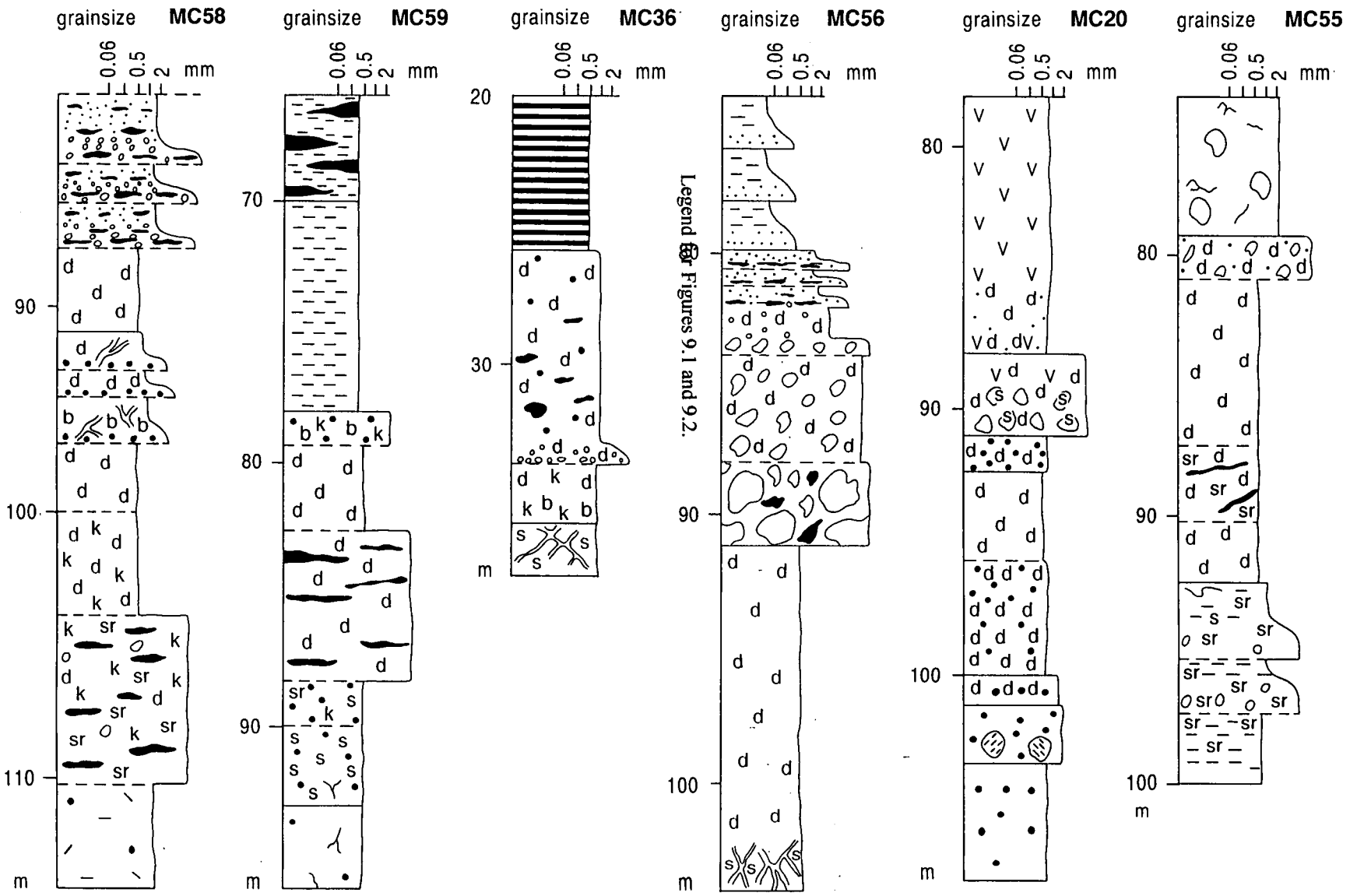

Legend for Figures 9.1 and 9.2.

Figure 9.2. Graphic logs of drill core from Mount Chalmers mine MC27A, MC43, MC22A and MC52. MC 27a and MC 43 are from the West Lode, MC22A and MC52 are from the Main Lode. The logs show that the dolomite occurs both below (MC27A, MC43 and MC49) and above the massive sulfide and gossan (MC22A, MC52).

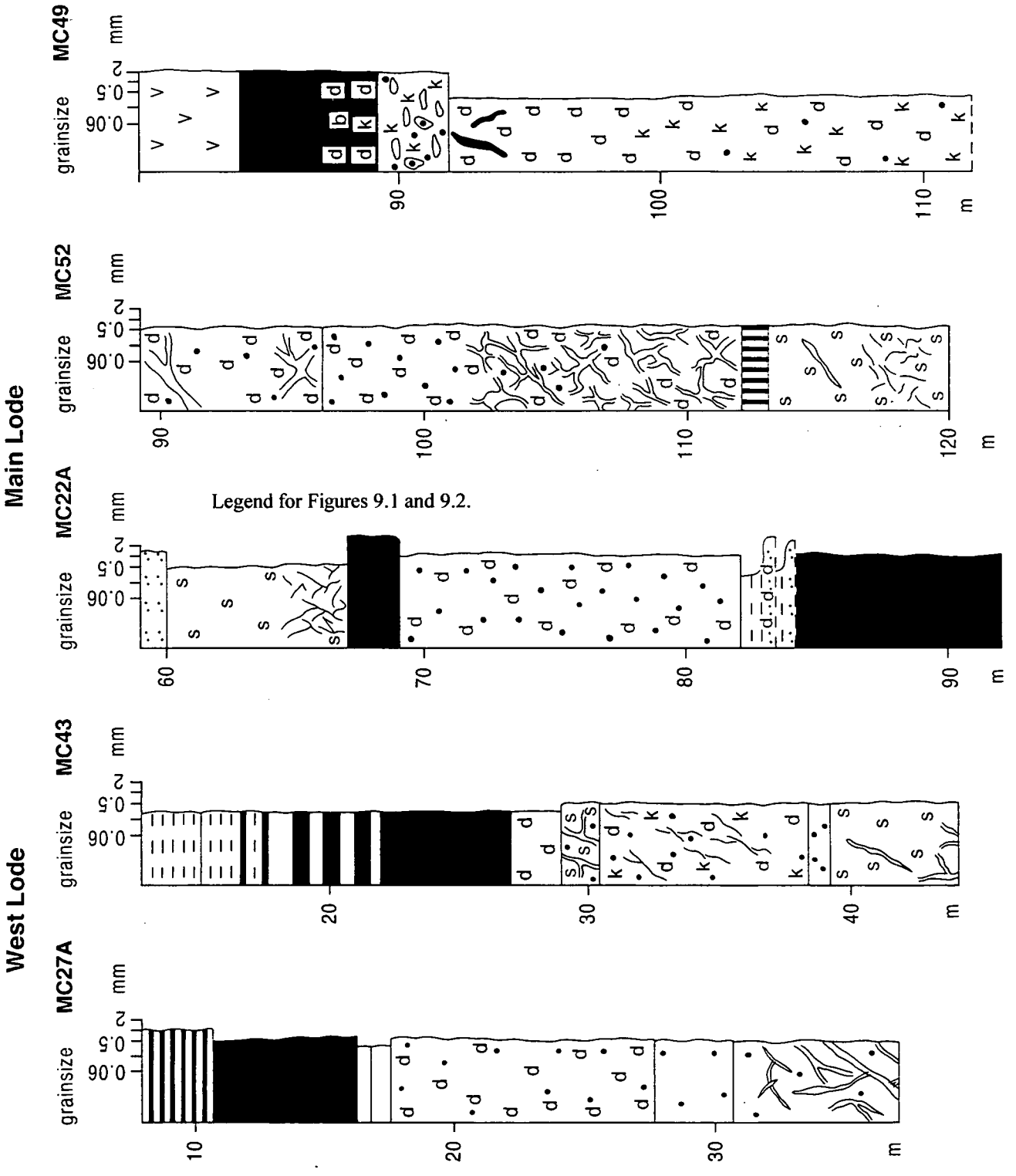

Legend for Figures 9.1 and 9.2.

9.3. DOLOMITE

The dolomite, like the massive sulphide, forms two major lenses and one minor lens. These occur both within the footwall and hangingwall and along strike from the massive sulphide ore. They vary in thickness from ~1 to 25 m (Fig. 9.3). They typically occur lateral to the massive sulphide and stringer vein system, but also occur immediately above and beneath the massive sulphide or gossanous zones (Fig. 9.2). The Main Lode dolomite lens (MLDL) is thicker and far more extensive than the West Lode lens (WLDL). The MLDL, like the massive sulphide lenses, is elongated in a northwesterly direction, while the long axis of the WLDL is oriented in a northerly direction (Fig. 9.3). The dolomite contains disseminated and veinlet pyrite with rare to minor chalcopyrite and sphalerite.

Macroscopically, the dolomite occurs in one of four modes: (1) massive very fine-grained dolomite (Fig. 9.4A); (2) massive dolomite with banding defined by veinlets of chlorite ± pyrite that have replaced the dolomite (Fig. 9.4A and 9.4B), (3) spotty dolomite, or (4) as late stage veins, vughs and fractures within the earlier formed massive dolomite. Late stage dolomite veins also occur throughout the mine stratigraphy and crosscut all rock types, including the massive dolomite, sulphide stringer veins and the massive sulphide (Fig. 9.4C).

Microscopically four generations of massive dolomite and one late stage dolomite vein and vugh filling generation are observed (Fig. 9.5):

1) cloudy anhedral to rhombohedral dolomite,
2) radiating blades of cloudy dolomite,
3) overgrowths of clear rhombohedral dolomite on the cloudy dolomite,
4) mosaics of interlocking euhedral clear dolomite within the cloudy dolomite,
5) late stage dolomite infilling veins, vughs and fractures.

Cloudy anhedral dolomite (Texture 1) consists of cloudy mosaics of irregularly shaped fine-grained (≤100 μm) interlocking anhedral to subhedral crystals (Fig. 9.5A). The cloudiness is due to abundant minute inclusions of phyllosilicates. The cloudy dolomite replaced earlier silica, leaving amoeboid-like patches of silica within the dolomite. Internally, the silica commonly has a poikilitic-like texture, while the outer margins commonly display dissolution margins adjacent to the dolomite (Fig. 9.5A).

Radiating blades of cloudy dolomite (Texture 2) were recognised in one sample, it is composed of radiating blades of cloudy dolomite that have replaced dolomite texture 1 (Fig. 9.5B).

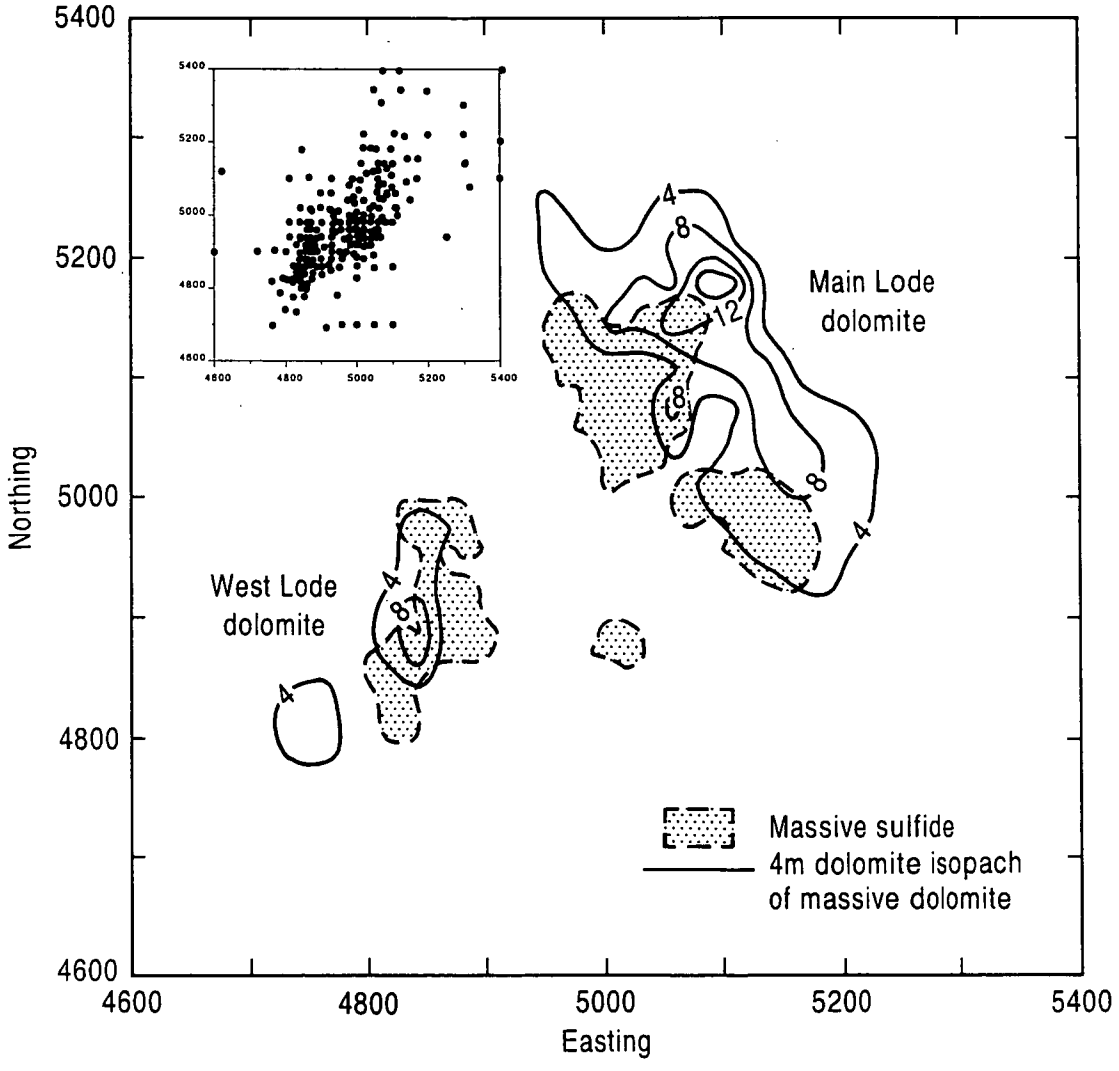

Figure 9.3. Isopachs of the dolomite and its spatial relationship to the massive sulfide mineralisation at Mount Chalmers. The inset shows the distribution of drillholes on which the contouring is based. The corner coordinates of the inset are identical to those of the main diagram. Grid coordinates are in meters.

Figure 9.4. Drill core samples of massive and late stage vein, vugh and fracture filling dolomite. a) and b) Massive fine grained dolomite, with later fine grained chlorite, forming layers and spotty textured (b)dolomite. c) late stage vein, vugh and fracture filling dolomite crosscutting and replacing earlier formed fine grained massive dolomite and up stratigraphy volcanolithic sandstones.


A
CM
B
C
CM

Figure 9.5. Photomicrographs of dolomite textures. A) Dolomite texture 1 — cloudy anhedral to rhombohedral dolomite replacing earlier formed silica alteration, producing amoeboid like shapes. MC31-25.9m. B) Dolomite texture 2 (dt2) — radiating blades of cloudy dolomite growing on earlier formed dolomite texture 1 (dt1). The clear areas of the photomicrograph are composed of fine grained quartz and phyllosilicates. MC50-101.56m. C) Dolomite texture 3 — overgrowths of clear rhombohedral dolomite on the cloudy dolomite. The overgrowths grade from zoned to clear dolomite on the margins. MC27A-27.5m. D) Dolomite texture 4 (dt4) — mosaics of interlocking euhedral clear dolomite within the cloudy dolomite. The clear domains surrounding the cloudy dolomite are composed of phyllosilicates (chlorite and kaolin) and quartz producing an apparent spotty texture. MC50-101.56m. In all photomicrographs, the opaque phase is pyrite and all photomicrographs were taken in plane polarised light.

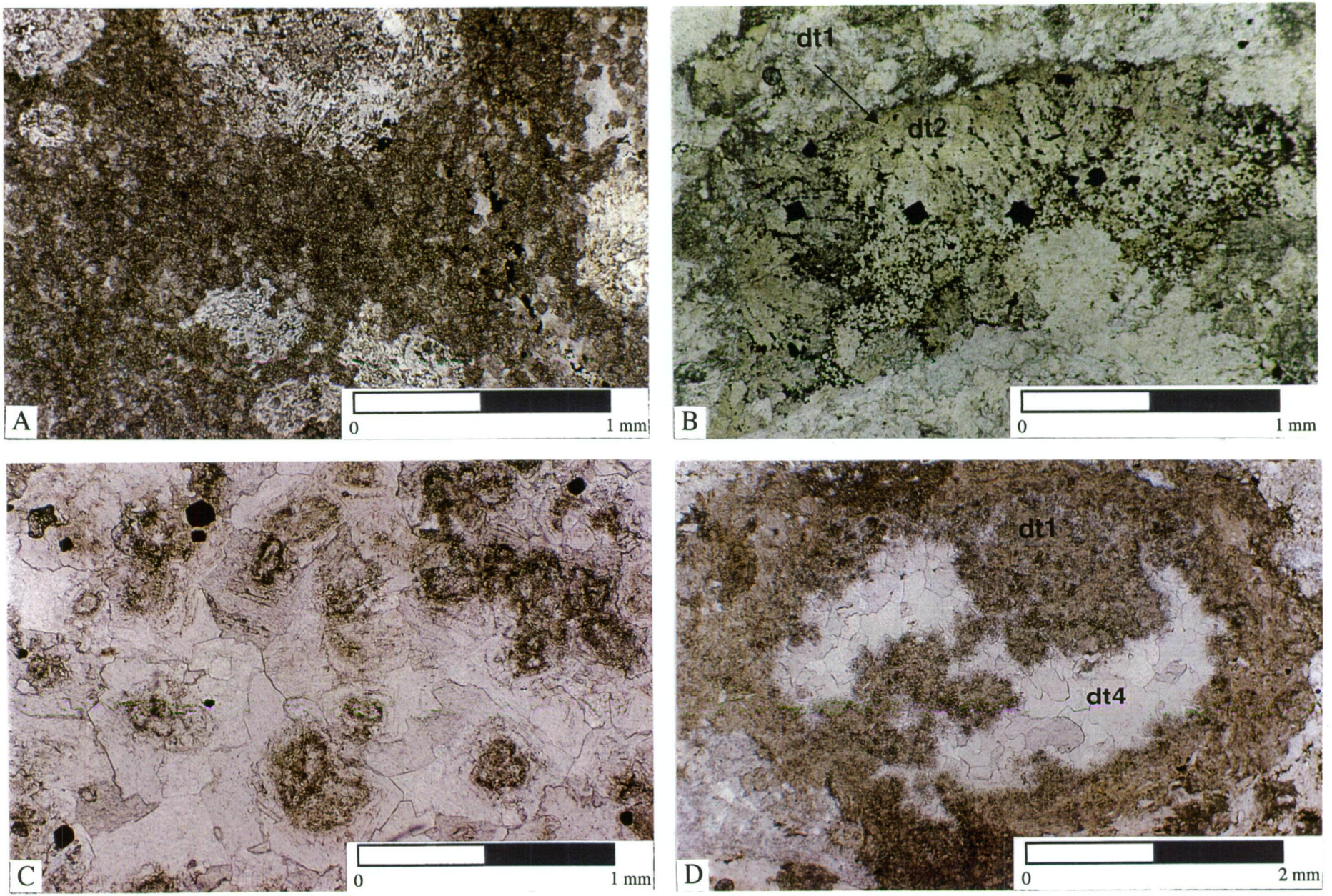
A
0
1 mm
B
dt1
dt2
0
1 mm
C
0
1 mm
D
dt1
dt4
0
2 mm

Dense mosaics of subhedral to euhedral crystals of clear dolomite occur as overgrowths with a core of cloudy dolomite (Texture 3). The cloudy cores commonly have relict rhombohedral outlines, and are commonly zoned with the growth zones marked by inclusions of very fine-grained phyllosilicates. The zonation may continue out into clear dolomite, but does not persist to the margins of the clear overgrowths (Fig. 9.5C).

Mosaics of interlocking subhedral clear dolomite (Texture 5) occur within the cloudy dolomite of texture 1 (Fig. 9.5D) and also forming cores to the dolomite spots. The clear dolomite is commonly zoned and may also have a rim of non-zoned dolomite.

Late stage clear dolomite fills veins, vughs and fractures (texture 5) and crosscuts dolomite textures 1, 2, 3 and 4 (Fig. 9.5C). Dolomite growing into open space filling commonly forms zoned dogtooth spar overgrowths on the cloudy dolomite.

Dolomite texture 1 is clearly an early replacive phase overprinting silica, barite, and a number of other minerals. Dolomite texture 2 post dates dolomite texture 1, but its relationship to the other dolomite texture is uncertain as it was only found in one sample. Based upon paragenetic relationships, dolomite texture 3 is interpreted as representing an intermediate stage of the hydrothermal activity responsible for the formation of the dolomite. Dolomite texture 4 is interpreted as void-filling dolomite, and possibly formed due to the dissolution replacement of earlier-formed dolomites. Dolomite texture 5 clearly cross cuts earlier formed dolomite textures 1, 2, 3 and 4.

Cathodoluminescence (CL) studies were undertaken using a Nuclide ELM-2B Luminoscope at 6-8 kV and approximately 0.5 mA current, and a focused beam 8-12 mm in diameter. All five generations of dolomite failed to luminescence. The failure of the dolomite to luminescence may be attributed to the presence of Fe^{2+} within the crystal lattice. In CL studies, the balance of activator and quencher centres controls the intensity of luminescence. The primary activator ion is Mn^{2+}, while Fe^{2+} is the commonest quencher ion (Miller, 1988). Complete quenching by Fe results in black luminescence distinct from non-luminescence (Amieux, 1992). Pierson (1981) found this to occur in dolomites where the Fe content exceeded 1.5 wt. percent. This was observed in samples studied, although many of them have higher Fe content

9.3.1. Replacement of Silica by Dolomite

Silica replacement by dolomite may have been caused by a number of different mechanisms. The solubility of silica increases with increasing temperature, pressure (Rimstidt, 1997), pH in solutions with pH $\geq$8 (Rimstidt, 1997), and in saline solutions (Fournier, 1983; Fournier and Marshall, 1983; Xie and Walther, 1993). Alternatively, replacement of silica by dolomite may occur by precipitation-controlled dolomite replacement of quartz along dolomite crystal faces, the contact surfaces of the quartz

grains being dissolved by pressure solution as the dolomite is being precipitated. The maximum pressure that a growing crystal could exert on its surroundings increases with the degree of supersaturation of the pore waters (Maliva and Siever, 1990).

9.3.2. Composition of Dolomites

Dolomite was identified as the dominant carbonate species by petrography, XRD and electron microprobe analysis. Rare calcite and siderite also were identified (Table 9.1). Dolomite compositions were determined quantitatively using the Cameca SX50 Electron Microprobe in the Central Science Laboratory at the University of Tasmania.

The $MgCO_3$ content ranges from 29.82 to 43.17 wt percent (median: 39.21 wt %); $CaCO_3$ from 47.25 - 57.56 wt percent (median: 52.93 wt %); $FeCO_3$ from 1.03 - 17.69 wt percent (median: 6.37 wt %) and for $MnCO_3$ between 0.0 to 0.47 wt percent (median: 0.23 wt %). The analyses form a tight cluster with a spread in the $FeCO_3$ content towards the siderite field and indicate that the dolomites contain negligible to very minor amounts of manganese (Fig. 9.6). The massive dolomites display little chemical compositional variation between the five recognised dolomite textures. Traverses across dolomite grains showed no compositional zoning. There is also no spatial variation in composition between the Main Lode and the West Lode. However, in the footwall, the dolomites show an increase in $MgCO_3$ and $CaCO_3$, and a decrease in $FeCO_3$ as the sulphide mineralisation is approached (Fig. 9.7).

9.4. ISOTOPIC MODELLING

Samples of late stage veins and the massive dolomite from the Main Lode and the West Lode were drilled from hand specimens, and carbon and oxygen isotopes were determined on a VG Micromass 602D mass spectrometer in the Central Science Laboratory, University of Tasmania, using the method of MacRae (1950). Dolomite separates were reacted with phosphoric acid for 24 hours at 50°C. The $\delta^{13}C$ data are quoted with respect to Peedee Formation Belemnite (PDB) and the $\delta^{18}O$ data are quoted with respect to Standard Mean Ocean Water (SMOW).

9.4.1 Results

Twenty-six hydrothermal dolomite samples analysed for this study are included with 14 unpublished analyses provided by David L. Huston (writ. comm.) (Table 9.2). The $\delta^{13}C$ values have a range of -6 to +1 ‰ and $\delta^{18}O$ values have a range of +11.0 to +18.0 ‰ (Fig. 9.8). Some dolomites from the Main Lode are enriched in $\delta^{18}O$ compared to the dolomites from the West Lode.

Table 9.1. XRD analysis and semi-quantitative compositions of mineral components of dolomites from Mount Chalmers.

Sample	>40%	25-40%	15-25%	10-15%	5-10%	<5%
MC27A-20.7m	Dolomite	Kaolinite			Quartz	Pyrite, ?Mica
MC27A-27.5m	Dolomite	Kaolinite		Mica		Pyrite, ?K-feldspar
MC31-25.9m	Dolomite			Kaolinite[1]	Quartz	Pyrite, Siderite
MC36-30.6m	Dolomite	Kaolinite		Pyrite	Mica	Chlorite, Gypsum, Quartz, ?K-feldspar, ?Calcite
MC36-30.7m	Dolomite		Kaolinite[1]	Mica	Pyrite, Mica	Quartz, Chlorite, ?Plagioclase, ?K-feldspar

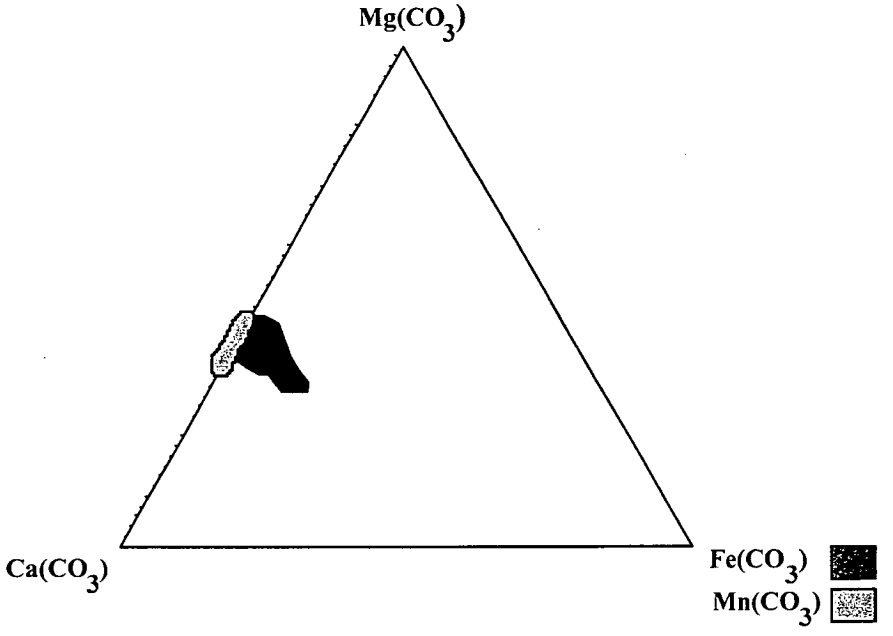

Figure 9.6. Ternary plot showing the chemical composition determined fromelectron microprobe analyses of the dolomites with respect to the major carbonate species

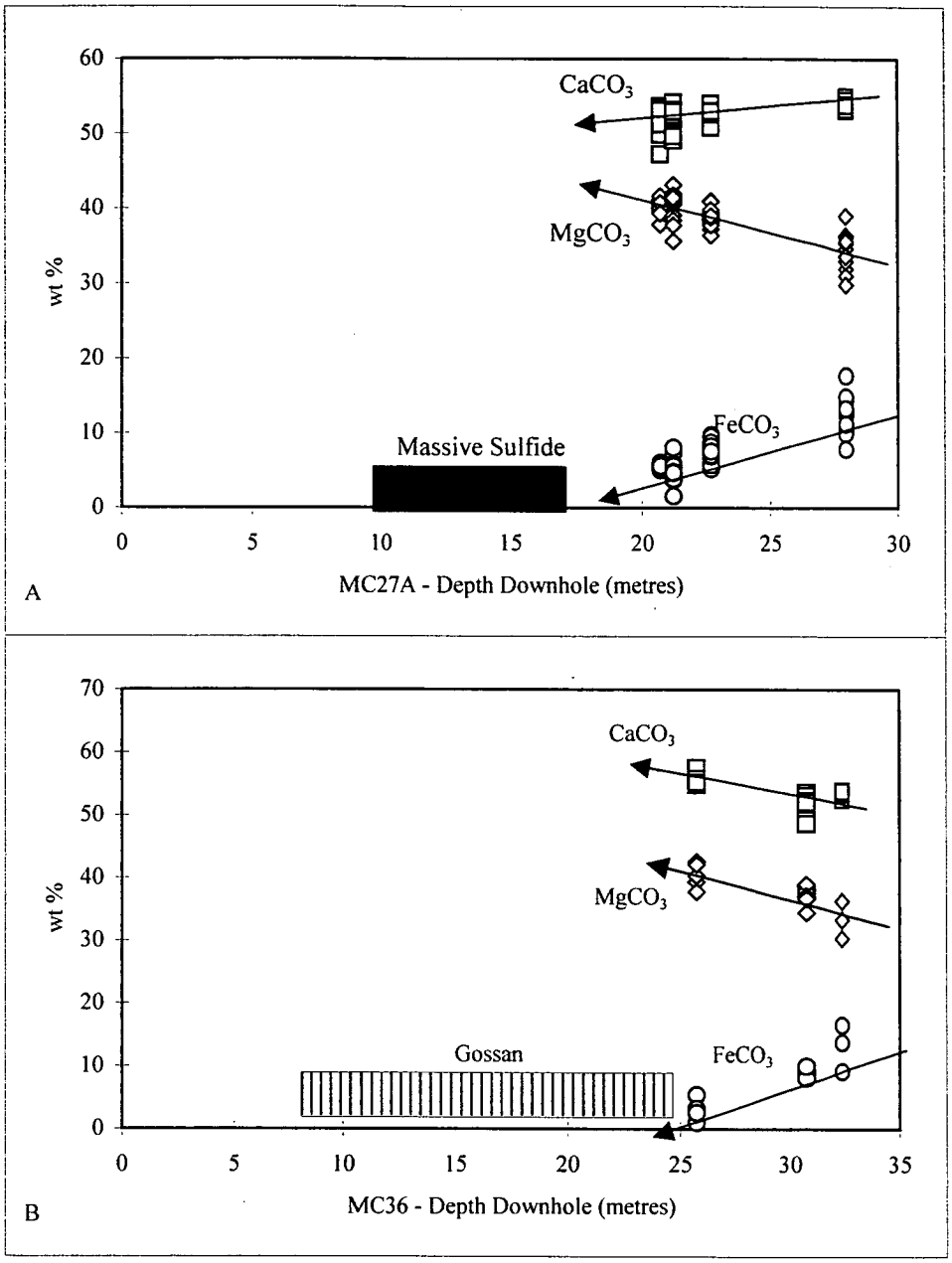

Figure 9.7. Downhole plots of electron microprobe analysis of dolomite for MC27A (Fig. 9.7A) and MC36 (Fig. 9.7B).

Table 9.2. Sample description, $\delta^{13}C_{PDB}$ and $\delta^{18}O_{SMOW}$ values for the Mount Chalmers dolomite and the Lake's Creek limestone. For the Mount Chalmers dolomite, the sample descriptions are as follows *e.g.*, MC34-50.6: Drill hole name (MC34) followed by the sample depth in metres (50.6). WL = West Lode; ML = Main Lode; FG = fine grained; LS = late stage.

Sample	Lode	Description	$\delta^{13}C_{PDB}$	$\delta^{18}O_{SMOW}$	Sample	Lode	Description	$\delta^{13}C_{PDB}$	$\delta^{18}O_{SMOW}$
MC22A-72.3	WL	FG massive dolomite	-1.98	12.62	FRD5-104.6	ML	LS dolomite vein	-4.25	13.11
MC22A-82.3	WL	FG massive dolomite	-2.89	12.45	FRD5-108.4	ML	FG massive dolomite	-2.92	15.20
MC25-52	WL	LS dolomite vein	-3.84	12.83	FRD5-108.4A	ML	LS dolomite vein	-4.16	18.39
MC25-57.3	WL	LS dolomite vein	-3.94	11.97	FRD5-108.4B	ML	LS dolomite vein	-5.17	18.27
MC25-67.5	WL	LS dolomite vein	-3.71	13.92	FRD15-111.5	ML	Dolomite spots	-5.58	15.07
MC27A-22.2	WL	LS dolomite vein	-1.87	13.10	FRD27-112.65	ML	FG massive dolomite	-4.36	16.32
MC27A-22.2A	WL	FG massive dolomite	-1.75	14.09	MC49-100.85	ML	FG massive dolomite	-4.76	16.20
MC27A-27.5	WL	FG massive dolomite	-1.76	14.28	MC49-93.5	ML	FG massive dolomite	-3.83	13.25
MC27A-28.0	WL	LS dolomite vein	-3.30	13.50	MC49-94.0	ML	FG massive dolomite	-5.30	11.90
MC27A-41	WL	LS dolomite vein	-5.30	12.40	MC49-97.2	ML	FG massive dolomite	-5.00	13.10
MC27A-44.2	WL	LS dolomite vein	-5.10	12.50	MC50-101.56	ML	Dolomite spots	-6.60	15.64
MC29-46.1	WL	LS dolomite vein	-4.25	16.01	MC50-101.56A	ML	FG massive dolomite	-6.12	15.96
MC31-25.9	WL	FG massive dolomite	-1.31	12.69	MC50-93.4	ML	FG massive dolomite	-5.25	16.04
MC31-32.4	WL	FG massive dolomite	-3.09	12.25	MC55-85.6	ML	FG massive dolomite	-5.20	13.00
MC34-35.6A	WL	LS dolomite vein	-3.49	13.41	MC55-91.2	ML	FG massive dolomite	-5.50	12.10
MC34-35.6B	WL	LS dolomite vein	-1.13	18.54	MC56-114.2	ML	LS dolomite vein	-3.55	12.29
MC34-50.6	WL	LS dolomite vein	-3.77	12.22	LQ1		Lakes Creek limestone	+2.48	16.94
MC36-25.7	WL	FG massive dolomite	-3.30	13.00	LQ2		Lakes Creek limestone	+0.89	16.20
MC36-27.8	WL	FG massive dolomite	-4.90	11.80	LQ3		Lakes Creek limestone	+1.13	16.58
MC36-30.6	WL	FG massive dolomite	-3.30	12.11	LQ4		Lakes Creek limestone	+1.78	16.94
MC36-31.8	WL	FG massive dolomite	-3.41	12.25	LQ5		Lakes Creek limestone	+1.20	16.51
MC36-32.4	WL	FG massive dolomite	-5.10	11.50	LQ6		Lakes Creek limestone	+1.04	16.96
MC43-45.5	WL	LS dolomite vein	-3.77	11.96	LQ7		Lakes Creek limestone	+2.39	21.01
MC47-99.1	WL	LS dolomite vein	-3.76	12.08	LQ8		Lakes Creek limestone	+0.80	18.09

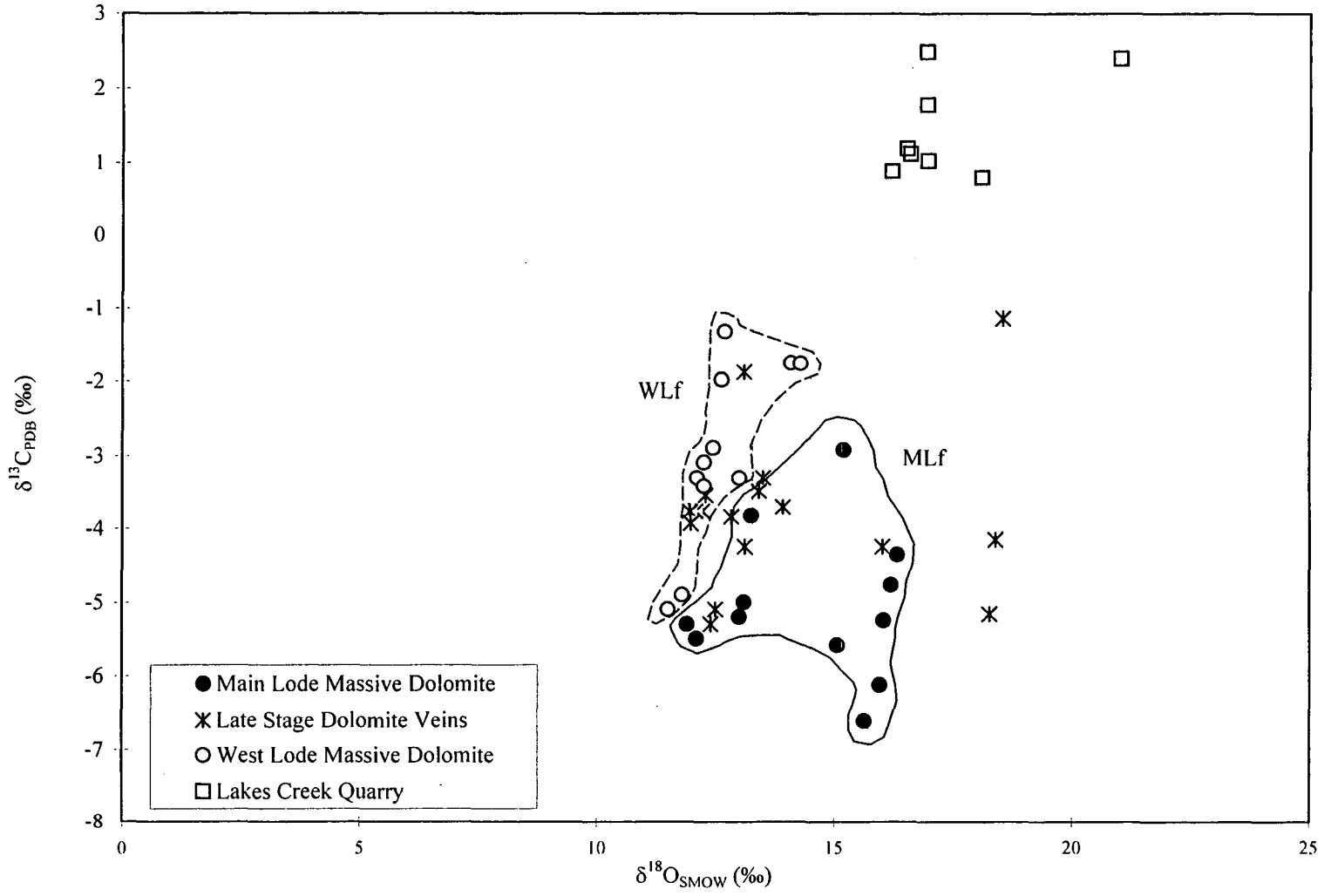

Figure 9.8 Carbon vs. Oxygen isotope variations of the Mount Chalmers dolomite and the Lake's Creek Quarry limestone. MLf - Main Lode field; WLf - West Lode field

The Main Lode field is dominated by fine-grained massive dolomite. The West Lode field is dominated by fine-grained massive dolomite and contains fine-grained pyrite. Dolomite from late-stage veins show considerable spread in their $\delta^{18}O$ and $\delta^{13}C$ values, overlapping both the Main and West Lode fields (Fig. 9.8).

Eight unmetamorphosed calcareous limestone samples from the Berserker beds at Lakes Creek Quarry (Fig. 1.1) were also analysed to provide data on carbonates precipitated from Permian seawater. The limestone has $\delta^{18}O$ and $\delta^{13}C$ values in the range +16.51 to +21.01 ‰ and +0.80 to +2.48 ‰ respectively (Table 9.2).

Carbonate mineral can be precipitated from hydrothermal solutions by one of four mechanisms: 1) heating of the solution; 2) degassing CO_2 in the pH where HCO_3^- is dominant over H_2CO_3; 3) decreasing salinity, and 4) increasing the pH (Rimstidt, 1997; as could be achieved by mixing or boiling). Further, dolomite formation is thermodynamically favoured with respect to calcite in solutions with low Ca^{2+}/Mg^{2+} and low Ca^{2+}/CO_3^{2-} (or Ca^{2+}/HCO_3^-) ratios and high temperatures (Deer *et al.*, 1992). The most important factors influencing dolomite precipitation are changes in temperature and fluid composition.

Dolomite precipitated in equilibrium with a fluid of constant composition will have $\delta^{13}C$ and $\delta^{18}O$ values that co-vary, with a slope of ~0.5 on a $\delta^{18}O$ versus $\delta^{13}C$ plot due to temperature dependent isotopic fractionation.

Changing temperature of deposition produces a positive correlation between $\delta^{18}O$ and $\delta^{13}C$ values in carbonates and this is not evident in Figure 9.8 (*e.g.* Rye and Williams, 1981; Khin Zaw and Large, 1992; Zheng and Hoefs, 1993). Also, if temperature change were the sole precipitation mechanism, oxygen isotope fractionation would produce a greater shift in $\delta^{18}O$.

Primary fluid inclusions in the dolomite are either absent or too small to be analysed, or were obscured by sericite in the "cloudy" dolomite phase, precluding direct measurements of the temperature and salinity of dolomite formation. Consequently, the possible influence of salinity on the formation of the dolomite is unresolvable. Calculated and measured temperatures in the range of 100° to 300°C have been reported for other carbonate formations associated with ancient (Dixon, 1980; Khin Zaw and Large, 1992; Hill, 1996; Huston, 1997) and modern day massive sulphide and hydrothermal carbonate deposits (Peter and Scott, 1988; Peter and Scott, 1991; Sagalevich *et al.*, 1992; Boni *et al.*, 1994).

9.4.2. Source of Dolomite-Forming Fluids

Hydrothermal fluids responsible for the formation of carbonates associated with both the ancient and modern day massive sulphide deposits are thought to be the principally derived from a mixed fluid source dominated by seawater with a minor magmatic and or meteoric component (Dixon, 1980; Khin Zaw and Large, 1992; Baker *et al.*, 1994; Duckworth *et. al.*, 1994; Hill, 1996; Huston, 1997). As the Mount Chalmers hydrothermal dolomite has lower $\delta^{18}O$ and $\delta^{13}C$ values of dissolved carbonate in equilibrium with seawater at surface temperatures, it is unlikely that the Mount Chalmers dolomites were formed by the direct precipitation from seawater. This suggests that fluid mixing or fluid/rock interaction are probable mechanisms for the precipitation of the Mount Chalmers dolomite. In this section the possible sources of dolomite-precipitating fluids at Mount Chalmers are considered.

Modern day seawater has $\delta^{18}O$ and $\delta^{13}C$ values very close to 0 ‰ (Taylor, 1987; Rollinson, 1993), and the values for Permian seawater are assumed too be isotopically similar. The unmetamorphosed Lake's Creek limestone values represent a carbonate precipitated from such seawater (Table 9.2). As the Mount Chalmers dolomite has lower $\delta^{13}C$ and has lower $\delta^{18}O$ values than Permian seawater, seawater derived HCO_3^- is unlikely to have been the dominant source of carbon.

Two models for dolomite formation are examined. The first examines fluid mixing between a hot fluid with C and O isotopes typical of a magmatic fluid or strongly evolved seawater and cold unmodified seawater. These processes can be modelled using mass-balance equations that examine the paired shift in C and O isotopes. Mass-balance modelling assumes an initial starting isotopic composition and then calculates the isotopic shifts that would be induced in an evolving fluid induced by temperature changes or mixing of fluids with differing components and varying isotopic values or carbon-species concentration. The second model examines fluid/rock interaction with a magmatic fluid or strongly evolved seawater.

9.4.3. Fluid Mixing

Modelling of the C and O covariance trends in the Mount Chalmers data will examine the mixing of Permian seawater and a hydrothermal fluid using mass-balance equations developed by Zheng and Hoefs (1991). Equation 9.1 (below) calculates $\delta^{13}C_{dol}$ and has three main elements. $\delta^{13}C_a + 10^3 \ln \alpha_y^x$ calculates the shift in fluid A due to equilibrium fractionation between components X and Y. The equilibrium isotopic fractionation factors for dolomite-H_2CO_3, dolomite-HCO_3^-, and dolomite-H_2O were derived from Deines *et al.* (1974) and Ohmoto and Rye (1979). The second element of the mass balance equations is X_a. This term is used to vary the mole fraction of fluid A in the mixed fluid and values can range between 1 and 0. A value of X_a=1 represents a fluid composed of only fluid A; if $X_a = 0$, only fluid B is present. The third part of the equation is P where $P = C_b/C_a$. This term measures the relative concentration of the total dissolved carbon in fluid B to that in fluid A.
Equation 9.2 has a similar appearance to Equation 9.1 in that it has a component that accounts for the equilibrium fractionation, a proportional term (X_a) and variables for the initial composition of fluids A and B.

$$\delta^{13}C_{dolomite} = \frac{X_a\left(\delta^{13}C_a + 10^3 \ln a^{dolomite}_{fluid\ A}\right) + P\left(1 - X_a\right)\left(\delta^{13}C_b + 10^3 \ln a^{dolomite}_{fluid\ B}\right)}{P + X_a - PX_a}. \quad \text{(Eqn. 9.1)}$$

$$\delta^{18}O_{dolomite} = \delta^{18}O_b + 10^3 \ln a^{dolomite}_{H_2O} + X_a\left(\delta^{18}O_a - \delta^{18}O_b\right). \quad \text{(Eqn. 9.2)}$$

Fluid A is taken to be Permian sub-polar seawater because during the Early Permian, the Berserker beds, were deposited in subpolar latitudes (Zeigler *et al.*, 1996), and during the Pleistocene glaciation, seawater was enriched by ~ 1.2 ‰ relative to that of modern day seawater (Shackelton and Opdyke, 1973). $\delta^{13}C$ and $\delta^{18}O$ values of +0 and +1.2 ‰ respectively were used for the composition of fluid A. The 5°C temperature of fluid A is used as modern seawater temperatures for subpolar regions of similar latitudes are in the range of 1° to 16°C (Rao and Adabi 1992; Rao 1996). The modelled isotope composition of fluid A is consistent with Lake's Creek limestone being precipitated from Permian sub-polar seawater, and this limestone plots at one end of the calculated mixing lines and is HCO_3^- dominant.

Fluid B is modelled with $\delta^{13}C$ = -8 and $\delta^{18}O$ = +2 ‰, a temperature of 200°C, and a CO_2 dominated carbon species. The temperature estimated for fluid B is within the range of calculated and estimated temperatures for the formation of carbonates associated with VHMS deposits. The modelled composition of fluid B is intended to represent a hydrothermal fluid that has had a significant input of juvenile CO_2, however, the CO_2 could either be sourced directly from an exsolving magmatic fluid (Gerlach, 1989; Butterfield *et al.*, 1990; Sedwick *et al.*, 1992) or extracted from basaltic vesicles or glass by the circulating hydrothermal fluid (Craig *et al.*, 1987; Wehlan *et al.*, 1987). The estimated $\delta^{13}C$ value of fluid B is within the range of $\delta^{13}C$ values (-8 to -5 ‰) for dissolved CO_2 in vent fluids from the Galapagos and the East Pacific Rise at 21°N hydrothermal fields (Taylor, 1987). These values are also consistent with CO_2 being derived from an underlying degassing magma chamber (Taylor, 1986). The $\delta^{18}O$ value chosen for fluid B of 2 ‰ is within the range of $\delta^{18}O$ values (-6 to +4 ‰) for fluids extracted from fluid inclusions in Kuroko VHMS (Pisutha-Arnond and Ohmoto, 1983).

Figure 9.10 shows trends of dolomite isotope values that would be in equilibrium with mixtures of fluids A and B and the relative total dissolved carbon contribution. Modelled fluid mixing trends with lower P values pass through the left-hand field of the WLf whereas higher P-value tend to pass through the MLf but with a greater spread of P-values in the MLf compared to the narrow range of P-values for the WLf. The WLf data plots within trends that have a higher mole fraction of fluid B to fluid A as represented by X_a.

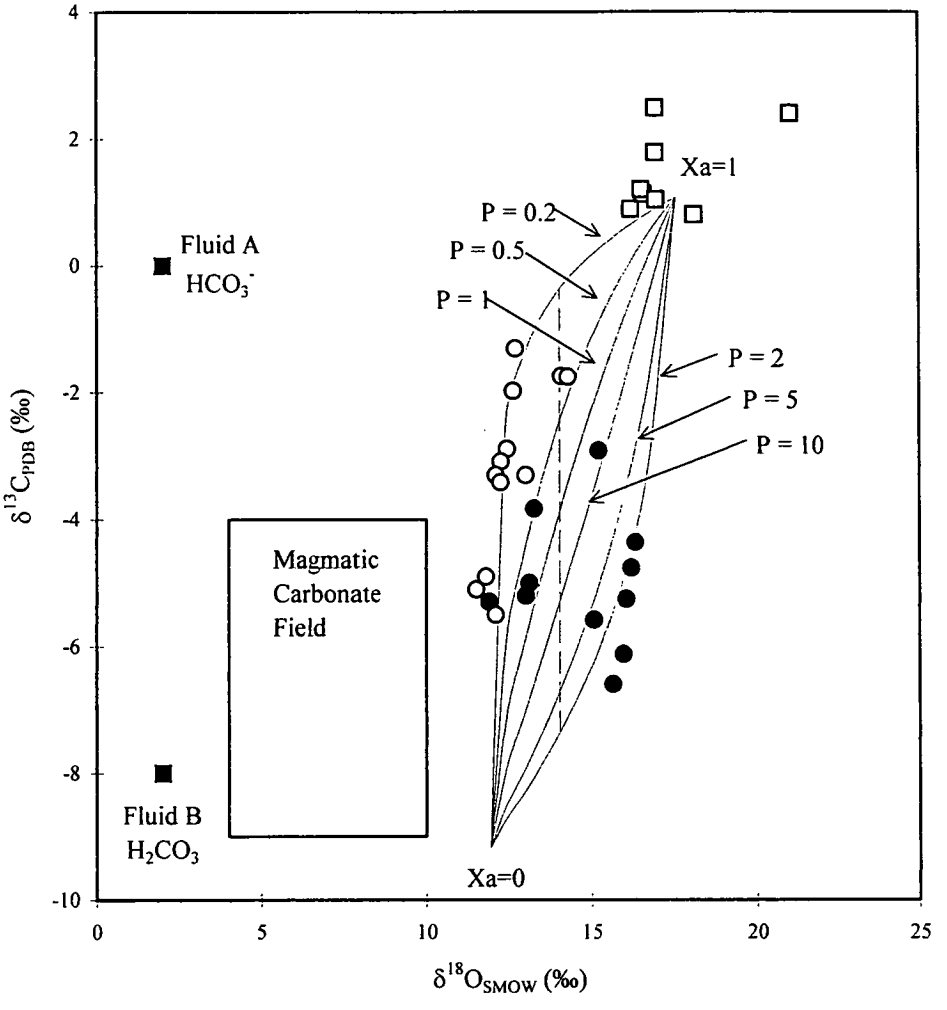

Figure 9.9 Mixing curves for dolomite, carbon and oxygen covariance diagram. Xa = proportion of the fluid A in the fluid mix. P represents the proportion of the carbon content in fluids A and B, so that P = Cb/Ca. The dashed vertical line is where the proportion of fluidA/ fluidB = 0.5 (Xa = 0.5). Fluid A (Permian seawater) = 5° C, $\delta^{18}O$ = 1.2 ‰; $\delta^{13}C$ = 0 ‰ and HCO_3^- is the most dominant carbon species. Fluid B (magmatic fluid) = 200° C, $\delta^{18}O$ = 2 ‰; $\delta^{13}C$ = -8 ‰ and H_2CO_3 is the dominat carbon species. Symbols as per Figure 9.8.

The P10 curve (Fig. 9.10) indicates that there is 10 times the concentration ratio of the total dissolved carbon in fluid B compared to fluid A. In other words the isotopic composition of fluid B is dominated by H_2CO_3 and not HCO_3^-. This dominance of CO_2 over HCO_3^- on the P10 curve may also indicate fluid temperatures were relatively hotter compared to the P1 curve. As at temperatures greater than 100°C, HCO_3^- becomes negligible compared to H_2CO_3 in a hydrothermal fluid (Ohmoto, 1986). The mass balance equations and fluid mixing curves suggest that it is isotopically consistent for the Mount Chalmers dolomites to have been formed by the mixing of two fluids; sub-polar seawater and a hydrothermal fluid containing magmatic CO_2, over a mixing range of 0.2 to 10 for molar proportion of $\frac{\text{Fluid A}}{\text{Fluid B}}$.

9.4.4. Fluid/Rock Interaction

At Mt Chalmers the dolomite is a replacive feature, suggesting interaction between the hydrothermal fluid and the wallrocks. Mass-balance equations of Zheng and Hoefs (1993) are used to model fluid/rock interaction. Equations 9.3 and 9.4 (Zheng and Hoefs, 1993) model the shift in isotopic composition of a fluid caused by 1) the change in temperature, and 2) the change in isotopic composition caused by interaction between a hydrothermal fluid and wallrock.

$$\delta^{13}C_{dolomite} = \delta^{13}C^{i}_{fluid} + 10^3 \ln \alpha^{dolomite}_{fluid} + \frac{R^i}{W^i} \cdot \Delta^{13}C^{i}_{fluid} . \qquad \text{(Eqn. 9.3)}$$

$$\delta^{18}O_{dolomite} = \delta^{18}O^{i}_{fluid} + 10^3 \ln \alpha^{dolomite}_{H_2O} + \frac{R}{W} \cdot \Delta^{18}O^{i}_{fluid} . \qquad \text{(Eqn. 9.4)}$$

The fluid/rock equations of Zheng and Hoefs (1993) (Equations 9.3 and 9.4) are comprised of three components, the first constrain the initial isotopic composition of the fluid (δ^{i}_{fluid}). The second accounts for the isotopic equilibrium fractionation with respect to temperature, fluid species, and precipitate product, and the third term relates to the fluid/rock interaction ($\frac{R}{W} \cdot \Delta^{i}_{fluid}$). The fluid/rock interaction term $\frac{R}{W} \cdot \Delta^{i}_{f}$ (where $\Delta^{i}_{f} = \delta^{i}_{rock} - \delta^{f}_{rock}$) was developed by Zheng and Hoefs (1993) from a simplified equation of Taylor (1977) and represents the change in the isotopic composition of the wall rock due to fluid/rock interaction. In many cases, this value can be measured from the unaltered and altered rocks.

Oxygen isotope analyses from the silica alteration zone beneath the massive sulphide have $\delta^{18}O$ values between ~ +9 to +13 ‰ (Hunns *et al.*, 1993). Using the median of ~+10 for $\delta^{18}O^{i}_{rock}$ and the range of +11.5 to +16.3 ‰ for $\delta^{18}O^{f}_{rock}$ (as measured on the dolomites) constrains $\Delta^{18}O^{i}_{f} = \delta^{i}_{rock} - \delta^{f}_{rock}$ to values between -1 and -6 ‰.

The initial carbon isotope ratio ($\delta^{13}C^{i}_{r}$) of the host-rocks is unknown and thus problematic in the calculation of $\frac{R}{W}\cdot\Delta^{13}C^{i}_{f}$. The pre-replacement lithologies include peperites, sediments, and the base of a basaltic-andesitic intrusion and silica-altered rock. However the package is dominated by volcanics therefore an estimated initial carbon isotope ratio of mantle or average crustal sources is used e.g. $\delta^{13}C \sim -7$ ‰ from Deines and Gold (1973) and Faure (1986). Using these estimates of $\delta^{13}C^{i}_{rock}$ and -1.3 to -6.6 ‰ from the Mount Chalmers dolomite for δ^{f}_{rock}, constrains $\Delta^{13}C^{i}_{f}$ between -5 to 7.5 ‰ and $\Delta^{13}C^{i}_{f} = \delta^{i}_{rock} - \delta^{f}_{rock}$ to values between –1 and -6 ‰.

Interaction of Permian seawater and the host rock would generate trends from the Lakes Creek limestone toward heavier isotope values. This suggests that seawater cannot be the responsible fluid in this mechanism. Figure 9.10 shows the results of fluid/rock modelling of an ascending, hot, hydrothermal fluid and wall rocks. The modelling suggests that the carbon species present within the hydrothermal fluid is less important, but that the carbon isotope ratio of the host lithology is a major influence. The isotopic starting composition of the hydrothermal fluid has the same $\delta^{18}O$ and $\delta^{13}C$ values (+1.2 and -8 ‰ respectively) as those used in the two fluid mixing model discussed above. As the hydrothermal fluids have passed through and reacted with a substantial thickness of igneous rocks. Any igneous carbon values that would have been assimilated into the hydrothermal fluid during the interaction (*e.g.* in fluid inclusions or from vesicles or glass by the circulating hydrothermal fluid) would have had magmatic values (Craig *et al.*, 1987; Wehlan *et al.*, 1987). Therefore the $\delta^{fluid}_{rock} = \delta^{13}C_{fluid} - \delta^{13}C_{rock}$ would have been very small, and the large spread seen in the $\delta^{13}C$ values could not have been generated.

The isotopic composition of fluid A has a lighter $\delta^{13}C$ value in the fluid/rock modelling compared to the initial isotopic composition of fluid B used in the two-fluid mixing model discussed earlier. However, it is still within the range of $\delta^{13}C$ values (-8 to -5 ‰) for dissolved CO_2 in vent fluids from the Galapagos and the East Pacific Rise at 21°N hydrothermal fields (Taylor, 1987). The modelling shows that the trend in the isotopic values for the Mount Chalmers dolomite can be formed by a cooling, ascending hydrothermal fluid reacting with the wallrocks that it passes through. The temperature range at which this interaction can occur over is between ~150° to 250°C. This temperature range is within the range of estimated and calculated temperatures for the formation of hydrothermal carbonates (e.g Huston, 1997).

Degassing of CO_2, where HCO_3^- is dominant over H_2CO_3 in a fluid is not considered to be a viable mechanism for the precipitation of dolomite (especially at elevated temperatures) at Mount Chalmers as HCO_3^- is negligible compared to H_2CO_3 in a hot (>200°C) hydrothermal fluid.

The removal of CO_2 for instance from the solution by boiling raises the pH of the fluid. The increase in pH causes more HCO_3^- to dissociate to H^+ and CO_3^{2-}, and the increased activity of the carbonate may cause carbonate precipitation (Rimstidt, 1997). Therefore, increasing pH of the hydrothermal fluid is considered a possible mechanism for the precipitation of the dolomites at Mount Chalmers.

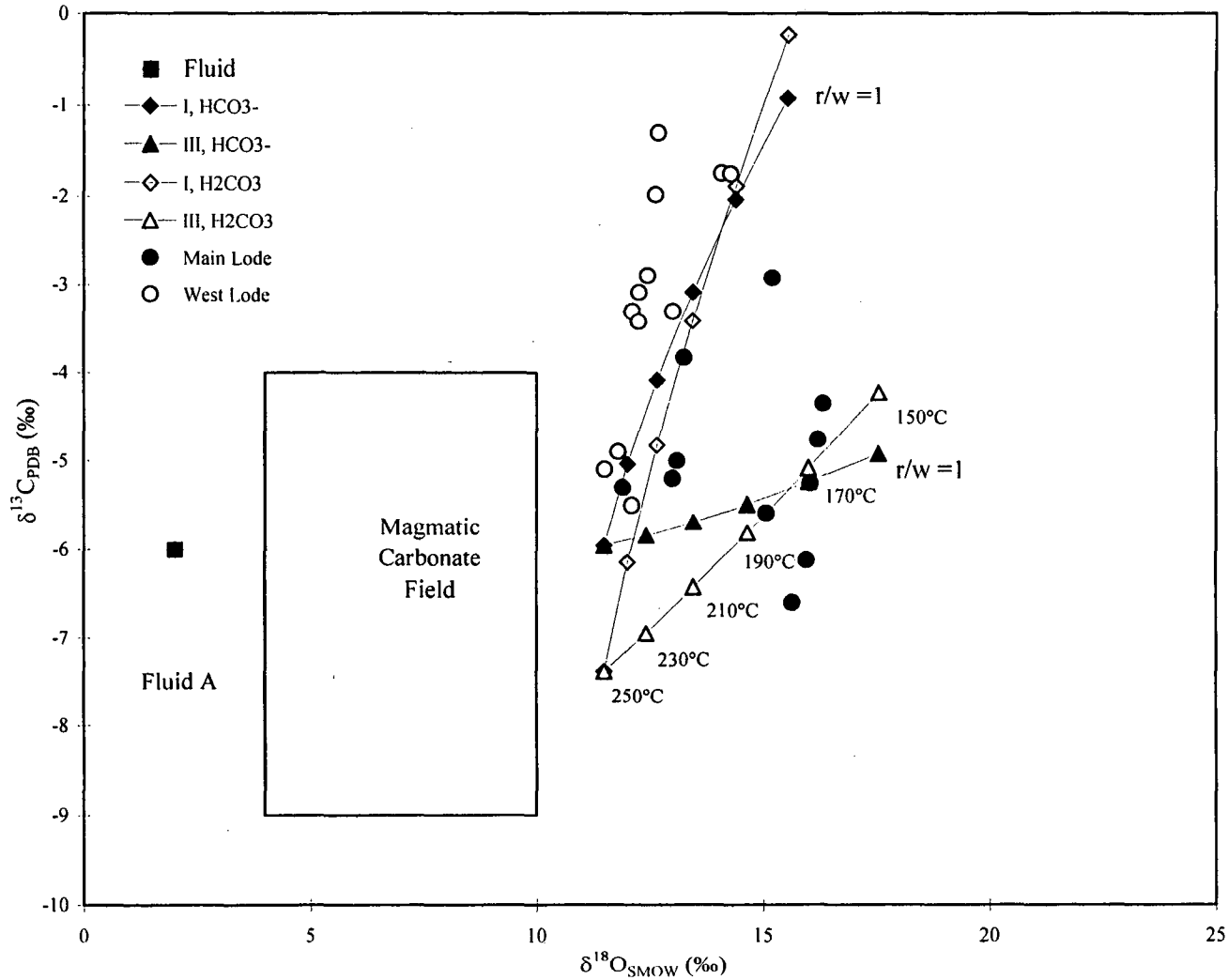

Figure 9.10. Carbon vs. Oxygen isotope variations of dolomite precipitated by fluid/rock interaction with progressively decreasing rock/water (r/w) and for a simultaneous change in temperature for either HCO_3^- or H_2CO_3 as the dominant dissolved carbon species. The curves were calculated under the following conditions: Fluid I: $\delta^{13}C_r^i$ - $\delta^{13}C_r^f$ 0 4 ‰ , $\delta^{18}O$ = -2 ‰; Fluid II: $\delta^{13}C_r^i$ - $\delta^{13}C_r^f$ = 0 ‰, $\delta^{18}O$ = -2 ‰. Symbols as per Figure 9.8

Circulating seawater under water-dominated conditions will not deposit carbonates during its descent into rock bodies. Thus, carbonates that are found coexisting with other alteration minerals in seafloor basalts must reflect low temperatures of alteration, as their stable isotope compositions commonly imply (Bischoff and Seyfried, 1978). The formation of dolomite in preference to calcite requires that Mg/Ca >1. Seawater loses Mg and to a lesser extent Ca upon heating. If the Ca was being depleted in a seawater derived circulating hydrothermal fluid, then Ca depletion must have been greater than that compared to modern day fluids, additionally the lithologies that the fluid passed must have also been depleted in Ca with respect to Mg.

Potential sources for the Mg required to form the Mount Chalmers dolomites include: Mg-bearing igneous silicates, chlorites related to an earlier hydrothermal alteration phase or high Mg, calcite-bearing, limestone.

9.5. SOURCE(S) OF MG AND CA CATIONS FOR DOLOMITE FORMATION: POSSIBLE ROLE OF SEAWATER

Modern-day seawater has a Mg content of ~ 53.0 mmol/kg (Krauskopf, 1979; Gill, 1989), whereas the Mg content of end-member hydrothermal fluids in modern day hydrothermal fluids is near zero (Koski *et al.*, 1985; Von Damm *et al.*, 1985A; Von Damm *et al.*, 1985B; Butterfield *et al.*, 1990; Butterfield *et al.*, 1994). In a convecting hydrothermal cell, seawater is modified by progressive heating and water rock interactions during its descent, leading to a loss of Mg^{2+}, Sr^{2+}, $SO_4^{=}$ and some Ca^{2+} (Bischoff and Dickson, 1975; Mottl and Holland, 1978; Butterfield *et al.*, 1994; Franklin, 1996). Experimental studies have shown that seawater becomes increasingly acid and depleted in Ca^{2+}, Mg^{2+}, and $SO_4^{=}$ as anhydrite and a magnesium oxysulfate are precipitated from seawater progressively heated to 350°C (Bischoff and Seyfried, 1978). This depletion of Mg^{2+} from seawater is thought to be the cause of the enrichment in Mg in alteration halos around VHMS deposits in felsic terranes (Urabe *et al.*, 1983; Franklin, 1996). The depletion in Mg from seawater therefore indicates that the Mg required for the formation of dolomite within VHMS ores cannot be sourced from modified circulating seawater alone, if at all.

However, hydrothermal fluids enriched in Mg^{2+} have recently been reported from hydrothermal vents associated with the Kasuga Seamounts, Northern Mariana Arc (27 % relative to ambient seawater), and the DESMOS caldera located in the eastern Manus Basin, Papua New Guinea (46 to 52 m*M*). The addition of Mg^{2+} is thought to be the result of interaction between CO_2 and igneous minerals or alteration phases (McMurty *et al.*, 1993; Gamo *et al.*, 1997). Mg^{2+} in Mount Chalmers may have also been derived from a CO_2 charged fluid-attacking limestone composed of high-Mg calcite or a dolomite deep within the footwall stratigraphy.

The Ca content of modern-day seawater is ~ 10 mmol/kg (Krauskopf, 1979; Gill, 1989), and of modern-day hydrothermal vent fluids varies between 10 to 81 mmol/kg (Von Damm *et al.*, 1985B; Sedwick *et al.*, 1992; Butterfield *et al.*, 1994; Campbell *et al*, 1994). For the Middle Valley hydrothermal vents, Butterfield *et al.*(1994) concluded that the excess Ca in the vent fluids

(compared to seawater) was derived from the interaction of circulating seawater with basalt. However at the Virgin Mound (Juan De Fuca Ridge) vent fluids are undersaturated in Ca. The Ca depletion at this site is attributed to the subsurface mixing (and subsequent cooling of the hydrothermal fluid) with cold alkaline seawater, resulting in the precipitation of anhydrite (Butterfield *et al.*, 1990).

9.6. CONCLUSIONS

The dolomite at Mount Chalmers forms semi-massive to massive lenses that occur beneath, above and lateral to the massive sulphide mineralisation. The dolomite occurs in two general modes, as massive dolomite and as late-stage veins, that crosscut both the footwall and hangingwall lithologies. Within the massive dolomite there are at least four generations: Dolomite texture 1 - anhedral to rhombohedral very fine-grained cloudy dolomite; Dolomite texture 3 – radiating blades of cloudy dolomite; Dolomite Texture 3 - overgrowths of clear rhombohedral dolomite on the cloudy dolomite; Dolomite Texture 4 - mosaics of interlocking subhedral clear dolomite within the cloudy dolomite. The cloudy dolomite replaced earlier formed silica alteration and barite blades, but was itself replaced by chlorite, sericite, muscovite and kaolinite. These four dolomite generations are all cut and replaced by a later fifth generation of vein, vugh and fracture-filling dolomite. The presence of five phases of dolomite indicates the formation of the hydrothermal dolomite was an ongoing, albeit episodic hydrothermal process.

Isotopic modelling indicates that there are two possible mechanisms for the formation of the Mount Chalmers dolomite: (1) two-fluid mixing and (2) fluid/rock interaction.

The two-fluid mixing model involves mixing of an ascending hot hydrothermal fluid, charged with juvenile CO_2 with cold seawater. Whether the ascending hydrothermal fluid was chemically- and isotopically modified seawater or magmatic in origin is uncertain. The addition of CO_2 into the hydrothermal fluid may either have been by direct addition of magmatic volatiles or by accumulation during fluid ascent and circulation. The addition of CO_2 to the fluid produced carbonic acid (H_2CO_3) which means that the fluid was able to chemically weather underlying high Mg-calcite bearing limestone, or any igneous rock containing mafic mineral phases, or mafic mineral alteration phases stripping Mg, Fe and Ca. The fluid continued to ascend and eventually precipitated dolomite principally by the exsolution of dissolved CO_2 and H_2O to H^+ and HCO_3^- (Fig. 9.11). The removal of CO_2 from the solution raised the pH of the hydrothermal fluid. The subsequent increase in the pH of the fluid caused HCO_3^- to dissociate to H^+ and CO_3^{2-}, and the increased activity caused carbonate precipitation. This increase in pH of the hydrothermal fluid facilitated the replacement of silica by the precipitating dolomite.

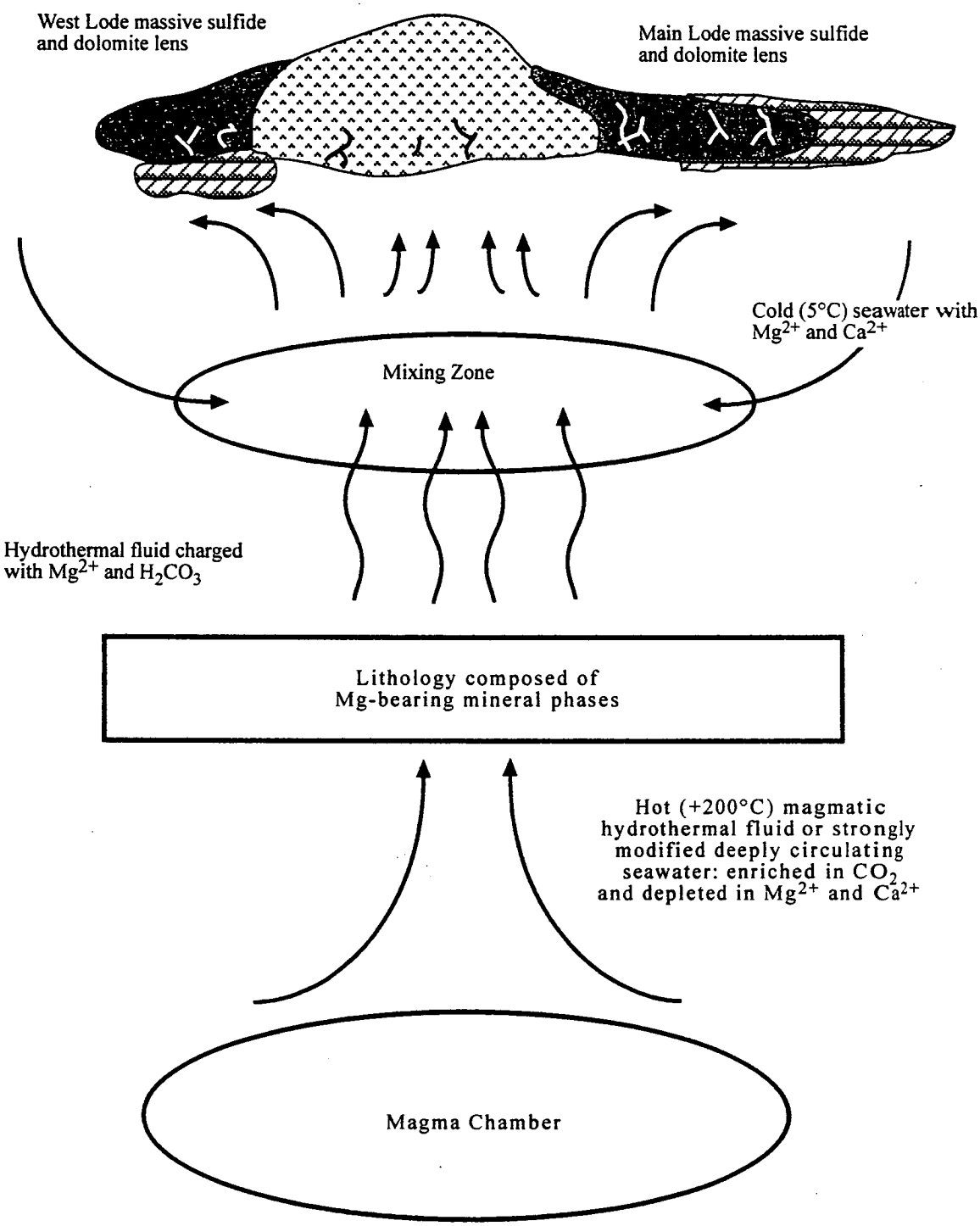

Figure 9.11 Schematic representation of the proposed 2 fluid mixing model for the formation of hydrothermal dolomite at Mount Chalmers.

The fluid/rock interaction model involves an ascending hot, but cooling hydrothermal fluid reacting with the wallrocks during its passage. Like the two-fluid mixing model discussed above, it is debatable as to whether the hydrothermal fluid was derived purely from a magmatic source or from chemically and isotopically modified seawater. The isotopic composition of the hydrothermal fluid is identical to fluid B in the two-fluid mixing model. The ascending hydrothermal fluid is charged with CO_2 and depleted in Mg^{2+} and Ca^{2+}. As the fluid reacted with the wallrocks, it underwent isotopic re-equilibration. During this process Mg and Ca are also stripped from the wallrocks, thus providing the necessary ions required for the formation of dolomite (Fig. 9.12). As in the two-fluid mixing model the removal of CO_2 from the solution raised the pH of the hydrothermal fluid, causing HCO_3^- to dissociate to H^+ and CO_3^{2-}, and the increased activity caused carbonate precipitation.

The isotopic modelling for the Mount Chalmers dolomite indicates that the fluids responsible for their formation were not derived either from a purely magmatic or seawater source, and that a sedimentary or seawater source was involved to some extent. In both models, the involvement of seawater occurred at or near the site of dolomite precipitation. But, in both cases the involvement of unmodified seawater was minimal.

The favoured model for the formation of the dolomite is the fluid/rock interaction model, as this model adequately explains the range in $\delta^{13}C$ by a cooling fluid and the range in $\delta^{18}O$ values by reacting with the wallrocks. This model is also consistent with geological relationships, in that the dolomite is a replacive phase and therefore, there must have been interaction between the fluid and the wallrocks that it passed through.

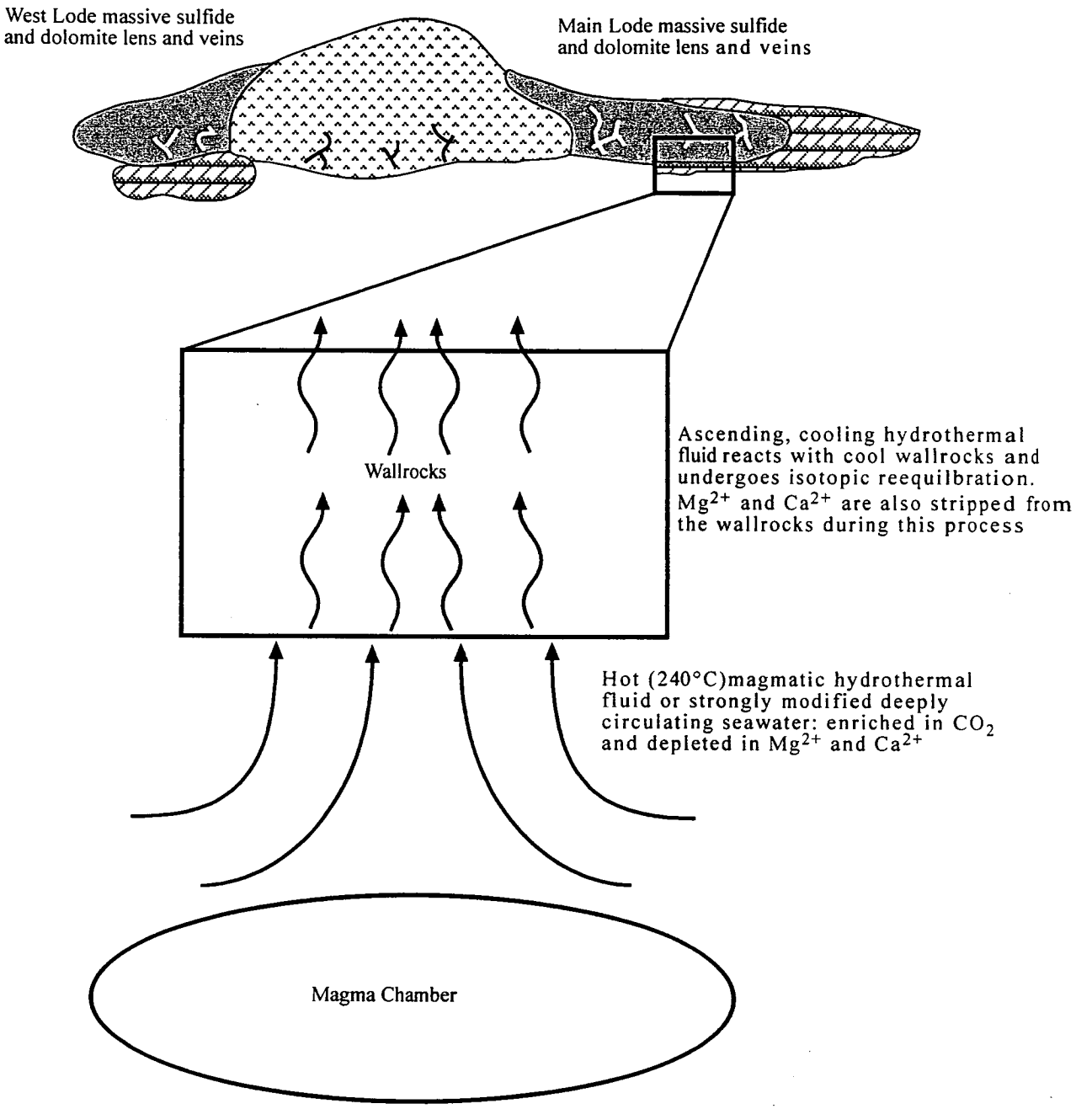

Figure 9.12 Schematic representation of the proposed fluid rock interaction model for the formation of hydrothermal dolomite at Mount Chalmers

CHAPTER 10
SULPHUR ISOTOPES

10.1 INTRODUCTION

In VHMS deposits the Cu, Pb and Zn are generally bound as sulphides, but the sulphur may not have necessarily experienced the same history as other components in the ore-forming fluids (Ohmoto and Goldhaber, 1997). Therefore an understanding of the geochemistry of sulphur through sulphur isotopes may aid in the understanding of the ore forming process, by providing temperature estimates of the ore forming minerals and potentially on the source of sulphur. This is based upon the different sulphur sources such as: igneous, biogenic and seawater sulphur having distinctive $\delta^{34}S$ values and patterns. The spatial variation of sulphur isotopes from VHMS deposits has provided valuable insights into not only the source of the sulphur but also the evolution of hydrothermal fluids through time. However, the mixing of reservoirs and redox reactions preclude the unambiguous resolution of sulphur sources (Huston, 1997).

Sulphur isotopes were determined predominantly for pyrite and chalcopyrite, along with sphalerite, galena and barite from the Mount Chalmers deposit in order to determine the source of the sulphur and to evaluate any possible spatial variation in the isotopic composition of the sulphur.

10.2 METHODS

Sulphide isotopes were determined on A VG Micromass 602D mass spectrometer in the Central Science Laboratory - University of Tasmania. Sulphide separates were drilled from hand specimens, combusted with excess Cu_2O in order to produce SO_2 (Coleman and Moore, 1978; Fritz *et al.*, 1974; Robinson and Kusakabe, 1975). Results have been combined with a database of unpublished sulphide and sulphate values determined for Ross Both (University of Adelaide) at Macquarie University, Australia. The results are presented as standard notation relative to the Cañon Diablo Troilite (CDT).

10.3 RESULTS

The $\delta^{34}S$ values of the sulphide species and barite from Mount Chalmers are shown in Figure 10.1. The range and median $\delta^{34}S$ values for pyrite, chalcopyrite, sphalerite, galena and barite from the Mount Chalmers deposit are listed in Table 10.1.

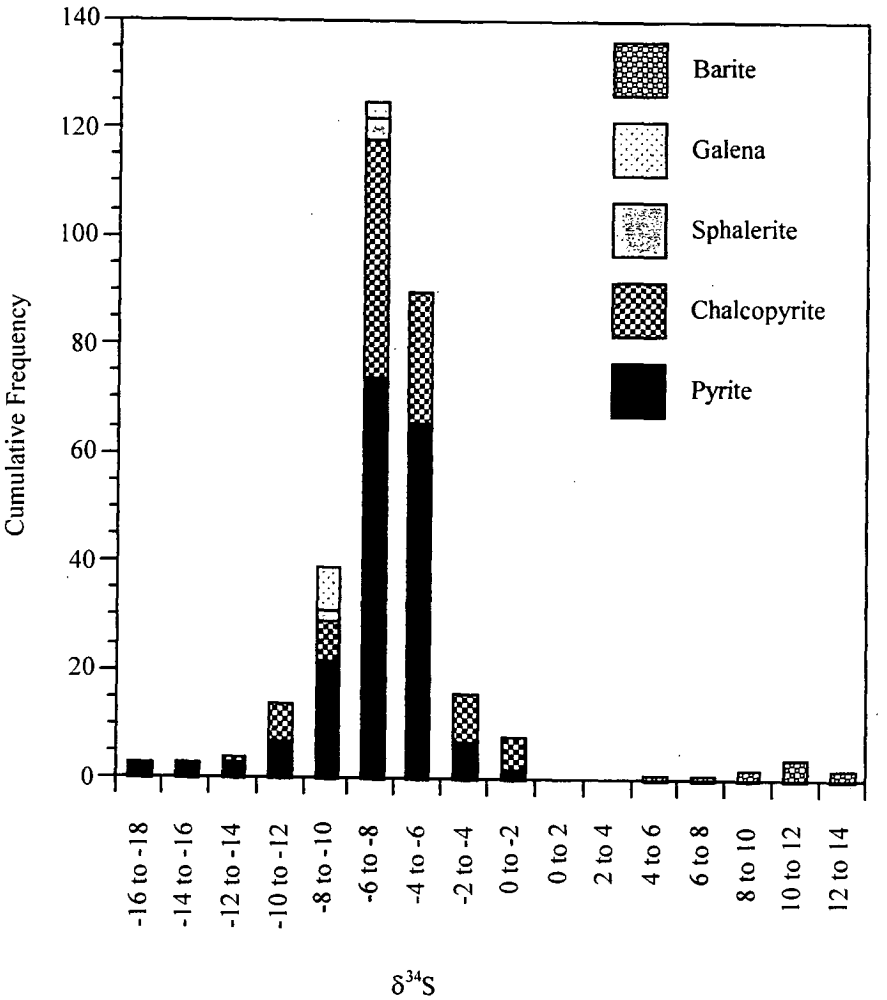

Figure 10.1 Frequency distribution of sulphur isotope values for Mount Chalmers

Table 10.1. Range and median $\delta^{34}S$ values for pyrite, chalcopyrite, sphalerite, galena and barite from Mt Chalmers (MC). Also listed are the range and median $\delta^{34}S$ values for pyrite and chalcopyrite subdivided for the Main Lode (ML) and West Lode (WL) lenses. Median $\delta^{34}S$ value for all samples from Mount Chalmers is -6.2 ‰

	Pyrite $\delta^{34}S$ - ‰ (range)	Chalcopyrite $\delta^{34}S$ - ‰ (range)	Sphalerite $\delta^{34}S$ - ‰ (range)	Galena $\delta^{34}S$ - ‰ (range)	Barite $\delta^{34}S$ - ‰ (range)
MC	-17.6 to -1.6	-13.0 to -3.0	-8.8 to -6.6	-10.0 to -7.5	+5.7 to +12.1
	median = -5.7	median = -6.5	median =-7.9	median = -8.9	median = +10.9
N°. samples	204	93	7	12	12
ML	-17.6 to -1.6	-13.0 to -3.9			
	median = -6.2	median = -6.8			
WL	-17.4 to -2.4	-9.2 to -3.0			
	median = -5.5	median = -6.2			

The $\delta^{34}S$ values for pyrite from Mount Chalmers range from -17.6 to -1.6 ‰, with a median value of -5.7 ‰ (Table 10.1) and has a skewed distribution (Fig. 10.1). Chalcopyrite has a narrower range of $\delta^{34}S$ values compared to that for pyrite (Table 10.1), and therefore the skewness of its distribution is not so pronounced as that for pyrite (Fig. 10.1). Both sphalerite and galena have restricted ranges in their $\delta^{34}S$ values compared to pyrite and chalcopyrite, but galena has a slightly broader range compared to sphalerite (Table 10.1; Fig. 10.1). One of the more obvious features of the range in $\delta^{34}S$ values for the sulphides is that they are all negative. The significance of this will be discussed further in sections 10.4.1.4 and 10.4.2. Barite has a broad range in $\delta^{34}S$ values and has a skewed distribution (Fig. 10.1).

The median $\delta^{34}S$ values of sulphides from the same sample at Mount Chalmers follow the pattern of $\delta^{34}S_{pyrite} > \delta^{34}S_{chalcopyrite} > \delta^{34}S_{sphalerite} > \delta^{34}S_{galena}$, which is somewhat different to isotopic equilibrium pattern documented by Sakai (1968), Ohmoto (1972) and Rye and Ohmoto (1974) of $\delta^{34}S_{pyrite} > \delta^{34}S_{sphalerite} > \delta^{34}S_{chalcopyrite} > \delta^{34}S_{galena}$. As some of the samples from Mount Chalmers do not follow this pattern, then isotopic disequilibrium conditions are thought to have prevailed, at least at the local scale.

10.3.1 Sulphides

10.3.1.1 $\delta^{34}S$ Values for Pyrite and Chalcopyrite Habits

Figures 10.2 a and b show the $\delta^{34}S$ values for pyrite and chalcopyrite plotted with respect to the three broad habits that they occur in; massive sulphide, in veins or as fine or coarse grained disseminations. The $\delta^{34}S$ values for pyrite within the massive sulphide have a narrow range between -10 to -4 ‰. The $\delta^{34}S$ values for the disseminated pyrite have a similar range compared to that of the massive sulphides. Whereas the $\delta^{34}S$ values for the vein pyrite shows a far greater spread in values from -18 to -1 ‰. Like the vein pyrite, the vein chalcopyrite also displays a wide spread in the $\delta^{34}S$ values (-14 to -4 ‰).

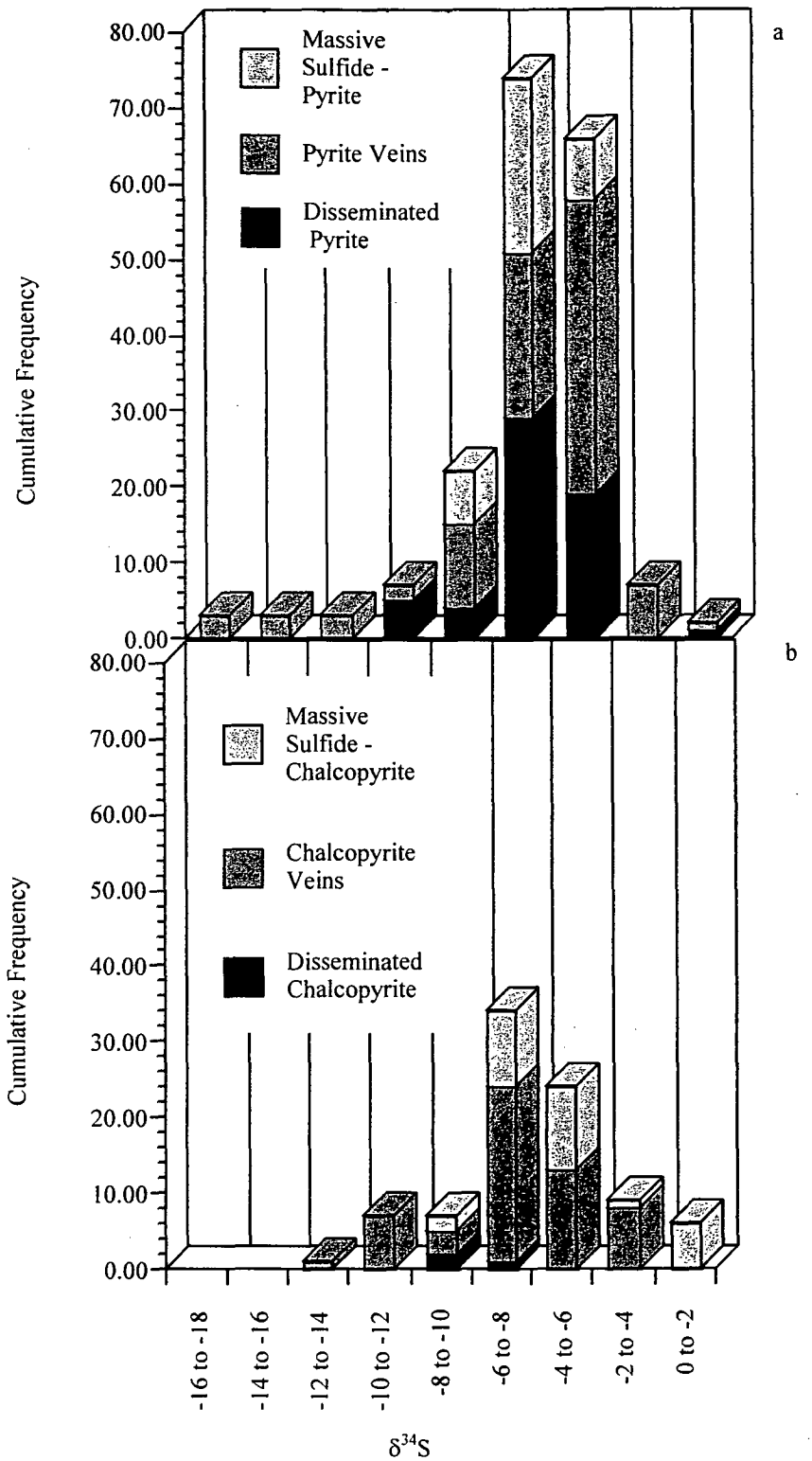

Figure 10.2. Frequency histograms for sulphur isotope values for pyrite (a) and chalcopyrite (b) versus the three broad habits that they occur in *i.e.* massive sulphide, disseminated and veined sulphide.

Whereas unlike the massive sulphide pyrite the $\delta^{34}S$ values for the massive sulphide chalcopyrite are not so tightly constrained. The $\delta^{34}S$ values for chalcopyrite are also skewed towards heavier values compared to the $\delta^{34}S$ values for pyrite.

10.3.1.2 Spatial Distribution of $\delta^{34}S$ Values

Table 10.1 also lists the range and median values for pyrite and chalcopyrite with respect to which of the massive sulphide lodes they occur in i.e the Main Lode or the West Lode. The distribution in $\delta^{34}S$ for both pyrite and chalcopyrite from the Main Lode and the west Lode are illustrated in Figure 10.3. The range in $\delta^{34}S$ values for pyrite for the Main Lode and the West Lode are similar, although the Main Lode has a slightly lighter median value (Table 10.1 and Fig. 10.3). Chalcopyrite has a slightly narrower range of -13.0 ‰ to -3.0 ‰ compared to pyrite. The Main Lode has a broader $\delta^{34}S$ range of -13.0 to -3.9 ‰ compared to -11.2 to -3.0 ‰ for the West Lode (Table 10.1 and Fig. 10.3). The Main Lode and the West Lode both have skewed distribution patterns for $\delta^{34}S$ values of pyrite (Fig. 10.3). Whereas the distribution patterns of $\delta^{34}S$ values for chalcopyrite for the two lodes are different. The Main Lode displays a bimodal distribution in the $\delta^{34}S$ values for chalcopyrite, while the West Lode has a slightly skewed distribution pattern and is more tightly constrained (Fig. 10.3).

10.3.1.3 Pyrite $\delta^{34}S$ Values — Lithology

The $\delta^{34}S$ values both for pyrite and chalcopyrite have been plotted as frequency histograms against the main lithological units that the $\delta^{34}S$ value was obtained from. These have been divided into 3 broad categories:

- 1) "Unaltered" lithologies;
- 2) Mineralisation;
- 3) Alteration.

Table 10.2 lists the $\delta^{34}S$ values for pyrite and chalcopyrite with respect to the broad lithologies, dominant alteration assemblages and styles of mineralisation that the $\delta^{34}S$ values were obtained from. The distribution of these of values are shown graphically in Figures 10.4a and b. Most of the lithologies and alteration phases tend to have a skewed distribution in their $\delta^{34}S$ values.

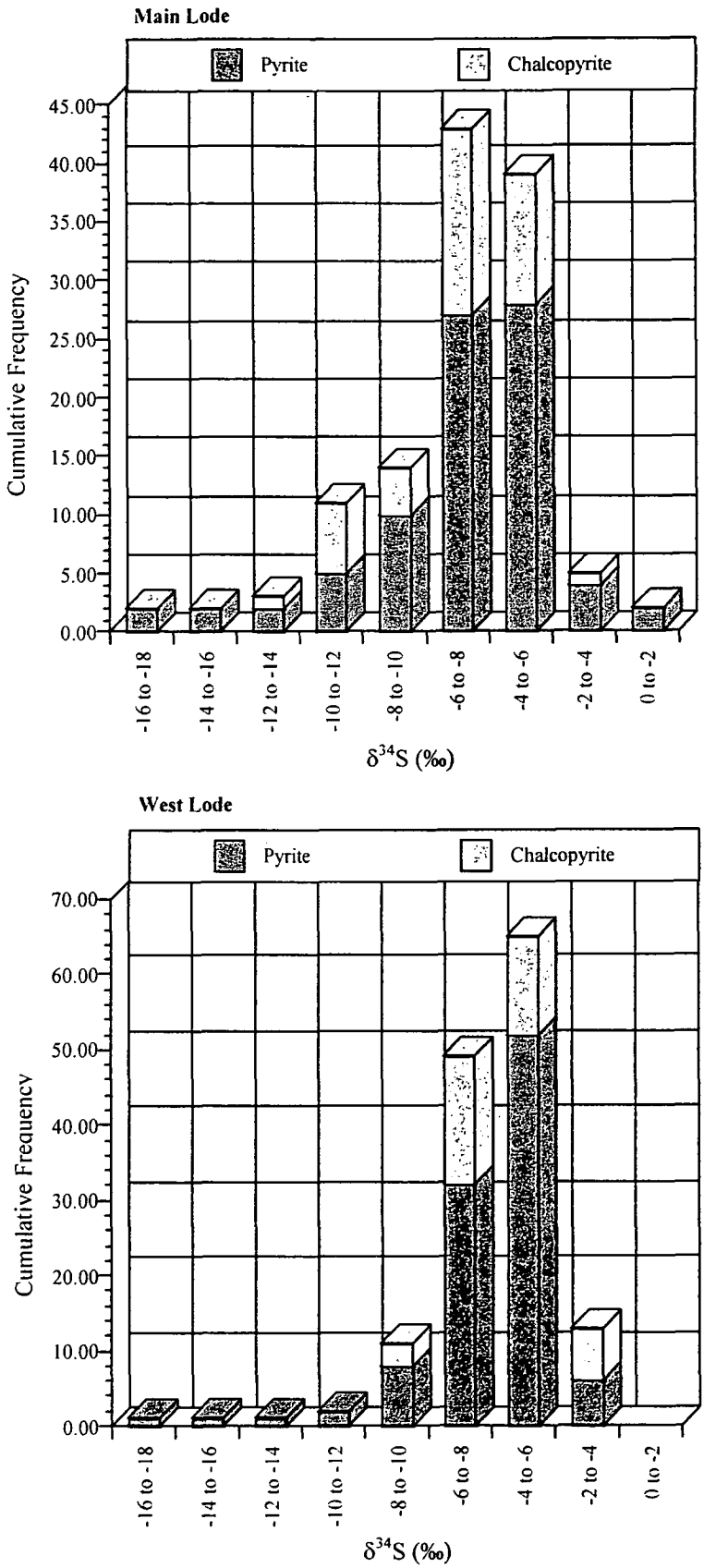

Figure 10.3. Frequency histograms showing the distribution of pyrite and chalcopyrite sulphur isotopes for the Main Lode and the West Lode.

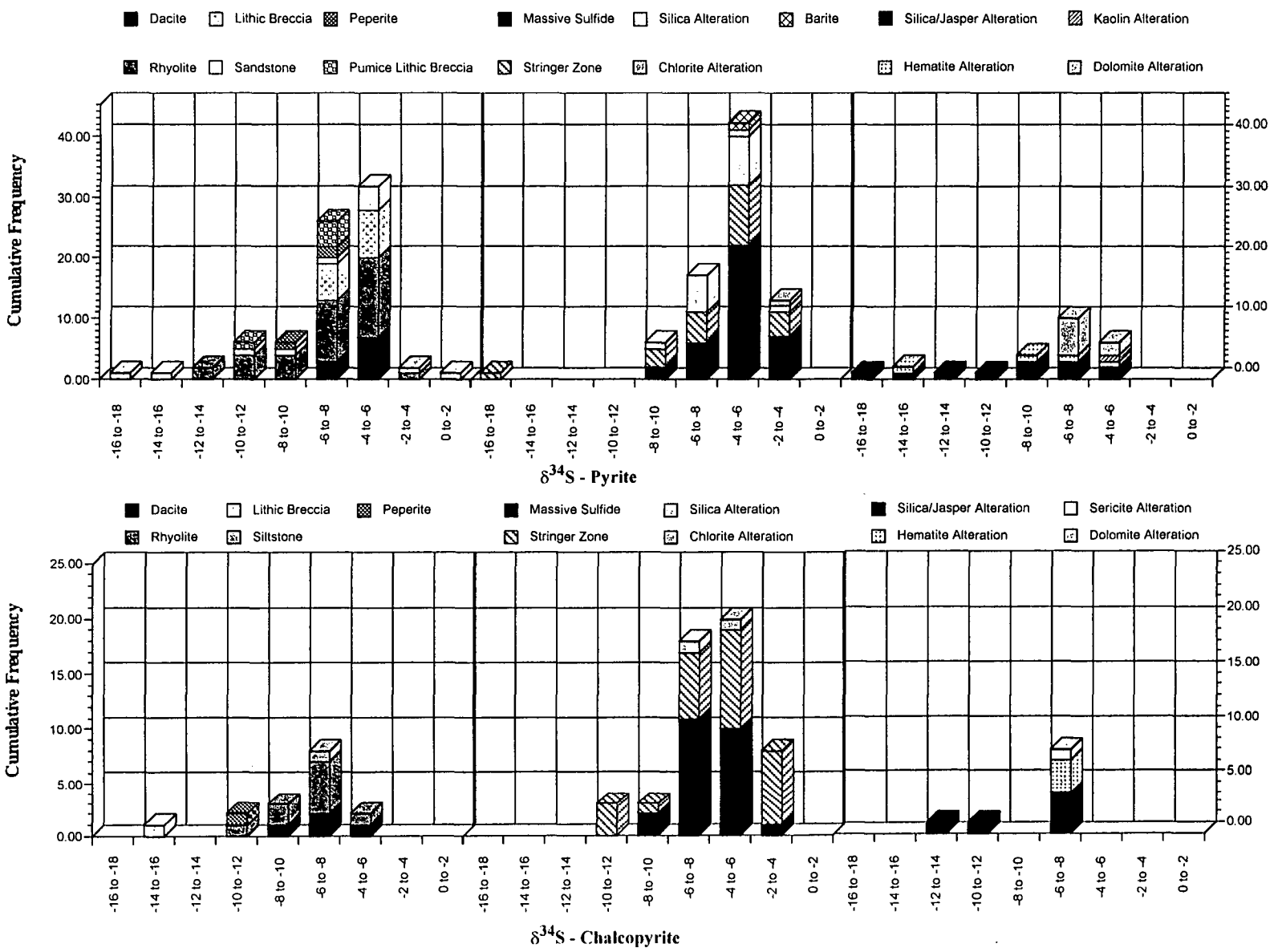

Figure 10.4. Frequency distribution of pyrite and chalcopyrite sulphur isotopes separated on the basis of the lithology that the isotopic value was obtained from.

Table 10.2. Range and median $\delta^{34}S$ values for pyrite and chalcopyrite grouped according to the major lithological, mineralised and alteration association the value was obtained from.

Lithology	Pyrite Range - $\delta^{34}S$ (‰)	Pyrite Median - $\delta^{34}S$ (‰)	N° of Analyses	Chalcopyrite Range - $\delta^{34}S$ (‰)	Chalcopyrite Median - $\delta^{34}S$ (‰)	N° of Analyses
Dacite	-6.9 → -4.7	-5.7	10	-8.2 → -5.6	-7.0	4
Rhyolite	-12.4 → -3.6	-6.6	34	-11.9 → -5.3	-7.3	9
Peperite	-8.8 → -6.7	-6.9	3	-10.8		1
Pumice lithic breccia	-10.5 → -6.2	-6.4	5			
Sandstone	-15.1 → -1.6	-5.5	7	-6.3 → -3.7	-5.1	4
Lithic breccia	-17.4 → -3.0	-6.0	18	-11.5		1
Massive sulphide	-8.5 → -2.1	-5.2	37	-8.5 → -3.1	-6.1	24
Stringer zone	-17.4 → -2.6	-5.7	23	-11.2 → -3.0	-5.0	26
Barite	-4.3		1			
Silica/jasper alteration	-17.6 → -5.6	-8.9	12	-13.0 → -7.0	-7.7	6
Hematite alteration	-15.2 → -5.7	-8.1	4			
Chlorite alteration	-4.5 → -4.0	-4.3	2	-4.4		1
Silica alteration	-8.2 → -4.0	-5.6	16	-9.2		1
Kaolin alteration	-5.9		1			
Sericite alteration	-9.5 → -4.8	-7.3	4	-7.3		1
Dolomite alteration	-7.8 → -5.5	-7.2	8			

Pyrite and chalcopyrite from the massive sulphide mineralisation have a relatively restricted range in their $\delta^{34}S$ values (Table 10.2). The pyrite from the stringer zone displays the greatest spread in $\delta^{34}S$ values, although this spread is the result of two outliers (Fig. 10.4a). Otherwise, the stringer zone values have a comparatively restricted range, comparable to that for majority of $\delta^{34}S$ values for the massive sulphide mineralisation (Fig. 10.4a). Chalcopyrite from the stringer zone displays a slightly broader range in $\delta^{34}S$ values compared to pyrite (Table 10.2 and Figs. 10.4a, b). Pyrite and chalcopyrite from the igneous lithologies (dacite, pumice lithic breccia and peperite) have narrow ranges in their $\delta^{34}S$ values, whereas, sulphides from footwall rhyolite have a much broader range in their $\delta^{34}S$ values (Table 10.2, Figs. 10.4a, b). Pyrite from the sedimentary facies (lithic breccia and sandstone) has the greatest spread in $\delta^{34}S$ values from -17.0 to -1.6 ‰ (Table 10.2). The phyllosilicate alteration assemblages (chlorite, kaolin and sericite) and dolomite have comparatively restricted ranges in their $\delta^{34}S$ values from -9.5 to -4.0 ‰ (Table 10.2) Whereas the $\delta^{34}S$ values for pyrite and chalcopyrite from the Fe-oxide dominated alteration assemblages have significantly broader range between -17.6 to -5.6 ‰ (Table 10.2). The $\delta^{34}S$ values from within the mineralisation types tend to have a more normal distribution in their $\delta^{34}S$ values, with chalcopyrite from the stringer zone showing the greatest spread in $\delta^{34}S$ values. All three groups display considerable spread in the $\delta^{34}S$ values for both pyrite and chalcopyrite but, the median values from these groups have a restricted range between -8.9 to -4.3 ‰. This restricted range in median $\delta^{34}S$ values from all three major groupings suggests that on the deposit scale neither the lithologies, the style of mineralisation or alteration type had a significant impact on the fractionation of the $\delta^{34}S$ values during precipitation of the sulphide species. Further suggesting that the $\delta^{34}S$ values of the sulphide species were largely controlled by the fluid chemistry and not fluid/rock interaction. However, at least at the local scale, where there have been major and rapid excursions to very light $\delta^{34}S$ values it is thought that fluid/rock interaction controlled the fluid chemistry .

10.3.1.4 Pyrite $\delta^{34}S$ Values — Drillhole Cross Sections

Sufficient sulphur analyses, especially on pyrite were collected to enable downhole plots of the $\delta^{34}S$ values versus lithology on both long sections (north-south orientation) and mine cross sections (east-west orientation) to be made. Five east-west cross sections were generated (Figs. 10.5a - 4970 mN; 10.5b - 5010 mN; 10.56c - 5060 mN; 10.5d - 5220 mN and 10.5e -- 5400 mN). Four north-south long sections were generated (Figs. 10.6a - 4840 mE; 10.6b - 4870 mE; 10.6c - 5010 mE and 10.6d - 5110 mE). The east-west cross sections primarily are located to the north of the West Lode massive sulphide mineralisation (Fig. 10.5a), through the Main Lode gossan (Fig. 10.5b) and massive sulphide mineralisation (Fig. 10.5c) and extend up 400 m northwards from the mineralisation (Figs. 10.5d, e). The north-south long sections provide two sections through the West Lode massive sulphide lens (Figs. 10.6a, b) one section through the Main Lode mineralisation (Fig. 10.6c) and one to the east of the mineralisation (Fig. 10.6d).

Both the cross sections and the long sections show that the $\delta^{34}S$ values of pyrite are reasonably consistent and generally fall within the -8 to -4 ‰ range (Table 10.2). The major excursions to lighter $\delta^{34}S$ values tend to coincide were the hydrothermal fluids precipitated pyrite within sedimentary lithologies (pumice lithic breccia, sandstone and lithic breccia), stringer zone and hematite/jasper mineralisation. Within the sedimentary lithologies and the rhyolite, the shifts to strongly negative $\delta^{34}S$ values tend to be a point value. *i.e* there is a rapid and radical isotopic shifts (up to -14 ‰) from "normal" values and then a rapid return to "normal" isotopic values (Figs. 10.5a-MC40; 10.5b-MC35; 10.5c-MC56; 10.6b-MC27A, MC35; 10.6d-MC56, MC69). The hematite/jasper-silica mineralisation shows one of two trends in the shift to very negative $\delta^{34}S$ values. Either there is gradual decline in the $\delta^{34}S$ values (Fig. 10.5b-MC45) or there is a single point departure and then a return to "normal" $\delta^{34}S$ values (Figs. 10.5b, 10.6c-MC63).

The $\delta^{34}S$ values for the massive sulphide, pyrite have a relatively restricted $\delta^{34}S$ range for both the Main Lode and the West Lode (Figs. 10.6b-4870 mE; 10.6c-5010 mE). Figure 10.6b-4870 mE show a north south oriented section through the West Lode mineralisation. In MC25, MC48 and MC27/27A there is a trend to heavier $\delta^{34}S$ values within both the massive sulphide and the stringer zone, and then a return to lighter $\delta^{34}S$ values. To the north of the West Lode massive sulphide, the $\delta^{34}S$ values tend to be with the "normal" range of $\delta^{34}S$ values for Mount Chalmers. Figure 10.6c-5010 mE show a north south oriented section through the Main Lode massive sulphide mineralisation. For MC65, the $\delta^{34}S$ values are very consistent with only one significant shift to heavier $\delta^{34}S$ values. A significant feature of the both the east-west and north-south cross sections show that there is very little if any significant lateral or vertical variation in the $\delta^{34}S$ values of pyrite.

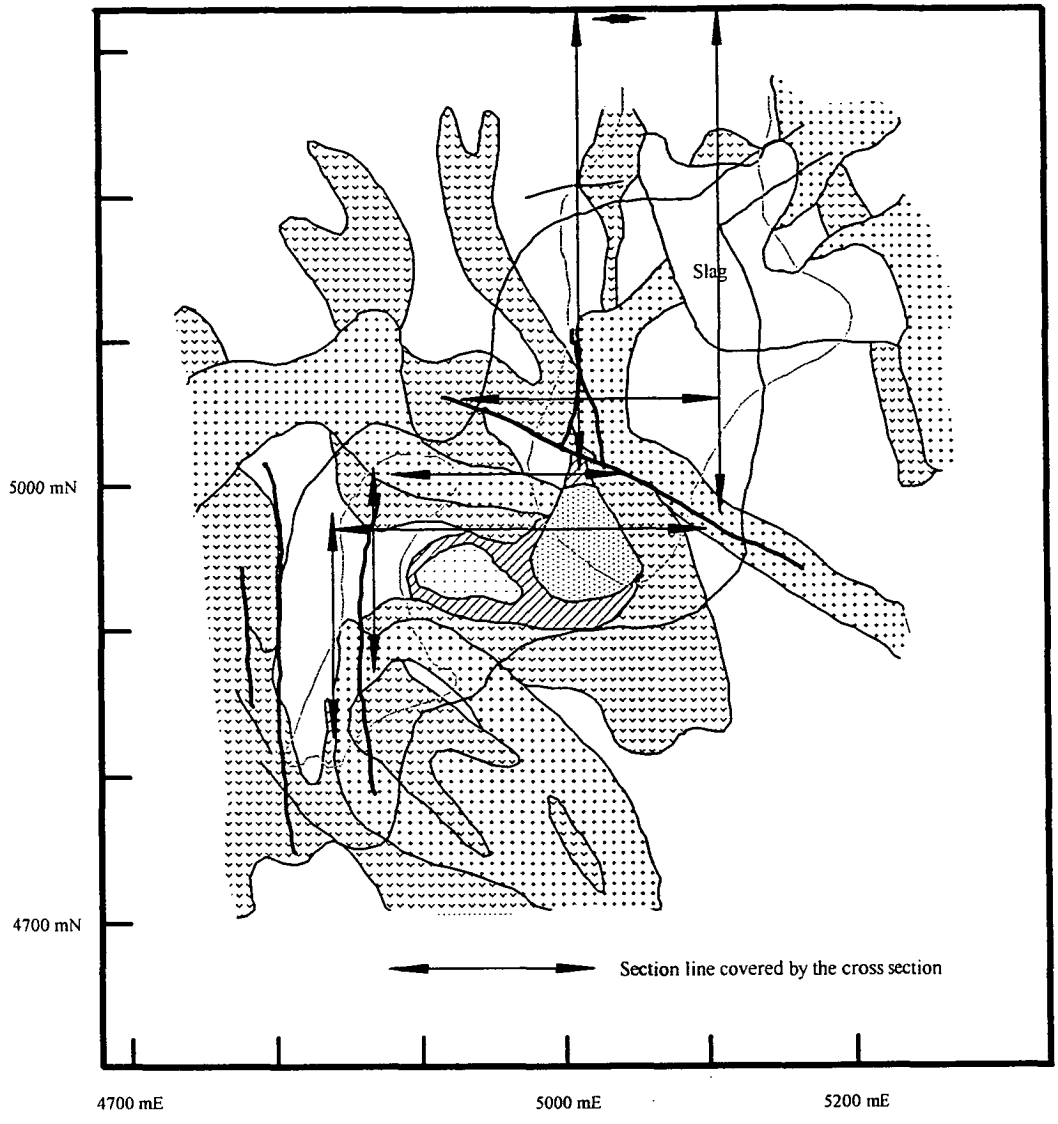

Figure 10.5a. Location of sulphur isotope cross sections.

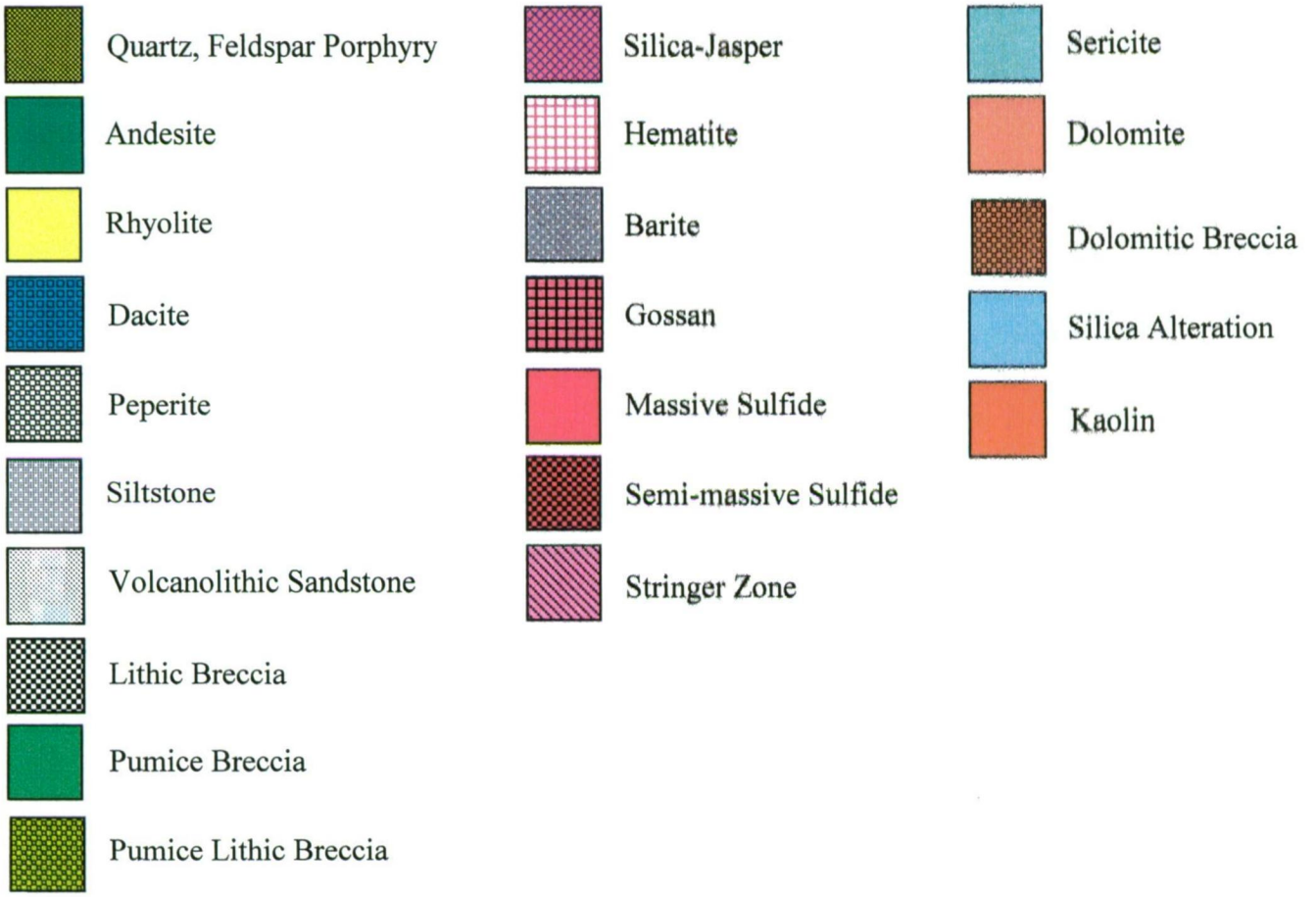

Geological Legend for Figures 10.5b – 10.5f and 10.6a – 10.6d

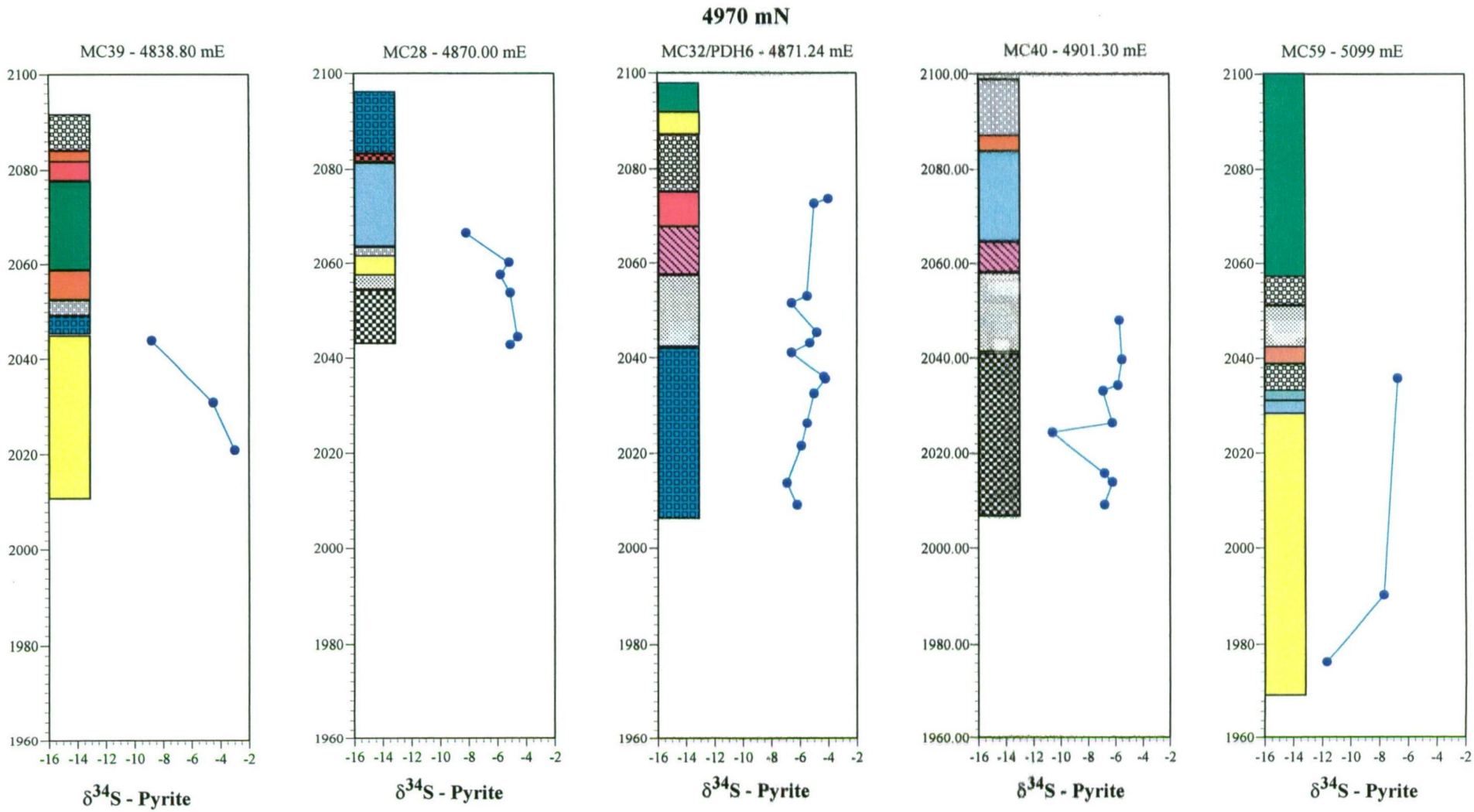

Figure 10.5b. Downhole sulphur isotope variation versus lithology – 4970 mN

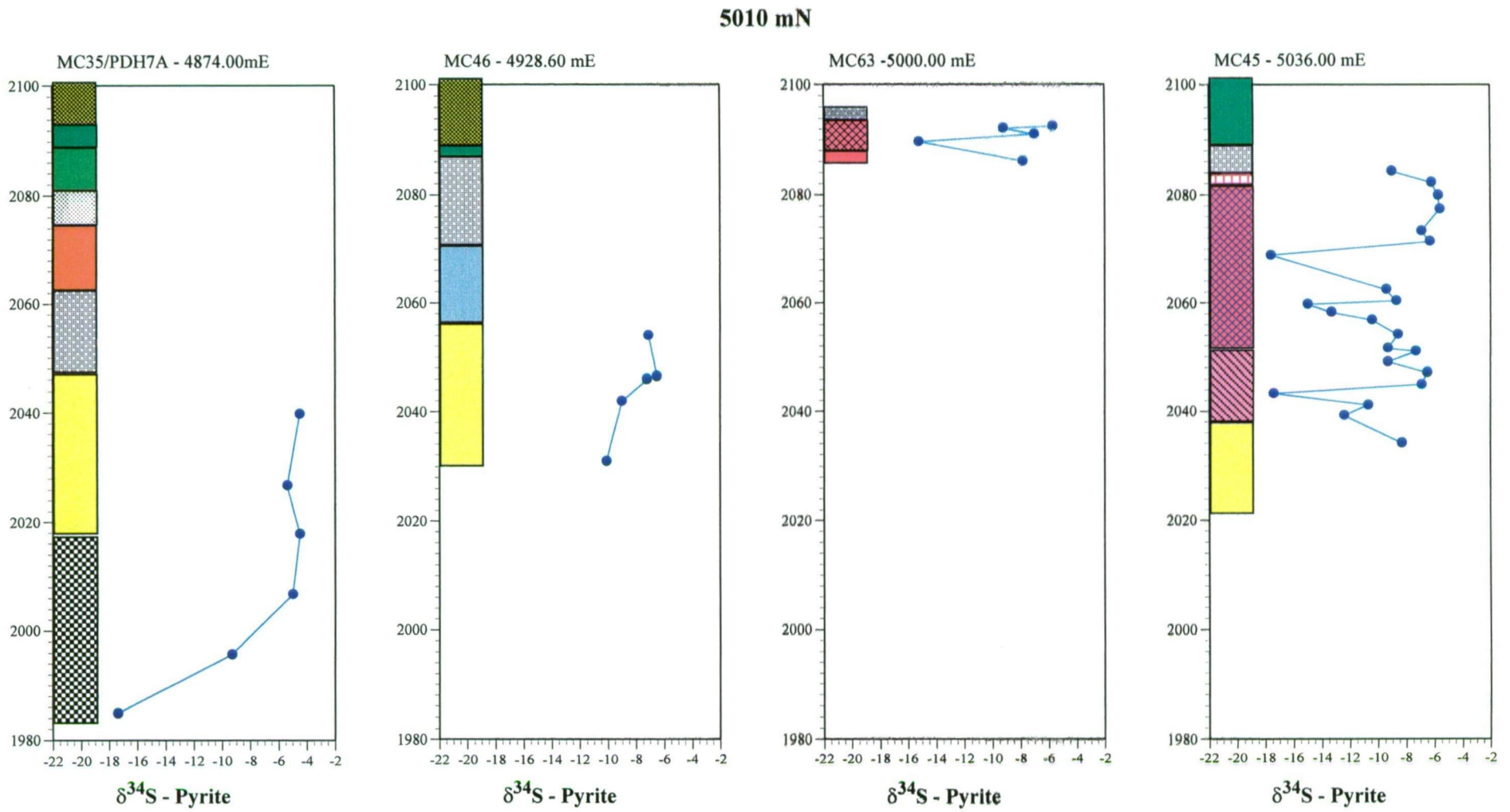

Figure 10.5c. Downhole sulphur isotope variation versus lithology – 5010 mN

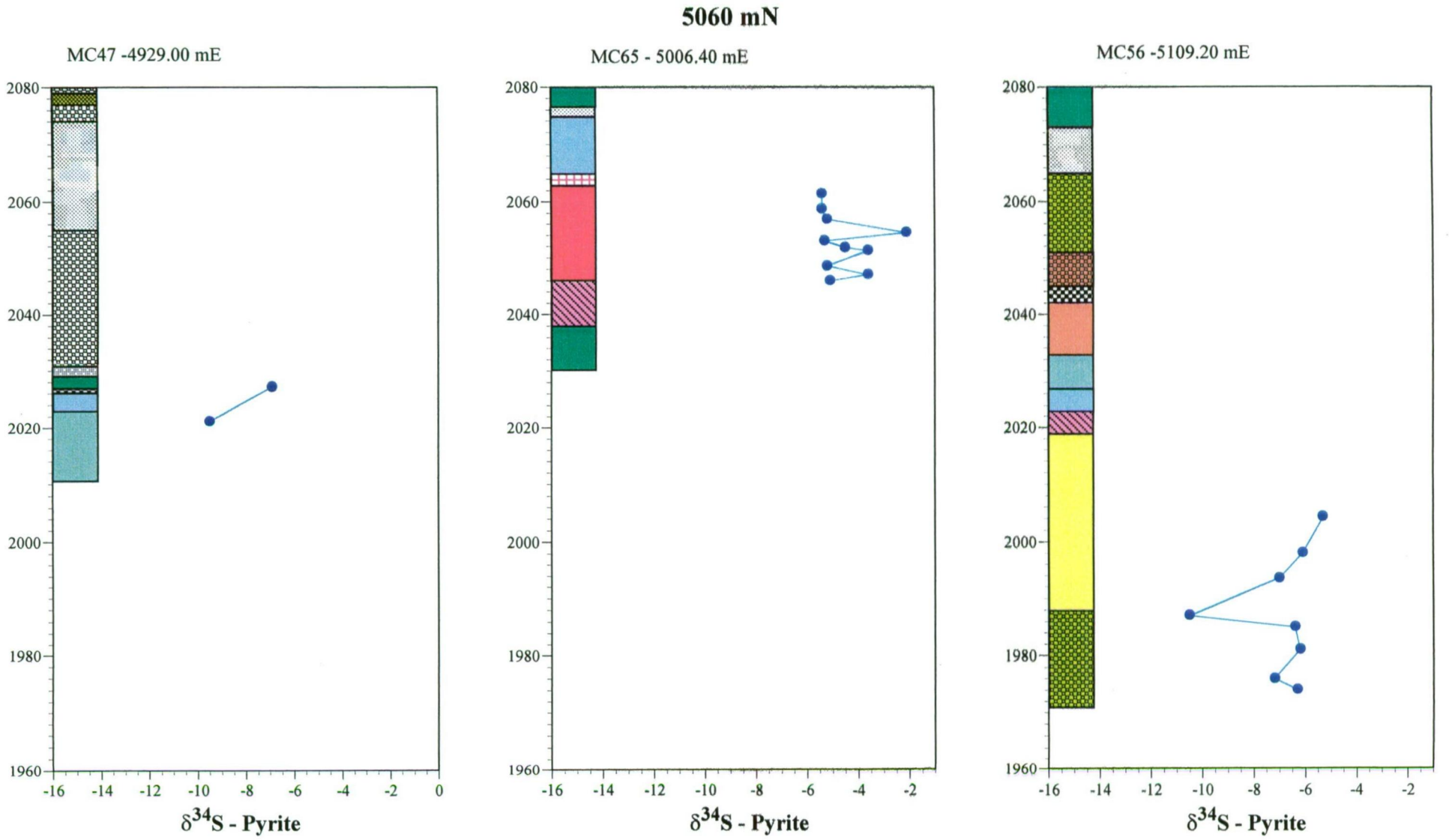

Figure 10.5d. Downhole sulphur isotope variation versus lithology – 5060 mN

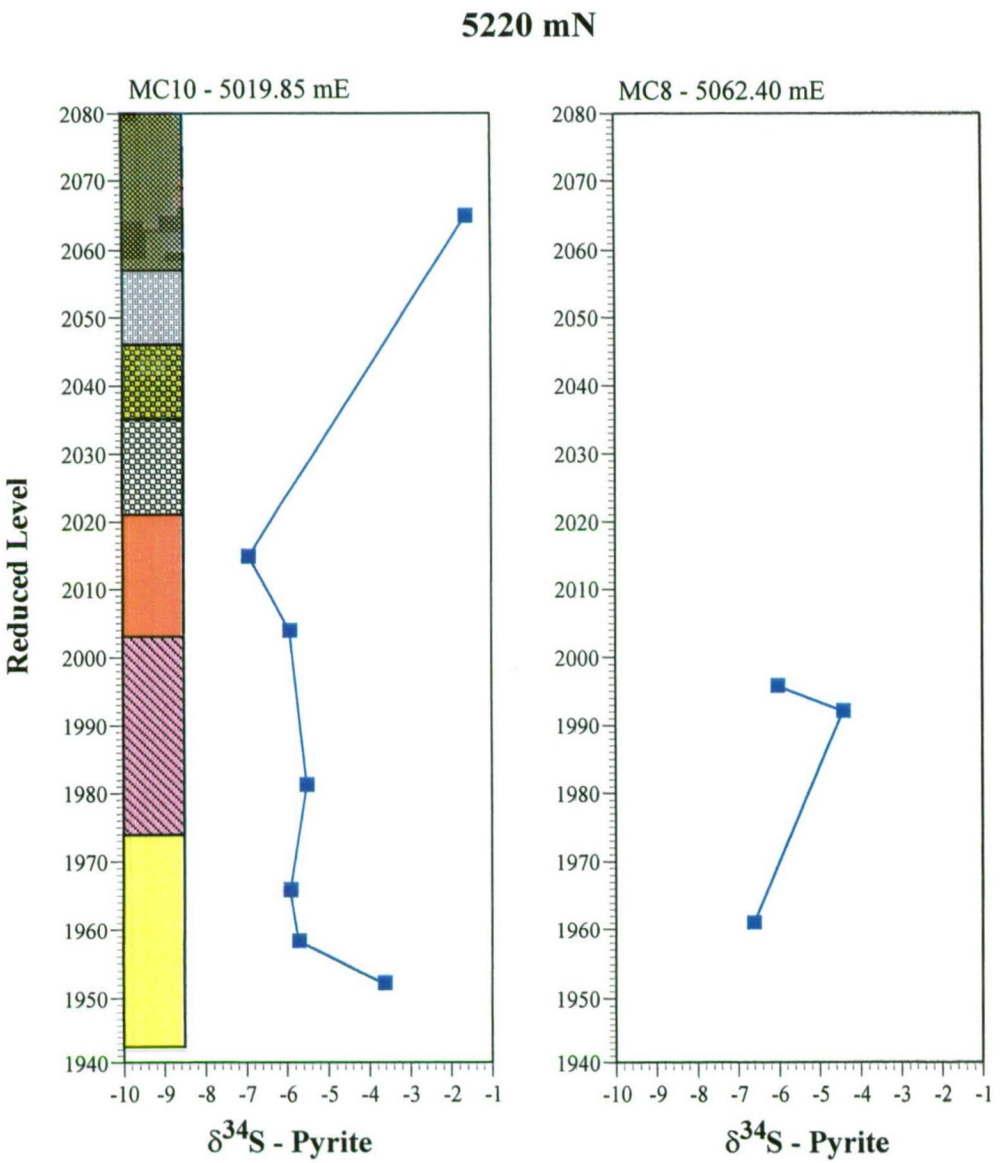

Figure 10.5e. Downhole sulphur isotope variation versus lithology – 5220 mN

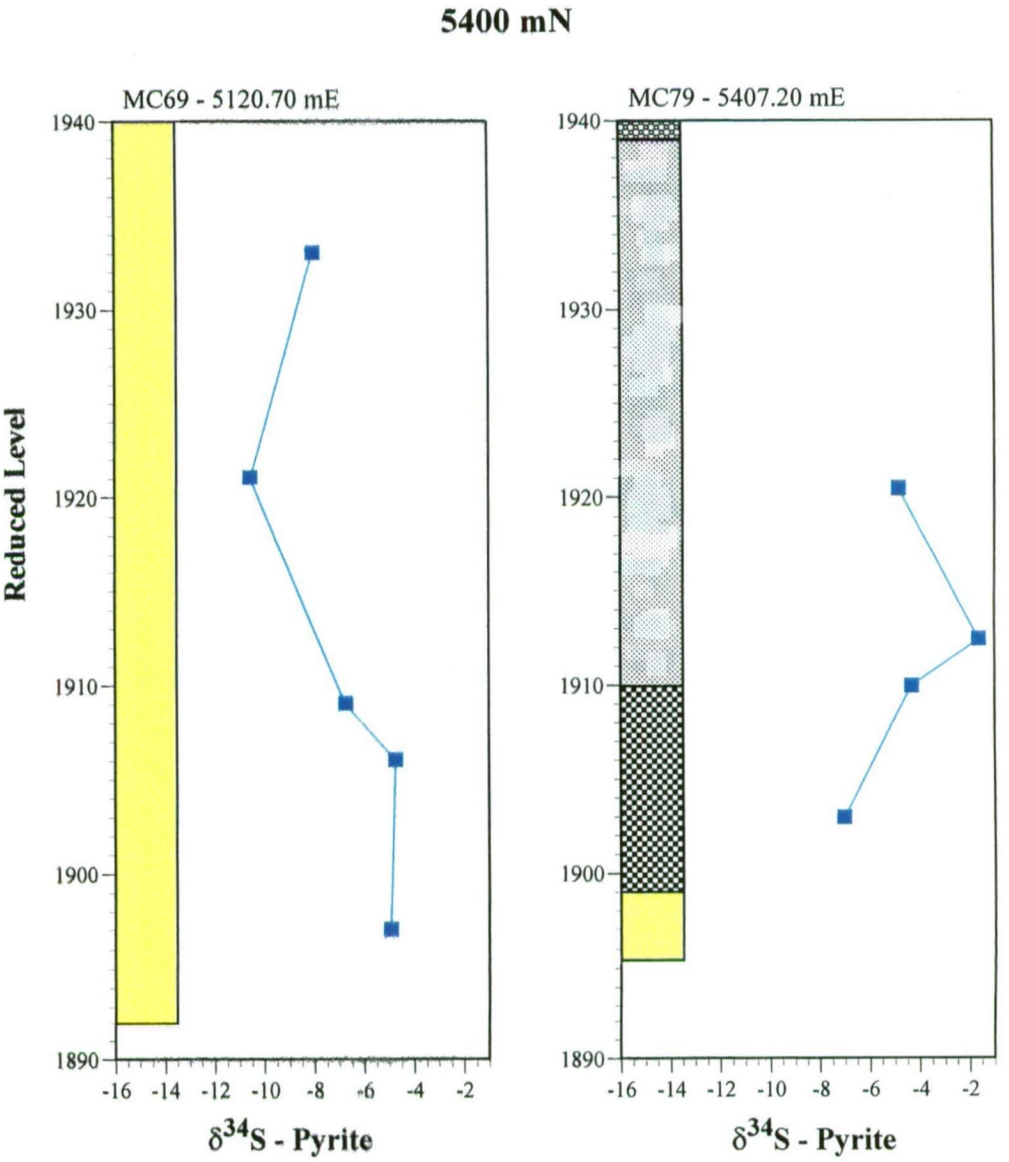

Figure 10.5f. Downhole sulphur isotope variation versus lithology – 5400 mN

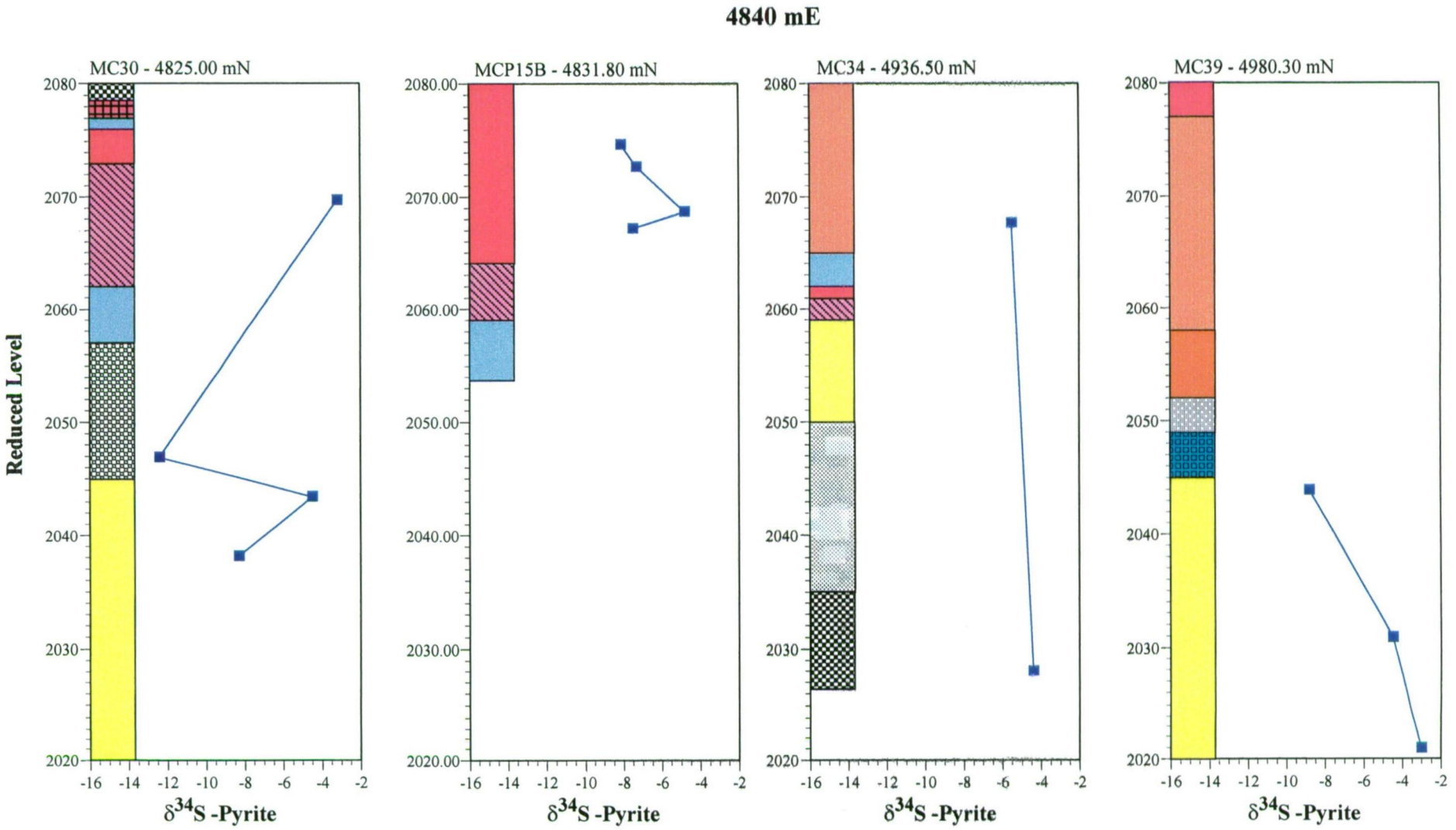

Figure 10.6a. Downhole sulphur isotope variation versus lithology – 4840 mE

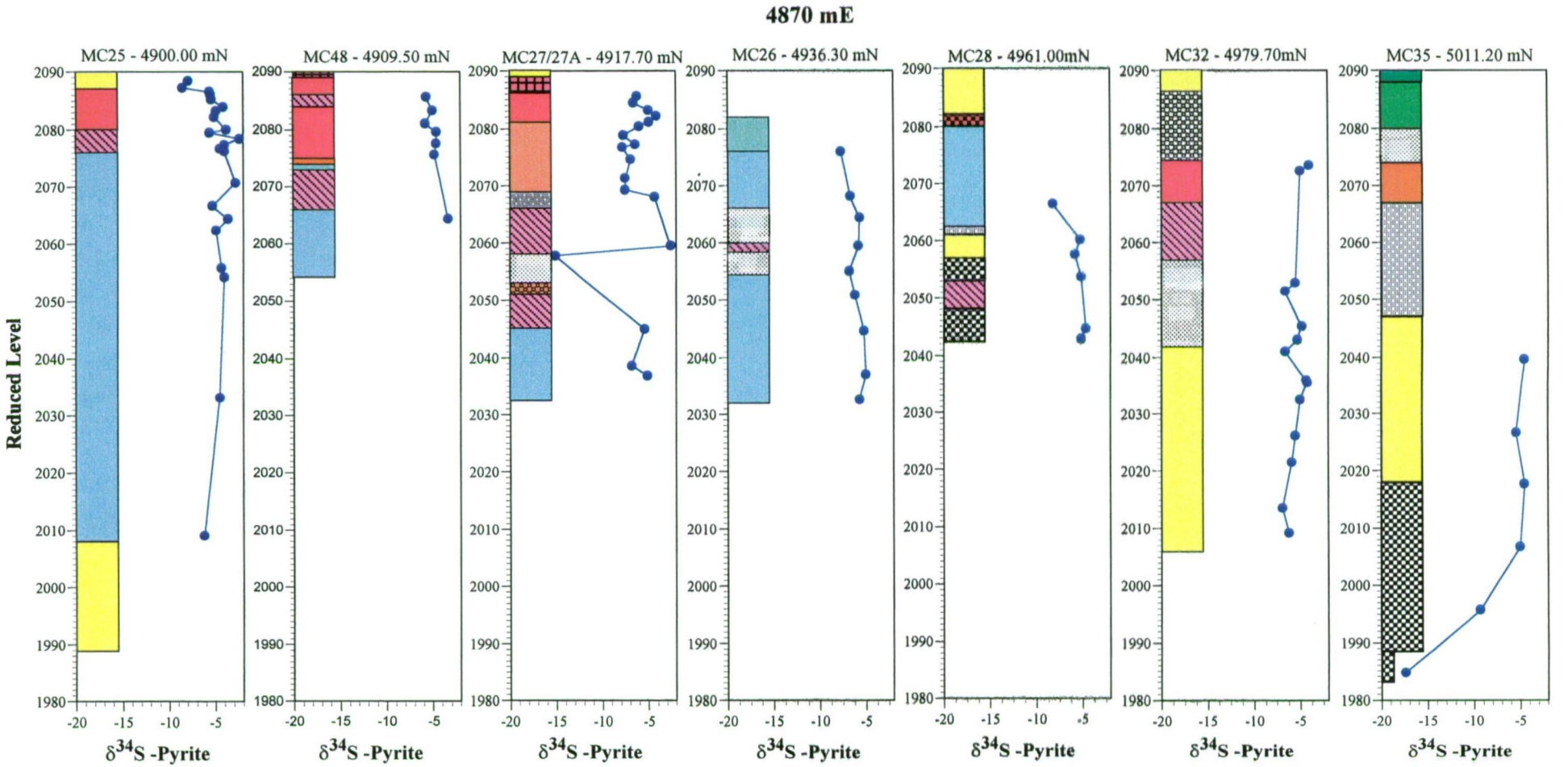

Figure 10.6b. Downhole sulphur isotope variation versus lithology – 4870 mE

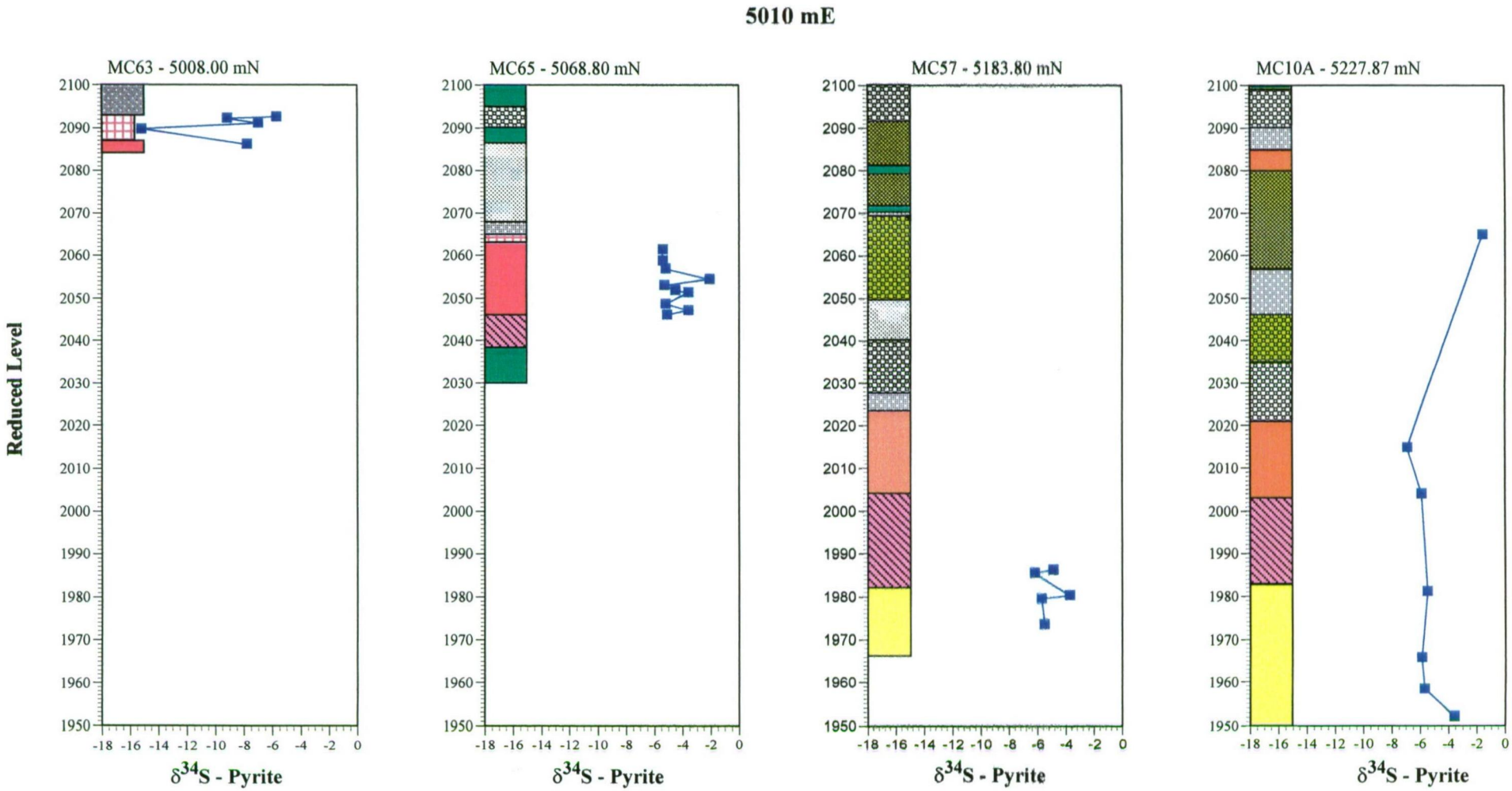

Figure 10.6c. Downhole sulphur isotope variation versus lithology – 5010 mE

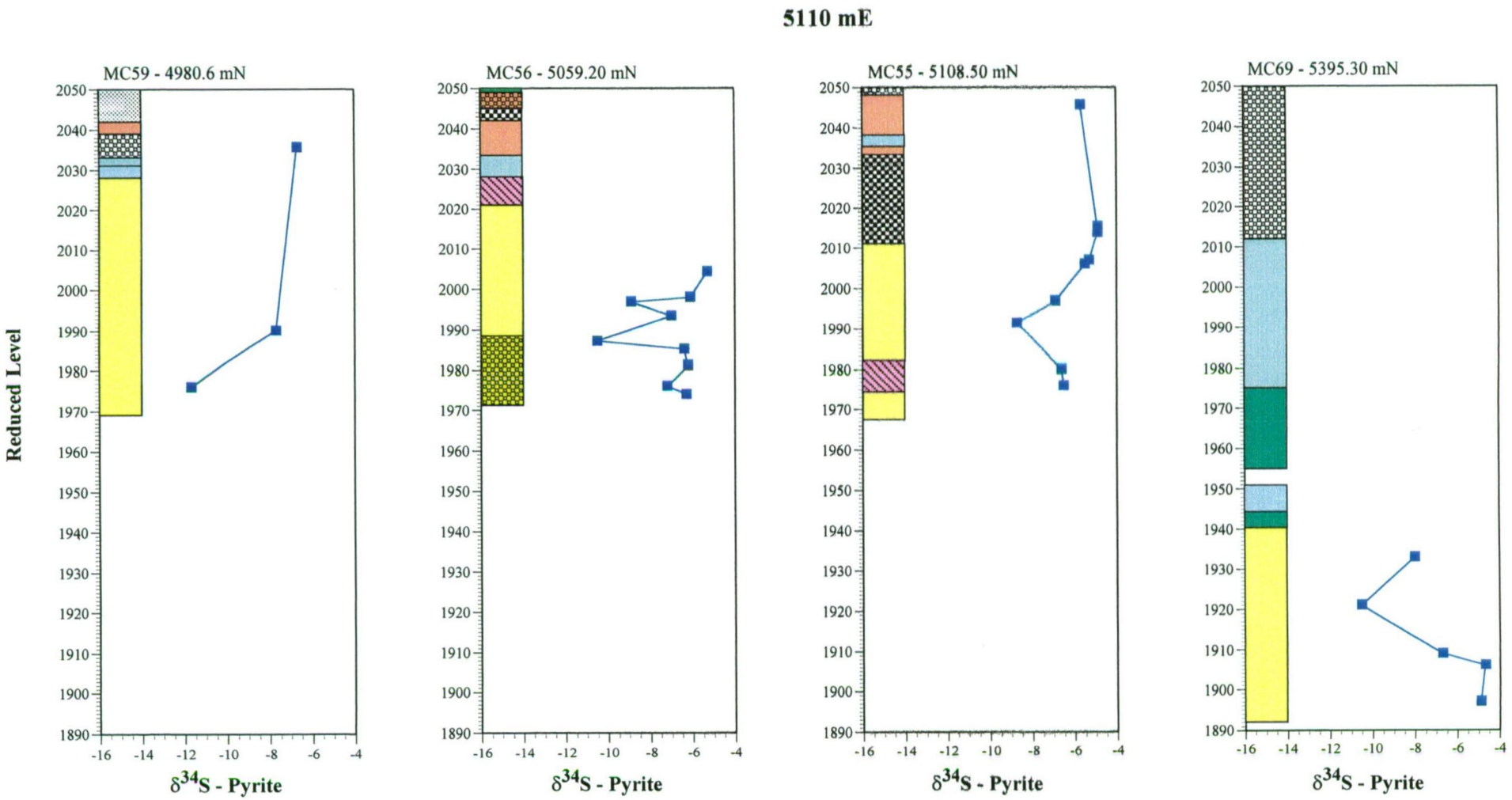

Figure 10.6d. Downhole sulphur isotope variation versus lithology – 5110 mE

10.3.2. Barite

Table 10.3 list the $\delta^{34}S$ values for barite obtained from Mount Chalmers. The majority of the samples come from the West Lode, except for MC63, which comes from the Main Lode. Except for one sample (MC63/31.5 - +5.7 ‰) the barite has a restricted range in $\delta^{34}S$ values of +7.3 to +12.1 ‰. Two samples, MC63/31.5 and PDH15B/20-22 were obtained from the southern margins of the Main Lode and West Lode massive sulphide lenses respectively. The remainder of the samples were obtained from barite lenses or from alteration and/or vein assemblages beneath the massive sulphide lenses. The sample with the lightest $\delta^{34}S$ value (+ 5.7 ‰) comes from within the massive sulphide lens of the Main Lode. The heaviest samples come from the West Lode massive sulphide lens (MC27/27A - +12.1 ‰ and PDH15B/20-22 - +12.1 ‰). Barite from within the massive sulphide lenses is the isotopically heaviest, while barite from vein and alteration assemblages are isotopically lighter. In MC63 (+7.3 to +10.3 ‰) and PDH15B (+11.4 to +11.7 ‰) the $\delta^{34}S$ values of the barite show little variation in their downhole isotopic composition, except for MC63/31.5 (+5.7 ‰).

Table 10.3 Sample location, $\delta^{34}S$ values and descriptions of barite from Mount Chalmers. All samples from the West Lode except for MC 63 (Main Lode).

Drill Hole	Sample Depth	$\delta^{34}S$ Barite (‰)	Comments
MC27/27A	28.7	+12.1	Pyrite-barite lens 13 m below the massive sulphide lens
MC47	84.0	+9.2	Barite occurs within the groundmass to sericite-silica altered lithic breccias
	85.6	+9.6	
West Lode open cut	RL 2072	+11.9	Grab sample from barite lens
MC63	25.0	+9.9	Pyrite-hematite-barite alteration and veins immediately overlying the massive sulphide
	25.4	+7.3	
	28.2	+10.3	
	31.5	+5.7	Barite within massive sulphide
PDH15B	20-22	+12.1	Barite within massive sulphide
	24-26	+11.7	Barite within dolomite
	26-28	+11.6	
	30-31	+11.4	

10.4 DISCUSSION

Excepting for Mount Chalmers and two other Permian VHMS deposits (see section 10.4.4), the vast majority of Phanerozoic VHMS deposits have $\delta^{34}S$ values for sulphides between 0 ‰ and that for coeval seawater sulphate. This relationship between the $\delta^{34}S$ value of seawater and sulphate evaporites was used initially used by Thode and Monster (1965) and later expanded upon by Thode and Monster (1967) and Claypool *et al.* (1980) to determine the $\delta^{34}S$ value of ancient seawater. Sangster (1968) noted a parallel variation between the $\delta^{34}S$ compositions of strata-bound sulphide deposits and the ancient seas throughout geologic time, and that barite was enriched by ~ 1 - 2 ‰ relative to the coeval seawater sulphate $\delta^{34}S$ value. The parallel relationship between the Phanerozoic VHMS deposits and the coeval seawater sulphate value has been used by a numerous authors to argue the dominance of seawater in VHMS hydrothermal systems (*e.g.* Kajiwara, 1971; Sasaki and Kajiwara, 1971; Ohmoto and Rye, 1974; Sasaki, 1974, Ripley and Ohmoto, 1977; Green *et al.*, 1981; Green, 1983; Solomon *et al.*, 1988; Gemmell and Large, 1992, 1993; Khin Zaw and Large, 1992; McGoldrick and Large, 1992; Hill, 1996).

10.4.1 Source of Sulphur

Unlike other studies on VHMS deposits (*e.g.* Green *et al*, 1981; Gemmel and Large, 1992, 1993; Hill, 1996) the $\delta^{34}S$ values of the Mount Chalmers VHMS provide equivocal evidence to their origin. Given the range in $\delta^{34}S$ for Mount Chalmers, then they may have been possibly sourced from one of three possible reservoirs of sulphur:

- *magmatic sulphur*: the $\delta^{34}S$ values of igneous rocks were thought to be within the range of 0 ‰ to ± 5 ‰. Mantle-derived sulphur has $\delta^{34}S$ values in the range of 0.0 ±3 ‰ (Chaussidon and Lorand, 1990). Mid-ocean ridge basalts have a $\delta^{34}S$ value of +0.3 ±0.5 ‰ (Sakai *et al.*, 1984), which contrasts with the $\delta^{34}S$ values for Japanese volcanic rocks of +5 ±10 ‰ (Ueda and Sakai, 1984). Granitic rocks have a wider range in $\delta^{34}S$ values between -10 to +8 ‰ (Coleman, 1977), compared to the average value of +7 ‰ for the continental crust (Chaussidon *et al.*, 1989). It can be seen that igneous rocks have a wider spread in their $\delta^{34}S$ values than previously thought. The $\delta^{34}S$ values in many igneous rocks are similar to the $\delta^{34}S$ values of the country rocks that they have intruded into. Suggesting that a considerable proportion of the sulphur within the igneous rocks was acquired by bulk-rock and/or selective assimilation (Ohmoto and Goldhaber, 1997).
- *sedimentary sulphur* with $\delta^{34}S$ values in the range of -70 to +70 ‰, but is more commonly depleted in the heavier isotope (Ohmoto and Rye, 1979);
- *seawater sulphur*: present day seawater has a $\delta^{34}S$ value of +20 ‰, although this value has varied through geological time (Thode and Monster (1965, 1967; Claypool *et al.* 1980).

Fluids and vapour phases containing sulphur derived from one of these three main reservoirs for sulphur may be modified by one or more of the following processes to produce the range in $\delta^{34}S$ values seen in VHMS deposits.

- bacterial reduction of seawater sulphate to sulphide (*e.g.* Sangster, 1968, 1971, 1976; Velasco *et al.*, 1998);
- admixture of magmatic hydrothermal fluid and seawater (*e.g.* Urabe and Sato, 1973; Bryndzia *et al.*, 1983; Gregory and Robinson, 1984);
- inorganic reduction of seawater sulphate ± leached volcanic rock sulphur (*e.g.* Kajiwara, 1971; Sasaki and Kajiwara, 1971; Ohmoto and Rye, 1974; Sasaki, 1974, Ripley and Ohmoto, 1977; Green *et al.*, 1981; Green, 1983; Solomon *et al.*, 1988; Gemmell and Large, 1992, 1993; Khin Zaw and Large, 1992; McGoldrick and Large, 1992; Hill, 1996);
- leaching of sulphate minerals with partial reduction (*e.g.* Ohmoto *et al.*, 1983)
- leached magmatic sulphur that has undergone little if any reduction (*e.g.* Ishihara and Sasaki, 1978; South and Taylor, 1985);
- direct contribution of magmatic vapour (*e.g.* Herzig *et al.*, 1998).

10.4.1.1 Inorganic/Organic Reduction of Seawater Sulphate

Sangster (1968), based upon the parallel variation between the $\delta^{34}S$ compositions of strata-bound sulphide deposits and the ancient seas throughout geologic time, observed that, on average, VHMS deposits show an average fractionation factor of -17.5 ‰ less than that of the coeval seawater sulphate value. A number of authors (e.g. Sasaki and Kajiwara, 1971; Large 1992;) have argued that this parallelism between the $\delta^{34}S$ of the sulphides from VHMS deposits and that of seawater sulphate implicates seawater as the major contributing source of sulphur for these types of deposits. From the data of Claypool *et al.* (1980), Early Permian seawater had a median $\delta^{34}S$ value of +13.1 ‰. If seawater was the main source of sulphur at Mount Chalmers and using the $\Delta_{SO_4^{2-}-H_2S}$ -17.5 ‰, then the $\delta^{34}S$ value for the sulphides should cluster around -4.2 ‰. As can be seen from Figure 10.1 the $\delta^{34}S$ values for the sulphides are clustered around -8/-6 ‰ division, with a median value of -6.2 ‰ (Table 10.1), some 2 ‰ lighter than that suggested by the simple reduction of seawater sulphate.

Assuming equilibrium conditions existed at Mount Chalmers then the empirical $\Delta_{SO_4^{2-}-H_2S}$ of -17.5 ‰ (Sangster, 1968) can be replaced by a more accurate estimate by the use of Equation 10.1 (Ohmoto and Lasaga, 1992).

$$\delta^{34}SO_{4\,(a.s)}^{2-} - \delta^{34}H_2S = 6.463\left(10^6/T^2\right) + 0.56‰ \qquad \text{(Eqn. 10.1)}$$

Where T =°K and SO_4^{2-}, either aqueous or solid sulphate.

For a temperature of 270°C the equilibrium fractionation value between coexisting sulphate and sulphide pairs is ~ -22 ‰. Early Permian seawater had a $\delta^{34}S$ value of ~ +13 ‰ (Claypool *et al.*, 1980). Therefore, sulphides precipitating from reduced Early Permian seawater sulphate at 270°C for Mount Chalmers would have $\delta^{34}S$ values in the range of -9 to +13 ‰ depending upon the amount of reduction. The majority of $\delta^{34}S$ values for sulphides from Mount Chalmers fall within range of the calculated and estimated $\delta^{34}S$ values of -9 to +13.1 ‰ suggesting that reduced seawater sulphate may have been a major but not the only source of sulphur for the Mount Chalmers hydrothermal system.

A major caveat to the approach of Ohmoto and Lasaga (1992) is the underlying assumption that the sulphate and sulphide minerals were precipitated under equilibrium conditions. However, at Mount Chalmers no evidence for this state has been recognised. Therefore, some other mechanism (other than the simple inorganic reduction of seawater) must be producing the negative $\delta^{34}S$ values, or there must be another source/reservoir of sulphur that contains very light isotopic sulphur contributing sulphur to the hydrothermal fluid.

10.4.1.2 Magmatic Fluid/Leached Magmatic Sulphur

Ohmoto and Rye (1979) showed that for low-temperature equilibrium systems magmatic fluids with $\delta^{34}S$ fluid between -3 and +7 ‰ are unlikely to produce sulphide minerals, such as pyrite and sphalerite with $\delta^{34}S$ values greater than +8 ‰ at temperatures above ~200° C. However, they may produce sulphide minerals with $\delta^{34}S$ values as low as ~ -30 ‰. This can be seen graphically in Figure 10.7 where the range in $\delta^{34}S$ for coexisting sulphide and sulphates are plotted both for an oxidised and a reduced magmatic fluid. Figure 11.8 shows that an oxidised magmatic fluid that precipitates sulphides and sulphates in a temperature range of 250° to 200°C could produce the range of $\delta^{34}S$ values at Mount Chalmers. Like the approach used by Ohmoto and Lasaga (1992) a major qualification to this approach is the that the sulphate-sulphide pairs were precipitated under equilibrium conditions.

Ohmoto, 1972 (Fig. 4 *in* Ohmoto 1972) showed that a hydrothermal fluid with an initial $\delta S^{34}_{\Sigma S}$ of 0.0 ‰ can produce pyrite with $\delta^{34}S$ values in the range of +5 to -27 ‰ and barite from about 0 to +32 ‰, within geologically reasonable limits of pH and f_{O_2} when $\delta^{34}S_{\Sigma S}$ = 0 ‰ and T° = 250° C. In a very recent study on an active hydrothermal site (the Hine Hina area at the southern Valu Fa ridge), Herzig *et al.*, (1998) on the basis of negative $\delta^{34}S$ values for pyrite (average = -4.0 ‰ and sphalerite (2 analyses: -4.0 and-5.7 ‰) and distinctive epithermal argillic alteration suggested a direct contribution of magmatic vapour to the hydrothermal fluid. Suggesting that magmatic volatiles are an important component of VHMS sulphide-forming hydrothermal systems.

Therefore, a purely magmatic fluid/vapour phase could produce the range in $\delta^{34}S$ value seen at Mount Chalmers. Alternatively, they could be contributing significant quantities of sulphur to a convecting hydrothermal fluid dominated by modified seawater. A third possibility is that the hydrothermal fluid, again modified seawater, leached significant quantities of igneous rock sulphur, such that the $\delta^{34}S$ rock sulphur values dominated the $\delta^{34}S_{fluid}$.

10.4.1.3 Oxidation State of the Ore-forming Fluids

The sulphide and Fe-oxide mineral species present at Mount Chalmers can be used to estimate the range of f_{O_2} for the hydrothermal fluids at Mount Chalmers. The sulphide mineralogy at Mount Chalmers is relatively simple, as it is dominated by pyrite with subordinate amounts of chalcopyrite, sphalerite and galena. Importantly no pyrrhotite was observed at Mount Chalmers. The dominant Fe-oxide species at Mount Chalmers is hematite with rare to minor magnetite. The absence of pyrrhotite and the presence of hematite ± magnetite indicates that the f_{O_2} of the initial fluid was high. Further evidence of the f_{O_2} state of the initial fluid at Mount Chalmers is provided by isotopic composition of the minerals relative to the fluid composition and the variation of isotopic composition caused by changes in f_{O_2} and pH (Table 10.4).

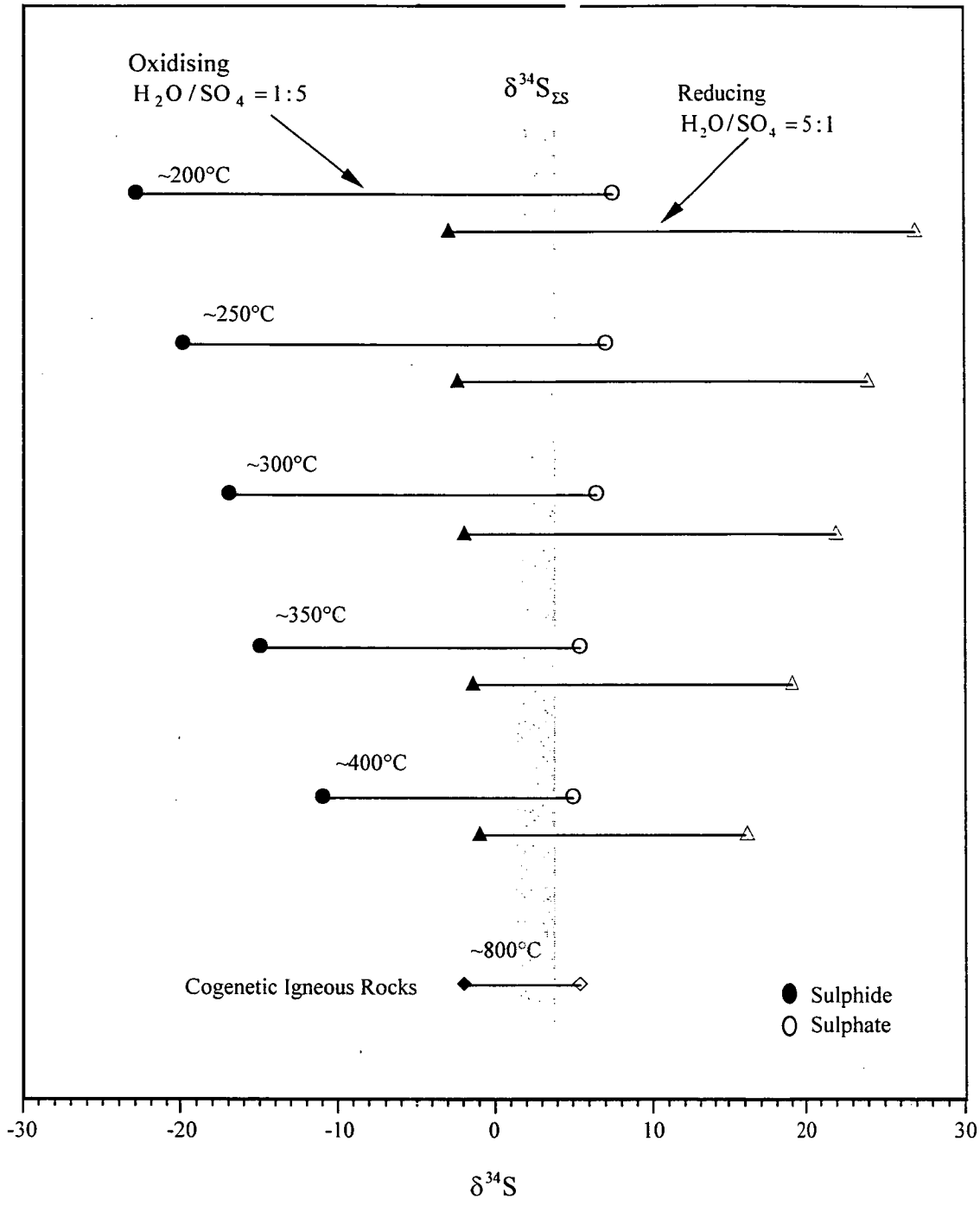

Figure 10.7. Idealised $\delta^{34}S$ systematics of coexisting sulphides and sulphates derived from evolved magmatic fluids with initial H_2S/SO_4 = 1 and precipitated over the temperature range 400° to 200° C. Circles show a fluid that followed an oxidising path, while the triangles show a fluid that followed a reducing path. If the $\delta^{34}S_{\Sigma S}$ of the system remains constant its value must lie between the values for sulphide and sulphate in cogenetic igneous rocks and here is assumed to be 2 ± 1‰. (From Rye 1993).

At Mount Chalmers both pyrite and chalcopyrite tend to have variable $\delta^{34}S$ values, while the $\delta^{13}C$ values for the dolomite at Mt Chalmers tend to have a uniform isotopic composition. This coupled with the sulphide mineralogy composed primarily of pyrite with no pyrrhotite and the presence of hematite/jasper both in the stringer zone and at the top of the sulphide indicates that the that the f_{O_2} of the initial fluid was moderate to high. Therefore, an oxidising hydrothermal fluid may have been responsible for the range, but not necessarily the whole spectrum of negative $\delta^{34}S_{sulphide}$ values at Mount Chalmers.

Table 10.4 Relationships between the chemical environments of ore depositions and the sulphur and carbon isotopic composition of hydrothermal minerals (From Ohmoto, 1972).

Area	Oxidation State	Possible Mineral Associations	Isotopic composition of minerals relative to fluid composition		Variation of isotopic composition by changes in f_{O_2} and pH	
			δS_i^{34}	δC_i^{13}	δS_i^{34}	δC_i^{13}
1	high	bar, calc.	$\delta S_{bar}^{34} \approx \delta S_{\Sigma S}^{34}$	$\delta C_{cc}^{13} \approx \delta C_{\Sigma C}^{13}$	uniform	uniform
2		bar, py, calc.	$\delta S_{bar}^{34} > \delta S_{\Sigma S}^{34}$ or $\delta S_{bar}^{34} < \delta S_{\Sigma S}^{34}$	$\delta C_{cc}^{13} \approx \delta C_{\Sigma C}^{13}$	variable	uniform
3		py, po, calc.	$\delta S_{py}^{34} \approx \delta S_{\Sigma S}^{34}$	$\delta C_{cc}^{13} \approx \delta C_{\Sigma C}^{13}$	uniform	uniform
4		py, po, calc, gr	$\delta S_{py}^{34} \approx \delta S_{\Sigma S}^{34}$	$\delta C_{cc}^{13} > \delta C_{\Sigma C}^{13}$ or $\delta C_{gr}^{13} < \delta C_{\Sigma C}^{13}$	uniform	variable
5	low	po	$\delta S_{po}^{34} \approx \delta S_{\Sigma S}^{34}$		uniform	

Minerals considered are pyrite (py), pyrrhotite (po), barite (bar), calcite (calc, cc) and graphite (gr) only. Sericite is stable in all areas. Presence or absence of pyrrhotite in areas 3 and 4 depend upon ΣS value.

10.4.1.4 Biogenic Reduction of Seawater Sulphur

A number of authors have implicated biogenic pyrite in the production of isotopically light sulphides within ancient VHMS deposits (*e.g.* Sangster, 1968, 1971, 1976; Rye *et al.*, 1974; Velasco *et al.*, 1998). Sangster (1968) proposed that the average reduction in $\delta^{34}S$ values between the coeval seawater sulphate and VHMS deposits (-17.5 ‰) and sedimentary-hosted massive sulphide deposits (-11.7 ‰) are very similar to the average fractionation factor (-15 ‰) for the bacterial reduction of seawater sulphate. Therefore concluded that sulphur within these deposits was the result of the biogenic reduction of seawater sulphate. However, Ohmoto *et al.*, (1990) showed that the isotopic fractionation between seawater sulphate and biogenic sulphides was much larger at -45 ± 20 ‰. Although for pre-Devonian oceans, the average $\Delta_{H_2S-SO_4}$ value may have been less negative than -40 ‰ (Ohmoto and Goldhaber, 1997).

Modern day marine sediments are generally reducing environments covered by a thin oxidised surface layer. This thin vertical zonation is maintained by the unidirectional flow of oxygen from the seawater above and by the benthic organisms and their metabolic rates (Jørgensen, 1977). The oxidised zone is dominated by organisms with an aerobic respiratory metabolism. Whereas the reducing zone is characterised by various types of anaerobic respiration and various types of fermentation processes (Jørgensen, 1977).

Although the modern day seafloor is oxygenated, this has not always been the case for the ancient seas, when periods of widespread anoxia existed (Goodfellow, 1987; Eastoe, 1994; Eastoe and Gustin, 1996). In modern marine sediments the dominant anaerobic bacteria is of the genus *Desulphovibrio*, which reduces SO_4^{2-} to H_2S via the reaction (Eqn. 10.2)

$$2CH_2O + SO_4^{2-} \rightarrow 2HCO_3^- + H_2S \qquad \text{(Eqn. 10.2)}$$

Where CH_2O is a proxy for the more complex organic compounds which are metabolised by sulphate reducing bacteria (Ohmoto *et al.*, 1990). Biogenic H_2S produced by Equation 10.2 will follow one of the following routes (Ohmoto *et al.*, 1990; Ohmoto and Goldhaber, 1997):

- escape from the sediment to the overlying seawater
- become oxidised by O_2 dissolved in the pore-fluid, ferric iron or sulphide-oxidising bacteria to S^0, $S_2O_3^{2-}$ and other oxidised compounds through reactions like (Eqn. 10.3)

$$H_2S + \tfrac{1}{2} O_2 \rightarrow S^0 + H_2O \qquad \text{(Eqn. 10.3)}$$

- react with Fe in the sediments to form acid soluble iron sulphides by reactions like (Eqn. 10.4)

$$Fe^{2+} + H_2S \rightarrow FeS + 2H^+ \qquad \text{(Eqn. 10.4)}$$

- react with organic matter in the sediments to form authigenic organosulphur compounds.

Velasco *et al.* (1998) in their sulphur isotope study on the Iberian Belt pyrite deposits argued that the negative $\delta^{34}S$ values they reported (as low as -26.5 ‰ for sphalerite and -15.1 ‰ for pyrite) were also produced by the bacterial reduction of seawater sulphate at or near the seawater-rock interface.

Strongly negative $\delta^{34}S$ values occur within the footwall lithologies of the Mount Chalmers VHMS deposit (Table 10.2). These values tend to occur in the graded tops to lithic breccias, volcano-lithic sandstone, silicified sedimentary rocks within the stringer zone and sediment component of peperites within the footwall rhyolites. The graded tops to the volcanolithic sandstones, lithic breccias and pumice lithic breccias are moderately to strongly bioturbated. The trace fossils are predominantly feeding traces. The presence of bioactivity within the sedimentary rocks indicates that there must have been sufficient organic matter for the animals responsible for the traces to live off. Therefore diagenetic pyrite may have formed as a result of the bacterial reduction of seawater sulphate by anaerobic bacteria that used the organic matter as a substrate, and hence was concentrated in organic-rich microenvironments within the sedimentary rocks (Thomsen and Vorren, 1984). Therefore, a hydrothermal fluid interacting with sediments containing diagenetically reduced sulphur can explain the major excursions to the extremely light $\delta^{34}S$ values for pyrite from within the footwall sedimentary rocks at Mount Chalmers.

10.4.2 Pyrite in Hematite/Jasper Mineralisation

Within the hematite and silica/jasper mineralisation the pyrite shows rapid shifts to strongly negative $\delta^{34}S$ values. Ohmoto (1972) and Ohmoto and Rye (1979) also showed that sulphide minerals formed in equilibrium with hematite will have $\delta^{34}S$ values much lower than $\delta^{34}S_{fluid}$. This can explain the significant shifts to very negative $\delta^{34}S$ values seen in MC45 and MC63 within the silica/jasper mineralisation (Fig. 10.5b 5010mN), assuming that the pyrite was formed in equilibrium with the hematite. Solomon *et al.*, (1988) argued that pyrite with negative $\delta^{34}S$ from barren pyrite-barite ± hematite lenses within the Cambrian Mount Read Volcanics of Tasmania ($\delta^{34}S_{seawater\ sulphate}$ = 30 ‰) were precipitated from oxidising fluids. Alternatively, the hydrothermal fluid may have reacted with the hematite/jasper mineralisation, causing the oxidation of the hydrothermal fluid to occur in microniches, and thereby producing the strongly negative shifts seen in the $\delta^{34}S$ values. The negative shifts in $\delta^{34}S$ values of pyrite may also be explained by biological reduction of seawater sulphate. Duhig *et al.*, (1992) interpreted strongly negative $\delta^{34}S$ values in pyrite from silica iron exhalites from the Mount Windsor volcanic belt (northern Queensland, Australia) as being due to biological reduction of seawater sulphate caused by filamentous microbial microfossils that were identified within the ironstones. However, at Mount Chalmers no evidence exists within the hematite/silica-jasper mineralisation of filamentous microbial microfossils.

10.4.3 Barite

The $\delta^{34}S$ values for barite from Mount Chalmers range from +5.7 to +12.1 ‰, with a median $\delta^{34}S$ value of +10.9 ‰ (Table 10.3). These values indicate that the barite from Mount Chalmers is depleted with respect to the $\delta^{34}S$ value for Early Permian seawater (~ +13.1 ‰). If reduced seawater sulphate was the sole source of sulphur for the formation of barite, then the $\delta^{34}S$ values of the barite should be enriched by ~1 to 2 ‰ relative to the contemporaneous seawater value (Sangster, 1968). This depletion in $\delta^{34}S$ values of the Mount Chalmers barite relative to the Early Permian seawater suggests that there must have been another isotopically lighter source of sulphur other than seawater. Barites with $\delta^{34}S$ less than that of contemporaneous seawater have also been reported from the Axial Seamount - Juan de Fuca Ridge (Hannington and Scott, (1988) and Hine Hina area, Valu Fa Ridge, southern Lau Basin (Herzig *et al.*, 1998). Hannington and Scott (1988) concluded that the mixing and incorporation of isotopically light sulphur from oxidised H_2S could account for the lighter $\delta^{34}S$ values for barite. Herzig *et al.*, (1998) concluded that for the Hine Hina area (Lau Basin) the isotopically light barite was produced by the oxidation of isotopically light sulphides (e.g. -5 ‰) to S^{32} –enriched SO_4 and mixing with heavy seawater SO_4. Solomon *et al.*, (1988) concluded that vein barite from south of Mount Lyell (Tasmania) with a range in $\delta^{34}S$ values from +21 to +30 ‰ (coeval Cambrian $\delta^{34}S_{seawater\ sulphate}$ = +30 ‰) were precipitated by oxidised fluids.

Two barite samples have $\delta^{34}S$ values approaching that of coeval seawater sulphate (Table 10.3; MC27/27A/28.7 - +12.1 ‰ and PDH15B/20-22 - +12.1 ‰). Sample PDH15B comes from near the top of the West Lode massive sulphide lens suggesting that mixing between the hydrothermal and cold seawater occurred at or near the seawater/rock interface on the margins of the West Lode sulphide mound. The $\delta^{34}S$ value from MC27/27A is somewhat more problematic in that the barite lens was intersected 13 metres below the massive lens. One possibility is that the barite was formed from the mixing of a cooling hydrothermal fluid, during the waning stages of hydrothermal activity and the downward ingress of cold seawater on the margins of the West Lode sulphide mound. Alternatively, the barite lens may have been formed prior to the formation of the overlying massive sulphide from the mixing of a hydrothermal fluid and cold seawater at or near the seawater/rock interface.

Barite samples from pyrite-hematite-barite alteration immediately overlying the massive sulphide in MC63 have a relatively restricted range of +7.3 to +10.3 ‰ (Table 10.3). The one barite sample from within the massive sulphide has the lowest $\delta^{34}S$ value for barite of +5.7 ‰. These values suggest that an oxidising hydrothermal fluid interacting with seawater precipitated hematite and barite. The $\delta^{34}S$ value within the massive sulphide suggests that there was only limited interaction between hydrothermal fluid and seawater. Suggesting that the Main Lode sulphide mound was effectively sealed to the ingress of seawater.

The range in $\delta^{34}S$ values for barite at Mount Chalmers can be adequately explained by the mixing of an oxidising hydrothermal fluid with cold Early Permian seawater. The consistency of the values in any one-drill hole and the narrow range of $\delta^{34}S_{barite}$ values suggest that the sulphate species were largely controlled by the fluid chemistry and not fluid/rock interaction, and that the fluid chemistry did not vary greatly during the formation of the barite.

10.4.4 Sulphur Isotopes of Other Permian VHMS Deposits

There are few Permian VHMS deposits known or described in the geological literature, especially with regard to their sulphur isotope composition. Other than Mount Chalmers, only three other Permian VHMS deposits have had sulphur isotope values reported from them; deposits from the Afterthought-Ignot area of Shasta County, California (Eastoe and Nelson, 1988), the Red Ledge deposit, Idaho (Fifarek, 1997) and Orange Point, Glacier Bay, Alaska (Newberry *et al.*, 1997). Except for the East Shasta mining district, Mount Chalmers along with the other known Permian VHMS deposits are all characterised by sulphides with negative $\delta^{34}S$ values. Whereas, the deposits from the East Shasta district are characterised by sulphides with positive $\delta^{34}S$ values, some of which exceed that of the coeval seawater sulphate value (Eastoe and Nelson, 1988).

Sulphides from the prospects of the East Shasta mining district have $\delta^{34}S$ values for pyrite in the range -28 to +33.2 ‰. The negative $\delta^{34}S$ values (-28 to 0 ‰) for pyrite tend to come from disseminated pyrite in rhyolites, andesite and bedded mudstones, siltstones and tuff, and were interpreted to have a biogenic origin.

Kuroko-type sulphide ores have a $\delta^{34}S$ range of +5 to +12 ‰ (which exceeds the $\delta^{34}S$ value for contemporaneous seawater sulphate), and were interpreted to have possibly been derived from partially reduced contemporaneous seawater sulphate, with a concealed rock-sulphur source of high $\delta^{34}S$ value more likely (Eastoe and Nelson, 1988).

The Red Ledge VHMS deposit has $\delta^{34}S$ values for sulphides between -9.5 to -0.6 ‰ and for barite between +11.1 to +14.0‰ for massive barite and between +12.6 to +15.9 ‰ for stringer barite. Based upon the temporal relationship between the $\delta^{34}S$ of seawater sulphate and contemporaneous VHMS deposits, Fifarek, (1997) argued that the isotopic composition of sulphide minerals is controlled by reduction of seawater sulphate at high temperatures and that the sulphate minerals contain essentially unfractionated oceanic SO_4^{2-}

The $\delta^{34}S$ values for the Orange Point VHMS are only presented as a range (~ -5 to ~ 0 ‰) within a diagram (Figure 22 *in* Newberry *et al.*, 1997), and no interpretation of the data is given.

10.4.5 $\delta^{34}S$ Zonation Within VHMS Deposits

The $\delta^{34}S$ zonation seen within VHMS deposits has been used by a number of authors to provide an understanding of the evolution of a hydrothermal system, not only through time but also with regards as to the source of sulphur (*e.g.* Green *et al.*, 1981; Gemmell and Large, 1992, 1993; McGoldrick and Large, 1992; Çagatay and Eastoe, 1995). A progressive upward increase in $\delta^{34}S$ sulphide values was recognised for the Hellyer (Gemmell and Large, 1993), Rosebery (Green *et al.*, 1981) and Thalanga (Hill, 1996) VHMS deposits. In contrast to the Hellyer, Rosebery and Thalanga VHMS deposits, a stratigraphically upward decrease in the $\delta^{34}S$ values for sulphides have been reported from a number of other VHMS deposits, Shakanai N°1 mine (Kajiwara, 1971), Que River (McGoldrick and Large, 1992) and Turkey (Çagatay and Eastoe, 1995). Regardless of whether the $\delta^{34}S$ values are increasing or decreasing towards the stratigraphic tops of the above mentioned VHMS deposits, all the authors agree that the variation in $\delta^{34}S$ values has been caused predominantly by mixing between an ascending hydrothermal fluid (± evolved seawater sulphate, ± igneous sulphur) and cold seawater. However, at Mount Chalmers except near the top of the sulphide lenses no apparent shift towards lighter or heavier $\delta^{34}S$ values is seen, although there are extreme shifts to very negative values throughout the deposit. This lack of spatial variation and restricted range in $\delta^{34}S$ values for all sulphides suggests that the sulphides and barite were formed by a single hydrothermal event of relatively constant isotopic composition, and that the fluid chemistry and not fluid/rock interaction largely controlled the $\delta^{34}S$ values. The Iron Mountain VHMS deposit (West Shasta district, California) has a restricted range in $\delta^{34}S$ values for pyrite (+3.2 to +5.3 ‰), that South and Taylor (1985) argued were precipitated from a fluid of rather constant isotopic composition and physiochemical state. This lack of apparent zonation in $\delta^{34}S$ is also seen in the Buchans VHMS deposits where the sulphur was derived from an evolving seawater dominated hydrothermal fluid, that did not interact with colder unmodified seawater at the site of deposition (Kowalik *et al.*, 1981).

10.5 CONCLUSIONS

The massive sulphides and sulphides in the stringer zone at Mount Chalmers have a broad range in $\delta^{34}S$ values between -17.6 to -1.6 ‰. However, the majority of the sulphides have a narrow range clustering between -8.0 to -6.0 ‰. The relatively restricted range in $\delta^{34}S$ values observed at Mount Chalmers in both the massive sulphide and the stringer zone mineralisation argues that the sulphides and sulphates were precipitated from a single hydrothermal event that maintained similar conditions of fO_2, pH and T. However, the total range in $\delta^{34}S$ values argues that there must have been another source of sulphur. One of four processes, or any combination of these four may have formed the sulphides at Mount Chalmers:

- *inorganic reduction of seawater at elevated temperatures*: $\delta^{34}S$ produced by the complete reduction of seawater sulphate to sulphide at elevated temperatures, although this does not explain the extremely light $\delta^{34}S$ values.
- *oxidised hydrothermal fluid*: evidence for a moderate to high oxidation state of the hydrothermal fluid is provided by the presence of hematite/jasper within the stringer zone and as a capping to the massive sulphide. In addition, the absence of pyrrhotite and a sulphide assemblage dominated by pyrite at Mount Chalmers also argues for a hydrothermal fluid of moderate to high fO_2.
- *oxidation of H_2S in an ascending magmatic fluid*: Using the mineral assemblages and the theoretical work of Ohmoto (1972), the negative range in sulphide $\delta^{34}S$ values at Mount Chalmers could be produced by a fluid with a $\delta^{34}S_{\Sigma S}$ of 0.0 ‰.
- *biogenic reduction of seawater sulphate*: can produce extremely light $\delta^{34}S$ values, however bioturbation only occurs at or near the tops of the sedimentary rocks, and evidence for widespread biogenic pyrite is not evident. Consequently, the role of biogenic sulphur is not considered to be important at Mount Chalmers except within microniches.

In combination with the fluid inclusion evidence, the favoured model to explain the $\delta^{34}S$ values in sulphides and barite is an oxidised hydrothermal fluid, that was probably dominated by evolved seawater, but one that had a minor, but not an insignificant input of sulphur from a magmatic source. The departures from the "normal" range of $\delta^{34}S$ values to values as low as -17.1 ‰ can be explained by the hydrothermal fluid interacting with biogenic sulphur within microniches with the sediments as the fluids passed through the volcano-sedimentary pile. The hydrothermal fluid also interacted with Fe-oxides both within the stringer zone and the overlying hematite/jasper-silica mineralisation to produce to departures to very light $\delta^{34}S$ values.

Barite from Mount Chalmers are isotopically lighter than what would be expected if barite was precipitated from Early Permian seawater sulphate. The $\delta^{34}S$ values for the barite also support the concept of an oxidising hydrothermal fluid that had an input from another source other than Early Permian seawater. The lighter $\delta^{34}S$ values for barite can also be explained by an oxidising hydrothermal fluid interacting with seawater either at or near the seawater/sulphide mound interface, or as the system waned and cold seawater entered the periphery of the sulphide mound and mixed with the cooling hydrothermal fluid.

CHAPTER 11
OXYGEN ISOTOPES - QUARTZ

11.1. INTRODUCTION

The $\delta^{18}O$ value of ore-forming fluids for ancient VHMS systems can be estimated either by direct or indirect methods, providing information on the source of water and the degree of water-rock interaction. The direct method involves the determination of the $\delta^{18}O$ value of fluids extracted from fluid inclusions. The indirect method is based upon the measurement of the $\delta^{18}O$ value of a mineral *e.g.* quartz. The isotopic composition of the mineral is then used with the estimated or measured temperature of mineralisation and an equation for the isotopic fractionation factor between the mineral and water (H_2O), to calculate the δ value of the ore-forming fluid (Ohmoto, 1986). The difference in $\delta^{18}O$ values between unaltered and altered rocks In VHMS deposits may be used either to define alteration halos in the surrounding lithologies associated with them (*e.g.* Aggarwal and Lonstaffe, 1987; Cathles, 1993; Green *et al*, 1983; Munha *et. al.*, 1986; Paradis *et al.*, 1993). A number of studies have shown that VHMS deposits are characterised by a zone of low $\delta^{18}O$ values that correspond to, and extend beyond the zone of most intense alteration associated with VHMS deposits (*e.g.* Beaty and Taylor, 1982; Green *et. al.*, 1983; Larson, 1983; Huston and Taylor, 1997 *in* Huston, 1997).

This chapter examines the oxygen isotope signature of the hydrothermal alteration within the stringer zone of the Mount Chalmers VHMS deposit as an aid for determining some of the hydrological characteristics such as water/rock (w/r) ratio and water flux estimates of the hydrothermal system.

11.2. ANALYTICAL METHODOLOGY

Preparation of the quartz samples was undertaken in the School of Earth Sciences, University of Tasmania. The quartz was ultrasonically cleaned in a water bath and then baked in an oven for 12 hours at 100°C. The samples were then reacted for 12 hours with BrF_5 in an evacuated nickel reaction vessels using the technique of Clayton and Mayeda (1963). The liberated oxygen was converted to CO_2 by reacting the gas with heated graphite (Taylor and Epstein, 1962). Isotope ratio measurements were carried out on a Finnigan Isogas mass spectrometer within the Central Science Laboratory, University of Tasmania. The results are expressed in the standard δ (‰) notation relative to Standard Mean Ocean Water (SMOW). XRD analysis conducted on all samples showed them to be composed of >95 % quartz (Table 11.1).

11.3. RESULTS

Eleven quartz samples from the silica alteration zone were selected for analysis: (1) immediately beneath a massive sulphide lens (MC25 – West Lode and MC65 – Main Lode); (2) immediately beneath semi-massive sulphide mineralisation (MC71 – Main Lode); and (3) from the stringer zone without any massive sulphide mineralisation (MC28 – West Lode; MC52, 53, and 56 – Main Lode). The samples were selected from sites immediately beneath the massive sulphide lenses and away from the massive sulphide mineralisation to determine whether there is any lateral and vertical zonation to the isotopic composition of the silica alteration associated with the Mount Chalmers VHMS mineralisation. It is possible that some of the sampled alteration was the result of syn-volcanic alteration and therefore not directly related to hydrothermal alteration processes. However, to avoid this problem, samples were selected as close as possible to mineralisation or where the silica alteration was enclosed by sulphide mineralisation. Furthermore, samples were also selected to ensure that they could be directly related to the samples taken for the fluid inclusion study, and therefore only quartz considered to be related to hydrothermal processes was sampled. Within the stringer zone, there are two phases of silica alteration. Phase 1 is composed of blue/grey cryptocrystalline quartz (Fig. 6.10c) and is interpreted to be late pre-mineralisation to early syn-mineralisation as it contains disseminated pyrite grains and is cross cut by the sulphide stringer veins. Phase 2 is composed of milky white cryptocrystalline quartz (Fig. 6.10db) and is interpreted to bepost-mineralisation, as it is replacing and cross cutting the Phase 1 silica, crosscutting some of the sulphide veins and is also locally replacing the massive sulphide mineralisation. None of the Phase 2 silica alteration was analysed. One sample from a late-stage (post-massive sulphide mineralisation) quartz vein was also analysed. The quartz-$\delta^{18}O$ values are listed in Table 11.1.

Except for two samples, the quartz alteration has a very restricted range in $\delta^{18}O$ values, between +9.1 to +9.8 ‰, regardless of the sample class, or whether the sample comes from immediately below a massive sulphide lens or at some vertical distance below a massive sulphide lens (Table 11.1).

Table 11.1. $\delta^{18}O$ and XRD analysis for quartz samples from the Mount Chalmers stringer zone. Vertical distance is measured from base of ore equivalent position. Sample description: *e.g.* MC25/32.8 = drill hole number followed by sample depth downhole. MC53* indicates no massive sulphide intersected in the drillhole.

Sample	Relative Level (metres)	Vertical Distance below Massive Sulphide Mineralisation	$\delta^{18}O$ ‰	Fluid Inclusion Th°C	XRD analysis
MC25/32.8	2065.4	10.9	9.7		quartz
MC25/34.2	2064.0	12.4	9.4	190	quartz
MC28/42.5	2052.5	28.2	9.4		quartz
MC52/130	1995.0	16.9	9.3		quartz
MC53/126.8	1998.7	27.8	9.2		quartz
MC53/133.2*	1992.3	34.2	9.8		quartz
MC53/154.4*	1971.1	55.4	13.8	260	quartz
MC56/136.1*	1996.9	44.9	9.7		quartz
MC56/136.1*	1996.9	44.9	9.1		quartz
MC65/68.4	2038.6	7.4	9.8		quartz
MC71/134.7	1991.2	39.7	7.1		quartz
			Mean = 9.7 S.D. = 1.5		

11.4. FLUID COMPOSITION

Potential sources for hydrothermal fluids responsible for the formation of VHMS deposits include; magmatic, seawater, metamorphic, connate, diagenetic and organic fluids or a combination of any of these fluids. Magmatic fluids have a restricted $\delta^{18}O$ value of between +5.5 to ~ 9.0 ‰ (Taylor, 1974; 1997). Modern seawater has a $\delta^{18}O$ value of 0 ‰ (Taylor, 1974; 1997). The composition of ancient seawater is also thought to have had a $\delta^{18}O$ value of ~ 0 ‰ (Muehlenbachs, 1986; Taylor, 1997), although, this value can only be safely assumed for the last 250 million years (Taylor, 1997).

Four processes are potentially capable of shifting the isotopic composition of seawater (Huston, 1997), assuming that seawater was the dominant fluid.

- evaporation
- isotopic exchange between water and rock
- boiling
- mixing with magmatic waters

All four processes are capable of producing fluids that are isotopically compatible with VHMS ore-forming fluids. If the hydrothermal fluid had a magmatic origin then evaporation of the fluid would not be a consideration. Evaporation produces a fluid evolution path that passes through the field of some high $\delta^{18}O$ fluids (see fig.8b in Huston, 1997). However, the formation of such a fluid requires that more than 90% of the fluid to be evaporated, which is geologically unreasonable for conditions under which VHMS deposits are normally thought to form (Huston, 1997). At Mount Chalmers, boiling is also not considered a viable mechanism as no evidence for boiling was observed in the fluid inclusions.

Meteoric waters have variable $\delta^{18}O$ values, but are generally depleted in ^{18}O compared to seawater and become lighter with increasing latitude and altitude (Taylor, 1979). An estimate of the $\delta^{18}O$ value of the quartz-forming fluid may be calculated using the quartz-H_2O fractionation of Matsuhisa *et al.* (1979) (Eqn. 11.1) and the temperature range in quartz from the stringer zone.

$$\delta^{18}O_{quartz-H_2O} = 3.34(10^6 / T^2_{(°K)}) - 3.31 \qquad \text{(Eqn. 11.1)}$$

Using the homogenisation temperature range determined from fluid inclusions (160° to 270°C) and the end member and average $\delta^{18}O$ values of +7.1, +13.8 and +9.7 ‰ (Table 11.1), the calculated $\delta^{18}O$ values for the hydrothermal fluids vary from -7.4 to +5.8 ‰. (Table 12.2).

Table 11.2. End member and average $\delta^{18}O$ values and calculated range in $\delta^{18}O$ values for an initial isotopic composition of fluids that may have been responsible for the formation of the Mount Chalmers massive sulphide.

End member and average $\delta^{18}O$ values - ‰		Calculated $\delta^{18}O^{i}_{f}$ values ‰
Low	7.1	-7.4 to -0.9 (160° to 270°C)
High	13.8	-0.7 to +5.8 (160° to 270°C)
Mean	9.7	-4.8 to +1.7 (160° to 270°C)

These values could be consistent with an initial fluid with meteoric, seawater or a magmatic origin, or any combination of these three. Although if the mean $\delta^{18}O$ value solely used then a magmatic origin for the hydrothermal fluids can be discounted, assuming no previous water-rock interaction had occurred. As Mount Chalmers is considered to have been formed in a shallow-marine environment, then any contribution of a meteoric fluid to the hydrothermal system is considered to be negligible, although it cannot be completely discounted. Therefore the hydrothermal fluids responsible for the formation of the Mount Chalmers VHMS deposit may have been derived from either seawater or a magmatic source or a combination of these two sources.

Ohmoto and Rye (1974) calculated that magmatic water and meteoric water may also attain the observed isotopic compositions of Kuroko hydrothermal fluids if the effective water/rock ratio (R) becomes sufficiently small ($R \leq 0.001$), and if the temperature of isotopic equilibration was approximately 200°C.

The measured and calculated $\delta^{18}O$ value of fluids that have formed most ancient and modern VHMS deposits are in the range of -1 to +4‰ (Huston, 1997). Figure 11.1 shows the estimated and calculated range in $\delta^{18}O$ values of ancient and modern VHMS deposits and shows that the estimated initial $\delta^{18}O$ values for hydrothermal fluids have not only a wide range in values for individual deposits but also for the whole spectrum of VHMS deposits. The calculated initial fluid composition for Mount Chalmers is comparable to those for other ancient and modern day VHMS deposits (Fig. 11.1). The range in calculated $\delta^{18}O^{i}_{f}$ values for Mount Chalmers is within the range of other ancient VHMS. The measured temperature of the hydrothermal fluid (fluid inclusions) at Mount Chalmers tends to be at the lower end of the temperature range for other ancient and recent VHMS deposits.

A comparison of $\delta^{18}O$ values of altered footwall rhyolites; felsic volcanics or intense silica alteration with other ancient VHMS is shown in Figure 11.2. The data shows that the except for the Mattagami deposit the ancient VHMS deposits have $\delta^{18}O$ values in the range of approximately +5 to +15 ‰ (quartz), which is comparable to the range for Mount Chalmers.

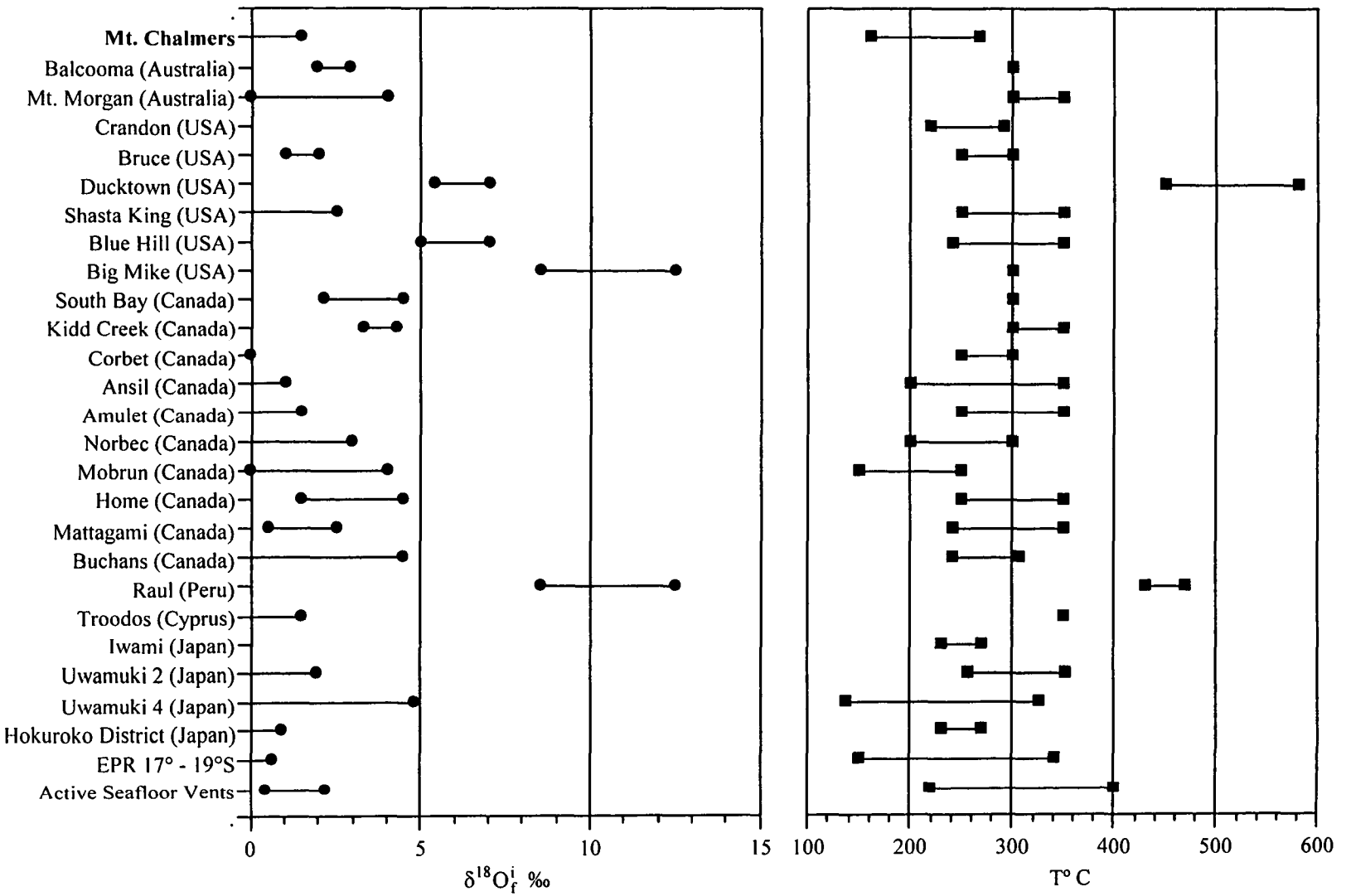

Figure 11.1. Estimated range in $\delta^{18}O$ values and measured and estimated temperatures for VHMS ore forming fluids. Data largely from Huston (1997) and the references therein. Data for Mount Chalmers this thesis. Data for Uwamuki 2 and 4 from Pisutha-Arnond and Ohmoto (1983). Data for EPR 17° to 19°S from Jean-Baptiste *et al.* (1997).

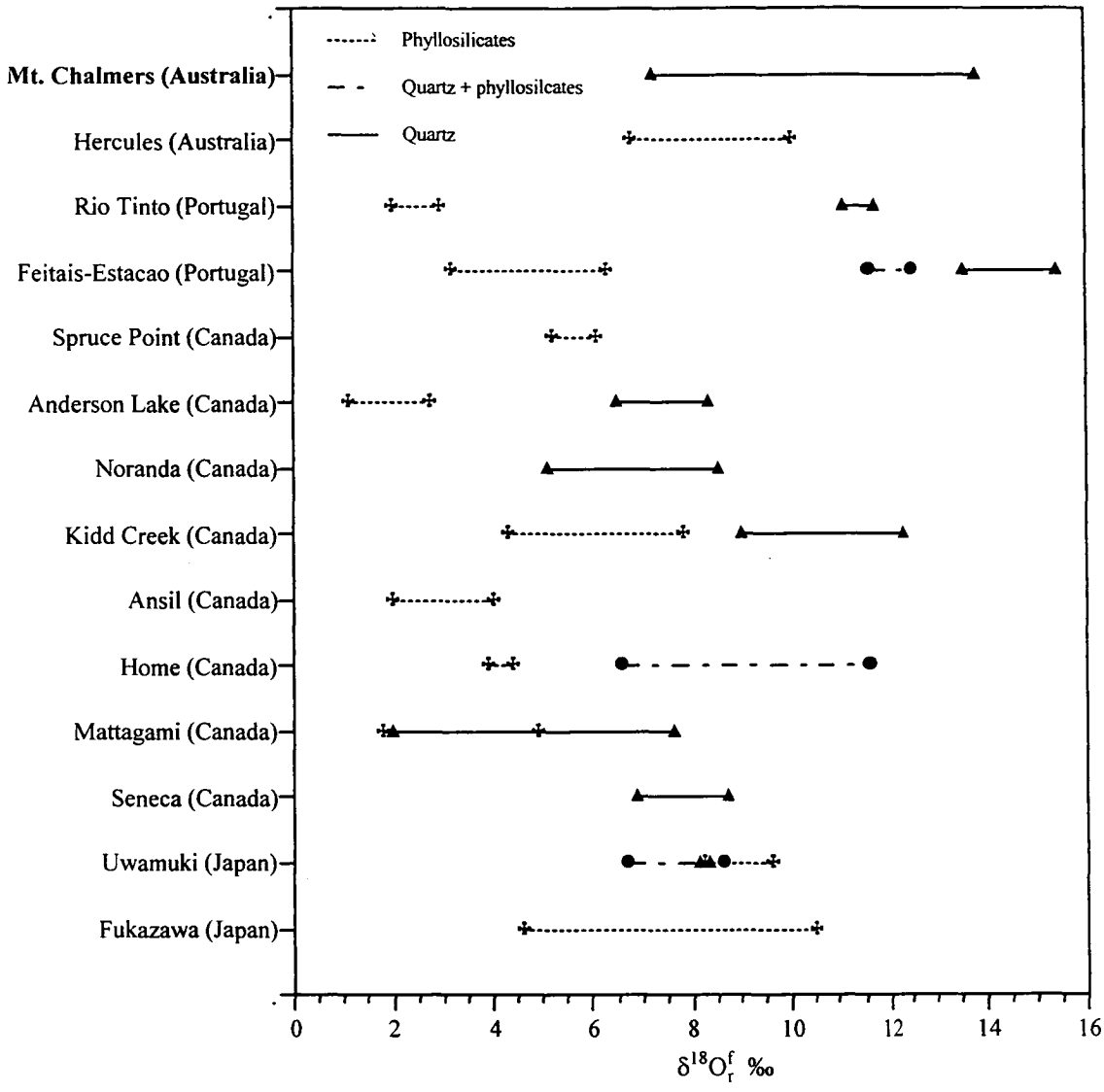

Figure 11.2. Range in $\delta^{18}O$ values of altered footwall rhyolites of selected VHMS deposits. Data largely from Huston (1997) and the references therein. Data for Mount Chalmers this thesis. Data for Anderson Lake and Spruce Point from Aggarwal and Longstaffe (1987). Data for Feitais-Estacao and Rio Tinto from Barriga and Kerrich (1984) and Munha *et al.* (1986).

11.5. WATER/ROCK RATIOS

The water/rock (w/r) ratio is a common a parameter used in the understanding of hydrothermal processes. The w/r ratio is used to provide an estimate of the relative amounts of water and rock that reacted with one another (Taylor and South, 1985). Isotopically estimated w/r ratios refer to the atom percent of oxygen exchanged during hydrothermal alteration (Sheppard *et al.*, 1971). Typically the w/r ratio is based upon the change in the oxygen isotope composition of feldspar due to its rapid exchange kinetics with a hydrothermal fluid of known or inferred oxygen isotope composition (Gregory and Taylor, 1981; Matthews *et al.*, 1981; O'Neil and Taylor, 1967; Taylor and South, 1985). Sheppard *et al.* (1971) concluded that the isotopic composition of quartz cannot be used as an indicator of the nature of the fluid associated with the alteration, unless there is specific evidence that quartz recrystallised in a certain mineral assemblage under new environmental conditions. At Mount Chalmers within the interpreted hydrothermal upflow zones the footwall lithologies have been completely altered to quartz and therefore the isotopic composition of quartz in this instance may be used as indicator of the nature of the hydrothermal fluid.

The footwall lithologies at the Mount Chalmers mine are dominated by rhyolites, dacites, rhyolitic pumice breccias, and to a lesser extent by sedimentary rocks. Rhyolites and dacites have unaltered whole rock $\delta^{18}O$ values of ~ +6 to ~ +10 ‰ (Taylor, 1974). The magnitude of the change in the $\delta^{18}O$ values of water by isotopic exchange reactions with the footwall volcanics depends upon a number of factors (Ohmoto and Rye, 1974):

- the initial isotopic composition of the water;
- the initial isotopic composition of the volcanics involved in the isotopic exchange reactions;
- the ratio of exchangeable oxygen atoms in the water to those in the rock (w/r);
- temperature, which determines the equilibrium isotopic fractionation between the rock and the water;
- the degree of isotopic equilibration.

The isotopic data was modelled for both an open system (Eqn. 11.2) and a closed system (Eqn. 11.3) using the equations of Taylor (1979). Equation 11.2 gives the w/r ratios intergrated over the lifetime of the hydrothermal system, assuming continuous recirculation and re-equilibration of the fluid (Closed System). Nevertheless, some of the hydrothermal fluid will be lost to the system, e.g by venting onto the seafloor. In the extreme case in which the water only passes the rocks once before venting onto the seafloor, the intergrated w/r ratio is given by Equation 11.3 (Open System) (Taylor, 1979).

$$\frac{w}{r} = \frac{\delta^{18}O_r^i - \delta^{18}O_r^f}{\delta^{18}O_w^f - \left(\delta^{18}O_r^f - \Delta^{18}O_w^r\right)} \qquad \text{Closed System} \qquad \text{(Eqn. 11.2)}$$

$$\frac{w}{r} = \ln\left[\frac{\delta^{18}O_w^i + \Delta^{18}O_w^r - \delta^{18}O_r^i}{\delta^{18}O_w^i - \left(\delta^{18}O_r^f - \Delta^{18}O_w^r\right)}\right] \qquad \text{Open System} \qquad \text{(Eqn. 11.3)}$$

Where:

- w/r is the water/rock ratio expressed in atom proportion of oxygen;
- $\delta^{18}O_r^i$ is the estimated or measured isotopic composition of the initial unaltered rock;
- $\delta^{18}O_r^f$ is the calculated isotopic composition of the final rock;
- $\delta^{18}O_w^i$ is the estimated isotopic composition of the altering fluid;
- Δ^r_w is the isotopic fractionation factor between the altered rock and the altering fluid.

A critical problem with the application of Equations 11.2 and 11.3 to natural systems is the selection of Δ^r_w values, because rocks are composed of more than one mineral phase and the mineral-water fractionation factors can either undergo equilibrium or kinetic isotopic fractionation. In previous studies Δ^r_w has been approximated by using single mineral-water fractionation which can be approximated by $\Delta^{oligoclase}_{water}$ (Taylor, 1979) or $\Delta^{muscovite}_{water}$ (*e.g.* Spooner *et al.*, 1977). In this study Δ^r_w has been estimated using the quartz-H_2O fractionation equation of Matsuhisa *et al* (1979) (Eqn. 11.1), as alteration assemblages are rarely dominated by plagioclase especially at elevated temperatures and therefore the fractionation between quartz-H_2O is considered to be more appropriate.

At Mount Chalmers, a predominance of rhyolitic volcanics within the footwall requires the adoption of $\delta^{18}O_r^i$ = +8.0 ‰ (Taylor, 1974; Taylor and Sheppard, 1986), although silicic magmas with low $\delta^{18}O$ values range (~ -1.0 to +5.0 ‰) are known (Taylor and Sheppard, 1986), but are rare. The $\delta^{18}O_w^i$ values of +1.2 and +9‰ represent respectively the end-member values for Permian glacial seawater (see Chapter 9) and a magmatic fluid that may have interacted with the volcanics at Mount Chalmers.

Rearranging Equations 11.2 and 11.3, the changes in the estimated $\delta^{18}O$ value (8 ‰) of the footwall volcanics from Mount Chalmers were calculated as a function of temperature (100 - 400° C) and water/rock under three conditions of $\delta^{18}O_w^i$ values for meteoric (-6 ‰), seawater (+1.2 ‰) and magmatic waters (+5.8 ‰). These values cover the range in calculated $\delta^{18}O_w^i$ values over the temperature range obtained from the fluid inclusion study.

$$\delta^{18}O_r^f = \frac{\delta^{18}O_r^i + \left(\delta^{18}O_w^i + \Delta^r_w\right)\frac{W}{r}}{1+\frac{W}{r}} \qquad \text{(Closed System)} \qquad \text{(Eqn. 11.4)}$$

$$\delta^{18}O_r^f = \delta^{18}_w{}^i + \Delta^r_w\left[\left(\delta^{18}O_w^i + \Delta^r_w - \delta^{18}O_r^i\right)^{-w/r}\right] \qquad \text{(Open System)} \qquad \text{(Eqn. 11.5)}$$

Comparisons of the calculated $\delta^{18}O_r^f$ values in Figures 11.3 and 11.4 with the temperatures measured from the fluid inclusions indicate the following possible conditions for the formation of the silica alteration with values $\delta^{18}O$ between 7.1 and 13.8 ‰ in a temperature range of 160° to 270° C.

For an open system:

$\delta^{18}O^{i}_{w}$ = -6.0 ‰ (meteoric) and w/r > ~0.01 OS-1

$\delta^{18}O^{i}_{w}$ = +1.2 ‰ (seawater) and w/r > ~0.01 OS-2

$\delta^{18}O^{i}_{w}$ = +5.8 ‰ (magmatic ± seawater) and w/r > ~0.01 to ~1.3 OS-3

And for a closed system:

$\delta^{18}O^{i}_{w}$ = -6.0 ‰ (meteoric) and w/r > 0.01 CS-1

$\delta^{18}O^{i}_{w}$ = 1.2 ‰ (seawater) and w/r > ~0.01 CS-2

$\delta^{18}O^{i}_{w}$ = +5.8 ‰ (magmatic ± seawater) and w/r > ~0.01 to ~ +40 CS-3

The $\delta^{18}O^{i}_{w}$ of 5.8 ‰ is thought to be a fluid that may have been a combination of a magmatic dominated water with some input from seawater, as this value is at the lower end of the range of $\delta^{18}O$ values for magmatic fluids (Taylor, 1974; 1997). From Figures 11.3a and 11.4a it can be seen that a magmatic water alone cannot produce the shift in $\delta^{18}O$ values from the assumed $\delta^{18}O^{i}_{r}$ value to the measured $\delta^{18}O^{f}_{r}$ values. In fact, a magmatic water produces little if any shift in $\delta^{18}O^{i}_{r}$ value and then only over a very restricted temperature interval of approximately 160° - 170° C. Seawater can produce the required shifts in $\delta^{18}O$ values in both the open and closed systems over the required temperature range at w/r ratios from >0.01 (Figs. 11.3b and 11.4 b). In contrast to this, a magmatic ± seawater fluid is only capable of producing the shift in $\delta^{18}O$ values within a closed system. If the two outside values +7.1 and +13.8 ‰ are omitted then the more restricted range of +9.1 to +9.8 ‰ for quartz (Table 11.1) places even greater restrictions on the conditions of formation. For a magmatic ± seawater fluid the shift in isotopic values for a rhyolite with $\delta^{18}O^{i}_{r}$ of +8 ‰ to $\delta^{18}O^{f}_{r}$ values in the range of +9.1 to +9.8 ‰ requires very tight w/r ratio $\leq$ ~0.6 *i.e.* rock dominated. If the hydrothermal fluid is dominated by seawater, the shift in isotopic values for a rhyolite with $\delta^{18}O^{i}_{r}$ of +8 ‰ to $\delta^{18}O^{f}_{r}$ values in the range of +9.1 to +9.8 ‰ will still occur over a range of w/r ratio $\geq$ ~0.1, but still within the temperature range deduced from the fluid inclusion study. Ohmoto *et al.* (1983) calculated that for the Kuroko deposits rocks within the montmorillonite zone the w/r ratio was ~2, and for rocks in the sericite-chlorite zone the w/r ratio was ~20. This would suggest that a magmatic ± seawater fluid could not produce the necessary shifts in $\delta^{18}O$ values seen at Mount Chalmers. However, Taylor (1997) argued the typical range of w/r ratios averaged over an entire hydrothermal system is seldom greater than 1. If a plausible length scale and flow vector are defined then these w/r ratios of ~1 translate into time-integrated H_2O fluxes of hundreds to thousands of kg/cm^2. Taylor (1997) further argues those w/r ratios much greater than 1 are not compatible with the limited quantities of heat energy available to drive convective systems, assuming a one-time only intrusion of a magma body. However, w/r ratios greater than unity maybe achieved where there have been multiple injections of magma into a volcanic pile.

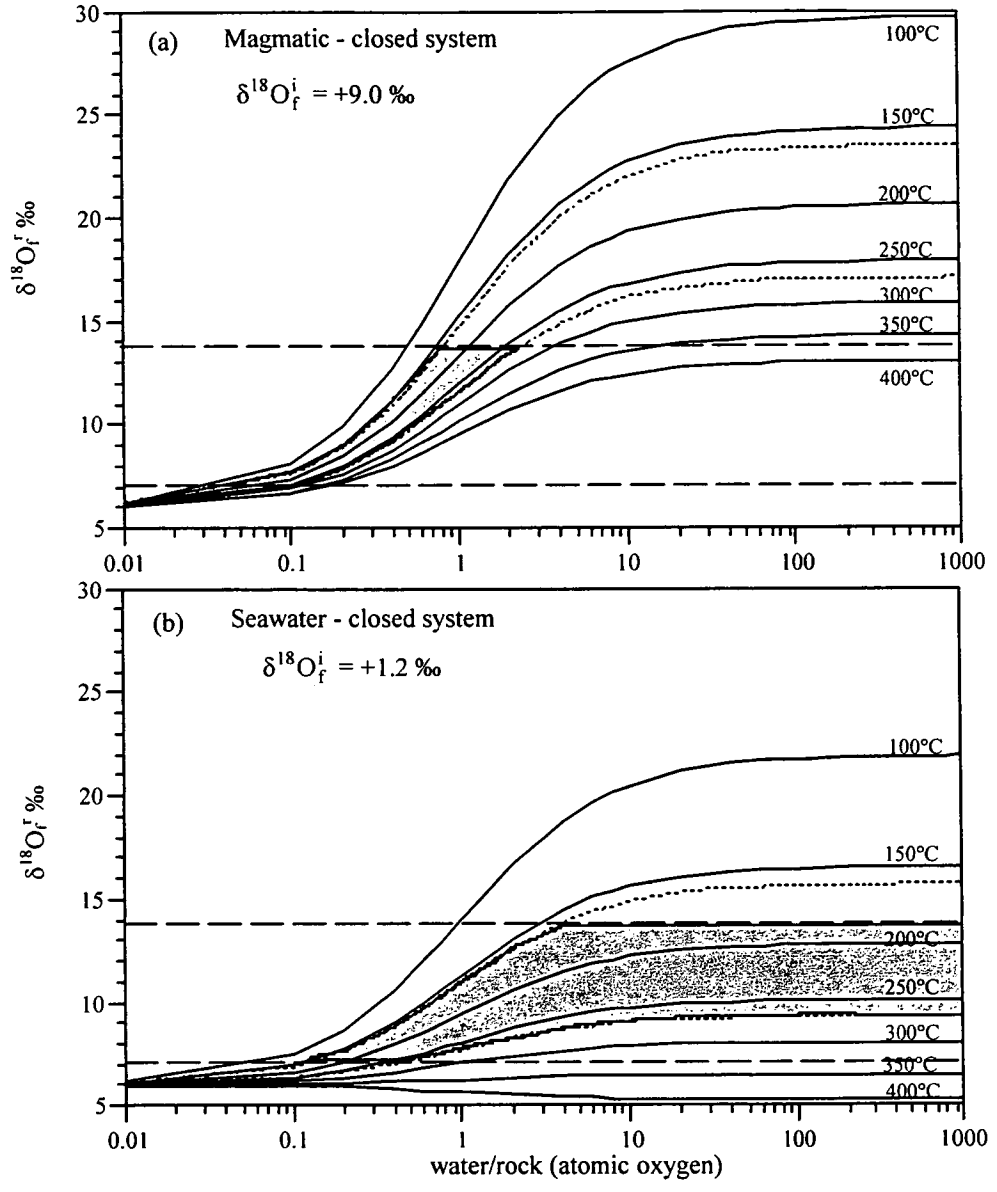

Figure 11.3. Calculated changes in the $\delta^{18}O$ values of rhyolite $\delta^{18}O$ = 7‰ in an open system as a result of equilibrium oxygen isotope exchange with a magmatic water (a) and seawate (b). The shaded areas represent the $\delta^{18}O$ range in values of altered rhyolite at Mount Chalmers.

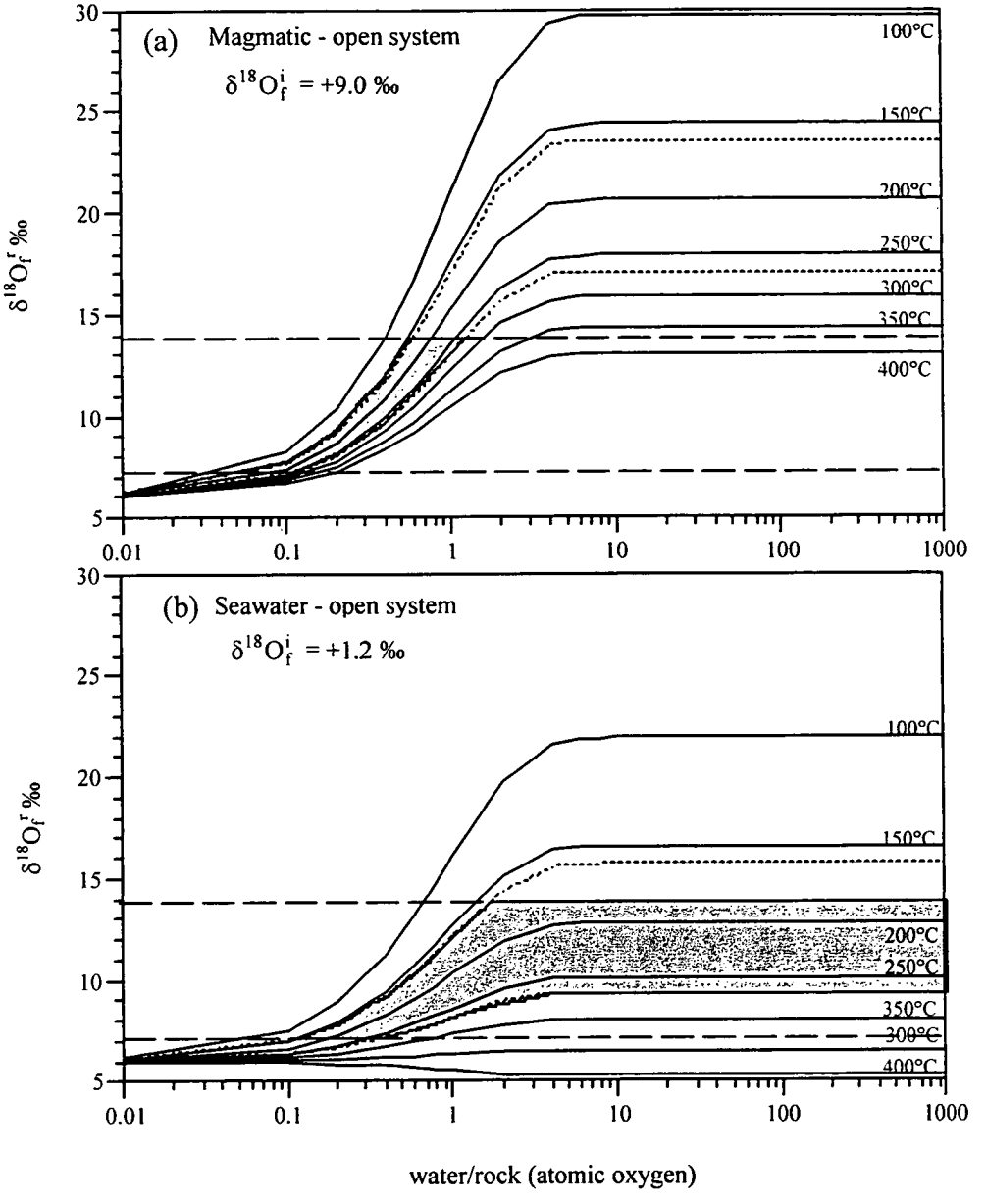

Figure 11.4. Calculated changes in the $\delta^{18}O$ values of rhyolite $\delta^{18}O$ = 7‰ in an open system as a result of equilibrium oxygen isotope exchange with a magmatic water and seawater. The shaded areas represent the $\delta^{18}O$ range in values of altered rhyolite at Mount Chalmers

The $\delta^{18}O^{i}_{w}$ values of +1.2 and +5.8 ‰ represent respectively the unmodified values of two types of water that may have interacted with the footwall volcanics and sedimentary rocks at Mount Chalmers: seawater and magmatic ± seawater. Base upon the above modelling the role of meteoric water at Mount Chalmers can be largely discounted. The other major factor to take into consideration is that the $\delta^{18}O_{w}$ of the fluid involved in the water rock interaction may not have maintained its original value, and thus may not be used as an indicator for the origin of the fluid (Green *et al.*, 1983). It is not possible to determine from any chemical or isotopic data the presence or absence of a small fraction (25%) of a magmatic component in hydrothermal fluid, as $\delta^{18}O^{i}_{w}$ of the magmatic fluid would change due to water-rock interaction (Ohmoto and Rye, 1974; Pisutha-Arnond and Ohmoto, 1983). Any fluid regardless of its origin may end with the same $\delta^{18}O$ if the w/r ratio was much less than 1 *i.e* rock dominated. Only when the w/r ratio of the hydrothermal system is water dominated *i.e* >1 can the $\delta^{18}O^{i}_{w}$ value estimated from the $\delta^{18}O^{f}_{r}$ value be used to identify the isotopic composition of the original fluid (Green *et al.*, 1983).

Therefore, any combination of the above condition(s) such as (OS-2), or (OS-2 + OS-3); (CS-2), (CS-3) or (CS-2 +CS-3) could theoretically produce the $\delta^{18}O$ values at Mount Chalmers. That is, in both the open and closed systems seawater alone can produce the shifts in $\delta^{18}O$ values seen at Mount Chalmers. A combination of seawater and a magmatic ± seawater fluid (seawater dominated) is also considered to be capable of producing the shifts in $\delta^{18}O$ values. In a closed system, magmatic ± seawater fluid is also considered to be capable of producing the shifts in $\delta^{18}O$ values at Mount Chalmers. However, if the more restricted range in $\delta^{18}O^{f}_{r}$ values (+9.1 to +9.8 ‰) is used then in both the open and closed systems only seawater is considered to be able to produce the change in $\delta^{18}O$ values seen at Mount Chalmers. However, the modelling would indicate that the most geologically reasonable hydrothermal fluid that was responsible for the shifts in the $\delta^{18}O$ values of the footwall rhyolite at Mount Chalmers was dominated by seawater.

11.6. WATER FLUX

Calculated w/r ratios only provide minimum estimates of the fluid mass that has flowed through and interacted with the volcanics. Water/rock ratios can be used to estimate the actual amounts of fluid that has flowed through and that has isotopically exchanged with a given volume of rock. One such method is too define an idealised time scale and flow geometry that approximates reality as much as possible. In this approach it is generally not worthwhile to define more than the length scale and a straight-line flow path Given a constant flow direction and geologically reasonable estimate for the length of time that the hydrothermal system has operated for, then the water/ratios can be transformed into actual fluid fluxes (Taylor, 1997). Therefore, it is convenient to normalise the silica alteration samples' w/r ratios to the mass of water that has exchanged oxygen with a representative equivalent volume (REV) of rock. For REV a volume equivalent to a 10 cm diameter sphere (523.60 cm^3) was used (Larson *et al.*, 1994).

The calculated molar ratios of oxygen in the fluid to that in the volcanics are converted to moles of water which have exchanged oxygen with an REV (*M*, in units of mole H_2O/REV) by multiplying w/r_{open} or w/r_{closed} by the inverse of the number of moles of water oxygen per mole of H_2O ($m_{o,water}$), and by the moles of rock oxygen per REV ($m_{o,rock}$) (Larson and Zimmerman, 1991).

$$M = \left(w / r_{open}\right)\left(m_{o,water}\right)^{-1}\left(m_{o,rock}\right) \text{ (Larson and Zimmerman, 1991)} \qquad \text{(Eqn. 11.6)}$$

Where:

- $m_{o,water} = 1$
- $m_{o,rock}$ is calculated by summing the contribution of oxygen from each major oxide in the least altered rhyolite

The average $m_{o,rock}$ for five of the least altered rhyolite samples from the Berserker beds is 51.35 moles per REV. The least altered rhyolites were selected by having an Alteration Index $\left(\left[\left(\frac{MgO+K_2O}{MgO+K_2O+Na_2O+CaO}\right)\times 100\right]\right.$ Ishikawa *et.al.*,1976$\left.\right)$ between ~35 to ~65. The average $m_{o,rock}$ value of 51.35
was used for all of the calculations of mole H_2O/REV. The upward flux of water through each REV cube (8.06 cm on a side) in the centre of the Mount Chalmers alteration system can be calculated by Equation 11.7 (Larson and Zimmerman, 1991):

$$f_{water} = 24,814\left(M\right)\left(\alpha_{REV}\right)^{-1}\left(t\right)^{-1} \qquad \text{(Eqn. 11.7)}$$

Where:

- *M* is determined from Eqn. (11.6);
- α_{REV} is the cross-sectional area of the REV (69.96 cm^2);
- *t* is the duration of the water/rock interaction in seconds.

The duration of hydrothermal activity at Mount Chalmers is not known. Modelling of the Kuroko VHMS hydrothermal systems (Cathles, 1983) found that they formed as a result of a number of small (1x3 km in cross section) intrusive pulses that cooled by convection and formed individual sulphide and sulfate ore lenses in less than 5,000 years and possibly in 100 years. Modelling by Cathles *et al.*, (1997) showed that a deep (16 to 18 km) large (40 x 2 km) single intrusion can sustain hydrothermal circulation and near-surface geothermal activity for ~800,000 years. The longevity of hydrothermal activity generated by these large intrusions may have the potential to produce isolated very large tonnage massive sulphide deposits. These figures therefore provide a time frame in which to calculate the amount of fluid flux in a given time period for the Mount Chalmers deposit.

Given the small tonnage and isolated nature of massive sulphide at Mount Chalmers, a short-lived hydrothermal system was modelled. The other unknown value required for these calculations is the vertical extent of the alteration system and hence the height of the hydrothermal plume that caused the alteration and the mineralisation. Estimates of the vertical extent of hydrothermal plumes associated with VHMS deposits range from 1 to 5 km or possibly deeper (*e.g.* Cathles, 1983; Galley, 1993). A hydrothermal plume with a vertical extent of 2 km was used in the calculation of f_{water}. The calculated water fluxes for w/r ratios between 0.5 to 2 vary from 6.2 $x10^{-8}$ to $2.5x10^{-7}$ mol/cm^2-s (Table 11.3). Integrated over the lifetime (5,000 years) of the hydrothermal system, this translates into a total water flux of ~9,800 - 39,000 mol/cm^2 (Table 11.3). These values are an order of magnitude greater than the values calculated for the Rico porphyry molybdenum deposit (Colorado) by Larson and Zimmerman (1991). The differences in water fluxes maybe influenced by the different environments that the two deposits were formed in. Mount Chalmers was formed in a submarine environment where there was an inexhaustible supply of water throughout the life of the hydrothermal system. Whereas, the Rico porphyry molybdenum deposit was formed in a subaerial environment and the hydrothermal fluids were largely of a meteoric origin and the volume and supply of water was possibly dictated by seasonal variations in the rainfall supply.

Table 11.3. Calculated f_{water} values for an open system with an assumed life of 5,000 years

Time years)	w/r ratios	f_{water} mol/cm^2-s	Intergrated water flux mol/cm^2	kg/cm^2
5,000	0.5	$6.2x10^{-8}$	9,800	180
5,000	1	$4.3x10^{-7}$	20,000	350
5,000	2	$2.5x10^{-7}$	39,000	710

From the above calculations it can be shown that a minimum of approximately 1.8 to 7.1 kg x 10^6 kg of H_2O must have passed through each square meter of cross section of the Mount Chalmers footwall rhyolite during the life of the hydrothermal system. For longer periods of time *e.g.* 10,000 years then the flow rates are doubled. From these figures minimum flow rates can be calculated, where q_{min} = 0.36 m/yr to q_{max} = 1.4 m/yr. These flow rates are an order of magnitude greater than the flow rates calculated for off-axis hydrothermal circulation at Deep Sea Drilling Project/Ocean Drilling Program Site 504 (central Pacific Ocean) by Fisher *et al.* (1994). It must be stressed that these are minimum values as considerable more H_2O may have moved through fractures within the rocks without undergoing isotopic exchange with the wallrocks, either as result of the wallrocks having already been depleted in ^{18}O, or because of slow kinetics (Taylor, 1997).

11.7. Discussion

Except for two samples the intense footwall silica alteration at Mount Chalmers has a very narrow range of $\delta^{18}O$ values (+9.1 to +9.8 ‰, Table 11. 1). MC53-154.4 is the deepest sample and has the heaviest $\delta^{18}O$ value (+13.8 ‰) and the highest recorded temperature from fluid inclusions. (Table 11.1). This, combined with the fluid inclusion temperature range, suggests that the deeper parts of the hydrothermal system were hotter and that the fluids were isotopically heavier (Table 11.1). Twenty metres vertically above sample MC53/154.4, the $\delta^{18}O_r$ value values decrease rapidly to +9.8 ‰ (MC53/133.2) and a further 6 metres uphole to 9.2 ‰ (MC53/126.8). The rapid decrease in $\delta^{18}O$ values suggests that large isotopic gradients over relatively short distances may have existed in the upwelling hydrothermal plume at Mount Chalmers. The fluid inclusion evidence shows that the fluids became cooler as they approached the seafloor-water interface. Sample MC71/134.7 (+7.1 ‰) was taken from the altered footwall rhyolite. If sample MC53/154.4 can be discounted due to dislocation between the isotopic value and the fluid inclusion data, then the shifts in isotopic composition seen in the footwall rhyolite at Mount Chalmers is comparable to what is typically seen in other VHMS deposits, where the $\delta^{18}O$ values of altered rocks deposits tend to decrease with depth and as the ore body is approached (*e.g.* Addy and Ypma, 1977; Costa *et al.*, 1983; Green *et al.*, 1983; Taylor and South, 1985; Paradis *et al.*, 1993).

The $\delta^{18}O_r^f$ of the quartz alteration represents the final product of interaction between the hydrothermal fluid and the footwall rhyolite as they obtained isotopic equilibrium or for some unknown reason the fluid flow decreased or stopped completely. The $\delta^{18}O_r^f$ further provides an estimate of the type of major chemical change occurring in the footwall as silica is precipitated and the hydrothermal fluid is locked out by mineral deposition. Isotopic modelling enables you back calculate to an estimate of the $\delta^{18}O_w^i$ value for the hydrothermal fluid, unless the $\delta^{18}O$ values are directly obtainable from fluid inclusions. Regardless of how these values are obtained they only give a snap shot in time of the fluid evolution and its interaction with the lithologies it has passed through and interacted with.

The calculated high water fluxes over a short time period (5,000 years) indicate that high water/rock ratios (≥ 1) prevailed throughout most of the life the hydrothermal system at Mount Chalmers. This conclusion is further reinforced by the modelling of w/r ratios for both open and closed systems that indicate that the hydrothermal fluid was dominated by seawater, with the possibility of the minor input of magmatic fluid. This conclusion is further reinforced by both the fluid inclusion and sulphur isotope evidence that indicate that the hydrothermal fluid was dominated by modified seawater with minor but not insignificant input from a magmatic fluid.

CHAPTER 12
METAL DISTRIBUTION, ZONATION AND ASSOCIATIONS

12.1 INTRODUCTION

A notable and consistent feature of VHMS deposits is the presence of vertical and/or lateral chemical and mineralogical zonation. This zonation was initially documented for two Canadian deposits by Price and Bancroft (1948) and Scott (1948) who recognised a vertical zonation from Cu-rich bases to Pb-Zn-rich tops for the Waite-Amulet and Quemont mines respectively. Horikoshi and Sato (1970), Eldridge *et al.* (1983), Ohmoto *et al.* (1983) and Shimazaki (1974) recognised a similar vertical mineralogical and chemical zonation for the VHMS deposit(s) of the Kuroko district of Japan. This vertical and lateral zonation has been further documented in general terms *i.e.* without reference to any specific deposit by Sangster, (1972); Large, (1977) and Franklin *et al.*, (1981). Metal zonation studies have been used by previous workers to delineate zones of hydrothermal activity within volcanic-hosted massive sulphide deposits (*e.g.* Khin Zaw *et al.*, 1988; Gemmell and Large, 1992; Hill, 1996). Metal zonation studies have also been used to determine stratigraphic younging directions in folded and deformed VHMS deposits (Large *et al.*, 1988) and to interpret the presence of folding within a massive sulphide ore lens, where other structural evidence is lacking (Khin Zaw *et al.*, 1988; Lees *et al.*, 1988).

12.2 ZINC RATIO

Huston and Large (1987) showed that the variations in the mean Zn ratio ({100 Zn/[Zn + Pb]}) between individual VHMS deposits of the Mount Read Volcanics (Tasmania) and their ore lenses indicate that the Pb-Zn saturation of the hydrothermal fluid rather than the Pb-Zn content in the footwall source lithologies was the major control on the Zn ratio of the deposits. The mean Zn ratio is also controlled by the temperature and salinity of the hydrothermal fluid and is independent of the pH and fO_2, and activity of dissolved sulfur. VHMS deposits typically have a restricted mean Zn ratio range between 60 - 77 and low standard deviations (< 15). Whereas other styles of mineralisation tend to have broader and a lower range of mean values and higher standard deviations (Huston and Large, 1987).

12.2.1 Methodology

The entire assay database for the Mount Chalmers deposit was compiled from mining and exploration company databases into a Microsoft Excel format. Assay data base was partly compiled by the author, Federation Resources, Outokumpu Exploration Australia and Great Fitzroy Mines from the original Geopeko drill logs. Assay intervals ranged between 0.5 - 3.0 m in length. The vast majority of the drill holes at Mount Chalmers were drilled vertically, with no downhole surveys conducted. It therefore has to be assumed that none of these holes deviated significantly from their vertical path.

This is considered to be a valid assumption as drill holes that have been surveyed and collared vertically have only deviated from the vertical by a maximum of 4.5° (Table 12.1).

Table 12.1 Sample downhole drill hole surveys.
Azimuth's are relative to the Mount Chalmers mine grid

Hole ID	Survey Depth	Azimuth	Dip
FDR19	0.00	360.00	-90
FDR19	92.00	313.00	-84.5
FDR19	122.00	94.00	-85.5
FDR19	152.00	179.00	-85
FDR25	120.45	72.00	-89
FDR25	150.00	173.00	-89
FDR25	180.50	360.00	-90
FDR26	0.00	360.00	-90
FDR26	120.00	135.00	-86.6
FDR26	150.20	126.00	-87
FDR26	177.00	340.00	-87

For the calculation of the Zn ratio the assays values were categorised according to the lens they came from and the style of mineralisation they came from, namely massive sulphide, stringer zone and mineralised horizon. To eliminate possible analytical error and to ensure that the Zn ratio is reflecting the hydrothermal activity and not the normal background values of the volcanics only assay values above 100 ppm were used.

12.2.2 Results

The mean Zn ratio values and standard deviations for Mount Chalmers as a whole, which ore lens and the style of mineralisation they pertain to are listed in Table 12.2.

Table12.2. Zn ratio (Zn x 100/Zn+Pb) mean and standard deviations for Mount Chalmers, the Main Lode and West Lode, and the main styles of mineralisation.

Ore Lens	Style of Mineralisation	Mean	S.D	N
Mount Chalmers		66.4	19.0	3844
Mount Chalmers	Massive sulphide	69.7	15.9	194
Main Lode	Au Pod	30.8	23.4	130
Main Lode + West Lode	Gossan	45.7	31.9	150
Main Lode		65.1	20.9	1475
Main Lode	Massive sulphide	70.3	14.8	61
Main Lode	Stringer zone mineralisation	70.0	17.7	1460
Main Lode	Mineralised horizon	63.6	20.1	128
West Lode		67.5	17.6	2002
West Lode	Massive sulphide	69.5	16.4	133
West Lode	Stringer zone mineralisation	66.1	18.2	818
West Lode	Mineralised horizon	64.8	20.3	132

For Mount Chalmers as a whole (massive sulphide, stringer zone mineralisation, dolomite, mineralised horizon, altered footwall lithologies), the shape of the histogram pattern is typical for Phanerozoic VHMS deposits (Fig. 12.1a).

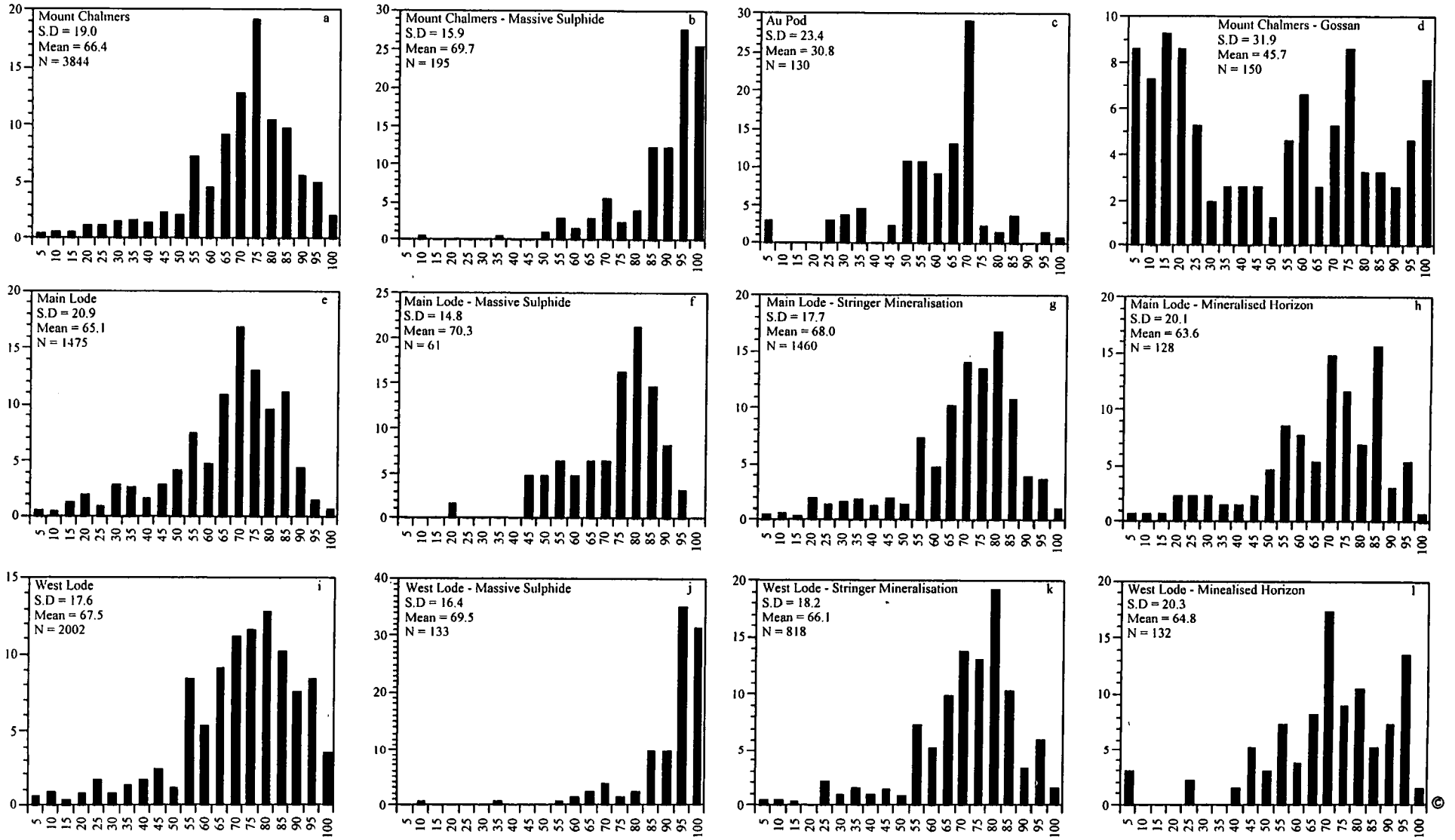

Figure 12.1. Zinc ratio histograms of (a) Mount Chalmers, (b) Mount Chalmers massive sulphide (combined Main Lode and West Lode), (c) Au Pod, (d) gossan, Main Lode (e) combined assays, (f) massive sulphide, (g) stringr zone mineralistion (h) mineralised horizon and West Lode (i) combined assays, (j) massive sulphide, (k) stringr zone mineralistion and (l) mineralised horizon.

Mount Chalmers has a mean Zn ratio of and a standard deviation of 66.4 and 19.0 respectively (Table 12.1). The mean value for Mount Chalmers falls within the range of mean values for Phanerozoic VHMS deposits, but has a higher standard deviation. The Mount Chalmers massive sulphide mineralisation (combined Main Lode and West Lode) has a histogram pattern that is skewed towards Zn and is an atypical pattern for Phanerozoic VHMS deposits (Fig. 12.1b). The histogram pattern for the Au Pod mineralisation has a broad similarity to Phanerozoic VHMS deposits, but the standard deviation (23.4) and mean (30.8) are well above those considered to be typical for Phanerozoic VHMS deposits (Fig. 12.1c). The gossan has a histogram pattern and standard deviation (31.9) and mean (45.7) values that have no resemblance to Phanerozoic VHMS deposits (Fig. 12.1d). This is a result of the enrichment of Pb in the gossan compared to Zn. This also illustrates the danger of using weathered or oxidised samples to finger print a VHMS Zn ratio pattern for a prospect in exploration.

The Main Lode (massive sulphide, stringer zone mineralisation, dolomite, mineralised horizon, altered footwall lithologies) has a histogram pattern and mean (65.1) and slightly higher standard deviation (20.9) that is typical for Phanerozoic VHMS deposits (Fig. 12.1e). The Main Lode massive sulphide, stringer zone mineralisation and mineralised horizon all have histograms pattens that may be considered typical for Phanerozoic VHMS deposits. Both the stringer zone and mineralised horizon have broader patterns than the massive sulphide with higher standard deviations (17.1 and 20.1 respectively, Figs. 12.1f, g and h).

The West Lode (massive sulphide, stringer zone mineralisation, dolomite, mineralised horizon, altered footwall lithologies) has a histogram pattern and mean (67.5) and a standard deviation (17.6) that may be considered to be typical for Phanerozoic VHMS deposits (Fig. 12.1i). The West Lode massive sulphide has a histogram pattern that skewed towards higher Zn ratios values and is atypical for Phanerozoic VHMS deposits. Whereas the stringer zone mineralisation and mineralised horizon have histograms pattens that may be considered typical for Phanerozoic VHMS deposits (Figs. 12.1k and l).

In either ore lens the mean values for the Zn ratio follows the pattern: massive sulphide > stringer zone > mineralised horizon. This pattern is also seen in the standard deviations for each of the ore lenses. This pattern indicates that the stringer zone mineralisation and the alteration envelope surrounding the massive sulphide mineralisation contains comparatively more Pb than the massive sulphide. This is also seen in the histograms where the Zn ratio for the stringer zone and the mineralised horizon tend to have a higher percentage of Zn ratio values towards the lower Zn ratio values.

The average Zn ratios (Table 12.2) for the Main Lode and West Lode massive sulphide lenses and stringer zone mineralisation are consistent with a fluid temperature between 200 and 250° C and a salinity of ≈5 -7 wt. % (see Fig. 18 *in* Cooke and Large, 1995). These values are in close agreement with the measured temperatures of homogenisation and equivalent wt. % NaCl for the Main Lode and West Lode.

12.3 METAL DISTRIBUTION

12.3.1 Copper

Figure 12.2a plots the percentage frequency of Cu values according to which lode they came from. These histograms are heavily skewed because of the number of analyses that have values of ≤1 %. It can be seen that both the Main Lode and the West Lode have similar distribution in assay values. The vast majority of analyses (> 84.2 % - Main Lode and > 88.2 % - West Lode) are ≤ 1 %. The Main Lode is more Cu-rich than the West Lode as 15.6 % of analyses from the Main Lode fall within the range of 1 to 8 % compared to 11.4 % for the West Lode.

Figure 12.2b plots the percentage frequency histogram of assay Cu values according to the lode and style of mineralisation the assays were obtained from (massive sulphide, stringer mineralisation, gossan and dolomite). For the massive sulphide and stringer zone mineralisation, the Main Lode is Cu-rich compared to West Lode. However, the West Lode massive sulphide has a higher percentage of assay values greater than 7 % compared to the Main Lode massive sulphide. In fact, the Main Lode massive sulphide has no significant Cu assay values above 8 %. In addition, the massive sulphide mineralisation for both lodes tends to have higher Cu values than the stringer mineralisation.

12.3.2 Zinc

Figure 12.3a is a histogram plot of the percentage frequency for Zn assay values for the Main Lode and the West Lode ore lenses at Mount Chalmers. The West Lode is comparatively more Zn-rich than the Main Lode, and has a greater percentage of values in the 1 to 2 % range than the West Lode (96.7 % versus 85.5 %). The Zn assay values have been further subdivided based upon the style of mineralisation the Zn is associated with *i.e* dolomite, massive sulphide, stringer zone and gossan (Fig. 12.3b). The Main Lode massive sulphide has 77.8 % of its Zn values in the 0 to 2 % compared to 32.4 % for the West Lode. This disparity in Zn values between the Main Lode and the West Lode is also maintained for the other two styles of mineralisation. Figure 12.3b also shows that in both lodes Zn is concentrated in the massive sulphide mineralisation compared to the stringer mineralisation or the dolomite alteration.

12.3.3 Lead

Like Zn, Pb predominantly occurs in the West Lode compared to the Main Lode (Fig. 12.4a). Pb occurs predominantly within the massive sulphide mineralisation and the gossan, where the Pb assays are evenly distributed (Fig. 12.4b). Negligible to minor amounts of Pb occurs within the stringer zone and Au Pod styles of mineralisation.

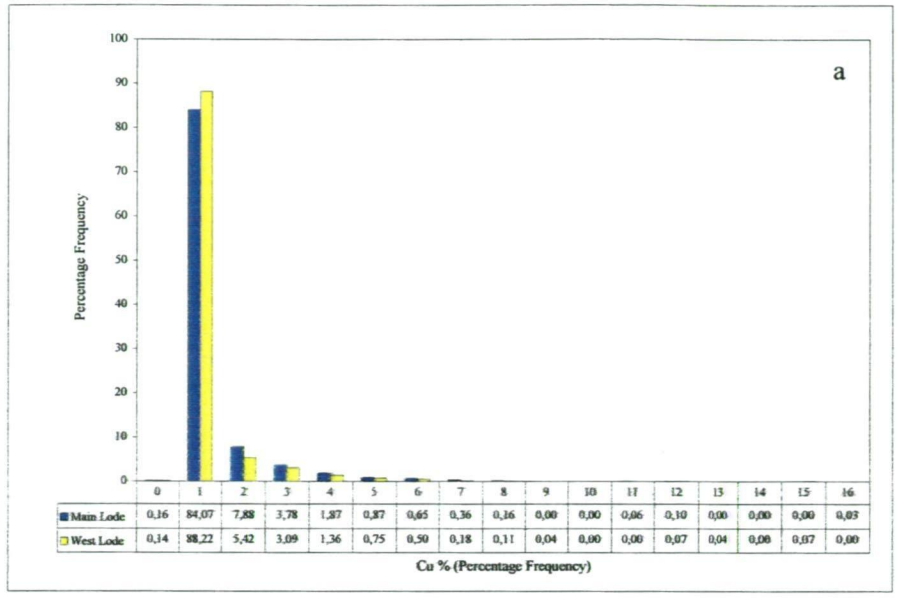

	0	1	2	3	4	5	6	7	8	9	10	11	12	13	14	15	16
Main Lode	0,16	84,07	7,88	3,78	1,87	0,87	0,65	0,36	0,16	0,00	0,00	0,06	0,10	0,00	0,00	0,00	0,03
West Lode	0,14	88,22	5,42	3,09	1,36	0,75	0,50	0,18	0,11	0,04	0,00	0,00	0,07	0,04	0,00	0,07	0,00

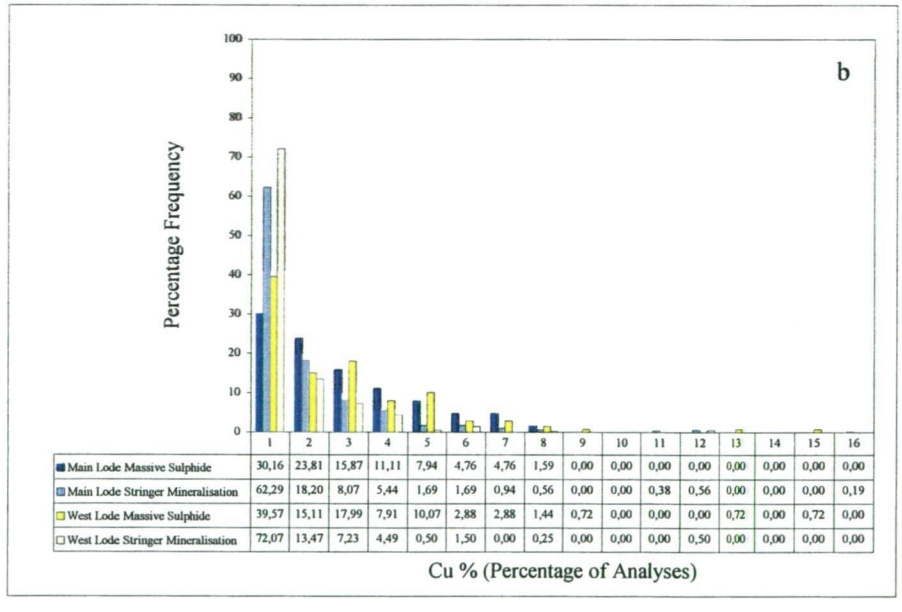

	1	2	3	4	5	6	7	8	9	10	11	12	13	14	15	16
Main Lode Massive Sulphide	30,16	23,81	15,87	11,11	7,94	4,76	4,76	1,59	0,00	0,00	0,00	0,00	0,00	0,00	0,00	0,00
Main Lode Stringer Mineralisation	62,29	18,20	8,07	5,44	1,69	1,69	0,94	0,56	0,00	0,00	0,38	0,56	0,00	0,00	0,00	0,19
West Lode Massive Sulphide	39,57	15,11	17,99	7,91	10,07	2,88	2,88	1,44	0,72	0,00	0,00	0,00	0,72	0,00	0,72	0,00
West Lode Stringer Mineralisation	72,07	13,47	7,23	4,49	0,50	1,50	0,00	0,25	0,00	0,00	0,00	0,50	0,00	0,00	0,00	0,00

Figures 12.2a & b. Histograms showing the distribution of Cu between the Main Lode and the West Lode and the massive sulphide and stringer zone mineralisation of the two lodes

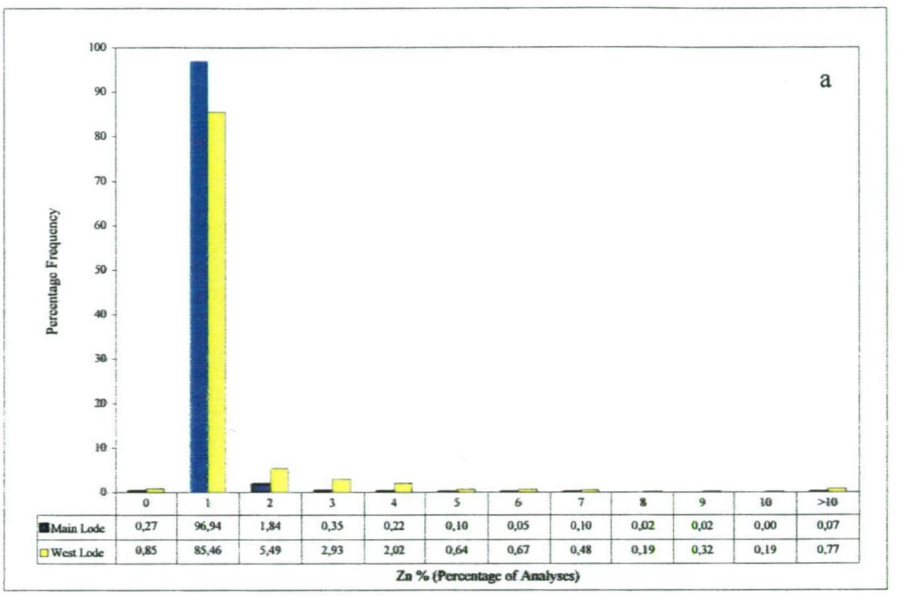

	0	1	2	3	4	5	6	7	8	9	10	>10
Main Lode	0,27	96,94	1,84	0,35	0,22	0,10	0,05	0,10	0,02	0,02	0,00	0,07
West Lode	0,85	85,46	5,49	2,93	2,02	0,64	0,67	0,48	0,19	0,32	0,19	0,77

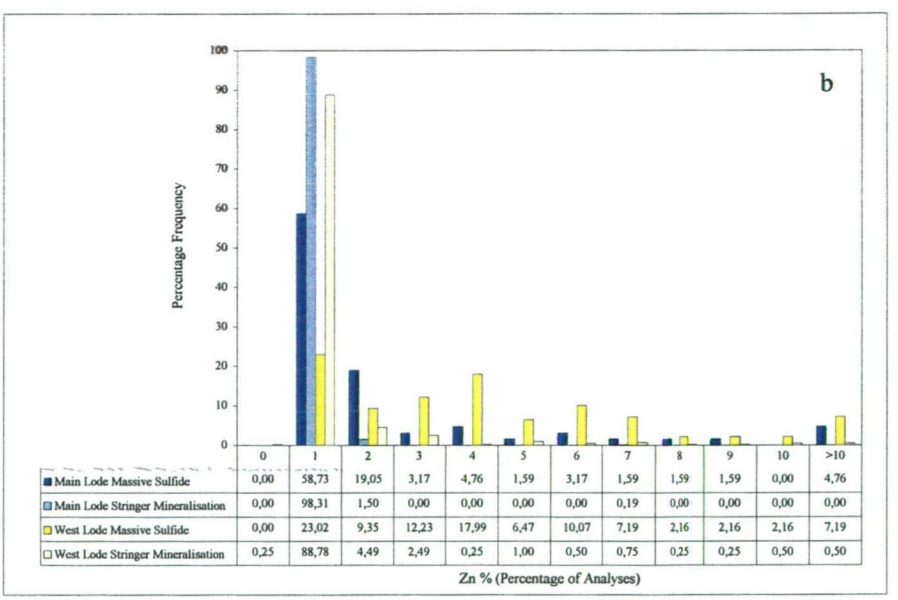

	0	1	2	3	4	5	6	7	8	9	10	>10
Main Lode Massive Sulfide	0,00	58,73	19,05	3,17	4,76	1,59	3,17	1,59	1,59	1,59	0,00	4,76
Main Lode Stringer Mineralisation	0,00	98,31	1,50	0,00	0,00	0,00	0,00	0,19	0,00	0,00	0,00	0,00
West Lode Massive Sulfide	0,00	23,02	9,35	12,23	17,99	6,47	10,07	7,19	2,16	2,16	2,16	7,19
West Lode Stringer Mineralisation	0,25	88,78	4,49	2,49	0,25	1,00	0,50	0,75	0,25	0,25	0,50	0,50

Figures 12.3a & b. Histograms showing the distribution of Zn between the Main Lode and the West Lode and the massive sulphide and stringer zone mineralisation of the two lodes

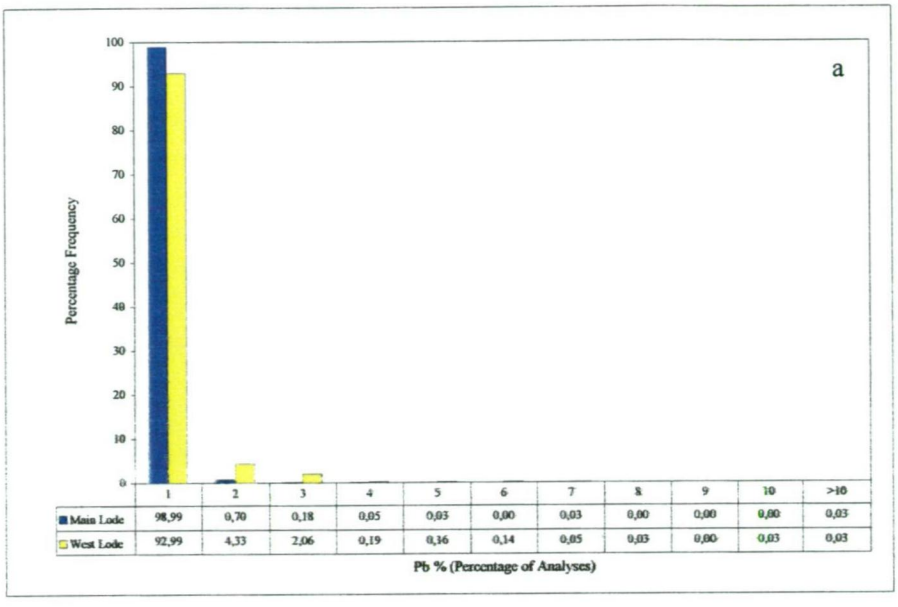

	1	2	3	4	5	6	7	8	9	10	>10
Main Lode	98,99	0,70	0,18	0,05	0,03	0,00	0,03	0,00	0,00	0,00	0,03
West Lode	92,99	4,33	2,06	0,19	0,16	0,14	0,05	0,03	0,00	0,03	0,03

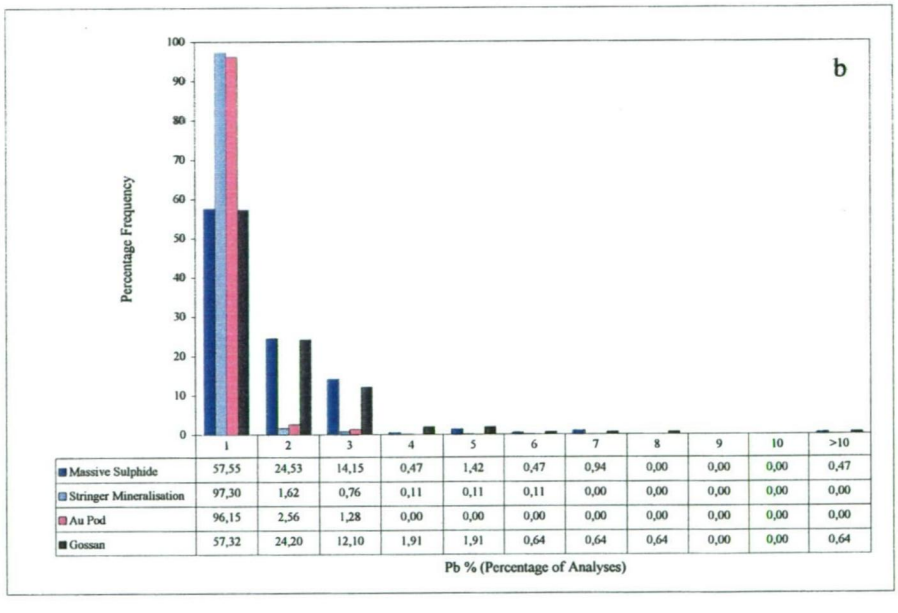

	1	2	3	4	5	6	7	8	9	10	>10
Massive Sulphide	57,55	24,53	14,15	0,47	1,42	0,47	0,94	0,00	0,00	0,00	0,47
Stringer Mineralisation	97,30	1,62	0,76	0,11	0,11	0,11	0,00	0,00	0,00	0,00	0,00
Au Pod	96,15	2,56	1,28	0,00	0,00	0,00	0,00	0,00	0,00	0,00	0,00
Gossan	57,32	24,20	12,10	1,91	1,91	0,64	0,64	0,64	0,00	0,00	0,64

Figures 12.4a & b. Histograms showing the distribution of Pb between the Main Lode and the West Lode and the massive sulphide, stringer zone, Au Pod and gossan mineralisation styles.

12.3.4 Gold

Both the Main Lode and the West Lode have a similar distribution pattern for their Au assays, although the West Lode appears to be slightly more Au-rich than the Main Lode (Fig. 12.5a). The higher Au grades (> 4 g/t) for both the Main Lode and the West Lode are concentrated in the massive sulphide (Fig. 12.5a). The Main Lode massive sulphide mineralisation dominates in the number of analyses in the 4 to 10 g/t range, whereas the West Lode massive sulphide mineralisation dominates in Au grades greater than 10 g/t (Fig. 12.5b). Figure 11.5b also shows that the gossan developed on the West Lode massive sulphide is significantly enriched in Au. The Au Pod is aptly named as it contains the majority of Au values in the 2 - 8 g/t ranges with high values continuing up into the 24 - 26 g/t ranges.

12.3.5 Silver

Ag like Au is concentrated in the West Lode compared to the Main Lode, and has a similar distribution pattern to that of Au (Figs. 12.6a and b). Also like Au, there is only minor Ag enrichment within the stringer zone mineralisation (Figs. 12.6b). Ag tends to be concentrated within the massive sulphide mineralisation compared to Au, but the majority of values (>100 g/t) are concentrated in the gossan.

12.4 METAL CONTOURS

12.4.1 Methodology

For the level contours a reduced level (RL) was calculated for the mid-point of each sample interval. The data was contoured at 10-m levels from 2100m RL to 1990m RL, giving 12 level contours (2,000m RL = sea level). This range provides a complete distribution of both the base and precious metals from the immediate hangingwall to the massive sulphide to deep within the footwall. Pb was not contoured, as there is not enough Pb within the deposit to enable to a complete set of contour plans to be made. Assay values within a 2-m range either side of the designated RL were then selected. Where inclined holes were drilled RLs, eastings for the mid-point of the assay sample intervals were calculated. Wherever for a given RL there was more than one assay value per hole, the assay values were averaged by a simple arithmetic mean. If the assay intervals were of unequal length, then a simple weighted average was calculated. The data was then transferred to the griding software package - MacGRIDZO™, and then contoured. The data were contoured using a weighted least squares griding algorithm, with a cell spacing of 60 in the x and y direction, a weighting exponent of four and the number of points equalling four. In order that the stratigraphic extent of a metal could be contoured, when metal values became less than the contour values selected (Cu = 0.2 %; Zn = 0.5 % and Au = 1 g/t) then a smaller contour interval was selected (Cu = 0.1 %; Zn = 0.2 % and Au = 0.5 g/t)

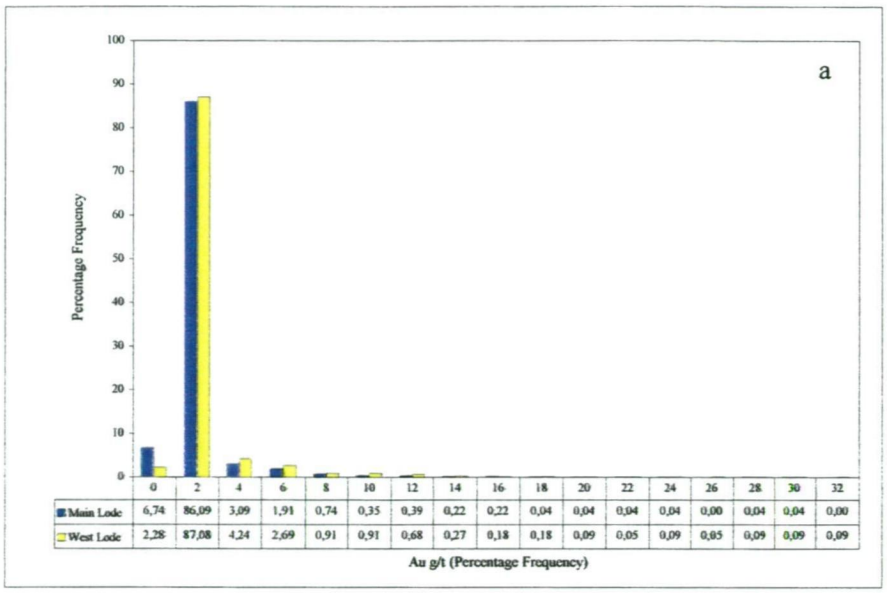

	0	2	4	6	8	10	12	14	16	18	20	22	24	26	28	30	32
Main Lode	6,74	86,09	3,09	1,91	0,74	0,35	0,39	0,22	0,22	0,04	0,04	0,04	0,04	0,00	0,04	0,04	0,00
West Lode	2,28	87,08	4,24	2,69	0,91	0,91	0,68	0,27	0,18	0,18	0,09	0,05	0,09	0,05	0,09	0,09	0,09

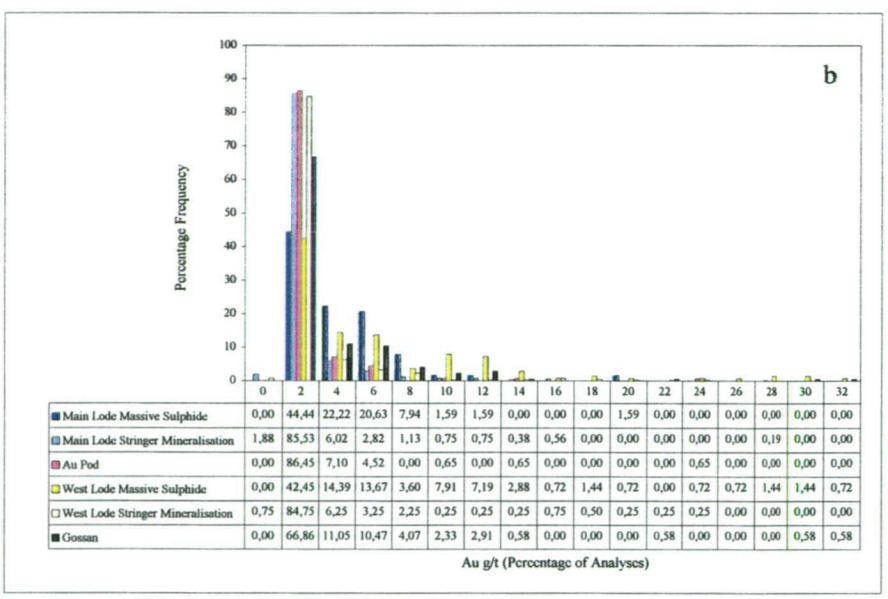

	0	2	4	6	8	10	12	14	16	18	20	22	24	26	28	30	32
Main Lode Massive Sulphide	0,00	44,44	22,22	20,63	7,94	1,59	1,59	0,00	0,00	0,00	1,59	0,00	0,00	0,00	0,00	0,00	0,00
Main Lode Stringer Mineralisation	1,88	85,53	6,02	2,82	1,13	0,75	0,75	0,38	0,56	0,00	0,00	0,00	0,00	0,00	0,19	0,00	0,00
Au Pod	0,00	86,45	7,10	4,52	0,00	0,65	0,00	0,65	0,00	0,00	0,00	0,00	0,65	0,00	0,00	0,00	0,00
West Lode Massive Sulphide	0,00	42,45	14,39	13,67	3,60	7,91	7,19	2,88	0,72	1,44	0,72	0,00	0,72	0,72	1,44	1,44	0,72
West Lode Stringer Mineralisation	0,75	84,75	6,25	3,25	2,25	0,25	0,25	0,25	0,75	0,50	0,25	0,25	0,25	0,00	0,00	0,00	0,00
Gossan	0,00	66,86	11,05	10,47	4,07	2,33	2,91	0,58	0,00	0,00	0,00	0,58	0,00	0,00	0,00	0,58	0,58

Figures 12.5a & b. Histograms showing the distribution of Au between the Main Lode, West Lode and the massive sulphide and stringer mineralisation of the two lodes, and the Au Pod and gossan styles of mineralisation.

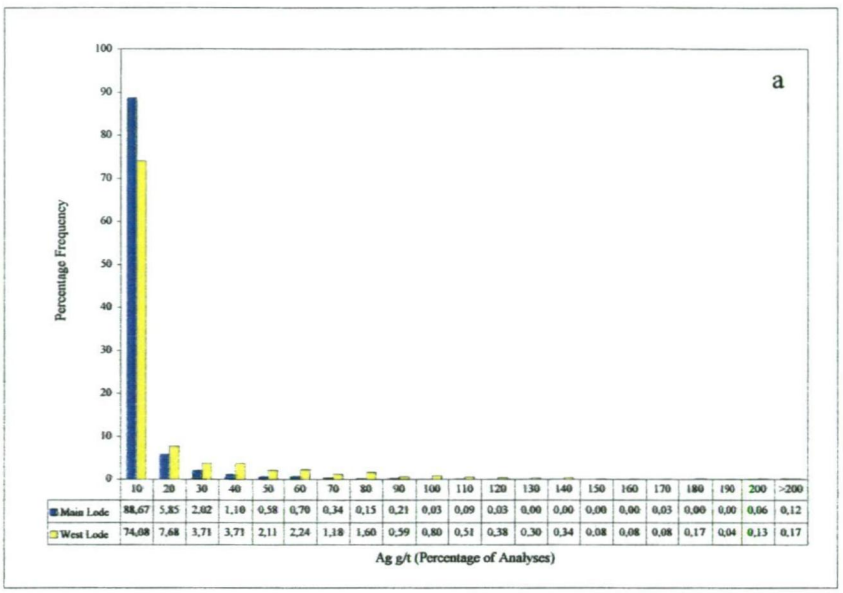

	10	20	30	40	50	60	70	80	90	100	110	120	130	140	150	160	170	180	190	200	>200
Main Lode	88,67	5,85	2,02	1,10	0,58	0,70	0,34	0,15	0,21	0,03	0,09	0,03	0,00	0,00	0,00	0,00	0,03	0,00	0,00	0,06	0,12
West Lode	74,08	7,68	3,71	3,71	2,11	2,24	1,18	1,60	0,59	0,80	0,51	0,38	0,30	0,34	0,08	0,08	0,08	0,17	0,04	0,13	0,17

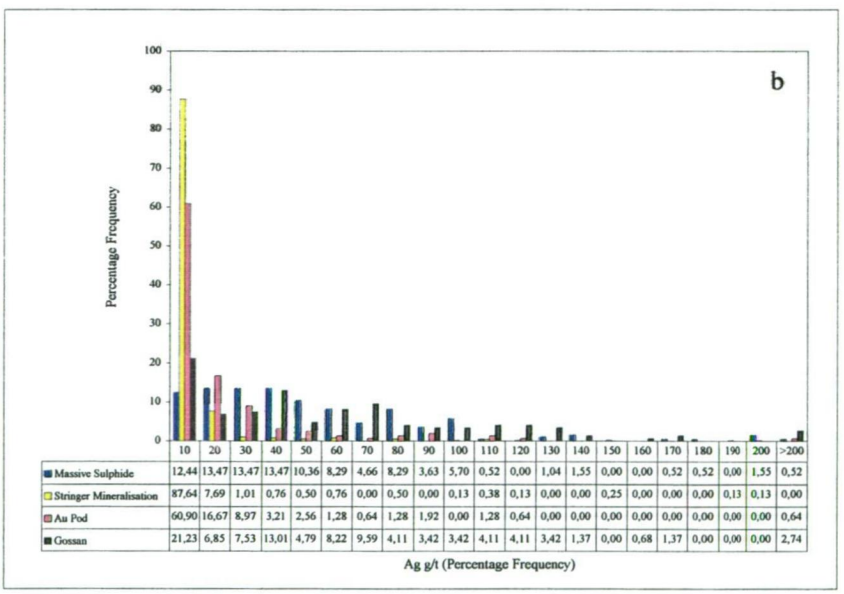

	10	20	30	40	50	60	70	80	90	100	110	120	130	140	150	160	170	180	190	200	>200
Massive Sulphide	12,44	13,47	13,47	13,47	10,36	8,29	4,66	8,29	3,63	5,70	0,52	0,00	1,04	1,55	0,00	0,00	0,52	0,52	0,00	1,55	0,52
Stringer Mineralisation	87,64	7,69	1,01	0,76	0,50	0,76	0,00	0,50	0,00	0,13	0,38	0,13	0,00	0,00	0,25	0,00	0,00	0,00	0,13	0,13	0,00
Au Pod	60,90	16,67	8,97	3,21	2,56	1,28	0,64	1,28	1,92	0,00	1,28	0,64	0,00	0,00	0,00	0,00	0,00	0,00	0,00	0,00	0,64
Gossan	21,23	6,85	7,53	13,01	4,79	8,22	9,59	4,11	3,42	3,42	4,11	4,11	3,42	1,37	0,00	0,68	1,37	0,00	0,00	0,00	2,74

Figures 12.6a & b. Histograms showing the distribution of Ag between the Main Lode and the West Lode and the massive sulphide, stringer, Au Pod and gossan mineralisation styles.

12.4.2 Results

The contours show that the distribution of Cu is distributed approximately in a NNW - SSE direction (Fig. 12.7a) and tends to be concentrated at or near the top of the massive sulphide lens. Copper values decrease down through the massive sulphide lenses, until they increase again within the stringer zone mineralisation. The Cu contours also show that the concentration of maximum Cu values varies from one level to another level. At the 2020m RL there is a shift in the concentration of Cu from the Main Lode to approximately 150-m north of the Main Lode (Fig. 12.7a).

The West Lode is more Zn rich than the Main Lode, with the Zn also being more widely distributed in the West Lode than in the Main Lode (Fig. 12.7b). In the West Lode, the contours show that the Zn mineralisation is aligned in a north-south direction, with the highest Zn values being concentrated above the interpreted faults. Significant Zn values in the West Lode do not occur below the 2050 m RL reflecting the absence or near absence of Zn from the stringer zone mineralisation. At the 2040m RL the Zn contours are concentrated in the South Lode (Fig. 12.7b).

Au tends to be concentrated within the Main Lode. The zones of high Au concentration within the Main Lode do not correspond to the zones of high Cu. In the Main Lode, below the 2040m RL Au concentration shifts northwards, towards the NW-SE structural displacement within the footwall. Within the West Lode Au is concentrated in a narrow N-S zone (Fig. 12.7c).

12.4.3 Location of Feeder Zones

As the ore lenses at Mount Chalmers are relatively undeformed the distribution of Cu, Zn and Au may be used as an indicator of palaeofluid channel ways. The concentration of high metal values within a limited number of areas within the both Main Lode and West Lode suggests that these may be reflecting the palaeofluid channel ways and possible palaeodischarge sites (*e.g.* Figs 12.7). The zones of high metal concentration have an uneven distribution within the massive sulphide and the footwall stringer zone. This uneven distribution suggests that the hydrothermal plumbing system was not static *i.e.* the preferred channel ways for the hydrothermal fluids shifted through time, and/or that multiple channel ways operating at the same time.

12.5 Downhole Metal Variability

The above discussions on the Zn ratio and metal distribution have largely been at the deposit scale. The downhole variability of anyone metal or combination of metals in an individual drillhole would reflect more accurately on a local scale the conditions under which the metals were deposited. For this reason the downhole variability of Cu, Zn, Au and Ag versus lithology from a number of drillholes from both the Main Lode and the West Lode were plotted.

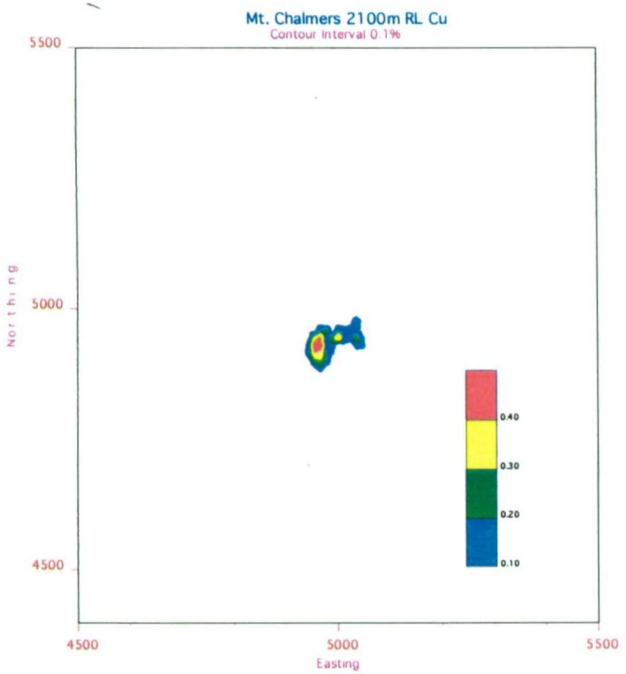
Mt. Chalmers 2100m RL Cu
Contour Interval 0.1%
5500
5000
4500
Northing
4500
5000
5500
Easting
0.40
0.30
0.20
0.10

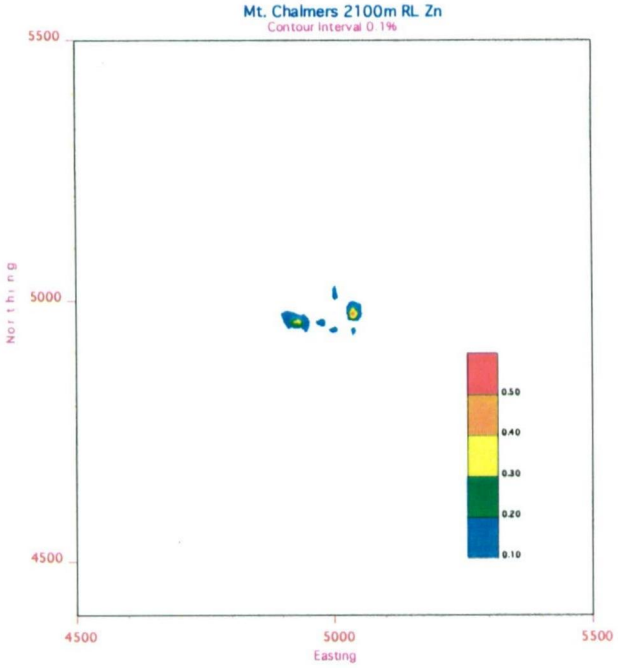
Mt. Chalmers 2100m RL Zn
Contour Interval 0.1%
5500
5000
4500
Northing
4500
5000
5500
Easting
0.50
0.40
0.30
0.20
0.10

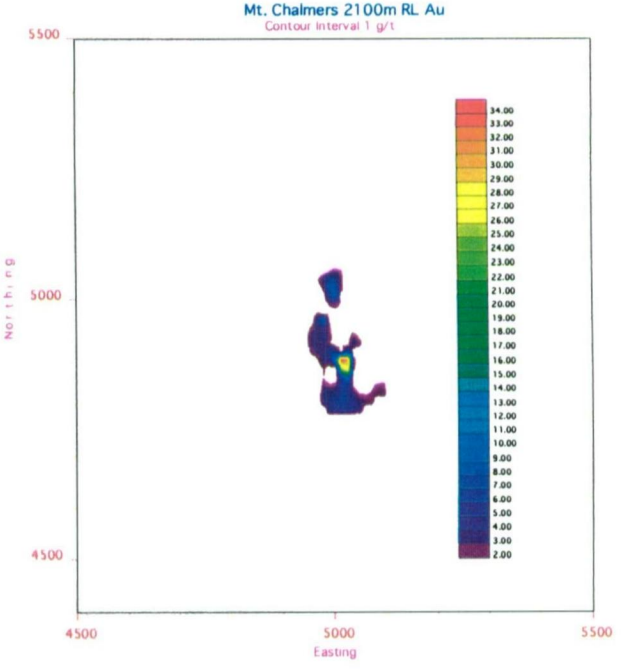
Mt. Chalmers 2100m RL Au
Contour Interval 1 g/t
5500
5000
4500
Northing
4500
5000
5500
Easting
34.00
33.00
32.00
31.00
30.00
29.00
28.00
27.00
26.00
25.00
24.00
23.00
22.00
21.00
20.00
19.00
18.00
17.00
16.00
15.00
14.00
13.00
12.00
11.00
10.00
9.00
8.00
7.00
6.00
5.00
4.00
3.00
2.00

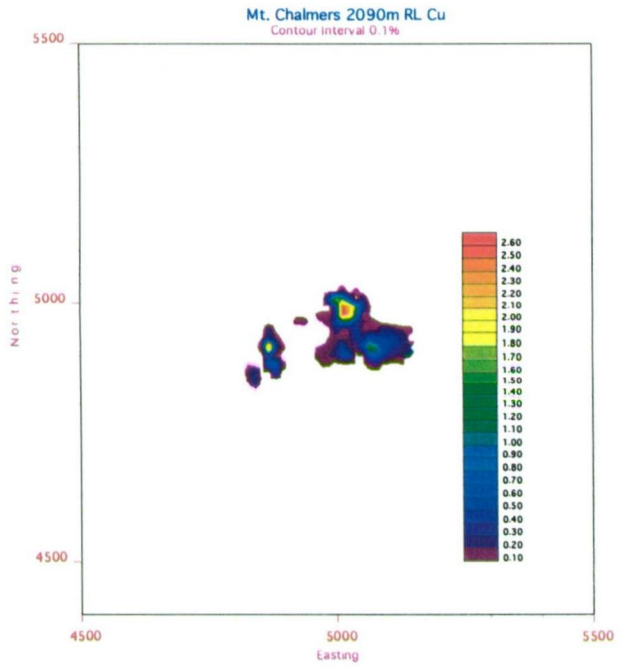
Mt. Chalmers 2090m RL Cu
Contour Interval 0.1%
5500
5000
4500
Northing
4500
5000
5500
Easting
2.60
2.50
2.40
2.30
2.20
2.10
2.00
1.90
1.80
1.70
1.60
1.50
1.40
1.30
1.20
1.10
1.00
0.90
0.80
0.70
0.60
0.50
0.40
0.30
0.20
0.10

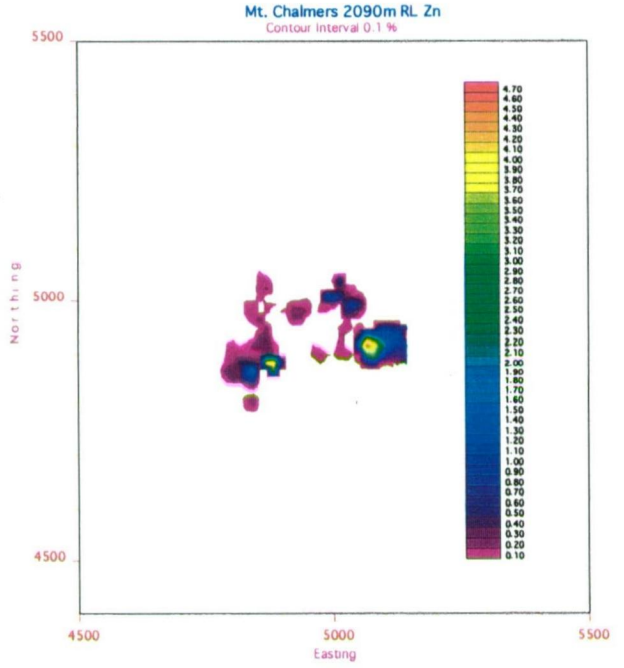
Mt. Chalmers 2090m RL Zn
Contour Interval 0.1 %
5500
5000
4500
Northing
4500
5000
5500
Easting
4.70
4.60
4.50
4.40
4.30
4.20
4.10
4.00
3.90
3.80
3.70
3.60
3.50
3.40
3.30
3.20
3.10
3.00
2.90
2.80
2.70
2.60
2.50
2.40
2.30
2.20
2.10
2.00
1.90
1.80
1.70
1.60
1.50
1.40
1.30
1.20
1.10
1.00
0.90
0.80
0.70
0.60
0.50
0.40
0.30
0.20
0.10

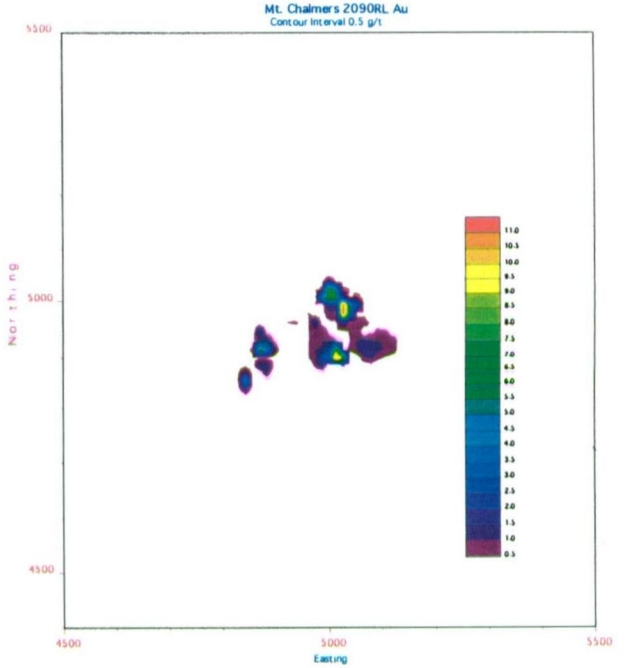
Mt. Chalmers 2090RL Au
Contour Interval 0.5 g/t
5500
5000
4500
Northing
4500
5000
5500
Easting
11.0
10.5
10.0
9.5
9.0
8.5
8.0
7.5
7.0
6.5
6.0
5.5
5.0
4.5
4.0
3.5
3.0
2.5
2.0
1.5
1.0
0.5

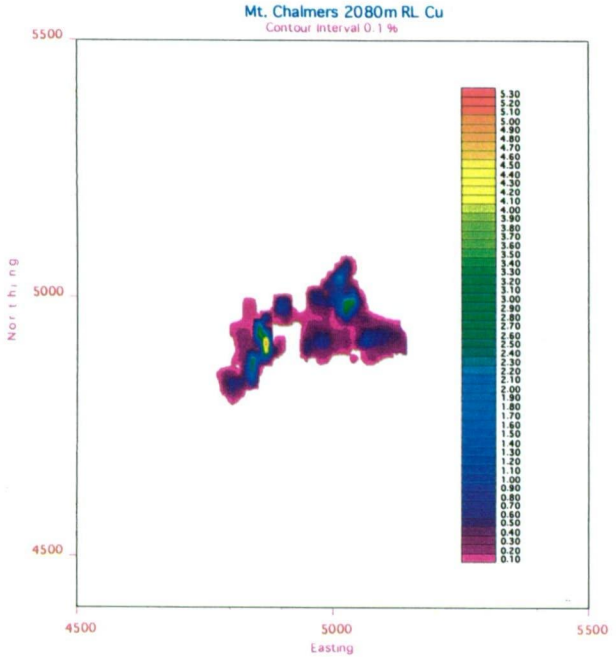
Mt. Chalmers 2080m RL Cu
Contour Interval 0.1 %
Northing
Easting
5500
5000
4500
5.30
5.20
5.10
5.00
4.90
4.80
4.70
4.60
4.50
4.40
4.30
4.20
4.10
4.00
3.90
3.80
3.70
3.60
3.50
3.40
3.30
3.20
3.10
3.00
2.90
2.80
2.70
2.60
2.50
2.40
2.30
2.20
2.10
2.00
1.90
1.80
1.70
1.60
1.50
1.40
1.30
1.20
1.10
1.00
0.90
0.80
0.70
0.60
0.50
0.40
0.30
0.20
0.10

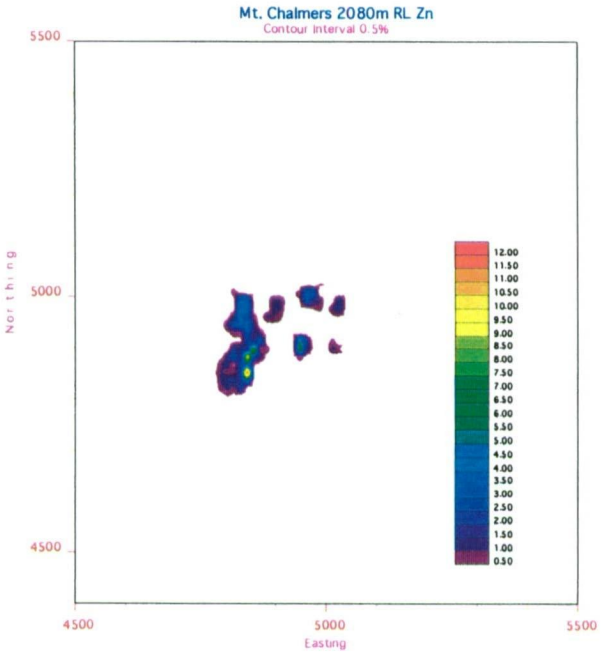
Mt. Chalmers 2080m RL Zn
Contour Interval 0.5%
Northing
Easting
5500
5000
4500
12.00
11.50
11.00
10.50
10.00
9.50
9.00
8.50
8.00
7.50
7.00
6.50
6.00
5.50
5.00
4.50
4.00
3.50
3.00
2.50
2.00
1.50
1.00
0.50

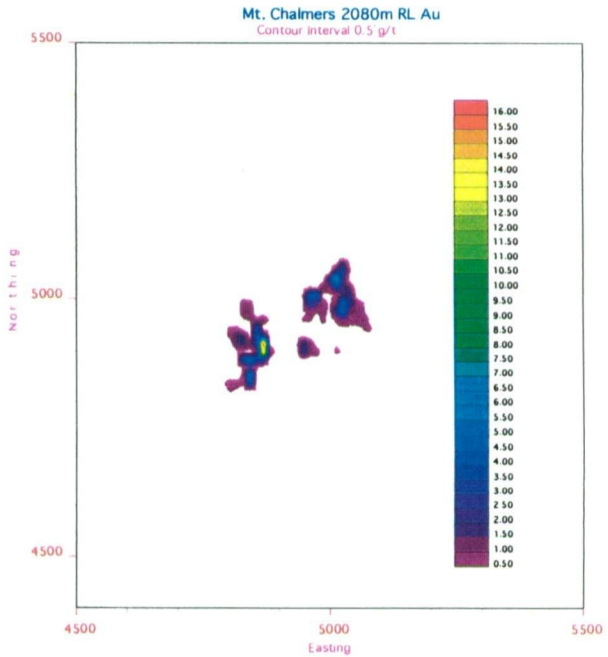
Mt. Chalmers 2080m RL Au
Contour Interval 0.5 g/t
Northing
Easting
5500
5000
4500
16.00
15.50
15.00
14.50
14.00
13.50
13.00
12.50
12.00
11.50
11.00
10.50
10.00
9.50
9.00
8.50
8.00
7.50
7.00
6.50
6.00
5.50
5.00
4.50
4.00
3.50
3.00
2.50
2.00
1.50
1.00
0.50

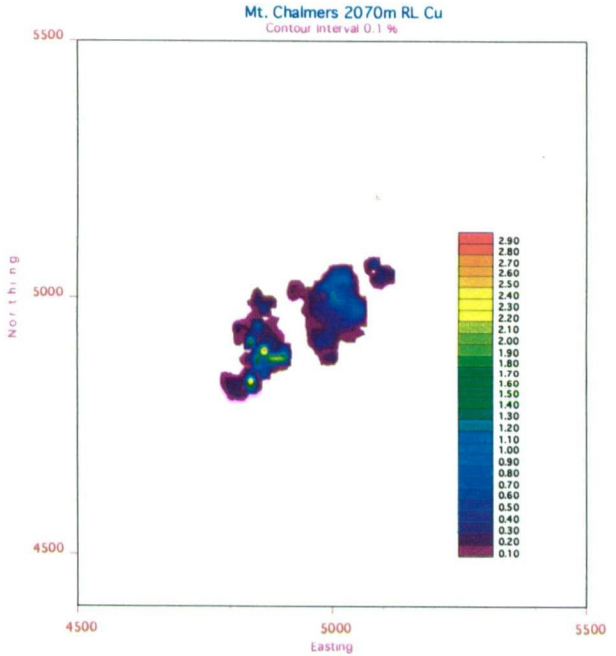
Mt. Chalmers 2070m RL Cu
Contour Interval 0.1 %
Northing
Easting
5500
5000
4500
2.90
2.80
2.70
2.60
2.50
2.40
2.30
2.20
2.10
2.00
1.90
1.80
1.70
1.60
1.50
1.40
1.30
1.20
1.10
1.00
0.90
0.80
0.70
0.60
0.50
0.40
0.30
0.20
0.10

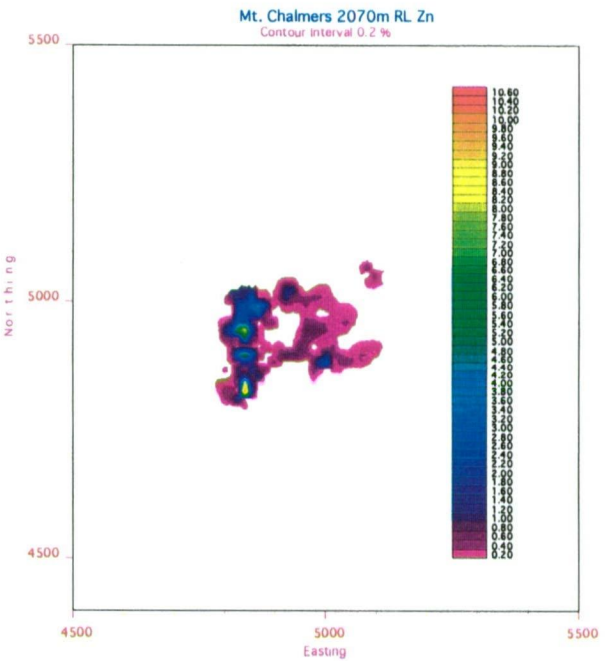
Mt. Chalmers 2070m RL Zn
Contour Interval 0.2 %
Northing
Easting
5500
5000
4500

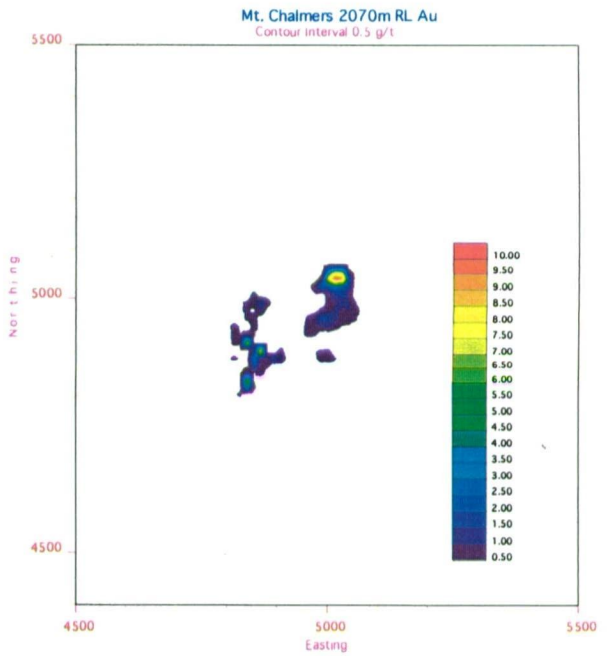
Mt. Chalmers 2070m RL Au
Contour Interval 0.5 g/t
Northing
Easting
5500
5000
4500
10.00
9.50
9.00
8.50
8.00
7.50
7.00
6.50
6.00
5.50
5.00
4.50
4.00
3.50
3.00
2.50
2.00
1.50
1.00
0.50

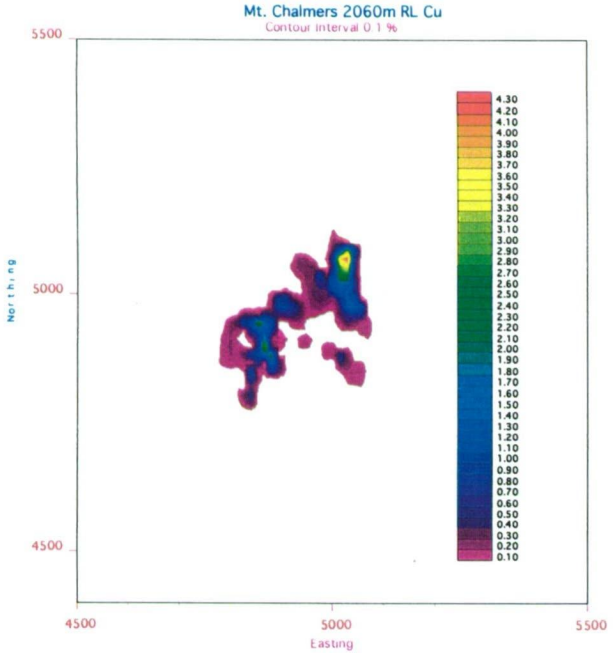
Mt. Chalmers 2060m RL Cu
Contour Interval 0.1 %
5500
5000
4500
Northing
4500
5000
5500
Easting
4.30
4.20
4.10
4.00
3.90
3.80
3.70
3.60
3.50
3.40
3.30
3.20
3.10
3.00
2.90
2.80
2.70
2.60
2.50
2.40
2.30
2.20
2.10
2.00
1.90
1.80
1.70
1.60
1.50
1.40
1.30
1.20
1.10
1.00
0.90
0.80
0.70
0.60
0.50
0.40
0.30
0.20
0.10

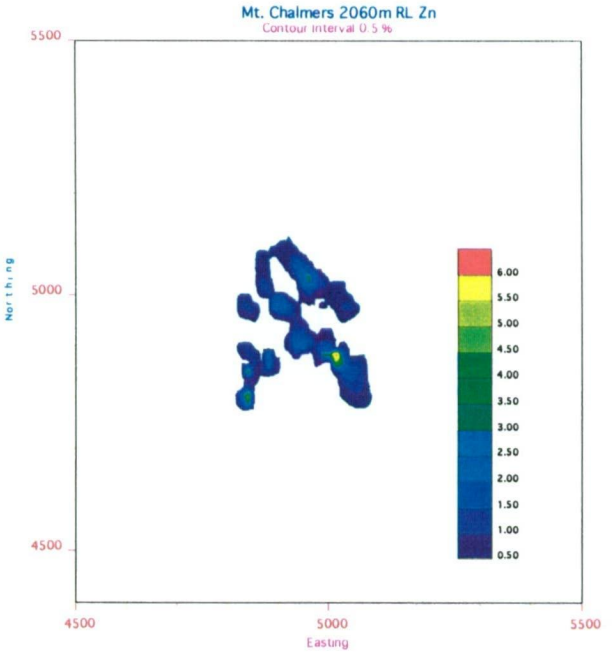
Mt. Chalmers 2060m RL Zn
Contour Interval 0.5 %
5500
5000
4500
Northing
4500
5000
5500
Easting
6.00
5.50
5.00
4.50
4.00
3.50
3.00
2.50
2.00
1.50
1.00
0.50

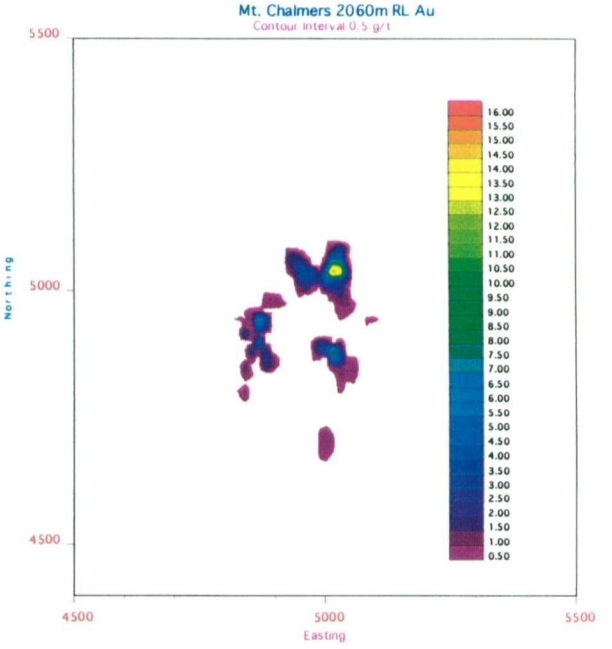
Mt. Chalmers 2060m RL Au
Contour Interval 0.5 g/t
5500
5000
4500
Northing
4500
5000
5500
Easting
16.00
15.50
15.00
14.50
14.00
13.50
13.00
12.50
12.00
11.50
11.00
10.50
10.00
9.50
9.00
8.50
8.00
7.50
7.00
6.50
6.00
5.50
5.00
4.50
4.00
3.50
3.00
2.50
2.00
1.50
1.00
0.50

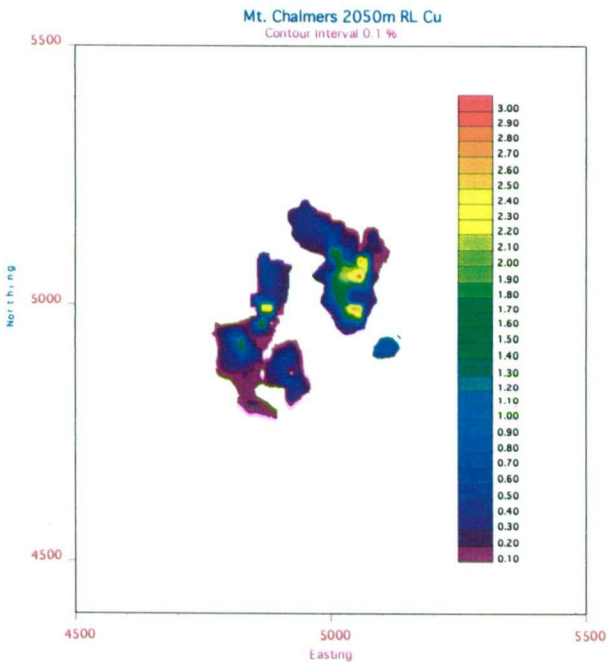
Mt. Chalmers 2050m RL Cu
Contour Interval 0.1 %
5500
5000
4500
Northing
4500
5000
5500
Easting
3.00
2.90
2.80
2.70
2.60
2.50
2.40
2.30
2.20
2.10
2.00
1.90
1.80
1.70
1.60
1.50
1.40
1.30
1.20
1.10
1.00
0.90
0.80
0.70
0.60
0.50
0.40
0.30
0.20
0.10

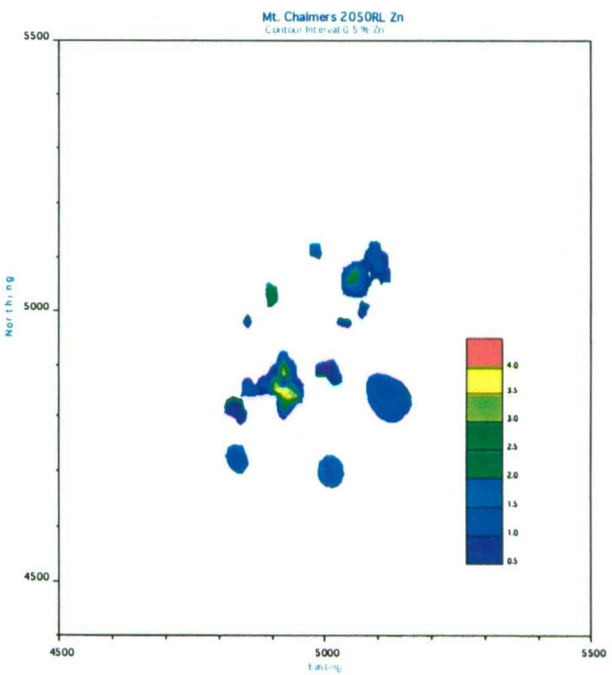
Mt. Chalmers 2050RL Zn
Contour Interval 0.5 % Zn
5500
5000
4500
Northing
4500
5000
5500
Easting
4.0
3.5
3.0
2.5
2.0
1.5
1.0
0.5

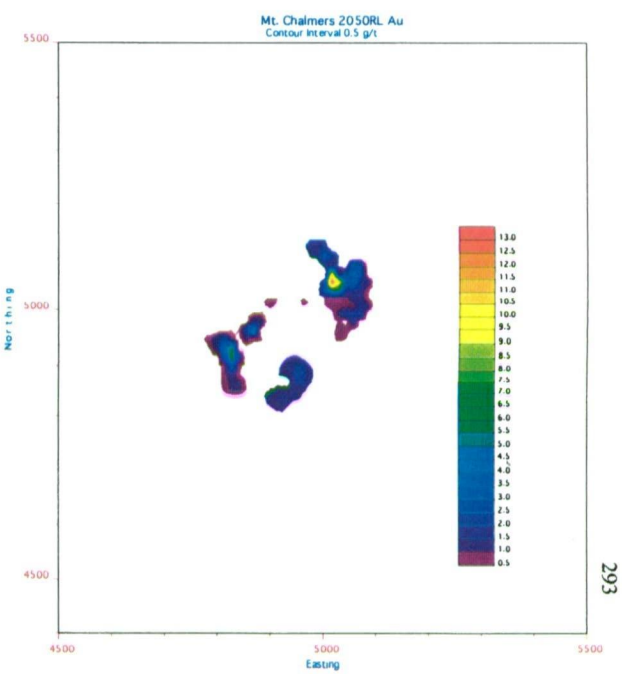
Mt. Chalmers 2050RL Au
Contour Interval 0.5 g/t
5500
5000
4500
Northing
4500
5000
5500
Easting
13.0
12.5
12.0
11.5
11.0
10.5
10.0
9.5
9.0
8.5
8.0
7.5
7.0
6.5
6.0
5.5
5.0
4.5
4.0
3.5
3.0
2.5
2.0
1.5
1.0
0.5

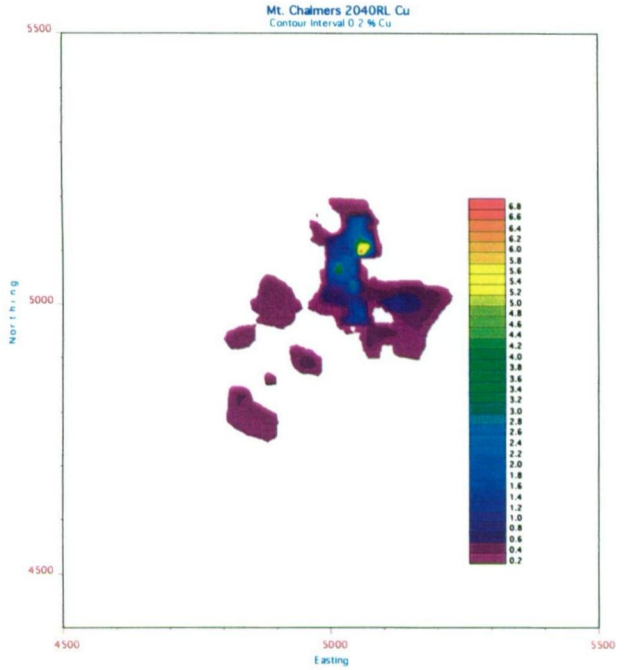
Mt. Chalmers 2040RL Cu
Contour Interval 0.2 % Cu
5500
5000
4500
Northing
4500
5000
5500
Easting

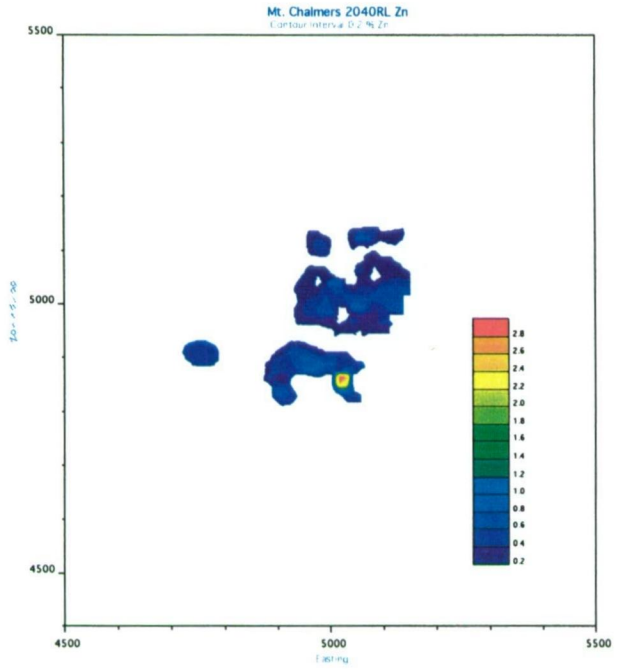
Mt. Chalmers 2040RL Zn
5500
5000
4500
4500
5000
5500

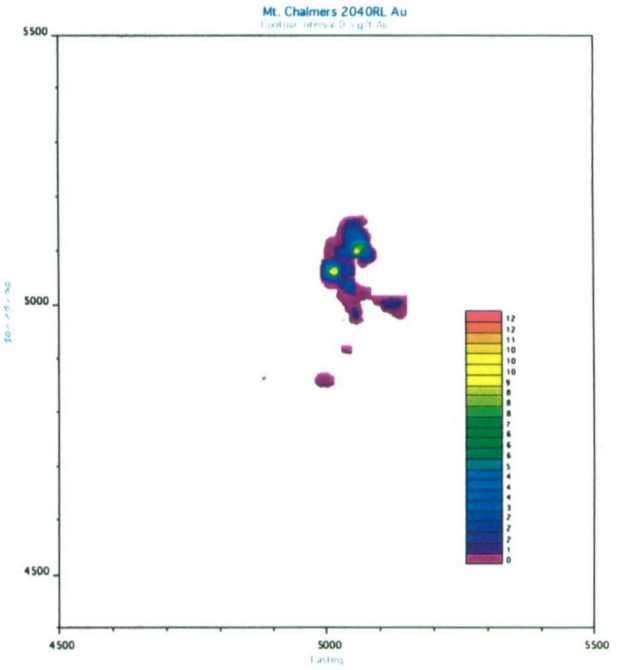
Mt. Chalmers 2040RL Au
5500
5000
4500
4500
5000
5500

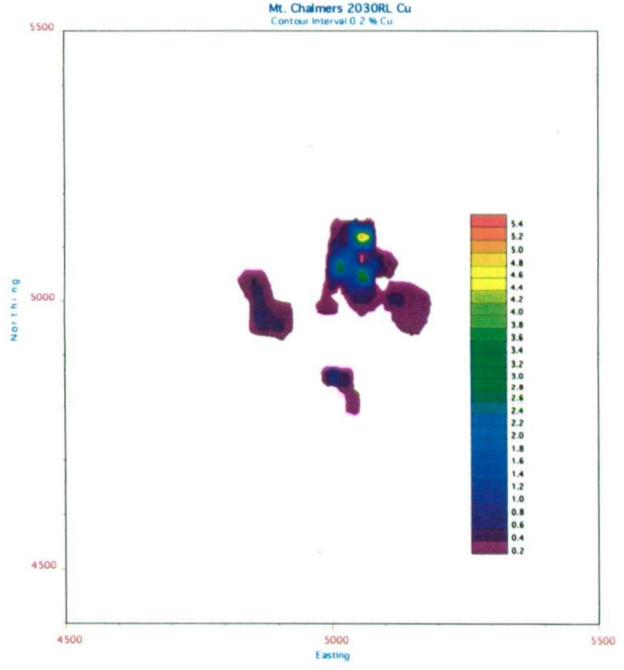
Mt. Chalmers 2030RL Cu
Contour Interval 0.2 % Cu
5500
5000
4500
Northing
4500
5000
5500
Easting

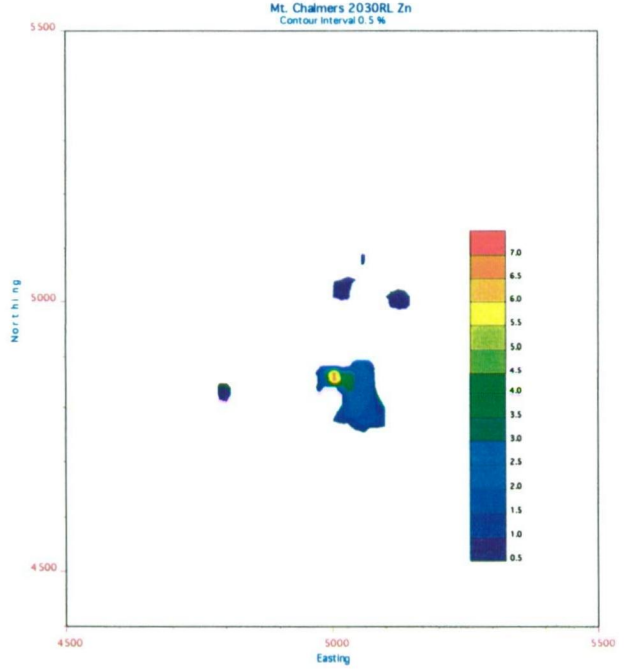
Mt. Chalmers 2030RL Zn
Contour Interval 0.5 %
5500
5000
4500
Northing
4500
5000
5500
Easting

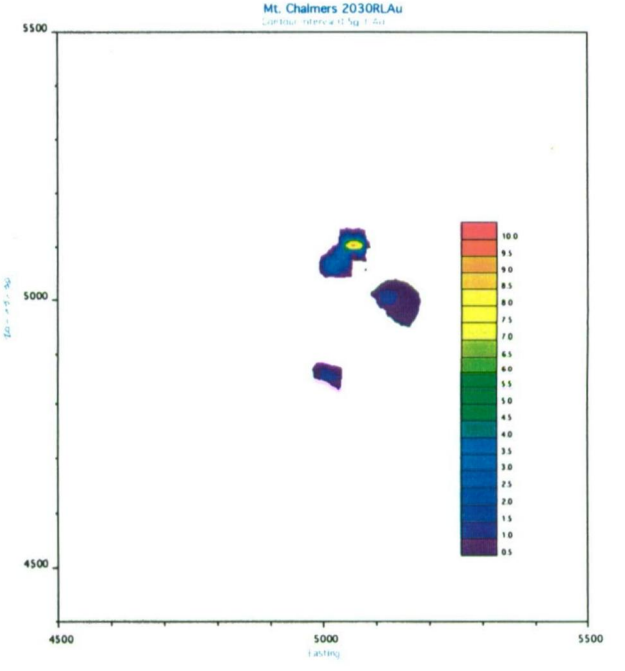
Mt. Chalmers 2030RLAu
5500
5000
4500
4500
5000
5500

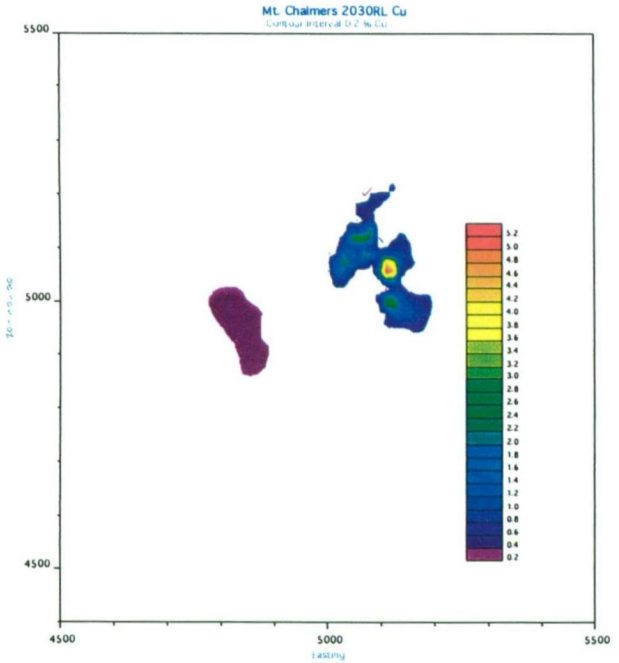
Mt. Chalmers 2030RL Cu
Contour Interval 0.2 % Cu
5500
5000
4500
4500
5000
5500
Easting

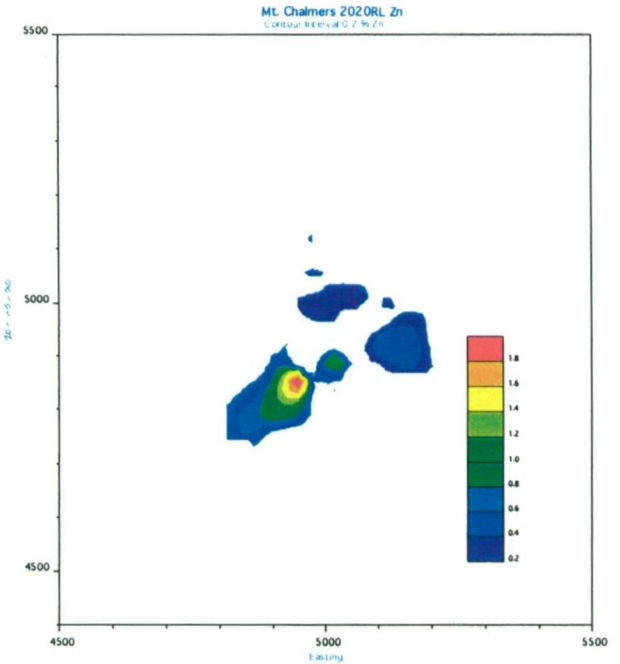
Mt. Chalmers 2020RL Zn
Contour Interval 0.2 % Zn
5500
5000
4500
4500
5000
5500
Easting

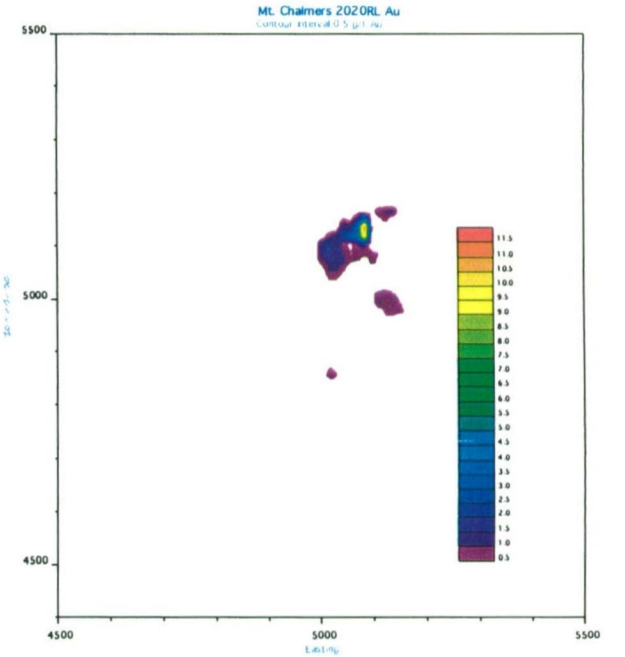
Mt. Chalmers 2020RL Au
Contour Interval 0.5 g/t Au
5500
5000
4500
4500
5000
5500
Easting

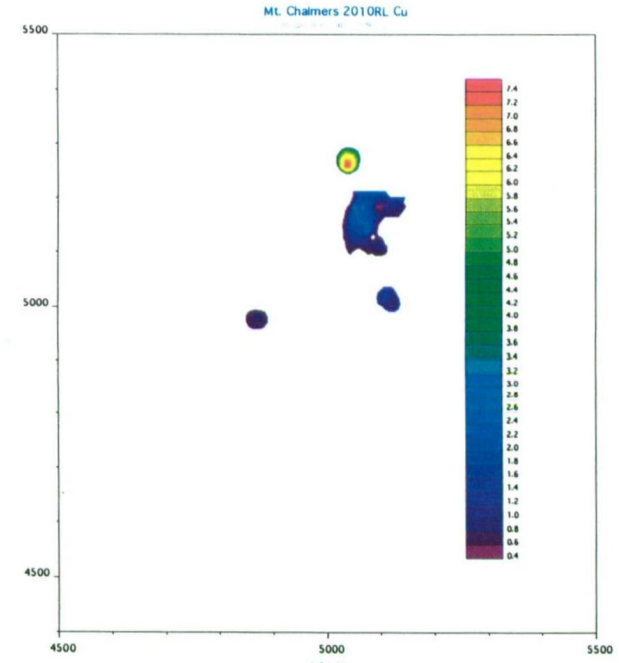
Mt. Chalmers 2010RL Cu
5500
5000
4500
4500
5000
5500

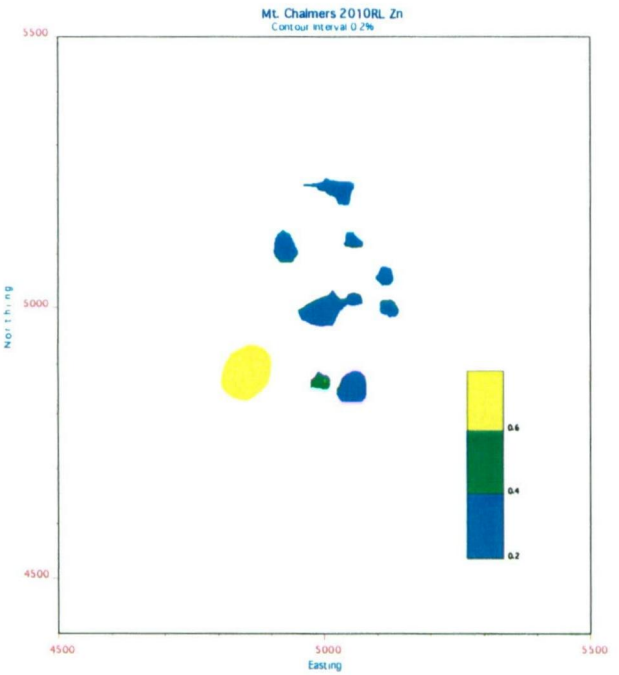
Mt. Chalmers 2010RL Zn
Contour Interval 0.2%
5500
5000
4500
Northing
4500
5000
5500
Easting

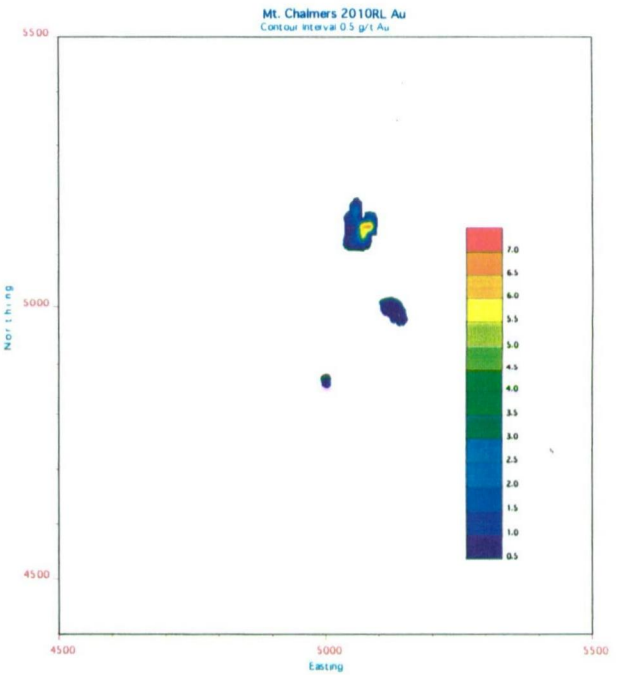
Mt. Chalmers 2010RL Au
Contour Interval 0.5 g/t Au
5500
5000
4500
Northing
4500
5000
5500
Easting

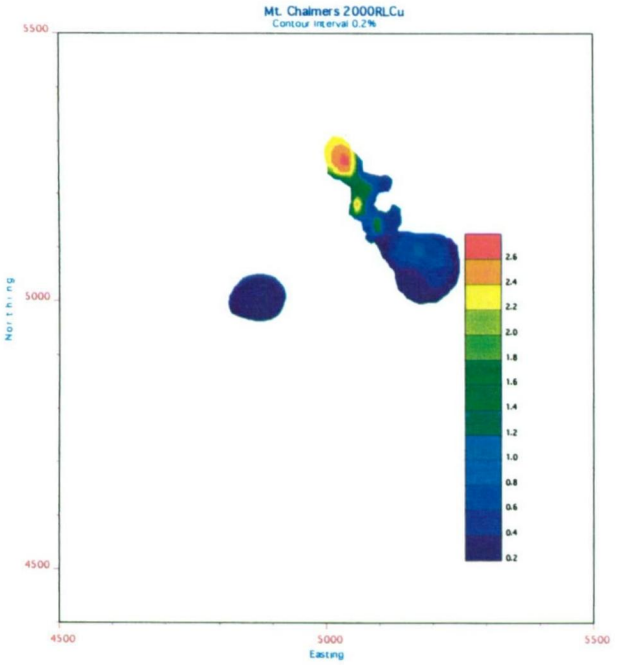
Mt. Chalmers 2000RLCu
Contour Interval 0.2%
5500
5000
4500
Northing
4500
5000
5500
Easting
2.6
2.4
2.2
2.0
1.8
1.6
1.4
1.2
1.0
0.8
0.6
0.4
0.2

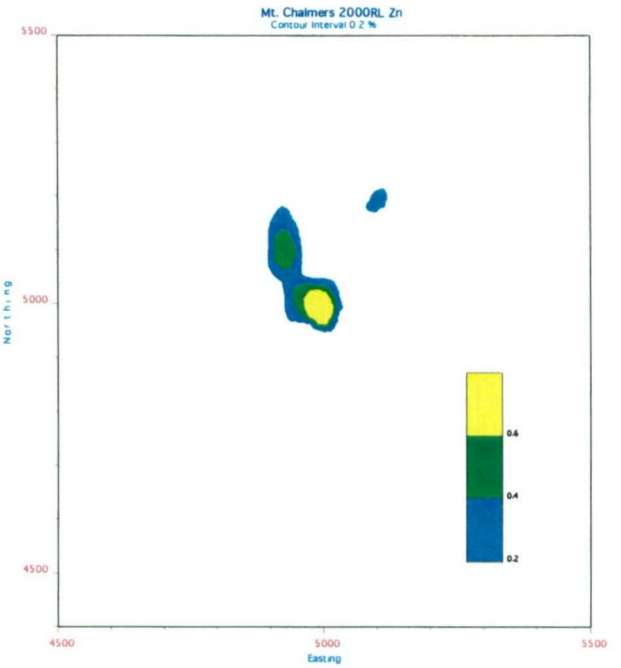
Mt. Chalmers 2000RL Zn
Contour Interval 0.2 %
5500
5000
4500
Northing
4500
5000
5500
Easting
0.6
0.4
0.2

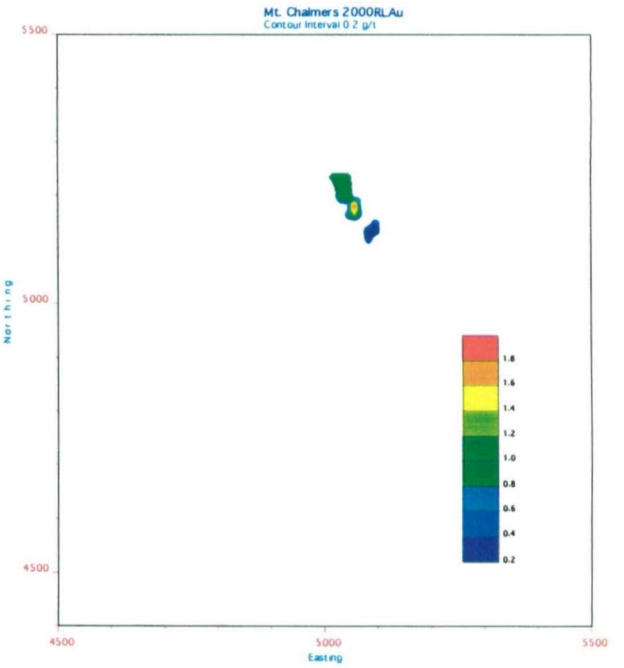
Mt. Chalmers 2000RLAu
Contour Interval 0.2 g/t
5500
5000
4500
Northing
4500
5000
5500
Easting
1.8
1.6
1.4
1.2
1.0
0.8
0.6
0.4
0.2

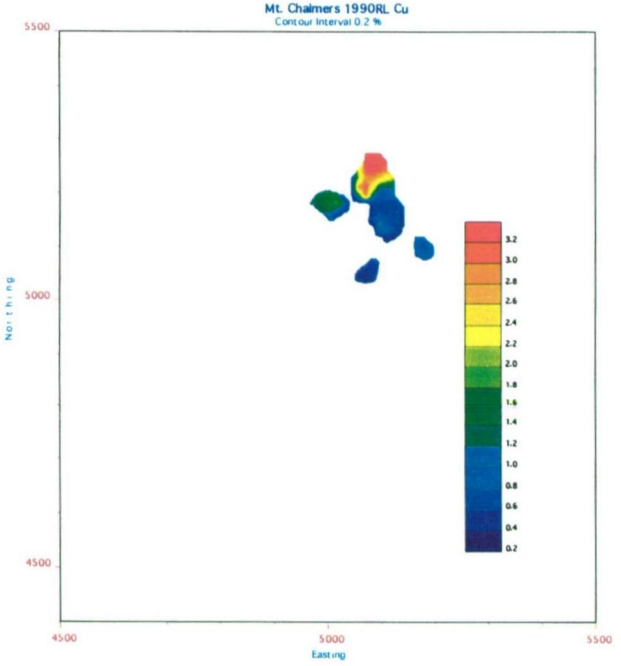
Mt. Chalmers 1990RL Cu
Contour Interval 0.2 %
5500
5000
4500
Northing
4500
5000
5500
Easting
3.2
3.0
2.8
2.6
2.4
2.2
2.0
1.8
1.6
1.4
1.2
1.0
0.8
0.6
0.4
0.2

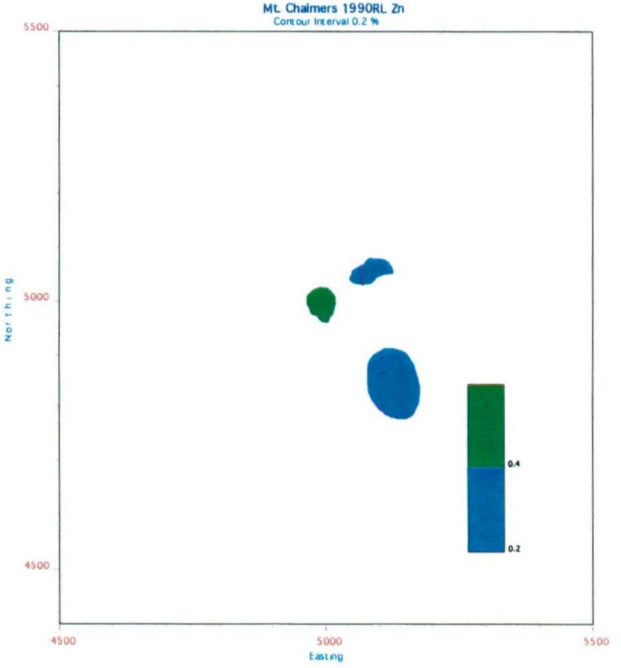
Mt. Chalmers 1990RL Zn
Contour Interval 0.2 %
5500
5000
4500
Northing
4500
5000
5500
Easting
0.4
0.2

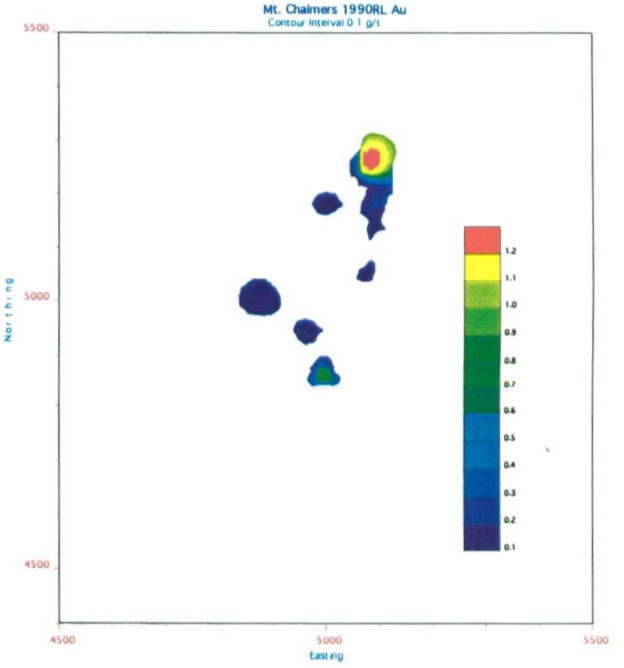
Mt. Chalmers 1990RL Au
Contour Interval 0.1 g/t
5500
5000
4500
Northing
4500
5000
5500
Easting
1.2
1.1
1.0
0.9
0.8
0.7
0.6
0.5
0.4
0.3
0.2
0.1

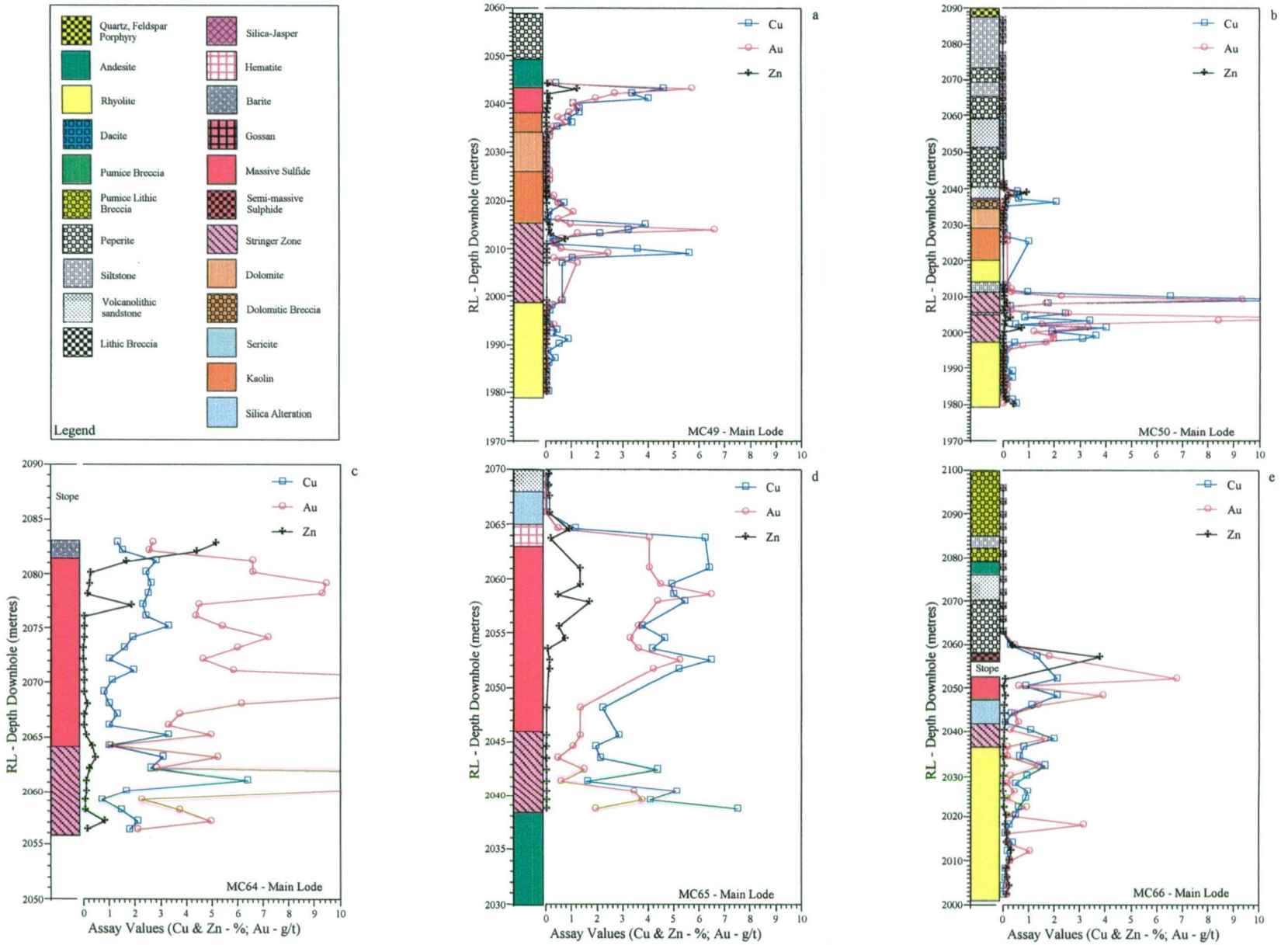

Figure 12.8. Downhole drill hole litholgies versus metal content for selected holes from the Main Lode.

12.5.1 Main Lode

Downhole assays for Cu, Zn and Au are plotted versus the downhole lithologies for five diamond drillholes from the Main Lode, MC49, MC50, MC64, MC65 and MC66 (Figs. 12.8a, b, c, d; e). These diamond drillholes were selected as they all have intersected massive sulphide mineralisation and have moderately to well develop stringer zones. MC64 and MC65 were selected as they also intersected the central and thickest portion of the Main Lode massive sulphide lens, while MC49, MC50 and MC64 were selected as they intersected the margins of the massive sulphide mound.

12.5.1.1 Au

Au enrichment occurs near the top of the massive sulphide intersected in MC49 MC64 and MC65 (Figs. 12.8a, c and d). In MC64 and MC65, a second zone of Au enrichment within the massive sulphide also occurs approximately half way along the massive sulphide (Figs. 12.8 c and d). High Au values were also intersected in the stringer zones to the massive sulphide mineralisation in MC49, MC50, MC64 and MC65 (Figs. 12.8a, b, c and d).

12.5.1.2 Zn

The Main Lode massive sulphide and stringer zone are essentially depleted in Zn. For all five holes plotted from the Main Lode, the maximum Zn values do not exceed approximately 4 % (MC66, Fig. 12.8e). There is minor Zn enrichment near the top of the massive sulphide mineralisation in MC65 (Fig. 12.8d). In MC64, there is a significant increase in the Zn values near the top of the massive sulphide with the values tending to increase up into the overlying barite mineralisation (Fig. 12.8c). This increase in the Zn content near the top of the massive sulphide is also seen in MC49 and MC50 (Figs. 12.8a and b). Except for these occasional spikes in the Zn content, the Main Lode mineralisation is essentially Zn-poor.

12.5.1.3 Cu

Cooper within the Main Lode tends to be concentrated near the top of the massive sulphide lens (Figs. 12.8a, b, c, d and e). In MC64 Cu is evenly distributed, with minor enrichment occurring in the top one third of the massive sulphide lens (Fig. 12.8c). In MC65 two zones of Cu-enrichment occur, the first occurs near middle of massive sulphide lens and the second near the top of the massive sulphide (Fig. 12.8d). Copper grades generally follow Au grades *i.e* that as Au content increases there is a corresponding increase in the Cu grade. However, near the top of the massive sulphide in MC65 as the Cu grade rises the Au grade falls. Copper within Main Lode stringer zone is controlled largely by the density and size of the sulphide bearing veins within the stringer zone.

12.5.2 West Lode

Downhole assays for Cu, Zn and Au are plotted versus the downhole lithologies for six diamond drillholes from the West Lode: MC25, MC27A, MC31, MC32, MC43 and MC48 (Figs. 12.9a, b, c, d, e and f). These diamond drillholes were selected as they all have intersected massive sulphide mineralisation with well-developed stringer mineralisation and variable alteration lithologies underlie the massive sulphide mineralisation. Several of the drill holes also have gossans associated with the massive sulphide mineralisation.

12.5.2.1 Au

Au tends to be concentrated in the in top of the massive sulphide and within the narrow gossanous zones, except in MC43 where the Au is concentrated near the base of the massive sulphide mineralisation (Figs. 12.9a, b, c, d, e and f). In MC48, highly elevated Au occurs throughout the massive sulphide. However, the Au is concentrated in a number of zones, as defined by the peak values of Au (see inset in Fig. 12.9f). Within the stringer zone mineralisation of the West Lode, erratic but high Au values were intersected (Figs. 12.9a, b, c, d, e and f). The various alteration lithologies generally have negligible to very low Au levels.

12.5.2.2 Zn

In the West Lode, Zn is concentrated near the top of the massive sulphide and within the overlying gossans (Figs. 12.9a, b, c, d, e and f). Immediately below the zone of Zn enrichment within the massive sulphide the Zn values decrease rapidly, except in MC48 where Zn is also enriched near the base of the massive sulphide (Fig. 12.9f). Within the underlying alteration lithologies and stringer zone mineralisation Zn values are significantly depressed compared to the massive sulphide mineralisation and gossan zones (Figs. 12.9a, b, c, d, e and f).

12.5.2.3 Cu

Within the West Lode Cu tends to be concentrated near the base of the massive sulphide (Figs. 12.9a, b, c, d, e and f) except in MC48 where the peak value occur near the top of the massive sulphide (Fig. 12.9f). Copper unlike Zn and Au shows minor enrichment within the overlying gossans (Figs. 12.9a, b, c, d, e and f). Like Au, Cu within the stringer zone mineralisation occurs as erratically but significant values, related to the density of the sulphide veining within the stringer zone (Figs. 12.9a, b, c, d, e and f).

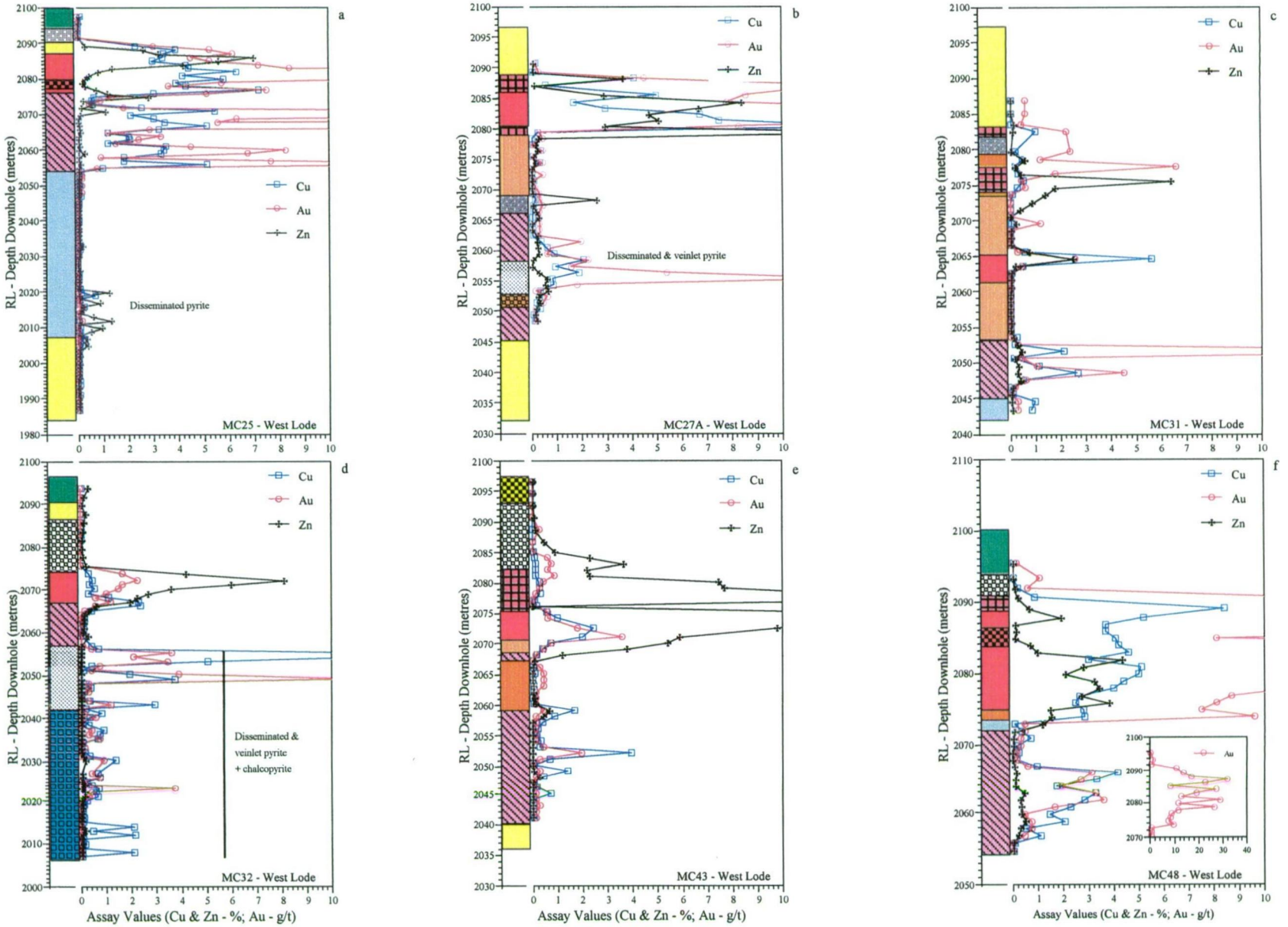

Figure 12.9. Downhle drill hole litholgies versus metal content for selected holes from the WestLode.

12.5.3 Discussion

The Main Lode is essentially a Cu- and Au-rich massive sulphide lens, that is depleted in Zn and Pb. In comparison, the West Lode is a Zn-, Cu- and Au-rich massive sulphide lens. In the West Lode Zn is enriched in the upper part of the massive sulphide mineralisation and is depleted in the stringer zone and alteration lithologies. A localised narrow zone of Zn enrichment occurs near the top of the Zn-poor Main Lode massive sulphide lens.

In both the Main Lode and West Lode Au enrichment tends to occur towards the top of the massive sulphide lenses, although the massive sulphide lenses tend to be Au-rich throughout. The stringer zone mineralisation for both lodes contains erratic but high Au grades, with the Au content being related to the density of sulphide veins within the stringer zone.

Within the Main Lode, Cu occurs throughout the massive sulphide lens, but with higher grades tending to occur near the top of the lens. Conversely, within the West Lode the higher Cu-grades occur at the base of the massive sulphide lens. However, in MC48 peak Cu grades occur towards the top of the massive sulphide lens. Within the Main Lode the Cu and Au grades are more consistent in MC64 and MC65 compared to the more spiky Cu and Au grades in the peripheral holes that intersected the massive sulphide, namely MC49 and MC66 (Figs. 12.8a, c, d and e). This suggests that within the core of the Main Lode massive sulphide mound hydrothermal fluid conditions were relatively stable and unaffected by the probable influx of seawater at the margins of the mound.

In both lodes wherever there is Zn enrichment, there is a corresponding depletion in the Cu and Au values and *vice versa*. In broad general terms, although the Cu and Au grades tend to follow one another their peak values do not always coincide.

The metal zonation seen especially within the West Lode, namely Zn-Au rich, Cu-poor top and a Cu-rich base may be explained by process of zone refining. Zone refining for VHMS deposits was initially proposed by Goldfarb *et al.* (1983), Hekinian *et al.* (1985) and Hekinian and Fouquet (1985) and a similar model for the Kuroko deposits was proposed by Eldridge *et al.* (1983). Zone refining is the process whereby low-temperature minerals that are initially precipitated by early cooler fluids in a sulphide mound are replaced, dissolved and remobilised to the outer margins of the mound. The constituents are reprecipitated in veins and open spaces near the seafloor. As a result nearly all of the Zn, Ag, Pb and Au are concentrated in the top 5 m of the mound, and any new metal precipitated by high-temperature end member fluids will eventually end up in the outermost Zn-rich zone of the mound (Hannington *et al.*, 1998). In other words, there is the upward and outward expansion of isotherms within the sulphide mound, resulting in the replacement of sphalerite in the mound core and the relative concentration of sphalerite in the mound crust. In MC48 there is a zone of Zn enrichment at the base of the massive sulphide that suggests that leaching and remobilisation of Zn was at least locally incomplete.

The concentration of Zn and Au in the upper part and Cu in the lower part of the West Lode massive sulphide lens reflects the process of zone refining outlined above. In that the lower temperature minerals *i.e* Zn and Au were probably initially precipitated by lower temperature hydrothermal fluids, and then subsequently were dissolved by higher temperature (Cu-bearing fluids) and reprecipitated in the outer margins of the growing sulphide mound. In contrast, the Main Lode massive sulphide lens has been virtually stripped of all of its Zn, and Cu and Au are concentrated at or near the top of the massive sulphide lens. This disparity in metal concentrations between the two massive sulphide lens is also seen in the fluid inclusion temperatures of homogenisation, in that the West Lode has lower temperatures compared to the Main Lode. This suggests one of two possible scenarios:

- that two different thermal regimes were operating at the same time (assuming synchronous precipitation of sulphides).
- the hydrothermal fluid responsible for the formation of the West Lode massive sulphide lens collapsed before thermal maturity (*cf.* to the Main Lode) was achieved.

12.5.4 Gossan – West Lode

The West Lode has a well-developed gossan that sits on and laterally to the massive sulphide of the West Lode. A gossan has also developed on the Main Lode but it is not as extensively developed as the West Lode gossan (Fig. 12.10). Assay values (Cu, Au, Zn and Ag) for one diamond drill hole (MC36) and three percussion drill holes (MCP87, MCP90 and MCP93) that intersected well developed gossan were plotted versus the down hole geology (Fig. 12.11a, b, c and d respectively). The gossan in MCP87 is also underlain by approximately five metres of massive sulphide.

12.5.4.1 Au

The downhole plots for MC36, MCP87 and MCP90 (Figs. 12.11a, b and c) shows that there is significant enhancement of Au in the gossan compared to the underlying massive sulphide and stringer mineralisation and alteration lithologies. In contrast, MCP93 shows no Au enrichment in either the gossan or the underlying alteration lithologies (Fig. 12.11d). The Au enrichment in the gossan intersected in MC36 and MCP87 is displaced relative to the zones of Cu and Zn enrichment (Figs. 12.11a and b). In MC36, MCP87 and MCP90 the Au enrichment extends upward from within the gossan into to the overlying lithologies (Figs. 12.11a, b and c). In MCP87 and MCP90 there are two zones of Au enrichment in the gossan; one near the top that extends up into the overlying lithologies and one that occurs near the base of the gossan (Figs. 12.11b and c). In MCP87, a third zone of Au enrichment also occurs near the top of the underlying massive sulphide. In MCP87, Au values remain erratic but high ($\geq$ 1 g/t) in the underlying massive sulphide, dolomite and stringer zone mineralisation (Fig. 12.11b). In MC36 Au enrichment occurs near the top of the gossan, and becomes strongly depleted downhole in the underlying mineralisation and alteration lithologies (Fig. 12.11a). Whereas in MCP90 and MCP93 Au is essentially depleted in the underlying mineralisation and alteration types (Fig. 12.11c and d).

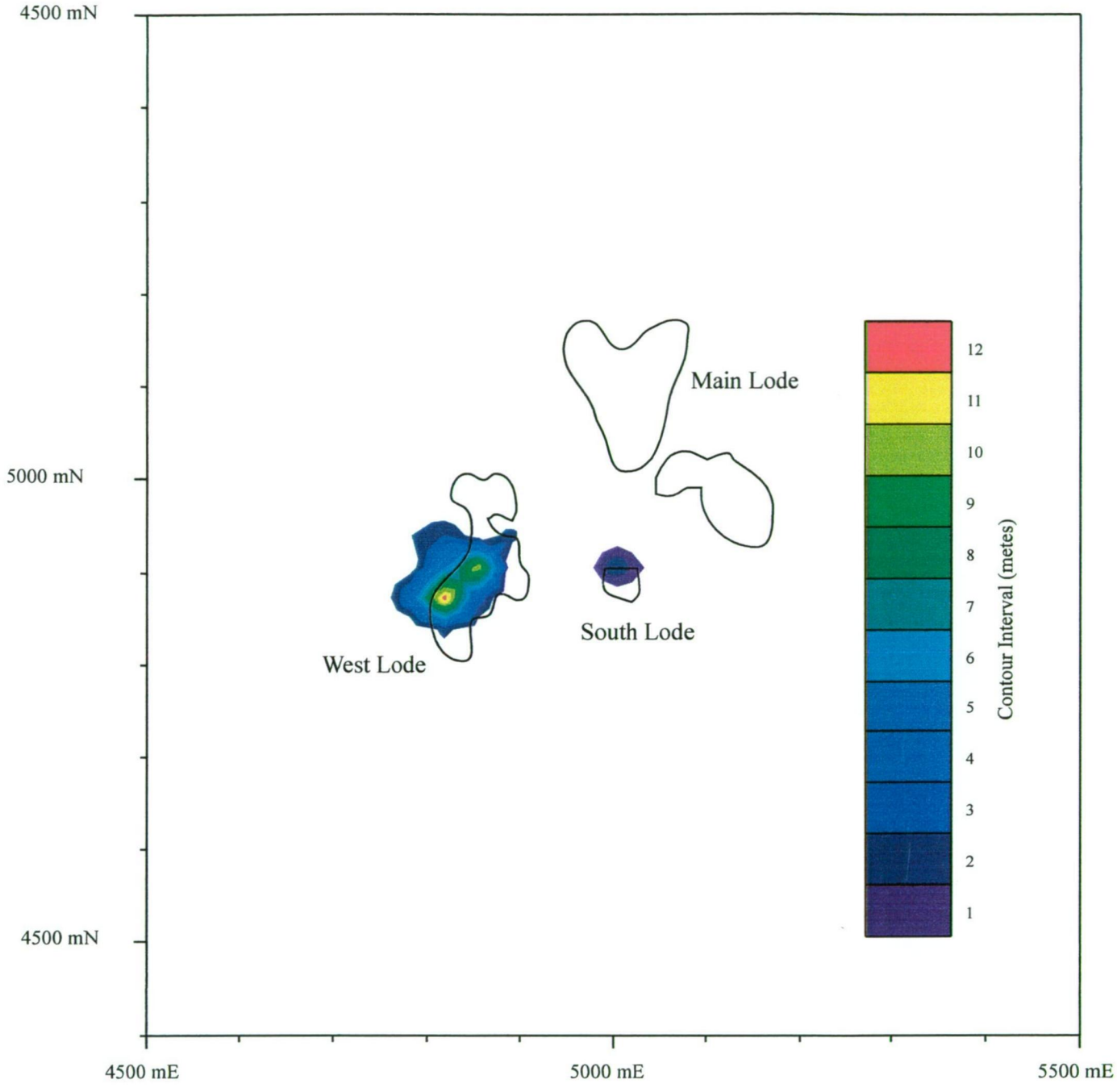

Figure 12.10. Isopachs of gossan thickness, with the outline of the massive sulphide lenses superimposed

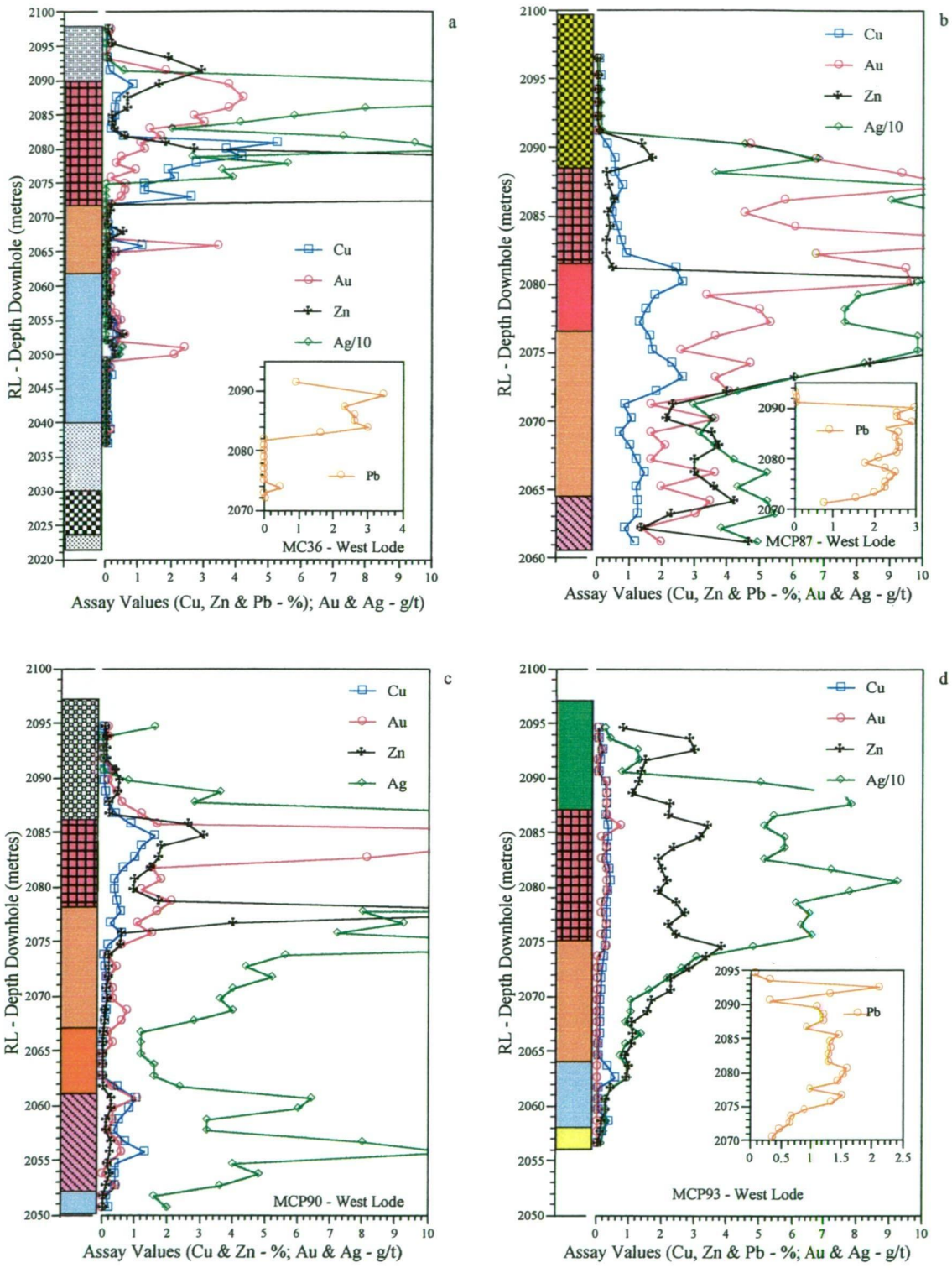

Figure 12.11 Downhole drill hole litholgies versus metal content for selected holes from the West Lode gossan. Legend is as for Figure 12.8.

12.5.4.2 Zn

In MC36 Zn, enrichment occurs within the bottom half of the gossan, which is in stark contrast to enrichment in Pb seen in the top half of the gossan (Fig. 12.11a). In MCP87, Zn is depleted in the gossan compared to MCP90 and MCP93 where Zn is enriched, especially in MCP93 (Figs. 12.11b, c and d). In all three-drill holes, there is significant enrichment of Zn at the top of the gossan that extends up into the overlying lithologies (Figs. 12.11b, c, and d). In MCP87 Zn is highly enriched in the underlying massive sulphide, and this enrichment extends well down into the underlying dolomite alteration to approximately 2071RL. Below which the Zn enrichment remains relatively high but erratic (Fig. 12.11b) This extension of Zn enrichment is also evident in MCP93 where Zn is enriched in the upper half of the dolomite, with the grades decreasing downhole (Fig. 12.11d). In contrast in MCP90 Zn is strongly depleted in the alteration lithologies that immediately underlie the gossan, but there is a major increase in Zn content at the top of the underlying dolomite (Fig. 12.11c).

12.5.4.3 Pb

Pb is strongly enriched in the West Lode gossan compared to the underlying massive sulphide and alteration lithologies. As for Zn and Ag, the Pb enrichment within the gossan continues up into the base of the overlying altered lithologies (Figs. 12.11a. b and d). In MCP87 Pb unlike Zn is depleted in the top of the massive sulphide and does not increase in content until the underlying dolomite is intersected (Fig. 12.11b).

12.5.4.4 Cu

Copper is depleted in the gossans intersected in MCP87 and MCP93 (Figs. 12.11b and d), but in MCP90, there is minor Cu enrichment near the top of the gossan (Fig. 12.11c). In MCP93 Cu is strongly depleted along the length of the drill hole (Fig. 12.11d). In MCP87, Cu enrichment occurs near the top of the massive sulphide and near the top of the underlying dolomite alteration (Fig. 12.11b). In contrast, Cu in MC36 is concentrated in the bottom half of the gossan, with maximum values occurring near the middle of the gossan (Fig. 12.11a)

12.5.4.5 Ag

In MC36, the gossan is highly enriched in Ag throughout its length and this enrichment continues into the overlying siltstone. This is in stark contrast to the Ag-poor underlying lithologies (Fig. 12.11a). MCP87 is enriched in Ag throughout its length. Within the gossan Ag is significantly enriched at its base (2081 - 2083mRL Ag averages 195 g/t) compared to the upper two thirds, even though values in this interval exceed 100 g/t (Fig. 12.11b). Within the underlying dolomite at approximately the 2072m RL there is a dramatic increase in the Ag content, with peak Ag values within the dolomite occurring at the top of the dolomite (Fig. 12.11b).

In MCP90 the Ag enrichment occurs within the gossan and continues upward into the overlying altered peperite. This enrichment continues downhole into the underlying dolomite alteration, but drops dramatically below the 2073m RL. The Ag enrichment then increases within the stringer zone, although not to the same levels as seen in the gossan (Fig. 12.11c). In MCP93, the Ag enrichment in the gossan extends well uphole into the overlying andesite, and extends down into and through the underlying dolomite (Fig. 12.11d).

12.5.4.6 Discussion

The West Lode massive sulphide lens has a well-developed gossan. It is commonly thought that the formation of gossans and the subsequent supergene enrichment of metals within the gossan are exclusively restricted to the subaerial environment. However, the presence of marine sedimentary rocks immediately above and lateral to the gossan indicates that the gossan must have formed without being exposed to near surface on land weathering processes.

Recent examples from both modern day seafloor massive sulphide deposits (*e.g.* TAG and Snakepit - Thompson *et al.*, 1988; 13° EPR - Hannington *et al.*, 1991; the Rodrigues Triple Junction. - Halbach, 1998 and the Cretaceous sulphide deposits of Cyprus - Constantinou and Govett, 1972; Constantinou, 1973 and Robertson, 1976) have also shown that massive sulphide deposits may be oxidised without being exposed to near surface on land weathering processes.

The relative depletion of Cu and Au within the West Lode gossan to the West Lode massive sulphide stands in contrast to the "normal" supergene enrichment of Cu typically seen with the ancient on-land examples of gossans. Table 12.2 shows that the average values of Cu, Zn and Au for the West Lode gossan are depleted relative to the average values within the massive sulphide lens. This is in stark contrast, to the "normal" supergene enrichment of Cu and Au typically seen within the ancient on-land (Krauskopf, 1979; Guilbert and Park, 1985; Hannington *et al.*, 1988b) and modern day seafloor examples of gossans or oxidised sulphides (Table 12.3; Hannington *et al.*, 1988b; Hannington *et al.* 1991).

Table 12.3. Comparison of average metal values between the West Lode gossan and massive sulphide lens.

		Sample N°	Cu %	Zn %	Pb %	Au g/t	Ag g/t
West Lode	Gossan		0.9	3.2	1.3	3.4	70
	Massive sulphide		2.3	5.4	1.4	5.4	52
TAG*	Primary Fe sulphides	1-10	0.09	2.09	0.1	1.6	17
		1-16	2.7	3.25	0.05	4.0	38
	Primary Cu-Fe sulphides	1-44	25.0	0.5	<0.01	0.8	14
	Secondary Cu-sulphides	1-26	32.5	1.2	0.02	5.6	45
		1-18	39.0	0.6	0.02	16.4	116

* Data from Hannington *et al.* (1988b)

One possible explanation as to why Cu is relatively depleted in the gossan compared to the massive sulphide is that chalcopyrite is readily broken down to form iron oxide and an acidic solution of cupric sulphate or it may be taken into solution by ferric sulphate. The sulphuric acid generated by these reactions or generated by oxidising iron sulphides aids in taking the Cu into solution as cupric sulphate (Guilbert and Park, 1985). Therefore, as long as the solutions remain acidic and oxidising (by influx of seawater of by dilute hydrothermal fluids) then the Cu will remain in solution and be removed by the fluids and not be precipitated.

The oxidation of Au requires the simultaneous presence of a powerful oxidising agent and a solution of chloride ion (Krauskopf, 1979). The oxidation of pyrite (most abundant sulphide present at Mount Chalmers) and other sulphides generates two strong oxidising agents, sulphuric acid and (Eqn. 12.1) and ferric sulphate (Eqn. 12.2). Seawater readily supplies solution rich in chloride ions as seawater contains approximately 19,000 ppm Cl^- (Krauskopf, 1979; Gill, 1989).

$$2FeS_2 + 7O_2 + 2H_2O \rightarrow 2FeSO_{4(aq)} + 2H_2SO_{4(aq)} \qquad \text{(Eqn. 12.1)}$$

$$2FeSO_{4(aq)} + H_2SO_{4(aq)} + 0.5O_2 \rightarrow Fe_2(SO_4)_{3(aq)} + H_2O \qquad \text{(Eqn. 12.2)}$$

Therefore the lack of an apparent enrichment in Au in the West Lode gossan as a whole may be attributed to the Au largely remaining in solution and being carried by percolating seawater and dilute hydrothermal fluids. Although enrichment of Au on a local scale is evident suggests that oxidation and leaching of Au did not occur uniformly throughout the gossan.

In the on land examples of gossans, Zn is dissolved in the presence of ferric sulphate and supergene enrichment is considered unlikely to occur due to the high solubility of sphalerite and its subsequent removal of Zn by surface or ground waters without being trapped (Krauskopf, 1979; Guilbert and Park, 1985). Such a process for the West Lode gossan may explain the depletion in Zn seen in the gossan relative to the massive sulphide (Table 12.2).

The apparent enrichment in Zn and Ag and to some extent Cu seen at the top of the dolomite lenses that underlie the West Lode gossan and the apparent downhole depletion in these metals, suggest that there has been a downward movement of Zn, Ag and Cu ions from the oxidised massive sulphide and their subsequent precipitation within the dolomite. The precipitation of Zn and Cu within the dolomite is caused by the neutralisation of acidic waters by the dolomite. Leggo (1980) identified smithsonite within the carbonate assemblage of the Mount Warminster gossan (see Chapter 6). Where smithsonite replaces dolomite, the $MgCO_3$ may be shown as reducing the acidity and so favouring precipitation (Eqn. 12.3).

$$ZnS + O_2 + H_2O + 2MgCO_3 \rightarrow ZnCO_3 + 2Mg^{2+} + 2HCO_3^- + SO_4^{2-} \qquad \text{(Eqn.12.3)}$$

In the presence of carbonates, cupriferous solutions react with CO_2 derived from the carbonates to form malachite (Eqn. 12.4) and azurite (Eqn. 12.5) (Guilbert and Park, 1985).

$$2CuO + CO_2 + H_2O \left[\text{or } 2Cu^{+2} + CO^{-2} + 2(OH)^-\right] \rightarrow Cu_2(OH)_2CO_3 \qquad \text{(Eqn. 12.4)}$$

$$3CuO + 2CO_2 + H_2O \left[\text{or } 3Cu^{+2} + 2CO_3^{-2} + 2(OH)^-\right] \rightarrow Cu3(OH)_2(CO_3)_2 \qquad \text{(Eqn. 12.5)}$$

Ag is the only metal that is enriched within the West Lode gossan compared to the underlying massive sulphide (Table 12.2). Galena within the West Lode massive sulphide contains up to 6900 ppm Ag (D. Huston *unpubl. data*). Huston *et al.* (1995) suggested that inclusions of argentiferous galena or tennantite might explain the high values of Ag within pyrite and chalcopyrite grains.

The relative enrichment of Pb and depletion of Cu and Zn seen in the top of the West Lode gossan may be explained by the difference in solubility between Pb and Zn and Cu and the armouring of galena by its common insoluble oxidation products (anglesite and cerussite) to prevent further oxidation and leaching. Leggo (1980) reported the presence of both cerussite and anglesite from the Mount Warminster gossan. Pb in galena can be oxidised directly to anglesite (Eqn. 12.6; Guilbert and Park, 1985).

$$PbS + 2O_2 \rightarrow PbSO_4 \qquad \text{(Eqn. 12.6)}$$

Alternatively, galena may be oxidised to anglesite by ferric sulphate (Eqn. 12.7; Guilbert and Park, 1985)

$$PbS + 2Fe^{+3} + 3SO4_4^{-2} + 1.5O_2 + H_2O \rightarrow PbSO_4 + 2Fe^{+2} + 2H^+ + 3SO_4^{-2} \qquad \text{(Eqn. 12.7)}$$

Therefore, the relative enrichment of Pb compared to Cu and Zn may be explained by the retention of some Pb within the gossan as galena armoured by cerussite and anglesite. While Cu and Zn have been oxidised, dissolved, mobilised and either reprecipitated elsewhere or lost to the seawater column.

The West Lode massive sulphide has undergone submarine weathering and oxidation, that has produced a gossan that is essentially depleted in Cu and is not enriched in Zn and Pb compared to the underlying massive sulphide. This is in stark contrast to the both the ancient on land examples and modern day sea floor examples of massive sulphides that have well developed gossans and supergene zones where enrichment especially of Cu and Au are common.

12.6 METAL ASSOCIATIONS

Contour diagrams can display the spatial distribution of metals within an ore deposit, but scatter diagrams are useful in illustrating the degree of correlation between the various ore metals present at within a deposit. In order to determine whether one metal may have a linear correlation with another metal, correlation coefficients (r) were calculated for the various metal associations (Eqn. 12.8).

$$r = \frac{\frac{\Sigma(x-\bar{x})(y-\bar{y})}{n-1}}{\left[\frac{\Sigma(x-\bar{x})^2}{n-1} \times \frac{\Sigma(y-\bar{y})^2}{n-1}\right]} \qquad \text{(Eqn. 12.8)}$$

where $\bar{x}$ and $\bar{y}$ are the mean values of x and y

However, a caveat must be attached to the use of scattergrams and r:

Metal values are generally quoted as percentages or parts per million (where 10,000 ppm = 1.0 %), if all the elements of interest are analysed in this case ore reserves (Cu, Au, Ag, Zn, Pb) then they will to total to 100 - x %. The remainder will be made of elements that have no economic interest are may be associated with the ore metals *e.g.* S and Fe or may be associated with the gangue minerals *e.g.* Al, Si, Mg, Mn and Ba are not of interest and may include Si, Fe, S, Mg and Ba Chayes (1960) pointed out that if one metal value is determined, *e.g.* Cu then the next metal or element is not free to take any value, but is restrained to be at most (100 - Cu). The next metal or element is again restrained to be less than (100 - Cu - second metal). The effect of a closed number system means that there is a tendency for negative correlations to be enhanced, and similarly positive values of r could be smaller than the tests would suggest (Till, 1984).

Given the above caveat, scattergrams were produced for the Mount Chalmers mineralised stratigraphy, Main Lode and West Lode and for the various mineralisation styles.

The Mount Chalmers assay database was divided into the

- Mount Chalmers mineralised stratigraphy (altered footwall lithologies, stringer zone mineralisation, semi and massive sulphide mineralisation, the ore equivalent horizon and dolomite)
- Main Lode and West Lode
- Mineralisation styles
  - massive sulphide mineralisation — West Lode and Main Lode
  - stringer zone mineralisation — West Lode and Main Lode
  - Au Pod

As only a limited number of elements were analysed (Cu, Zn, Pb, Au and Ag) by the various mining companies then an array of scatter diagrams was generated in order to determine if a relationship between any of the analysed metals exists (Table. 12.4).

Table 12.4. Schematic representation of the array of scatter diagrams discussed in the following sections.

Cu vs Au	Cu vs Ag	Cu vs Pb	Cu vs Zn
Zn vs Au	Zn vs Ag	Zn vs Ag	
Pb vs Au	Pb vs Ag		
Ag vs Au			

12.6.1 Mount Chalmers

For Mount Chalmers, the mineralised stratigraphy includes the altered footwall lithologies, stringer zone, semi and massive sulphide, dolomite and the ore equivalent horizon. Scatter diagrams were not generated for the hangingwall stratigraphy, as the assay values are very low and no meaningful conclusions could be drawn from them. The data is present as series of scattergrams and have been tabulated (Table 12.5). For the mineralised stratigraphy there is a moderate correlation between Cu and Au (r = 0.47: Fig. 12.12a) and a weak correlation between Cu and Ag (r = 0.29: Fig. 12.12b). For Cu versus Pb and Zn there is no correlation between Cu and Pb (r = 0.17: Fig. 12.12c) and Zn (r = 0.17: Fig. 12.12d). Zn has a weak correlation with Au (r = 0.25: Fig. 12.12e), and a moderate correlation with Ag (r = 0.66: Fig. 12.12f) and Pb (r = 0.75: Fig. 12.12g) respectively. Like Zn, Pb has a weak positive correlation with Au (r = 0.23: Fig. 12.12h) and a moderate correlation with Ag (r = 0.69: Fig. 12.12i). Ag has a weak correlation with Au (r = 0.32: Fig. 12.12j).

Table 12.5. Correlation matrix for Mount Chalmers mineralised stratigraphy

	Cu	*Au*	*Zn*	*Pb*
Cu				
Au	0.47			
Zn	0.19	0.25		
Pb	0.17	0.23	0.75	
Ag	0.29	0.32	0.66	0.69

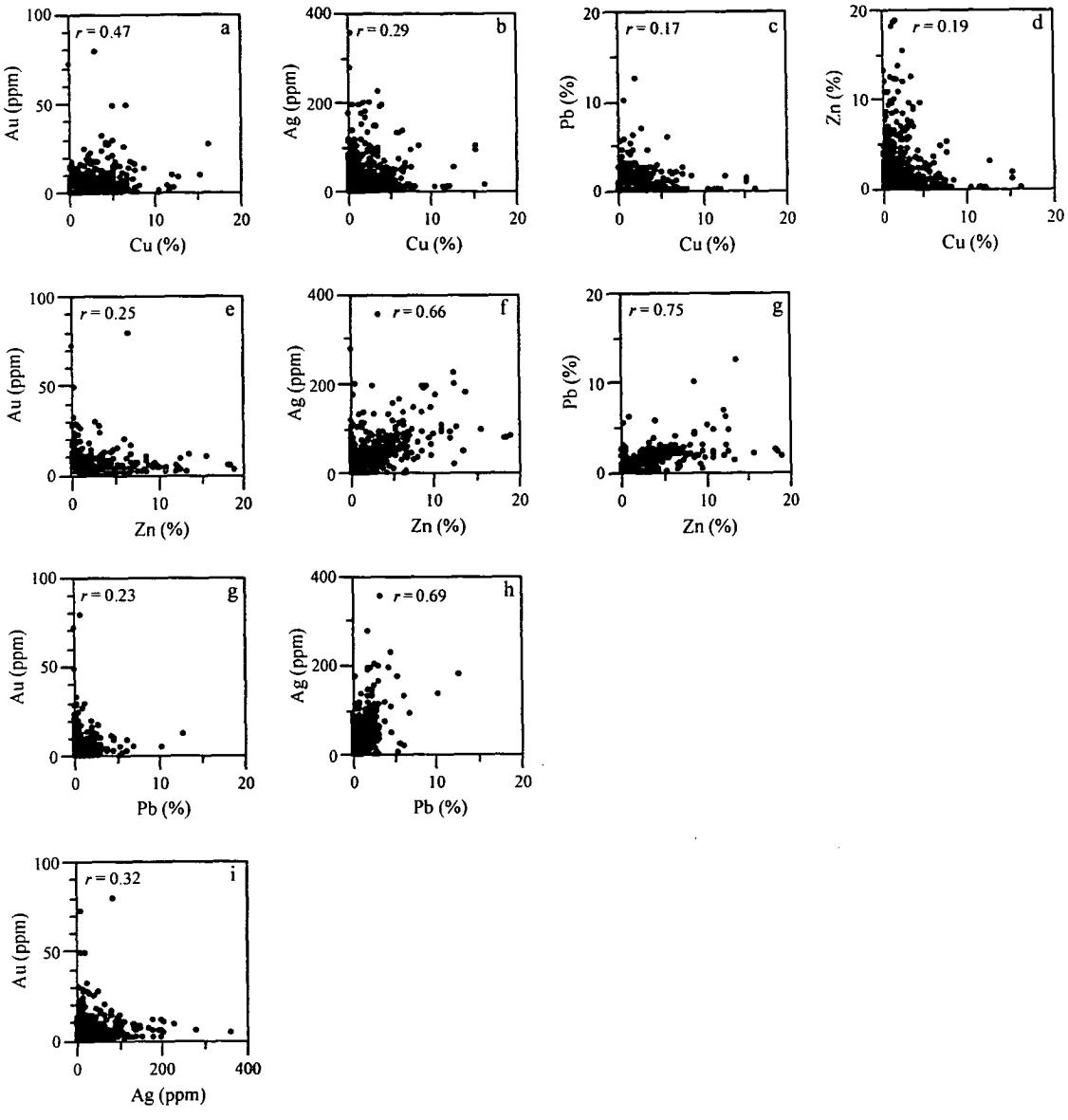

Figure 12. 12 Scatter diagrams depicting the relationship between the various ore metals within the Mount Chalmers mineralised stratigraphy

12.6.2 Main Lode versus West Lode

The data is present as series of scattergrams and have been tabulated (Table 12.6). Copper from the Main Lode has weak correlation with Au (r = 0.36: Fig. 12.13a) and a weak correlation with Ag (r = 0.21: Fig. 12.13b), and has no correlation with either Pb (r = 0.06: Fig. 12.13c) or Zn (r = 0.12: Fig. 12.13d). The West Lode has a higher and stronger correlation coefficient between Cu and Au (r = 0.64: Fig. 12.13e) and for Ag (r = 0.40: Fig. 12.13f) compared to the Main Lode. Unlike the Main Lode, the West Lode has a stronger but weak correlation between Pb and Cu (r = 0.28: Fig. 12.13g) and Zn and Cu (r = 0.282: Fig. 12.13h). Although the higher grades for Cu and Pb tend to be independent of each other.

Zn has a weak correlation with Au for both the Main Lode (r = 0.25: Fig. 12.13i) and West Lode (r = 0.31: Fig. 12.13l). Although the higher grades for both Zn and Au are generally independent of each other. Zn from the Main Lode has a moderate correlation with Ag (r = 0.54: Fig. 12.13j) and Pb (r = 0.67: Fig. 12.13k). While for the West Lode Zn is more strongly correlated with Ag (r = 0.71: Fig. 12.13m) and Pb (r = 0.76: Fig. 12.13n) compared to the Main Lode.

Pb from both lodes has a very weak correlation with Au (Main Lode; r = 0.21: Fig. 12.13o: West Lode; r = 0.31: Fig. 12.13q), with the higher grades for both metals being independent of each other. For both lodes Pb has a strong correlation with Ag (Main Lode; r = 0.67: Fig. 12.13p: West Lode; r = 0.74: Fig. 12.13r).

Ag for both the Main Lode (r = 0.32: Fig. 12.13s) and the West Lode (r = 0.36: Fig. 12.13t) has a weak correlation with Au, with the higher assay grades for both precious metals generally being independent of each other.

Table 12.6. Correlation matrices for the mineralised stratigraphies of the Main Lode and West Lode

Main Lode

	Cu	*Au*	*Zn*	*Pb*
Cu				
Au	0.36			
Zn	0.12	0.25		
Pb	0.06	0.21	0.66	
Ag	0.21	0.32	0.54	0.67

West Lode

	Cu	*Au*	*Zn*	*Pb*
Cu				
Au	0.64			
Zn	0.28	0.31		
Pb	0.28	0.31	0.76	
Ag	0.40	0.36	0.71	0.74

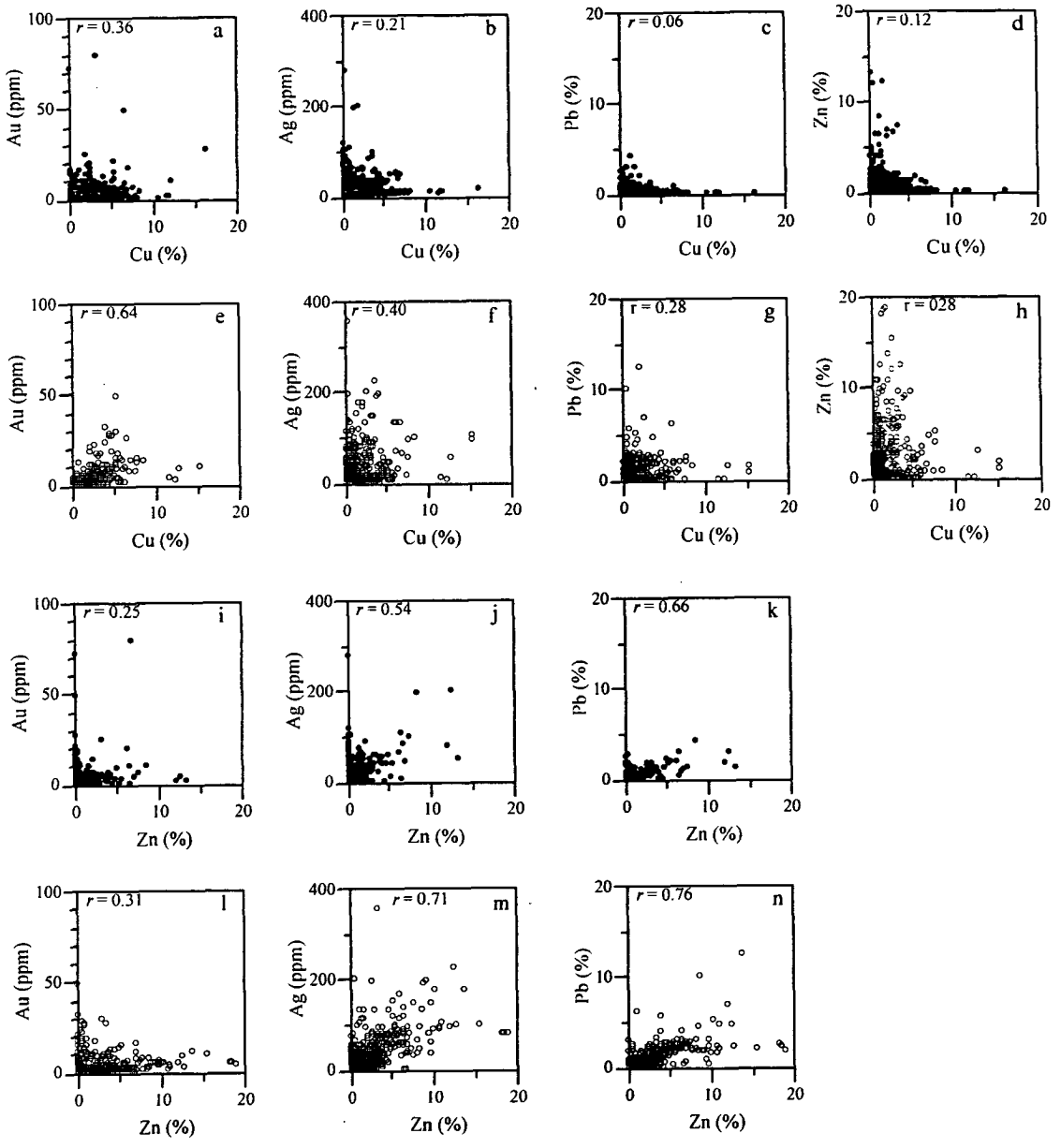

Figure 12.13 Scatter diagrams depicting the relationship between the various ore metals for the Main Lode and the West Lode.
● = Main Lode; O = West Lode

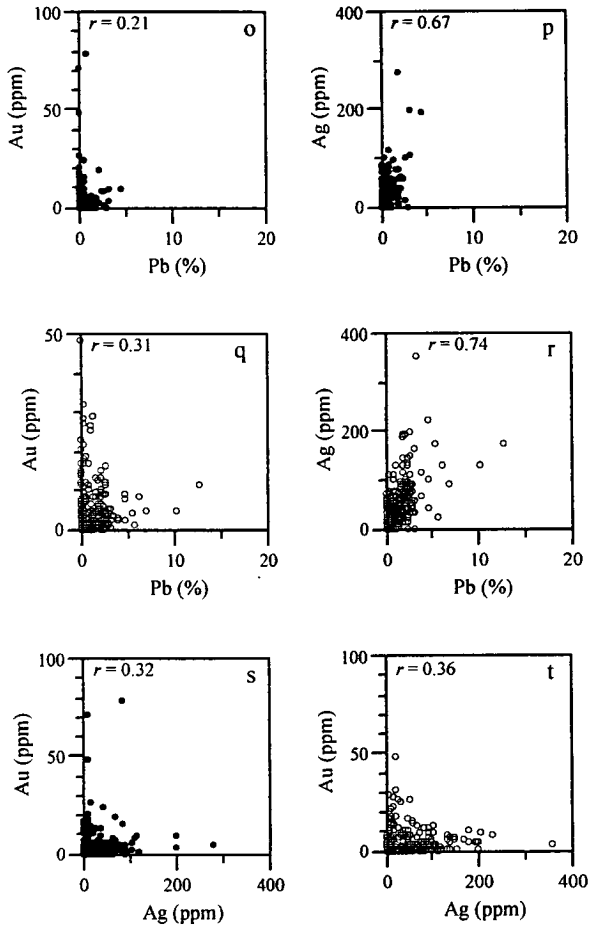

Figure 12.13 con't. Scatter diagrams depicting the relationship between the various ore metals for the Main Lode and the West Lode. ● = Main Lode; ○ = West Lode

12.6.3 Mineralisation Styles

In this section only assays from the massive sulphide (includes semi-massive sulphide), stringer zone and Au Pod mineralisation are discussed, because the metal values within the these zones has a significantly higher probability of reflecting the partition of metals directly within the hydrothermal plumbing system.

12.6.3.1 Massive Sulphide Mineralisation

The data is present as series of scattergrams and have been tabulated (Table 12.7). Copper has a weak correlation with Au for the Main Lode (r = 0.30: Fig. 12.14a) compared to a moderate correlation for the West Lode (r = 0.60: Fig. 12.14e). For the Main Lode Cu has no correlation with Ag (r = 0.09: Fig. 12.14b) compared to a weak correlation with Ag from the West Lode (r = 0.26: Fig. 12.14f). For both the Main Lode and the West Lode Cu has no correlation with either Pb (Main Lode; r = -0.17: Fig. 12.14c: West Lode; r = 0.04: Fig. 12.14g). Cu is negatively correlated with Zn for both the Main Lode and West Lode (Main Lode; r = -0.21: Fig. 12.14d: West Lode; r = -0.11: Fig. 12.14h).

Zn from both the Main Lode has a weak correlation with Au (Main Lode; r = 0.26: Fig. 12.14) and a negative correlation with Au from the West Lode (r = -0.08: Fig. 12.14l). Zn from the Main Lode has a strong correlation with both Ag and Pb (Ag; r = 0.75: Fig. 12.14j: Pb; r = 0.80: Fig. 12.14k). Compared to a moderate correlation with Ag and Pb from the West Lode (r = 0.47: Fig. 12.14m; Pb; r = 0.53: Fig. 12.14n).

Pb from the Main Lode has a moderate correlation Au (r = 0.44: Fig. 12.14o) compared to the West Lode were Pb has no correlation with Au (r = 0.03: Fig. 12.14q). Pb from the Main Lode has very strong correlation with Ag (r = 0.88: Fig. 12.14p) and a moderate correlation with Ag from the West Lode (r = 0.60: Fig. 12.14r).

Ag has a moderate correlation with Au in the Main Lode (r = 0.44: Fig. 12.14s) compared to having no correlation with Au in the West Lode massive sulphide mineralisation (r = 0.07: Fig. 12.14t).

Table 12.7. Correlation matrices for the Main Lode and West Lode massive sulphide lenses

Main Lode Massive Sulphide

	Cu	*Au*	*Zn*	*Pb*
Cu				
Au	0.30			
Zn	-0.21	0.26		
Pb	-0.17	0.44	0.80	
Ag	0.08	0.44	0.75	0.88

West Lode Massive Sulphide

	Cu	*Au*	*Zn*	*Pb*
Cu				
Au	0.60			
Zn	-0.11	-0.08		
Pb	0.04	0.03	0.53	
Ag	0.26	0.07	0.47	0.60

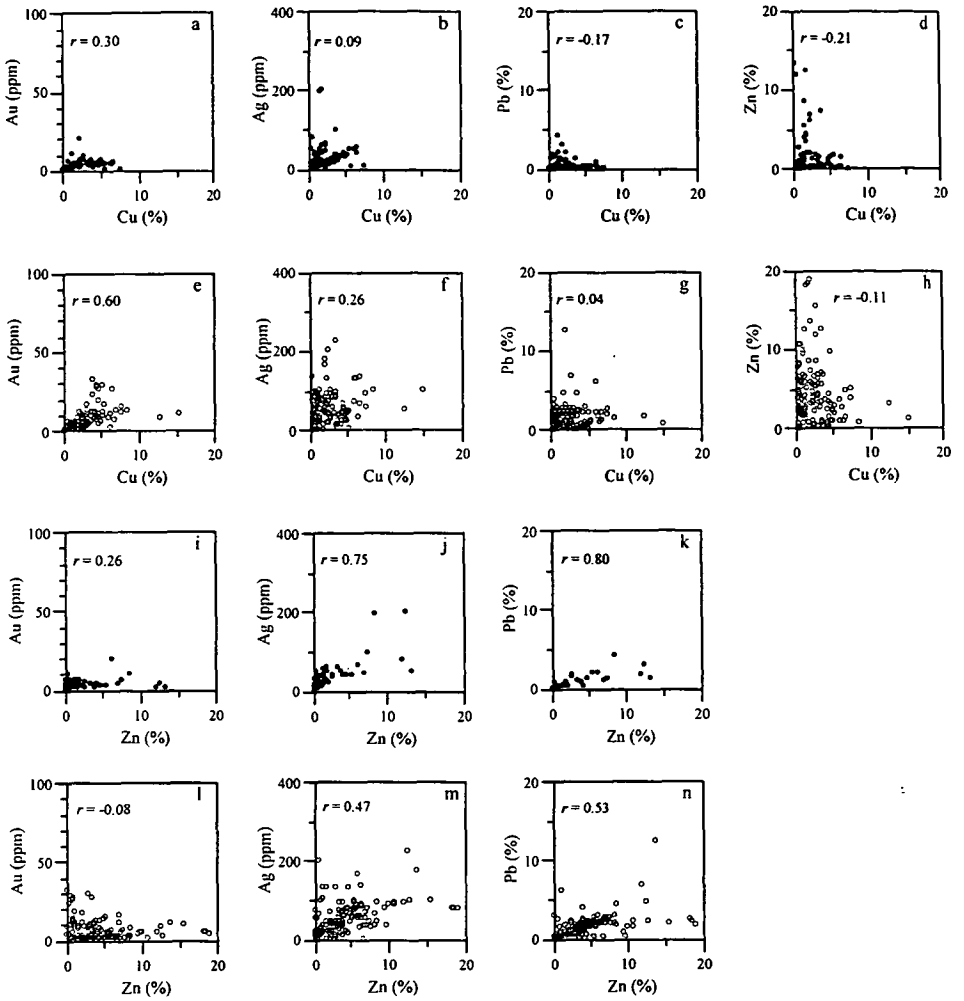

Figure 12.14 Scatter diagrams depicting the relationship between the various ore metals within the massive sulphide mineralisation for the Main Lode and the West Lode.
● = Main Lode, O = West Lode

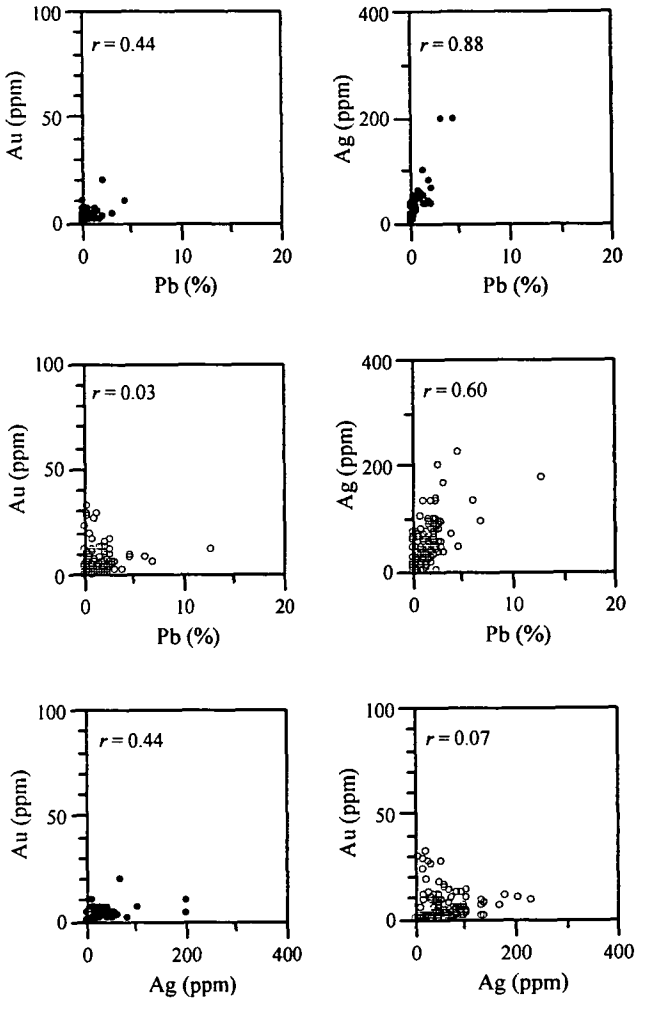

Figure 12.14 con't Scatter diagrams depicting the relationship between the various ore metals within the massive sulphide mineralisation for the Main Lode and the West Lode.
● = Main Lode, o = West Lode

*12.6.3.2. **Stringer Zone and Au Pod Mineralisation***

The data is present as series of scattergrams and have been tabulated (Stringer zone mineralisation - Table 12.8 and Au Pod - Table 12.9). Copper within the stringer zone mineralisation for both the Main Lode and the West Lode has a moderate correlation both with Au (Main Lode; r = 0.43: Fig. 12.15a: West Lode; r = 0.51: Fig. 12.15e) and Ag (Main Lode; r = 0.39: Fig. 12.15b: West Lode; r = 0.22: Fig. 12.15f) and has no correlation with either Pb (Main Lode; r = 0.03: Fig. 12.15c: West Lode; r = 0.09: Fig. 12.15g) or Zn (Main Lode; r = 0.02: Fig. 12.15d: West Lode; r = 0.16: Fig. 12.15h). Within the Au Pod mineralisation, Cu (as in the Main Lode and West Lode stringer zone mineralisation) has moderate correlation with Au (r = 0.49: Fig. 12.15i), but has no correlation with Ag (r = 0.07: Fig. 12.15j) or Pb (r = 0.10: Fig. 12.15k). However, Cu has moderate correlation with Zn within the Au Pod mineralisation (r = 0.55: Fig. 12.15i).

Zn from the Main Lode stringer zone has no correlation with Au (r = 0.02: Fig. 12.15m), and only has weak correlation with Ag (r = 0.25: Fig. 12.15n) and a moderate correlation with Pb (r = 0.62: Fig. 12.15o). Zn from the West Lode stringer zone has no correlation with Au (r = 0.13: Fig. 12.15p), a very strong correlation with Ag (r = 0.90: Fig. 12.15q) and a strong correlation with Pb (r = 0.85: Fig. 12.15r). Conversely compared to the Main Lode and West Lode stringer mineralisation, Zn from the Au Pod has an apparent near perfect (1:1) correlation with Au (r = 0.95: Fig. 12.15s). The near perfect correlation between Zn and Au from the Au Pod can be explained by the three outlying points (Fig. 12.15s). When these three points are ignored and r is recalculated then the correlation coefficients for Zn and Au is 0.21. Zn from the Au Pod has a very weak correlation with Ag (r = 0.18: Fig. 12.15t) and Pb (r = 0.11: Fig. 12.15u). If the three outlying data points are removed as for (Zn vs. Au) and new correlation coefficients are calculated then Zn has no correlation with either Ag (r = 0.02) or Pb (r = 0.03).

Pb has no correlation with Au from either the Main Lode or the West Lode stringer zone mineralisation (Main Lode; r = 0.04: Fig. 12.15v: West Lode; r = 0.07: Fig. 12.15y), but has a weak correlation within the Au Pod (r = 0.23: Fig. 12.15z). Pb from the Main Lode and the Au Pod has a moderate correlation with Ag (Main Lode; r = 0.41: Fig. 12.15w: Au Pod; r = 0.55: Fig. 12.15aa). While Pb from the West Lode has a very strong correlation with Ag (r = 0.81: Fig. 12.15y).

Ag has a weak correlation with Au from the Main Lode (r = 0.25: Fig. 12.15bb) and West Lode (r = 0.18: Fig. 12.15cc) stringer zone mineralisation as well as from the Au Pod mineralisation (r = 0.31: Fig. 12.15dd).

Table 12.8. Correlation matrices for the Au Pod

	Cu	*Au*	*Zn*	*Pb*
Cu				
Au	0.49			
Zn	0.55	0.95		
Pb	0.10	0.23	0.11	
Ag	0.07	0.31	0.18	0.55

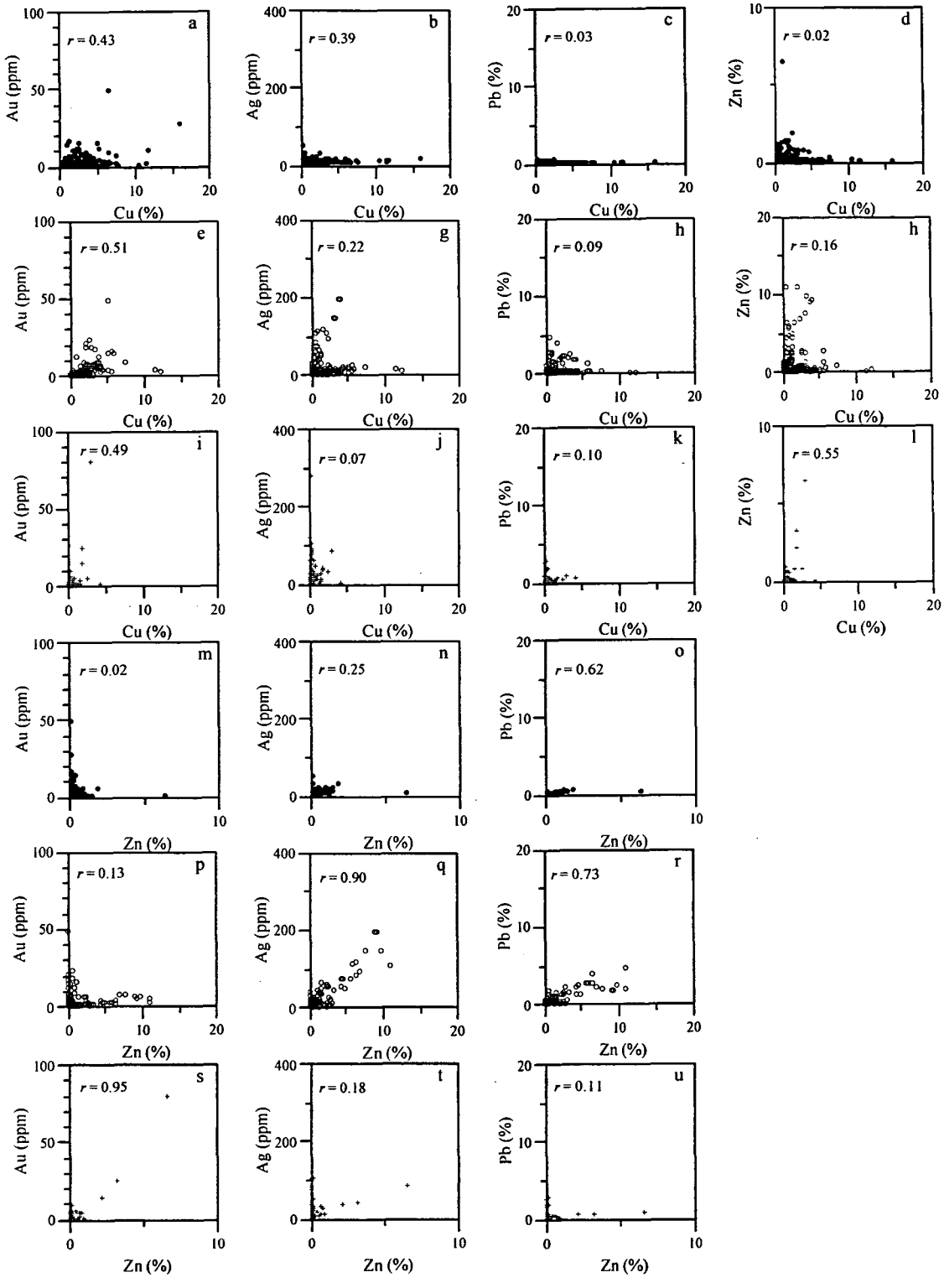

Figure 12.15 Scatter diagrams depicting the relationship between the various ore metals within the stringer zone mineralisation for the Main Lode, West Lode and the Au Pod.
● = Main Lode; ○ = West Lode; + = Au Pod

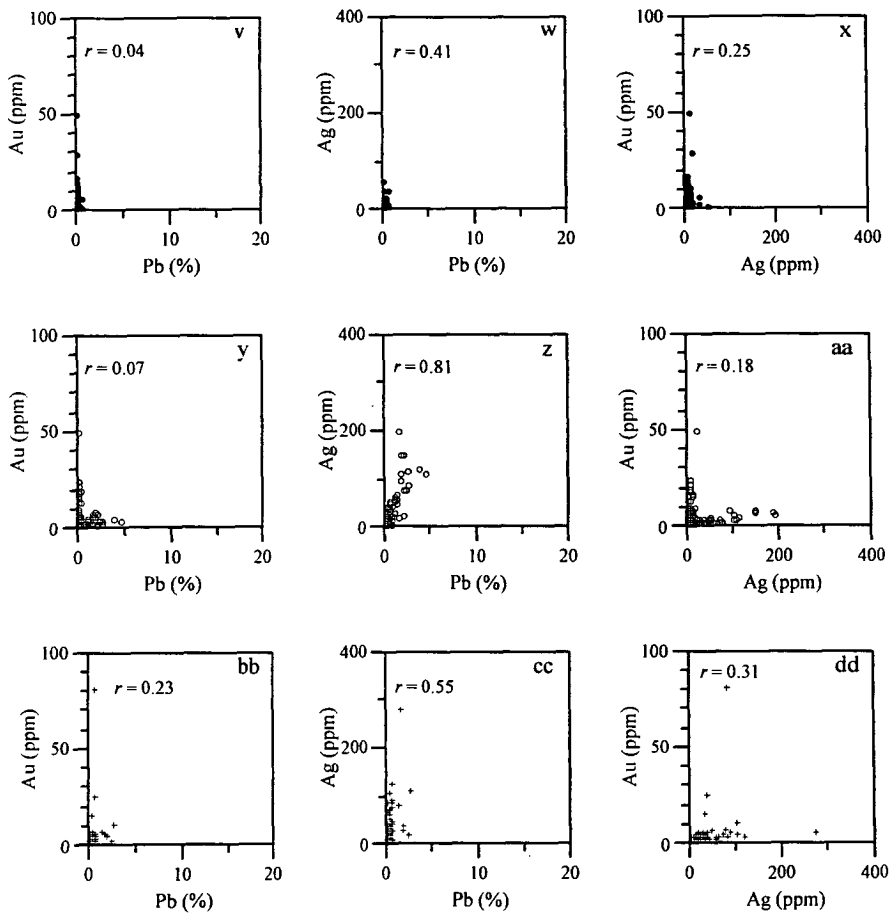

Figure 12.15 Scatter diagrams depicting the relationship between the various ore metals within the stringer zone mineralisation for the Main Lode, West Lode and the Au Pod.
● = Main Lode; ○ = West Lode; + = Au Pod

Table 12.9. Correlation matrices for the Main Lode and West Lode stringer zone mineralisation

Main Lode stringer zone

	Cu	*Au*	*Zn*	*Pb*
Cu				
Au	0.43			
Zn	0.02	0.02		
Pb	0.03	0.04	0.62	
Ag	0.39	0.25	0.28	0.41

West Lode stringer zone

	Cu	*Au*	*Zn*	*Pb*
Cu				
Au	0.51			
Zn	0.16	0.13		
Pb	0.09	0.07	0.85	
Ag	0.22	0.18	0.90	0.81

12.6.4 Discussion

The West Lode massive sulphide was formed from a low-temperature hydrothermal fluid compared to a higher temperature fluid for the Main Lode (see Chapter 8). The West Lode massive sulphide has a statistically significant *r*-value between Cu and Au and low r-values for Zn, Ag and Pb. This is opposite of what should be expected from a seafloor massive sulphide formed from low-temperature hydrothermal fluids. Conversely, the lack of a statistically significant correlation between Cu Au and Ag in the Main Lode massive sulphide is compatible with a seafloor massive sulphide formed from higher-temperature hydrothermal fluids (Herzig *et al.*, 1998; *cf.* Hannington, 1991).

The Main and West Lode have a similar distribution pattern for Cu, although the Main Lode is Cu-rich compared to the West Lode. Like Cu, Au has a similar distribution for both the Main Lode and the West Lode, with the West Lode having the higher Au-grades compared to the Main Lode. The higher correlation coefficient between Au and Cu for the West Lode suggests that the higher Cu and Au grades are related to each other, whereas for the Main Lode, the lower correlation coefficient and observationally the higher Cu and Au grades are not related to each other.

12.7 Classification of the Mount Chalmers VHMS Deposit

Until recently four schemes have been proposed for classifying VHMS deposits, of which the first tends to predominate in the geological literature, namely:

- metal content (*e.g.*, Hutchinson, 1973; Solomon, 1976; Franklin *et al.*, 1981; Large 1992), in which the actual metal content of the deposit determines what type of VHMS deposit it is *e.g.*, Cu-Zn; Zn-Cu; Zn-Pb-Cu and Pb-Zn,
- metal ratios and pyrite $\delta^{34}S$ values (Lydon, 1988) and only Zn-Pb-Cu and Cu-Zn types were recognised,
- tectonic setting (*e.g.*, Sawkins, 1976; Hutchinson, 1980),
- host rock lithology (*e.g.*, volcanic, volcano-sedimentary, sedimentary divisions: Sangster and Scott, 1976).

Using a limited assay database from Mount Chalmers, Large (1992) correctly pointed out a major shortcoming of classifying VHMS deposits based solely on their metal content. In that individual ore lenses or segments of a deposit may fall into separate groups of the classification. Using a much larger assay data base than what was available to Large (1992), the average assay grades (using a cut off of 0.5 % Cu, lower limit for the economic mining of Cu) for Mount Chalmers, the Main Lode, West Lode, and the Au-pod were plotted using the metal classification scheme of Large (1992) (Figs. 12.16). Using this classification scheme Mount Chalmers deposit would be classified as a Zn-Pb-Cu-type VHMS deposit, while the Main Lode and West Lode would be classified as Cu-type and Zn-Pb-Cu-type respectively. However, Mount Chalmers only has an average assay grade for Zn of 0.78 % and for Pb of 0.34 %. The Au-pod from the Main Lode (average Au = 2.79 g/t), is enigmatic as its average assay grade and the majority of its assays plot outside of the three types of VHMS deposits classified by Large (1992), but contains relatively higher grades of Pb compared to Cu and Zn than the Main Lode or West Lode. The assay database for the massive sulphide lenses and stringer zone mineralisation from the Main Lode and the West Lode were also plotted using the classification scheme of Large (1992). The assay grades from both lodes straddle the Cu-type and Zn-Pb-Cu-type deposits. Interestingly, the average assay grades for the Main Lode massive sulphide lens and the stringer zone plot in two different fields, with the stringer zone mineralisation controlling the overall average assay grade for the Main Lode.

On the basis of a deposit's bulk Zn/(Zn+Pb) ratio Lydon (1988) recognised two types of VHMS deposits:

- Zn-Pb-Cu type, with a ratio between 0.70 and 0.80, and
- Cu-Zn type with a ratio greater than 0.95.

Mount Chalmers has an average Zn/(Zn+Pb) ratio of 0.66, according to the above classification would not be classified either as a Zn-Pb-Cu- or Cu-Zn-type VHMS deposit. Lydon (1988) further argued that the sulphur isotope ratios of the two types of VHMS deposits form two distinct populations based upon their $\delta^{34}S$ value of pyrite from the massive sulphide lenses and the Cu/(Cu+Zn) ratios. The ratios of the Cu-Zn type generally having significantly lighter $\delta^{34}S$ values (Figure 12.17). Mount Chalmers has a Cu/(Cu+Zn) ratio of 0.46 and an average $\delta^{34}S$ value for pyrite from the massive sulphide mineralisation of -5.2‰ (Fig. 12.17); and therefore would be classified as a Cu-Zn type of VHMS deposit.

The classification scheme outlined by Lydon (1988) produces the greatest ambiguity in attempting to classify Mount Chalmers. Using the Zn/(Zn+Pb) ratio Mount Chalmers cannot be classified either as a Zn-Pb-Cu- or a Cu-Zn-type VHMS deposit. However, plotting the Cu/(Cu+Zn) vs $\delta^{34}S$ for pyrite, Mount Chalmers plots within the Cu-Zn type deposit field. Therefore, based upon metal content what type of VHMS deposit is Mount Chalmers? As whole using the scheme outlined by Large (1992) Mount Chalmers is a Zn-Pb-Cu-type VHMS deposit, but the individual lodes would be classified differently.

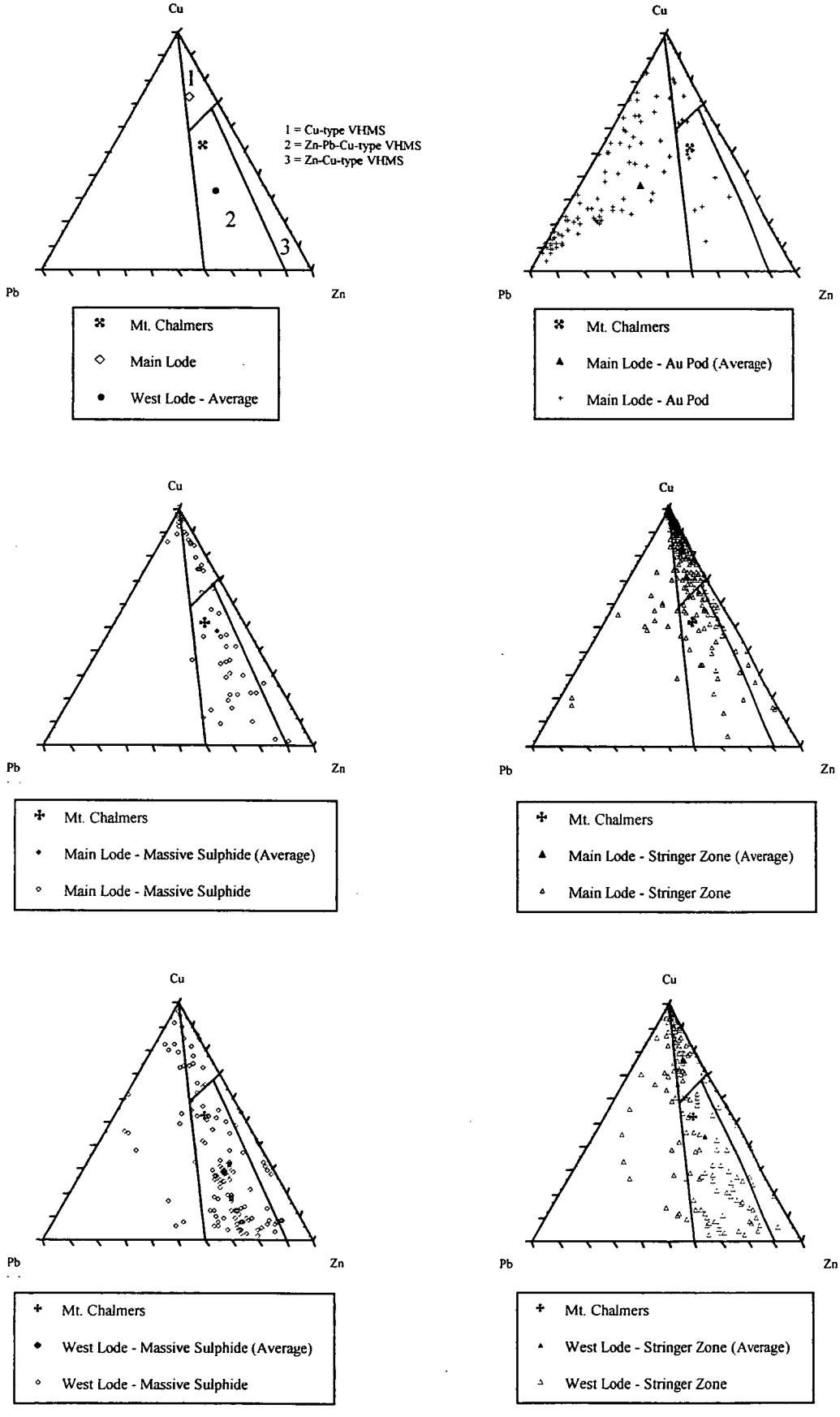

Figure 12.16 Variation in Cu, Zn and Pb for drill hole assays for Mount Chlamers (all assays), Main Lode, West Lode and the Au Pod mineralisation styles.

12.8 SUMMARY

Mount Chalmers has a Zn ratio histogram that can be considered typical of Phanerozoic VHMS deposits. The average Zn ratios for the Main Lode and West Lode massive sulphide lenses and stringer zone mineralisation are consistent with a fluid temperature between 200 and 250° C and a salinity of ≈5-7 wt. %. These values are in close agreement with the measured fluid inclusion temperatures salinities from the West Lode and Main Lode.

The metal contours show that metals are aligned roughly in a north-south direction and that alignment of the metals is coincident with mapped faults. This indicates that there is a strong structural control on the distribution of the massive sulphide and stringer zone mineralisation and that the hydrothermal plumbing system was largely controlled by high angle normal faults. The distribution of Cu, Zn and Au within both the Main Lode and the West Lode can be used to interpret the location of the palaeofluid channel ways. This indicates that the hydrothermal system was dynamic and that the hydrothermal fluids were discharged into the seawater column through a number of vents.

The Main Lode is essentially a Cu-Au-rich massive sulphide that has been a virtually stripped of all of its Zn and Pb compared to the West Lode, which is a Zn-, Cu- Au-rich. Zn within the West Lode tends to be concentrated at the top of the massive sulphide lens while Cu tends to be concentrated at its base. In both lodes, Au enrichment tends to occur towards the top of the massive sulphide lenses. This enrichment of Au The metal zonation seen especially within the West Lode, namely Zn-Au rich, Cu-poor top and a Cu-rich base may be explained by process of zone refining. Within the Main Lode the zone refining process has essentially stripped the massive sulphide of all of its Zn and Pb and left behind only Cu, pyrite and Au.

The West Lode massive sulphide has a well-developed gossan that was formed in a submarine environment. The gossan is essentially depleted in Cu and is not enriched in Zn and Pb compared to the underlying massive sulphide. This is in contrast to the both the ancient on land examples and modern day sea floor examples of massive sulphides that have well developed gossans and supergene zones where enrichment especially of Cu and Au are common.

Contrary to the assertion of Large *et al.*, (1989) there is no positive correlation between Cu and Au throughout the Mount Chalmers deposit. The West Lode has a statistically significant *r*-value between Au and Cu and low *r*-values for Zn, Ag and Pb, This is the opposite of what should be expected from a seafloor massive sulphide deposit formed from low-temperature hydrothermal fluids. Conversely, the Main Lode lacks a statistically significant correlation between Cu, Au and Ag that is compatible with a seafloor massive sulphide formed from higher-temperature hydrothermal fluids.

CHAPTER 13
CONCLUSIONS

"All good science is cumulative; no one can get everything right the first time."
Stephen Jay Gould from an essay titled "Unenchanted Evening" in Eight Little Piggies: Reflections in Natural History (1993)

Mount Chalmers is a pyrite dominated VHMS deposit with accessory chalcopyrite, sphalerite, galena and gold that formed in a shallow-marine (≤300 m) environment. The isotopic, fluid inclusion, and fluid chemistry evidence indicates that the hydrothermal activity was mainly associated with evolved, seawater-derived oxidised acidic hydrothermal fluids, but seawater was not the only fluid involved but there was also a magmatic component to the hydrothermal fluids. The close spatial association between the massive sulphide ore lenses and the proximal facies of the footwall rhyolite argue that there was a link between the hydrothermal activity and magmatic processes. The principal conclusions related to the aims of this study are summarised below.

Volcanic and volcano-sedimentary facies

The Berserker beds are a complex sequence of rhyolitic to andesitic volcanics and volcanolithic siltstones and mudstones. The volcanics are comprised mainly comprised of graded mass-flow emplaced pumiceous breccias, volcanolithic sandstone units, graded polymict, feldspar phyric pumiceous breccias, rhyolite intrusives, coherent to auto-brecciated rhyolite flows and their autoclastic products, basaltic intrusions, andesitic intrusions, lavas and their autoclastic products.

- The footwall lithologies known only from drill holes, principally at Mount Chalmers, but also from some of the surrounding prospects, and are comprised mainly of::
    - graded cobble to sandstone siltstone units, that are interpreted as volcaniclastic massive flow deposits;
    - graded, sericite-silica-chlorite altered polymictic lithic breccia that is interpreted as volcaniclastic massive flow deposits.
    - feldspar-phyric, lithic pumice breccia
    - feldspar-phyric rhyolite, that forms a small dome complex comprised of autobrecciated to resedimented autobrecciated rhyolite

The hangingwall facies of the Berserker beds at Mount Chalmers are dominated by primary and secondary volcanic facies. The primary volcanic facies include rhyolite lavas and their autoclastic products, andesitic intrusions and lavas and their autoclastic products. Voluminous and areally extensive feldspar-phyric, pumice-lithic breccia and feldspar-phyric breccia dominate the secondary volcanic facies. Volcanolithic sandstone and siltstone interpreted as turbites occur throughout the hangingwall stratigraphy.
Within the Berserker beds three types of pumiceous breccias have been recognised:

- graded feldspar-phyric, pumice-lithic breccia - characterised by the presence of polymict lithics,
- feldspar-phyric pumice breccia - characterised by the presence of monomict rhyolitic lithics.

- feldspar-phyric, pumice-lithic breccia - characterised by the presence of rhyolitic and andesitic lithics

Although composed of pumice, presumably of pyroclastic origin, the units show no signs of hot emplacement and their internal organisation is consistent with deposition from water supported, submarine, high particle concentration, volcaniclastic mass flows. The abundance of pumice clasts and the large volumes represented by the units strongly suggests that the parent mass flows were syn-eruptive.

Andesitic intrusions, lavas and resedimented andesitic breccias occur in the southern half of the field area, and occur at two stratigraphic levels, separated by feldspar-phyric pumice breccias. The two andesitic breccias have facies and textures in common:

- coherent to brecciated andesite is interpreted as being produced from the sequential build up of and intrusion of andesitic magma into a pile of contemporaneous unconsolidated hyaloclastite of the same composition.
- poorly sorted polymictic andesitic breccia is thought to have been derived from debris flow that was initiated from the partial collapse of an andesitic cone. The presence of normally graded beds within the polylithic breccia suggests that the deposits were formed from deposition of low concentration turbidity currents.

The eruption and intrusion of the Ellrott Rhyolite mark the last phase of effusive volcanism within the study area. The Ellrott Rhyolite is composed of two facies variants:

- brecciated rhyolite and massive to flow banded coherent feldspar-phyric rhyolite, and
- graded sandstone and lithic breccias

Reconstruction of the volcanic facies architecture

In the vicinity of the Mount Chalmers mine, the Berserker beds are represented by a dynamic and constantly evolving stratigraphic succession of proximal and distal volcanics interbedded with distally derived turbidites. A significant feature of this evolving and variable stratigraphy is the cyclic nature of the volcanism that is represented by the change in volcanism from rhyolite dominant to andesite dominant and back to rhyolite dominant again. The differing volcanic facies indicate that both subaerial and submarine volcanism was occurring within the general vicinity of each other.

Submarine volcanism is represented by the eruption and emplacement of the

- footwall rhyolite,
- coherent to brecciated andesite
- Ellrott Rhyolite.

Subaerial volcanism is possibly represented by the submarine emplacement of subaerially derived pumice breccias. The abundance of pumice clasts and the large volumes represented by the units strongly suggests that the parent mass flows were syn-eruptive. Resedimentation of temporarily stored, non-welded, pumice-rich, primary pyroclastic deposits is also plausible.

VHMS mineralisation at Mount Chalmers

- Palaeontolgical evidence shows that the Berserker beds as a whole as well as the volcanolithic sandstone and siltstone that host VHMS mineralisation were deposited in a shallow-marine ($\lesssim$300 m) environment;

- the Mount Chalmers massive sulphide ore lenses were formed and grew from a continuing cycle of chimney growth and decay and collapse, as well as from circulating hydrothermal fluids within the mound growth;

- gossan development over the West Lode and South Lode massive sulphide lenses argues that the Mount Chalmers VHMS was formed in an oxygenated water column;

- preservation potential of other VHMS deposits formed within an oxygenated water column is limited unless the massive sulphide is rapidly buried before complete oxidation has occurred;

- presence of limited hangingwall alteration and the extension of hydrothermal veins up into the hangingwall lithologies indicates that hydrothermal activity continued after burial of the massive sulphide ore lenses by the hangingwall lithologies;

- close spatial relationship between the proximal facies of the footwall rhyolite and the massive sulphide ore lenses argues that a link exists between the hydrothermal and magmatic processes;

- elongate form of both the massive sulphide and stringer zone mineralisation and the close spatial relationship between the massive sulphide mineralisation and mapped faults indicates that the mineralisation was also largely structurally controlled.

Alteration at Mount Chalmers

- Five main alteration mineral phases have been recognised at Mount Chalmers: two varieties of chlorite: (sudoite, a Li poor, aluminous di, trioctahedral chlorite; trioctahedral chlorite); kaolinite; sericite/muscovite; two generations of silica (phase 1 and phase 2) and dolomite;

- five alteration phases can occur separately or with one another, presenting a complex history of interacting mineral phases;

- interaction between the different mineral phases has produced complex alteration assemblages;

- style of alteration at Mount Chalmers has similarity to both the stratabound and semiconformable alteration, and the pipe-like alteration style;

- alteration assemblages generally being centred on interpreted high angle normal faults, which are interpreted as being the conduits for the hydrothermal fluids;

- silica alteration is extensively developed within the footwall lithologies and increases in intensity stratigraphically upwards;

- chlorite is developed within and adjacent to the sulphide veins and within the dolomite;

- sericite alteration is possibly the result of the destruction of feldspars and volcanic glass;

- dolomite, kaolin and pyrite alteration is very important on a local scale and are associated with known mineralised occurrences

Fluid inclusion and fluid chemistry

- Primary fluid inclusions in quartz from the stringer zone of the Main Lode yielded homogenisation temperatures in the range of 207.5° to 276.6°C and salinities of 4.8 to 7.8 eq. NaCl wt %;

- fluid inclusions from the West Lode yielded homogenisation temperatures in the range of 157.8° to 231.6°C and salinities of 4.9 to 11.2 eq. NaCl wt %;

- ore fluid salinities are higher than seawater ;

- no evidence for boiling, such as simultaneously formed inclusions of both liquid and vapour phases were recognised either from the Main Lode or from the West Lode;

- PIXE analysis of fluid inclusions suggests that the high concentrations of Ba, Cu, Fe, and Pb and the presence of significant concentrations of As and K cannot be solely derived form the leaching of footwall stratigraphy by circulating modified seawater, but that there was a magmatic input of these elements;

Isotopic constraints on the formation of the Mount Chalmers VHMS deposit

- $\delta^{18}O$ values from the footwall silica alteration have a very narrow range (+9.1 to +9.8 ‰);

- calculated $\delta^{18}O$ values could be consistent with an initial fluid with meteoric, seawater or a magmatic origin, or any combination of these three. Although if the mean $\delta^{18}O$ value was solely used then a magmatic origin for the hydrothermal fluids can be discounted, assuming no previous water-rock interaction had occurred;

- modelled w/r ratios for both an open and closed systems indicate that the hydrothermal fluid was dominated by modified seawater, with minor contribution of magmatic fluid;

- calculated water fluxes indicate that high w/r ratios (≥ 1) prevailed throughout most of the life of the hydrothermal system at Mount Chalmers;

- Mount Chalmers has uniformly negative $\delta^{34}S$ values for pyrite (-17.6 to -1.6 ‰), chalcopyrite (-13.0 to -3.0 ‰), sphalerite (-8.5 to -6.6 ‰) and galena (-10 to -7.5 ‰); the majority of the sulphides however have a narrow range clustering between -8.0 to -6.0 ‰; relatively restricted range in $\delta^{34}S$ values were at Mount Chalmers in both the massive sulphide and the stringer zone mineralisation argues that the sulphides and sulphates were precipitated from a single hydrothermal event that maintained similar conditions of $\delta^{18}O$, pH and T;

- however, the total range in $\delta^{34}S$ values argues that there must have been another source of sulphur; the extremely low $\delta^{34}S$ values (down to -17 ‰) may be explained by the interaction of hydrothermal fluid with biogenic sulphur within microniches within the volcano-sedimentary pile;

- barite has values between +7.5 to +12.1 ‰, which are isotopically lighter than what would be expected from Early Permian seawater sulphate with a median $\delta^{34}S$ value of +13.1 ‰; lighter $\delta^{34}S$ values for barite may be explained by an oxidising hydrothermal fluid interacting with seawater either at or near the seawater/sulphide mound interface, or as the system waned and cold seawater entered the periphery of the sulphide mound and mixed with the cooling hydrothermal fluid.

- $\delta^{34}S$ values in sulphides and barite can be explained by an oxidised hydrothermal fluid, that was probably dominated by evolved seawater, but one that had a significant input of sulphur from a magmatic source.

Origin of dolomite at Mount Chalmers

- Lenses of semi-massive to massive dolomite associated with massive sulfide at Mount Chalmers have replaced hangingwall and footwall rocks;

- five generations of dolomite are distinguished based on textural relations: texture 1 - anhedral to subhedral very fine-grained cloudy dolomite; texture 2 - radiating blades of cloudy dolomite; texture 3 - clear rhombohedral dolomite overgrowths on the cloudy dolomite; texture 4 - mosaics of interlocking subhedral clear dolomite within the cloudy dolomite and texture 5 - late stage dolomite infilling veins, vugs and fractures.;

- the five phases of dolomite indicate evolving, episodic hydrothermal replacement;

- carbon and oxygen isotopes are consistent with dolomite formation either: (1) fluid mixing, between an ascending hydrothermal fluid charged with juvenile CO_2 and cold seawater, or (2) fluid/rock interaction between an ascending CO_2-rich fluid and mafic minerals that provide cations for dolomite formation; in both models, it is envisaged that contribution of seawater to the formation of dolomite was minor and occurred at or near the site of dolomite precipitation. Geological observations favour derivation of the dolomite by fluid/rock interaction.

REFERENCES

Addy, S. K., and Ympa, P. J. M., 1977, Origin of massive sulfide deposits at Ducktown, Tennessee: An oxygen, carbon, and hydrogen isotope study: Economic Geology, v. 72, p. 1245-1268.

Aggarwal, P. K., and Longstaffe, F. J., 1987, Oxygen-isotope geochemistry of metamorphosed, massive sulfide deposits of the Flin Flon — Snow Lake Belt, Manitoba: Contributions to Mineralogy and Petrology, v. 96, p. 314-325.

Allen, J. R. L., 1977, The possible mechanics of convolute lamination in graded beds: Journal of the Geological Society of London, v. 134, p. 19-31.

Allen, R. L., 1988, False pyroclastic textures in altered silicic lavas, with implications for volcanic-associated mineralization: Economic Geology, v. 83, p. 1424-1446.

Allen, R. L., 1992, Reconstruction of the tectonic, volcanic, and sedimentary setting of strongly deformed Zn-Cu massive sulfide deposits at Benambra, Victoria: Economic Geology, v. 87, p. 825 - 855.

Allen, R. L., and Cas, R. A. F., 1990, The Rosebery controversy: Distinguishing prospective submarine ignimbrite-like units from true subaerial ignimbrites in the Rosebery-Hercules ZnCuPb massive sulfide district, Tasmania: Gondwana: Terranes and Resources. Tenth Australian Geological Convention, Hobart, 1990, 1990, p. 31-32.

Allen, R. L., Weihed, P., and Svenson, S., 1997, Setting of Zn-Cu-Au-Ag massive sulfide deposits in the evolution and facies architecture of a 1.9 Ga marine volcanic arc, Skellefte district, Sweden: Economic Geology, v. 91, p. 1022-1053.

Amieux, P., 1982, La cathodoluminscence: methode d'étude sedimentologique des carbonates.: Bulletin des Centres de Recherches Exploration - Production; Elf Aquitane, v. 6, p. 437-483.

Anderson, J. J., 1969, Development of snowflake texture in a welded tuff, Davis Mountains, Texas: Geological Society of America Bulletin, v. 80, p. 2075-2080.

Armstrong, J. D., Dear, J. F., and Runnegar, B., 1967, Permian ammonoids from eastern Australia.: Journal of the Geological Society of Australia, v. 14, p. 87-96.

Asano, K., Ingle, J., and Takayanagi, Y., 1969, Neogene planktonic foraminiferal sequence of northeastern Japan, *In* Bronnimann, P., and Renz, H., eds., Proceedings of the First International Conference on Planktonic Microfossils, 1: Leiden, E. J. Brill, p. 15-25.

Baker, P. A., Cross, S. L., and Burns, S. J., 1994, Geochemistry of carbonate nodules and implications for hydrothermal circulation, Middle Valley, Juan de Fuca Ridge, *In* Mottl, M. J., Davis, E. E., Fisher, A. T., and Slack, J. F., eds., Proceedings of the Ocean Drilling Programme, Scientific Results, 139: College Station, Texas, Ocean Drilling Program, p. 313-328.

Banks, D. A., 1986, Hydrothermal chimneys and fossil worms from the Tynagh Pb-Zn deposit, Ireland, *In* Andrew, C. J., Crowe, R. W. A., Finlay, S., Pennell, W. M., and Pyne, J. F., eds., Geology and Genesis of Mineral Deposits in Ireland: Dublin, Irish Association for Economic Geology Ltd., p. 441-447.

Barrett, T. J., and Sherlock, R. L., 1996, Quartz, *In* Thompson, A. J. B., and Thompson, J. F. H., eds., Atlas of Alteration, Geological Association of Canada, Mineral Deposits Division, p. 86-87.

Barrett, T. J., Thompson, J. F. H., and Sherlock, R. L., 1996, Stratigraphic, lithogeochemical and tectonic setting of the Kutcho Creek massive sulfide deposit, northern British Columbia: Exploration and Mining Geology, v. 5, p. 309-338.

Barrie, C. T., and Hannington, M. D., 1997, Classification of VMS deposits based on host rock compositions, *In* Barrie, C. T., and Hannington, M. D., eds., Volcanic-Associated Massive Sulfide Deposits: Processes and Examples in Modern and Ancient Settings: Ottawa, Canada, Geological Association of Canada(GAC), Mineral Deposits Subdivision of the GAC, and the Society of Economic Geologists., p. 1-12.

Bates, R. L., and Jackson, J. A., 1995, Glossary of Geology: Alexandria, Virginia, American Geological Institute.

Baur, M. E., Hayes, J. M., Studley, S. A., and Walter, M. R., 1985, Millimeter-scale variations of stable isotope abundances in carbonates from banded-iron formation in the Hamersley Group of Western Australia: Economic Geology, v. 80, p. 270-282.

Beaty, D. W., and Taylor, H. P., 1982, Some petrologic and oxygen isotopic relationships in the Amulet Mine, Noranda, Quebec, and their bearing on the origin of Archean massive sulfide deposits: Economic Geology, v. 77, p. 95-108.

Beaty, D. W., Taylor, H. P. J., and Coads, P. R., 1988, An oxygen isotope study of the Kidd Creek, Ontario, volcanogenic massive sulfide deposit: Evidence for a high $\delta^{18}O$ ore fluid: Economic Geology, v. 83, p. 1-17.

Bence, A. E., and Taylor, B. E., 1985, Rare earth element systematics of West Shasta metavolcanic rocks: petrogenesis and hydrothermal alteration.: Economic Geology, v. 80, p. 2164-2176.

Bernier, L. R., and MacLean, W. H., 1993, Lithogeochemistry of a metamorphosed VMS alteration zone at Montauban, Grenville Province, Quebec: Exploration and Mining Geology, v. 2, p. 367-386.

Bigger, S. E., and Hanson, R. E., 1992, Devitrification textures and related features in the Carlton Rhyolite in the Blue Creek Canyon area, Wichita Mountains, southwestern Oklahoma: Oklahoma Geological Survey, Geological Notes 52, p. 124-142.

Bischoff, J. L., and Dickson, F. W., 1975, Seawater-basalt interaction at 200°C and 500 bars: implications for origin of seafloor heavy metal deposits and regulation of seawater chemistry: Earth and Planetary Science Letters, v. 25, p. 385-397.

Bischoff, J. L., and Seyfried, W. E., 1978, Hydrothermal chemistry of seawater from 25° to 350°C: American Journal of Science, v. 278, p. 838-860.

Blake, P. R., Simpson, G. A., Fordham, B. G., and Hayward, M. A., 1998, The Yarrol fore-arc basin: a complex suite of volcanic facies and allochthonous limestone blocks: Geoscience for the New Millennium, Townsville, Australia, 1998.

Bodnar, R. J., 1993, Revised equation and table for determining the freezing point depression of H_2O-NaCl solutions: Geochimica et Cosmochimica Acta, v. 57, p. 683-684.

Bonnichsen , B., and Kauffman, D. F., 1987, Physical features of rhyolite lava flows in the Snake River Plain volcanic province, southwestern Idaho, *In* Fink, J. H., ed., The Emplacement of Silicic Domes and Lava Flows, Geological Society of America Special Paper 212, p. 119 - 145.

Boulter, C. A., 1993, High-level peperitic sills at Rio Tinto, Spain: implications for stratigraphy and mineralisation: Transactions of the Institute for Mining and Metallurgy (Section B: Applied earth Science), v. 102, p. B30-B37.

Boyce, A. J., Coleman, M. L., and Russell, M. J., 1983, Formation of fossil hydrothermal chimneys and mounds from Silvermines, Ireland: Nature, p. 545-550.

Boyd, F. R., 1961, Welded tuffs and flows in the rhyolite plateau of Yellowstone Park, Wyoming: Geological Society of America Bulletin, v. 72, p. 387-426.

Braithwaite, R. L., 1974, Origin of the Rosebery ore deposit: Economic Geology, v. 69, p. 1086-1101.

Branney, M. J., and Sparks, R. S. J., 1990, Fiamme formed by diagenesis and burial-compaction in soils and subaqueous sediments: Journal Geological Society of London, v. 147, p. 919-922.

Brooks, E. R., 1995, Paleozoic fluidization, folding, and peperite formation, northern Sierra Nevada, California: Canadian Journal of Earth Science, v. 32, p. 314-324.

Brooks, E., R, Wood, M., M, and Garbutt, P. L.,1982, Origin and metamorphism of peperite and associated rocks in the Devonian Elwell Formation, northern Sierra Nevada, California: Geological Society of America Bulletin, v. 93, p. 1208-1231.

Bryndzia, L. T., Scott, S. D., and Farr, J. E., 1983, Mineralogy, geochemistry, and mineral chemistry of siliceous ore and altered footwall rocks in the Uwamuki 2 and 4 deposits, Kosaka Mine, Hokuroku District, Japan, *In* Ohmoto, H., and Skinner, B. J., eds., The Kuroko and Related Volcanogenic Massive Sulfide Deposits, Economic Geology Monograph No.5, p. 507-522.

Burnham, C. W., 1983, Deep submarine pyroclastic eruptions, *In* Ohmoto, H., and Skinner, B. J., eds., The Kuroko and Related Volcanogenic Massive Sulfide Deposits, Economic Geology Monograph No. 5, p. 142-148.

Busby-Spera, C. J., and White, J. D. L., 1987, Variation in peperite textures associated with differing host-sediment properties: Bulletin of Volcanology, v. 49, p. 765-775.

Butterfield, D. A., McDuff, R. E., Franklin, J., and Wheat, C. G., 1994, Geochemistry of hydrothermal vent fluids from Middle Valley, Juan de Fuca Ridge, *In* Mottl, M. J., Davis, E. E., Fisher, A. T., and Slack, J. F., eds., Proceedings of Ocean Drilling Program. Scientific Results, 139: College Station, Texas, Ocean Drilling Program, p. 395-410.

Butterfield, D. A., Massoth, G. J., McDuff, R. E., Lupton, J. E., and Lilley, M. D., 1990, Geochemistry of hydrothermal fluids from Axial Seamount Hydrothermal Emissions Study vent field, Juan de Fuca Ridge: subseafloor boiling and subsequent fluid-rock interaction: Journal of Geophysical Research, v. 95, p. 12,895-12,921.

Çagatay, M. N., and Eastoe, C. L., 1995, A sulfur isotope study of volcanogenic massive sulfide deposits of the Eastern Black Sea province, Turkey: Mineralium Deposita, v. 30, p. 55-66.

Campbell, A. C., and Edmond, J. M., 1989, Halide systematics of submarine hydrothermal vents: Nature, v. 342, p. 168-170.

Campbell, A. C., German, C. R., Palmer, M. R., Gamo, T., and Edmond, J. M., 1994, Chemistry of hydrothermal fluids from Escanaba Trough, Gorda Ridge, *In* Morton, J. L., Zierenberg, R. A., and Reiss, C. A., eds., Geologic, Hydrothermal, and Biologic Studies at Escanaba Trough, Gorda Ridge, Offshore Northern California, Bulletin 2022, Unites States Geological Survey, p. 201-221.

Campbell, A. R., 1995, The evolution of a magmatic fluid: a case history from the Capitan Mountains, New Mexico, *In* Thompson, J. F. H., ed., Magmas, Fluids, and Ore Deposits, Short Course Vol 23: Victoria, Canada, Mineralogical Association of Canada.

Cas, R. A. F., 1992, Submarine volcanism: Eruption styles, products, and relevance to understanding the host-rock successions to volcanic-hosted massive sulfide deposits: Economic Geology, v. 87, p. 511-541.

Cas, R. A. F., and Wright, J. V., 1987, Volcanic Successions, modern and ancient: London, Allen and Unwin Ltd, 487 p.

Cashman, K. V., and Fiske, R. S., 1991, Fallout of pyroclastic debris from submarine volcanic eruptions.: Science, p. 275 - 280.

Cathles, L. M., 1983, An analysis of the hydrothermal system responsible for massive sulfide deposition in the Hokuroku Basin of Japan, *In* Ohmoto, H., and Skinner, B. J., eds., The Kuroko and Related Volcanogenic Massive Sulfide Deposits, Economic Geology Monograph No. 5, p. 439-487.

Cathles, L. M., 1993, Oxygen isotope alteration in the Noranda mining district, Abitibi Greenstone Belt, Quebec: Economic Geology, v. 88, p. 1483-1511.

Cathles, L. M., Erendi, A. H. J., and Barrie, T., 1997, How long can a hydrothermal system be sustained by a single intrusive event?: Economic Geology, v. 92, p. 766-771.

Cathles, L. M., Guber, A. L., Lenagh, T. C., and Dudás, F. Ö., 1983, Kuroko-type massive sulfide deposits of Japan: Products of an aborted island-arc rift, *In* Ohmoto, H., and Skinner, B. J., eds., *The Kuroko and Related Volcanogenic Massive Sulfide Deposits, Economic Geology Monograph No. 5*, p. 96-114.

Charlou, J. L., Fouquet, Y., Donval, J. P., Auzende, J. M., Jean-Baptiste, P., Stievenard, M., and Michel, S., 1996, Mineral and gas chemistry of hydrothermal fluids on an ultrafast spreading ridge: East Pacific Rise, 17° to 19°S (Naudur cruise, 1993) phase separation processes controlled by volcanic and tectonic activity: *Journal of Geophysical Research*, v. 101, p. 15,899-15,919.

Chaussidon, M., Albarède, F., and Sheppard, M. F., 1989, Sulphur isotope variations in the mantle from ion microprobe analyses of micro-sulphide inclusions: Earth and Planetary Science Letters, v. 92, p. 144-156.

Chaussidon, M., and Lorand, J. P., 1990, Sulphur isotope composition of orogenic spinel lherzolite from Ariege (N.E. Pyrenees, France): An ion microprobe study: Geochimica et Cosmochimica Acta, v. 54, p. 2835-2846.

Chayes, F., 1960, On correlation between variables of constant sum: *Journal of Geophysical Research*, v. 65, p. 4185-4193.

Christiansen, R. L., and Lipman, P. W., 1996, Emplacement and thermal history of a rhyolite lava flow near Forty mile Canyon, southern Nevada: Geological Society of America Bulletin, v. 77, p. 671-684.

Clark, L. A., 1971, Volcanogenic ores: Comparison of cupriferous pyrite deposits of Cyprus and Japanese Kuroko deposits, *In* Takéuchi, Y., ed., Proceedings of the IMA-IAGOD '70 Meetings, Special Issue No. 3., Society of Mining Geologists of Japan, p. 206-215.

Clark, L. A., 1983, Genetic implications of fragmental ore texture in Japanese kuroko deposits: Canadian Institute of Mining, p. 105-114.

Claypool, G. E., Holser, W., T, Kaplan, I. R., Sakai, H., and Zak, I., 1980, The age curves of sulfur and oxygen isotopes in marine sulfate and their mutual interpretation: Chemical Geology, v. 28, p. 199-260.

Clayton, R. N., and Mayeda, T. K., 1963, The use of bromine pentafluoride in the extraction of oxygen from oxides and silicates: Geochimica et Cosmochimica Acta, v. 27, p. 43-52.

Clough, B. J., Wright, J. V., and White, J. D. L., 1981, An unusual bed of giant pumice in Mexico: Nature, v. 289, p. 49-50.

Coleman, J. M., 1969, Brahmaputra River: Channel processes and sedimentation: Sedimentary Geology, v. 3, p. 129-239.

Coleman, J. M., and Gagliano, S. M., 1965, Sedimentary structures: Mississippi River deltaic plain, *In* Middleton, G. V., ed., Primary Sedimentary Structures and their Hydrodynamic Interpretation, Special Publication 12, Society of Economic Paleontologists and Mineralogists, p. 133-148.

Colley, H., 1993, Shallow-water kuroko-type mineralisation in Fiji: IAVCEI - Ancient Volcanism and Modern Analogues, Canberra, 1993, p. 22.

Colley, H., and Rice, C. M., 1975, A Kuroko-type ore deposit in Fiji: Economic Geology, v. 70, p. 1373-1386.

Collinson, J. D., and Thompson, D. B., 1989, Sedimentary Structures: London, Chapman and Hall, 207 p.

Concetta, G., and Maugeri, T. L., 1993, Chemolithotrophic, sulfur-oxidizing bacteria from marine, shallow hydrothermal vent of Vulcano (Italy): Geomicrobiology Journal, v. 11, p. 109-120.

Constantinou, G., 1973, Geology, geochemistry, and genesis of Cyprus sulphide deposits: Economic Geology, v. 68, p. 843-858.

Constantinou, G., and Govett, G. J. S., 1972, Genesis of sulphide deposits, ochre and umber of Cyprus: Transactions of the Institute of Mining and Metallurgy (Section B, Applied Earth Science), v. 81, p. 34-36.

Conybeare, C. E. B., and Crook, K. A. W., 1982, Manual of Sedimentary Structures: Canberra, Bureau of Mineral Resources, 327 p.

Cooke, D. R., and Large, R. R., 1995, Hydrothermal geochemistry, Exploration Geochemistry and Hydrothermal Geochemistry Part 2, Master of Economic Geology Course Manual 12: Hobart, CODES SRC, University of Tasmania, p. 1-38.

Costa, U. R., Barnett, R. L., and Kerrich, R., 1983, The Matagami Lake Mine Archean Zn-Cu sulfide deposit, Quebec: Hydrothermal coprecipitation of the talc and sulfides in a sea-floor brine pool—evidence from geochemistry, $^{18}O/^{16}O$, and mineral chemistry: Economic Geology, v. 78, p. 1144-1203.

Cran, J. N., 1985, Authority to Prospect 4020M: New Berserker. Report on Exploration for the period June 14, to 1985 to December 14, 1985 and final report, Newmont Holdings Pty Ltd., unpublished company report, p. 11.

Crockford, J., 1945, A bryozoan fauna from the Lake's Creek quarry, Rockhmapton, Queensland. Proceedings of the Linnean Society of New South Wales, v. 70, p.125-134.

Crouch, S., and Parfrey, S., 1998, Geology of the Berserker Province, northern New England Orogen: Queensland Government Mining Journal, p. 15-25.

Curran, H. A., 1985, The trace fossil assemblage of a Cretaceous nearshore environment: Englishtown Formation of Delaware, U.S.A, *In* Curran, H. A., ed., Biogenic Structures: Their Use In Interpreting Depositional Environments, Special Publication N° 35, Society of Economic Paleontologists and Mineralogists, p. 261-276.

Dadd, K. A., 1992, Structures within large volume rhyolite lava flows of the Devonian Comerong Volcanics, southeastern Australia, and the Pleistocene Ngongotaha lava dome, New Zealand: Journal of Volcanology and Geothermal Research, v. 54, p. 33-51.

Dando, P. R., Hughes, J. A., and Thiermann, F., 1995, Preliminary observations on biological communities at shallow hydrothermal vents in the Aegean Sea, *In* Parson, L. M., Walker, C. L., and Dixon, D. R., eds., Hydrothermal Vents and Processes, Geological Society Special Publication No. 87, p. 303-317.

Date, J., Watanabe, Y., and Saeki, Y., 1983, Zonal alteration around the Fukazawa kuroko deposits, Akita Prefecture, northern Japan, *In* Ohmoto, H., and Skinner, B. J., eds., The Kuroko and Related Volcanogenic Massive Sulfide Deposits, Monograph 5, Economic Geology, p. 365-386.

David, T. W. E., 1950, The Geology of the Commonwealth of Australia: London, Edward Arnold & Co.

Davies, H. G., 1965, Convolute lamination and other structures from the Lower Cole Measures of Yorkshire: Sedimentology, v. 5, p. 305-325.

Day, R. W., Murray, C. G., and Whitaker, W. G., 1978, The eastern part of the Tasman Orogenic Zone: Tectonophysics, v. 48, p. 327-364.

Day, R. W., Whitaker, W. G., Murray, C. G., Wilson. I. H. and Grimes., 1983, Queensland Geology. A Companion Volume to the 1:2 500 000 Sclae Geological Map (1975): Geological Survey of Queensland Publication 383, 186 p.

De Boer, P. L., 1979, Convolute lamination in modern sands of the estuary of the Oosterschelde, the Netherlands, formed as result of entrapped air: Sedimentology, v. 26, p. 283-294.

De Rosen-Spence, A. F., Provost, G., Dimroth, E., Gochnauer, K., and Owen, V., 1980, Archean subaqueous felsic flows, Rouyn-Noranda, Quebec, Canada, and their Quaternary equivalents: Precambrian Research, v. 12, p. 43-77.

Deer, W. A., Howie, R. A., and Zussman, J., 1992, An Introduction to the Rock Forming Minerals: Harlow, England, Longman Scientific and Technical, 696 p.

Deines, P., and Gold, D. P., 1973, The isotopic composition of carbonatite and kimberlite carbonates and their bearing on the isotopic composition of deep-seated carbon: Geochimica et Cosmochimica Acta, v. 37, p. 1709-1733.

Deines, P., Langmuir, D., and Harmon, R. S., 1974, Stable isotope ratios and the existence of a gas phase in the evolution of carbonate groundwater: Geochimica et Cosmochimica Acta, v. 38, p. 1147-1164.

Dimroth, E., and Yamagishi, H., 1987, Criteria for the recognition of ancient subaqueous pyroclastic rocks: Report of the Geological Survey of Hokkaido, v. Report No. 58, p. 55-88.

Dixon, G. H., 1980, Geological, Geochemical and Stable Isotope Studies of the Carbonates at Rosebery: Unpub. BSc(Hons) thesis, University of Tasmania, 173 p.

Donchak, P. J.T., and Holmes, K.H., 1991, Gladstone Sheet 9150. 1:100 000 Geological Map Commentary: Brisbane, Department of Resource Industries, Queensland, 46 p.

Duckworth, R. C., Fallick, A. E., and Rickard, D., 1994, Mineralogy and sulfur isotopic composition of the Middle Valley massive sulfide deposit, northern Juan de Fuca Ridge, *In* Mottl, M. J., Davis, E. E., Fisher, A. T., and Slack, J. F., eds., Proceedings of Ocean Drilling Program. Scientific Results, Ocean Drilling Program: College Station, Texas, p. 373-385.

Duffield, W., A, Bacon, C., R, and Delaney, P. T., 1986, Deformation of poorly consolidated sediment during shallow emplacement of a basalt sill, Coso Range, California: Bulletin of Volcanology, v. 48, p. 97-107.

Duhig, N. C., Stolz, J., Davidson, G. J., and Large, R. R., 1992, Cambrian microbial and silica gel textures in silica iron exhalites from the Mount Windsor volcanic belt, Australia: their petrography, chemistry and origin: Economic Geology, v. 87, p. 764-784.

Eastoe, C. J., 1994, Volcanogenic massive sulphide deposits and chemical events in the Phanerozoic oceans: 12th Australian Geological Convention, Perth, 1994, p. 94.

Eastoe, C. J., and Gustin, M. M., 1996, Volcanogenic massive sulfide deposits and anoxia in the Phanerozoic oceans: Ore Geology Reviews, v. 10, p. 179-197.

Eastoe, C. J., and Nelson, S. E., 1988, A Permian Kuroko-style hydrothermal system, Afterthought-Ignot area, Shasta County, California: Lateral and vertical sections, and geochemical evolution: Economic Geology, v. 83, p. 588-605.

Einsele, G., 1963, "Convolute bedding" und ähnliche Sedimentstrukturen im rheinischen Oberdevon und anderen Ablagerungen: Neues Jabrb. Geol. Palaentol. Abhandl, v. 116, p. 162-198.

Eldridge, C. S., Barton Jr, P. B., and Ohmoto, H., 1983, Mineral textures and their bearing on formation of the Kuroko orebodies, *In* Ohmoto, H., and Skinner, B. J., eds., The Kuroko and Related Volcanogenic Massive Sulfide Deposits, Economic Geology Monograph 5.

Eldridge, C. S., Compston, W., Willians, I. S., Both, R. A., Walshe, J. L., and Ohmoto, H., 1988, Sulfur isotope variability in sediment-hosted massive sulfide deposits as determined using the ion microprobe SHRIMP: I. An example from the Rammelsberg orebody: Economic Geology, v. 83, p. 443-449.

Embley, R. W., Jonasson, I. R., Perfit, M. R., Franklin, J. M., Malahoff, A., Smith, M. F., and Francis, J. G., 1988, Submersible investigation of an extinct hydrothermal system on the Galapagos Ridge: Sulfide mounds, stockwork zone, and differentiated lavas.: Canadian Mineralogist, v. 26, p. 517-539.

Faure, G., 1986, Principles of Isotope Geology: New York, John Wiley and Sons, 589 p.

Fifarek, R. H., 1997, Stable isotope geochemistry of the Red Ledge massive sulfide deposit, Idaho, USA: Evidence for equilibrium mixing of hydrothermal fluids and seawater in the vent and stockwork feeder zones.: SEG Field Conference 1997 - Neves Corvo, Lisbon, 1997, p. 50.

Fink, J. H., and Manley, C. R., 1987, Origin of pumiceous and glassy textures in rhyolite flows and domes, *In* Fink, J. H., ed., The Emplacement of Silicic Domes and Lava Flows, Geological Society of America Special Paper 212, p. 77 - 88.

Fisher, N. H., and Owen, H. B., 1952, Mount Chalmers copper and gold mine Queensland, Bureau of Mineral Resources, Geology and Geophysics.

Fisher, R. V., and Schmincke, H.-U., 1984, Pyroclastic Rocks: Berlin, Springer-Verlag, 472 p.

Fiske, R. S., Cashman, K. V., Shibata, A., and Watanabe, K., 1998, Tephra dispersal from Myojinsho, Japan, during its shallow submarine explosion: Bulletin of Volcanology, v. 59, p. 262-275.

Fletcher, R. J., 1975, Mount Chalmers gold-copper deposit, *In* Knight, C. L., ed., Economic Geology of Australia and Papua New Guinea., 1. Metals: Melbourne, Australasian Institute of Mining and Metallurgy, p. 786-787.

Foley, N. K., 1986, Fluid inclusion study of ores from the Fukazawa mine, Hokuroko District, Akita Prefecture, Japan: Mining Geology, v. 36, p. 11-20.

Fouquet, Y., Henry, K., Knott, R., and Cambon, P., 1998, Geochemical section of the TAG hydrothermal mound, *In* Herzig, P. M., Humphris, S. E., Miller, D. J., and Zierenberg, R. A., eds., Proceedings of the Ocean Drilling Program, Scientific Results, 158: College Station, Texas (Ocean Drilling Program).

Fouquet, Y., von Stackelberg, U., Charlou, J. L., Donval, J. P., Foucher, J. P., Erzinger, J., Herzig, P., Mühe, R., Wiedicke, M., Soaki, S., and Whitechurch, H., 1991, Hydrothermal activity in the Lau back-arc basin: Sulfides and water chemistry: Geology, v. 19, p. 303-306.

Fouquet, Y., von Stackelberg, U., Charlou, J. L., Erzingere, J., Herzig, P. M., Mühe, R., and Wiedicke, M., 1993, Metallogenesis in back-arc environments: The Lau basin example: Economic Geology, v. 88, p. 2154-2181.

Franklin, J. M., 1986, Volcanic-associated massive sulphide deposits—an update, *In* Andrew, C. J., Crowe, W. A., Finlay, S., Pennell, W. M., and Pyne, J. F., eds., Geology and Genesis of Mineral Deposits in Ireland: Dublin, Irish Association for Economic Geology, p. 49-69.

Franklin, J. M., 1996, Volcanic-associated massive sulphide base metals, *In* Eckstrand, O. R., Sinclair, W. D., and Thorpe, R. I., eds., Geology of Canadian Mineral Deposits, Geology of Canada, No. 8. Geological Society of America's Geology of North America, Geological Survey of Canada, p. 158-183.

Franklin, J. M., Lydon, J. W., and Sangster, D. F., 1981, Volcanic-associated massive sulfide deposits, *In* Skinner, B. J., ed., Seventy-fifth Anniversary Volume: El Paso, Texas, Economic Geology Publishing Company, p. 485-627.

Frey, R. W., and Pemberton, S. G., 1984, Trace fossil facies models, *In* Walker, R. G., ed., Facies Models, Geoscience Canada Reprint Series 1.

Furnes, H., Friedleifsson, I. B., and Atkins, F. B., 1980, Subglacial volcanics—on the formation of acid hyaloclastites: Journal of Volcanology and Geothermal Research, v. 8, p. 95-110.

Galley, A. G., Bailes, A. H., and Kitzler, G., 1993, Geological setting and hydrothermal evolution of the Chisel Lake and North Chisel Zn-Pb-Cu-Ag-Au massive sulfide deposits, Snow Lake, Manitoba: Exploration and Mining Geology, v. 2, p. 271-295.

Gamberi, F., Marani, M., and Savelli, C., 1997, Tectonic, volcanic and hydrothermal features of a submarine portion of the Aeolian arc (Tyrrhenian Sea): Marine Geology, v. 140, p. 167-181.

Gamo, T., Okamura, K., Charlou, J.-L., Urabe, T., Auzende, J.-M., Ishibashi, J., Shitashima, K., Chiba, H., and Ship Board Party of the ManusFlux Cruise., 1997, Acidic and sulfate-rich hydrothermal fluids from the Manus back-arc basin, Papua New Guinea: Geology, v. 25, p. 139-142.

Gemmell, J. B., 1996, Alteration and stringer zones associated with VHMS deposits, Ore Deposit Studies and Exploration Models: Volcanic-hosted Massive Sulphide Deposits, CODES Master of Economic Geology Course Work Manual 3 (4th Ed.): Hobart, CODES, University of Tasmania, p. 4.1-4.65.

Gemmell, J. B., and Large, R. R., 1992, Stringer system and alteration zones underlying the Hellyer Volcanic-hosted massive sulfide deposit, Tasmania, Australia: Economic Geology, v. 87, p. 620-649.

Gemmell, J. B., and Large, R. R., 1993, Evolution of a VHMS hydrothermal system, Hellyer deposit, Tasmania, Australia: Sulphur isotope evidence: Resource Geology, v. Special Issue 17, p. 108-119.

Gemmell, J. B., and Sharpe, R., 1998, Detailed sulfur-isotope investigation of the TAG hydrothermal mound and stockwork zone, 26°N, Mid-Atlantic Ridge, *In* Herzig, P. M., Humphris, S. E., Miller, D. J., and Zierenberg, R. A., eds., Proceedings of the Ocean Drilling Program, Scientific Results, 158: College Station, Texas, Ocean Drilling Program, p. 71-85.

Gerlach, T. M., 1989, Degassing of carbon dioxide from basaltic magma at spreading centres: II. Mid-oceanic ridge basalts: Journal of Volcanology and Geothermal Research, v. 39.

German, C. R., Briem, J., Chin, C., Danielsen, M., Holland, S., James, R., Jósdóttir, A., Ludford, E., Moser, C., Ólafsson, J., Palmer, M. R., and Rudnicki, M. D., 1994, Hydrothermal activity on the Reykjanes Ridge: the Steinahóll vent-field at 63°06'N: Earth and Planetary Science Letters, v. 121, p. 647-654.

Gifkins, C. C., McPhie, J., and Allen, R. L., 1996, Fiamme associated with silicic pumiceous lavas and intrusions: Supplement to EOS Transactions, v. 77(22), p. W125.

Gill, R., 1989, Chemical Fundamentals of Geology: London, Unwin Hyman, 291 p.

Goldfarb, M. S., Converse, D. R., Holland, H. D., and Edmond, J. M., 1983, The genesis of hot springs on the East Pacific Rise, 21°N, *In* Ohmoto, H., and Skinner, B. J., eds., The Kuroko and Related Volcanogenic Massive Sulfide Deposits, Economic Geology Monograph 5, p. 184-197.

Golding, S. D., McNaughton, N. J., Turner, J. V., Barley, M. E., Groves, D. I., Ho, S. E., and Rock, N. M. S., 1988, Fluid sources and circulation paths for Archaean gold deposits: constraints from carbon and oxygen isotope studies: Geological Society of America Abstracts, v. 22, p. 217-224.

Golubic, S., and Knoll, A. H., 1993, Prokaryotes, *In* Lipps, J. H., ed., Fossil Prokaryotes and Protists: Boston, Blackwell Scientific Publications, p. 51-77.

Goodfellow, W. D., 1987, Anoxic stratified oceans as source of sulphur in sediment-hosted stratiform Zn-Pb deposits (Selwyn Basin, Yukon, Canada): Chemical Geology (Isotope Geoscience Section), v. 65, p. 359-382.

Goodfellow, W. D., 1998, SEDEX Zn-Pb-Ag deposits of North America, Ore Deposit Studies and Exploration Models: Sediment-hosted Zn-Pb Deposits: North American SEDEX Deposits, Genetic Considerations, CODES Short Course Manual 3, CODES SRC. University of Tasmania, p. 1.1-1.50.

Goodfellow, W. D., Lydon, J. W., and Turner, R., 1993, Geology and genesis of stratiform sedimented-hosted (SEDEX) zinc-lead-silver sulphide deposits, *In* Kirkham, R. V., Sinclair, W. D., Thorpe, R. I., and Duke, J. M., eds., Ore Deposit Models, Special Paper 40, Geological Association of Canada, p. 201-251.

Goto, Y., and McPhie, J., 1996, A Miocene basanite peperitic dyke at Stanley, northwestern Tasmania, Australia: Journal of Volcanology and Geothermal Research, v. 74, p. 111-120.

Graf, J. L., 1977, Rare earth elements as hydrothermal tracers during the formation of massive sulfide deposits in volcanic rocks: Economic Geology, v. 72, p. 527-548.

Green, G. R., 1983, The Geological Setting and Formation of the Rosebery Volcanic-hosted Massive Sulfide Orebody, Tasmania: Unpub. PhD thesis, University of Tasmania, 288 p.

Green, G. R., Ohmoto, H., Date, J., and Takahashi, T., 1983, Whole-rock oxygen isotope distribution in the Fukazawa-Kosaka area, Hokuroku district, Japan, and its potential application to mineral exploration, *In* Ohmoto, H., and Skinner, B. J., eds., The Kuroko and Related Volcanogenic Massive Sulfide Deposits, Economic Geology Monograph 5, p. 395-411.

Green, G. R., Solomon, M., and Walshe, J. L., 1981, The formation of the Rosebery volcanic-hosted massive sulfide deposit at Rosebery, Tasmania: Economic Geology, v. 76, p. 304-338.

Gregory, P. W., and Robinson, B. W., 1984, Sulphur isotope studies of the Mt Molloy, Dianne and O. K. Stratiform sulphide deposits, Hodgkinson Province, north Queensland, Australia: Mineralium Deposita, v. 19, p. 36-43.

Gregory, R. T., and Taylor, H. P. J., 1981, An oxygen isotope profile in a section of Cretaceous crust, Samail ophiolite, Oman: Evidence for ^{18}O buffering of the oceans by deep (>5km) seawater-hydrothermal circulation at midocean ridges: Journal of Geophysical Research, v. 86, p. 2737-2755.

Guber, A. L., and Green, G. R., 1983, Aspects of the sedimentologic and structural development of the eastern Hokuroku district, Japan, *In* Ohmoto, H., and Skinner, B. J., eds., The Kuroko and Related Volcanogenic Massive Sulfide Deposits, Economic Geology Monograph 5, p. 71-95.

Guilbert, J. M., and Park, J. C. F., 1985, The Geology of Ore Deposits: New York, W. H. Freeman and Co.

Gustin, M. S., 1990, Stratigraphy and alteration of the host rocks, United Verde massive sulfide deposit, Jerome, Arizona: Economic Geology, v. 85, p. 29-49.

Haas, J. L., 1971, The effect of salinity on the maximum thermal gradient of a hydrothermal system at hydrostatic pressure: Economic Geology, v. 66, p. 940-946.

Halbach, P., Blum, N., Münch, U., Plüger, W., Garbe-Schönberg, D., and Zimmer, M., 1998, Formation and decay of a modern sulfide deposit in the Indian Ocean: Mineralium Deposita, v. 33, p. 302-309.

Hannington, M. D., Galley, A. G., Herzig, P. M., and Petersen, S., 1998, Comparison of the TAG mound and stockwork complex with Cyprus-type massive sulfide deposits, *In* Herzig, P. M., Humphris, S. E., Miller, D. J., and Zierenberg, R. A., eds., Proceedings of the Ocean Drilling Program, Scientific Results, 158: College Station, Texas, Ocean Drilling Program, p. 389-415.

Hannington, M. D., and Herzig, P. M., 1993, Shallow submarine hydrothermal systems in modern island arc settings: Geological Association of Canada Program with Abstracts, v. 18, p. A40.

Hannington, M. D., Herzig, P. M., and Scott, S. D., 1991, Auriferous hydrothermal precipitates on the modern seafloor, *In* Foster, R. P., ed., Gold Metallogeny and Exploration: Glasgow, Blackie and Son, p. 249-282.

Hannington, M. D., and Scott, S. D., 1988a, Mineralogy and geochemistry of a hydrothermal silica-sulfide-sulfate spire in the caldera of the Axial Seamount, Juan de Fuca Ridge: Canadian Mineralogist, v. 26, p. 603-625.

Hannington, M. D., Thompson, G., Rona, P. A., and Scott, S. D., 1988b, Gold and native copper in supergene sulphides from the Mid-Atlantic Ridge: Nature, v. 333, p. 64-66.

Hanson, R. E., 1991, Quenching and hyaloclastic disruption of andesitic to rhyolitic intrusions in a submarine island-arc sequence, northern Sierra Nevada, California: Geological Society of America Bulletin, v. 103, p. 804-816.

Hanson, R. E., and Schweickert, R. A., 1982, Chilling and brecciation of a Devonian rhyolite sill intruded into wet sediment, northern Sierra Nevada, California: Journal of Geology, v. 90, p. 717-724.

Hanson, R. E., and Wilson, T. J., 1993, Large-scale rhyolite peperites (Jurassic, southern Chile): Journal of Volcanology and Geothermal Research, v. 54, p. 247-264.

Hashiguichi, H., 1983, Penecontemporaneous deformation of Kuroko ore at the Kosaka Mine, Akita, Japan, *In* Ohmoto, H., and Skinner, B. J., eds., The Kuroko and Related Volcanogenic Massive Sulfide Deposits, Economic Geology Monograph 5, p. 167-183.

Hayakawa, N., Shimada, I., Shibata, T., and Suzuki, S., 1974, Geology of the Aizu metalliferous district, northeast Japan, *In* Ishihara, S., ed., Geology of Kuroko Deposits, Mining Geology Special Issue N° 6: Tokyo, The Society of Mining Geologists of Japan.

Haymon, R. M., Fornari, D. J., von Damm, K. L., Lilley, M. D., Edmond, J. M., Shanks, W. C., Lutz, R. A., Grebmeier, J. M., Carbotte, S., Wright, D., McLaughlin, E., Smith, M., Beedle, N., and Olson, E., 1993, Volcanic eruption of the mid-ocean ridge along the East Pacific Rise crest at 9 degrees 45-52'N; direct submersible observations of seafloor phenomena associated with an eruption event in April, 1991: Earth and Planetary Science Letters, v. 119, p. 85-101.

Hawkins, B. W., and Whitcher, I. G., 1962, Mount Morgan investigation. Report to Department of Mines, Queensland, for year ended 30th May, 1962. A to P 161/162M. Unpublished Company Report. Consolidatd Zinc Pty. Ltd. Exploration Division. Held by Queensland Department Mines as CR803.

Haymon, R. M., Koski, R. A., and Sinclair, C., 1984, Fossils of hydrothermal vent worms from Cretaceous sulfide ores of the Samail Ophiolite, Oman: Science, p. 1407-1409.

Heaton, T. H. E., and Sheppard, S. M. F., 1977, Hydrogen and oxygen isotope evidence for sea-water-hydrothermal alteration and ore deposition, Troodos Complex, Cyprus, Volcanic Processes in Ore Genesis, Special Publication N. 7, Geological Society of London, p. 42-57.

Hedenquist, J. W., 1992, Recognition of magmatic contributions to active and extinct hydrothermal systems, *In* Hedenquist, J. W., ed., Magmatic Contributions to Hydrothermal Systems and The Behaviour of Volatiles in Magma, Report No. 279, Geological Survey of Japan, p. 68-79.

Hedenquist, J., and Reid, F., 1985, Epithermal Gold: Sydney, The Earth Resources Foundation, University of Sydney, 318 p.

Heiken, G., Worhletz, K., and Eichelberger, J., 1989, Fracture fillings and intrusive pyroclasts, Inyo Domes, California.: Journal of Geophysical Research, v. 93, p. 45 - 4350.

Heinrich, C. A., Ryan, C. G., Mernagh, T. P., and Eadington, P. J., 1992, Segregation of ore metals between magmatic brine and vapor. A fluid inclusion study using PIXE microanalysis: Economic Geology, v. 87, p. 1566-1583.

Hekinian, R., and Fouquet, Y., 1985, Volcanism and metallogenesis of axial and off-axial structures on the East Pacific Rise: Economic Geology, v. 80, p. 221-249.

Hekinian, R., Francheteau, J., and Ballard, R. D., 1985, Morphology and evolution of hydrothermal deposits at the axis of the East Pacific Rise: Oceanology Acta, v. 8, p. 147-155.

Hemley, J. J., and Jones, W. R., 1964, Chemical aspects of hydrothermal alteration with emphasis on hydrogen metasomatism: Economic Geology, v. 59, p. 538-569.

Hemley, J. J., Montoya, J. W., Marinenko, J. W., and Luce, R. W., 1980, Equilibria in the system Al2O3-SiO2-H2O and some general implications for alteration/mineralization processes: Economic Geology, v. 75, p. 210-228.

Henley, R. W., and Thornley, P., 1979, Some geothermal aspects of polymetallic massive sulfide formation: Economic Geology, v. 74, p. 1600-1612.

Henderson, R. A., Fergusson, C. L., Leitch, E. C., Morand, V. J., Reinhard, J. J., and Carr, P. F., 1993, Tectonics of the northern New England Fold Belt, *In* Flood, P. G., and Aitchison, J. C eds., New England Orogen, Eastern Australia. Conference Papers. Dept. Geology and Geophysics, University Of Armidale, Australia. p. 505-515.

Herrington, R. J., and Little, C. T. S., 2000, Life in the dark: Geoscientist, v. 10, No.4, p. 4-5.

Herzig, P. M., Hannington, M. D., and Arribas Jr, A., 1998, Sulfur isotopic composition of hydrothermal precipitates from the Lau back-arc: implications for magmatic contributions to seafloor hydrothermal systems: Mineralium Deposita, v. 33, p. 226-237.

Herzig, P. M., Hannington, M. D., Fouquet, Y., von Stackelberg, U., and Petersen, S., 1993, Gold-rich polymetallic sulfides from the Lau back arc and implications for the geochemistry of gold in sea-floor hydrothermal systems of the southwest Pacific: Economic Geology, v. 88, p. 2182-2209.

Hessler, R. R., and Kaharl, V. A., 1995, The deep-sea hydrothermal vent community: an overview, *In* Humphris, S. E., Zierenberg, R. A., Mullineaux, L. S., and Thomson, R. E., eds., Seafloor Hydrothermal Systems: Physical, Chemical, Biological, and Geological Interactions, Geophysical Monograph 19: Washington, D. C, American Geophysical Union, p. 72-84.

Hill, P. A., 1996, Structure, Volcanic Setting, Hydrothermal Alteration and Genesis of the Thalanga Massive Sulphide Deposit: Unpub. PhD thesis, University of Tasmania, 404 p.

Hoffman, A., Gruszczynski, M., and Malkowski, K., 1991, On the interrelationship between temporal trends in $\delta^{13}C$ and $\delta^{18}O$, and $\delta^{34}S$ in the world ocean: Journal of Geology, v. 99, p. 355-370.

Holland, H. D., and Malinin, S. D., 1979, The solubility and occurrence of non-ore minerals, *In* Barnes, H. L., ed., Geochemistry of Hydrothermal Ore Deposits: New York, John Wiley & Sons, p. 461-508.

Horikoshi, E., and Sato, T., 1970, Volcanic activity and ore deposition in the Kosaka mine, *In* Tatsumi, T., ed., Volcanism and Ore Genesis: Tokyo, University of Tokyo Press, p. 181-195.

Hou, Z., and Mo, X., 1993, Geology, geochemistry and genetic aspects of kuroko-type volcanogenic massive sulfide deposits in Sanjiang region, southwestern China: Exploration and Mining Geology, v. 2, p. 17-29.

Hunns, S. R., 1994, Geology of the Mount Chalmers volcanic-hosted massive sulphide and implications for its formation, in Holcombe, R. J., Stephens, C. J., and Fielding, C. R., ed., 1994 Field Conference Guide Book Capricorn Region Central Coastal Queensland., Geological Society of Australia. Queensland Division, p. 80-92.

Hunns, S. R., and Kuronen, U., 1993, Exploration Permit 8640 - Berserker Project, Queensland: Annual Report for the Period Ending 5th March, 1993, Unpublished Company Report: Mining Project Investors Pty. Ltd, p. 13.

Hunns, S. R., Kuronen, U., and Taube, A., 1993, Volcano-sedimentary stratigraphy of the Mount Chalmers ore body: IAVCEI - Ancient Volcanism and Modern Analogues, Canberra, 1993, p. 51.

Hunns, S. R., and McPhie, J., 1999, Pumiceous peperite in a submarine volcanic succession at Mount Chalmers, Queensland, Australia: Journal of Volcanology and Geothermal Research, v. 88, p. 239-254.

Hunns, S. R., Zaw, K., Large, R. R., Dean, J. A., Ryan, C. G., and McPhie, J., 1994, Preliminary geochemical results constraining the formation of the Mount Chalmers volcanic-hosted massive sulfide deposit: New Developments in Geology and Metallogeny: Northern Tasman Orogenic Zone, Townsville, 1994, p. 117-124.

Hunns, S. R., and Zaw, K., 1997, Mount Chalmers - a shallow water exhalative VMS deposit: GAC/MAC Annual Meeting: Ottawa '97, Ottawa, 1997, p. 70.

Huston, D. L., 1997, Stable isotopes and their significance for understanding the genesis of volcanic-hosted massive sulfide deposits: a review, *In* Barrie, C. T., and Hannington, M. D., eds., Volcanic-Associated Massive Sulfide Deposits: Processes and Examples in Modern Ancient Settings, GAC-MDD-SEG, p. 157-181.

Huston, D. L., and Large, R. R., 1987, Genetic and exploration significance of the zinc ratio (100/Zn(Zn + Pb)) in massive sulfide systems: Economic Geology, v. 82, p. 1521-1539.

Huston, D. L., Sie, S. H., Suter, G. F., Cooke, D. R., and Both, R. A., 1995, Trace elements in sulfide minerals from eastern Australian volcanic-hosted massive sulfide deposits: Part I. Proton microprobe analyses of pyrite, chalcopyrite, and sphalerite, and Part II. Selenium levels in pyrite: Comparison with $\delta^{34}S$ values and implications for the source of sulfur in volcanogenic hydrothermal systems: Economic Geology, v. 90, p. 1167-1196.

Huston, D. L., Taylor, T., Fabray, J., and Patterson, D. J., 1992, A comparison of the geology and mineralization of the Balcooma and Dry River South volcanic-hosted massive sulfide deposits, northern Queensland: Economic Geology, v. 87, p. 785-811.

Hutchinson, R. W., 1973, Volcanogenic sulfide deposits and their metallogenic significance.: Economic Geology, v. 68, p. 1223-1246.

Hutchinson, R. W., 1980, Massive base metal sulphide deposits as guides to tectonic evolution, *In* Strangway, D. W., ed., Geological Association of Canada Special Paper 20, p. 659-684.

Iijima, A., 1974, Clay and zeolitic alteration zones surrounding Kuroko deposits in the Hokuroku district, northern Akita, as submarine hydrothermal-diagenetic alteration products, *In* Ishihara, S., ed., Geology of Kuroko Deposits, Mining Geology Special Issue, No. 6: Tokyo, The Society of Mining Geologists of Japan, p. 267-289.

Ishibashi, J., and Urabe, T., 1995, Hydrothermal activity related to arc-backarc magmatism in the western Pacific, *In* Taylor, B., ed., Tectonics and Magmatism: New York, Plenum Press, p. 451-495.

Ishihara, S., and Sasaki, A., 1978, Sulfur of Kuroko deposits—a deep seated origin?: Mining Geology, v. 28, p. 361-367.

Ishihara, S., and Terashima, S., 1974, Base metal content of the basement rocks of Kuroko deposits, *In* Ishihara, S., ed., Geology of Kuroko Deposits, Mining geology Special Issue, No. 6, The Society of Mining geologists of Japan, p. 421-428.

Ishikawa, Y., Sawaguchi, T., Iwaya, S., and Horiuchi, M., 1976, Delineation of prospecting targets for Kuroko deposits based on modes of volcanism of underlying dacite and alteration haloes: Mining Geology, v. 26, p. 105117.

Ishikawa, Y., and Yanagisawa, Y., 1974, Geology of the Ainai Mine, with special reference to syngenetic origin of the Daikoku deposits, *In* Ishihara, S., ed., Geology of Kuroko Deposits: Tokyo, The Society of Mining Geologists of Japan, p. 79-97.

Ito, T., Matsumoto, R., Kanao, K., and Sakuyama, M., 1984, Welding of acidic tuff and altered rhyolite fragments caused by the intrusion of magma examples in the Neogene Shirahama Group in the southern part of the Izu Peninsula, central Japan: Journal of the Geological Society of Japan, v. 90, p. 191-205.

Jack, R. L., and Etheridge, R. J., 1892, The geology and palaeontology of Queensland and New Guinea: Geological Survey of Queensland Publication, v. 92, 2 vols.

James, R. H., and Eldefield, H., 1996, Chemistry of ore-forming fluids and mineral formation rates in an active hydrothermal sulfide deposit on the Mid-Atlantic Ridge: Geology, v. 24, p. 1147-1150.

Jannasch, H. W., 1995, Microbial Interactions with hydrothermal fluids, *In* Humphris, S. E., Zierenberg, R. A., Mullineaux, L. S., and Thomson, R. E., eds., Seafloor Hydrothermal Systems: Physical, Chemical, Biological, and Geological Interactions, American Geophysical Union, p. 273-296.

Jean-Baptiste, P., Charlou, J. L., Stievenard, M., Donval, J. P., Bougault, H., and Mevel, C., 1991, Helium and methane measurements in hydrothermal fluids from the mid-Atlantic ridge: the Snake Pit site at 23° N: Earth and Planetary Science Letters, v. 106, p. 17-28.

Jean-Baptiste, P., Dapoigny, A., Stievenard, M., Charlou, J. L., Fouquet, Y., Donval, J. P., and Auzende, J. M., 1997, Helium and oxygen isotope analyses of hydrothermal fluids from the East Pacific Rise between 17°S and 19°S: Geo-Marine Letters, v. 17, p. 213-219.

Johnson, H. D., and Baldwin, C. T., 1986, Shallow siliclastic seas, *In* Reading, H. G., ed., Sedimentary Environments and Facies (2nd Edition): Oxford, Blackwell Scientific Publications, p. 229-282.

Johnson, H. D., and Baldwin, C. T., 1996, Shallow clastic seas, *In* Reading, H. G., ed., Sedimentary Environments; Processes, Facies and Stratigraphy (3rd Edition): Oxford, Blackwell Science, p. 232-280.

Jørgensen, B. B., 1977, Bacterial sulfate reduction within reduced microniches of oxidized marine sediments: Marine Biology, v. 41, p. 7-17.

Juniper, S. K., and Fouquet, Y., 1988, Filamentous iron-silica deposits from modern and ancient hydrothermal sites: Canadian Mineralogist, v. 26, p. 859-869.

Kajiwara, Y., 1970, Syngenetic features of the Kuroko ore from the Shakani Mine, *In* Tatsumi, T., ed., Volcanism and Ore Genesis: Tokyo, University of Tokyo Press, p. 197-206.

Kajiwara, Y., 1971, Sulfur isotope study of the Kuroko-ores of the Shakanai No. 1 deposits Akita Prefecture, Japan: Geochemical Journal, v. 4, p. 157-181.

Kano, K., 1989, Interactions between andesitic magma and poorly consolidated sediments: Examples in the Neogene Shirahama Group, south Izu, Japan: Journal of Volcanology and Geothermal Research, v. 37, p. 59-75.

Kano, K., Yamamoto, T., and Ono, K., 1996, Subaqueous eruption and emplacement of the Shinjima Pumice, Shinjima (Moeshima) Island, Kagoshima Bay, SW Japan: Journal of Volcanology and Geothermal Research, v. 71, p. 187-206.

Kato, I., Murio, I., Yamazaki, T., and Abe, M., 1971, Subaqueous pyroclastic flow deposits in the Upper Donzurubo Formation, Nijo-san district, Osaka, Japan: Journal of the Geological Society of Japan, v. 77, p. 193-206.

Kato, Y., 1987, Woody pumice generated with submarine eruption: Journal of the Geological Society of Japan, v. 93, p. 11-20.

Kerr, D. J., and Gibson, H. L., 1993, A comparison of the Horne volcanogenic massive sulfide deposit and intracauldron deposits of the Mine sequence, Noranda, Quebec: Economic Geology, v. 88, p. 1419-1442.

Kirkegaard, A. G., Shaw, R. D., and Murray, C. G., 1970, Geology of the Rockhampton and Port Clinton 1:250,000 sheet areas: Brisbane, Geological Survey of Queensland.

Kirkham, R. V., and Thurlow, J. G., 1987, Evaluation of a resurgent caldera and aspects of ore deposition and deformation at Buchans, *In* Kirkham, R. V., ed., Buchans Geology, Newfoundland, Geological Survey of Canada Paper 86-24, p. 177-194.

Klug, C., and Cashman, K. V., 1996, Permeability development in vesiculating magmas: implications for fragmentation.: Bulletin of Volcanology, v. 58, p. 87 - 100.

Knott, R., Fouquet, Y., Honnorez, J., Petersen, S., and Bohn, M., 1998, Petrology of hydrothermal mineralisation: a vertical section through the TAG mound, *In* Herzig, P. M., Humphris, S. E., Miller, D. J., and Zienenberg, R. A., eds., Proceedings of the Ocean Drilling Program, Scientific Results, 158: College Station, Texas, Ocean Drilling Program, p. 5-46.

Kokelaar, B. P., 1982, Fluidization of wet sediments during emplacement and cooling of various igneous bodies: Journal of the Geological Society of London, v. 139, p. 21-33.

Kolpack, R. L., 1965, Abyssal sand ripples in the Drake Passage, Antarctica: Special Publication Geological Society of America, v. 82, p. 112.

Kornhauser, K. O., and Ferris, F. G., 1996, Diversity of iron and silica precipitation by microbial mats in hydrothermal waters, Iceland: Implications for Precambrian iron formations: Geology, v. 24, p. 323-326.

Koski, R., A, Lonsdale, P. F., Shanks, W., C, Berndt, M., E, and Howe, S., S, 1985, Mineralogy and geochemistry of a sediment-hosted hydrothermal sulfide deposit from the southern trough of Guaymas Basin, Gulf of California: Journal of Geophysical Research, v. 90, p. 6695-6707.

Kouda, R., and Koide, H., 1978, Ring structures, resurgent cauldron and ore deposits in the Hokuroko volcanic field, northern Akita, Japan: Mining Geology, v. 28, p. 233-244.

Kowalik, J., Rye, R. O., and Sawkins, F. J., 1981, Stable-isotope study of the Buchans, Newfoundland, polymetallic sulphide deposits, *In* Swanson, E. A., Strong, D. F., and Thurlow, J. G., eds., The Buchans Orebodies: Fifty Years of Geology and Mining, Special Paper 22, Geological Association of Canada, p. 229-254.

Kranidiotis, P., and MacLean, W. H., 1987, Systematics of chlorite alteration at the Phelps Dodge massive sulfide deposit, Matagami, Quebec: Economic Geology, v. 82, p. 1898-1911.

Krasnov, S., Stepanova, T., and Stepanov, M., 1994, Chemical composition and formation of a massive sulfide deposit, Middle Valley, northern Juan de Fuca Ridge (Site 856), *In* Mottl, M. J., Davis, E. E., Fisher, A. T., and Slack, J. F., eds., Proceedings of the Ocean Drilling Program, Scientific Results, 139: College Station, Texas, Ocean Drilling Program, p. 353-372.

Krauskopf, K. B., 1979, Introduction to Geochemistry: New York, McGraw-Hill, 617 p.

Kulm, L. D., Suess, E., and Snavely, P. D., 1986, The role of carbonate chimneys in the fluid venting history of the accretio nary complex off Oregon: AGU 1986 Fall Meeting and ASLO Meeting., 1986, p. 1205.

Kurnosov, V., Murdmaa, I., Rosanova, T., Kashintzev, G., Eroshchev-Shak, V., and Krasnov, S., 1994, Mineralogy of hydrothermally altered sediments and igneous rocks at Sites 856-858, Middle Valley, Juan de Fuca Ridge, Leg 139, *In* Mottle, M. J., Davis, E. E., Fisher, A. T., and Slack, J. F., eds., Proceedings of the Ocean Drilling Program, Scientific Results, 139: College Station, Texas, Ocean Drilling Program.

Kurokawa, A., 1991, Formation of felsic pumiceous hyaloclastites: a case study from Tadami district, Fukushima Prefecture, Japan.: Journal of Mineralogy, Petrology and Economic Geology, v. 86, p. 439 - 458.

Kuznetov, A. P., Maslennikov, V. V., Zaikov, V. V., and Sobetski, V. A., 1988, Fossil fauna in the sulfide hydrothermal hills from the middle Devonian paleo-ocean of the Ural area: Proceedings of the Academy of Science, U.S.S.R, v. 303, p. 1477-1481.

Kuznetov, A. P., Maslennikov, V. V., Zaikov, V. V., and Zonenshin, L. P., 1991, Fossil hydrothermal vent fauna in Devonian sulfide deposits Uralian ophiolites: Deep Sea Newsletter, v. 19, p. 9-11.

Large, R. R., 1979, Mt. Chalmers Mine Geological and Assay Plans and Sections: Mt. Morgan, Queensland, Geopeko Limited.

Large, R. R., 1992, Australian volcanic-hosted massive sulfide deposits: features, styles and genetic models: Economic Geology, v. 87, p. 471-510.

Large, R. R., and Both, R. A., 1980, The volcanogenic ores at Mount Chalmers, eastern Queensland: Economic Geology, v. 75, p. 992-1009.

Large, R. R., Huston, D. L., McGoldrick, P. J., Ruxton, P. A., and McArthur, G., 1989, Gold distribution and genesis in Australian volcanogenic massive sulfide deposits and their significance for gold transport models, Monograph 6, Economic Geology, p. 520-535.

Large, R. R., McGoldrick, P. J., and Berry, R. F., 1988, A tightly folded, gold-rich, massive sulfide deposit: Que River Mine, Tasmania: Economic Geology, v. 83, p. 681-693.

Larocque, A. C. L., and Hodgson, C. J., 1993, Carbonate-rich footwall alteration at the Mobrun Mine, a possible Mattabi-type VMS deposit in the Noranda Camp: Exploration and Mining Geology, v. 2, p. 165-169.

Larson, P. B., 1984, Geochemistry of the alteration pipe at the Bruce Cu-Zn volcanogenic massive sulfide deposit, Arizona: Economic Geology, v. 79, p. 1880-1896.

Larson, P. B., and Zimmerman, B. S., 1991, Variations in $\delta^{18}O$ values, water/rock ratios, and water flux in the Rico paleothermal anomaly, Colorado, *In* Taylor, H. P. J., O'Neil, J. R., and Kaplan, I. R., eds., Stable Isotope Geochemistry: A Tribute to Samuel Epstein, Special Publication No. 3. Levinson, A. A: San Antonio, The Geochemical Society, p. 463-469.

Larson, P. B., Cunningham, C. G., and Naeser, C. W., 1994, Large-scale alteration effects in the Rico Paleothermal Anomaly, southwest Colorado: Economic Geology, v. 89, p. 1769-1779.

Lebedev, L. M., 1967, Metalloids in Endogenic Deposits: New York, Plenum Press.

Lee, M. S., Miyajima, T., and Mizumoto, H., 1974, Geology of the Kamikita Mine, Aomori Prefecture, with special reference to genesis of fragmental ores, *In* Ishihara, S., ed., Geology of Kuroko Deposits: Tokyo, The Society of Mining Geologists of Japan, p. 53-66.

Lees, T., Zaw, K., Large, R. R., and Huston, D. L., 1988, Economic geology of the Rosebery-Hercules area, western Tasmania, Ore Deposits of Western Tasmania. Excursion Guide, Ore Deposit Research Team, University of Tasmania.

Leggo, N. L., 1980, The Geology of the Mount Warminster Cu - Pb - Zn - Ag Deposit, East-Central Queensland: Unpub. B.Sc(Hons) thesis, University of Queensland, 157 p.

Leybourne, M. I., and Goodfellow, W. D., 1994, Mineralogy and mineral chemistry of hydrothermally altered sediment, Middle Valley, Juan de Fuca Ridge, *In* Mottl, M. J., Davis, E. E., Fisher, A. T., and Slack, J. F., eds., Proceedings of the Ocean Drilling Programme, Scientific Results, 139: College Station, Texas, Ocean Drilling Program, p. 155-289.

Liaghat, S., and MacLean, H., 1995, Lithogeochemistry of altered rocks at the New Insco VMS deposit, Noranda, Quebec: Journal of Geochemical Exploration, v. 52, p. 333-350.

Lindberg, P. A., 1985, A volcanogenic interpretation for massive sulfide origin, West Shasta district, California: Economic Geology, v. 80, p. 2240-2254.

Little, C. T. S., Herrington, R. J., Haymon, R. M., and Danelian, T., 1999, Early Jurassic hydrothermal vent community from the Franciscan Complex, San Rafael Mountains, California: Geology, v. 27, p. 167-170.

Little, C. T. S., Herrington, R. J., Maslennikov, V. V., Morris, N. J., and Zaykov, V. V., 1997, Silurian hydrothermal-vent community from the southern Urals, Russia: Nature, v. 385, p. 146-148.

Little, C. T. S., Herrington, R. J., Maslennikov, V. V., and Zaykov, V. V., 1998, The fossil record of hydrothermal vent communities, *In* Mills, R. A., and Harrison, K., eds., Modern Ocean Floor Processes and the Geological Record, Special Publications 148: London, Geological Society, p. 259-270.

Lofgren, G., 1971a, Spherulitic textures in glassy and crystalline rocks: Journal of Geophysical Research, v. 76, p. 5635-5648.

Lofgren, G., 1971b, Experimentally produced devitrification textures in natural rhyolite: Geological Society of America Bulletin, v. 82.

Lowell, R. P., Rona, P. A., and Von Herzen, R. P., 1995, Seafloor hydrothermal systems: Journal of Geophysical Research, v. 100, No. B1, p. 327-352.

Lucchi, F. R., 1995, Sedimentographica. Photographic Atlas of Sedimentary Structures: New York, Columbia University Press, 255 p.

Lydon, J. W., 1984, Volcanogenic massive sulphide deposits Part 1: A descriptive model: Geoscience Canada, v. 11, p. 195-202.

Lydon, J. W., 1988, Volcanogenic massive sulphide deposits. Part 2: Genetic Models: Geoscience Canada, v. 15, p. 43-65.

MacLean, W. H., and Kranidiotis, P., 1987, Immobile elements as monitors of mass transfer in hydrothermal alteration: Phelps Dodge Massive sulfide deposit, Matagami, Quebec: Economic Geology, v. 82, p. 951-962.

MacRae, J. M., 1950, The isotope chemistry of carbonates and a paleotemperature scale: Journal Chemical Physics, v. 18, p. 849-857.

Magenheim, A. J., and Gieskes, J. M., 1994, Evidence for hydrothermal fluid flow through surficial sediments, Escanaba Trough, *In* Morton, J. L., Zierenberg, R. A., and Reiss, C. A., eds., Geologic, Hydrothermal, and Biologic Studies at Escanaba Trough, Gorda Ridge, Offshore Northern California, U. S. Geological Survey Bulletin 2022, p. 241-256.

Malahoff, A., Embley, R. W., Cronan, D. S., and Skirrow, R., 1983, The geological setting and chemistry of hydrothermal sulfides and associated deposits from the Galapagos Rift at 86°W: Marine Mining, v. 4, p. 123-137.

Maliva, R. G., and Siever, R., 1989, Influences of dolomite precipitation on quartz surface textures: Journal of Sedimentary Petrology, v. 60, p. 820-826.

Manley, C. R., 1992, Extended cooling and viscous flow of large, hot rhyolite lavas: Implications of numerical modelling results: Journal of Volcanology and Geothermal Research, v. 53, p. 27-46.

Hannington, M. D., Galley, A. G., Herzig, P. M., and Petersen, S., 1998, Comparison of the TAG mound and stockwork complex with Cyprus-type massive sulfide deposits, *In* Herzig, P. M., Humphris, S. E., Miller, D. J., and Zierenberg, R. A., eds., Proceedings of the Ocean Drilling Program, Scientific Results, 158, p. 389-415.

Marumo, K., 1989, Genesis of kaolin minerals and prophyllite in Kuroko deposits of Japan: Implications for the origins of hydrothermal fluids from mineralogical and stable isotope data: Geochimica et Cosmochimica Acta, v. 53, p. 2915-2924.

Matsuhisa, Y., Goldsmith, J. R., and Clayton, R. N., 1979, Oxygen isotope fractionation in the system quartz-albite-anorthite-water: Geochimica et Cosmochimica Acta, v. 43, p. 1131-1140.

Matsuhisa, Y., Morishita, Y., and Sato, T., 1985, Oxygen and carbon isotope variations in gold-bearing hydrothermal veins in the Kushikino mining area, southern Kyushu, Japan: Economic Geology, v. 80, p. 283-293.

Matsukuma, T., 1974, Geology of the Kuroko-style deposits of the Tsuchihata Mine, Iwate Prefecture, *In* Ishihara, S., ed., Geology of Kuroko Deposits, Mining Geology Special Issue, N° 6: Tokyo, Society of Mining Geologists of Japan, p. 169-181.

Matsukuma, T., and Horikoshi, E., 1970, Kuroko deposits in Japan, a review, *In* Tatsumi, T., ed., Volcanism and Ore Genesis: Tokyo, University of Tokyo Press, p. 153-179.

Matthews, A., Goldsmith, J. R., and Clayton, R. N., 1983, On the mechanisms and kinetics of oxygen isotope exchange in quartz and feldspars at elevated temperatures and pressures: Geological Society of America Bulletin, v. 94, p. 396-412.

McArthur, G. J., and V, D. E., 1990, Que River and Hellyer zinc-lead deposits, *In* Hughes, F. E., ed., Mineral Deposits of Australia and Papua and New Guinea, Monograph 15, Australasian Institute of Mining and Metallurgy, p. 1331-1339.

McBirney, A. R., 1963, Factors governing the nature of submarine volcanism: Bulletin of Volcanology, v. 26, p. 455-469.
McGoldrick, P. J., and Large, R. R., 1992, Geologic and geochemical controls on gold-rich stringer mineralization in the Que River deposit, Tasmania: Economic Geology, v. 87, p. 667-685.
McKee, E. D., 1966, Significance of climbing-ripple structures: U.S. Geological Survey Professional Papers, v. 550-d, p. D94-D103.
McKellar, R. G., 1969, Permian pelmatozoan echinoderms from Nerimbera, near Rockhampton, Queensland. Geological Survey of Queensland Publication, v. 337, p. 19-28.
McKellar, R. G., Dear, J. F., and Fleming, P. J. G., 1970, Devonian, Carboniferous and Permian fossils from the Rockhmapton 1:250 000 Sheet area, *In* Kirkegaard, A. G., Shaw, R. D., and Murray, C. G., Geology of the Rockhampton and Port Clinton 1:250 000 Sheet aareas. Geolgical Survey of Queensland, Report 38, p. 138-155.
McLeod, R. L., 1987, Alteration associated with volcanogenic sulphide ores at Mount Chalmers, Queensland, Australia: Transactions of the Institute of Mining and Metallurgy (Sect. B: Applied Earth Sciences), v. 96, p. B117-B127.
McMurty, G. M., Sedwick, P. N., Fryer, P., Von der Haar, D. L., and Yeh, H.-W., 1993, Unusual geochemistry of hydrothermal vents on submarine arc volcanoes: Kasuga Seamounts, Northern Mariana Arc.: Earth and Planetary Science Letters, v. 114, p. 517-528.
McPhie, J., 1993, The Tennant Creek porphyry revisited: a synsedimentary sill with peperite margins, Early Proterozoic, Northern Territory: Australian Journal of Earth Science, v. 40, p. 545-558.
McPhie, J., Doyle, M., and Allen, R. L., 1993, Volcanic Textures: A Guide to the Interpretation of Textures in Volcanic Rocks: Hobart, CODES Key Centre, University of Tasmania, 196 p.
McPhie, J., and Hunns, S. R., 1995, Secondary welding of submarine, pumice-lithic breccia at Mount Chalmers, Queensland, Australia: Bulletin of Volcanology, v. 57, p. 170-178.
McPhie, J., and Goto, Y., 1996, Lobe and layered structure in dacite sills of the Archaean Strelley succession, Western Australia: Supplement to EOS, American Geophysical Union, Wester Pacific Geophysics Meeting, p. 77 (22) W125.
Miller, J., 1988, Cathodluminescence microscopy, *In* Tucker, M., ed., Techniques in Sedimentology: Oxford, Blackwell Scientific Publications, p. 174-190.
Minniti, M., and Bonavia, F. F., 1984, Copper-ore grade hydrothermal mineralization discovered in a seamount in the Tyrrhenian Sea (Mediterranean): is the mineralization related to porphyry-copper or to base metal lodes?: Marine Geology, v. 59, p. 271-282.
Moore, D. G., 1962, Bearing strength and other physical properties of some shallow and deep-sea sediments from the north Pacific: Geological Society of America Bulletin, v. 73, p. 1163-1166.
Moore, D. W., Young, L. E., Modene, S., and Plahuta, J. T., 1986, Geologic setting of the Red Dog zinc-lead-silver deposit, Western Brooks Range, Alaska: Economic Geology, v. 81, p. 1696-1727.
Morton, R. L., Walker, J. S., Hudak, G. J., and Franklin, J. M., 1991, The early development of an Archean submarine caldera complex with emphasis on the Mattabi Ash-Flow Tuff and its complex relationship to the Mattabi massive sulfide deposit: Economic Geology, v. 86, p. 1002-1011.
Motegi, M., 1974, Kuroko deposits of the Kurosawa Mine, Fukushima Prefecture, *In* Ishihara, S., ed., Geology of the Kuroko Deposits, Mining Geology Special Issue, N° 6: Tokyo, Society of Mining Geologists of Japan, p. 203-207.
Mottl, M. J., and Holland, H. D., 1978, Chemical exchange during hydrothermal alteration of basalt by seawater. I. Experimental results for major and minor components of seawater: Geochimica et Cosmochimica Acta, v. 42.
Mottl, M. J., and Seyfried, W. E., 1980, Sub-seafloor hydrothermal systems - rock - vs. seawater-dominated, *In* Rona, P. A., and Lowell, R. P., eds., Seafloor Spreading Centers: Hydrothermal Systems: Stroudsberg, Pa, Dowden, Hutchinson and Ross.
Muehlenbachs, K., 1986, Alteration of the oceanic crust and the ^{18}O history of seawater, *In* Valley, J. W., Taylor, H. P. J., and O'Neil, J. R., eds., Stable Isotopes in High Temperature Geological Processes, 16: Washington D. C, Mineralogical Society of America, p. 425-444.
Mungall, J. E., Bagdassarov, N. S., Romamo, C., and Dingwell, D. B., 1996, Numerical modelling of stress generation and microfracturing of vesicle walls in glassy rocks: Bulletin of Volcanology and Geothermal Research, v. 73, p. 33-46.
Munha, J., Barriga, J. A. S., and Kerrich, R., 1986, High ^{18}O ore-forming fluids in volcanic-hosted base metal massive sulfide deposits: Geologic, $^{18}O/^{16}O$, and D/H from the Iberian Pyrite Belt; Crandon, Wisconsin; and Blue Hill, Maine: Economic Geology, v. 81, p. 530-552.
Murray, C. G., 1975, Rockhampton, Queensland – 1:250 000 Geological Series. Bureau fo Mineral Resources, Geology and Geophysics,Australia, Explanatory Notes SF/56-13, 43 p.

Mutti, E., Remacha, E., Tinterri, R., Mavilla, N., Angella, S., and Fava, L., 1999, An introduction to the analysis of ancient turbidite basins from an outcrop perspective, PESBG - Turbidite Training Course: London, p. 45.

Nakada, S., 1992, Lava domes and pyroclastic flows of the 1991 - 1992 eruption at Unzen Volcano, *In* Yanagi, T., Okada, H., and Ohta, K., eds., Unzen Volcano, The 1990-1992 Eruption, Nishinippon and Kyushu University Press, p. 56-66.

Natland, J. H., and Hekinan, R., 1982, Hydrothermal alteration of basalts and sediments at Deep Sea Drilling Project Site 456, Mariana Trough, Initial Reports, Deep Sea Drilling Project, Leg 60: Washington D.C, U. S. Government Printing Office, p. 759-768.

Newberry, R. J., Crawford, T. C., Newkirk, S. R., Young, L. E., W, N. S., and Duke, N. A., 1997, Volcanogenic massive sulfide deposits of Alaska, 9, Society of Economic Geologists, p. 120-150.

O'Neil, J. R., and Taylor, H. P. J., 1967, The oxygen isotope and cation exchange chemistry of feldspars: American Mineralogist, v. 52, p. 1414-1437.

Ohmoto, H., 1972, Systematics of sulfur and carbon isotopes in hydrothermal ore deposits: Economic Geology, v. 67, p. 551-578.

Ohmoto, H., 1983, Geologic setting of the Kuroko deposits, Japan: Part I. Geologic history of the Green Tuff region, *In* Ohmoto, H., and Skinner, B. J., eds., The Kuroko and Related Volcanogenic Massive Sulfide Deposits, Economic Geology Monograph 5, p. 9-24.

Ohmoto, H., 1986, Stable isotope geochemistry of ore deposits, *In* Valley, J. W., Taylor, H. P. J., and O'Neil, J. R., eds., Stable Isotopes in High Temperature Geological Processes, 16. Reviews in Mineralogy, Mineralogical Society of America, p. 491-560.

Ohmoto, H., Kaiser, C. J., and Geer, K. A., 1990, Systematics of sulphur isotopes in recent marine sediments and ancient sediment-hosted basemetal deposits, *In* Herbert, H. K., and Ho, S. E., eds., Stable Isotopes and Fluid Processes in Mineralization, 23: Perth, The University of Western Australia, p. 70-120.

Ohmoto, H., and Goldhaber, M. B., 1997, Sulfur and carbon isotopes, *In* Barnes, H. L., ed., Geochemistry of Hydrothermal Ore Deposits: New York, John Wiley & Sons, Inc., p. 517-611.

Ohmoto, H., and Lasaga, A. C., 1982, Kinetics of reactions between aqueous sulfates and sulfides in hydrothermal systems: Geochimica et Cosmochimica Acta, v. 46, p. 1727-1745.

Ohmoto, H., Mizukami, M., Drummond, S. E., Eldridge, C. S., Pisutha-Arnond, V., and Lenagh, T. C., 1983, Chemical processes of Kuroko formation, *In* Ohmoto, H., and Skinner, B. J., eds., The Kuroko and Related Volcanogenic Massive Sulfide Deposits, Economic Geology Monograph 5, p. 570-604.

Ohmoto, H., and Rye, R. O., 1974, Hydrogen and oxygen isotopic compositions of fluid inclusions in the Kuroko deposits, Japan: Economic Geology, v. 69, p. 947-953.

Ohmoto, H., and Rye, R. O., 1979, Isotopes of sulfur and carbon, *In* Barnes, H., L, ed., Geochemistry of Hydrothermal Ore Deposits: New York, John Wiley & Sons, p. 509-567.

Ohmoto, H., and Takahashi, T., 1983, Geologic setting of the Kuroko deposits, Japan: Part III. Submarine calderas and Kuroko genesis, *In* Ohmoto, H., and Skinner, B. J., eds., The Kuroko and Related Volcanogenic Massive Sulfide Deposits, Economic Geology Monograph 5, p. 39-54.

Okill, R., 1974, Distribution and genesis of the Mt. Chalmers Cu-Au mineralization. South-east Queensland: Carpentaria Exploration Company.

Orth, K., and Hill, A. P., 1994, Textures and origins of carbonate associated with the Rosebery VHMS deposit: Contentious Issues in Tasmanian Geology, Hobart, 1994, p. 105.

Oshima, T., Hashimoto, T., Kamono, H., Kawabe, S., Suga, K., Tanimura, S., and Ishikawa, Y., 1974, Geology of the Kosaka Mine, Akita Prefecture, *In* Ishihara, S., ed., Geology of the Kuroko Deposits, Mining Geology Special Issue, N° 6: Tokyo, Society of Mining Geologists of Japan, p. 89-100.

Oudin, E., and Constantinou, G., 1984, Black smoker chimney fragments in Cyprus sulphide ore deposits: Nature, v. 308, p. 349-353.

Paradis, S., Taylor, B. E., Watkinson, D. H., and Jonasson, I. R., 1993, Oxygen isotope zonation and alteration in the northern Noranda district, Quebec: Evidence for hydrothermal fluid flow: Economic Geology, v. 88, p. 1512-1525.

Pecover, R. S., Buchanan, D. J., and Ashby, D. E., 1973, Fuel-coolant interaction in submarine volcanism: Nature, v. 245, p. 307-308.

Peltz, S., and Kafri, U., 1992, Neogene pyroclastics containing peperites in the Zalmon Valley, central Galilee, Israel: Israeli Journal of Earth Science, v. 41, p. 45-49.

Pemberton, S. G., and Frey, R. W., 1982, Trace fossil nomenclature and the Planolites—Palaeophycus dilemma: Journal of Paleontology, v. 56, p. 843-881.

Peter, J. M., 1986, Genesis of Hydrothermal Vent Deposits in the Southern Trough of the Guaymas Basin, Gulf of California: A Mineralogical and Chemical Study: Unpub. M.Sc thesis, University of Toronto.

Peter, J. M., and Scott, S. D., 1988, Mineralogy, composition, and fluid-inclusion microthermometry of seafloor hydrothermal deposits in the southern trough of Guaymas Basin, Gulf of California: Canadian Mineralogist, v. 26, p. 567-587.

Peter, J. M., and Scott, S. D., 1991, Hydrothermal mineralization in the Guaymas Basin, Gulf of California, *In* Dauphin, J. P., and Simoneit, B. R. T., eds., The Gulf and Peninsular Province of the Californias, 47, American Association of Petroleum Geologists, p. 721-741.

Phillips, W. R., 1981, Optical Mineralogy: The Nonopaque Minerals: San Francisco, W. H. Freeman and Co., 677 p.

Pichler, T., and Dix, G. R., 1996, Hydrothermal venting within a coral reef ecosystem, Ambitle Island, Papua New Guinea: Geology, v. 24, p. 435-438.

Pickering, K. T., Hiscott, R. N., and Hein, F. J., 1989, Deep Marine Environments: London, Unwin Hyman Ltd, 416 p.

Pierson, B. J., 1981, The control of cathodluminscence in dolomite by iron and manganese: Sedimentology, v. 28.

Pisutha-Arnond, V., and Ohmoto, H., 1983, Thermal history and chemical and isotopic compositions of the ore-forming fluids responsible for the Kuroko massive sulfide deposits in the Hokuroku District of Japan, *In* Ohmoto, H., and Skinner, B. J., eds., The Kuroko and Related Volcanogenic Massive Sulfide Deposits, Economic Geology Monograph No. 5, p. 523-558.

Price, P., and Bancroft, W., 1948, Waite-Amulet Mine, Structural Geology of Canadian Ore Deposits: Montreal, Canadian Institute of Mining and Metallurgy, p. 748-754.

Purser, B. H., Tucker, M. E., and Zenger, D. H., 1994, Problems, progress and future research concerning dolomites and dolomitization, *In* Purser, B. H., Tucker, M. E., and Zenger, D. H., eds., Dolomites. A Volume in Honour of Dolomieu, Special Publication No. 21 of the International Association of Sedimentologists: Oxford, Blackwell Scientific Publications, p. 3-20.

Rao, C. P., 1996, Modern Carbonates: Tropical, Temperate, Polar. Introduction to Sedimentology and Geochemistry: Hobart, Carbonates, 206 p.

Rao, C. P., and Adabi, M. H., 1992, Carbonate minerals, major and minor elements and oxygen and carbon isotopes and their variation with water depth in cool, temperate carbonates, western Tasmania, Australia: Marine Geology, v. 103, p. 249-273.

Rawlings, D. J., 1993, Mafic peperite from the Gold Creek Volcanics in the Middle Proterozoic McArthur Basin, Northern Territory: Australian Journal of Earth Science, v. 40, p. 109-113.

Reed, M. H., 1997, Hydrothermal alteration and its relationship to ore fluid composition, *In* Barnes, H. L., ed., Geochemistry of Hydrothermal Ore Deposits: New York, John Wiley and Sons, p. 303-365.

Reid, J. H., and Morton, C. C., 1928, Central Queensland geological section: Queensland Government Mining Journal, v. 29, p. 384-389.

Reid, J. H., 1930, The Queensland Upper Palaeozoic succession: Geological Survey of Queensland Publication, v. 28.

Reid, J. H., 1935, Kuala Lumpur mine, Geological Survey of Queensland, unpublished file report.

Reid, J. H., 1936, Operations in the New Zealand Gully: Queensland Government Mining Journal, v. 37, p. 197.

Reid, J. H., 1938a, Report on the Golden Crest, New Zealand Gully. Geological Survey of Queensland unpublished file report: .

Reid, J. H., 1938b, Mount Chalmers ore reserves.: Queensland Government Mining Journal, v. 39, p. 224-225.

Reineck, H.-E., and Singh, I. B., 1980, Depositional Sedimentary Environments. With Reference to Terrigenous Clastics: Berlin, Springer-Verlag, 543 p.

Reyes, A. G., 1990, Petrology of Philippine geothermal systems and the application of alteration mineralogy to their assessment: Journal of Volcanology and Geothermal Research, v. 43, p. 279-309.

Reynolds, M. S. A., and Best, J. G., 1976, Summary of the 1953-57 eruption of Tuluman volcano, Papua New Guinea, *In* Johnson, R. W., ed., Volcanism in Australasia: Amsterdam, Elsevier, p. 287-296.

Rhoads, D. C., 1975, The paleoecological and environmental significance of trace fossils, *In* Frey, R. W., ed., The Study of Race Fossils: A Synthesis of Principles, Problems and Procedures in Ichnology: Berlin, Springer Verlag, p. 147-160.

Rimstidt, J. D., 1997, Gangue mineral transport and deposition, *In* Barnes, H. L., ed., Geochemistry of Hydrothermal Ore Deposits: New York, John Wiley and Sons, Inc, p. 487-515.

Ripley, E. M., and Ohmoto, H., 1977, Mineralogic, sulfur isotope, and fluid inclusion studies of the stratabound copper deposits at the Raul Mine, Peru: Economic Geology, v. 72, p. 1017-1041.

Robertson, A. H. F., 1976, Origins of ochres and umbers: evidence from Skouriotissa, Troodos Massif, Cyprus: Transactions of the Institute of Mining and Metallurgy (Section B, Applied Earth Science), v. 85, p. 245-251.

Roedder, E., 1984, Fluid Inclusions, 644 p.

Rollinson, H. R., 1993, Using Geochemical Data: Evaluation, Presentation, Interpretation: London, Longman, 352 p.

Rona, P. A., 1988, Hydrothermal mineralization at oceanic ridges: The Canadian Mineralogist, v. 26, p. 431-466.

Rubin, J. N., Henry, C. D., and Price, J. G., 1993, The mobility of zirconium and other "immobile" elements during hydrothermal alteration: Chemical Geology, v. 110, p. 29-47.

Runnegar, B., 1979, Ecology of Eurydesma and the Eurydesma fauna, Permian of eastern Australia: Alcheringa, v. 3, p. 261-285.

Runnegar, B., and Campbell, K. S. W., 1976, Late Palaeozoic faunas of Australia: Earth Science Reviews, v. 12, p. 235-257.

Ryan, C. G., Cousens, D. R., Heinrich, C. A., Griffins, W. L., Sie, S. H., and Mernagh, T. P., 1991, Quantitative PIXE microanalysis of fluid inclusions based on a layered yield model: Nuclear Instruments and Methods in Physics Research, v. B54, p. 292-297.

Ryan, C. G., Heinrich, C. A., and Mernagh, T. P., 1993a, PIXE microanalysis of fluid inclusions and its application to study ore metals in segregation between magmatic brine and vapour: Nuclear Instruments and Methods in Physics Research, v. B77, p. 463-471.

Ryan, C. G., Heinrich, C. A., Griffins, W. L., Mernagh, T. P., Ballhaus, V., and Van Achterberg, E., 1994a, PIXE analysis of fluid inclusions. Microprobing ore forming fluids: 12th Australian Geological Convention, Perth, p. 389-390.

Ryan, C. G., Heinrich, C. A., Griffins, W. L., Mernagh, T. P., Ballhaus, V., Van Achterberg, E., and Churms, C. L., 1993b, Quantitative microanalysis of fluid inclusions in minerals using the proton microprobe: International Conference of Applied Mineralogy, Perth, p. 1-4.

Ryan, C. G., Heinrich, C. A., Griffins, W. L., Mernagh, T. P., Ballhaus, V., Van Achterberg, E., and Churms, C. L., 1994b, Microanalysis of ore-forming fluids using the scanning proton microprobe: 4th International Conference on Nuclear Microprobe Technology and Applications, Shanghai, 1994b.

Rye, R. O., and Ohmoto, H., 1974, Sulfur and carbon isotopes and ore genesis: a review: Economic Geology, v. 69, p. 826-842.

Rye, R. O., and O'Neil, J. R., 1968, The O18 content of water in primary fluid inclusions from Providencia, north-central Mexico: Economic Geology, v. 63, p. 232-238.

Rye, R. O., Roberts, R. J., Snyder, W. S., Lahusen, G. L., and Motica, J. E., 1974, Textural and stable isotope studies of the Big Mike cupriferous volcanogenic massive sulfide deposit, Pershing County, Nevada: Economic Geology, v. 79, p. 124-140.

Rye, D. M., and Williams, N., 1981, Studies of the base metal sulfide deposits at McArthur River, Northern Territory, Australia: III. The stable isotope geochemistry of the H.Y.C., Ridge and Colley deposits: Economic Geology, v. 76, p. 1-26.

Sagalevich, A. M., Torokhov, P. V., Matveyenkov, V. V., Galkin, S. V., and Moskalev, L. I., 1992, Hydrothermal manifestations at Piyp submarine volcano, Bering Sea: International Geology Reviews, v. 34, p. 1200-1209.

Sainty, R. A., 1992, Shallow-water stratigraphy at the Mount Chalmers volcanic-hosted massive sulfide deposit, Queensland, Australia: Economic Geology, v. 87, p. 812-824.

Sakai, H., 1968, Isotopic properties of sulfur compounds in hydrothermal processes: Geochemical Journal, v. 2, p. 29-49.

Sakai, H., Osaki, S., and Tsukagishi, M., 1970, Sulfur and oxygen isotopic geochemistry of sulfate in the black ore deposits of Japan: Geochemical Journal, v. 4, p. 27-39.

Sakai, H., Des Marias, D. J., Ueda, A., and Moore, J. G., 1984, Concentrations and isotope ratios of carbon, nitrogen and sulfur in ocean-floor basalts: Geochimica et Cosmochimica Acta, v. 48, p. 2433-2441.

Sanders, I. S., and Johnston, J. D., 1989, The Torridonian Stac Fada Member: an extrusion of fluidised peperite?: Transaction of the Royal Society of Edinburgh: Earth Sciences, v. 80, p. 1-4.

Sangster, D. F., 1968, Relative sulphur isotope abundances of ancient seas and strata-bound sulphide deposits: The Geological Association of Canada, Proceedings, v. 19.

Sangster, D. F., 1971, Sulphur isotopes, stratabound sulphide deposits, and ancient seas, *In* Takéuchi, Y., ed., International Association of the Genesis of Ore Deposits., Special Issue No. 3, Society of Mining Geologists of Japan, p. 295-299.

Sangster, D. F., 1976, Sulfur and lead isotopes in strata-bound deposits, *In* Wolf, K. H., ed., Handbook of Stratabound and Strataform Deposits, 2: Amsterdam, Elsevier Publishing Co., p. 219-226.

Sangster, D., F, and Scott, S. D., 1976, Precambrian stratabound massive Cu-Zn-Pb sulfide ores of North America, *In* Wolf, K. H., ed., Handbook of Strata-bound and Stratiform Ore Deposits: Amsterdam, Elsevier, p. 129-222.

Sasaki, A., 1974, Isotopic data of Kuroko deposits, *In* Ishihara, S., ed., Geology of Kuroko Deposits, Mining Geology Special Issue, No. 6: Tokyo, The Society of Mining Geologists of Japan, p. 389-397.

Sasaki, A., and Kajiwara, Y., 1971, Evidence of isotopic exchange between seawater sulfate and some syngenetic sulfide ores, *In* Takéuchi, Y., ed., International Association of the Genesis of Ore Deposits., Special Issue No. 3, Society of Mining Geologists of Japan, p. 289-294.

Sato, T., 1974, Distribution and geological setting of the Kuroko deposits, *In* Ishihara, S., ed., Geology of the Kuroko Deposits, Mining Geology Special Issue, N° 6: Tokyo, Society of Mining Geologists of Japan, p. 1-11.

Sato, N., and Kusaka, H., 1974, Geology of the Matsuki Mine, Ohdate City, Akita Prefecture, *In* Ishihara, S., ed., Geology of the Kuroko Deposits, Mining Geology Special Issue, N° 6: Tokyo, Society of Mining Geologists of Japan, p. 141-146.

Sawkins, F. J., 1976, Massive sulphide deposits in relation to geotectonics: Geological Association of Canada Special Paper 14, p. 221-240.

Sawkins, F. J., and Kowalik, J., 1981, The source of ore metals at Buchans: magmatic versus leaching models., *In* Swanson, E. A., Strong, D. F., and Thurlow, J., G, eds., The Buchans Orebodies: Fifty Years of Geology and Mining, Special Paper 22, Geological Association of Canada.

Scott, J., 1948, Quemont Mine, Structural geology of Canadian Ore Deposits: Montreal, Canadian Institute of Mining and Metallurgy, p. 773-776.

Scrope, G. P., 1825, Considerations on volcanoes: London, W. Phillips and G. Yard, 270 p.

Sedwick, P. N., McMurty, G. M., Hilton, D. R., and Goff, F., 1994, Carbon dioxide and helium in hydrothermal fluids from Loihi Seamount, Hawaii, USA: Temporal variability and implications for the release of mantle volatiles: Geochimica et Cosmochimica Acta, v. 58, p. 1219-1227.

Sedwick, P. N., McMurty, G. M., and MacDougall, J. D., 1992, Chemistry of hydrothermal solutions from Pele's Vents, Loihi seamount, Hawaii: Geochimica et Cosmochimica Acta, v. 56, p. 3643-3667.

Sedwick, P., and Stüben, 1996, Chemistry of shallow submarine warm springs in an arc-volcanic setting: Vulcano Island, Aeolian Archipelago, Italy: Marine Chemistry, v. 53, p. 147-161.

Sheppard, S. M. F., 1977, Identification of the origin of ore-forming solutions by the use of stable isotopes, Volcanic Processes in Ore Genesis, Special Publication No. 7, Geological Society of London, p. 25-41.

Sheppard, S. M. F., Nielsen, R. L., and Taylor, H. P. J., 1971, Hydrogen and oxygen isotope ratios in minerals from porphyry copper deposits: Economic Geology, v. 66, p. 515-542.

Shimazaki, Y., 1974, Ore minerals of the Kuroko-type deposits, *In* Ishihara, S., ed., Geology of Kuroko Deposits, Mining Geology Special Issue, N°6: Tokyo, The Society of Mining Geologists of Japan, p. 311-322.

Shirozu, H., 1974, Clay minerals in altered wall rocks of the Kuroko-type deposits, *In* Ishihara, S., ed., Geology of Kuroko Deposits, Mining Geology Special Issue, No. 6: Tokyo, The Society of Mining Geologists of Japan, p. 303-310.

Sibley, D. F., 1982, The origin of common dolomite fabrics: clues form the Pliocene: Journal of Sedimentary Petrology, v. 52, p. 1087-1100.

Sillitoe, R. H., Hannington, M. D., and Thompson, J. F. H., 1996, High sulfidation deposits in the volcanogenic massive sulfide environment: Economic Geology, v. 91, p. 204-212.

Solomon, M., 1976, "Volcanic" massive sulphide deposits and their host rocks - a review and an explanation, *In* Wolf, K. H., ed., Handbook of Strata-bound and Stratiform Ore Deposits: II: Regional Studies and Specific Deposits: Amsterdam, Elsevier, p. 1307-1328.

Solomon, M., 1981, An introduction to the geology and metallic mineral resources of Tasmania: Economic Geology, v. 76, p. 194-208.

Solomon, M., Eastoe, C. J., Walshe, J. L., and Green, G. R., 1988, Mineral deposits and sulfur isotope abundances in the Mount Read Volcanics between Que River and Mount Darwin, Tasmania: Economic Geology, v. 83, p. 1307-1328.

South, B. C., and Taylor, B. E., 1985, Stable isotope geochemistry and metal zonation at the Iron Mountain mine, West Shasta District, California: Economic Geology, v. 80, p. 2177-2195.

Spooner, E. T. C., and Fyfe, W. C., 1973, Subsea floor metamorphism, heat and mass transfer: Contributions to Mineralogy and Petrology, v. 42, p. 287-304.

Spooner, E. T. C., Beckinsdale, R. D., England, P. C., and Senior, A., 1977, Hydration, ^{18}O enrichment and oxidation during ocean floor hydrothermal, metamorphism of ophiolite metabasic rocks from E. Liguria, Italy: Geochimica et Cosmochimica Acta, v. 41, p. 857-871.

Stanton, R. L., 1985, Stratiform ores and geological processes: Royal Society of New South Wales, v. 118, p. 77-100.

Stanton, R. L., 1990, Magmatic evolution and the ore type-lava type affiliations of volcanic exhalative ores, Monograph 15, Australasian Institute of Mining and Metallurgy, p. 101-107.
Stanton, R. L., 1994, Ore Elements in Arc Lavas: Oxford, Oxford Science Publications, 391 p.
Stolz, J., and Large, R. R., 1992, Evaluation of the source-rock control on precious metal grades in volcanic-hosted massive sulfide deposits from western Tasmania: Economic Geology, v. 87, p. 720-738.
Stow, D. A. V., Reading, H. G., and Collinson, J. D., 1996, Deep seas, *In* Reading, H. G., ed., Sedimentary Environments: Processes, Facies and Stratigraphy: Oxford, Blackwell Science, p. 395-453.
Stüben, D., Sedwick, P., and Colantoni, P., 1996, Geochemistry of submarine warm springs in the limestone cavern of Grotta Azzurra, Capo Palinuro, Italy: evidence for mixing-zone dolomitisation: Chemical Geology, v. 131, p. 113-125.
Sudarikov, S. M., and Galkin, S. V., 1995, Geochemistry of the Snake Pit vent filed and its implications for vent and non-vent fauna, *In* Parson, L. M., Walker, C. L., and Dixon, D. R., eds., Hydrothermal Vents and Processes, Special Publications 87: London, Geological Society, p. 319-327.
Takakashi, T., and Suga, K., 1974, Geology of the ore deposits of the Hanaoka Kuroko belt, Akita Prefecture, *In* Ishihara, S., ed., Geology of Kuroko Deposits: Tokyo, Society of Mining Geologists of Japan, p. 101-112.
Tanaka, T., Kuroda, H., and Kusaka, H., 1974, Geology of the Furotobe Mine, Akita Prefecture, *In* Ishihara, S., ed., Geology of Kuroko Deposits, Mining Geology Special Issue N° 6: Tokyo, The Society of Mining Geologists of Japan.
Taube, A., 1986, The Mount Morgan gold-copper mine and environment, Queensland: A volcanogenic massive sulfide deposit associated with penecontemporaneous faulting: Economic Geology, v. 81, p. 1322-1340.
Taube, A., 1987, Report on Drilling Investigation of MLA 1106, Rockhampton - New Zealand Gully, 1987, Nobelex Limited, p. 13.
Taube, A., 1990, Mount Chalmers gold-copper deposit, *In* Hughes, F. E., ed., Mineral Deposits of Australia and Papua and New Guinea, Monograph 15, Australasian Institute of Mining and Metallurgy, p. 1493-1497.
Taube, A., and van der Helder, P., 1983, The Mount Chalmers mine and environment - a Kuroko style volcanogenic sulphide environment, Permian Geology of Queensland: Brisbane, Geological Society of Australia, Queensland Division, p. 387-399.
Taylor, A. M., and Goldring, R., 1993, Description and analysis of bioturbation and ichnofabric: Journal of the Geological Society of London, v. 150, p. 141-148.
Taylor, B. E., 1987, Stable isotope geochemistry of ore-forming fluids, *In* Kyser, T. K., ed., Stable Isotope Geochemistry of Low Temperature Processes, 13: Toronto, Mineralogical Association of Canada, p. 337-418.
Taylor, B. E., and South, B. C., 1985, Regional stable isotope systematics of hydrothermal alteration and massive sulfide deposition in the West Shasta District, California: Economic Geology, v. 80, p. 2149-2163.
Taylor, G. F., and Thornber, M. R., 1992, Gossan and ironstone surveys, *In* Butt, C. R. M., and Zeegers, H., eds., Handbook of Exploration Geochemistry: Regolith Exploration Geochemistry in Tropical and Subtropical Terrains, 4, Elsevier, p. 139-188.
Taylor, H. P. J., 1974, The application of oxygen and hydrogen isotope studies to problems of hydrothermal alteration and ore deposition: Economic Geology, v. 69, p. 843-883.
Taylor, H. P. J., 1977, Water/rock interactions and the origin of H_2O in granitic batholiths: Journal of Geological Society of London, v. 133, p. 509-558.
Taylor, H. P. J., 1979, Oxygen and hydrogen isotope relationships in hydrothermal mineral deposits, *In* Barnes, H. L., ed., Geochemistry of Hydrothermal Ore Deposits: New York, John Wiley & Sons, p. 236-277.
Taylor, H. P. J., 1997, Oxygen and hydrogen isotope relationships in hydrothermal mineral deposits, *In* Barnes, H. L., ed., Geochemistry of Hydrothermal Ore Deposits: New York, John Wiley and Sons Inc, p. 229-302.
Taylor, H. P. J., and Sheppard, S. M. F., 1986, Igneous rocks: I. Processes of isotopic fractionation and isotope systematics, *In* Valley, J. W., Taylor, H. P. J., and O'Neil, J. R., eds., Stable Isotopes in High Temperature Geological Processes, 16. Reviews in Mineralogy, Mineralogical Society of America, p. 227-272.
Thode, H. G., and Monster, J., 1965, Sulfur-isotope geochemistry of petroleum, evaporites and ancient seas: American Association of Petroleum Geologists Memoir, v. 4, p. 367-377.
Thode, H. G., and Monster, J., 1967, The sulfur isotope abundances in evaporites and in the ancient oceans, *In* Vinogradov, A. P., ed., Chemistry of the Earth's Crust: Proceedings of the Geochemical Conference Commemorating the Centenary of Academician V. I. Vernadskii's Birth: Jerusalem, Israel Program for Scientific Translations, p. 630-641.

Thompson, G., Humphris, S. E., Schroeder, B., Sulanowska, M., and Rona, P. A., 1988, Active vents and massive sulfides at 26°N (TAG) and 23°N (Snakepit) on the Mid-Atlantic Ridge: Canadian Mineralogist, v. 26, p. 697-711.

Thomsen, E., and Vorren, T. O., 1984, Pyritization of tubes and burrows from Late Pleistocene continental shelf sediments off Norway: Sedimentology, v. 31, p. 481-492.

Thornber, M. R., and Taylor, G. F., 1992, The mechanisms of sulphide oxidation and gossan formation, *In* Butt, C. R. M., and Zeegers, H., eds., Handbook of Exploration geochemistry: Regolith Exploration Geochemistry in Tropical and Subtropical Terrains, 4: Amsterdam, Elsevier, p. 119-137.

Thurlow, J. G., 1977, Occurrence, origin and significance of mechanically transported sulphide ores at Buchans, Newfoundland, Volcanic Processes in Ore Genesis: Proceedings of a Joint Meeting of the Volcanic Studies Group of the Geological Society of London and the Institution of Mining and Metallurgy held in London on 21 and 22 January, 1976, Geological Society of London Special Publication No. 7, p. 127.

Thurlow, J. G., 1988, Geology of the Buchans orebodies — a 1988 summary, *In* Swinden, H. S., and Kean, B. F., eds., The Volcanogenic Sulphide Districts of Central Newfoundland. A Guidebook and Reference Manual for Volcanogenic Sulphide Deposits in the Early Paleozoic Oceanic Volcanic Terranes of Central Newfoundland, Geological Association of Canada - Mineral Deposits Division, p. 111-116.

Till, R., 1984, Statistical Methods for the Earth Scientist. An Introduction: London, Macmillan, 154 p.

Tiwary, A., and Deb, M., 1997, Geochemistry of hydrothermal alteration at the Deri massive sulphide deposit, Sirohi district, Rajasthan, NW India: Journal of Geochemical Exploration, v. 59, p. 99-121.

Tufar, W., 1991, Paragenesis of complex massive ores from the Tyrrhenian Sea: Mitteilungen der Österreichischen Geologischen Gesellschaft, v. 84, p. 265-300.

Ueda, A., and Sakai, H., 1984, Sulfur isotope study of Quaternary volcanic rocks from the Japanese Islands Arc: Geochimica et Cosmochimica Acta, v. 48, p. 1837-1848.

Urabe, T., 1987, Kuroko deposit modelling based on magmatic hydrothermal theory: Mining Geology, v. 37, p. 159-176.

Urabe, T., and Marumo, K., 1991, A new model for Kuroko-type deposits of Japan: Episodes, v. 14, p. 246-251.

Urabe, T., and Sato, T., 1978, Kuroko deposits of the Kosaka Mine, northeast Honshu, Japan—Products of submarine hot springs on Miocene sea floor: Economic Geology, v. 73, p. 161-179.

Urabe, T., Scott, S. D., and Hattori, K., 1983, A comparison of footwall-rock alteration and geothermal systems beneath some Japanese and Canadian volcanogenic massive sulfide deposits, *In* Ohmoto, H., and Skinner, B. J., eds., The Kuroko and Related Volcanogenic Massive Sulfide Deposits, Economic Geology Monograph No. 5, p. 345-364.

Utada, M., Minato, H., Ishikawa, T., and Yoshizaki, Y., 1974, The alteration zones surrounding Kuroko-type deposits in Nishi-Aizu District, Fukushima Prefecture, with emphasis on the analcime zone as an indicator in exploration for ore deposits, *In* Ishihara, S., ed., Geology of Kuroko Deposits, Mining Geology Special Issue, No. 6: Tokyo, The Society of Mining Geologists of Japan, p. 291-302.

Veizer, J., Fritz, P., and Jones, B., 1986, Geochemistry of brachiopods: Oxygen and carbon isotopic records of Paleozoic oceans: Geochimica et Cosmochimica Acta, v. 50, p. 1679-1696.

Velasco, F., Sáncheez-España, J., Boyce, A. J., Fallick, A. E., Sáez, R., and Almodóvar, G. R., 1998, A new sulphur isotopic study of some Iberian Pyrite Belt deposits: evidence of a textural control on sulphur isotope composition: Mineralium Deposita, v. 34, p. 4-18.

von Bitter, P. H., Scott, S. D., and Schenk, P. E., 1990, Early Carboniferous low-temperature hydrothermal vent communities from Newfoundland: Nature, v. 344, p. 145-147.

Von Damm, K. L., 1995, Controls on the chemistry and temporal variability of seafloor hydrothermal fluids, *In* Humphris, S. E., Zierenberg, R. A., Mullineaux, L. S., and Thomson, R. E., eds., Seafloor Hydrothermal Systems: Physical, Chemical, Biological, and Geological Interactions, Geophysical Monograph 91: Washington DC, American Geophysical Union, p. 222-247.

Von Damm, K. L., Edmond, J. M., Grant, B., Measures, C. I., Walden, B., and Weiss, R. F., 1985a, Chemistry of submarine hydrothermal solutions at 21°N, East Pacific Rise: Geochimica et Cosmochimica Acta, v. 49, p. 2197-2220.

Von Damm, K. L., Edmond, J. M., Grant, B., and Measures, C. I., 1985b, Chemistry of hydrothermal solutions at Guaymas Basin, Gulf of California: Geochimica et Cosmochimica Acta, v. 49, p. 2221-2237.

Walker, R. G., and Plint, A. G., 1992, Wave- and storm-dominated shallow marine systems, *In* Walker, R. G., and James, N. P., eds., Facies Models; Response to Sea Level Change: St. Johns, Canada, Geological Association of Canada, p. 219-238.

Walter, M. R., Bauld, J., and Brock, T. D., 1972, Siliceous algal and bacterial stromatolites in hot spring and geyser effluents of Yellowstone National Park: Science, v. 178, p. 402-405.

Westrich, H. R., Stockman, H. W., and Taylor, B. E., 1985, Volatile content of Obsidian Dome and the Inyo Dike (abstract): EOS (American Geophysical Union Transactions, v. 66, p. 387.
White, M. J., 1996, Stratigraphy, Volcanology and Sedimentology of the Cambrian Tyndall Group, Mount Read Volcanics, Western Tasmania: Unpub. PhD thesis, University of Tasmania.
Whitehouse, F. W., 1928, Central Queensland geology: Queensland Government Mining Journal, v. 29, p. 441-442.
Whitman, A. G., and Sparks, R. S. J., 1986, Pumice: Bulletin of Volcanology, v. 48, p. 209 - 223.
Williams, H., and McBirney, A. R., 1979, Volcanology: San Francisco, Freeman, Cooper and Co, 397 p.
Willmot, W. F., O'Flynn, M. L., and Trezise, D. L., 1984, Rockhampton Region 1: 100 000 Geological Map Sheet 99051 and Part Sheet 8951: Brisbane, Department of Mines, Queensland.
Willmott, W. F., O'Flynn, M. L., and Tresize, D. L., 1986, Rockhampton Region, 1:100 000 Geological Map Commentary: Brisbane, Department of Mines, Queensland Geological survey, 43 p.
Winkler, H. G. F., 1976, Petrogenesis of Metamorphic Rocks: New York, Springer International Student Edition, 334 p.
Winn, C. D., Karl, D. M., and Massoth, G. J., 1986, Microorganisms in deep-sea hydrothermal plumes: Nature, v. 320, p. 744-746.
Wirsen, C. O., Jannasch, H. W., and Molyneaux, S. J., 1993, Chemosynthetic microbial activity at Mid-Atlantic Ridge hydrothermal sites: Journal of Geophysical Research, v. 98, p. 9696-9703.
Wood, D. A., Gibson, I. L., and Thompson, R. N., 1976, Elemental mobility during zeolite facies metamorphism of the Tertiary basalts of eastern Iceland: Contributions to Mineralogy and Petrology, v. 55, p. 241-254.
Wood, S. A., and Williams-Jones, A. E., 1994, The aqueous geochemistry of the rare-earth elements and yttrium 4. Monzanite solubility and REE mobility in exhalative massive sulfide-depositing environments: Chemical Geology, v. 115, p. 47-60.
Wunderlich, F., 1967, Die Entstehung von "convolute bedding" an Platenrändern.: Senckenbergiana Lethaea, v. 48, p. 345-349.
Yamada, E., 1984, Subaqueous pyroclastic flows: their development and their deposits, *In* Kokelaar, B. P., and Howells, M. F., eds., Marginal Basin Geology: Volcanic and associated sedimentary and tectonic processes in modern and ancient marginal basins: Oxford, The Geological Society, p. 29-35.
Yamagishi, H., 1987, Studies on the Neogene subaqueous lavas and hyaloclastites in Southwest Hokkaido: Geological Survey of Hokkaido, v. Report 59, p. 55-101.
Yamazaki, T., Kato, I., Muroi, I., and Abe, M., 1974, Textural analysis and flow mechanism of the Donzurubo subaqueous pyroclastic flow deposits: Bulletin Volcanologique, v. 37, p. 231-244.
Yang, K., and Mo, X., 1993, Characteristics of the Laochang volcanogenic massive sulfide deposit, southwestern Yunnan, China: Exploration and Mining Geology, v. 2, p. 31-40.
Zaikov, V. V., Shadlun, T. N., Maslennikov, V. V., and Bortnikov, N. S., 1995, Yaman-Kasy sulfide lode as an ancient black smoker of the Urals paleocean: Geology of Ore Deposits, v. 36, p. 446-463.
Zaw, K., 1991, The Effect of Devonian Metamorphism and Metasomatism on the Mineralogy and Geochemistry of the Cambrian VMS Deposits in the Rosebery-Hercules District, Western Tasmania: Unpub. PhD thesis, University of Tasmania, 302 p.
Zaw, K., and Cooke, D. R., 1995, Fluid Inclusions, Exploration Geochemistry and Hydrothermal Geochemistry, Master of Economic Geology Course Manual 12: Part 2: Hobart, CODES SRC University of Tasmania, p. 161-225.
Zaw, K., Gemmell, J. B., Hunns, S. R., Mernagh, T. P., Ryan, C. G., Large, R. R., and Both, R. A., 1995, Composition of fluid inclusions from the Hellyer and Mt. Chalmers VHMS deposits, Australia: implications for ore-forming fluids: PACRIM '95, 1995, p. 663-668.
Zaw, K., Gemmell, J. B., Large, R. R., Mernagh, T. P., and Ryan, C. G., 1994, Evolution of VHMS fluids in the footwall stringer zone, Hellyer deposit, western Tasmania: Constraints from fluid inclusion microthermometry and geochemistry: 12th Australian Geological Convention, Perth, Australia, 1994, p. 482.
Zaw, K., Gemmell, J. B., Large, R. R., Mernagh, T. P., and Ryan, C. G., 1996, Evolution and source of ore fluids in the stringer zone system, Hellyer VHMS deposit, Tasmania, evidence from fluid inclusion microthermometry and geochemistry: Ore Geology Reviews, v. 10, p. 251-278.
Zaw, K., Huston, D. L., and Large, R. R., 1988, Ore Metal Distribution, Zonation and Structural Relationships at Rosebery, Western Tasmania (Final Report), Electrolytic Zinc Company of Australasia, p. 26.
Zaw, K., and Large, R. R., 1992, The precious metal-rich South Hercules mineralization, western Tasmania: A possible subsea-floor replacement volcanic-hosted massive sulfide deposit: Economic Geology, v. 87, p. 931-952.

Zeigler, A. M., Hulver, M. L., and Rowley, D. B., 1996, Permian world topography and climate, *In* Marini, I. P., ed., Late Glacial and Postglacial Environmental Changes—Quaternary, Carboniferous-Permian and Proterozoic: New York, Oxford University Press.

Zheng, Y.-F., and Hoefs, J., 1993, Carbon and oxygen isotopic covariations in hydrothermal calcites. Theoretical modelling on mixing processes and applications to Pb-Zn deposits in the Harz Mountains, Germany: Mineralium Deposita, v. 28, p. 79-89.

Zierenberg, R. A., and Shanks III, W. C., 1994, Sediment alteration associated with massive sulfide formation in Escanaba Trough, Gorda Ridge: The importance of seawater mixing and magnesium metasomatism, *In* Morton, J. L., Zierenberg, R. A., and Reiss, C. A., eds., Geologic, Hydrothermal, and Biologic Studies at Escanaba Trough, Gorda Ridge, Offshore California, US Geological Survey Bulletin, 2022, p. 257-278.

Appendix A

ELSEVIER

Journal of Volcanology and Geothermal Research 88 (1999) 239–254

Journal of volcanology and geothermal research

Pumiceous peperite in a submarine volcanic succession at Mount Chalmers, Queensland, Australia

Steven R. Hunns, Jocelyn McPhie *

Centre for Ore Deposit Research, University of Tasmania, GPO Box 252-79, Hobart 7001, Tasmania, Australia

Received 10 July 1998; accepted 6 January 1999

Abstract

Pumiceous peperite comprising irregularly shaped apophyses of feldspar-phyric rhyolitic tube pumice and siltstone occurs within well-bedded volcaniclastic sandstone and siltstone facies of the Early Permian Berserker beds at Mount Chalmers, Australia. The tube pumice structure is preserved where sericite or silica have replaced the glass of vesicle walls and vesicles have been infilled by silica. In some instances, the peperite occurs gradationally above or below intervals of coherent feldspar-phyric rhyolite that are also predominantly pumiceous. The siltstone in the pumiceous peperite is texturally homogeneous, locally vesicular and contains shards and crystals derived from disintegration of the pumiceous rhyolite. Pumiceous rhyolite and peperite occur at various positions in the stratigraphy and may represent interconnected intrusive digits or lobes. Intrusion of the lobes was accommodated by expansion of the pore water and possible fluidisation of the host sediment, resulting in local destruction of bedding. The lobes developed chilled margins at contacts with wet sediment and inflated in response to vesiculation and the supply of new magma. Cooling of the lobes was possibly accompanied by development of microfractures in the glassy vesicle walls. Rupture of the chilled margin and propagation of fractures into the interior could have temporarily and locally depressurised the lobes, resulting in failure, disintegration and mixing with the adjacent wet and/or steam-rich sediment. Hot pumiceous rhyolite in lobe interiors may have interacted directly with the wet sediment and been dismembered by quench fragmentation and/or steam explosions. Bubbles of magmatic gas and/or steam were trapped in the sediment that mixed with the pumiceous rhyolite. The development of pumiceous texture in the sills was favoured by emplacement beneath a thin cover of wet sediment in a relatively shallow, submarine shelf setting in which the confining pressure was sufficiently low to permit vesiculation. This setting was also important in limiting the extent of degassing of the pumiceous rhyolite during cooling.

Keywords: Pumiceous peperite; Wet sediment; Vesicle; Submarine volcanic succession; Berserker beds

1. Introduction

Peperite is formed when hot magma or lava comes into contact with wet unconsolidated sediments and the two components are dynamically mixed. The most common circumstances for peperite formation occur at the contacts between an intrusion or lava and sediment. Peperite may involve a wide range of sediment types and the full spectrum of magma compositions, and forms in diverse settings (e.g., Brooks et al., 1982; Hanson and Schweickert, 1982; Kokelaar, 1982; Busby-Spera and White, 1987; Kano, 1989; Sanders and Johnston, 1989; Hanson, 1991;

* Corresponding author. Tel.: +61-3-6226-2476; Fax: +61-3-6226-7662; E-mail: j.mcphie@utas.edu.au

0377-0273/99/$ - see front matter
PII: S0377-0273(99)00015-3

Peltz and Kafri, 1992; Boulter, 1993; Hanson and Wilson, 1993; McPhie, 1993; Rawlings, 1993; Brooks, 1995; Goto and McPhie, 1996).

The igneous component of peperite is commonly nonvesicular to poorly vesicular and may be totally glassy or almost entirely crystalline. Here we report an example of peperite composed predominantly of formerly glassy, rhyolitic tube pumice. The peperite is associated with sills that are also substantially pumiceous. This example is unusual because the host sediment is vesicular.

The internal textures and facies relationships of the pumiceous peperite and host sediment are described and used to constrain a genetic model. The peperite developed at the margins of rhyolitic intrusions emplaced into a relatively shallow submarine, mixed volcanic and sedimentary succession. Intrusion evidently took place beneath a thin cover of wet sediment that did not impede vesiculation of the rhyolite and that trapped bubbles of steam and/or magmatic volatiles generated during mixing. Such a setting could also have been important in the development of microfractures in vesicle walls (cf. Mungall et al., 1996) that facilitated disintegration of the intrusions and mixing with adjacent wet sediment.

2. Geological setting

Pumiceous peperite occurs within the Early Permian Berserker beds in the Mount Chalmers district, northeastern Australia. The Berserker beds occupy an elongate (~110 km long), northwest-trending, 5–15 km wide, fault-bounded block (Fig. 1), and amount to approximately 3000 m in thickness (Kirkegaard et al., 1970). Mid to Late Permian regional deformation produced open, upright, NNW-trending folds. Dips of bedding rarely exceed 40° and a weak, vertical, N to NNW-trending cleavage is locally present (McPhie and Hunns, 1995). The succession is unmetamorphosed although hydrothermal alteration is locally intense.

The Berserker beds comprise a mixture of sedimentary and volcanic facies associations. In the Mount Chalmers district where the pumiceous peperite occurs, the volcanic facies association is dominant and represented by rhyolitic and andesitic

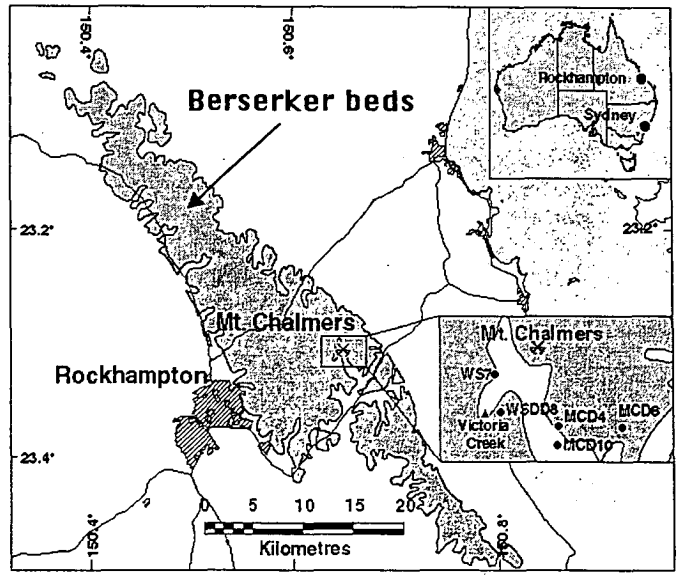

Fig. 1. Setting of the Early Permian Berserker beds in central Queensland and locations of drill holes that intersected pumiceous sills and pumiceous peperite in the Mount Chalmers district. Pumiceous peperite is exposed in outcrop in Victoria Creek. Modified from Willmott et al. (1984).

lavas, autoclastic breccia, rhyolite–mudstone peperite, very thick, graded beds of rhyolitic pumice-lithic breccia and late-stage rhyolitic and andesitic intrusions (sills and dykes) (Fig. 2). None of the components in the volcaniclastic facies are still glassy although relic volcanic textures are well preserved. Originally glassy components are now composed of quartzo-feldspathic or phyllosilicate assemblages. The sedimentary facies association consists of thinly to thickly bedded, volcanolithic, graded and massive sandstone, and laminated to thinly bedded mudstone. Slightly reworked and in situ mollusc, brachiopod and bryozoan body fossils typical of submarine shelf environments occur at several localities, and many intervals of both sandstone and mudstone contain trace fossils characteristic of the ichnofacies *Cruziana* (Sainty, 1992).

Pumiceous peperite was initially recognised in diamond drill core from the Mount Chalmers massive sulfide mine and also at other widely scattered locations (Fig. 1). The peperite is exposed in only two outcrops, on the eastern bench of the Mount Chalmers mine and in Victoria Creek (Fig. 1). Because outcrop is very limited, the descriptions pre-

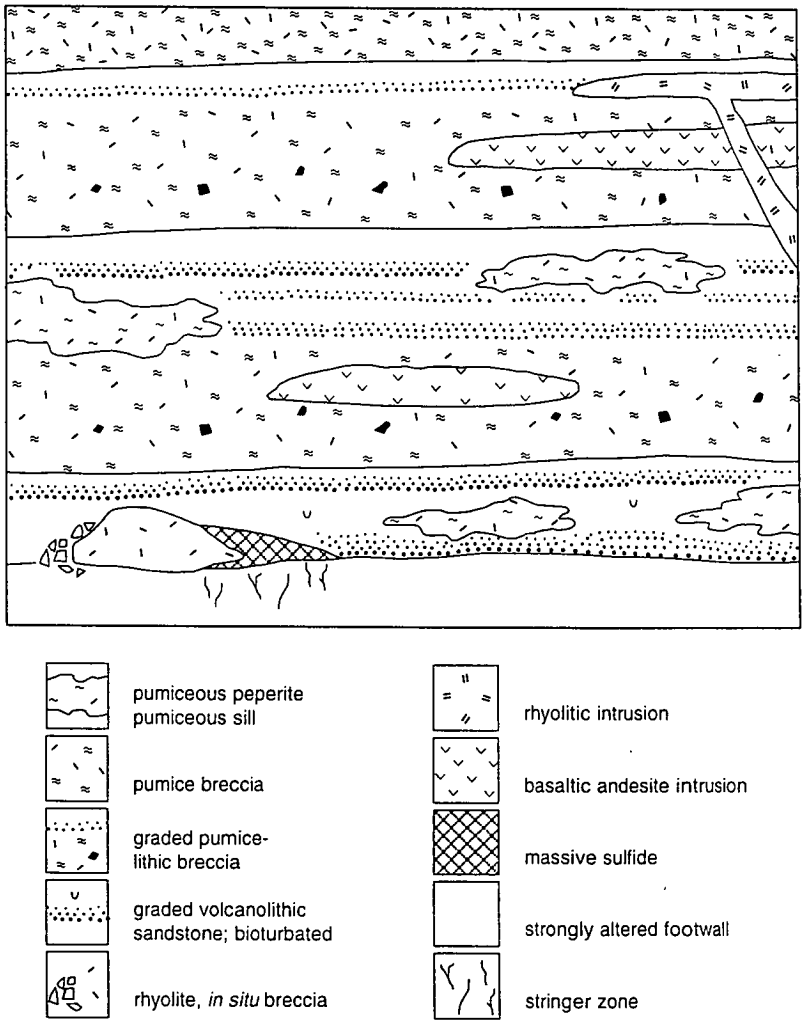

Fig. 2. Schematic facies architecture of the Berserker beds in the Mount Chalmers district. Pumiceous rhyolite sills and pumiceous peperite occur within intervals of volcanolithic sandstone and the fine-grained tops of graded pumice-lithic breccia units in the hangingwall stratigraphy to the Mount Chalmers massive sulfide ore body.

sented here concentrate on drill core examples. Their context and stratigraphic relationships are very well constrained by detailed logging and correlation of more than 120 diamond drill holes through the Berserker beds.

3. Field relationships of the pumiceous peperite

Pumiceous peperite has been identified throughout the hangingwall stratigraphy to the Mount Chalmers massive sulfide mineralisation and is not confined to one particular stratigraphic position. The peperite occurs within thick sequences of interbedded graded sandstone and siltstone, or within the laminated siltstone to sandstone tops of very thick, graded units of pumice-lithic breccia. In some instances, the peperite is associated with coherent pumiceous rhyolite. Where well constrained by adjacent drill hole intersections, the intervals of pumiceous rhyolite appear to be conformable with the enclosing units. They are thus interpreted to be sills. However, the facies geometry is complex in detail, comprising a number of relatively thin (< 20 m) intervals of pumiceous rhyolite and/or pumiceous peperite of limited lateral extent (less than a few tens of metres) intercalated with sedimentary facies. Macroscopic textures in the host sedimentary facies, the pumiceous rhyolite (igneous component) and the peperite are described in this section.

3.1. Sedimentary facies

The sedimentary facies that host the Mount Chalmers pumiceous peperite are dominated by normally graded beds of volcaniclastic siltstone, sandstone and pebbly sandstone. Single beds vary from 15 mm to 2.5 m thick. The framework grains are predominantly volcanic lithic fragments, relic pumice clasts and crystals (mainly feldspar, subordinate quartz); minor components are clasts of siliceous siltstone and intraclasts of fine-medium sandstone. The thicker beds of sandstone have sharp bases and commonly grade upward into siltstone, displaying Bouma divisions ABD. The siltstone intervals are massive to delicately laminated; however, in many cases, any original bedding has been destroyed by bioturbation.

The sediment component within and immediately adjacent to the peperite is dominantly siltstone to fine sandstone with a homogeneous texture. Neither bedding nor grading is present. Typically, bedding, grading and bioturbation structures occur and are undisturbed beyond about 0.5 m from the peperite.

The sediment component that occurs mixed with rhyolite in the peperite contains vesicles that are now filled by fine-grained quartz, chlorite or quartz–chlorite assemblages (Fig. 3A,B and Fig. 4A,B). The vesicles are generally spherical, although elliptical to lenticular forms are also present, and range from < 1 mm to 3 mm in diameter. They occur singularly or in groups, and in some cases, they define 'trails' that parallel the irregular sediment–rhyolite contacts. Importantly, vesicles have been observed only in the sedimentary facies immediately adjacent to the rhyolite component of the peperite. The sediment component within the peperite is also commonly paler (Fig. 3) and more siliceous along contacts with the rhyolite than elsewhere away from the rhyolite.

3.2. Rhyolite

The igneous component of the peperite has an evenly porphyritic texture comprising euhedral feldspar phenocrysts (10–20%, 1–2 mm in size; plagioclase and K-feldspar) and glomerocrysts set within a formerly glassy, variably vesicular groundmass. The feldspars have been altered to sericite, quartz or quartzo-feldspathic assemblages. Next to contacts with the sedimentary component, some of the feldspars are highly fractured in situ. The formerly glassy groundmass has been completely altered to sericite and/or silica. Sericite alteration of the groundmass predominates, whereas silica alteration is largely confined to groundmass adjacent to contacts with the host sediment. The phenocryst assemblage suggests that the igneous component is broadly felsic in composition. Texturally similar, but less altered feldspar-phyric pumice breccias elsewhere in the succession are predominantly rhyolitic in composition (Ti/Zr ranges from 3 to 22; SR Hunns, unpublished data). Thus, the igneous component was probably originally rhyolitic.

The groundmass of the rhyolite has three textural domains, all of which are transitional to each other: nonvesicular, round vesicle and tube pumice do-

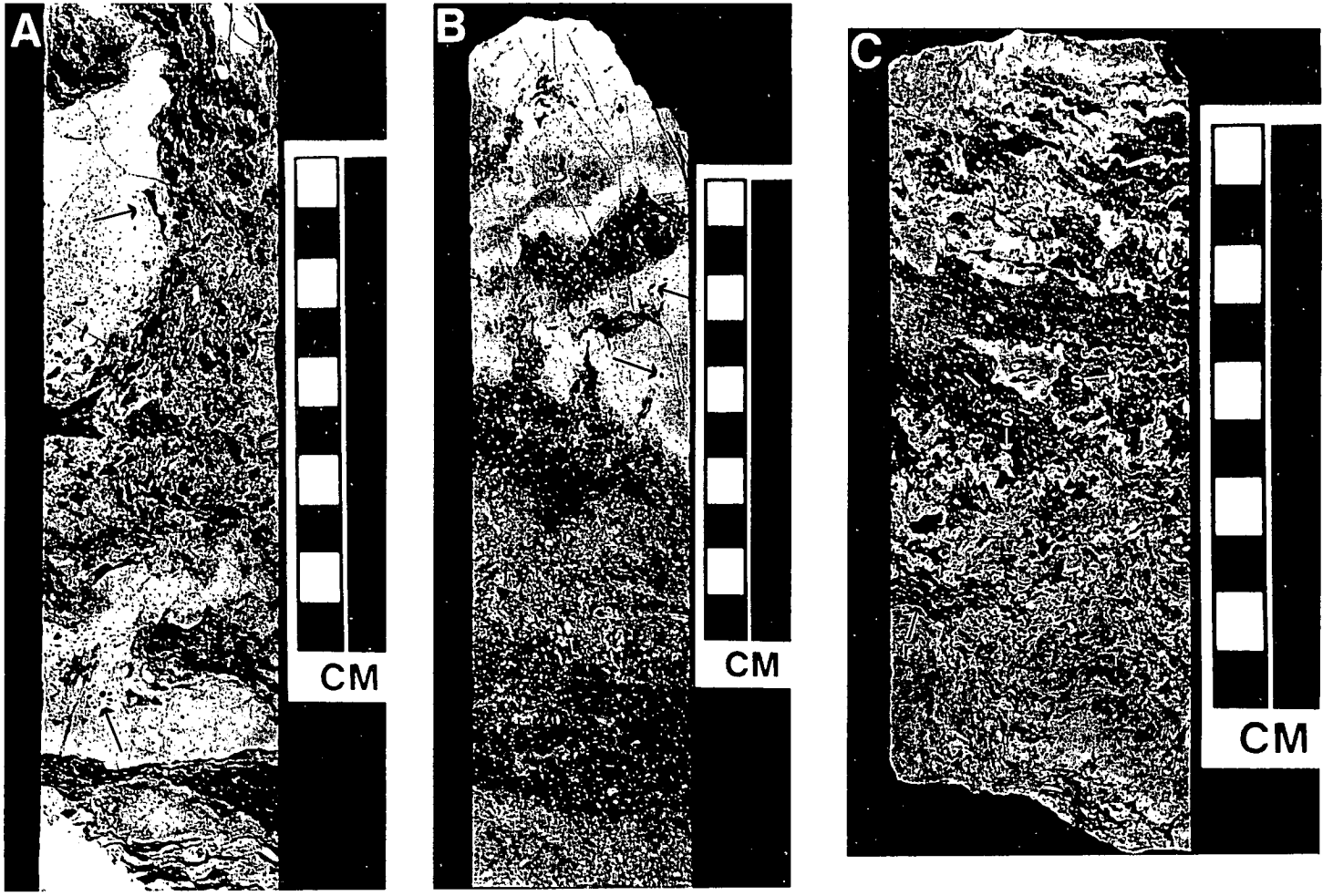

Fig. 3. Drill core samples of pumiceous peperite composed of highly irregular domains of pumiceous rhyolite (dark grey) and homogeneous host sediment (pale grey). In A and B, the sediment in contact with the pumiceous rhyolite is bleached and contains chlorite- and/or quartz-filled vesicles (arrows). In places, the vesicles define trails parallel to the contacts. In C, the formerly vesicular rhyolite clasts (r) have been compacted and now resemble wispy fiamme. They include intricately crenulated 'veins' of sediment (s). (A) MCD 10, 217.7 m; (B) MCD 10, 175.3 m; (C) WS 8, 79.6 m. Long dimension of each sample is approximately perpendicular to bedding.

mains. The transition from one domain to the next occurs over short distances (≤ 2–3 mm). In the nonvesicular domains, the groundmass is uniformly and completely altered to sericite ± silica. The round vesicle domains are composed of round quartz-filled vesicles less than 0.1 mm in diameter within sericitic

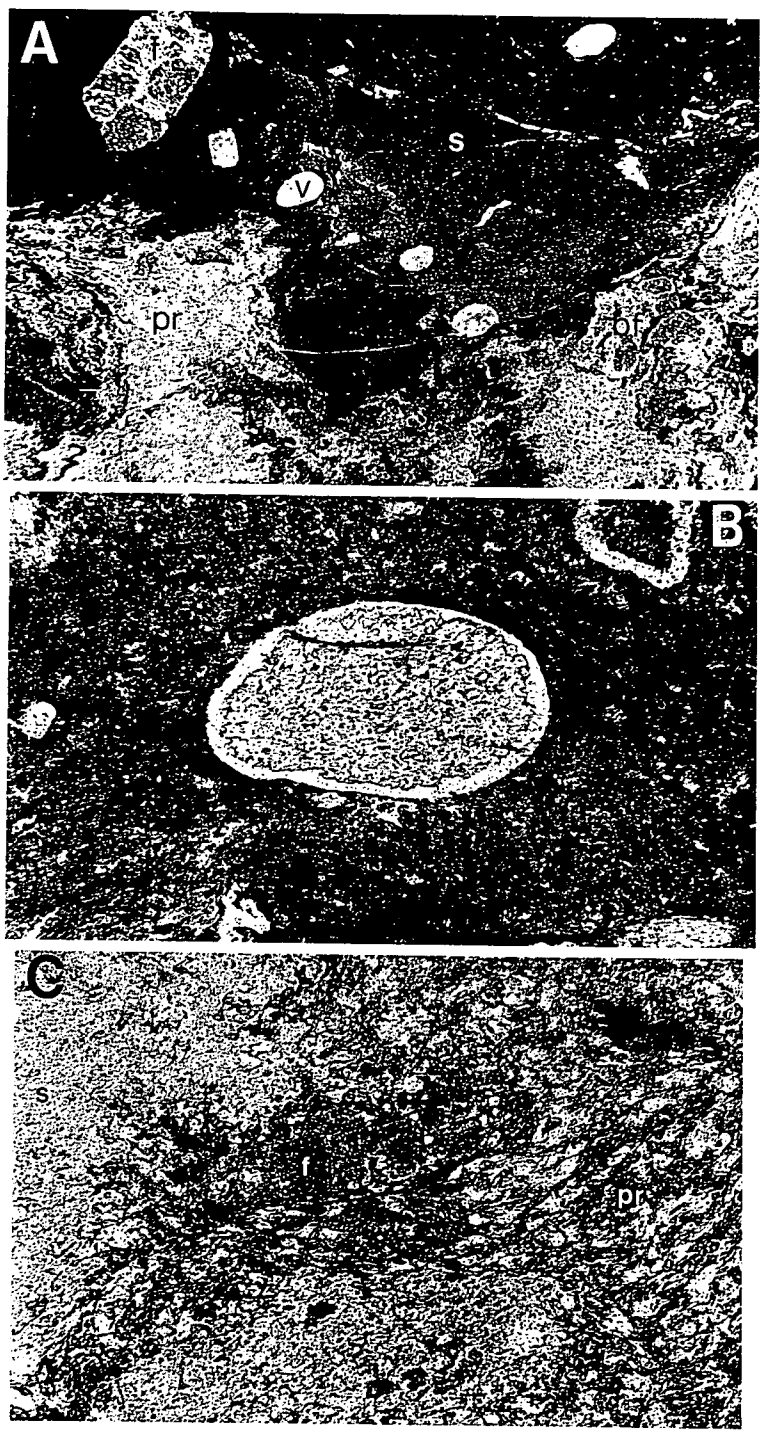

groundmass. The vesicles comprise up to 60% of the round vesicle domains. These round vesicle domains grade into tube pumice domains. In the tube pumice domains, vesicles are infilled by quartz and the vesicle walls have been completely altered to sericite.

The rhyolite is internally massive throughout drill core intersections up to 15 m in thickness. It includes up to 2 modal % feldspar-phyric clasts which have the same size and abundance of feldspar phenocrysts as the surrounding rhyolite, but within a nonvesicular, quartz–feldspar–sericite groundmass that was probably originally glassy. These probable rhyolite clasts range up to 25 mm across and are angular to subangular.

3.3. Pumiceous rhyolite–siltstone peperite

Peperite composed of pumiceous rhyolite and siltstone at Mount Chalmers occurs in two main settings: (1) peperite associated with intervals of coherent to in situ fractured rhyolite (Fig. 5); and (2) peperite not associated with coherent rhyolite (Fig. 6). The latter category includes a spectrum of rhyolite–siltstone mixtures that range from rhyolite-dominated to sediment-dominated peperite. The distinction between the rhyolite- and sediment-dominated types is based on a visual estimate of the relative proportions of the two components.

Examples of peperite associated with coherent rhyolite (1) were intersected in diamond drill holes WSDD 8, MCD 4 and MCD 10 (Fig. 5). Intervals of coherent pumiceous rhyolite range from 1 m to 10 m in thickness and have gradational to sharp upper and lower contacts with both rhyolite-dominated and sediment-dominated peperite. The coherent rhyolite is composed of euhedral feldspars set within a sericite–silica-altered pumiceous groundmass. Irregularly shaped lobes and worm-like stringers of homogeneous sediment a few millimetres across also occur within the intervals of coherent pumiceous rhyolite, and apophyses of rhyolite locally extend for relatively short distances ($\leq$ 10 cm) into the host sediment.

Peperite that is not associated with coherent rhyolite (2) dominates the peperite occurrences intersected by the Mount Chalmers drill holes (Fig. 6). The peperite is composed of predominantly irregular, ragged clasts and stringers of either rhyolite in sediment (e.g., MCD 6) or sediment in rhyolite (e.g., WS 7), although peperite comprising blocky sediment or rhyolite domains was also intersected. In these types, the rhyolite groundmass has been completely altered to sericite, and the sediment lacks bedding and is texturally homogeneous.

In some cases, the rhyolite clasts in the peperite have very wispy, lenticular shapes and are aligned sub-parallel to bedding (Fig. 3C), resembling fiamme. In these clasts, the vesicular texture is not preserved and the groundmass is composed of fine-grained structureless sericite. Similar intensely sericitic, wispy domains that lack pumiceous textures occur within some intervals of coherent pumiceous rhyolite. It is likely that initial alteration of the glassy pumiceous rhyolite was patchy. Where the vesicles were infilled and the glassy walls replaced, the tube pumice structure was preserved. However, where alteration of the glassy walls involved mainly sericite (or a clay precursor), and the vesicles remained open, the pumiceous structure did not survive. These more porous domains would have compacted during diagenesis, whereas the domains with infilled vesicles were not strongly affected by compaction. Early (pre- or syn-diagenetic compaction), patchy alteration appears to be a relatively common feature of submarine pumiceous facies (e.g., Allen and Cas, 1990; McPhie et al., 1993).

In thin section, intricate mixing of the rhyolite component and the sedimentary component is visible (Fig. 4A,C). Delicate, semi-detached to completely detached apophyses of tube pumice extend a few

Fig. 4. Photomicrographs of the pumiceous peperite and host sediment. (A) The highly irregular contact between pumiceous rhyolite (pr; pale tone) and the host siltstone (s; dark) at 175.3 m in MCD 10. Feldspar crystals (f) from the pumiceous rhyolite and vesicles (v) occur within the host siltstone near the contact. Note the broken feldspar phenocryst (bf) in the rhyolite adjacent to the contact. Plane-polarised light. Field of view ~ 7.5 mm across. (B) Detail of a chlorite–quartz-filled vesicle in the host siltstone adjacent to pumiceous rhyolite at 175.3 m in MCD 10. Plane-polarised light. Field of view ~ 1.25 mm across. (C) Tube pumice texture in feldspar-phyric (f) pumiceous rhyolite (pr) that intrudes siltstone (s; pale tone) at 175.3 m in MCD 10. Note the delicate wispy terminations of the pumiceous rhyolite domain. Plane-polarised light. Field of view ~ 3 mm across.

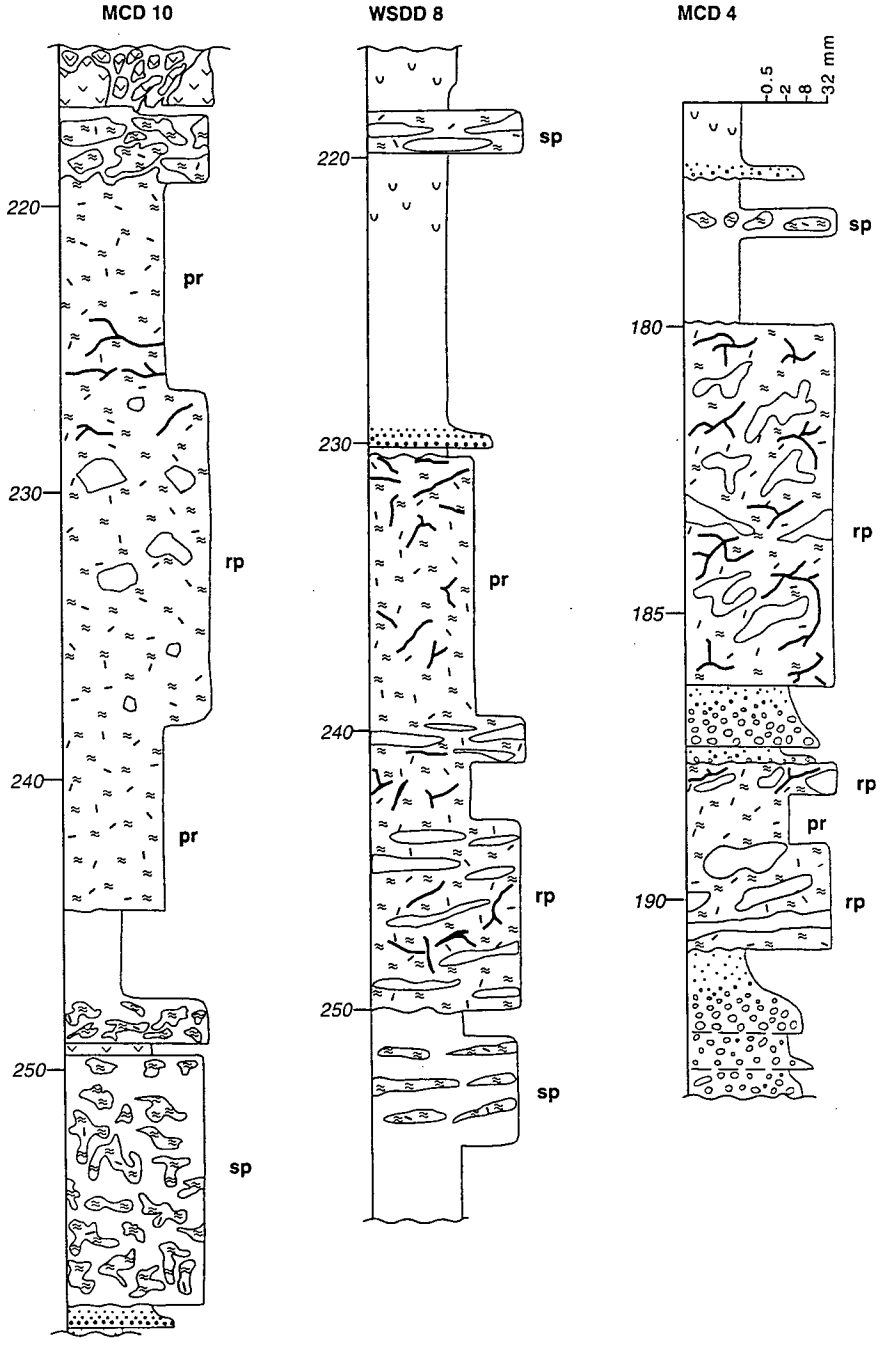

Fig. 5. Graphic logs of diamond drill holes MCD 10 (215–259 m), WSDD 8 (216–257 m) and MCD 4 (176–193.5 m), each of which intersected pumiceous peperite that is associated with intervals of coherent pumiceous rhyolite (pr). Examples of both rhyolite-dominated (rp) and sediment-dominated (sp) peperite are also present in each intersection. The rhyolite-dominated peperite in MCD 10 (227–238 m) includes a small proportion of nonvesicular, feldspar-phyric probable rhyolite clasts. Legend for symbols is given on Fig. 6.

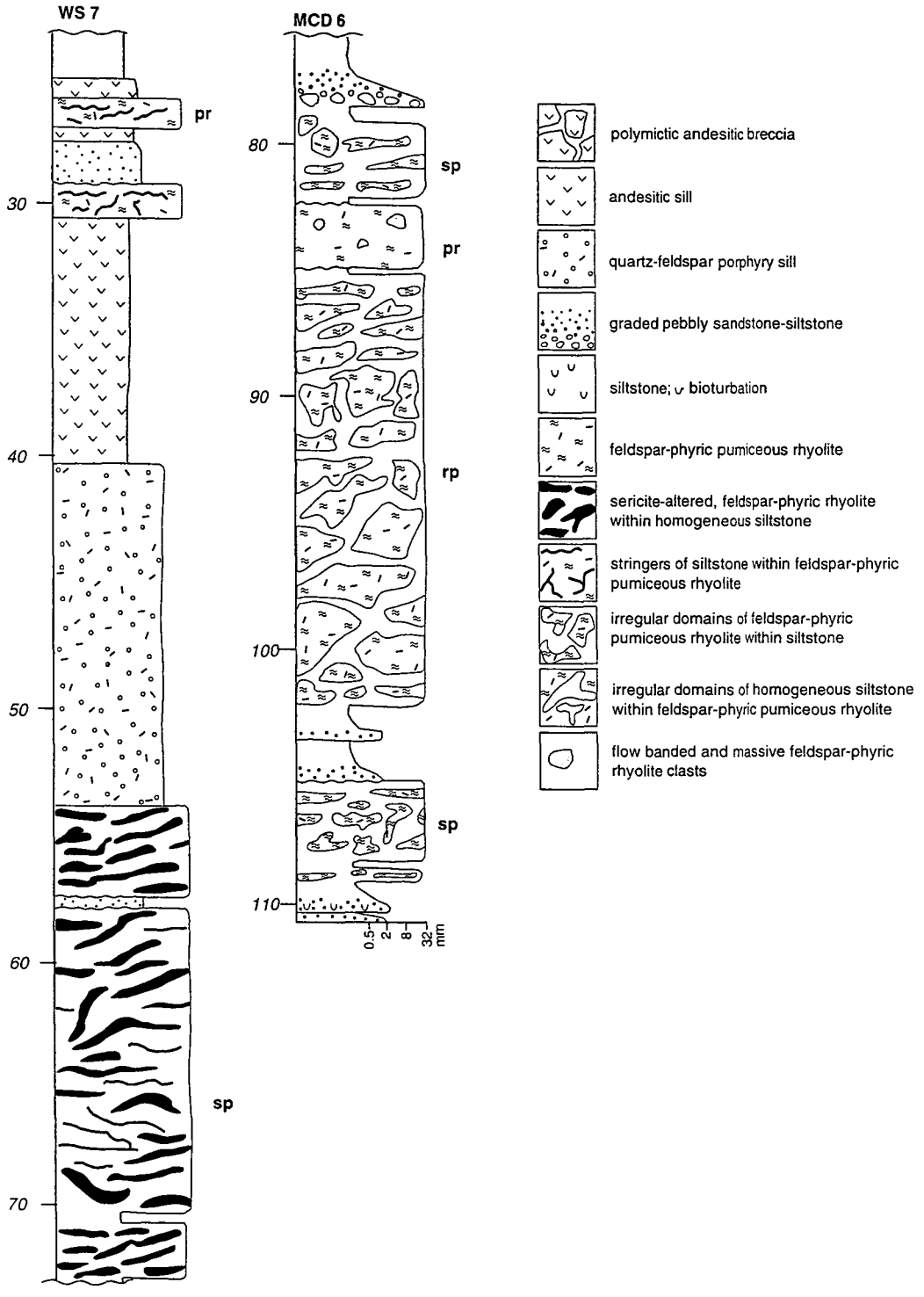

Fig. 6. Graphic logs of diamond drill holes WS 7 (23–73 m) and MCD 6 (76–111 m) which intersected intervals of pumiceous peperite dominated by either the igneous (pumiceous rhyolite; rp) or by the sediment (siltstone; sp) component. In the sediment-dominated peperite of WS 7, the formerly pumiceous rhyolite is altered to sericite and compacted into lenses and wisps that resemble fiamme.

millimetres into the host sediment; feldspar crystals, some of which have rinds of tube pumice, occur adjacent to the tube pumice apophyses. Shards derived from the pumiceous rhyolite are also a common feature of the peperite. They occur isolated within the sediment adjacent to tube pumice apophyses, or else are connected to the tube pumice. The shards are dominantly cuspate and platy bubble wall shards and pumice shreds. None of the shards show evidence for plastic deformation while still hot, as seen in welded ignimbrites. Some of the vesicles within the tube pumice shreds have been infilled by the host sediment.

4. Identification of pumiceous peperite

Peperite is a variety of volcanic breccia that results from dynamic mixing of unconsolidated, typically wet sediment and molten lava or magma. Positive identification therefore rests on evidence that the sediment was unconsolidated at the time of mixing and that the igneous component was hot. The Mount Chalmers examples are very well constrained as peperite by the following several arguments:

(1) The host sediment involved in the peperite is homogeneous in texture and unstratified, whereas elsewhere, it is bedded and beds are graded. Local destruction of bedding and grading requires considerable re-arrangement of the original grain packing which can only take place in sediment that is unconsolidated or weakly consolidated.

(2) The sediment immediately adjacent to the rhyolite is vesicular. The vesicles indicate that gas-filled bubbles were trapped within the sediment. Formation of vesicles requires small-scale rearrangements of the sediment grains and intergranular movement of the entrapped gas phase, both of which can only be accomplished in wet, unconsolidated sediment.

(3) The presence of vesicles in the host sediment indicates that the rhyolite was hot when the two components were mixing. Vesicles do not occur elsewhere in the sedimentary facies and show a close spatial relationship with the rhyolite. In this instance, the gas phase could have been steam generated from heating of the pore fluids by the intruding rhyolite and/or magmatic volatiles exsolving from the rhyolite or released from rupturing vesicles within it.

(4) Away from the rhyolite, the host sediment is green–grey, but it fades to cream or very pale green in a zone about 1–2 cm wide adjacent to the rhyolite. The colour change is gradational and closely mirrors the sediment–rhyolite contacts. The paler sediment at the contacts is more silicified than the host sedimentary facies elsewhere. The subtle, gradational colour change and local silicification of the sediment are interpreted to result from thermal metamorphism of the sediment in contact with hot rhyolite.

(5) The shapes of many of the rhyolite clasts in the peperite are highly irregular and suggest that part of the rhyolite was behaving, at least momentarily, in a ductile and plastic fashion during mixing. However, in some cases, the highly irregular and ragged shape of the rhyolite domains is not entirely primary, but a consequence of variable compaction of the original pumiceous structure.

In submarine settings, pumice–sediment mixtures can result from mechanisms other than dynamic mixing of a pumiceous intrusion with wet sediment. Large clasts of pumice generated by submarine eruptions, both effusive and explosive, are initially buoyant, but eventually become water-logged and sink, together with fine sediment from other sources settling from suspension (e.g., Reynolds and Best, 1976; Clough et al., 1981; Kano et al., 1996; Fiske et al., 1998). This process yields a deposit composed of outsize (up to several metres across) pumice clasts in mudstone or siltstone, which after compaction, can strongly resemble the complicated and intricate mixtures of sedimentary and igneous components typical of pumiceous peperite. However, water-settled pumice blocks may be distinguished by the presence of stratification in the enclosing sediment, especially stratification that drapes contacts with the pumice blocks. Water-settled pumice blocks are typically concentrated in laterally continuous beds, and evidence for thermal metamorphism of the sediment component is lacking. Neither do they show gradational relationships with intervals of coherent pumiceous component. On all counts, features of the pumiceous rhyolite–siltstone mixtures at Mount Chalmers are not consistent with an origin involving water-logged pumice, but are best interpreted as the result of dynamic mixing of a pumiceous intrusion with wet sediment. The two main categories of

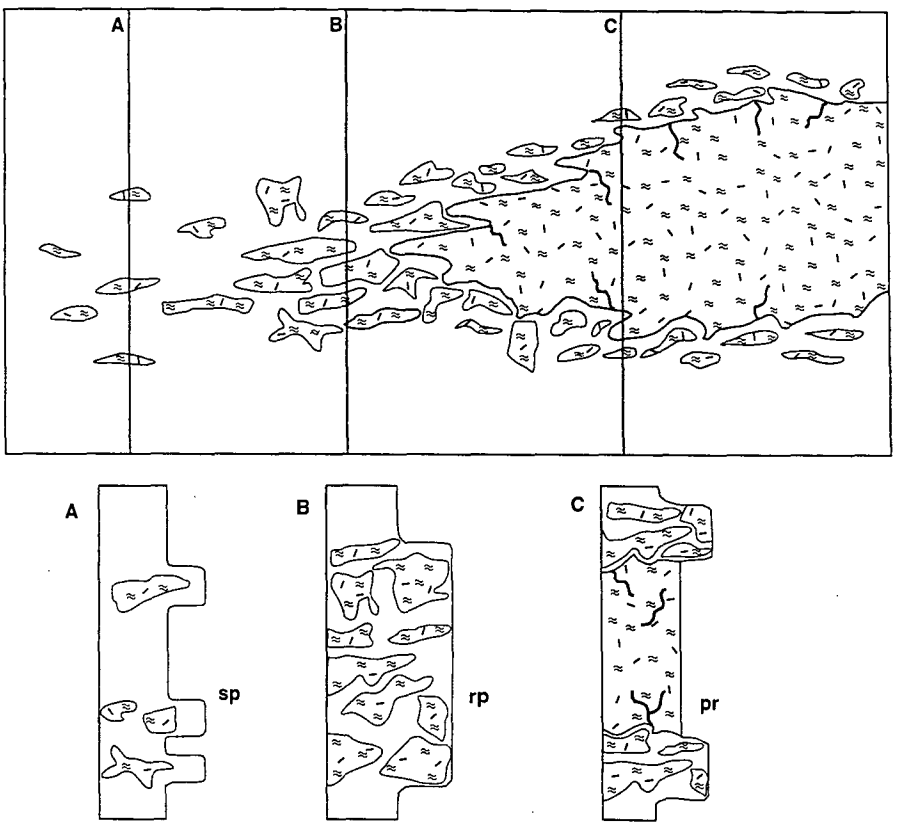

Fig. 7. Cartoon showing inferred relationships between drill core intersections that include pumiceous peperite associated with coherent pumiceous rhyolite (pr) and those that include peperite only. It is likely that the latter intersections (A,B) represent settings beyond the margins of the sills where the peperite facies was dominant. In these settings, the peperite ranges from rhyolite-dominated (rp) near the sills (B), to sediment-dominated peperite (sp) farther from the sills (A).

pumiceous peperite described above (associated with or separate from coherent rhyolite) are most likely related, representing sections that have intersected either the parent intrusion (1) or its peperitic margins (2) (Fig. 7).

5. Formation of pumiceous sills and pumiceous peperite

The setting, facies relationships and textures in the pumiceous sills and peperite at Mount Chalmers provide some constraints on the sequence of events, especially the means by which the pumiceous rhyolite was dismembered and mixed with the enclosing sediment.

5.1. Setting and confining pressure

Significant vesiculation of rhyolitic magmas with average water contents (~ 3 wt.%) is probably limited to confining pressures less than 10 MPa (McBirney, 1963). Both the presence of vesicles in the host sediment and the pumiceous nature of the rhyolite at Mount Chalmers imply that the confining pressure was substantially below that limit. The sedimentary succession that hosts the pumiceous rhyolite has facies characteristics and trace fossil and body fossil assemblages consistent with a shallow submarine shelf setting (Sainty, 1992). The abundance of turbidites suggests that the setting was below storm wave base. These constraints provide an indication that the water depth most likely ranged from a

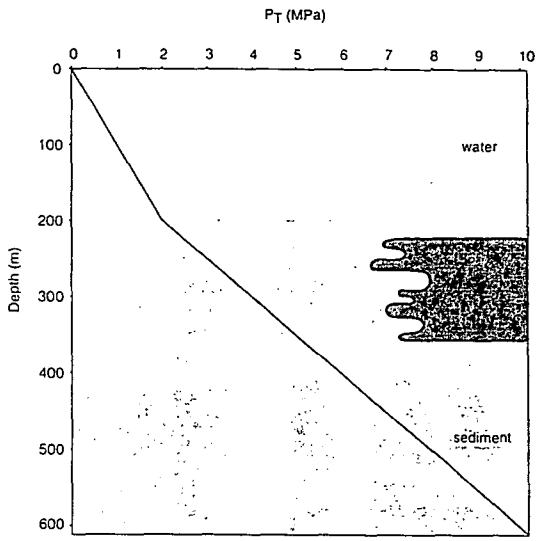

Fig. 8. Graph showing the likely range of confining pressure (P_T) experienced by the Mount Chalmers pumiceous rhyolite sills. P_T includes the pressure exerted by the seawater and the pressure exerted by the wet sediment covering the sills. The depth of the seawater was probably less than 200 m. The thickness of the wet sediment cover is poorly constrained, but may have been in the range of 30–150 m. P_T exerted by a 150-m thick layer of wet sediment with density 2000 kg/m^3 (e.g., Moore, 1962) and 200 m of sea water is ~5 MPa. Vesiculation of rhyolite can occur for confining pressures up to about 10 MPa (McBirney, 1963), which corresponds to a sediment cover of ~400 m.

minimum of a few tens of metres to a maximum of about 200 m.

Constraints on the thickness of sediment cover above the rhyolite sills at Mount Chalmers are less precise. The position of the palaeoseafloor at the time of intrusion cannot be recognised in the stratigraphy above the sills. However, the sediment cover may have been as little as a few tens of metres up to more than 100 m thick. At the likely maximum water depth of 200 m, the confining pressure limit of 10 MPa would not have been exceeded until the wet sediment cover was more than about 400 m thick (Fig. 8). Thus, the confining pressure did not prevent vesiculation.

5.2. Geometry and size of the pumiceous intrusions

The lack of correlation among intervals of pumiceous rhyolite and associated peperite suggests that the initial rhyolitic intrusion comprised separate lobes or digits with dimensions in the order of 10 m across and up to a few tens of metres thick (Fig. 9A). Such a facies geometry has been described in felsic, submarine and subglacial rhyolites (e.g., De Rosenspence et al., 1980; Furnes et al., 1980; Yamagishi, 1987), and in subaerial felsic lavas (e.g., Nakada, 1992) and in felsic intrusions (e.g., McPhie and Goto, 1996).

5.3. Model for intrusion, fragmentation and mixing

The rhyolite lobes intruded wet sediment and rapidly developed chilled, glassy margins that thermally insulated the interior (Fig. 9A,B). Intrusion was accommodated by expansion of the enclosing water-saturated sediment in response to heating of the pore fluid, progressive disruption of grain contacts and displacement of the sediment cover. The confining pressure exerted by the sediment cover and the overlying shallow seawater was sufficiently low to allow vesiculation of the hot interior of the rhyolite lobes. Concurrently, new magma was being fed into the lobe interiors. Thus, the lobes inflated (Fig. 9C) in response to vesiculation and to continued magma supply. Early formed vesicles became increasingly elongate in the direction of shear within the growing lobes.

The intricate mixtures of pumiceous rhyolite and sediment in the Mount Chalmers peperite indicate that at some point, the rhyolite lobes were dismembered and invaded by wet sediment. The nonvesicular, formerly glassy rhyolite clasts in the pumiceous sills could represent fragments of the ruptured chilled margin. A number of processes probably contributed to fragmentation of the lobes. Depressurisation of the inflated lobes may have triggered fragmentation. Mungall et al. (1996) have shown that cooling of vesicular shallow intrusions is accompanied by development of microfractures in vesicle walls due to dehydration and shrinkage. This greatly reduces the strength of the vesicular glass, so that a small reduction in confining pressure can cause disintegration. This process would have affected portions of the vesicular rhyolite that had cooled below the glass transition temperature and were subject to small, probably local reductions in confining pressure. Cooling and microfracturing of the rhyolite were heterogeneous, proceeding faster in proximity to the

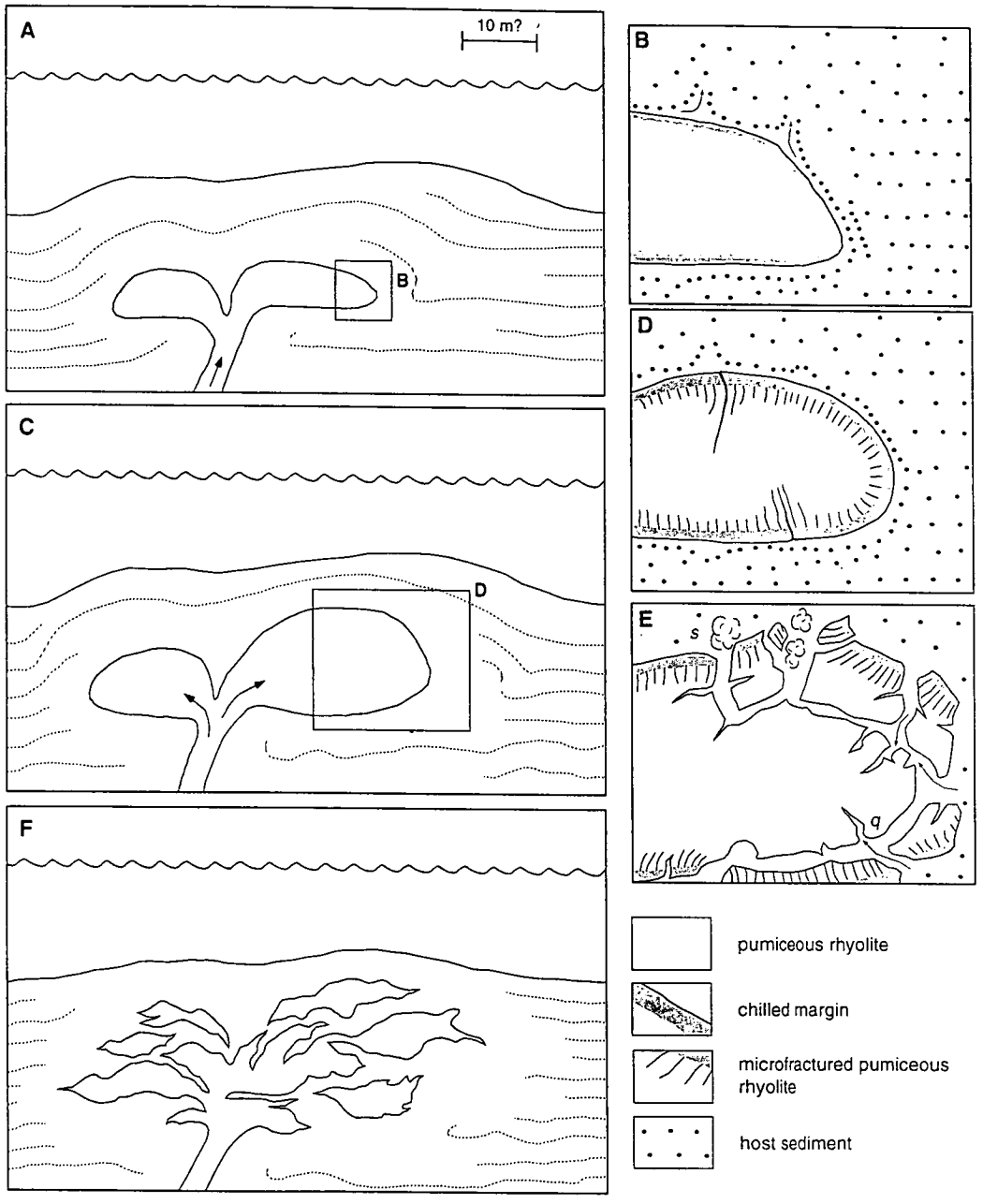

Fig. 9. Schematic reconstruction of the sequence of events involved in the formation of pumiceous sills and associated peperite at Mount Chalmers. (A) Intrusion of rhyolite lobes into wet silt and fine sand. (B) Space was created by expansion and fluidisation of the sediment at the contact. The lobes developed a glassy, nonvesicular chilled margin. (C) Inflation of the lobes occurred in response to vesiculation and to continued magma supply. (D) Parts of the lobes that cooled through the glass transition temperature developed microfractures in the walls of vesicles. (E) Failure of the microfractured vesicular domains dismembered the lobes and allowed the ingress of wet sediment. Direct interaction of wet sediment with the hot rhyolite resulted in further disintegration and mixing caused by steam explosions (s) and/or quench fragmentation (q). (F) Fragmentation of the intrusive lobes and mixing with the wet host sediment produced a complex arrangement pumiceous rhyolite, rhyolite-dominated peperite and sediment-dominated peperite. Bedding in the host sediment was destroyed where mixing with the pumiceous rhyolite occurred, but was undisturbed elsewhere.

chilled margins and quench fractures (Fig. 9D). Mechanisms for reducing confining pressure in these circumstances include (1) local unloading by slumping of the overlying, up-domed sediment pile, and/or (2) propagation of fractures through the chilled margins of the lobes and into the more slowly cooled vesicular domains. Microfracture-driven disintegration could yield fragments ranging from millimetre size, being bubble-wall shards from disruption of vesicles, to several metres, governed by the distribution of domains that had cooled through the glass transition. Wet and/or steam-rich sediment would have immediately invaded fractures propagating through the rhyolite and engulfed detached apophyses of rhyolite.

Failure of the cooler parts of the lobes allowed wet sediment to interact directly with hot rhyolite that remained in the interior of the lobes (Fig. 9E). Because the confining pressure was relatively low, direct contact between the hot rhyolite and wet sediment may have generated steam-driven explosions capable of fragmenting the rhyolite. Also, dismembering of the lobes would have been promoted by rapid cooling and contraction of the hot rhyolite in contact with wet sediment. Quench fractures that opened in the hot vesicular rhyolite were rapidly invaded by the host sediment.

Gas released by rupture of vesicles in the rhyolite and/or steam from vaporised pore fluid formed bubbles in the sediment immediately adjacent to the rhyolite. Intrusion of the rhyolite into the sediment together with heating, expansion and possible fluidisation by the pore fluid led to destruction of bedding and other original structures in the host sediment adjacent to the rhyolite. Heat and magmatic fluids released from the rhyolite resulted to induration, bleaching and silicification of the sediment in direct contact with it.

5.4. Other examples of pumiceous peperite

Although by no means common, pumiceous peperite is not unique to the Mount Chalmers locality. Other examples of felsic pumiceous intrusions and associated peperite have been reported from the Miocene submarine successions of the Green Tuff Belt on Honshu, Japan and the Mount Read Volcanics of western Tasmania (e.g., Gifkins et al., 1996). These are also known from drill core intersections and involve complex arrangements of coherent pumiceous to nonvesicular rhyolite enclosed by in situ intrusive hyaloclastite and pumiceous peperite. The apparent paucity of examples most likely reflects a combination of the rarity of the special circumstances required for vesiculation of intrusions, and the difficulty of identifying the critical diagnostic features of such facies. In particular, extensive vesiculation requires low confining pressure and delayed quenching which are conditions not easily met by intrusions into water-saturated sediments. The first condition places limits on the thickness of the sediment cover and on the water depth. The second condition depends on the development of an insulating chilled margin that impedes cooling and promotes the build-up of internal volatile pressure.

6. Conclusions

The Early Permian submarine volcanic and sedimentary succession at Mount Chalmers includes syn-volcanic sills and associated peperite in which the igneous component is pumiceous rhyolite. Key features of the pumiceous peperite are: (1) the highly irregular contacts between pumiceous rhyolite and host sediment, (2) the gradational to sharp contacts between coherent pumiceous rhyolite and pumiceous peperite, (3) the presence of vesicles and thermal metamorphic effects in the host sediment adjacent to the rhyolite, and (4) local destruction of bedding in the sediment involved in the peperite.

Formation of the pumiceous sills and associated pumiceous peperite involved intrusion of rhyolite lobes that developed chilled margins. The lobes inflated in response to magma supply and vesiculation. A number of processes may have operated to fragment and dismember the lobes. In this setting, microfracturing of vesicle walls probably occurred during cooling, weakening the vesicular rhyolite, so that even a small reduction in confining pressure would have been sufficient to cause disintegration (e.g., Mungall et al., 1996). Where hot rhyolite came in direct contact with wet sediment, both quench fragmentation and steam explosions may have operated. Heating of the sediment pore fluid led to expansion and possible vaporisation that disrupted grain packing and completely destroyed bedding in the vicinity

of the lobes. Gas released from the pumiceous rhyolite and/or steam from vaporised pore fluid was entrapped as bubbles in the host sediment.

The formation of pumiceous sills and peperite in a water-saturated host sedimentary succession requires a special combination of low confining pressure, vesiculation and delayed quenching. The facies characteristics of the Mount Chalmers pumiceous sills and peperite suggest that the depositional setting was a submarine shelf below wave base, but no more than a couple of hundred metres deep and possibly substantially shallower. Delayed quenching was achieved by development of a chilled margin that effectively insulated the interior from the surrounding wet sediment.

Acknowledgements

The research for this manuscript was in part funded by the Australian Research Council's Special Research Centres program, and by an APA(I) scholarship held by SRH and sponsored by Great Fitzroy Mines. Outokumpu Exploration Australia and Mining Project Investors also contributed financial and logistic support for the research. Federation Resources are thanked for allowing access to recently completed diamond drill holes. Critical comments from Yoshi Goto, Sharon Allen, Paolo Papale and an anonymous referee are gratefully acknowledged.

References

Allen, R.L., Cas, R.A.F., 1990. The Rosebery controversy: distinguishing prospective submarine ignimbrite-like units from true subaerial ignimbrites in the Rosebery-Hercules ZnCuPb massive sulfide district, Tasmania. Geol. Soc. Aust. 25, 31–32. Abstracts.

Boulter, C.A., 1993. High-level peperitic sills at Rio Tinto, Spain: implications for stratigraphy and mineralisation. Trans. Inst. Min. Metall. (Section B: Applied Earth Science) 102, B30–B37.

Brooks, E.R., 1995. Paleozoic fluidization, folding, and peperite formation, northern Sierra Nevada, California. Can. J. Earth Sci. 32, 314–324.

Brooks, E.R., Wood, M.M., Garbutt, P.L., 1982. Origin and metamorphism of peperite and associated rocks in the Devonian Elwell Formation, northern Sierra Nevada, California. Geol. Soc. Am. Bull. 93, 1208–1231.

Busby-Spera, C.J., White, J.D.L., 1987. Variation in peperite textures associated with differing host-sediment properties. Bull. Volcanol. 49, 765–775.

Clough, B.J., Wright, J.V., Walker, G.P.L., 1981. An unusual bed of giant pumice in Mexico. Nature 289, 49–50.

De Rosen-spence, A.F., Provost, G., Dimroth, E., Gochnauer, K., Owen, V., 1980. Archean subaqueous felsic flows, Rouyn-Noranda, Quebec, Canada, and their Quaternary equivalents. Precambrian Res. 12, 43–77.

Fiske, R.S., Cashman, K.V., Shibata, A., Watanabe, K., 1998. Tephra dispersal from Myojinsho, Japan, during its shallow submarine eruption of 1952–1953. Bull. Volcanol. 59, 262–275.

Furnes, H., Friedleifsson, I.B., Atkins, F.B., 1980. Subglacial volcanics—on the formation of acid hyaloclastites. J. Volcanol. Geotherm. Res. 8, 95–110.

Gifkins, C.C., McPhie, J., Allen, R.L., 1996. Fiamme associated with silicic pumiceous lavas and intrusions. Supplement to EOS Trans., Am. Geophys. Union, Western Pacific Geophysics Meeting 77 (22) W125.

Goto, Y., McPhie, J., 1996. A Miocene basanite peperitic dyke at Stanley, northwestern Tasmania, Australia. J. Volcanol. Geotherm. Res. 74, 111–120.

Hanson, R.E., 1991. Quenching and hyaloclastic disruption of andesitic to rhyolitic intrusions in a submarine island-arc sequence, northern Sierra Nevada, California. Geol. Soc. Am. Bull. 103, 804–816.

Hanson, R.E., Schweickert, R.A., 1982. Chilling and brecciation of a Devonian rhyolite sill intruded into wet sediment, northern Sierra Nevada, California. J. Geol. 90, 717–724.

Hanson, R.E., Wilson, T.J., 1993. Large-scale rhyolite peperites (Jurassic, southern Chile). J. Volcanol. Geotherm. Res. 54, 247–264.

Kano, K., 1989. Interactions between andesitic magma and poorly consolidated sediments: examples in the Neogene Shirahama Group, south Izu, Japan. J. Volcanol. Geotherm. Res. 37, 59–75.

Kano, K., Yamamoto, T., Ono, K., 1996. Subaqueous eruption and emplacement of the Shinjima Pumice, Shinjima (Moeshima) Island, Kagoshima Bay, SW Japan. J. Volcanol. Geotherm. Res. 71, 187–206.

Kirkegaard, A.G., Shaw, R.D., Murray, C.G., 1970. Geology of the Rockhampton and Port Clinton 1:250000 sheet areas. Geol. Surv. Queensland Rep. 38, 155 pp.

Kokelaar, B.P., 1982. Fluidization of wet sediments during emplacement and cooling of various igneous bodies. J. Geol. Soc. London 139, 21–33.

McBirney, A.R., 1963. Factors governing the nature of submarine volcanism. Bull. Volcanol. 26, 455–469.

McPhie, J., 1993. The Tennant Creek porphyry revisited: a synsedimentary sill with peperite margins. Early Proterozoic, Northern Territory. Aust. J. Earth Sci. 40, 545–558.

McPhie, J., Goto, Y., 1996. Lobe and layered structure in dacite sills of the Archaean Strelley succession, Western Australia. Supplement to EOS, Trans. Am. Geophys. Union, Western Pacific Geophysics Meeting 77 (22) W125.

McPhie, J., Hunns, S.R., 1995. Secondary welding of submarine

pumice-lithic breccia at Mount Chalmers, Queensland, Australia. Bull. Volcanol. 57, 170–178.

McPhie, J., Dole, M., Allen, R.L., 1993. Volcanic Textures: A Guide to the Interpretation of Textures in Volcanic Rocks. CODES Key Centre, University of Tasmania, Hobart, 196 pp.

Moore, D.G., 1962. Bearing strength and other physical properties of some shallow and deep-sea sediments from the north Pacific. Geol. Soc. Am. Bull. 73, 1163–1166.

Mungall, J.E., Bagdassarov, N.S., Romano, C., Dingwell, D.B., 1996. Numerical modelling of stress generation and microfracturing of vesicle walls in glassy rocks. J. Volcanol. Geotherm. Res. 73, 33–46.

Nakada, S., 1992. Lava domes and pyroclastic flows of the 1991–1992 eruption at Unzen Volcano. In: T. Yanagi, H. Okada, K. Ohta (Eds.), Unzen Volcano, The 1990–1992 Eruption. Nishinippon and Kyushu University Press, pp. 56–66.

Peltz, S., Kafri, U., 1992. Neogene pyroclastics containing peperites in the Zalmon Valley, central Galilee, Israel. Israeli J. Earth Sci. 41, 45–49.

Rawlings, D.J., 1993. Mafic peperite from the Gold Creek Volcanics in the Middle Proterozoic McArthur Basin, Northern Territory. Aust. J. Earth Sci. 40, 109–113.

Reynolds, M.S.A., Best, J.G., 1976. Summary of the 1953–57 eruption of Tuluman volcano, Papua New Guinea. In: Johnson, R.W. (Ed.), Volcanism in Australasia. Elsevier, Amsterdam, pp. 287–296.

Sainty, R.A., 1992. Shallow-water stratigraphy at the Mount Chalmers volcanic-hosted massive sulfide deposit, Queensland, Australia. Econ. Geol. 87, 812–824.

Sanders, I.S., Johnston, J.D., 1989. The torridonian stac fada member: an extrusion of fluidised peperite? Trans. R. Soc. Edinburgh, Earth Sci. 80, 1–4.

Willmott, W.F., O'Flynn, M.L., Trezise, D.L., 1984. Rockhampton Region 1:100000 Geological Map Sheet 99051 and Part Sheet 8951, 1st edn. Department of Mines, Brisbane, Australia.

Yamagishi, H., 1987. Studies on the Neogene subaqueous lavas and hyaloclastites in Southwest Hokkaido. Geol. Surv. Hokkaido, Report 59: 55–101.

Bull Volcanol (1995) 57:170–178

ORIGINAL PAPER

J. McPhie · S. R. Hunns

Secondary welding of submarine, pumice–lithic breccia at Mount Chalmers, Queensland, Australia

Received: June 15, 1994 / Accepted: February 27, 1995

Abstract Very thick units of massive pumice and lithic clast-rich breccia in the Early Permian Berserker beds at Mount Chalmers, Queensland, are deposits from cold, water-supported, volcaniclastic mass flows emplaced in a below-wave base submarine setting. Adjacent to syn-volcanic andesitic and rhyolitic sills and dykes, the pumice–lithic breccia shows a well-developed eutaxitic texture. The eutaxitic foliation is parallel to intrusive contacts and extends as far as a few metres away from the contact. At these sites, pumice clasts are strongly flattened and tube vesicles within the pumice clasts are compacted and aligned parallel to the direction of flattening. Some lenticular pumice clasts contain small ($\leqslant$2 mm), round, quartz-filled amygdales and spherulites. Further away from the sills and dykes, the pumice clasts have randomly oriented, delicate tube vesicle structure and are blocky or lensoid in shape. Round amygdales were generated by re-vesiculation of the glass and the spherulites indicate devitrification of the glass at relatively high temperatures. The eutaxitic texture is therefore attributed to re-heating and welding compaction of glassy pumice–lithic breccia close to contacts with intrusions. In cases involving sills, secondary welding along the contacts formed extensive, conformable, eutaxitic zones in the pumice–lithic breccia that could be mistaken for primary welding compaction in a hot, primary pyroclastic deposit.

Key words Submarine pumice breccia · Eutaxitic textures · Secondary welding · Compaction · Glass · Spherulites · Syn-volcanic intrusions

Editorial responsibility: T. Ui

Jocelyn McPhie (✉) · Steven R. Hunns
CODES, University of Tasmania,
GPO Box 252C Hobart, Tasmania 7001, Australia

Introduction

Compaction of pumice and bubble-wall shards may occur during high-temperature welding of hot, primary pyroclastic flow and fall deposits (Smith 1960; Ross and Smith 1961; Sparks and Wright 1979). Thoroughly welded pyroclastic deposits have much lower porosity than their non-welded counterparts, and display eutaxitic texture (Ross and Smith 1961) comprising plastically deformed, compacted, aligned (commonly bedding-parallel) pumice lenses in a matrix of flattened shards. Here we report eutaxitic texture in Permian, mass-flow emplaced pumice and lithic clast-rich breccia deposited in a below-wave base submarine setting at Mount Chalmers, Queensland (Fig. 1). In this instance, the mass-flow deposit was cold and the eutaxitic texture was generated by re-heating and high-temperature compaction of initially glassy pumice adjacent to syn-volcanic intrusions, a process we refer to as secondary welding. This example adds to the growing number of circumstances where eutaxitic textures can occur and emphasizes the need for care in the interpretation of rocks displaying such textures.

One type of secondary welding is already well documented. Glassy pyroclastic deposits and tuffaceous sediments underlying and adjacent to younger subaerial lavas may undergo secondary welding compaction that results in zones of 'fused tuff' (Smith 1960; Ross and Smith 1961; Christiansen and Lipman 1966; Schmincke 1967). Christiansen and Lipman (1966), following Smith (1960: 800) used the term 'fused' for the induration and deformation of glassy clasts resulting from heating by adjacent lava, but emphasized that the term should not be taken to imply that melting (fusion) had occurred. Similarly, there is no evidence that melting occurred in the Mount Chalmers case, but the term 'fused tuff' is nevertheless inappropriate because the pumice–lithic breccia is not a primary pyroclastic deposit (that is, not 'tuff'). It is clear that any glassy pumiceous deposits, whether primary non-welded pyroclas-

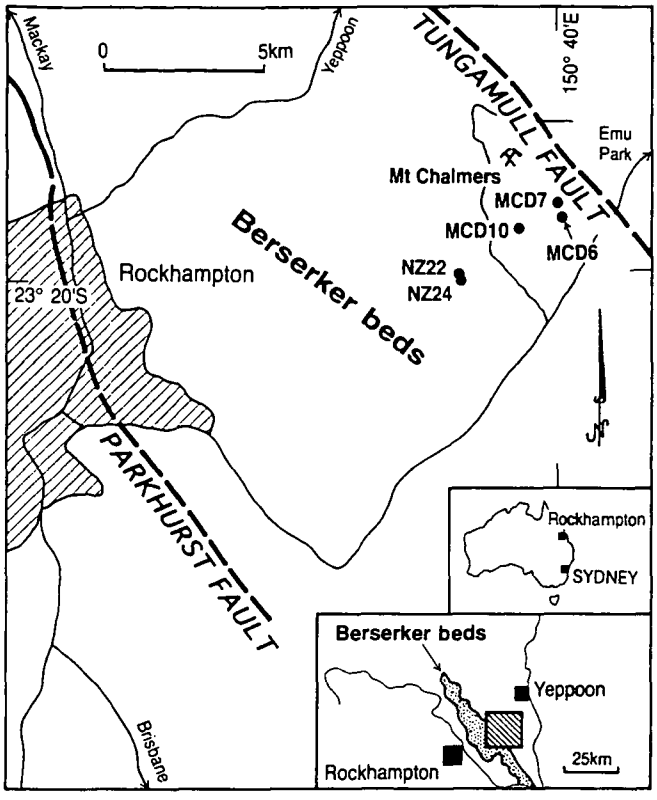

Fig. 1 Map showing the location of outcrops and drillholes discussed in the text. The Early Permian Berserker beds occur between the Tungamull and Parkhurst faults. The shaded area outlines Rockhampton city limits

tic deposits or resedimented and reworked deposits, can be affected by secondary welding adjacent to lava flows, intrusions and other sufficiently hot pyroclastic deposits.

Eutaxitic texture is characteristic of, but not restricted to, welded pyroclastic deposits and can also be generated by processes other than either primary or secondary welding compaction. These processes include: (1) diagenetic compaction of pumiceous deposits (Branney and Sparks 1990; McPhie et al. 1993); (2) devitrification and hydrothermal alteration of coherent lavas and intrusions (Allen 1988, 1992); or (3) re-heating and plastic deformation of autoclastic breccia associated with lava flows (Boyd 1961; Dadd 1992; Sparks et al. 1993). Eutaxitic texture resulting from primary welding is limited to volcaniclastic aggregates that are deposited hot, and is most commonly found in subaerial or very shallow subaqueous pyroclastic deposits. Eutaxitic texture resulting from secondary welding has no specific connotations for emplacement processes, nor for depositional setting, but does imply proximity to a lava flow or intrusion and is restricted to pumiceous (or scoriaceous), initially porous, glassy deposits. Eutaxitic textures generated by other processes can occur in a wide range of volcaniclastic deposits, lavas and shallow intrusions in diverse environments.

Geological setting

The eutaxitic texture recognized in the Mount Chalmers district occurs in pumice–lithic breccia of the Early Permian Berserker beds. The Berserker beds are approximately 3000 m thick and occupy an elongate, ~110 km long, north-west trending, 5–15 km wide fault block (Fig. 1; Kirkegaard et al. 1970). Regional deformation, most probably during the Mid- to Late Permian, produced open, upright, NNW trending folds. Dips of bedding rarely exceed 40° and a weak, vertical, N to NNW trending cleavage is locally present.

The Berserker beds comprise a mixture of sedimentary and volcanic facies associations. The sedimentary facies association is dominated by thinly to thickly bedded, volcanolithic, graded and massive sandstone, and laminated to thinly bedded mudstone. Transported and *in situ* fossils thought to be typical of shelf environments occur at several localities, and many intervals of both sandstone and mudstone contain trace fossils characteristic of the *Cruziana* ichnofacies (Sainty 1992). The volcanic facies association comprises rhyolitic, dacitic and andesitic lavas and related autoclastic breccia, peperite, pumice–lithic breccia and syn-volcanic intrusion (Hunns et al. 1993).

There are regional variations in the proportions of sedimentary versus volcanic facies associations in the Berserker beds. In the Mount Chalmers district where the secondary welding textures occur, the volcanic facies association is dominant and represented by: rhyolitic and andesitic lavas, and autoclastic breccia; dacite–mudstone peperite; rhyolitic and andesitic intrusions (sills and dykes); and very thick, graded dacitic pumice–lithic breccia (Fig. 2). Although relict volcanic textures are well preserved, the originally glassy components are now composed of quartzo-feldspathic or phyllosilicate assemblages. Rhyolitic intrusions are principally dykes and are strongly discordant to bedding. Andesitic intrusions are mainly sills or else are slightly discordant to bedding, and up to 200 m in thickness. In the vicinity of Mount Chalmers mine, andesitic sills have been intersected in drillholes over an area of 6 × 4 km.

The Berserker beds at Mount Chalmers host a gold- and copper-rich massive sulfide ore body, mining of which ceased in 1982 (Taube and van der Helder 1983). The ore body is considered to be a kuroko-style massive sulfide deposit that formed on the Early Permian seafloor (Okill 1974; Large and Both 1980; Taube and van der Helder 1983; Taube 1990). Eutaxitic textures occur in pumice–lithic breccia exposed in the Mount Chalmers pit, in drillcore that intersected laterally equivalent sequences about 2 km to the south and south-east (MCD 6, MCD 7, MCD 10) and in outcrops about 4 km to the south-west (NZ-22, NZ 24; Fig. 1). The pumice–lithic breccia in each instance is within the hangingwall stratigraphy relative to the massive sulfide mineralization (Fig. 2).

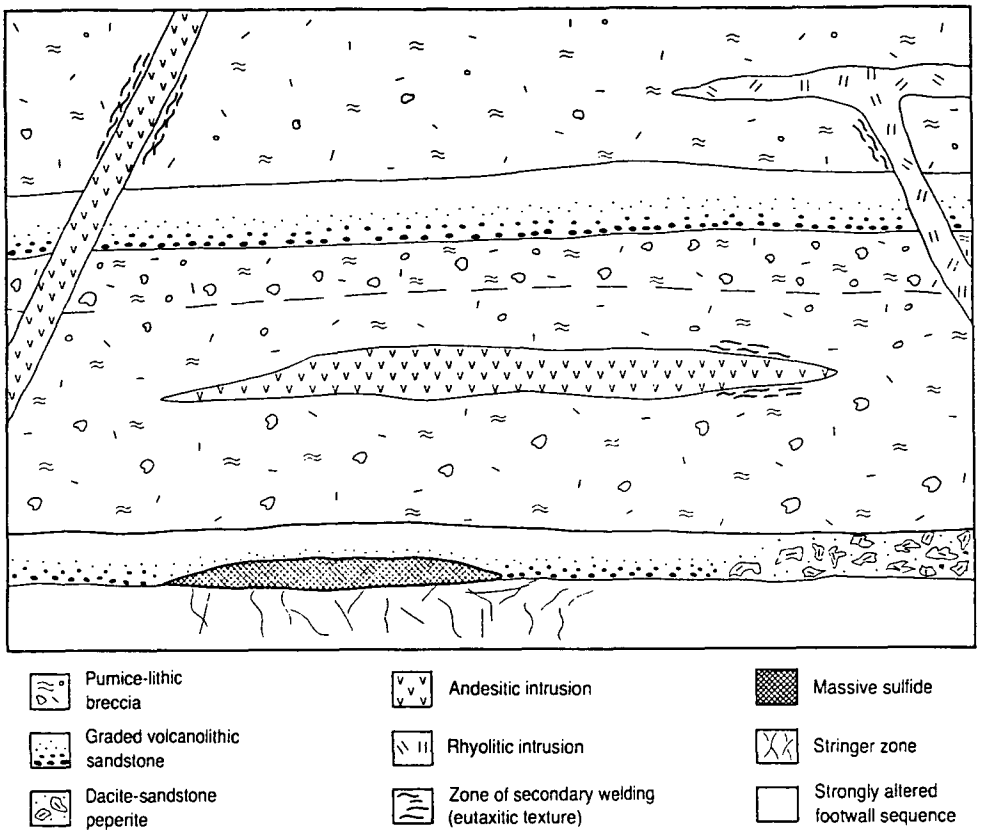

Fig. 2 Schematic reconstruction, not to scale, of the facies geometry of the Berserker beds near Mount Chalmers. The sedimentary interval between the thick, pumice–lithic breccia units contains *in situ* trace fossils of the *Cruziana* ichnofacies (Sainty 1992). Eutaxitic foliation occurs in the pumice–lithic breccia close to contacts with syn-volcanic rhyolitic and andesitic intrusions (dykes and sills). The total stratigraphic thickness represented is approximately 300 m

Eutaxitic texture in pumice–lithic breccia at Mount Chalmers

Pumice–lithic breccia

Pumice–lithic breccia units in the drillcore intersections, pit exposures and outcrops are texturally very similar. The units are generally very thick, some in excess of 100 m, and have sharp basal contacts above which there is a massive to weakly graded interval overlain gradationally by diffusely bedded tuffaceous sandstone and mudstone. The units are very poorly sorted and comprise feldspar-phyric tube pumice and less abundant volcanic lithic clasts. Delicate tube vesicles are preserved within the pumice clasts and, overall, there is a very weak alignment due to diagenetic compaction. However, many pumice clasts are uncompacted and randomly oriented. *In situ* trace fossils in interbedded sedimentary facies indicate that the depositional environment was submarine. Although composed of pumice, presumably of pyroclastic origin, the units show no signs of hot emplacement and have an internal organization (sharp base; massive-graded coarse lower part; diffusely stratified fine upper part) that is consistent with deposition from water-supported, submarine, high particle concentration, volcaniclastic mass flows. The abundance of pumice clasts and the large volumes represented by single sedimentation units strongly suggest that the submarine mass flows were fed directly from major pyroclastic eruptions – that is, they were syn-eruptive. Re-sedimentation of non-welded, pumice-rich, primary pyroclastic deposits temporarily stored in coastal environments is also plausible.

Pumice–lithic breccia adjacent to sills

Pumice–lithic breccia in drillholes MCD 6, MCD 7 and MCD 10 is intruded by andesitic sills (Figs 1 and 3). In two instances (MCD 6 and MCD 10) a single interval of andesite occurs within very thick, massive pumice–lithic breccia. In the third instance (MCD 7), there are five intervals of andesite, the uppermost two of which have faulted contacts. Where contacts between the andesite and the pumice–lithic breccia are preserved and are not fault contacts, a well-developed eutaxitic texture occurs in the pumice–lithic breccia adjacent to the contacts. There is a gradual transition towards these contacts from randomly oriented, slightly compacted pumice clasts to strongly aligned and compacted pumice clasts adjacent to the andesite (Fig. 4). The compacted pumice clasts are plastically deformed around lithic clasts close to the contacts (e.g. MCD 7, Fig. 4). In addition, pumice–lithic breccia close to the andesite is indurated and silicified. The eutaxitic texture, induration and silicification extend as far as 3 m from the contact with the andesite. Contacts of the sills, the eutaxitic foliation, the weak compaction foliation and regional bedding are all more or less parallel and subhorizontal. In these drillhole sections, the eutaxitic texture, induration and

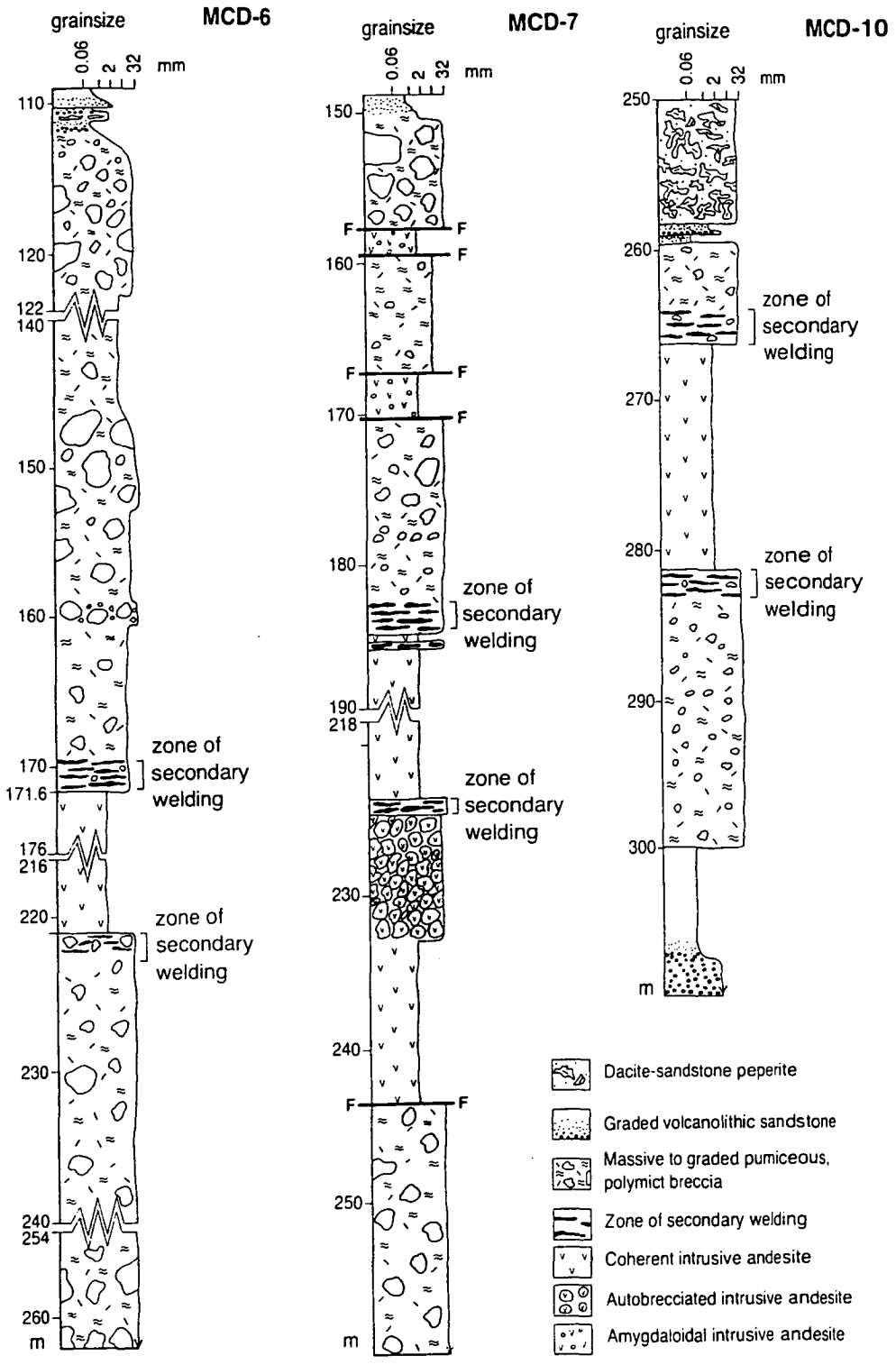

Fig. 3 Graphic logs of drill-core from part of MCD 6, MCD 7 and MCD 10. MCD 6 and MCD 7 are both located within about 3 km SE of Mount Chalmers pit (Fig. 1). The pumice–lithic breccia units in each section are correlated (SR Hunns, unpublished data). Eutaxitic texture occurs at both contacts of a single, 50 m thick andesite sill in MCD 6. Of the five intervals of andesite in MCD 7, only three have unfaulted contacts; in each instance the adjacent pumice–lithic breccia shows eutaxitic foliation. Drill-core samples from one zone of secondary welding and the andesite in MCD 7 are illustrated in Fig. 4. MCD 10 is located about 2 km S of Mount Chalmers pit (Fig. 1). Eutaxitic foliation occurs in pumice–lithic breccia adjacent to both the lower and upper contacts of a 15 m thick andesite sill. F, Faulted contact

silicification occur in the pumice–lithic breccia *only* where it is in contact with intrusive andesite.

Similar relationships between a gently south-dipping, 3 m thick andesite sill and pumice–lithic breccia are exposed on the east face of the Mount Chalmers pit. Away from the andesite, the pumice–lithic breccia is massive. Within about 1 m of both the upper and lower contacts of the sill, the pumice–lithic breccia shows a distinct foliation, which is parallel to the contacts and defined by strongly flattened relict pumice clasts. Although everywhere sharp, the lower contact of the sill is locally highly irregular. Flame-like protrusions of pumice–lithic breccia extend upwards into the andesite, suggesting that the pumice–lithic breccia was unconsolidated at the time of intrusion.

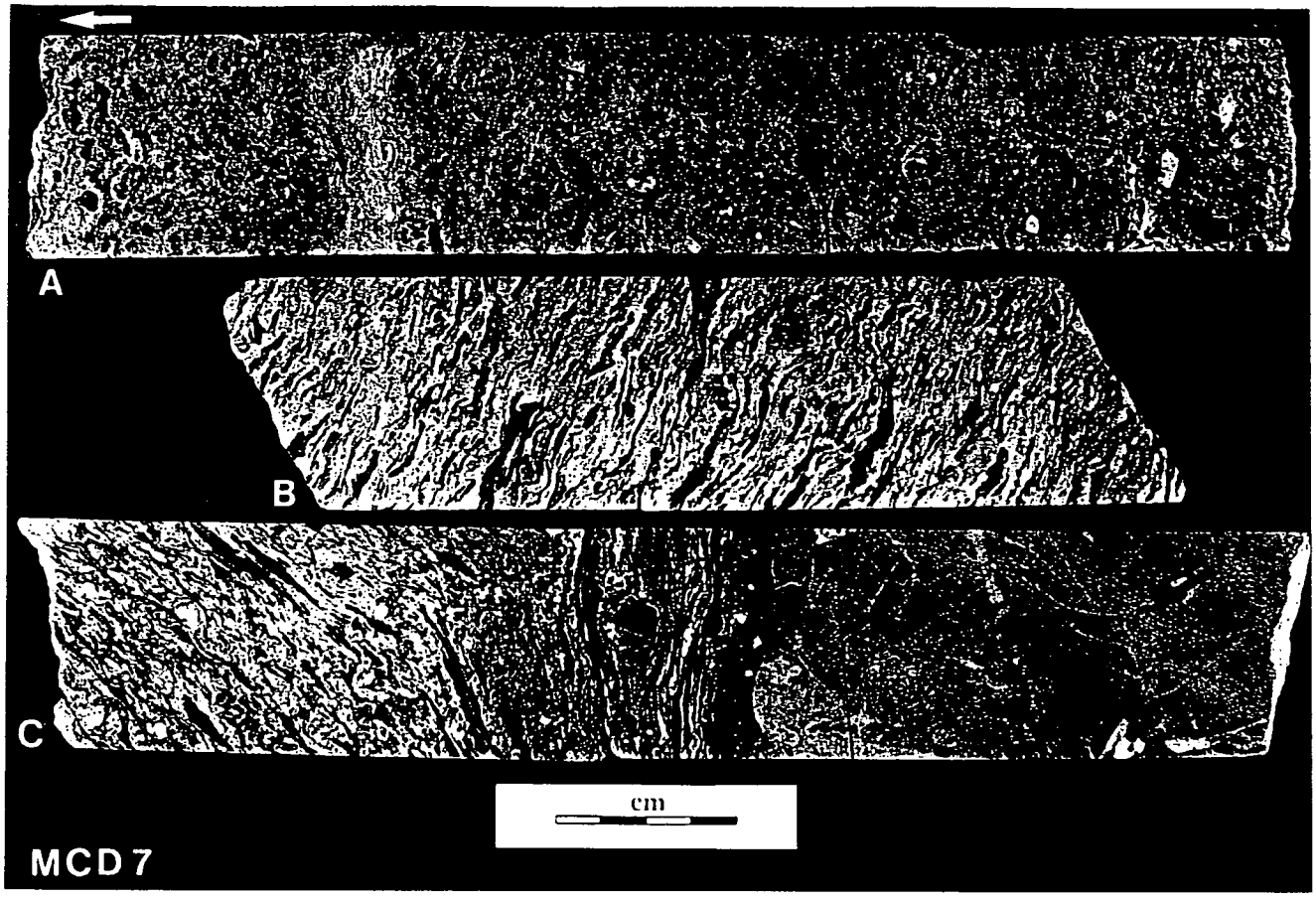

Fig. 4 Drillcore samples from MCD 7 (Fig. 3), showing well-developed eutaxitic texture in pumice–lithic breccia adjacent to an andesite sill. The eutaxitic foliation is subparallel to the sill contacts and to regional bedding. The samples come from the uppermost zone of secondary welding: **A** (181.6 m), **B** (184.3 m) and **C** (184.7 m). The contact with the andesite occurs at 184.6 m. Sample depths have been measured from the centre of the drillcore. Arrow, uphole direction

Pumice–lithic breccia adjacent to dykes

Pumice–lithic breccia in New Zealand Gully, about 4 km south-west of Mount Chalmers pit (Fig. 1), is intruded by rhyolitic and andesitic dykes. The orientation of bedding is not evident along the gully because all outcrops are within a very thick (at least 200 m) unit of massive pumice–lithic breccia. However, regional bedding dips gently (<20°) to the west. Contacts between dykes and the pumice–lithic breccia are exposed at localities NZ 22 (258245mE 7417432mN; Rockhampton 1:100000), and NZ 24 (258400mE 7417340mN; Rockhampton 1:100000). The dyke at NZ 22 is rhyolite and about 50 m wide; the single exposed contact with pumice–lithic breccia is oriented 70°/105° (dip/dip azimuth). The dyke at NZ 24 is andesite and about 1.2 m wide; its contacts with the pumice–lithic breccia are oriented 80°/016°. Away from the dykes, the pumice–lithic breccia is massive, apart from a very weak, near vertical, N–S trending regional cleavage. In both instances, a well-developed eutaxitic foliation is present in the pumice–lithic breccia adjacent to the dykes (Fig. 5) and is oriented parallel to the dyke contacts. The texture dies out beyond about 3 m from the contact with the rhyolite (NZ 22) and beyond about 1 m from the andesite (NZ 24). The eutaxitic texture is defined by compacted, aligned pumice clasts; the pumice clasts adjacent to the lithic fragments are the most strongly deformed (Fig. 5).

A poorly exposed contact between andesite and pumice–lithic breccia occurs on a track leading to the hilltop above the northern face of the Mount Chalmers pit. Relationships are similar to those observed at New Zealand Gully. The contact is near vertical and trends north-easterly. Eutaxitic foliation developed in adjacent pumice–lithic breccia is more or less parallel to the contact and dies out within 1–2 m.

Eutaxitic texture in thin section

The pumice–lithic breccia consists of close-packed, granule-size and coarser, feldspar–phyric, tube pumice clasts together with lithic fragments. Feldspar crystals are mainly phenocrysts within pumice clasts. Although euhedral, many show jigsaw-fit fracture patterns, indicating they have broken *in situ*, perhaps reflecting brit-

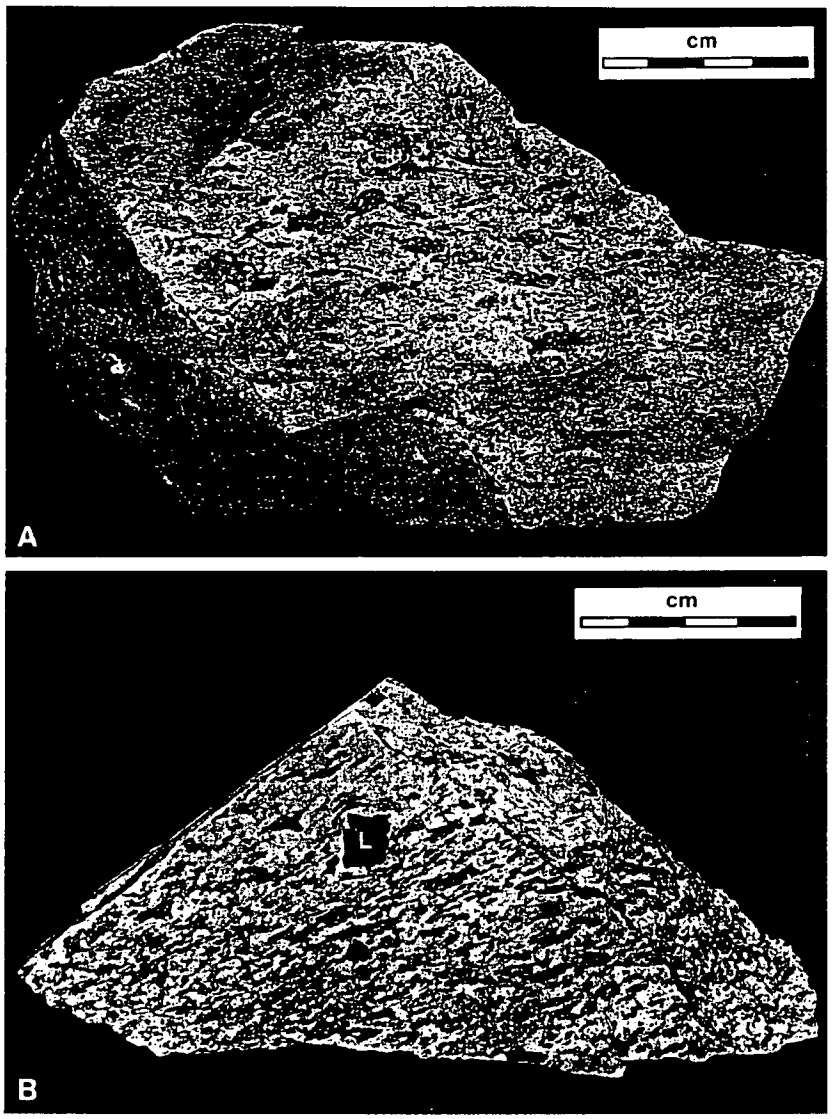

Fig. 5A, B Samples of pumice–lithic breccia from New Zealand Gully, about 4 km SW of Mount Chalmers (Fig. 1). **A** NZ 22, Adjacent to a rhyolite dyke, weathered surface. **B** NZ 24, Adjacent to an andesite dyke, sawn and polished surface. Both samples show well-developed eutaxitic texture defined by dark grey, wispy, compacted relict tube pumice clasts. The eutaxitic foliation in each instance is oriented parallel to the steeply dipping contacts of the dykes. In **B**, the pumice clasts adjacent to lithic fragments (L) are the most strongly deformed

tle fracturing during compaction of the enclosing pumice. In massive pumice–lithic breccia, the tube pumice clasts are randomly oriented and vary from equant to lenticular. Closer to the contacts with the intrusions, most pumice clasts are aligned and the tube vesicles are compacted, but some retain a tube vesicle texture oriented at high angles to the eutaxitic foliation. Adjacent to the intrusions, relict pumice clasts have been deformed into long thin 'strands' that wrap around rigid phenocrysts and lithic fragments.

In thin section, the tube pumice structure is clearly preserved where the glass has been replaced by a very fine grained quartzo-feldspathic mosaic (Fig. 6A). In instances where phyllosilicates (principally sericite or chlorite) have replaced the glass, the relict pumice clasts are represented by wispy phyllosilicate lenses and patches in which the original vesicular microtextures are less distinct (Fig. 6B). Strongly flattened pumice in samples from close to the intrusions contain abundant, round and ovoid, quartz-filled amygdales (Fig. 6C). These were small vesicles, generated by secondary vesiculation during re-heating by the adjacent intrusions (cf. Schmincke 1967; Yamamoto et al. 1991). Furthest from the intrusions, the vesicles are very small (0.1 mm diameter) and they increase in size up to about 2 mm across at the contacts of the intrusions.

Spherical structures are especially conspicuous in pumice lenses replaced by phyllosilicates (Fig. 7A). Some are composed of radially arranged, fine, quartz or feldspar crystals and are interpreted to be spherical spherulites (cf. Lofgren 1971a). Others that are identical in mineralogy, size, shape and distribution, but lacking distinct radial structure, may be recrystallized spherical spherulites. There is a range in size from less than 0.04 mm in the least compacted samples to about 0.1 mm close to the intrusions. Also close to the intrusions, some samples show interlocking quartz patches that overprint the relict pumice and strongly resemble micropoikilitic (or 'snowflake') texture (Fig. 7B and 7C; cf. Anderson 1969; Lofgren 1971a; Bigger and Hanson 1992). Samples that contain amygdales (Fig. 6C) are also spherulitic and characterized by sheath spheru-

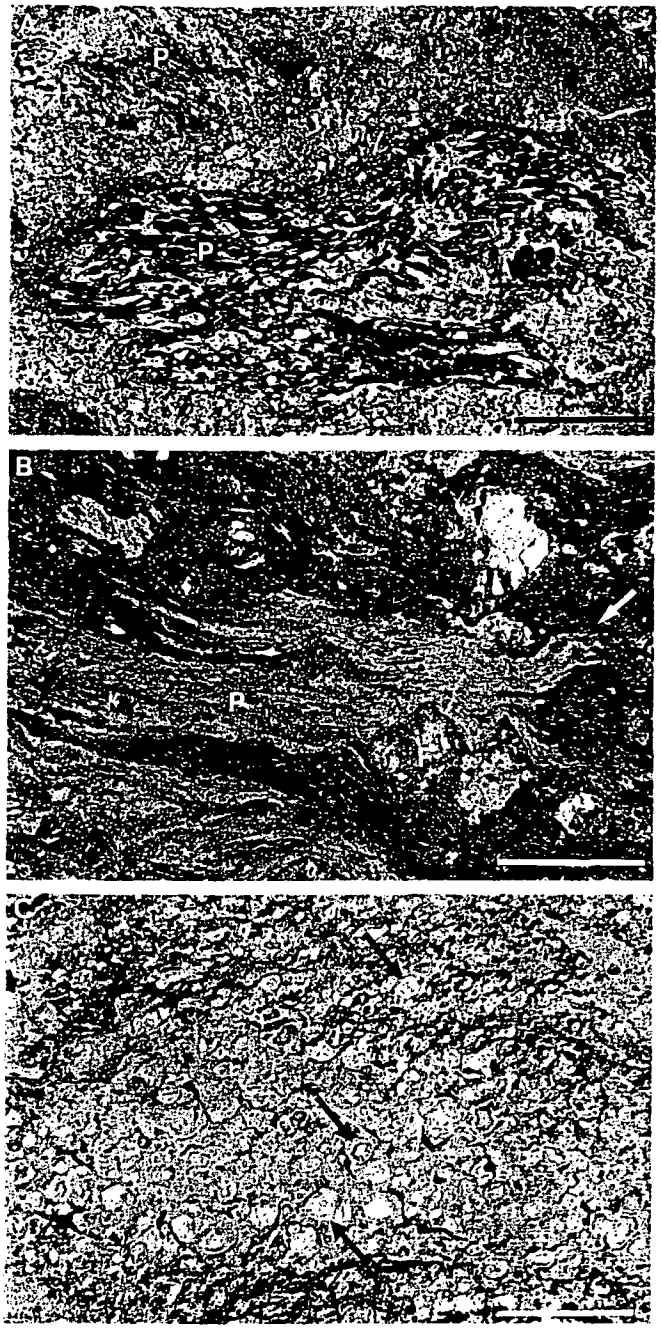

Fig. 6A–C Photomicrographs of pumice–lithic breccia in the Berserker beds. **A** Tube vesicle texture preserved in relict pumice (P) in massive pumice–lithic breccia from the New Zealand Gully area (sample NZ 1b). The tube vesicles within the pumice clasts are uncompacted and the pumice clasts have different orientations. Plane polarized light, scale bar 0.5 m. **B** Sericite-altered tube pumice (P) clasts in pumice–lithic breccia that shows good eutaxitic foliation (NZ 22, Fig. 5A). Pumice clasts have wispy terminations (arrow). Tube vesicles are compacted and deformed adjacent to feldspar (F) phenocrysts. Plane polarized light, scale bar 1 mm. **C** Abundant amygdales (e.g. arrows) within a compacted pumice clast from pumice–lithic breccia with good eutaxitic foliation (MCD 6, 170.4 m, Fig. 3). The pumice clast fills the field of view and is crowded with round or ovoid, quartz-filled amygdales up to about 0.3 mm diameter. Between the amygdales are abundant impinging sheath spherulites (cf. Lofgren 1971a), evident only with crossed nicols. The amygdales record secondary vesiculation of compacted pumice as a result of re-heating by an adjacent andesite sill. Plane polarized light, scale bar 1 mm

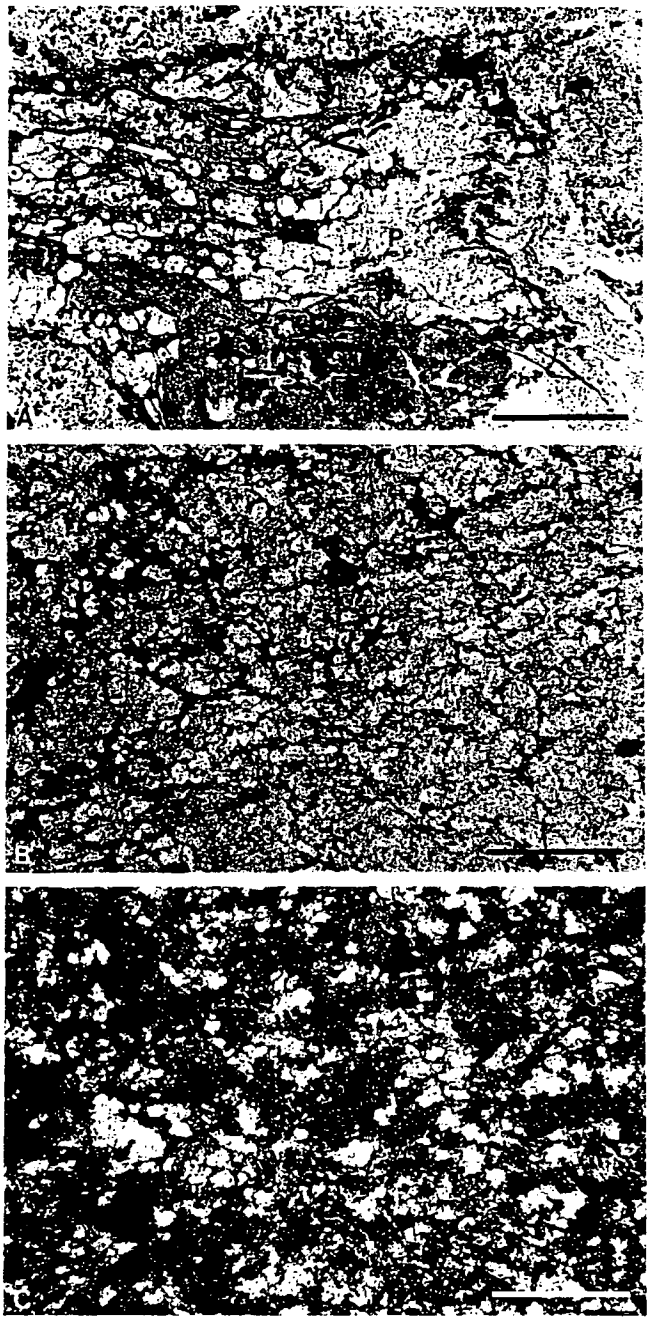

Fig. 7A–C Photomicrographs showing devitrification textures in pumice–lithic breccia affected by secondary welding. **A** Spherulites (e.g. arrows; about 0.8 mm diameter) in a compacted pumice (P) clast from pumice–lithic breccia that shows well-developed eutaxitic foliation (NZ 24, Fig. 5B). On the left-hand side, spherulites are isolated within chlorite that replaces compacted former glass; on the right-hand side, the spherulites have coalesced. Plane polarized light, scale bar 0.5 mm. **B, C** Micropoikilitic texture in pumice–lithic breccia affected by secondary welding adjacent to an andesite sill (MCD 10, 265.5 m, Fig. 3). The poikilitic quartz patches are about 0.05–0.1 mm diameter. They include abundant very fine feldspar microlites replaced by sericite and are outlined by narrow seams of very fine phyllosilicates and opaque grains. In both thin section and hand specimen, pumice clasts are less distinct where the micropoikilitic texture occurs. The micropoikilitic texture overprints the eutaxitic foliation and is the result of devitrification during slow cooling after secondary welding of the pumice–lithic breccia. **B** Plane polarized light; **C** crossed nicols; scale bar 0.5 mm

lites, many of which nucleated on the amygdale margins.

Origin: secondary welding compaction adjacent to intrusions

In most outcrops and drillcore sections, the pumice–lithic breccia at Mount Chalmers is non-welded and entirely massive or else displays a weak, bedding-parallel, diagenetic compaction foliation. The parent pumice-rich mass flows were submarine, although they may have originated from a shallow water or subaerial source. Juvenile pumiceous clasts can remain very hot during transport and after deposition from syn-eruptive, water-supported mass flows (e.g. Tamura et al. 1991; Cashman and Fiske 1991). Nevertheless, primary welding compaction is uncommon in submarine pumiceous mass-flow deposits, either because the clasts are cooler than the minimum welding temperatures, or because the lithostatic load is insufficient. A primary welding origin for the eutaxitic foliation observed in pumice–lithic breccia at Mount Chalmers is untenable because the texture is strictly confined to the vicinity of intrusions, including dykes, and dies out a few metres away from the intrusive contacts. Instead, the texture is interpreted to be secondary, and resulted from re-heating and compaction of tube pumice close to the intrusions. The presence of spherulites and round amygdales in flattened relict pumice provides critical evidence that compaction involved high-temperature welding, rather than low-temperature compaction of pumice that was more altered and, hence, mechanically weak, adjacent to intrusions.

Secondary welding compaction of cold pumice can occur providing: (1) the pumice is still glassy and porous at the time of intrusion; (2) there is sufficient directed stress, either lithostatic load or stress related to the intrusion of dykes or sills; and (3) enough heat is transferred to the pumice–lithic breccia so that the glass can deform plastically and compact. Previous workers have highlighted the importance of water vapour pressure, in addition to temperature and load, in promoting primary welding (Smith 1960; Boyd 1961; Sparks et al. 1980), and steam generated in porous deposits under lava flows may play a part in the heat transfer involved in forming 'fused tuffs' (Christiansen and Lipman 1966; Schmincke 1967). The water-saturated condition of the submarine pumice–lithic breccia at Mount Chalmers may thus have been a factor favouring the development of secondary welding compaction when the intrusions were emplaced (cf. Ito et al. 1984).

The eutaxitic foliation in the Mount Chalmers pumice–lithic breccia is parallel to the intrusive contacts. In the instances involving sills, this orientation is subparallel to bedding and perpendicular to the direction of the greatest principal stress (σ_1) generated by lithostatic load. In instances involving dykes, the foliation defined by flattened pumice clasts reflects the local stress field related to the emplacement of the dykes, rather than the lithostatic load. That is, the subhorizontally directed stress associated with the intrusion of the dykes was evidently more important than lithostatic load during secondary welding of the adjacent pumice–lithic breccia and produced steeply dipping, contact-parallel eutaxitic foliations. Indeed, the volume reduction in the pumice–lithic breccia reflected by the secondary welding compaction may have facilitated intrusion of the dykes.

Re-heating of the glassy pumice–lithic breccia adjacent to intrusions resulted not only in secondary welding compaction, but also in high-temperature devitrification of the glass. Spherulities and micropoikilitic textures develop during cooling of felsic glass and result from crystallization at relatively high temperatures (Lofgren 1971a, 1971b), probably above the glass transition temperature (Manley 1992). Furthermore, such textures develop only in continuous glass and therefore are common in the interiors of lavas, shallow intrusions and thick, densely welded ignimbrites (Anderson 1969; Lofgren 1971a, 1971b; Bigger and Hanson 1992; Manley 1992). Lofgren (1971a, 1971b) concluded that spherulitic textures generated during first cooling and during re-heating would be similar and that such textures do not alone indicate a particular origin for the glass. Their presence in pumice–lithic breccia at Mount Chalmers can only be explained as a result of re-heating and secondary welding compaction of the tube pumice to continuous non-vesicular glass, followed by spherulitic and micropoikilitic devitrification. Very similar textures were recognized immediately north of the Mount Chalmers pit by Sainty (1992) and interpreted by him to indicate primary welding. However, another possibility suggested by this study is that his samples were affected by re-heating adjacent to a concealed intrusion.

Conclusions

We interpret eutaxitic textures within pumice–lithic breccia at Mount Chalmers to be the result of secondary welding compaction adjacent to intrusions. The critical evidence indicating that re-heating was responsible for the compaction is the presence of amygdales, due to re-vesiculation, and spherulities, generated by high-temperature devitrification, within flattened pumice clasts adjacent to intrusions. As predicted by Lofgren (1971a, 1971b) the high-temperature devitrification textures are the same as those formed during initial cooling of hot glass.

Secondary welding is probably common in submarine volcanic sequences because these typically include thick, glassy pumice-rich deposits and syn-volcanic intrusions (McPhie and Allen 1992). For example, very similar secondary welding is present in submarine pumice-rich volcaniclastic rocks re-heated by syn-volcanic andesitic and dacitic intrusions in the southern Izu Pen-

insula, Japan (Ito et al. 1984). Such occurrences of secondary welding compaction differ from 'fused tuff' (Smith 1960; Christiansen and Lipman 1966; Schmincke 1967) in two main respects: (1) the affected units are submarine-emplaced pumice-rich volcaniclastic mass-flow deposits rather than subaerial, primary pyroclastic deposits; and (2) syn-volcanic intrusions rather than lava flows were involved.

Zones of secondary welding compaction at Mount Chalmers extend to a few metres away from the intrusive contacts of both dykes and sills, and the eutaxitic foliation is parallel to the contacts. Away from the intrusions the pumice–lithic breccia is massive, non-welded and shows no evidence for having been emplaced hot. In instances involving sills, the eutaxitic foliation is approximately parallel to bedding and large areas (km^2) of pumice–lithic breccia have been affected. Where exposure is poor and the sills or their contacts are concealed, the more or less conformable zones of welded pumice–lithic breccia could easily have been mis-interpreted as welded, primary, pyroclastic flow deposits (ignimbrite).

Acknowledgements Rod Allen, Ray Cas, Mark Doyle and Bob Christiansen provided critical reviews of early versions of this paper. Mining Project Investors, Outukumpu Exploration Australia Pty Ltd and the ARC contributed financial support for the research.

References

Allen RL (1988) False pyroclastic textures in altered silicic lavas, with implications for volcanic-associated mineralization. Econ Geol 83:1424–1446

Allen RL (1992) Reconstruction of the tectonic, volcanic, and sedimentary setting of strongly deformed Zn–Cu massive sulfide deposits at Benambra, Victoria. Econ Geol 87:825–855

Anderson JE Jr (1969) Development of snowflake texture in a welded tuff, Davis Mountains, Texas. Geol Soc Am Bull 80:2075–2080

Bigger SE, Hanson RE (1992) Devitrification textures and related features in the Carlton Rhyolite in the Blue Creek Canyon area, Wichita Mountains, southwestern Oklahoma. Oklahoma Geol Surv, Geol Notes 52:124–142

Boyd FR (1961) Welded tuffs and flows in the rhyolite plateau of Yellowstone Park, Wyoming. Geol Soc Am Bull 72:387–426

Branney MJ, Sparks RSJ (1990) Fiamme formed by diagenesis and burial-compaction in soils and subaqueous sediments. J Geol Soc London 147:919–922

Cashman KV, Fiske RS (1991) Fallout of pyroclastic debris from submarine volcanic eruptions. Science 253:275–279

Christiansen RL, Lipman PW (1966) Emplacement and thermal history of a rhyolite lava flow near Fortymile Canyon, southern Nevada. Geol Soc Am Bull 77:671–684

Dadd KA (1992) Structures within large volume rhyolite lava flows of the Devonian Comerong Volcanics, southeastern Australia, and the Pleistocene Ngongotaha lava dome, New Zealand. J Volcanol Geotherm Res 54:33–51

Hunns SR, Kuronen U, Taube A (1993) Volcano-sedimentary stratigraphy of the Mount Chalmers ore body. IAVCEI General Assembly, Canberra, Abstracts, p 51

Ito T, Matsumoto R, Kano K, Sakuyama M (1984) Welding of acidic tuff and altered rhyolite fragments caused by the intrusion of magma examples in the Neogene Shirahama Group in the southern part of the Izu Peninsula, central Japan. J Geol Soc Jpn 90:191–205

Kirkegaard AG, Shaw RD, Murray CG (1970) Geology of the Rockhampton and Port Clinton 1:250000 sheet areas. Geol Surv Qld Rep 38:155 pp

Large RR, Both RA (1980) The volcanogenic sulfide ores at Mount Chalmers, eastern Queensland. Econ Geol 75:992–1009

Lofgren G (1971a) Spherulitic textures in glassy and crystalline rocks. J Geophys Res 76:5635–5648

Lofgren G (1971b) Experimentally produced devitrification textures in natural rhyolitic glass. Geol Soc Am Bull 82:111–124

Manley CR (1992) Extended cooling and viscous flow of large, hot rhyolite lavas: implications of numerical modeling results. J Volcanol Geotherm Res 53:27–46

McPhie J, Allen RL (1992) Facies architecture of mineralised submarine volcanic sequences: Cambrian Mount Read Volcanics, western Tasmania. Econ Geol 87:587–596

McPhie J, Doyle MG, Allen RL (1993) Volcanic Textures. Centre for Ore Deposit and Exploration Studies, University of Tasmania, 198 pp

Okill R (1974) Distribution and genesis of the Mount Chalmers Cu–Au mineralization, Southeast Queensland. Carpentaria Exploration Company, Unpubl Rep:34 pp

Ross CS, Smith RL (1961) Ash-flow tuffs: their origin, geologic relations and identification. USGS Prof Pap 366:81 pp

Sainty RA (1992) Shallow-water stratigraphy at the Mount Chalmers volcanic-hosted massive sulfide deposit, Queensland, Australia. Econ Geol 87:812–824

Schmincke H-U (1967) Fused tuff and pépérites in south-central Washington. Geol Soc Am Bull 78:319–330

Smith RL (1960) Ash flows. Geol Soc Am Bull 71:795–842

Sparks RSJ, Wright JV (1979) Welded air-fall tuffs. Spec Pap Geol Soc Am 180:155–166

Sparks RSJ, Sigurdsson H, Carey SN (1980) The entrance of pyroclastic flows into the sea, II. Theoretical considerations on subaqueous emplacement and welding. J Volcanol Geotherm Res 7:97–105

Sparks RSJ, Stasiuk MV, Gardeweg M, Swanson DA (1993) Welded breccias in andesite lavas. J Geol Soc London 150:897–902

Tamura Y, Koyama M, Fiske RS (1991) Paleomagnetic evidence for hot pyroclastic debris flow in the shallow submarine Shirahama Group (Upper Miocene–Pliocene), Japan. J Geophys Res 96:21779–21787

Taube A (1990) Mount Chalmers gold–copper deposits. In: Hughes FE (ed) Mineral Deposits of Australia and Papua New Guinea. The Australasian Institute of Mining and Metallurgy, Melbourne, pp 1493–1497

Taube A, van der Helder P (1983) The Mount Chalmers mine and environment – a Kuroko-style volcanogenic sulphide environment. In: Permian Geology of Queensland. Geol Soc Aust Qld Div, Brisbane, pp 387–399

Yamamoto T, Soya T, Suto S, Uto K, Takada A, Sakaguchi K, Ono K (1991) The 1989 submarine eruption off eastern Izu Peninsula, Japan: ejecta and eruption mechanisms. Bull Volcanol 53:301–308

Composition of fluid inclusions from the Hellyer and Mt. Chalmers VHMS deposits, Australia: implications for source of ore-forming fluids

Khin Zaw
CODES Key Centre, University of Tasmania, Hobart, Tasmania, AUSTRALIA 7001

J. B. Gemmell
CODES Key Centre, University of Tasmania, Hobart, Tasmania, AUSTRALIA 7001

S. R. Hunns
CODES Key Centre, University of Tasmania, Hobart, Tasmania, AUSTRALIA 7001

T. P. Mernagh
Australian Geological Survey Organisation, Canberra, ACT, AUSTRALIA 2601

C. G. Ryan
CSIRO Division of Exploration and Mining, North Ryde, NSW, AUSTRALIA 2113

R. R. Large
CODES Key Centre, University of Tasmania, Hobart, Tasmania, AUSTRALIA 7001

R.A. Both
Geology Department, University of Adelaide, Adelaide, SA, AUSTRALIA 5005

ABSTRACT

The Hellyer and Mt. Chalmers deposits are mound-style volcanic-hosted massive sulphide (VHMS) deposits in Australia. Textural, petrographic and microthermometric investigations of fluid inclusions in the Hellyer stringer system indicate that Type I, primary, liquid-vapour inclusions are 10-15 μm in size, and yield homogenisation temperatures of 170-220°C in early 2A veins, 165-322°C in main-stage 2B veins and 190-256°C in late-stage 2C veins. These data suggest a waxing and waning thermal history. However, the average salinity remained between 8-11 NaCl equiv. wt % in all Stage 2 veins. At Mt. Chalmers, Type I inclusions up to 20 μm are found in quartz from the mineralised zone, and these inclusions yielded homogenisation temperatures of 160-268°C and salinities of 5-8 NaCl equiv. wt %. Laser Raman spectroscopic (LRS) analysis indicates the presence of CO_2 (<1 mole %) in the Hellyer and Mt. Chalmers VHMS systems. Semi-quantitative SEM/WDS microprobe analyses of fluid inclusion decrepitates indicate that the Hellyer and Mt. Chalmers ore fluids were enriched in potassium and calcium but depleted in magnesium relative to seawater. PIXE microanalysis of fluid inclusions in quartz also indicates a significant base metal concentration in these fluids. Cation composition and higher salinities relative to seawater suggest that recycled seawater alone cannot be the sole source of the ore fluids. High base metal content and the presence of CO_2 in the fluid inclusions imply that magmatic input of ore metals during seawater leaching of the footwall volcanic pile is a distinct possibility.

KEYWORDS: *VHMS, Hellyer, Mt. Chalmers, fluid inclusions, PIXE, Laser Raman.*

INTRODUCTION

The Hellyer and Mt. Chalmers deposits are important volcanic-hosted massive sulphide (VHMS) deposits in Australia (Figure 1). The Hellyer massive sulphide deposit in western Tasmania is a high grade polymetallic deposit with ore reserves of 17 million tonnes at 13.0 % Zn, 6.8 % Pb, 0.3 % Cu, 160 g/t Ag, and 2.3 g/t Au (Gemmell and Large, 1992). The Mount Chalmers deposit in Queensland consists of two ore lenses, the Main Lode and the West Lode, with a total pre-mining resource of 4.3 million tonnes grading 1.76% Cu and 2.15 g/t Au (Hunns, 1994; Hunns *et al.*, 1994). The major aim of this study is to use the fluid inclusion compositional variation as constraints for the source of the ore-forming fluids at the Hellyer and Mt. Chalmers deposits.

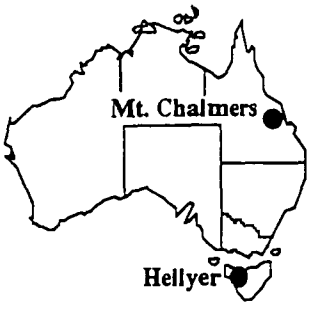

Figure 1 Location of the Hellyer and Mt. Chalmers deposits, Australia.

GEOLOGICAL SETTING

The Hellyer deposit lies in the Cambrian Mt Read Volcanics, which occur in an arcuate, longitudinal belt of 200 km long and up to 15 km wide (Figure 2). The Mt Read Volcanics consist of calc-alkaline volcanic rocks which are predominantly rhyolite, dacite and andesite with minor basalt (Gemmell and Large, 1992). The Mt Read Volcanics are subdivided into several sequences, one of which, the felsic Central Volcanic Complex (CVC), is host to several important VHMS deposits in western Tasmania, the Mount Lyell, Hercules and Rosebery deposits.

The Hellyer and Que River deposits are hosted in the Que-Hellyer sequence which is inferred by regional mapping to overlie the CVC. The Que-Hellyer sequence is dominated by andesitic lava, breccia and volcaniclastic rocks consisting of basaltic lava and breccia, and minor amounts of dacitic lava, intrusions and breccia (McArthur and Dronseika, 1990). The surface geology of the Hellyer deposit is shown in Figure 2. The footwall unit consists of feldspar-phyric, massive and fragmental andesitic and basaltic lavas with intercalated polymict epiclastic mass-flow sediments. The Hellyer mineralised sequence consists of a poorly sorted, polymict mass-flow breccia of dominantly andesitic composition and fine-grained, massive to well-laminated ash units. Overlying the mineralised sequence are polymict breccia, ash and shale, basaltic pillow lava, Que River shale and interbedded rhyolitic volcaniclastics, graded greywacke, shale and siltstone (McArthur and Dronseika, 1990; Gemmell and Large, 1992). The Que-Hellyer area was subjected to deformation during the Middle Devonian Tabberabberan Orogeny, producing two major fold trends. A major synclinal axis passes through the Que River deposit and a major parallel anticlinal axis passes through the Hellyer deposit. Regional metamorphism in the area is prehnite-pumpellyite facies (McArthur and Dronseika, 1990).

The Mt. Chalmers deposit is hosted within the Early Permian Berserber beds, a volcaniclastic sequence in Queensland (Large and Both, 1980; Taube, 1990; Hunns, 1994; Hunns *et al*, 1994). The generalised surface geology (pre-mining) of the Mount Chalmers area is shown on Figure 3. The host stratigraphy is relatively flat lying and appears to be continuous for at least a few kilometres around the mine. The footwall units include: graded sericite-silica-chlorite altered polymict lithic breccia, feldspar-phyric, lithic and pumice rich breccias, massive to autobrecciated feldspar-phyric rhyolitic intrusions/flows and dacitic-andesitic quartz-chlorite altered lithic breccia. The hangingwall lithologies are composed of pumiceous, polymict lithic mass-flow deposits, mass-flow emplaced pumiceous breccia, peperite, graded and well-bedded bioturbated turbidites and late-stage cross-cutting andesitic dykes and quartz-feldspar porphyry dykes (Hunns, 1994; Hunns *et al*, 1994).

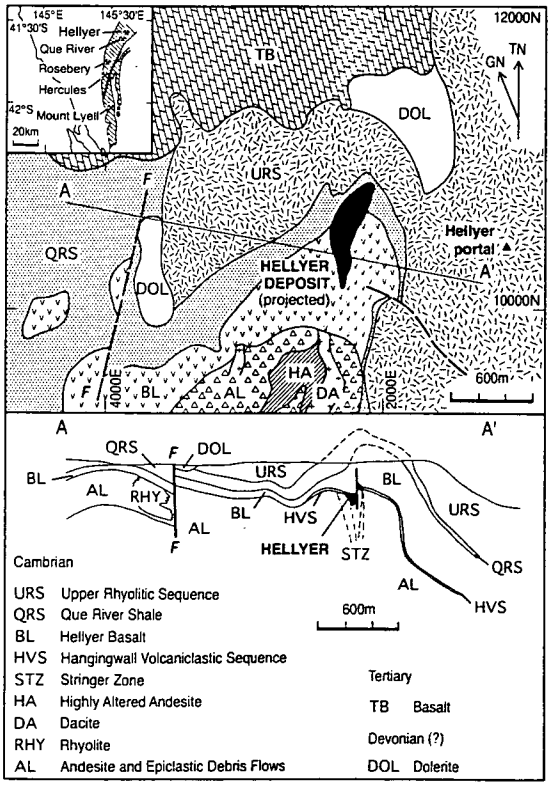

Figure 2 Geology surrounding the Hellyer deposit, Tasmania (after Gemmell and Large, 1992).

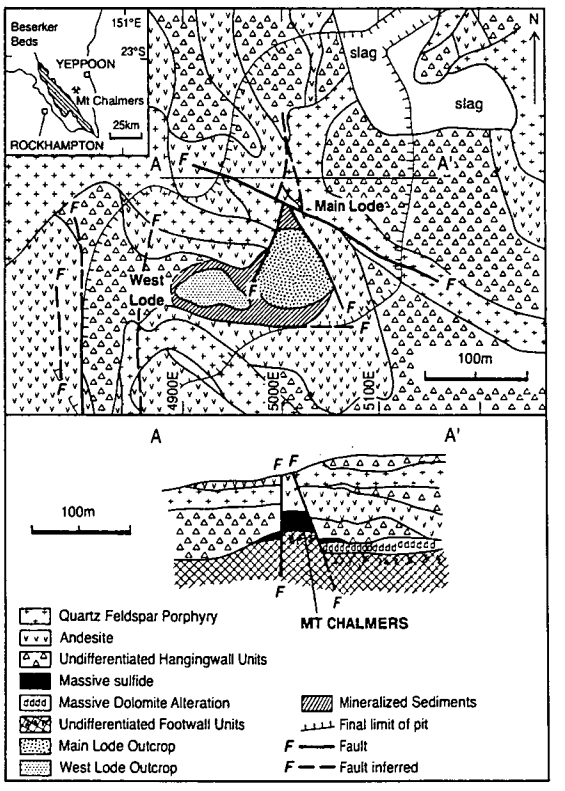

Figure 3 Geology surrounding the Mt Chalmers deposit, Queensland (after Hunns *et al*, 1994).

MINERALISATION

Hellyer and Mt. Chalmers occur as mound-shaped massive sulphide bodies with extensively altered footwall stringer zones. Gemmell and Large (1992) documented one stage of premineralisation, three stages of synmineralisation, and four stages of postmineralisation veins in the stringer system at Hellyer. The vein paragenesis indicates that premineralisation Stage 1 veins consist entirely of quartz, and occurs throughout the alteration pipe. The synmineralisation Stage 2 veins are most abundant veins and consist of three sub-stages: Stage 2A veins of crustiform quartz, pyrite, and carbonate with minor footwall amounts of chalcopyrite, sphalerite and galena, Stage 2B veins with abundant base metal sulphides with minor quartz, carbonate and barite gangue and Stage 2C veins of coarsely crystalline barite with variable amounts of pyrite, sphalerite, galena and carbonate. Stages 3-6 veins are postmineralisation veins that are related to the Devonian Tabberabberan Orogeny.

The massive sulphide mineralisation at Mt. Chalmers is hosted within well-bedded, graded, moderately to strongly quartz-sericite-pyrite altered volcaniclastic turbidites. The massive sulphide mineralisation comprises an upper massive zone, in part layered and fragmental, and underlain by a more extensive silica alteration cut by stringer sulphides veins. The massive sulphide contains gold, copper and silver plus minor zinc and lead. The stringer zone is much less pyritic and contains copper and gold with only traces of zinc, silver and lead (Taube, 1990; Hunns, 1994; Hunns *et al,* 1994).

FLUID INCLUSION STUDIES

A Fluid Inc. modified USGS heating/freezing stage was used in this study. The precision of the temperature measurements is better than ±1°C for heating and ±0.3°C for freezing. The fluid inclusions from Hellyer and Mt. Chalmers can be classified into three major types based on the phases observable in the inclusions at room temperature and their paragenesis. Fluid inclusions were also classified in a temporal sense as primary, secondary and pseudosecondary relative to the time of trapping as defined by Roedder (1984). The following inclusion types are observed:

Type I: Primary two-phase, liquid and vapour inclusions.

Type II: Primary three-phase with liquid, vapour and chalcopyrite daughter minerals.

Type III: Secondary two-phase, liquid-rich inclusions with variable liquid and vapour ratios.

Primary fluid inclusions can be distinguished in relation with textural criteria of the host minerals (e.g. growth zoning in quartz and colour banding in sphalerite). Negative shape or isolated, solitary nature are not considered as evidence for primary origin in this study.

FLUID INCLUSION PETROGRAPHY

Characteristics of fluid inclusions from Hellyer and Mt. Chalmers are shown in Figure 4. Type I inclusions are found in quartz, sphalerite and barite. In this study, only fluid inclusions in quartz and sphalerite have been investigated. Type I inclusions from Heyller occur within growth planes of the host quartz (Figure 4A). Type I inclusions are also found in quartz from the mineralised zone of the Mt Chalmers deposit (Figure 4B) but Type II inclusions are only found in quartz and sphalerite from the synmineralisation Stage 2B veins at Hellyer (Figures 4C and 4D). Chalcopyrite daughter minerals were identified by microscopy and by Laser Raman Spectroscopy. Similar chalcopyrite daughter mineral bearing fluid inclusions in sphalerite have been reported in the Fukazawa mine, Hokuroko district, Japan (Foley, 1986).

Type III inclusions are found in all minerals from both Heyller and Mt. Chalmers. They cross-cut all other inclusion types and also grain boundaries of host minerals. Their irregular shape and cross-cutting nature indicate a secondary origin. The randomly distributed array of these secondary Type III inclusions and their textural features suggest that they were probably formed during later metamorphic recrystallisation and deformation.

MICROTHERMOMETRY

Microthermometric investigation of Type I fluid inclusions in Stage 2 synmineralisation from the Hellyer stringer system yielded homogenisation temperatures of 170-220°C in early 2A veins, 165-322°C in main-stage 2B veins and 190-256°C in late-stage 2C veins. However, salinity varies between 8-11 NaCl equiv. wt % in all Stage 2 veins (Khin Zaw *et al,* 1994, 1995). In comparison, Type I fluid inclusions in the mineralised quartz from the Mt Chalmers deposit yielded homogenisation temperatures of 160-268°C and salinities of 5-8 NaCl equiv. wt % (Hunns *et al,* 1994). First melting temperatures of –25.0°C to –50.0°C indicate that the fluid is not a simple NaCl brine, and suggest that other salts of magnesium, potassium, calcium, iron and manganese may be present.

LASER RAMAN ANALYSIS

A DILOR MICRODIL-28® Raman microprobe at the Australian Geological Survey Organisation (AGSO), Canberra was used to quantitatively determine the gaseous components with a detection limit of 0.1 mole % for some species and to identify the daughter minerals in fluid inclusions. Gaseous components (H_2S, CO, CO_2, CH_4, SO_2, H_2, NH_3, N_2) in fluid inclusions from Hellyer and Mt. Chalmers were scanned by LRS method. Only CO_2 was present and other gas species were not detected.CO_2 was recorded in the Stage 2B veins (Figure 5A), but no detectable CO_2 in 2A and 2C vein stages at Hellyer. CO_2 was also found in fluid inclusions in quartz from the mineralised zone of the Mt. Chalmers deposit (Figure 5B).

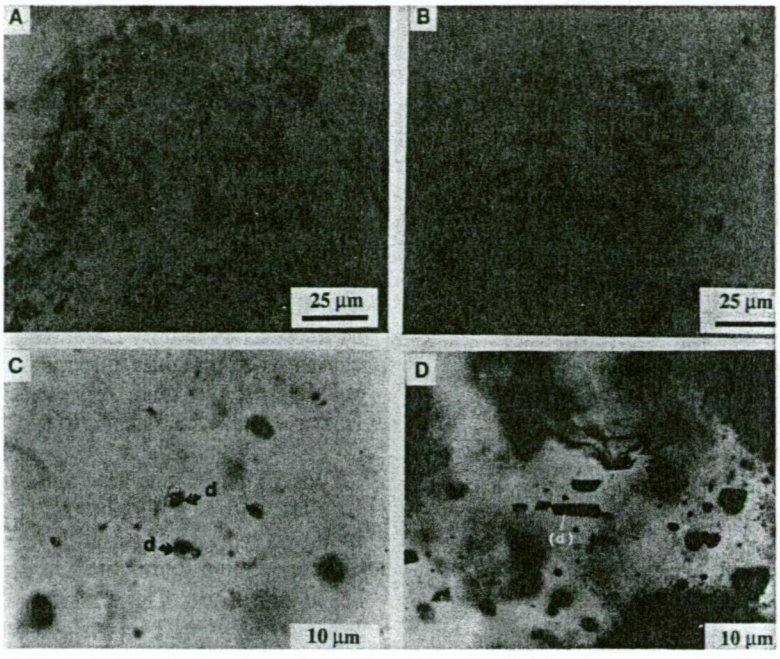

Figure 4 Photomicrographs showing primary fluid inclusions: **(A)** Type I fluid inclusions lining the growth planes in quartz from Stage 2B vein, Hellyer, **(B)** Type I inclusions in quartz from the mineralised zone, Mt. Chalmers, **(C)** Type II chalcopyrite-bearing inclusions in quartz from Stage 2B vein, Hellyer, and **(D)** Type II chalcopyrite-bearing inclusion in sphalerite from Stage 2Bvein, Hellyer.

The relatively low intensity of the CO_2 bands at 1383-1378 and 1281-1287 cm^{-1} suggests that the CO_2 content is near the detection limits of 0.1 mole %. Type II chalcopyrite-bearing primary fluid inclusions in the base metal-rich Stage 2B veins at Hellyer have been also confirmed by LRS method (Figure 5C).

SEM/WDS ANALYSIS

The major element chemistry of fluid inclusion decrepitates from the Hellyer and Mt. Chalmers deposits was studied by electron microprobe. Fluid inclusions were thermally decrepitated at 350-400°C to produce salt precipitates and these were analysed semi-quantitatively by SX 50 CAMECA microprobe. The semi-quantitative SEM/WDS microprobe analyses of fluid inclusion decrepitates indicate that the Hellyer ore fluid was enriched in potassium and calcium but depleted in magnesium relative to seawater (Figure 6A). Similar to the Hellyer deposit, the semi-quantitative SEM/WDS analysis of fluid inclusion decrepitates from quartz in the West Lode indicates significant potassium and calcium in the ore fluids (Figure 6B).

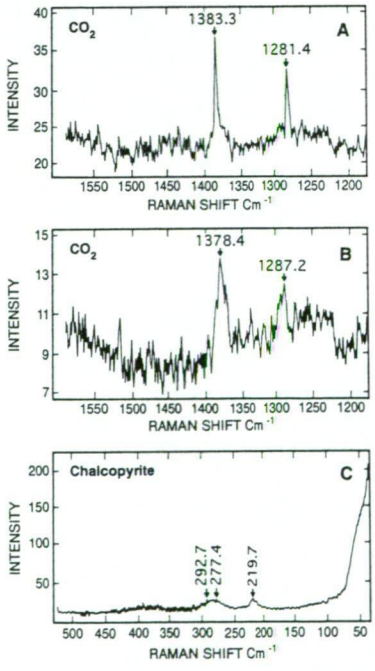

Figure 5 A. Laser Raman spectra of CO_2 in Type I fluid inclusion in quartz from Stage 2B vein, Hellyer. **B.** Laser Raman spectra of CO_2 in Type I inclusion in quartz from the ore zone, Mt. Chalmers, and **C.** Laser Raman spectra of chalcopyrite daughter mineral in Type II inclusion in quartz from Stage 2B vein, Hellyer. Laser power 40 mW (at sample) with 3 cm^{-1} band pass. Spectra were averaged from 10 accumulations at 10 second counting times.

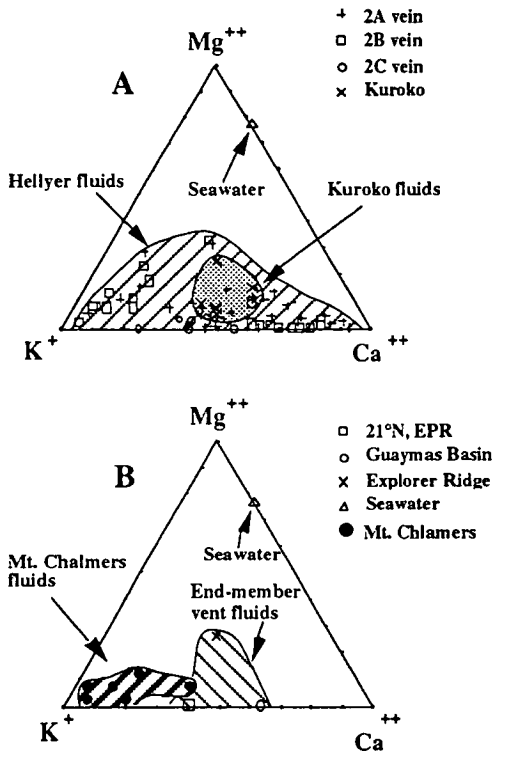

Figure 6 **A.** K-Ca-Mg plot of fluid inclusion decrepitates for the synmineralisation veins from the Hellyer stringer zone, western Tasmania together with fluid inclusion composition of the Kuroko deposits, Japan (after Pisutha-Arnond and Ohmoto, 1983); **B.** K-Ca-Mg plot of end-member vent fluids from 21° N, East Pacific Rise, Guaymas basin, Explorer Ridge and present-day sea water (after Hannington and Scott, 1988) together with fluid inclusion decrepitates composition from the Mt. Chalmers mineralised zone, central Queensland.

PIXE ANALYSIS

The development of non-destructive PIXE (Proton Induced X-ray Emission) microanalysis of the chemical composition of fluid inclusions (Ryan *et al*, 1991, 1993) has enabled quantitative determination of individual fluid inclusion compositions. Quantitative PIXE micro-analysis of fluid inclusions confirms the SEM/WDS analysis that significant amounts of potassium and calcium are present in the Hellyer and Mt. Chalmers ore fluids. PIXE results also indicate that the Stage 2A veins at Hellyer have 100-900 ppm Zn and 150-200 ppm Cu, whereas the Stage 2B veins contain 300-700 ppm Zn and 200-10000 ppm Cu. The Stage 2B ore fluids have a significantly higher base metal concentration compared to the Stage 2A veins. Quantitative PIXE micro-analysis of fluid inclusions in the mineralised quartz from the Main Lode at Mt. Chalmers yielded 65-300 ppm Cu and 79-101 ppm Zn.

DISCUSSION AND CONCLUSIONS

The Hellyer and Mt. Chalmers deposits are the least metamorphosed VHMS deposits in Australia. Detailed petrographic and textural studies indicate that primary fluid inclusions are present in these VHMS systems. At Hellyer, Type I fluid inclusions in quartz yielded homogenisation temperatures of 170-220°C in early 2A veins, 165-322°C in main-stage 2B veins and 190-256°C in late-stage 2C veins. This is comparable with results obtained by fluid inclusion studies of stringer zones from the Kuroko deposits by Pisutha-Arnond and Ohmoto (1983) and supports the interpretation of waxing and waning thermal history (e.g. Eldridge *et al*, 1983).

However, no consistent salinity variation was recognised. Salinity values remained within 8-11 NaCl equiv. wt % at Hellyer and 5-8 NaCl equiv. wt % at Mt. Chalmers. These ore fluid salinity values are higher than seawater. In this study, no fluid inclusion evidence of boiling (e.g. vapour-rich inclusions and liquid-rich inclusions together in the same healed micro-fracture) was recorded. Cation composition, higher salinities relative to seawater and the presence of CO_2 together with significant base metal concentration in the fluid inclusions suggest that recycled seawater alone cannot be the sole source of the VHMS ore fluids.

Fluid inclusion compositional data suggest that magmatic input of ore elements during the convective circulation of seawater and leaching of the footwall volcanic pile during the VHMS mineralisation cannot be ruled out. This interpretation is in agreement with stable isotopic studies (Gemmell and Large, 1992). They suggested that mineralising fluid at Hellyer initially consisted of totally to partially reduced seawater sulphate that evolved into a fluid dominated by an igneous sulphur as the convection system intensified and penetrated deeper into footwall. The enrichment of base metals (copper and zinc) in the fluid inclusions from the mineralised system suggests a possible use of the composition of ore fluids in determining the fluid flow pathway and vector to the high-grade mineralised zone.

ACKNOWLEDGEMENTS

The authors would like to thank geologists from the Aberfoyle Resources Limited and staff members of the Key Centre for Ore Deposit and Exploration Studies at the University of Tasmania for their critical discussions. Research was supported by Aberfoyle Resources Limited and Australian Research Council.

REFERENCES

Eldridge, C S, Barton, P B Jr and Ohmoto, H, 1983. Mineral textures and their bearing on formation of the Kuroko orebodies, *Econ Geol Mon*, 5: 241-281.

Foley, N K, 1986. Fluid inclusion study of ores from the Fukazawa mine, Hokuroko District, Akita Prefecture, Japan, *Mining Geology*, 36: 11-20.

Gemmell, J B, and Large, R R, 1992. Stringer system and alteration zones underlying the Hellyer volcanic-

hosted massive sulphide deposit, Tasmania, Australia, *Econ Geol*, 87: 620-649.

Hannington, M D and Scott, S D, 1988. Mineralogy and geochemistry of a hydrothermal silica-sulphide-sulphate spire in the caldera of Axial Seamount, Juan de Fuca Ridge, *Can Mineral*, 26: 603-625.

Hunns, S R, 1994. Geology of the Mount Chalmers volcanic-hosted massive sulphide and implications for its formation, *1994 Field Conference guidebook, Capricorn region, central coastal Queensland*, (Ed: R J Holcombe *et al*), p 80-92, (Geol Soc Australia).

Hunns, S R, Khin Zaw, Large, R R, Dean, J A, Ryan, C G, and McPhie, J, 1994. Preliminary geochemical results constraining the formation of the Mount Chalmers volcanic-hosted massive sulphide deposit: *New Developments in Geology and Metallogeny: Northern Tasman Orogenic Zone*, (Ed: R A Henderson), Extended Conference Abstracts Volume, Contributions of the Economic Geology Research Unit, No. 50: 117-124.

Khin Zaw, Gemmell, J B, Large, R R, Mernagh, T P, and Ryan, C G, 1994. Evolution of VHMS fluids in the footwall stringer zone, Hellyer deposit, western Tasmania: Constraints from fluid inclusion microthermometry and geochemistry: 12th Australian Geological Convention, Perth, Australia, *Geol Soc Aust Abstr*, 37: 482.

Khin Zaw, Gemmell, J B, Large, R R, Mernagh, T P, and Ryan, C G, 1995. Fluid evolution and source of ore fluids in the stringer system, Hellyer VHMS deposit, western Tasmania: evidence from fluid inclusion microthermometry and geochemistry, Wisdom of Solomon Special Volume, *Ore Geol Review* (in press).

Large, R R, and Both, R A, 1980. The volcanogenic sulphide ores at Mount Chalmers, eastern Australia, *Econ Geol*, 75: 992-1009.

McArthur, G J, and Dronseika, E V, 1990. Que River and Hellyer zinc-lead deposits. *Australasian Inst Mining and Metallurgy Mon*, 15: 1331-1339.

Pisutha-Arnond, V, and Ohmoto, H, 1983. Thermal history, and chemical and isotopic compositions of the ore-forming fluids responsible for the Kuroko massive sulphide deposits in the Hokuroko district of Japan, *Econ Geol Mon*, 5: 523–558.

Roedder, E, 1984. Fluid Inclusions, *Miner Soc Amer Reviews in Mineralogy* 12, 644 pp.

Ryan, C G, Cousens, D R, Heinrich, C A, Griffins, W L, Sie, S H and Mernagh, T P, 1991. Quantitative PIXE microanalysis of fluid inclusions based on a layered yield model, *Nuclear Instruments and Methods in Physics Research*, B54: 292-297.

Ryan, C G, Heinrich, C A, and Mernagh, T P, 1993. PIXE microanalysis of fluid inclusions and its application to study ore metals segregation between magmatic brine and vapour. *Nuclear Instruments and Methods in Physics Research*, B77: 463-471.

Taube, A, 1990. Mount Chalmers gold-copper deposit, in *Mineral deposits of Australia and Papua and New Guinea*, (Ed: F E Hughes), pp 1493-1497, Australasian Institute of Mining and Metallurgy.